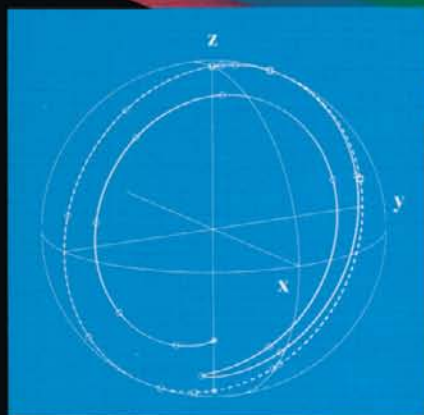


Analytical  
Spectroscopy  
Library

8



# Methods for Structure Elucidation by High-Resolution NMR

edited by  
Gy. Batta, K.E. Kövér and Cs. Szántay, Jr.

Elsevier

**Analytical Spectroscopy Library – Volume 8**

**Methods for Structure Elucidation  
by High-Resolution NMR**

**applications to organic molecules  
of moderate molecular weight**

## **Analytical Spectroscopy Library**

A Series of Books Devoted to the Application of Spectroscopic Techniques to Chemical Analysis

---

- Volume 1 **NMR for Liquid Fossil Fuels**, by L. Petrakis and D. Allen
- Volume 2 **Advances in Standards and Methodology in Spectrophotometry**, edited by C. Burgess and K.D. Mielenz
- Volume 3 **Introduction to Inductively Coupled Plasma Atomic Emission Spectrometry**, by G.L. Moore
- Volume 4 **Sample Introduction in Atomic Spectroscopy**, edited by J. Sneddon
- Volume 5 **Atomic Absorption Spectrometry. Theory, Design and Applications**, edited by S.J. Haswell
- Volume 6 **Spectrophotometry, Luminescence and Colour; Science and Compliance**, edited by C. Burgess and D.G. Jones
- Volume 7 **Applications of Synchrotron Radiation to Materials Analysis**, edited by H. Saisho and Y. Gohshi
- Volume 8 **Methods for Structure Elucidation by High-Resolution NMR**, edited by Gy. Batta, K.E. Kövér and Cs. Szántay, Jr.

Analytical Spectroscopy Library – Volume 8

# Methods for Structure Elucidation by High-Resolution NMR

applications to organic molecules  
of moderate molecular weight

edited by

Gy. Batta

*Research Group for Antibiotics of the Hungarian Academy of Sciences  
Department of Chemistry, L. Kossuth University,  
H-4010 Debrecen, Hungary*

K.E. Kövér

*Department of Organic Chemistry, L. Kossuth University,  
H-4010 Debrecen, Hungary*

Cs. Szántay, Jr.

*Chemical Works of Gedeon Richter Ltd., Spectroscopic Research Division,  
H-1475 Budapest 10, Hungary*



1997

ELSEVIER

Amsterdam – Lausanne – New York – Oxford – Shannon – Singapore – Tokyo

ELSEVIER SCIENCE B.V.  
Sara Burgerhartstraat 25  
P.O. Box 521, 1000 AM Amsterdam, The Netherlands

ISBN: 0-444-82157-0

© 1997 Elsevier Science B.V. All rights reserved.

No part of this publication may be reproduced, stored in a retrieval system or transmitted in any form or by any means, electronic, mechanical, photocopying, recording or otherwise, without the prior written permission of the publisher, Elsevier Science B.V., Copyright & Permissions Department, P.O. Box 521, 1000 AM Amsterdam, The Netherlands.

Special regulations for readers in the USA. This publication has been registered with the Copyright Clearance Center Inc. (CCC), 222 Rosewood Drive, Danvers, MA 01923. Information can be obtained from the CCC about conditions under which photocopies of parts of this publication may be made in the USA. All other copyright questions, including photocopying outside of the USA, should be referred to the copyright owner, Elsevier Science B.V., unless otherwise specified.

No responsibility is assumed by the publisher for any injury and/or damage to persons or property as a matter of products liability, negligence or otherwise, or from any use or operation of any methods, products, instructions or ideas contained in the material herein.

This book is printed on acid-free paper.

Printed in The Netherlands

---

# Preface

---

Nuclear Magnetic Resonance Spectroscopy (NMR) is now widely regarded as having evolved into a discipline in its own right. The field has become immensely diverse, ranging from medical use through solid state NMR to liquid state applications, with countless books and scientific journals devoted to these topics. The theoretical as well as experimental advances continue to be rapid, and have in fact been accelerated by many novel innovations.

This book is part of the “Analytical Spectroscopy Library” series, and is devoted to high-resolution NMR, specifically applications in the structure elucidation of organic molecules of moderate molecular weight. The book contains 16 loosely connected chapters written by some of today’s most accomplished NMR scientists. Much emphasis has been given to the latest developments in NMR, in particular to selective pulses and pulsed field gradients.

We aimed at presenting a book which conceptually offers something different from basic educational texts, hard-core scientific papers and regular review articles. The chapters are the authors’ personal accounts of the special insights and results that have crystallized after several years of research into a given topic. The book does not revolve around a single theme, but offers a selection of scientific “gems” of various colors, reflecting the great diversity of NMR. We hope that there will be future editions to provide a platform for information of similar flavor.

As for the scope of this book, it is intended mainly for chemists, other scientists and students with some background in NMR. Some of the chapters have slight overlap in the topics discussed, which we consider to be particularly exciting in terms of gaining insight into the same area from different angles.

The Editors

This Page Intentionally Left Blank

---

# CONTENTS

---

Preface . . . . .	v
Contents . . . . .	vii
List of Contributors . . . . .	ix
1. Selective Pulses in NMR S.J.F. Vincent and C. Zwanen . . . . .	1
2. Multiple Selective Excitation: A Method to Improve the Efficiency of Selective 1D and 2D Experiments P. Bigler . . . . .	19
3. Concatenation of Polarization Transfer Steps in 1D Homonuclear Chemical Shift Correlated Experiments. Application to Oligo- and Polysaccharides D. Uhrin . . . . .	51
4. The Selective Reverse INEPT Experiment G.A. Morris and I.C. Clements . . . . .	91
5. GROESY, Gradient-enhanced Selective 1D ROE Measurements P. Adell, T. Parella, F. Sánchez-Ferrando and A. Virgili . . . . .	107
6. The DANTE-Z Experiment D. Canet and C. Roumestand . . . . .	121
7. One-Dimensional TOCSY and Related 1D Techniques T.C. Wong . . . . .	131
8. Use of High-Power Spin-Lock Purge Pulses in High-Resolution NMR Spectroscopy G. Otting . . . . .	149
9. Decoupled HMBC (D-HMBC), an Improved Version of HMBC H. Seto and K. Furihata . . . . .	173

10. Optimal Acquisition and Presentation of HoMQC Spectra	
I. Pelczer and K.D. Bishop . . . . .	187
11. High Resolution Diffusion Ordered Spectroscopy	
G.A. Morris and H. Barjat . . . . .	209
12. Chemical Exchange Measurements in NMR	
A.D. Bain and G.J. Duns . . . . .	227
13. Homonuclear Two-Dimensional Cross-Relaxation Spectroscopy	
N. Juranić, Zs. Zolnai and S. Macura . . . . .	265
14. Reference Deconvolution	
G.A. Morris and H. Barjat . . . . .	303
15. The Super Fast Inversion Recovery (SUFIR) Experiment	
D. Canet, P. Mutzenhardt and J.-B. Robert . . . . .	317
16. Measurements of Relaxation Rates for Low Natural Abundance $I = 1/2$ Nuclei	
J. Kowalewski and L. Mäler . . . . .	325
Subject Index . . . . .	349

---

## List of Contributors

---

- P. Adell, Departament de Química, Universitat Autònoma de Barcelona, 08193 Bellaterra, Barcelona, Catalonia, Spain
- A.D. Bain, Department of Chemistry, McMaster University, Hamilton, ON, Canada L8S 4M1
- H. Barjat, Department of Chemistry, University of Manchester, Oxford Road, Manchester M13 9PL, United Kingdom
- P. Bigler, Department of Chemistry and Biochemistry, University of Berne, Freiestrasse 3, 3012 Bern, Switzerland
- K.D. Bishop, Department of Chemistry, Michigan State University, East Lansing, MI 48824, USA
- D. Canet, Laboratoire de Méthodologie RMN (URA CNRS 406 – LESOC; FU CNRS E008 – INCM), Université Henri Poincaré, Nancy 1, B.P. 239, 54506 Vandoeuvre les Nancy Cedex, France
- I.C. Clements, Department of Chemistry, University of Manchester, Oxford Road, Manchester M13 9PL, United Kingdom
- G.J. Duns, Department of Chemistry, McMaster University, Hamilton, ON, Canada L8S 4M1
- K. Furihata, Division of Agriculture and Agricultural Life Sciences, University of Tokyo, Yayoi, Bunkyo-ku, Tokyo 113, Japan
- N. Juranić, Department of Biochemistry and Molecular Biology, Mayo Graduate School, Mayo Clinic and Foundation, Rochester, MN 55905, USA
- J. Kowalewski, Division of Physical Chemistry, Arrhenius Laboratory, Stockholm University, S-106 91 Stockholm, Sweden
- S. Macura, Department of Biochemistry and Molecular Biology, Mayo Graduate School, Mayo Clinic and Foundation, Rochester, MN 55905, USA
- L. Mäler, Division of Physical Chemistry, Arrhenius Laboratory, Stockholm University, S-106 91 Stockholm, Sweden

- G.A. Morris, Department of Chemistry, University of Manchester, Oxford Road, Manchester M13 9PL, United Kingdom
- P. Mutzenhardt, Laboratoire de Méthodologie RMN, (URA CNRS 406 – LESOC; FU CNRS E008 – INCM) Université Henri Poincaré, Nancy 1, B.P. 239, 54506 Vandoeuvre les Nancy Cedex, France
- G. Otting, Department of Medical Biochemistry and Biophysics, Karolinska Institute, S-171 77 Stockholm, Sweden
- T. Parella, Departament de Química, Universitat Autònoma de Barcelona, 08193 Bellaterra, Barcelona, Catalonia, Spain
- I. Pelczer, Department of Chemistry, Frick Laboratory, Princeton University, Princeton, NJ 08544, USA
- J.-B. Robert, Centre de Recherches sur les Très Basses Températures, Laboratoire associé à l'Université J. Fourier-Grenoble I/CNRS, B.P. 166, 38042 Grenoble Cedex, France
- C. Roumestand, Centre de Biochimie Structurale, (UMR CNRS 9955 – U 414 INSERM/Université de Montpellier I), 15 Avenue Charles Flahault, 34060 Montpellier Cedex, France
- F. Sánchez-Ferrando, Departament de Química, Universitat Autònoma de Barcelona, 08193 Bellaterra, Barcelona, Catalonia, Spain
- H. Seto, Institute of Molecular and Cellular Biosciences, University of Tokyo, Yayoi, Bunkyo-ku, Tokyo 113, Japan
- D. Uhrín, University of Edinburgh, Department of Chemistry, West Mains Road, Edinburgh EH9 3JJ, United Kingdom
- S.J.F. Vincent, National High Magnetic Field Laboratory (NHMFL), 1800 E. Paul Dirac Drive, Tallahassee, FL 32310, USA
- A. Virgili, Departament de Química, Universitat Autònoma de Barcelona, 08193 Bellaterra, Barcelona, Catalonia, Spain
- T.C. Wong, Department of Chemistry, University of Missouri, Columbia, MO 65211, USA
- Zs. Zolnai, Department of Biochemistry and Molecular Biology, Mayo Graduate School, Mayo Clinic and Foundation, Rochester, MN 55905, USA
- C. Zwahlen, National High Magnetic Field Laboratory (NHMFL), 1800 E. Paul Dirac Drive, Tallahassee, FL 32310, USA

# chapter 1

---

## Selective Pulses in NMR

---

Sébastien J.F. Vincent and Catherine Zwanen

*National High Magnetic Field Laboratory (NHMFL)*

*1800 E. Paul Dirac Drive*

*Tallahassee, FL 32310*

*USA*

Methods for Structure Elucidation by High-Resolution NMR

Edited by Gy. Batta, K.E. Kövér and Cs. Szántay, Jr.

© 1997 Elsevier Science B.V. All rights reserved

This Page Intentionally Left Blank

## Abstract

The properties of some widely used selective pulses are described, together with methods for calibration. The emphasis is on an overview of what may be expected from a given pulse shape in terms of selectivity, duration, quality of profile, sensitivity to relaxation, and range of applicability.

## 1. Introduction

Insufficient resolution is often an obstacle to the extraction of information from conventional multi-dimensional nuclear magnetic resonance spectra. Non-selective experiments often do not allow one to accurately determine the information contained within the fine structure of multiplets. Moreover, non-selective pulses affect all spins in the system more or less uniformly. As more and more subtle structural details are being investigated by nuclear magnetic resonance, separate manipulation of the spins of interest in selective experiments will probably gain in importance. Using selective pulses, it is possible to record spectra with very small spectral windows, typically 20 to 1000 Hz, in all proton dimensions. It has readily been recognized that this turns out to be an important advantage [1, 2] especially in homonuclear multi-dimensional experiments where selective preparation pulses allow one to use a smaller number of time increments. A further advantage resulting from the use of selective pulses is the simplification of complex spectra. The use of *fully* selective experiments, i.e., experiments that are selective in all frequency domains, allows one to focus on the desired information which concerns the chosen active spins. This approach highlights the relevant information (existence of multiplets, fine structure, and scalar couplings) with a precision enabling an accurate extraction of parameters.

This contribution will describe the manipulation of spin multiplets as a whole, and the word *selective* – or “soft” – will be used for multiplet-selective pulses, in contrast to *band-selective*, which refers to a broader bandwidth which may affect several spins, and to *transition selective* when only one line is affected. The discussion will be based on proton spectra, but all aspects are similar for other nuclei. Soft pulses use lower amplitudes and much longer irradiation times than non-selective “hard” pulses. Typical durations for soft pulses are of the order of 1 to 500 ms with a peak amplitude

of 1 to 100 Hz, which are to be compared with the 1 to 50  $\mu\text{s}$  and 1 to 50 kHz for hard pulses. In addition to require low rf amplitudes and long durations, selective pulses are generated using a time-dependent amplitude envelope. The envelopes – the *pulse shapes* – must be optimized, usually by numerical simulations, in order to obtain the best possible frequency-domain response. Another way to implement soft pulses, which will not be described in this contribution, consists in applying a sequence of equally spaced non-selective pulses with small flip angles, which can be used for selective manipulation of spins because of precession during the interleaved delays. This technique, referred to as DANTE [3, 4], has been applied to most families of NMR experiments [5–9]. Not all existing selective pulses will be analyzed here, but only some amongst the most widely applied ones. Reviews on other aspects of selective pulses and their applications can be found in the literature [10–14]. This contribution will focus on practical advices in the choice, implementation and calibration of some chosen shaped pulses.

The manipulation of different homonuclear spins on the basis of their chemical shift differences is made possible by the use of selective pulses. Soft pulses have to present a constant response, typically either an ideal excitation or a perfect inversion of magnetization, over a given bandwidth, without significant frequency-dependent phase distortions, and a minimum amount of perturbations outside this chosen bandwidth. The *transition regions*, defined as the frequency regions between the bandwidth of constant response and the rest of the unperturbed spectrum, should be kept as small as possible because the response of the spins in this region is not optimal and cannot be controlled. This problem has been partially solved by the introduction of various shaped pulses providing a refocalisation within the time-course of the pulse. The four families of such pulses considered in this work are the Gaussian pulse [1, 15], the Gaussian cascades ( $G^3$  and  $G^4$ ) [16], the BURP pulses [12, 17], and the Quaternions cascades ( $Q^3$  and  $Q^5$ ) [18], in addition to the rectangular pulse used as a reference.

## 2. Selective excitation pulses

Similarly to non-selective experiments, the first operation needed to perform experiments involving selective pulses is the transformation of longitudinal order (Zeeman polarization  $I_z$ ) into transverse magnetization ( $I_x$  or  $I_y$ ). This can be achieved by a *selective excitation* pulse. The first “successful” shaped pulse described in the literature is the Gaussian  $90^\circ$  pulse [1]. This analytical function has been chosen because its Fourier transform is also a Gaussian. In a first order approximation, the Fourier transform of a time-domain envelope can be considered to describe the frequency response of the shaped pulse. This amounts to say that the response of the spin system to a radio-frequency (rf) pulse is linear. An exact description of the

TABLE 1  
Commonly used selective excitation pulses.

Pulse name	Reference	Universal pulse?	Peak rf amplitude/ rectangular 90° <sup>a</sup>
Rectangular	–	Yes	1
Gaussian 270° <sup>b</sup>	[15]	Yes	6.7
Quaternion cascade (Q <sup>5</sup> )	[18]	Yes	19.3
E-BURP-1	[12]	No	13.7
E-BURP-2	[12]	No	17.0
Gaussian cascade (G <sup>4</sup> )	[16]	No	18.2

<sup>a</sup> The peak rf amplitude required to achieve optimum excitation with a selective excitation pulse is given in comparison to the rf amplitude required to achieve an on-resonance 90° flip-angle with a selective rectangular pulse, the simplest conceivable shape.

<sup>b</sup> The Gaussian pulse is truncated at 2.5% in order to keep its duration finite without introducing distortions in the profile; its half-height full width is 43.5% of its total duration. The flip angle is calibrated to 270° in order to use the “self-refocussing” properties of this pulse [15].

TABLE 2  
Description of the selectivity of the selective excitation pulses of table 1, all numbers given for properly calibrated 30 ms pulses.

Pulse name	rf amplitude [Hz] <sup>a</sup>	$\Delta\Omega(95\%)$ [Hz] <sup>b</sup>	$\Delta\Omega(90\%)$ [Hz]	$\Delta\Omega(80\%)$ [Hz]	$\Delta\Omega(70\%)$ [Hz]
Rectangular	8.3	6	8	10	14
Gaussian 270° (G <sup>1</sup> )	54.5	23	28	36	41
Quaternion cascade (Q <sup>5</sup> )	151.0	176	183	191	198
E-BURP-1	113.3	133	141	151	158
E-BURP-2	141.0	135	143	154	162
Gaussian cascade (G <sup>4</sup> )	154.0	205	217	239	253

<sup>a</sup> The rf amplitude given were calibrated by numerical simulation, as described in the text.

<sup>b</sup> The bandwidths  $\Delta\Omega$  are given  $\pm 1$  Hz for various percentages, where a percentage describes the minimal amplitude of signals within the corresponding bandwidth  $\Delta\Omega$ .

frequency response can be obtained either by solving the Bloch equations, or by numerical solution of the equation of motion in a stepwise fashion to ensure that the Hamiltonian is time-independent over the integration intervals. Many variants of selective excitation pulses have been described and only some of the most successful are listed in table 1.

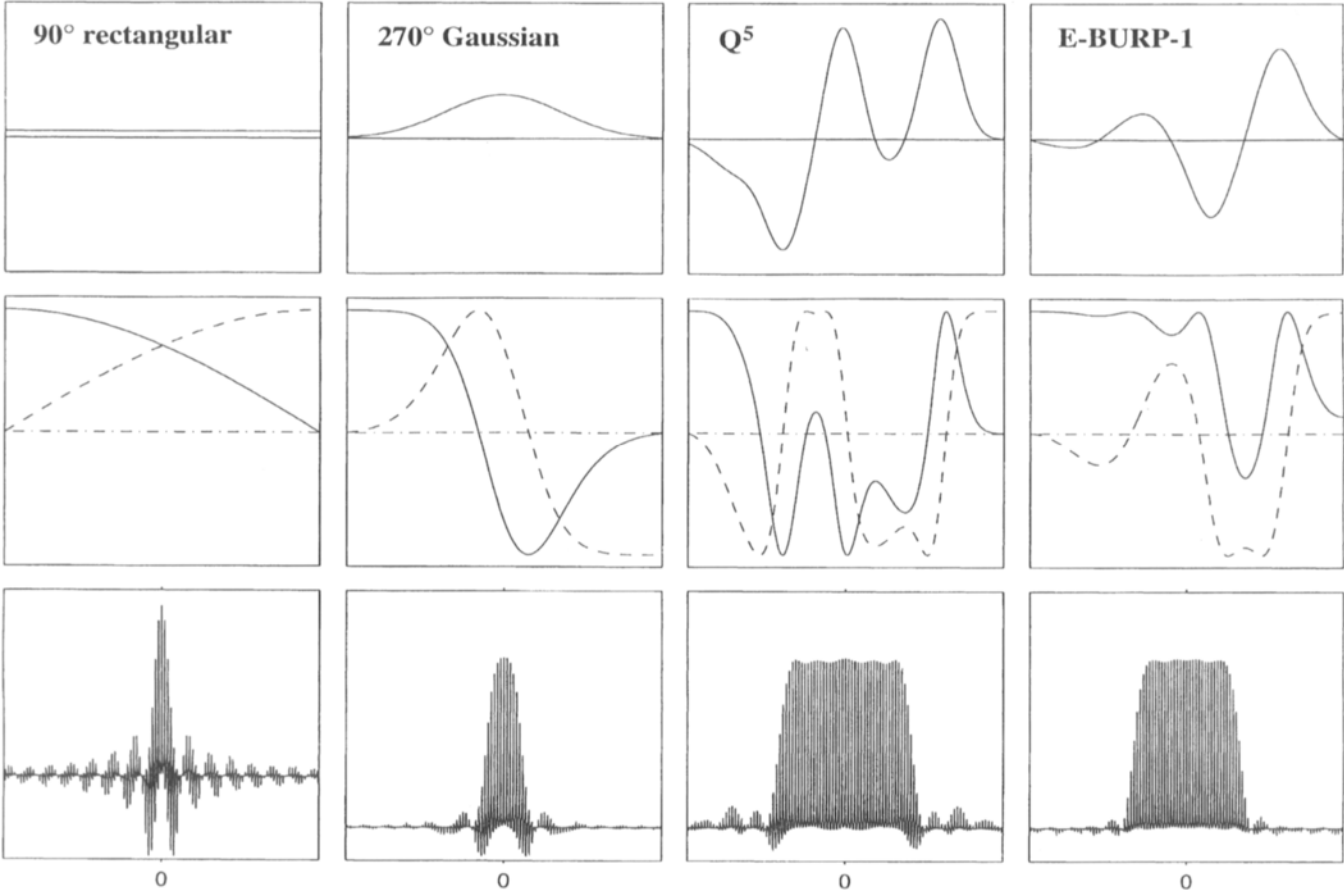
The last three pulses listed in table 1, namely the two E-BURPs and the G<sup>4</sup>, are non-universal pulses designed to transfer Zeeman polarization ( $I_z$ ) into detectable transverse magnetization ( $I_x$  or  $I_y$ ), but not to achieve the reverse operation. The conversion of  $I_x$  or  $I_y$  into  $I_z$  can be achieved by using the time-reversal of the considered pulse shape. An alternative

consists in using *universal pulses*, examples of which are the rectangular pulse, the  $270^\circ$  Gaussian, and the  $Q^5$ , which are all intended to rotate any initial condition by an angle of  $90^\circ$  (or  $270^\circ$ ), in particular both  $I_z$  into  $I_x$  or  $I_y$  and vice-versa.

Figure 1 shows the pulse shapes, magnetization components trajectories, and excitation profiles for four pulses. The rectangular pulse has the sharpest excitation profile for a given duration (bottom left of fig. 1 and table 2), as can be seen from the small frequency region effectively excited by the pulse, but the response is uniform only over a very limited region. Moreover, broad transition regions are perturbed by the rf irradiation, and therefore this pulse should not be used for selective excitation. The profile of the  $270^\circ$  Gaussian is much better: the peak rf amplitude of 54.5 Hz for a duration of 30 ms excites almost uniformly a multiplet of 35 Hz width, while a multiplet of 50 Hz across requires a somewhat harder pulse of about 20 ms duration. The negative excursions in the transition region can become a problem either if the spins under scrutiny have a small separation in chemical shifts, or if several multiplets must be excited in a band-selective experiment. Under these circumstances, one should turn to more efficient pulses with a more regular response within the excitation window and which have smaller and cleaner transition regions. These advantages are obtained at the expense of selectivity, as shown by the broader excitation regions obtained for the same duration (bottom row of fig. 1 and table 2), meaning that the required peak rf amplitudes for a given duration are higher. The selectivity of the different pulses of table 1 for a typical pulse length of 30 ms is described in table 2.

For a system with scalar coupling(s), antiphase terms such as  $2I_y^A I_z^X$  arise in the course of the pulse, as shown in fig. 2, which illustrates the creation and subsequent disappearance of this term during a  $270^\circ$  Gaussian pulse.

→  
 Fig. 1. Computer simulations of four selective excitation pulses. (Top) Pulse shapes. From left to right:  $90^\circ$  rectangular pulse,  $270^\circ$  Gaussian truncated at 2.5%, Quaternion cascade  $Q^5$ , and E-BURP-1. The vertical axis shows the relative rf amplitudes, whereas the horizontal axis shows the time. (Middle) Trajectories of Cartesian operators in the rotating frame during the rf pulses, neglecting relaxation:  $I_x$  (---),  $I_y$  (-·-·-), and  $I_z$  (—). The initial density operator was set to  $\sigma = I_z$  in all cases, and the phase of the pulses was set parallel to the  $y$  axis. (Bottom) Simulated excitation profiles obtained with pulses of 30 ms. The carrier frequency was stepped through 500 Hz in 5 Hz increments between  $\Omega_A \pm 250$  Hz. No phase correction was made within the series. All pulse rf amplitudes were calibrated for a 30 ms duration: 8.3 Hz amplitude for the  $90^\circ$  rectangular pulse, 54.5 Hz peak amplitude for the  $270^\circ$  Gaussian, 151.0 Hz for the  $Q^5$ , and 113.3 Hz for the E-BURP-1. The simulations were achieved using a numerical simulation program based on the Liouville–von Neumann equation. The code was developed with MATLAB [25], a data handling program specialized in matrix operations and data visualization.



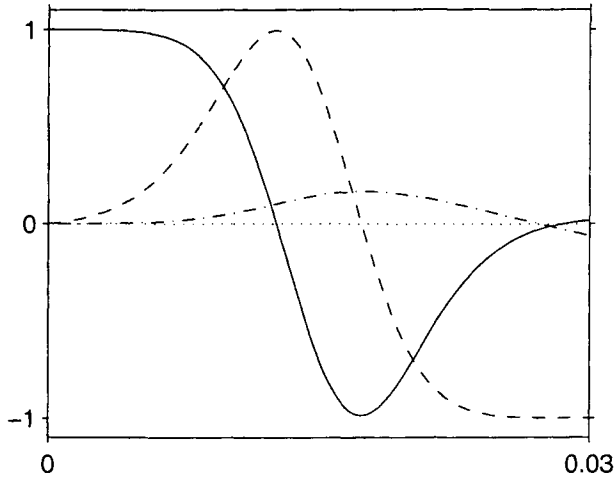


Fig. 2. Trajectories of some Cartesian product operators of a two-spin system under a  $270^\circ$  Gaussian pulse,  $I_x^A$  (---),  $I_y^A$  (····),  $I_z^A$  (—), and  $2I_y^A I_x^A$  (-·-·-), neglecting relaxation. The initial density matrix was  $\sigma = I_z^A$ , the coupling constant  $J_{AX} = 7$  Hz and the chemical shift difference between the two spins  $\Delta\Omega = 500$  Hz. The pulse was applied to spin A with a duration of 30 ms, amplitude of 54.5 Hz and phase parallel to the  $y$  axis. All other conditions as in fig. 1.

This phenomenon is due to the “self-refocussing” effect [15], which leaves only a small amount of antiphase term at the end of the pulse and is necessary in extended spin systems. All pulses described in this contribution, except the rectangular, the  $90^\circ$  Gaussian, and the  $180^\circ$  Gaussian pulses, feature some degree of “self-refocussing” effect.

### 3. Selective inversion and refocussing

For selective irradiations with a flip angle of  $180^\circ$ , one can distinguish two groups of shaped pulses: *inversion pulses*, which change the sign of Zeeman

Fig. 3. Numerical simulations of four different selective inversion pulses. (Top) Pulse shapes. From left to right:  $180^\circ$  rectangular,  $180^\circ$  Gaussian truncated at 2.5%, Quaternion cascade  $Q^3$ , and I-BURP-2. (Middle) Trajectories of Cartesian operators in the rotating frame during rf pulses, neglecting relaxation:  $I_x$  (---),  $I_y$  (-·-·-), and  $I_z$  (—). The initial density operator was set to  $\sigma = I_z$  in all cases, and the phases of the pulses were along the  $y$ -axis. (Bottom) Inversion profiles obtained with pulses of 30 ms followed by a hard “read” pulse applied on resonance, phase-cycled  $\pm x$  with the receiver. The  $180^\circ$  rectangular pulse requires an rf amplitude of 16.7 Hz, the  $180^\circ$  Gaussian 36.4 Hz, the Quaternion cascade  $Q^3$  110.0 Hz, and the I-BURP2 165.0 Hz. Other conditions as in fig. 1.

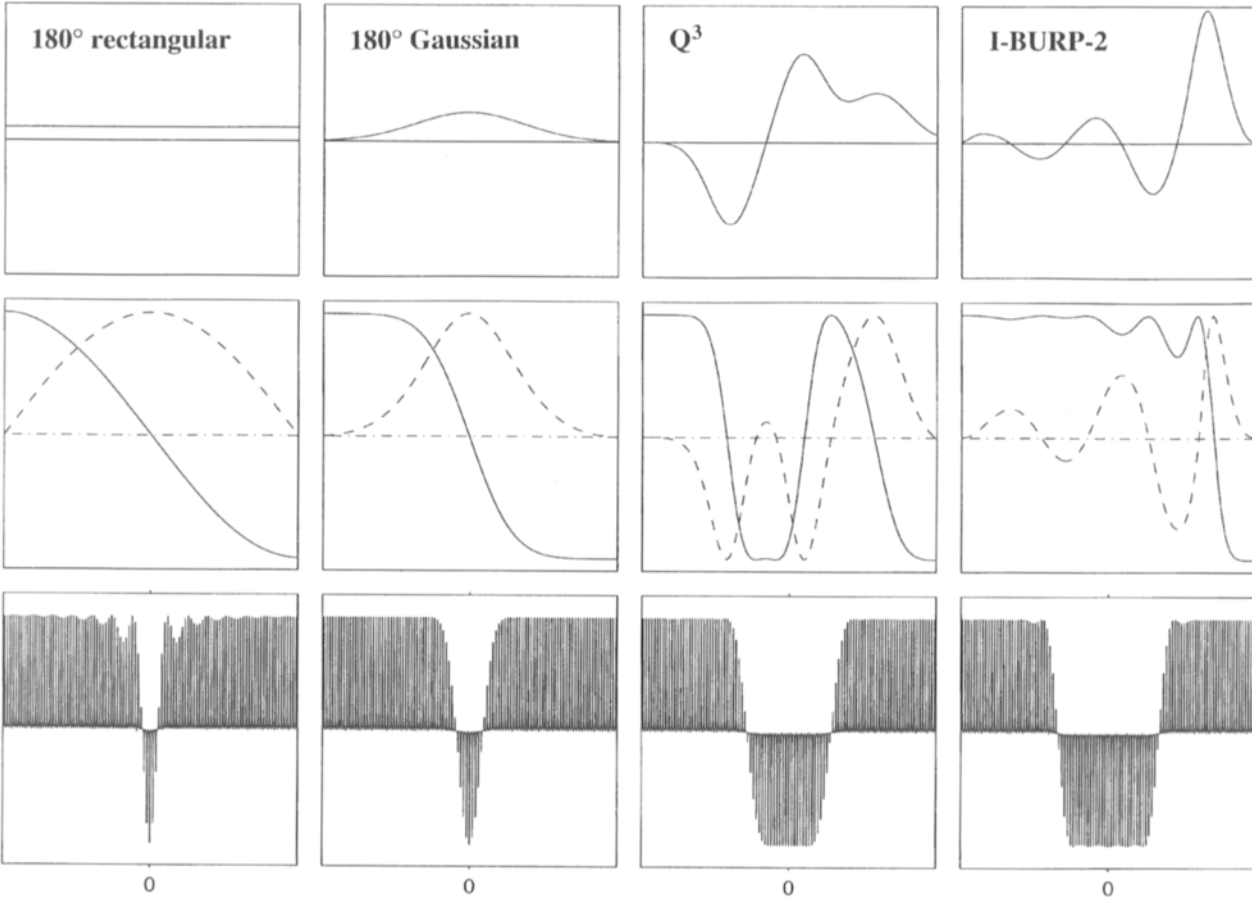


TABLE 3  
Most commonly used selective inversion and selective refocussing pulses.

Pulse name	Reference	Universal pulse? <sup>a</sup>	Peak rf amplitude/ rectangular 90° <sup>b</sup>
Rectangular 180°	–	Yes	2.0
Gaussian 180°	[1]	Yes	4.8
Quaternion cascade (Q <sup>3</sup> )	[18]	Yes	13.0
RE-BURP	[12]	Yes	24.0
Gaussian cascade (G <sup>3</sup> )	[16]	No	12.1
I-BURP-1	[12]	No	13.9
I-BURP-2	[12]	No	19.9

<sup>a</sup> A universal inversion pulse can also be used for selective refocussing.

<sup>b</sup> The peak rf amplitude required to achieve optimum inversion with a selective inversion pulse is given in comparison to the rf amplitude required to achieve an on-resonance 90° flip-angle with a selective rectangular pulse, the simplest conceivable shape.

TABLE 4  
Selectivity of the selective inversion pulses of table 3, all numbers given for properly calibrated 30 ms pulses.

Pulse name	rf amplitude	$\Delta\Omega(95\%)$	$\Delta\Omega(90\%)$	$\Delta\Omega(80\%)$	$\Delta\Omega(70\%)$
	[Hz] <sup>a</sup>	[Hz] <sup>b</sup>	[Hz]	[Hz]	[Hz]
Rectangular 180°	16.7	6	8	10	14
Gaussian 180°	36.4	9	12	18	22
Quaternion cascade (Q <sup>3</sup> )	110.0	91	98	107	114
RE-BURP	208.0	133	140	149	155
Gaussian cascade (G <sup>3</sup> )	120.0	97	103	112	118
I-BURP-1	111.5	135	139	145	150
I-BURP-2	165.0	135	140	146	151

<sup>a</sup> The rf amplitude given were calibrated by numerical simulation, as described in the text.

<sup>b</sup> The bandwidths  $\Delta\Omega$  are given  $\pm 1$  Hz for various percentages, where a percentage describes the minimal amplitude of signals within the corresponding bandwidth  $\Delta\Omega$ .

polarization, and *refocussing pulses*, which rotate transverse magnetization. Both actions can be realized by universal 180° pulses (table 3), whereas non-universal inversion pulses should not be used for selective refocussing.

Figure 3 shows four selective inversion pulses: a rectangular pulse, a 180° Gaussian, a Q<sup>3</sup>, and a I-BURP2. The profiles, shown in the bottom row of fig. 3, have been calculated for selective-inversion pulses with a duration of 30 ms, followed by a hard rectangular 90° “read” pulse applied on resonance and alternated in phase in concert with the receiver. Both the rectangular 180° and the 180° Gaussian pulses lack a uniformly inverted region in the inversion profiles (fig. 3). The best profiles are obtained for

the Quaternion cascade  $Q^3$  and for the I-BURP2. Both have a well-behaved inversion region and a narrow transition region. The  $Q^3$  is 1.5 times more selective than the I-BURP2, as illustrated in table 4, and in addition, the  $Q^3$  is universal whereas the I-BURP-2 is not. For a given pulse duration, the two sophisticated pulses are less selective than a  $180^\circ$  Gaussian or a rectangular  $180^\circ$  pulse.

#### 4. Calibration of selective pulses

Similarly to their non-selective counterparts, selective pulses need to be calibrated in order to obtain a reasonable response. This means either varying the length of the pulse for a constant rf amplitude, or changing the peak rf amplitude for a fixed duration. From an experimental point of view, a duration can be precisely adjusted as defining a pulse duration with a  $\mu\text{s}$  precision on a spectrometer is routine, while setting a given intensity, say in Hz, is more difficult. But varying an amplitude is preferable as it leads to a calibrated pulse with *known selectivity*. The calibration of selective pulses should result from experimental tests carried out on “representative” multiplets, i.e., signals with typical relaxation properties of the spin system under consideration, similar total multiplet width, same dielectric properties of the solution, and identical spectrometer setup.

The first – and simplest – calibration is for the selective rectangular and Gaussian pulses. In both cases, the amplitude of the signal has a sinusoidal dependence on the amplitude of the pulse, as can be expected from the on-resonance trajectory of the magnetization (middle row of fig. 1 and figure 2). It is therefore straightforward to identify the signal amplitude values corresponding to  $90^\circ$ ,  $180^\circ$  and  $270^\circ$ , *provided the curve is recorded completely*. The first maximum in signal amplitude – when the rf amplitude is increased – amounts to a on-resonance flip angle of  $90^\circ$ , the first zero-crossing point to a on-resonance flip angle of  $180^\circ$ , and the first minimum corresponds to  $270^\circ$ , provided a constant phasing is applied to the whole series of spectra.

It is slightly more difficult to calibrate more sophisticated excitation pulses such as Gaussian cascades, Quaternion cascades, or BURP pulses: the optimum response does not necessarily correspond to a maximum signal amplitude, but rather to the most uniform profile in frequency domain. The experimental recording of pulse profiles is a time-consuming process, except if one uses a “one-shot” method using pulsed field gradients as recently proposed by Decors and co-workers [19]. Other criteria can be considered in order to recognize an optimum response: a signal should have *minimal antiphase contributions* and be close to the *maximum signal amplitude*. To obtain minimal antiphase contributions within the desired region is the most important criterion, while a maximum signal amplitude is a secondary

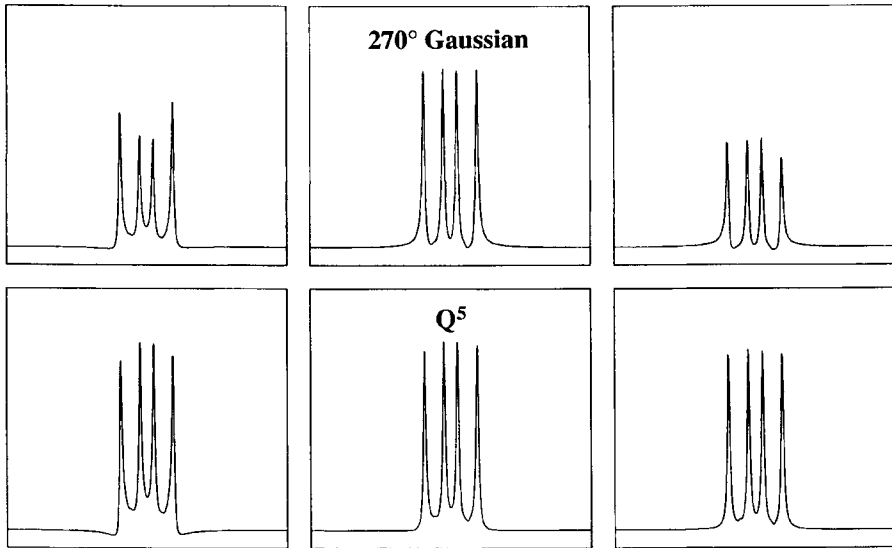


Fig. 4. Numerical simulations showing the effect of  $\pm 20\%$  miscalibration of the rf amplitudes of two selective excitation pulses: (Top) A  $270^\circ$  Gaussian of 30 ms duration (peak amplitudes from left to right: 43 Hz, 54 Hz, and 65 Hz) and (Bottom) a Quaternion cascade  $Q^5$  of 30 ms duration (peak amplitudes from left to right: 121 Hz, 151 Hz, and 181 Hz). The multiplets were obtained by simulating a three-spin system with couplings  $J_{AM} = 7$  Hz,  $J_{AX} = 12$  Hz, and  $J_{MX} = 0$  Hz. The vertical axes show a constant arbitrary amplitude, whereas the horizontal axis gives the frequencies  $\Omega_A \pm 50$  Hz.

concern. For separated multiplets, the criterion is straightforward, since the desired multiplet should be identical to the corresponding multiplet obtained in a non-selective one-dimensional spectrum. If signals overlap in the region of interest, the peaks within the region of constant response must be as similar as possible to the corresponding region in a non-selective one-dimensional spectrum. The intensities anomalies originating from phase distortions should be kept to a minimum, and the transition regions should exhibit minimal phase distortions. Figure 4 shows simulated multiplets illustrating the effect of a peak rf amplitude error of  $\pm 20\%$  for a  $270^\circ$  Gaussian and for a Quaternion cascade  $Q^5$ . As described before, the  $270^\circ$  Gaussian pulse has a clear optimum defined almost exclusively by the maximum amplitude of the in-phase term. For the same errors, the  $Q^5$  pulse leads to very small variations in signal amplitude, but the asymmetrical phase distortions are significant. This becomes more crucial in crowded spectra, as can be seen in the experimental example shown in fig. 5. The experimental variation of the rf amplitude of the band-selective E-BURP-1 clearly shows that the optimum (central multiplet highlighted by an arrow) is not obtained for maximal signal amplitude, but for minimal phase distortions.

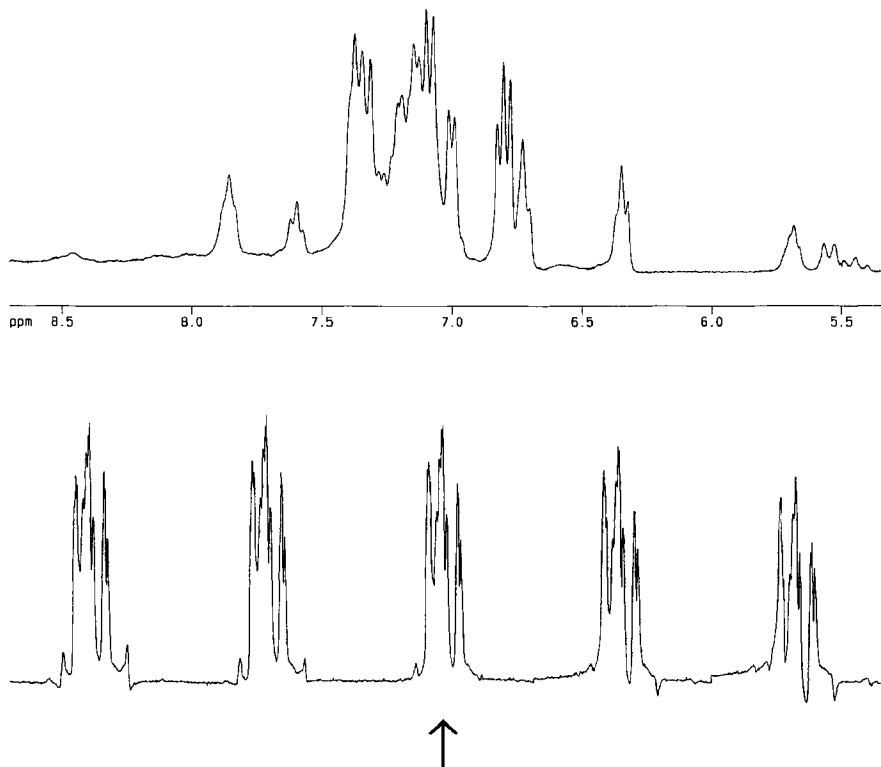


Fig. 5. Experimental calibration of a 15 ms E-BURP-1 around the optimum amplitude value on a DMX300. (Top) Excerpt of the one-dimensional spectrum of BPTL. (Bottom) Same region centered around 7 ppm excited by a 15 ms E-BURP-1 with amplitudes increasing from left to right by 1 dB steps. The optimum is located at the intermediate value (determined by smaller amplitude steps, typically of 0.1 dB).

Computer simulations allow one to calculate the ideal rf amplitude  $\nu_1$  [Hz] needed for a pulse of duration  $\tau$  on the basis of the chosen selectivity. In order to experimentally apply an amplitude  $\nu_1$ , one can calibrate a rectangular pulse with a duration  $\tau_{\text{calib}} = 1/(4\nu_1)$  [s] to a  $90^\circ$  flip angle and subsequently use this value as a starting point to optimize the shaped pulse according to the above mentioned criteria, i.e., obtaining a minimal amount of phase dispersion. For example, if one wants to calibrate a 30 ms  $Q^5$ , computer simulations show that the optimum amplitude has to be 151.0 Hz (table 2). By applying a rectangular pulse of duration  $1/(4 \times 151.0 \text{ Hz}) = 1.656 \text{ ms}$  and calibrating the  $90^\circ$  nutation angle as described above, the rf amplitude value on the spectrometer should be nearly identical as the one required by the 30 ms  $Q^5$ .

Inversion pulses can be calibrated either by the crude method which consists of applying the pulse to an isolated multiplet and searching the

zero-crossing point by variation of the rf amplitude, or in a more satisfactory manner by using a selective inversion pulse directly followed by a non-selective  $90^\circ$  excitation pulse alternated in phase together with the receiver phase. This leads to a normal one-dimensional spectrum, except that the chosen multiplet should tend towards a minimum of phase distortions and maximum negative signal when the calibration is optimal, similarly to the discussion concerning selective excitation pulses. This procedure avoids miscalibrations due to an erroneous estimation of the amplitude of the residual signal.

### 5. Relaxation during selective pulses

Selective pulses are of finite durations and contrarily to “infinitely” short hard pulses, transverse and longitudinal relaxation occur *during* the pulses.

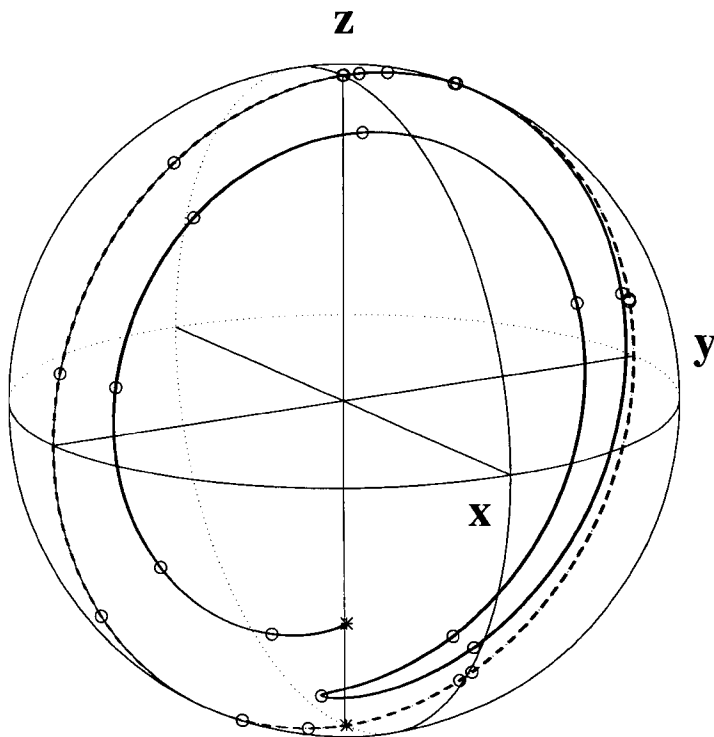


Fig. 6. Simulation of the effect of longitudinal and transverse relaxation during a 30 ms selective inversion  $Q^3$  pulse. The trajectories are shown on a Bloch sphere and in the rotating frame: relaxation “off” (---), and relaxation “on” (—) described by a  $T_1$  and a  $T_2$  chosen for the sake of illustration. Circles have been drawn on the trajectory at equal intervals of 2 ms. Both curve begin along the  $+z$  axis and the stars (\*) depict the end of the trajectories, along the  $-z$  axis.

Figure 6 illustrates the loss in magnetization in the course of a selective inversion  $Q^3$  pulse. The dashed line starting from the  $+z$  axis down to  $-z$ , back up to  $+z$  and finally  $-z$  (represented by the lower \* at the end of the trajectory), shows the trajectory with no relaxation. When both a transverse ( $T_2$ ) and longitudinal relaxation ( $T_1$ ) are assumed, the trajectory changes, as illustrated by the full line. The final result is a reduction of the intensity of the inverted signal (upper \* along  $-z$ ). Although the selective pulses have not been originally optimized with relaxation properties taken into account [12, 15, 16, 18], more recent work by Lerner and co-workers [20–22] and by Nuzillard and Freeman [23] attempt to tackle these effects. The approach taken here consist in using existing pulses and take their relaxation properties into account depending on the experiment under consideration. In most experiments at the exclusion of relaxation measurements, relaxation during selective pulses will just act as a loss of signal that can be assessed between different pulse shapes. In the case of relaxation measurements, these effects are to be taken into account quantitatively, and in this case, relaxation-compensated pulse shapes offer no improvement.

## 6. Conclusions

To summarize the analysis of the various shaped pulses presented in this contribution, the following points can be formulated:

- 1) The properties of a pulse have to be evaluated by applying the pulse directly to the spin system under study in order to account for parameters such as multiplet width, relaxation, sample properties, and setup and behavior of the spectrometer. This practical approach can be supported by numerical simulations, especially for complicated shapes.
- 2) For selective excitation, the  $270^\circ$  Gaussian pulse offers the best ratio of selectivity versus duration and its excitation profile is generally sufficiently flat for typical multiplets to be excited in a satisfactory fashion. The requirement of a short duration is often so critical that it overwhelms arguments about the top-hat profile and the transition regions, especially when the emphasis is on fast relaxing spins such as in macromolecules and chemically exchanging systems. The  $270^\circ$  Gaussian pulse is also the easiest one to calibrate, and it is a universal pulse. The only restriction lies in the frequency domain response which has undesired “wiggles” outside the desired bandwidth (fig. 1). Generally, these have a negligible effect if the selectivity – i.e., the length of the pulse – is chosen appropriately.

- 3) Better profiles may sometimes be needed, in which case an E-BURP-1 is recommended, particularly for band-selective experiments. The calibration is relatively easy and very narrow transition regions are very useful (fig. 1). If a universal pulse is needed, the E-BURP-1 may either be replaced by a  $Q^5$  pulse, or if only a conversion of  $I_x$  or  $I_y$  into  $I_z$  is required, by a time-reversed E-BURP-1.
- 4) For selective inversion or refocussing, a universal  $Q^3$  pulse is a good choice. In cases where singlets are to be inverted and where relaxation or exchange during pulses is critical, one may need to use a  $180^\circ$  Gaussian pulse which is the shortest selective inversion pulse available [24].

### Acknowledgements

We are indebted to G. Bodenhausen for invaluable discussions. This research was supported by the National High Magnetic Field Laboratory (NHMFL), Tallahassee.

### References

- [1] C. Bauer, R. Freeman, T. Frenkiel, J. Keeler and A.J. Shaka, *J. Magn. Reson.* **58** (1984) 442–457.
- [2] C. Griesinger, O.W. Sørensen and R.R. Ernst, *J. Am. Chem. Soc.* **109** (1987) 7227–7228.
- [3] G. Bodenhausen, R. Freeman and G.A. Morris, *J. Magn. Reson.* **23** (1976) 171–175.
- [4] G.A. Morris and R. Freeman, *J. Magn. Reson.* **29** (1978) 433–462.
- [5] P. Blondet, J.P. Albrand, M. v. Kienlin and M. Decorps, *J. Magn. Reson.* **71** (1987) 342–346.
- [6] D. Boudot, D. Canet, J. Brondeau and J.C. Boubel, *J. Magn. Reson.* **83** (1989) 428–439.
- [7] E. Kupce and R. Freeman, *J. Magn. Reson.* **100** (1992) 208–214.
- [8] E. Kupce and R. Freeman, *J. Magn. Reson. Ser. A* **101** (1993) 225–228.
- [9] C. Roumestand, D. Canet, N. Mahieu and F. Toma, *J. Magn. Reson. Ser. A* **106** (1994) 168–181.
- [10] J. Keeler, in: NATO Advanced Science Institute (ASI) Series, eds P. Granger and R.K. Harris (Kluwer, Dordrecht, 1990) pp. 201–238.
- [11] H. Kessler, S. Mronga and G. Gemmecker, *Magn. Reson. Chem.* **29** (1991) 527–557.
- [12] H. Geen and R. Freeman, *J. Magn. Reson.* **93** (1991) 93–141.
- [13] R. Freeman, *Chem. Rev.* **91** (1991) 1397–1412.
- [14] L. Emsley, *Methods Enzymol.* **239** (1994) 207–246.
- [15] L. Emsley and G. Bodenhausen, *J. Magn. Reson.* **82** (1989) 211–221.
- [16] L. Emsley and G. Bodenhausen, *Chem. Phys. Lett.* **165** (1990) 469–476.
- [17] H. Geen, S. Wimperis and R. Freeman, *J. Magn. Reson.* **85** (1989) 620–627.
- [18] L. Emsley and G. Bodenhausen, *J. Magn. Reson.* **97** (1992) 135–148.
- [19] V. Belle, G. Cros, H. Lahrech, P. Devoulon and M. Decorps, *J. Magn. Reson. Ser. A* **112** (1995) 122–125.

- [20] P.J. Hajduk, D.A. Horita and L.E. Lerner, *J. Magn. Reson. Ser. A* **103** (1993) 40–52.
- [21] D.A. Horita, P.J. Hajduk and L.E. Lerner, *J. Magn. Reson. Ser. A* **103** (1993) 53–60.
- [22] J. Shen and L.E. Lerner, *J. Magn. Reson. Ser. A* **112** (1995) 265–269.
- [23] J.-M. Nuzillard and R. Freeman, *J. Magn. Reson. Ser. A* **107** (1994) 113–118.
- [24] C. Zwiahlen, S.J.F. Vincent, M. Schwager and G. Bodenhausen, *Chem. Europ. J.* **1** (1996) 137–141.
- [25] MATLAB, © Copyright 1984–1994 The Mathworks Company, Inc., Version 4.2a.

This Page Intentionally Left Blank

## chapter 2

---

# Multiple Selective Excitation: A Method to Improve the Efficiency of Selective 1D and 2D Experiments

---

Peter Bigler

*Department of Chemistry and Biochemistry  
University of Berne  
Freiestrasse 3, 3012 Bern  
Switzerland*

This Page Intentionally Left Blank

## **Abstract**

A solution to improve the overall efficiency of selective 1D and 2D experiments is described and demonstrated. It is based on the principle of multiple selective excitation with subsequent data processing to disentangle the superimposed responses of the selectively and simultaneously excited spin systems. Several inherent insensitive and correspondingly modified experiments are presented together with typical applications.

## **1. Introduction**

The popularity of high resolution NMR has many reasons and is mainly based on its ability to detect and measure a variety of weak interactions between nuclei, forming a rich source of information about the structures and conformations of molecules in solution. Among the various technical developments of the last years, the introduction of frequency selective pulses to selectively excite or perturb the spins resonating within one or several narrow spectral regions and their incorporation into a series of pulse experiments has at least partly revolutionized today's NMR and has opened new perspectives. Selective excitation of nuclear spins, however, is not a novelty and has been applied since the first days of NMR spectroscopy. The first continuous wave (CW-) NMR spectrometers used selective excitation to record  $^1\text{H}$ -,  $^{19}\text{F}$ - and  $^{31}\text{P}$ -spectra. The frequency of a narrow band radiofrequency source was either held constant (field sweep type spectrometers) or was continuously increased or decreased (frequency sweep type spectrometers) thereby scanning the corresponding spectral region and exciting spins at different resonance frequencies selectively, one after the other. Today selective continuous wave (CW) excitation has survived in a few double resonance experiments, with the 1D decoupling experiment and the 1D NOE experiment representing the most popular ones.

Structural problems subject to an NMR analysis may be subdivided into two main classes. The solution of part of the problems necessitates a maximum of structural information, including the spectral parameters of all the nuclei of the investigated molecule. Typical representatives of this kind of problems are the conformational analysis of biomolecules or the elucidation of the unknown structure of an isolated natural product by NMR

methods. Such problems are probably best and most efficiently solved by the application of adequate multidimensional NMR experiments, yielding all the necessary information to establish and characterize the full spin-spin interaction network in one single experimental step.

For other problems the constitution of the corresponding molecule is well known and the investigator's interest is focused to one or only a few local structural regions, i.e., to obtain relative configurations or to determine the conformational or dynamic behaviour within this/these structural fragment(s). It is usually sufficient to acquire data of nuclei located within these structural regions and to study the corresponding interactions between typically a few rather than all the nuclei of a molecule. As a consequence of the limited amount of information it is, however, important in such cases to get the corresponding parameters as accurate as possible and within reasonable measuring time. For this kind of problems one usually applies selective 1D instead of 2D experiments, since they yield NMR data of higher quality, mainly due to a higher digital resolution, within shorter measuring time and with less wasting valuable disk storage space. It is therefore this class of problems which takes best advantage of new developments with the design of selective pulses and their incorporation in pulse sequences.

Frequency selective low-power pulses were developed to overcome the strong limitations and the disadvantages of selective excitation using the continuous wave method and to enlarge the range of applications. They form the last member in the chain of developments for selective excitation methods using pulses rather than continuous irradiation. It seems that with the availability of the corresponding hard- and software, with the easy set-up of the corresponding experiments on modern NMR spectrometers and with the high potential of applications, frequency selective pulses more and more displace the DANTE [1] methods originally introduced as the first pulse alternative, using trains of hard, non-selective, rather than single low-power pulses for selective excitation. Frequency selective pulses have meanwhile been incorporated in many 1D and 2D homo- and heteronuclear experiments and have been applied as single pulses, as pulse-sandwiches or very recently as trains of selective pulses, i.e., to perform broadband decoupling under even more power sparing conditions as needed at the highest magnetic fields.

There exists meanwhile a variety of frequency selective experiments still using the conventional CW irradiation as the 1D NOE experiment, or "upgraded" with one or more selective pulses, as the 1D TOCSY or the 1D COSY experiment. These experiments and their many variants are probably the best choice in such cases as long as the response of a spin system to the perturbation of only one single spin or one single group of equivalent spins is of interest. If, however, and this is the most common situation, informations on several rather than only one spin-spin interaction is needed,

these single selective experiments are hampered by their inherent low efficiency. In such situations the corresponding single selective experiment has to be repeated several times, with the spin selected for selective perturbation changed from experiment to experiment, giving longer measuring time.

In this contribution and – in more detail – in the corresponding publications [2–6], a solution to overcome this problem and to at least partially improve the overall efficiency of frequency selective experiments is presented. This solution is based on the principle of multiple selective excitation combined with spectral editing. It is a modification to “up-grade” existing but inherently insensitive standard experiments, including the selective 1D TOCSY experiment, the selective 1D heteronuclear NOE experiment, the selective 1D INADEQUATE experiment or the selective 1D heteronuclear long-range COSY experiment, with the latter dedicated to detect heteronuclear spin–spin connectivities through two or more bonds. Furthermore the same principle has been applied in a modified selective 2D TOCSY–COSY experiment, and in a selective 2D HMBC experiment.

These experiments fill the gap between the non-efficient single selective experiments and in some sense the “over-killing” 2D experiments, producing a huge amount of mainly non-exploited informations. They circumvent the problem with 2D experiments to be either too time consuming when yielding the data at equal quality or to yield data of unacceptable quality within short measuring time.

In the first part of this contribution the general principle of multiple frequency selective excitation is explained, followed by a short presentation of correspondingly “updated” selective 1D and 2D pulse sequences and by a few applications and results for demonstration. The contribution concludes with a critical discussion of advantages and limitations for this kind of experiments and the perspectives for further developments. Readers interested in a more detailed description and in experimental details such as spectrometer settings are referred to the corresponding publications [2–6].

## **2. The principle of multiple selective excitation**

The basic principle common to all the above mentioned selective experiments is the selective and more or less simultaneous perturbation of not only one but of several predefined spins with different resonance frequencies or of groups of spins each resonating within a narrow spectral region. This may be achieved by single selective pulses each tuned to a selected frequency and either applied as a series of pulses one after the other, using the same transmitter channel, or applied simultaneously using different channels of the spectrometer. As a promising but in this context not yet tested alternative, the selective perturbation of several spins could also be achieved by a single multiselective pulse designed accordingly. Due to former hardware

and software limitations of our spectrometer either DANTE [1] pulse trains or series of single selective pulses have been applied. Very recently a modified 2D HMBC experiment has been performed on our new spectrometer with the simultaneous application of single selective pulses on different transmitter channels.

The simultaneous and selective perturbation of several selected spins leads in the course of the pulse sequence to a perturbation of coupled spins and finally to a superposition of responses of the corresponding coupled spin systems. To disentangle these individual, superimposed responses the modified experiment must be performed several times with the data stored separately and with the individual responses labeled uniquely and differently for each of the subexperiments. This allows to correlate each response with the corresponding coupled spin system and allows to finally calculate subspectra by simple linear combinations of the separately stored data sets. These calculated subspectra correspond to the spectra acquired with the basic single selective experiment. To compare one of these subspectra with the corresponding spectrum of the basic single selective experiment, the total measuring time for the multiple selective and the basic single selective experiment must be the same, of course. This is accomplished by simply reducing the number of scans for each of the subexperiments in the modified variant accordingly.

Properties of the selective pulses are used therefore twofold in such experiments. Firstly, a selective pulse selectively perturbs the selected spin and the perturbation is distributed in the course of the experiment among the coupled spins, depending on the type of coupling (scalar, dipolar) and depending on the type of exchange mechanism (polarization transfer, cross polarization or cross relaxation). Secondly, the phase (selective  $90^\circ$  pulse) or the frequency (selective  $180^\circ$  pulse) of the selective pulse serve to label the response of both the selected and the residual coupled spins as positive or negative.

As an example and to clarify the principle, the acquisition and the processing schemes for the modified heteronuclear inverse detected 1D COSY experiment (pulse sequence IVa in fig. 1) are shown below (tables 1 and 2).

In this experiment a series of selective  $180^\circ$  pulses serves to individually label selected carbon spins prior to the series of  $^{13}\text{C}$ - and  $^1\text{H}$ -pulses used for refocusing and polarization transfer. Therefore the frequency of any of these initial  $180^\circ$  pulses is set either on-resonance to the resonance of carbon  $i$  ( $f_i$ ), or set off-resonance ( $f_{\text{off-res.}}$ ), which simply inverts (label  $-$ ) or not inverts (label  $+$ ) the corresponding spin polarization respectively. In the example below three target spins with resonance frequencies  $f_1$ ,  $f_2$  and  $f_3$  are chosen. A series of three selective pulses has to be applied and at least four experiments have to be performed with the frequencies of the selected pulses set as shown in the acquisition scheme below and four separately

TABLE 1

Acquisition scheme for the multiple selective heteronuclear inverse detected 1D COSY experiment. Four experiments have to be performed with 3 carbon resonances selected for selective perturbation. The frequencies are set either on-resonance ( $f_1$ ,  $f_2$ ,  $f_3$ ) or off-resonance to the selected resonance frequencies.

Experiment	Frequency of selective Pulse 1	Frequency of selective Pulse 2	Frequency of selective Pulse 3	Data
1	$f_1$	$f_2$	$f_3$	a
2	$f_1$	$f_{\text{off-res.}}$	$f_{\text{off-res.}}$	b
3	$f_{\text{off-res.}}$	$f_2$	$f_{\text{off-res.}}$	c
4	$f_{\text{off-res.}}$	$f_{\text{off-res.}}$	$f_3$	d

TABLE 2

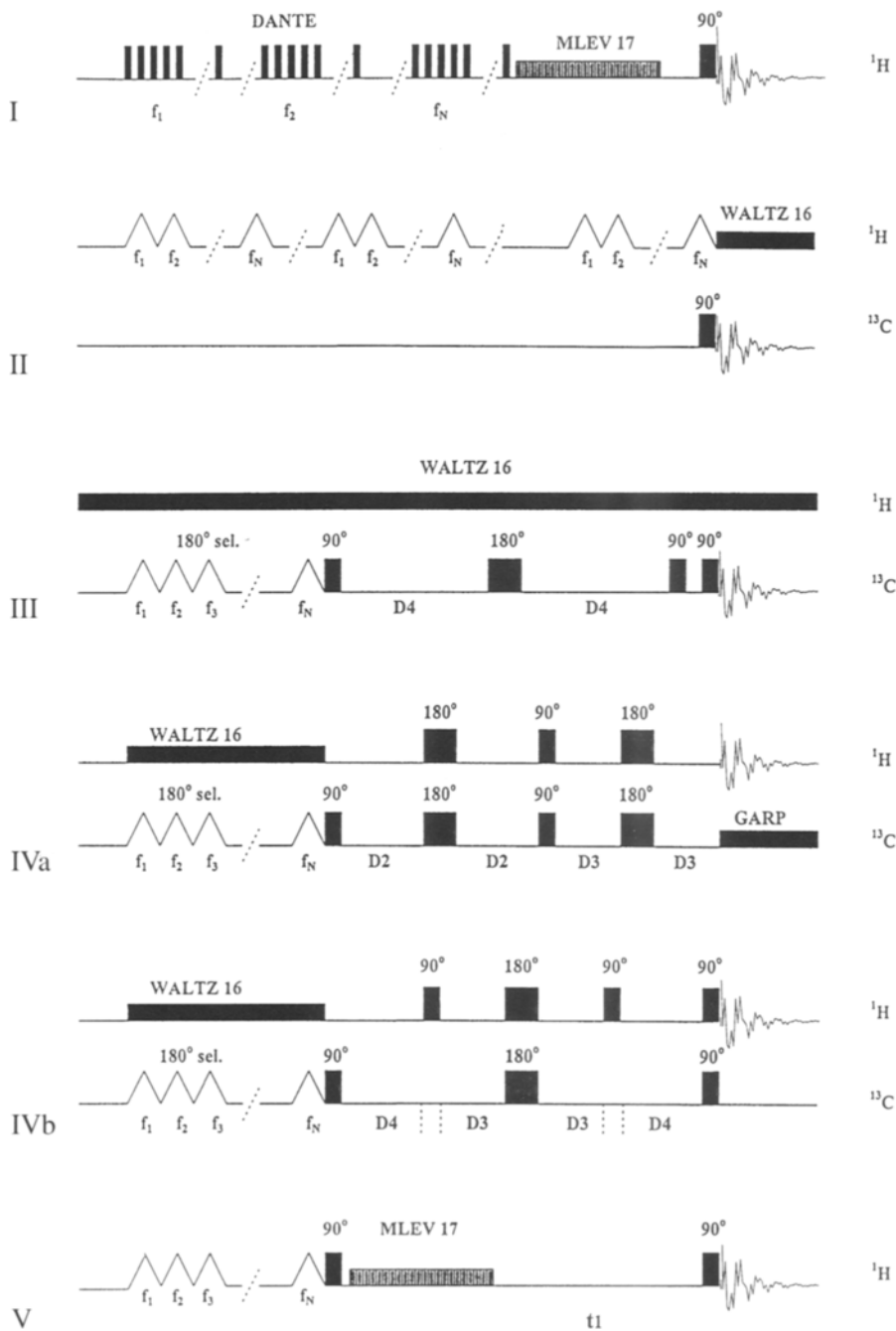
Processing scheme for the multiple selective heteronuclear inverse detected 1D COSY experiment. The final spectra A, B, C corresponding to the selective perturbation of three carbons resonating at frequencies  $f_1$ ,  $f_2$ , and  $f_3$  are obtained by linear combination of the original data a, b, c and d acquired in accordance with the acquisition scheme (table 1).

Processing step	Data a	Data b	Data c	Data d	Spectrum
1	–	–	+	+	A
2	–	+	–	+	B
3	–	+	+	–	C

stored data sets a, b, c and d are obtained. If for the basic inverse 1D heteronuclear COSY experiment NS scans are acquired, then NS/4 scans must be used in this case for each of the subexperiments to compare the results of the two experiments on the basis of equal total measuring time. The four data sets a–d are linearly combined in three different ways as outlined in the processing scheme above (processing steps 1–3) and allow to calculate the corresponding subspectra A, B and C. These schemes may easily be expanded accordingly, if more target spins to be selectively perturbed have been selected.

### 3. Pulse sequences

The principle of multiple selective excitation has been incorporated into a few 1D and 2D experiments, the schemes of which are shown below (fig. 1). Depending on the experiment, either a DANTE pulse train (1D TOCSY [2]), frequency selective  $180^\circ$  pulses (1D NOE [3], 1D INADEQUATE [4], 1D C/H COSY [5] and 2D TOCSY-COSY [6]) or frequency selective  $90^\circ$  pulses (2D HMBC [11]) are applied to selectively perturb and uniquely label selected spins. Besides the DANTE “pulse”, composed itself of a series of non-selective rectangular pulses, Gaussian-shaped  $180^\circ$  and



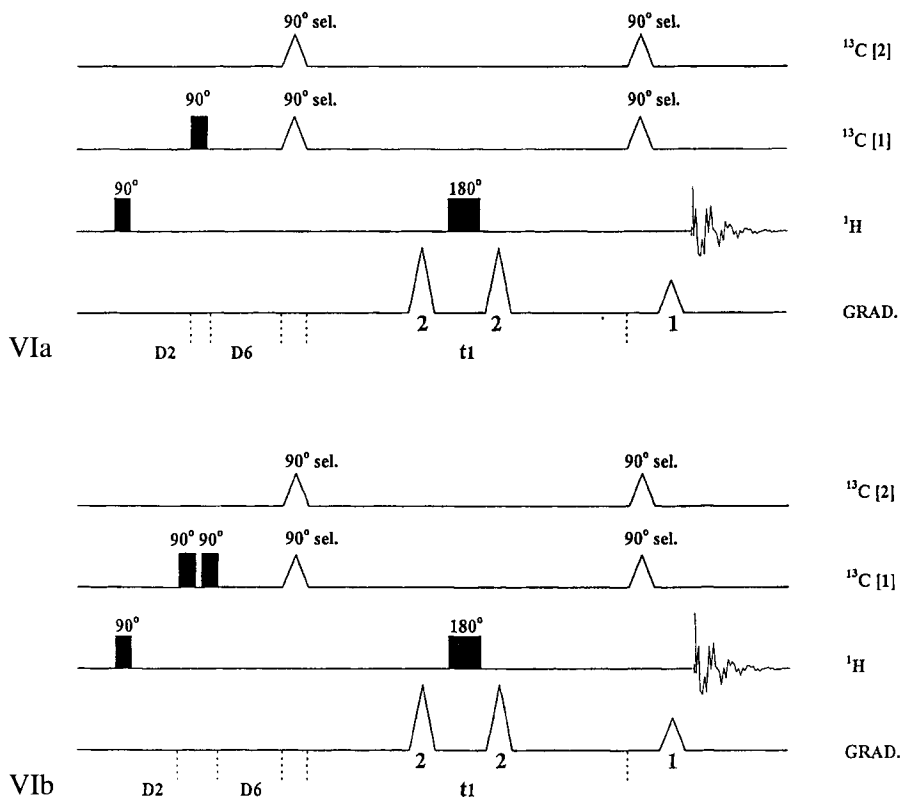


Fig. 1. Pulse sequences modified for multiple selective excitation. I: 1D TOCSY, II: heteronuclear 1D NOE, III: 1D INADEQUATE, IVa: heteronuclear 1D COSY (optimized to detect  $^1J_{\text{CH}}$ ), IVb: heteronuclear 1D COSY (optimized to detect  $^nJ_{\text{CH}}$ ), V: 2D TOCSY-COSY, VIa: 2D HMBC (designed to detect heteronuclear long-range couplings  $^nJ_{\text{CH}}$  only), VIb: 2D HMBC (extended pulse sequence to detect both heteronuclear long-range  $^nJ_{\text{CH}}$  and one-bond  $^1J_{\text{CH}}$  couplings).

TOPHAT-shaped 90° pulses are used in other cases as the best compromise with respect to the excitation profile, the phase homogeneity and length. Depending on the type of the detected spin-spin interaction – being either scalar or dipolar coupling – each selected spin is initially perturbed only once (1D TOCSY, 1D INADEQUATE, 1D C/H COSY, 2D TOCSY-COSY and 2D HMBC), or for several times (1D NOE). With each of the selected spins initially perturbed only once the inherently smaller transient NOEs would be detected in the latter case, whereas with the multiple excitation of a selected spin within the NOE build-up period the stronger steady-state NOEs are more or less approximated.

The use of selective 180° pulses at the beginning of the pulse sequence to initially perturb the spins is not a necessity and other possibilities exist.

They could well be replaced today by a single multiselective  $90^\circ$  or  $180^\circ$  pulse somewhere in the pulse sequence leading to probably superior variants as demonstrated with the modified 2D HMBC experiment. Former hardware and software limitations, however, forced us to use the variant with initially applied trains of selective  $180^\circ$  pulses.

#### 4. Applications and results

The modified pulse sequences have been applied to several compounds with the corresponding structures shown in fig. 2.

##### 4.1. 1D TOCSY [2]

The TOCSY or HOHAHA experiments have proved to be a valuable tool in the case of molecules composed of a series of coupled spin systems isolated

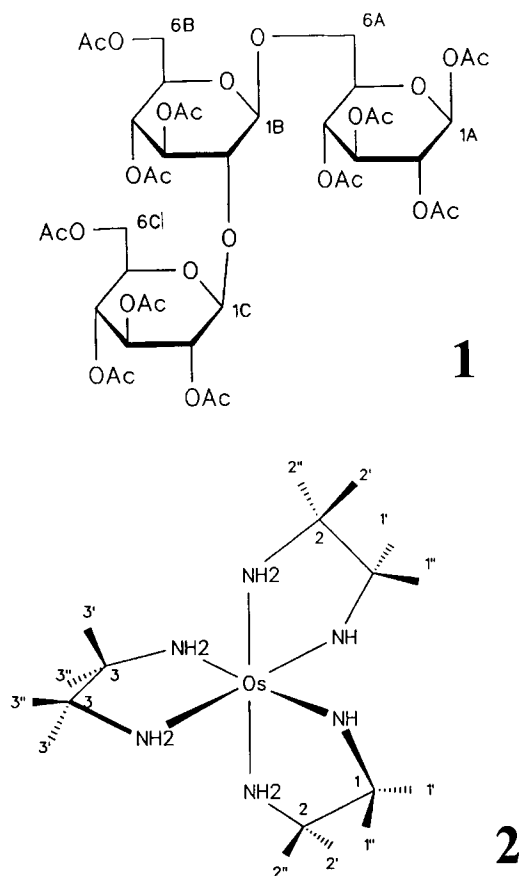


Fig. 2. Structural formulas.

from each other to evaluate coupling networks. This kind of isolated spin systems is most common in biomolecules, i.e., polysaccharides, polypeptides and polynucleotides. The experiments are based on the concept of spin propagation via a homonuclear Hartmann–Hahn coherence transfer process. Two variants of the basic experiment are in use, with the application of a selective  $180^\circ$  pulse set on- and off-resonance in two subsequent experiments – the TOCSY spectrum is calculated from the difference of the two data sets – or more simply with the application of a selective  $90^\circ$  pulse set on resonance in a single experiment. The results of these two variants with respect to sensitivity are the same.

We had to use the first variant (pulse scheme I in fig. 1) for the modified multiple selective experiment with a series of selective  $180^\circ$  DANTE pulse trains, since our spectrometer was not yet equipped with pulse shaping hardware and software at that time. It is important to note, that for the  $90^\circ$ -variant a single multiselective  $90^\circ$  pulse rather than a series of single selective  $90^\circ$  pulses must be used in order to circumvent severe phasing and sensitivity problems. Following the general acquisition scheme shown above  $2^{N-1}$  experiments have to be performed for  $N$  selected target spins, with the frequencies  $f_i$  for the  $N$  selective  $180^\circ$  pulses set either on- or off-resonance accordingly.

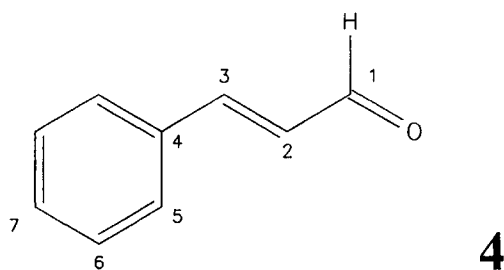
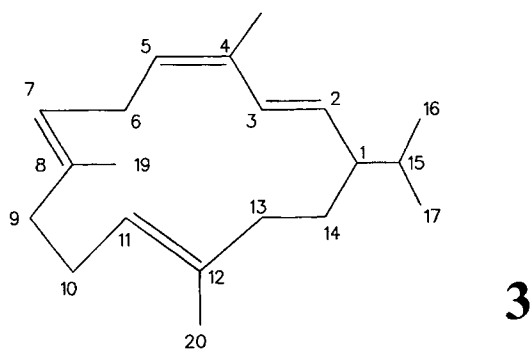


Fig. 2. (Continued) Structural formulas.

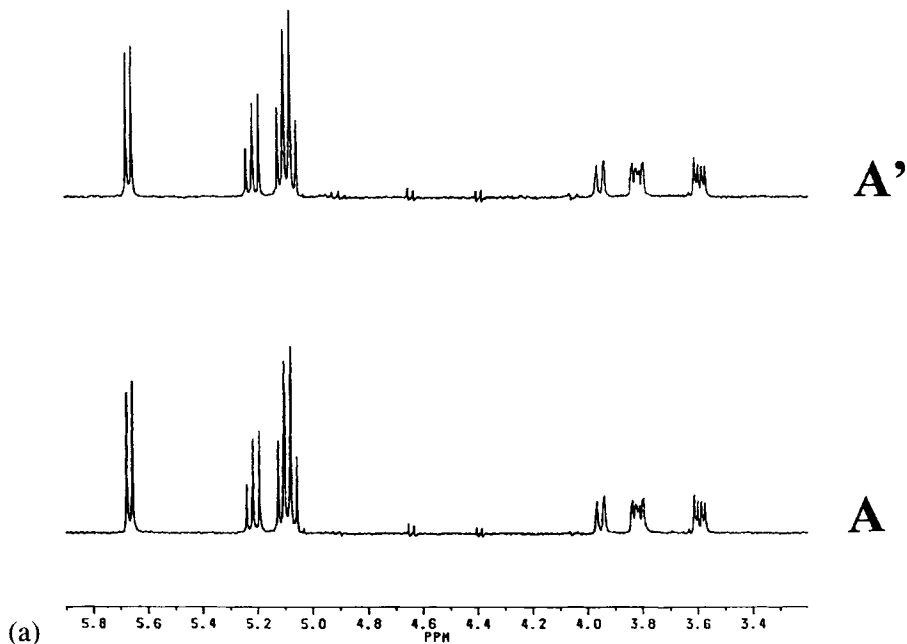


Fig. 3. (a) Comparison of subspectra A and A' as obtained from equal number of scans within the same total measuring time with the modified and the basic experiment respectively.

Following the general processing scheme shown above  $N$  spectra are calculated, corresponding to the 1D TOCSY spectra, measured with the basic single selective experiment. Whereas with this basic 1D TOCSY experiment only one of the spectra is acquired, all  $N$  subspectra are obtained within the same total measuring time with pulse sequence I, modified for multiple selective excitation. In accordance to theory and confirmed experimentally the same signal-to-noise ratios are measured with the modified and the basic pulse sequences, as long as relaxation may be neglected. However, longitudinal relaxation processes, being effective in the preparation period, affect the amount of  $z$ -polarization of those spins initially inverted by a selective  $180^\circ$  pulse. This subsequently decreases the overall sensitivity and sets an upper limit to the number  $N$  of target spins to be selectively perturbed.

As an example the three subspectra of a carbohydrate **1** (peracetylated triglucose) obtained with the modified pulse sequence I and with the frequencies of the selective  $180^\circ$  pulses adjusted to the frequencies of the three anomeric protons 1A, 1B and 1C are shown in fig. 3(b). One of these spectra is compared with the corresponding spectrum measured within exactly the same total measuring time with the basic single selective 1D TOCSY experiment (fig. 3(a)).

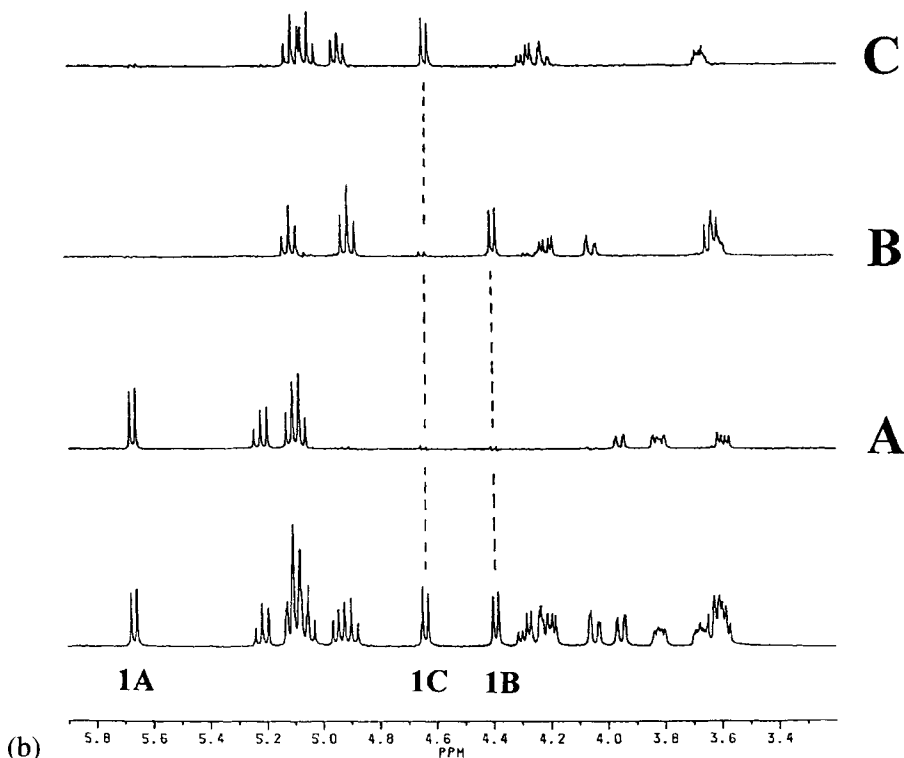


Fig. 3. (Continued) (b) Spectrum of peracetylated triglucose **1** dissolved in  $\text{CDCl}_3$  (bottom) and 1D TOCSY spectra A, B and C of the corresponding three glucose subunits, simultaneously acquired with pulse sequence I.

These spectra demonstrate that with the multiselective method a clean separation of the subspectra of the three independent spin systems may be achieved. They furthermore prove that – compared to the basic 1D TOCSY experiment – spectra of the same quality with respect to the suppression of residual signals originating from the other spin systems and with respect to the signal-to-noise ratios can be measured.

#### 4.2. 1D heteronuclear NOE [3]

Heteronuclear NOE experiments yield additional, but due to their inherent low sensitivity only sparsely exploited information on molecular structures. They are most useful to unravel structural features in the vicinity of quaternary carbons often behaving as barriers when exposed to standard routine experiments dedicated to evaluate coupling networks. Heteronuclear NOE data – in some sense complementary to the data from heteronuclear long-range couplings – are based on dipolar spin–spin interactions and strongly depend on internuclear distances. In contrast to the sometimes similar  $^2J_{\text{CH}}$

and  $^3J_{\text{CH}}$  coupling constants no ambiguities arise. The major problem with heteronuclear NOE experiments, however, is their sensitivity, since insensitive and less abundant nuclei with relatively long  $T_1$  values for quaternary centers are measured.

We have implemented the principle of multiple selective excitation (pulse sequence II in fig. 1) thereby replacing the low-power CW irradiation in the preparation period of the basic 1D experiment by a series of selective  $180^\circ$  pulses. The whole series of selective pulses at frequencies  $f_1, f_2, \dots, f_n$  is applied for several times in the NOE build-up period to achieve sequential saturation of the selected protons. Compared with the basic heteronuclear 1D experiment, in this new variant the sensitivity is improved by the combined application of sequential, selective pulses and the more efficient data accumulation scheme. Quantitation of NOEs is no longer straightforward since neither pure steady-state nor pure transient effects are measured and since cross-relaxation in a multi-spin system after perturbation of a single proton (as in the basic experiment) or of several protons (as in the proposed variant) differs. These attributes make this modified experiment most suitable for the qualitative recognition of heteronuclear dipole–dipole interactions rather than for a quantitative evaluation of the corresponding effects.

The improved pulse sequence was applied to correlate the signals of each of the quaternary carbons of compound **2** with the resonances of the the closely spaced methyl and amino protons. The resulting connections of chemical shifts served to overcome  $^2J_{\text{CH-}}$ ,  $^3J_{\text{CH-}}$  ambiguities left in the long-range  $J$ -correlated COLOC and FLOCK spectra and allowed, together with other data, to assign all proton and carbon resonances unequivocally. The modified experiment was performed three times with different numbers of simultaneously saturated protons, providing three series of NOE spectra (fig. 4 series a, b and c). In the first experiment the protons of one of five selected methyl groups were saturated by a series of  $180^\circ$  pulses. The experiment – it corresponds to the basic scheme with a series of selective  $180^\circ$  pulses rather than CW-irradiation at one single frequency – had to be repeated six times including an experiment with the decoupler frequency set off-resonance giving the NOE difference spectra shown in series a. This data served as a standard for comparison with the data correspondingly obtained with the two other experiments with simultaneous saturation of 5 (series b) and 10 (series c) protons. For the second experiment five of the six methyl signals and for the third experiment all the six methyl and four of the five amine signals of compound **2** were selected for simultaneous saturation.

The results may be summarized as follows. The NOE responses, obtained with the second and the third experiment with the simultaneous saturation of 5 and 10 resonances, respectively, agree with the results of the first (reference) experiment, if compared on a qualitative level. The results prove

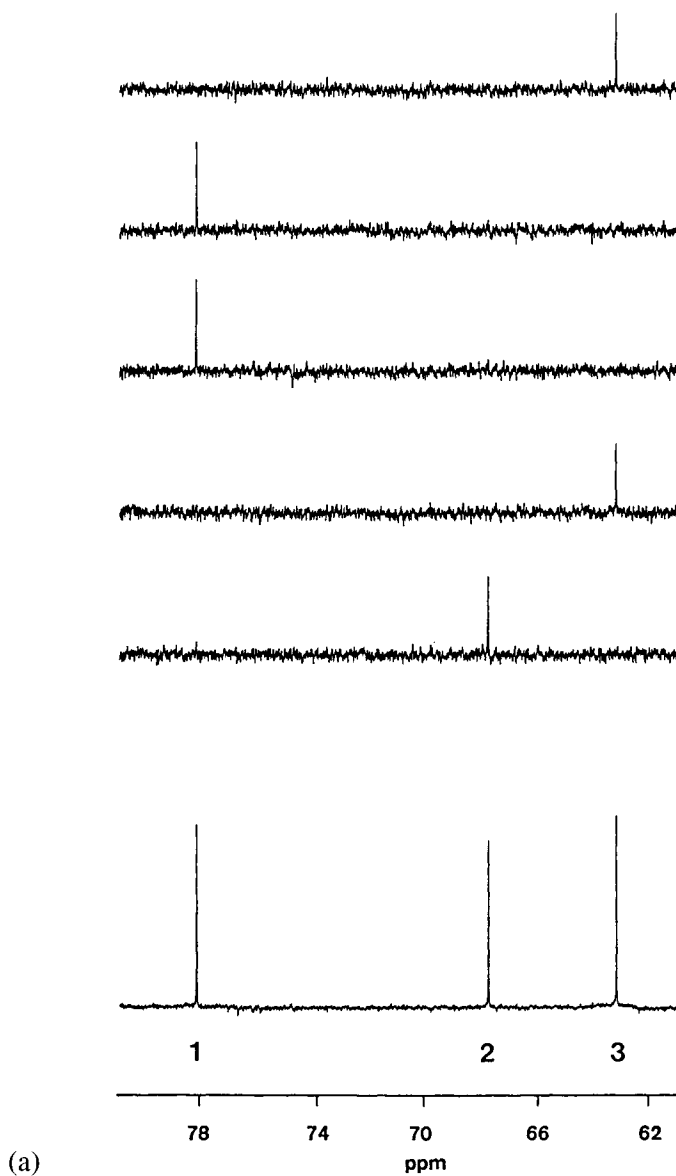


Fig. 4.  $^{13}\text{C}$  spectrum showing the three quaternary carbons C1, C2 and C3 of compound **2** dissolved in  $\text{CD}_3\text{CN}$  (bottom) and heteronuclear NOE spectra simultaneously acquired with pulse sequence II. Three data blocks a, b and c corresponding to three experiments with the number  $N$  of proton resonances selected for simultaneous saturation set to 1 (a), 5 (b) and 10 (c) are depicted. Five spectra with the initial saturation of protons  $3'$ ,  $1'$ ,  $1''$ ,  $3''$  and  $2'$  are presented. The additional five NOE difference spectra acquired in case c, with the irradiation of the sixth methyl and of four NH ( $\text{NH}_2$ ) proton resonances are not shown. (Continued on subsequent pages)

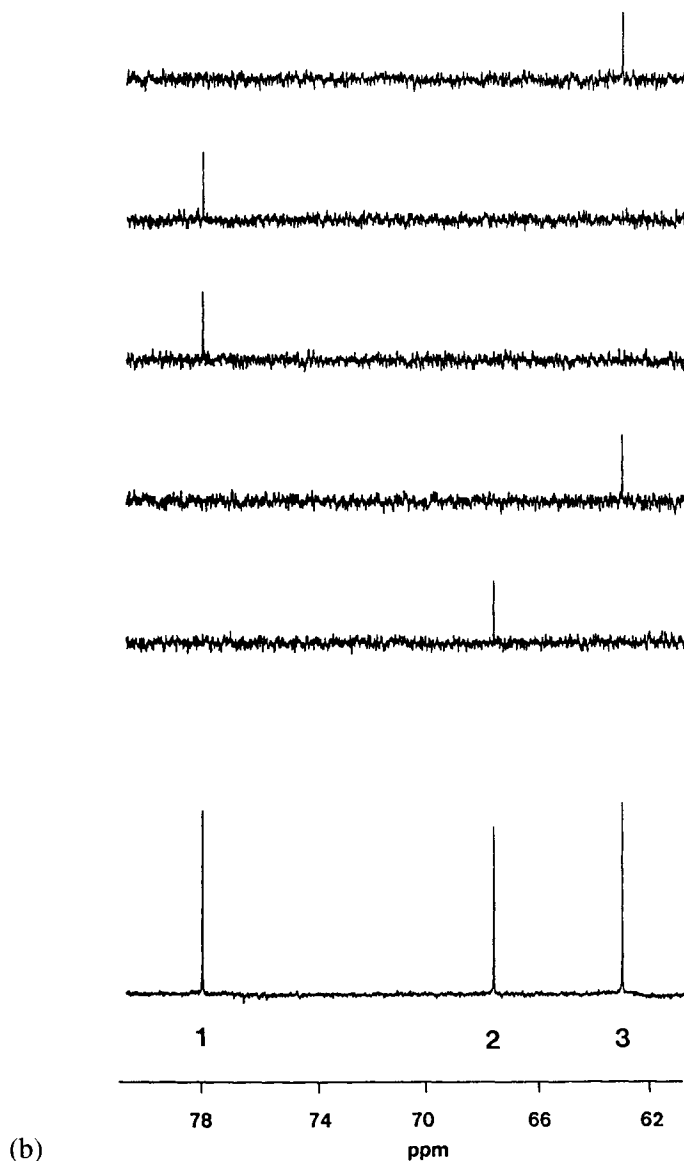


Fig. 4. (Continued)

that substantial gains in measuring times can indeed be obtained. Whereas with the first experiment only one NOE spectrum could be acquired, five and ten NOE spectra with the given quality were obtained with the second and the third experiment, respectively, within the same total measuring time. It is obvious, however, and in full agreement with theory that each NOE decays if the number of simultaneously saturated protons is increased.

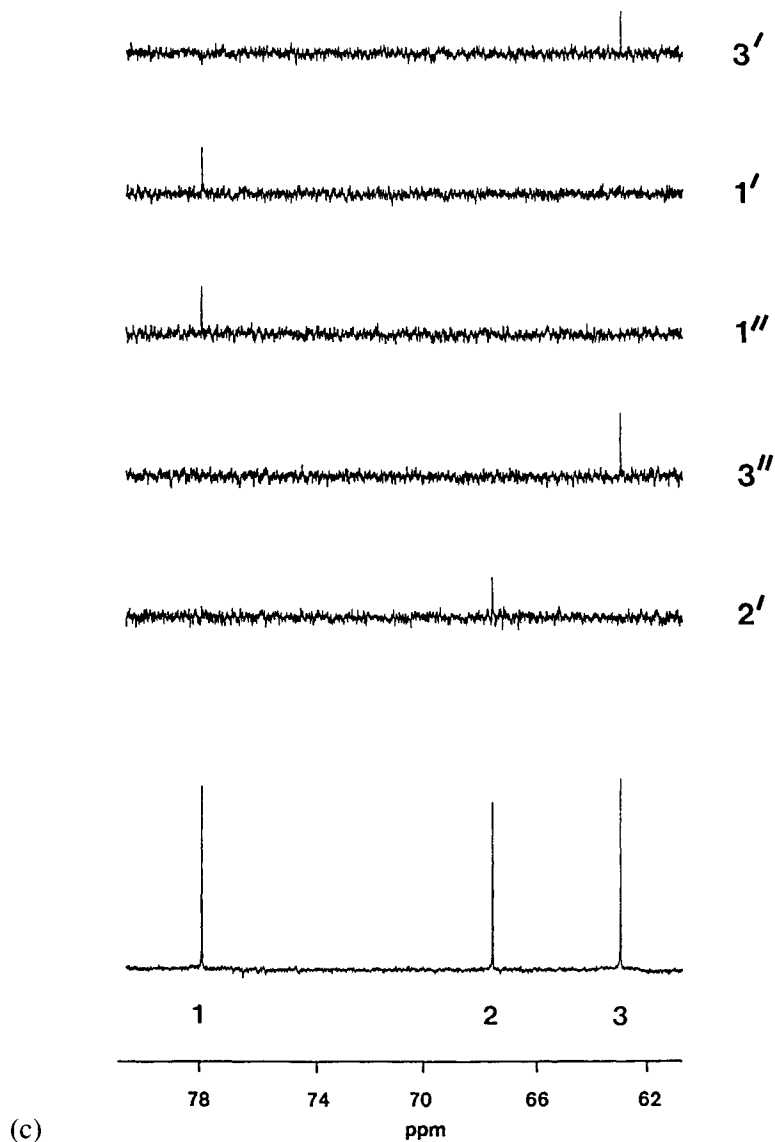


Fig. 4. (Continued)

Furthermore it could be shown that this decay of carbon signal intensity depends on the  $T_1$  of the correspondingly saturated proton and is most pronounced for short proton  $T_1$  values.

#### 4.3. 1D INADEQUATE [4]

Detailed structural information about the carbon skeleton of molecules, such as connectivities, bond orders and dihedral angles, can be derived from one-

bond and long-range carbon–carbon coupling constants. The inherent low sensitivity of such experiments if applied to  $^{13}\text{C}$  non-enriched samples, and the problems associated with the strong residual central signals of the correspondingly single labeled isotopomer, which particularly affects the measurement of carbon–carbon long-range couplings, drastically confines the range of their application. Two ways have recently been proposed to improve the inherent low sensitivity of these experiments. The initial heteronuclear polarization transfer takes advantage of the higher proton polarization and the usually shorter proton longitudinal relaxation time, which allows to use shorter intervals between subsequent scans. The final polarization transfer as applied in inverse INADEQUATE experiments takes advantage of the higher sensitivity of proton detection as generally incorporated in inverse techniques. Both of these improvements are restricted, however, to cases in which at least one of the coupled carbon nuclei is directly bound to protons. The corresponding experiments do not allow the measurement of coupling constants between quaternary carbons. Further, if highly accurate carbon–carbon one-bond or – even more demanding – carbon–carbon long-range coupling constants are of interest, neither the basic 2D INADEQUATE nor the sensitivity enhanced inverse techniques with final proton detection are of advantage. 2D techniques suffer from their usually low digital resolution and the evaluation of carbon–carbon coupling constants from the corresponding proton spectra obtained with inverse techniques with additional homo- and heteronuclear spin–spin interactions is certainly not straightforward. A selective 1D INADEQUATE experiment (SELINQUATE [7]) has been proposed, which allows to detect carbon–carbon connectivities and to measure accurately the corresponding coupling constants. It suffers, however, from its low efficiency if the connectivities and coupling constants of not a single but of a few carbons are of interest. Furthermore the  $90^\circ$  selective pulse used in this experiment shows an unfavourable excitation profile and its phase must be adjusted carefully relative to the phase of the non-selective pulses in the sequence. We incorporated the principle of multiple selective excitation into the basic selective 1D INADEQUATE experiment (pulse sequence III in fig. 1). Instead of the final selective  $90^\circ$  pulse we applied a series of selective  $180^\circ$  pulses in the preparation period for the reasons mentioned above. To reduce relaxation losses and to achieve the highest sensitivity the selective pulses are set as short as possible. On the other hand they are set as long as possible to be selective, but still short enough to fully affect the two carbon satellite signals caused by carbon–carbon couplings. Gaussian  $180^\circ$  pulses offer the best compromise for this purpose and have the advantage that no phase adjustments with respect to the phases of the hard pulses are necessary. In this version and compared with the normal INADEQUATE or the single selective SELINQUATE experiment, only half of the signal intensity can be obtained. This inherent

handicap, however, is compensated for and converted into increased overall sensitivity if the number of target carbons is increased.

The improved pulse sequence was applied to cembrene **3** to obtain carbon-carbon connectivity information and the corresponding one-bond and long-range coupling constants. Therefore the parameters of the experiment were adjusted to detect one-bond and long-range coupling constants within the same experiment. Figure 5a shows the selective INADEQUATE spectra obtained with the experiment modified for multiple selective excitation. Figure 5b demonstrates the comparison of corresponding results obtained within exactly the same total measuring times with the basic non-selective (left) and the modified (right) experiment.

The spectra in fig. 5a demonstrate that both one-bond and long-range connectivities and the corresponding coupling constants can be measured at the same time. Figure 5b shows that, in agreement with theory, only half of the intensity with respect to the basic experiment is obtained with the modified version and, more interestingly, that the additional loss of sensitivity caused by relaxation is extremely small. Furthermore, fig. 5b shows the almost perfect suppression of the unwanted central signals obtained with the modified experiment, which is especially useful when measuring long-range coupling constants. This high suppression degree must be attributed to the "cleaning effect" generally observed for double difference techniques, used in the final data processing with multiple selective excitation. These long-range coupling constants are usually not accessible in the spectra of the basic INADEQUATE experiment owing to the superposition of all the  $^{13}\text{C}$  satellites in the vicinity of the main isotopomer signal and to the overlap with the residual center signal itself.

#### 4.4. 1D C/H-COSY [5]

Correlations between protons and carbons have profound importance for structural elucidation of organic molecules. Whereas the knowledge of direct connectivities is essential for unambiguous resonance assignments of  $\text{CH}_n$  fragments, heteronuclear long-range couplings are used to connect these fragments within the molecule, to assign the resonances of quaternary carbons, and, most important, to deduce stereochemical information. If, as outlined before, the knowledge of a few spin-spin interactions suffices for structure elucidation, heteronuclear 1D shift-correlation experiments can be performed. For the task of detecting and quantifying proton-carbon couplings over one or more bonds, one-dimensional frequency selective analogues of inverse-detected 2D shift correlation methods have been designed [8, 9], which show quite satisfying results. They suffer, however, from their low efficiency, especially for a greater number of selected spins, as the individual excitations must be performed in separate experiments one after the other. We have developed two basic sequences, with the con-

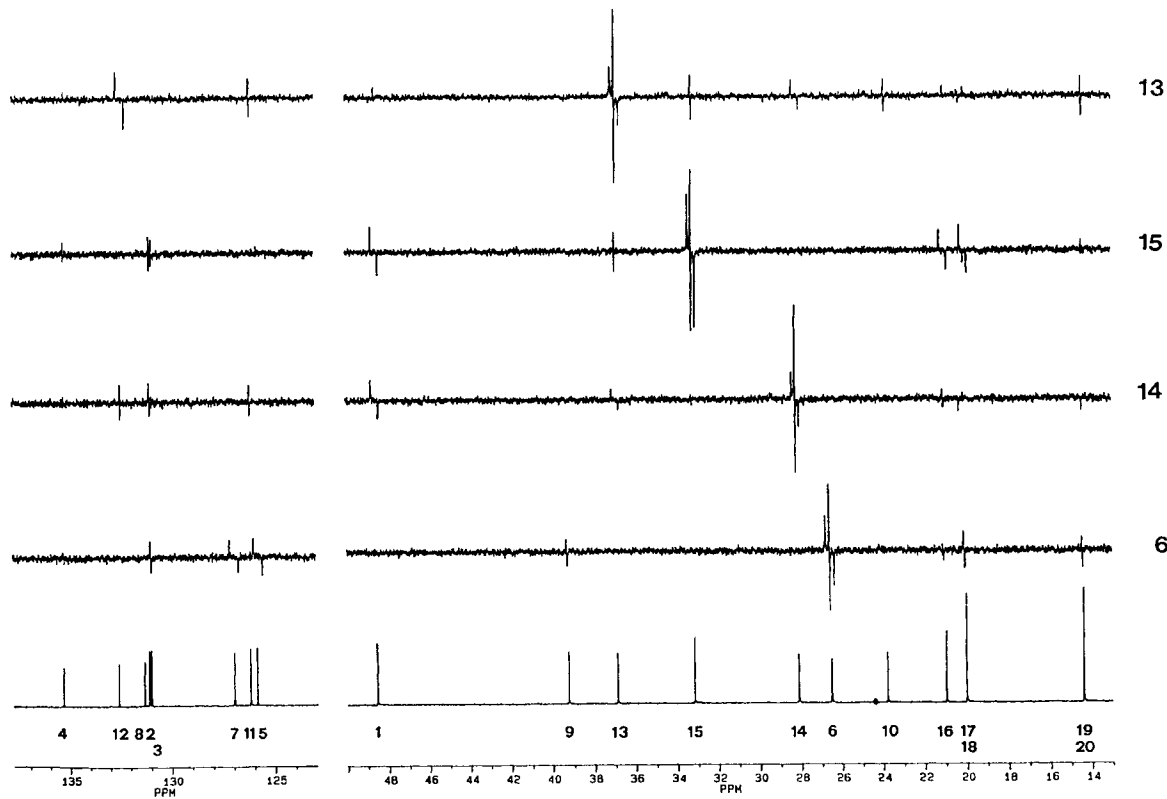


Fig. 5a. Part of the spectra obtained with the 1D multiple selective INADEQUATE experiment III applied to cembrene 3 dissolved in  $\text{CDCl}_3$ . The spectra were obtained after appropriate processing, showing the responses in the olefinic and the aliphatic regions after selective inversion of carbons C-13, C-15, C-14 and C-6. Normal  $^{13}\text{C}$  spectrum at the bottom.

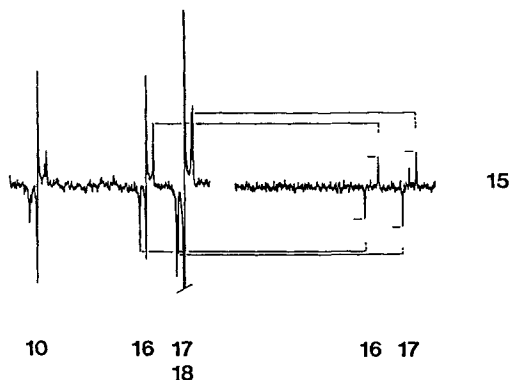


Fig. 5b. Comparison of the results obtained with the basic (left) and the multiple selective (right) INADEQUATE experiment. The signals of C-10, C-16, C-17 and C-18 are shown and are compared with the responses measured with the modified experiment after perturbation of C-15. Corresponding satellite signals are connected by horizontal lines.

cept of multiple selective excitation incorporated, adapted to evaluate either heteronuclear one-bond (pulse sequence IVa in fig. 1) or heteronuclear long-range couplings (pulse sequence IVb in fig. 1), respectively. Selectively labeled carbon magnetization is transferred to protons by polarization transfer either via  $^1J_{CH}$  or  $^nJ_{CH}$  couplings. Broadband proton decoupling is used while a train of selective  $180^\circ$  Gaussian shaped pulses is applied. Two versions with/without an initial INEPT part exist. We further combined both versions of sequence IVa with a subsequent COSY or TOCSY transfer to enlarge the connectivity region around the selected carbons. Whereas for sequence IVb (long-range couplings) proton antiphase magnetization is detected, in-phase proton magnetization may be detected as well with sequence IVa (one-bond coupling), if an additional delay is introduced. This allows to acquire the proton signal with concomitant carbon broadband decoupling thereby simplifying the spectra and increasing the sensitivity. The various delays in both sequences must carefully be adjusted to the expected coupling constant values and the influence of carbon multiplicities must be taken into account. Suppression of unwanted central signals is managed, on the one hand by phase cycling and, most effectively, by the application of purge pulses.

A solution of cinnamic aldehyde **4** was used to test the two pulse sequences, the results of which are shown in fig. 6. Three frequencies were selected to simultaneously perturb C1, C3 and C7 for experiment IVa and C1, C4 and C7 for experiment IVb to correlate directly and long-range coupled spins respectively. To minimize a decrease in sensitivity due to relaxation effects during the pulse cascade, the frequencies in the pulse train were ordered according to their estimated spin-lattice relaxation times. The

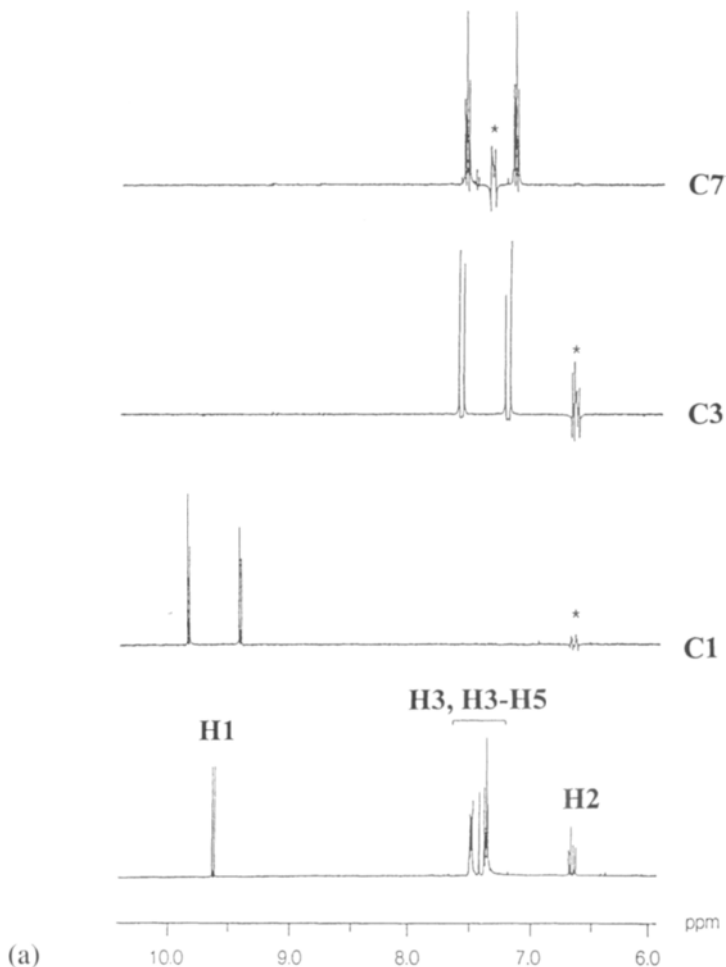


Fig. 6. Spectra of cinnamic aldehyde **4** dissolved in  $\text{CDCl}_3$  and obtained with the heteronuclear multiple selective COSY experiments. (a) Spectra acquired with pulse sequence IVa dedicated to detect and measure  $^1J_{\text{CH}}$  connectivities after selective perturbation of carbons C7, C3 and C1. Spurious TOCSY peaks caused by short purge pulses (not shown in fig. 1) are marked with an asterisk. (b) Spectra acquired with pulse sequence IVb dedicated to detect and measure  $^nJ_{\text{CH}}$  connectivities after selective perturbation of carbons C-7, C-1 and C-4. Normal  $^1\text{H}$  spectra at the bottom.

delays for coupling evolution were adjusted to averages of values expected for the investigated compound.

Looking at the series of subspectra obtained with both sequences, the perfect suppression of central signals is noticeable. This must be attributed on the one hand to the highly effective combination of proton broadband decoupling, the purge pulses and phase cycling and on the other hand to

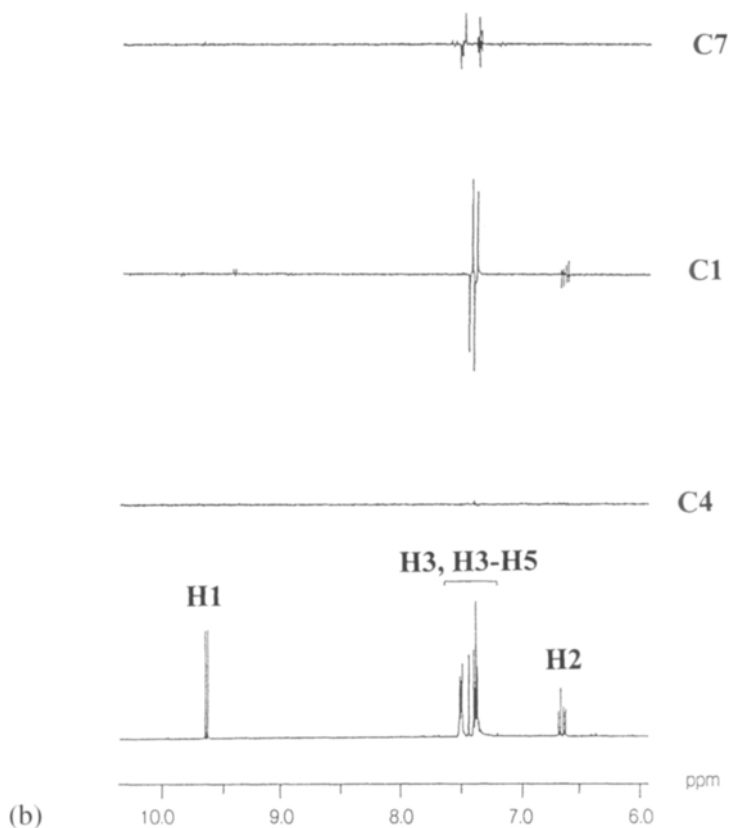


Fig. 6. (Continued)

the “cleaning effect” of double difference techniques, as subsequently applied with multiple selective excitation, when processing the acquired data. Most of the small residual signals (marked with an asterisk) observed with sequence IVa originate from partial TOCSY transfer induced by one of the purge pulses, which acts as short spin lock pulses. If experiment IVb is applied to C1 and C7, the expected long-range responses appear in pure antiphase mode and almost unperturbed by residual central signals. For the quaternary carbon C4, no response was obtained under these experimental conditions, mainly because of its long  $T_1$  value. Compared to the experimental results obtained with the single selective SELINCOR [8] and the single selective HMBC [9] experiment (not shown), performed with the same acquisition parameters within the same total measuring time and selectively exciting the same carbon resonances, almost the same signal-to-noise ratios were obtained throughout. Deviations are negligibly small with both experiments and are more than compensated by the fact that within the same

total measuring time not only one, as with the basic sequences, but in this case three subspectra are obtained with the multiple selective methods. The gain in sensitivity increases with the number of carbon targets exposed to the train of selective pulses. However, as with the other multiple selective experiments, an upper limit for the number of “simultaneously” inverted carbon resonances is given due to relaxation effects. Starting with carbon evolution has two main consequences: The influence of proton–proton couplings on the intensity of the detected proton signal, most troublesome for the determination of heteronuclear long-range couplings, may be neglected, but sensitivity is lost by a factor of 2 and 3 for  $\text{CH}_2$  and  $\text{CH}_3$  groups, respectively, compared to the corresponding pulse sequences starting with proton evolution.

#### 4.5. 2D TOCSY/COSY [6]

Among the multidimensional techniques for assignment of proton resonances, the recently proposed 3D HOHAHA-COSY experiment [10] is most promising and useful since it combines the advantages of two techniques designed for selective detection of spin subsystems (HOHAHA) and for the evaluation of coupling pathways (COSY). It further circumvents critical parameter adjustments even in the case of strong coupling, and it offers increased sensitivity compared to techniques in which heteronuclei are involved. On the other hand, longer measuring time has to be taken into account with 3D experiments, which is a disadvantage if spectral information on only a few but not all the spin systems is of interest. Powerful data systems with high computing and data storage capacities, including 3D data-handling software, are a prerequisite for efficient 3D data processing. We have proposed a 2D analog of the 3D HOHAHA-COSY experiment, using again the principle of multiple selective excitation (pulse sequence V in fig. 1) to improve the inherent poor sensitivity of a single selective experiment. Its application is advisable if a limited number of isolated spin systems are to be disentangled, i.e., the spin systems of few monomers of an oligomer or polymer, or spin systems of the individual components of a mixture. A series of selective inversion pulses uniquely labels a few selected proton resonances. Cross polarization effective in the subsequent spin-lock period transfers these labels to all the protons of the corresponding isolated systems of coupled spins. The individual labeling of all the protons of a spin system finally allows to disentangle the superimposed COSY spectra, in accordance to table 2 in the final data processing step.

The modified pulse sequence was applied to the trisaccharide **1**. A series of three Gaussian shaped  $180^\circ$  pulses were applied to initially invert the three anomeric proton spins. As a result the three COSY spectra, showing the coupling connectivities for the corresponding three monomer units were obtained, as shown in fig. 7 after appropriate data processing.

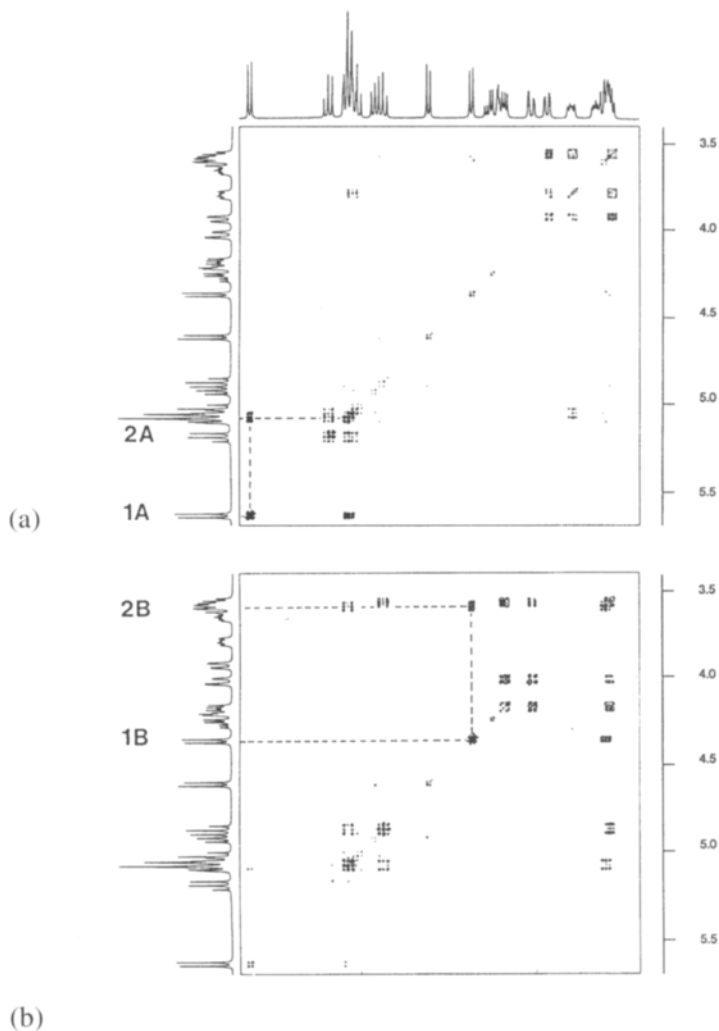


Fig. 7. Normal COSY spectrum (expansion of the ring-protons) of the trisaccharide **1** dissolved in  $\text{CDCl}_3$  (d). Individual COSY subspectra A, B and C ((a), (b) and (c)) of the three monomer units, obtained with the optimized 2D TOCSY-COSY experiment V. The three anomeric protons were used to selectively perturb the three spin systems. They are assigned and their connectivities to protons 2A, 2B and 2C, respectively, are indicated. (Continued on the next page)

The decomposition of a COSY spectrum as acquired with a normal non-selective COSY experiment into a series of 2D subspectra with a selective HOHAHA-COSY variant certainly simplifies spectral analysis especially in more demanding cases with severe signal overlap. Compared to the single selective experiment a substantial gain in sensitivity was obtained with the

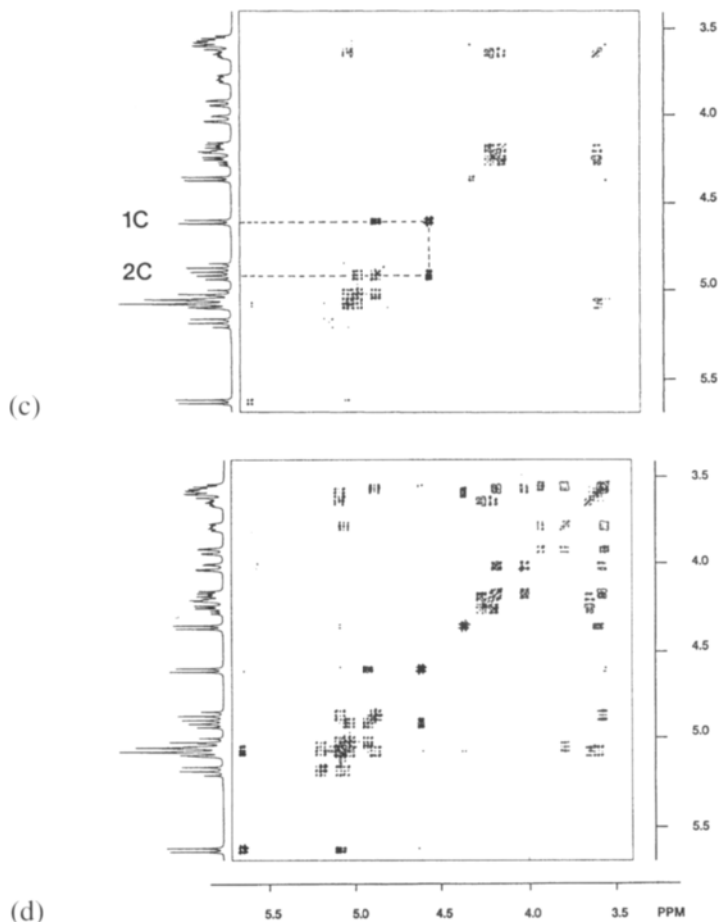


Fig. 7. (Continued)

experiment modified for multiple selective excitation. The losses due to relaxation were negligibly small in this case, but nevertheless set an upper limit to the number of target spins to be selectively inverted at the beginning of the pulse sequence. The substantial gain in the overall sensitivity or in spectrometer time and the increased clarity of the much simpler COSY subspectra compensates, at least partially, for the inherently lower sensitivity of the HOHAHA-COSY compared to the basic COSY experiment.

#### 4.6. 2D HMBC [11]

The detection of heteronuclear long-range spin-spin interactions and the measurement of the corresponding coupling constants serve to assign the signals of heteronuclei, especially of quaternary centers and yield most important structural informations, i.e., connectivities between molecular frag-

ments to establish molecular structures or of dihedral angles for the solution of conformational or stereochemical problems. If such information is needed not only for a few but eventually for all the heteronuclear spins of a molecule, the 2D HMBC experiment is probably the best choice. The use of  $^1\text{H}$  detection (inverse mode) and of gradients to select the desired coherence pathways offers maximum sensitivity and the best spectral quality. The initial low-pass filter removes or at least suppresses unwanted responses of one-bond heteronuclear interactions, eventually giving rise to problems and ambiguities in spectral analysis and interpretation. With the basic HMBC experiment the whole chemical shift range of the heteronucleus must be taken into account when setting up the experiment to circumvent folding problems of resonance signals being outside the spectral window in the second frequency domain  $F_1$ . This may give data matrices of respectable size, if at the same time high digital resolution is needed to resolve spectral ranges with high signal densities or to resolve the cross peak fine structure to obtain values for the corresponding heteronuclear coupling constants. Large data matrices not only require much storage space, but could lead to problems with remote data processing on less powerful computers, i.e., PCs. We have applied a modified  $^{13}\text{C}$ - $^1\text{H}$ - HMBC experiment (pulse sequences VIa and VIb in fig. 1), in which one or two – as in this case – non-selective carbon pulses are replaced by their selective counterparts. This allows to define not only the  $^1\text{H}$ - but also the  $^{13}\text{C}$ - spectral region of interest, yielding the corresponding section of the 2D spectrum without any folded cross-peaks, with high digital resolution, but reasonable data size. If not only one carbon region is of interest, this experiment must be repeated several times. We incorporated the principle of multiple selective excitation to improve the overall efficiency by using additional carbon channels on our spectrometer. Sequence VIa was used to excite two different carbon regions simultaneously with the corresponding selective carbon pulses on both channels adjusted accordingly. Two sub-experiments with half the number of scans each were performed within the same total measuring time as used for the single selective experiment carried out for comparison. Different phase combinations ( $x, x$ ;  $x, -x$ ) for the last pair of simultaneously applied pulses were used in these two sub-experiments to label differently the corresponding superimposed responses. Final data processing according to the general scheme outlined above was accomplished to disentangle the two subspectra. If additional spectrometer channels are available, not only two but more carbon regions to be selectively excited may be defined.

In most cases where long-range couplings are exploited to solve a structural problem corresponding information on heteronuclear one-bond interactions is needed as well. Instead of suppressing this valuable information with a low-pass filter as in the basic HMBC experiment, we additionally modified our pulse sequence – the second non-selective  $90^\circ$   $^{13}\text{C}$  pulse is

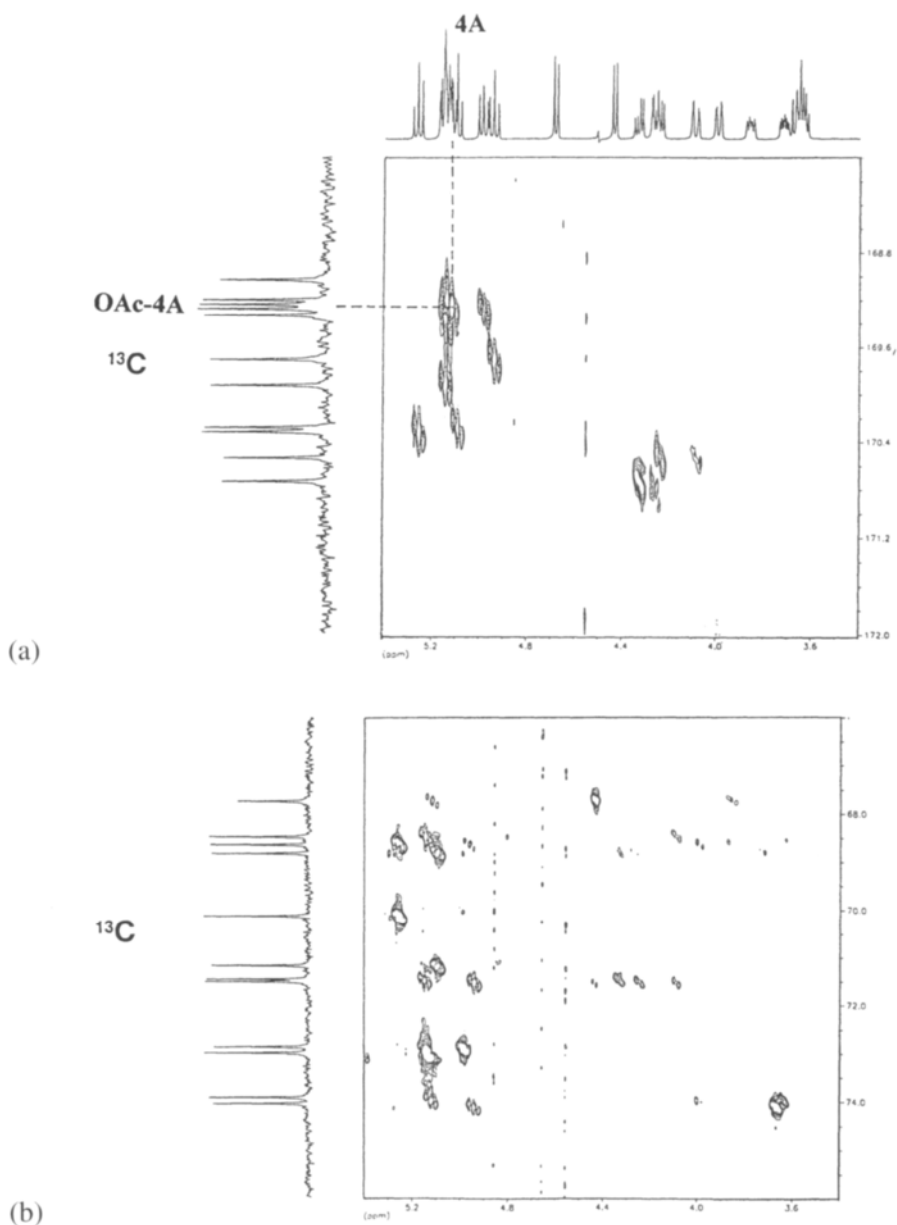


Fig. 8. Normal HMBC spectrum (expansion of the ring carbons and ring protons) of the trisaccharide **1** dissolved in  $\text{CDCl}_3$  (b). Equivalent spectrum obtained with the multiple frequency selective experiment further modified to discriminate between  ${}^nJ_{\text{CH}}$  and  ${}^1J_{\text{CH}}$  (c). Additional spectra acquired within the same experiment, which show  ${}^nJ_{\text{CH}}$  connectivities between the ring protons and the carbonyl carbons (a), and which show the  ${}^1J_{\text{CH}}$  connectivities between the ring protons and the ring carbons (d).

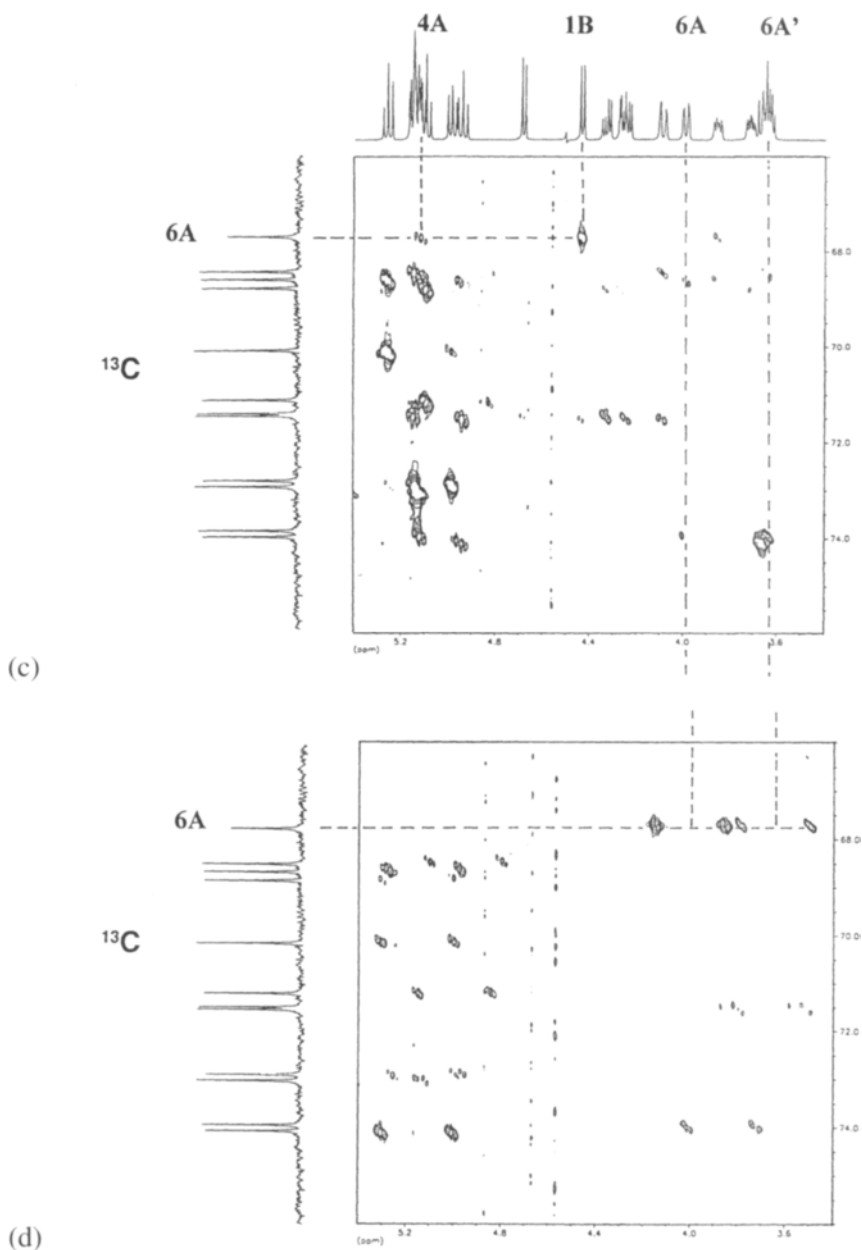


Fig. 8. (Continued) The fourth (empty) spectrum obtained within the same experiment and showing  $^1J_{\text{CH}}$  connectivities between the ring protons and the carbonyl carbons is not shown. A few connectivities starting with the assigned  $^1J_{\text{CH}}$  correlation C-6A - H-6A, H-6A' and leading to the assignment of H-1B, H-4A and carbonyl carbon-4A are indicated.

replaced by two  $90^\circ$  pulses – to acquire one-bond responses as well (sequence VIb in fig. 1). The delay D6 has to be adjusted to the values of long-range and one-bond coupling constants. To disentangle the superimposed long-range and one-bond responses we used the same principle as applied before to disentangle the responses of different  $^{13}\text{C}$  ranges. Different phase combinations ( $x, x$  and  $x, -x$ , respectively) were used for the two  $90^\circ$   $^{13}\text{C}$  pulses to differently label the one-bond and long-range responses. Four sub-experiments with NS/4 scans each have to be performed therefore to uniquely label responses with respect to one-bond/long-range couplings and to couplings with carbons resonating in the two spectral regions.

The modified pulse sequence VIb was applied to the trisaccharide **1**. Two  $^{13}\text{C}$  spectral regions, i.e., the region of the carbonyl and the ring carbons, were selectively perturbed with the selective pulses on the two channels  $^{13}\text{C}$  [1] and  $^{13}\text{C}$  [2]. As a result four spectra were obtained after appropriate data processing, showing either long-range or one-bond coupling interactions from either the carbonyl- or the ring-carbon region. Three of these spectra – the one-bond spectrum of the carbonyl region is empty and was omitted – are shown together with the spectrum obtained within exactly the same total measuring time with the single selective HMBC adjusted to the ring carbon region in fig. 8.

Compared to the single selective HMBC experiment (spectrum b) a substantial gain in sensitivity – the relaxation losses with the modified experiment were negligibly small – was obtained (spectrum c), since two (spectrum a and c) or even more subspectra may be acquired within the same total spectrometer time. Additionally not only long-range but also one-bond connectivities can be measured. The two types of connectivities are clearly separated as confirmed by spectra c and d.

Due to its improved efficiency and its economical use of data storage capacities the modified “HMBC” experiment is a valuable alternative for all those structural problems for which the knowledge of long-range and one-bond connectivities and values of the corresponding coupling constants is essential and for which only small sample amounts are available.

## 5. Conclusion

We have demonstrated that the principle of multiple selective excitation with subsequent data processing appropriate to disentangle the superimposed responses may successfully be incorporated into selective 1D and 2D pulse sequences. This allows to improve the overall efficiency especially of experiments with an inherent low sensitivity. In most of the presented examples a series of single selective pulses has been applied, giving rise to unwanted relaxation losses and setting an upper limit to the number of perturbed nuclear spins. With the application of single multiple selec-

tive  $90^\circ$  or  $180^\circ$  pulses, rather than trains of single selective  $180^\circ$  pulses applied in an initial preparation period, even better or more promising variants can be expected. Such variants with multiple selective single pulses, or variants using different transmitter channels – demonstrated with the 2D HMBC experiment – may be performed on modern spectrometers and other pulse sequences could be “up-dated” as well. There is, however, one final point which should be carefully taken into account when performing this kind of experiments. The individual spectra of the various excited spin systems obtained after appropriate processing fully correspond to the spectra measured with the corresponding basic single selective experiments, if the excited spin systems are completely isolated from each other, otherwise data interpretation, especially when carried out on a quantitative level, is no longer straightforward.

## References

- [1] G.A. Morris and R. Freeman, *J. Magn. Reson.* **29** (1978) 433.
- [2] H.R. Bircher, C. Mueller and P. Bigler, *J. Magn. Reson.* **89** (1990) 146.
- [3] C. Mueller, H.R. Bircher and P. Bigler, *Magn. Reson. Chem.* **30** (1992) 466.
- [4] L. Ma and P. Bigler, *Magn. Reson. Chem.* **30** (1992) 1247.
- [5] A. Steck and P. Bigler, *J. Magn. Reson., Series A* **110** (1994) 90.
- [6] H.R. Bircher, C. Mueller and P. Bigler, *Magn. Reson. Chem.* **29** (1991) 726.
- [7] S. Berger, *Angew. Chem., Int. Ed. Engl.* **27** (1988) 1196.
- [8] S. Berger, *J. Magn. Reson.* **81** (1989) 561.
- [9] M.A. Keniry and G.A. Poulton, *Magn. Reson. Chem.* **29** (1991) 46.
- [10] C. Griesinger, O.W. Sorensen and R.R. Ernst, *J. Magn. Reson.* **73** (1987) 574.
- [11] In preparation.

This Page Intentionally Left Blank

## chapter 3

---

# Concatenation of Polarization Transfer Steps in 1D Homonuclear Chemical Shift Correlated Experiments. Application to Oligo- and Polysaccharides

---

Dušan Uhrín

*University of Edinburgh  
Department of Chemistry  
West Mains Road, Edinburgh EH9 3JJ  
United Kingdom*

This Page Intentionally Left Blank

## 1. Introduction

Chemical shift correlated NMR experiments are the most valuable amongst the variety of high resolution NMR techniques designed to date. In the family of homonuclear techniques, four basic experiments are applied routinely to the structure elucidation of molecules of all sizes. The first two, COSY [1, 2] and TOCSY [3, 4], provide through bond connectivity information based on the coherent ( $J$ -couplings) transfer of polarization between spins. The other two, NOESY [5] and ROESY [6] reveal proximity of spins in space by making use of the incoherent polarization transfer (nuclear Overhauser effect, NOE). These two different polarization transfer mechanisms can be looked at as two complementary vehicles which allow us to move from one proton atom of a molecule to another proton atom: this is the essence of a structure determination by the  $^1\text{H}$  NMR spectroscopy.

Depending on the size of a molecule and the dispersion of chemical shifts of its protons the task of establishing individual chains of coupled spins from 2D COSY and TOCSY spectra might be hampered seriously by spectral overlaps. For the same reason, the assignment of crosspeaks in 2D NOESY or ROESY spectra might also be ambiguous. Under these circumstances a crucial bit of information can be provided by concatenating coherent and incoherent polarization transfer steps in a single homonuclear experiment. This class of experiments is referred to here as the “combined” NMR techniques. They provide, in principle, identification of networks of coupled spins as well as information concerning through-space proximity between adjacent spin systems. Combined experiments allow us to use simultaneously the two different vehicles, “fueled” by  $J$  couplings and NOEs, on our metaphorical journey along the proton atoms.

The pioneering work in this field, a two-dimensional relayed-NOE experiment proposed by Wagner [7], was quickly followed by the appearance of several related NMR techniques [8–17]. Application of isotropic mixing during the  $J$ -transfer period yielded the 2D TOCSY-NOESY [11, 15] and NOESY-TOCSY [12, 14] experiments. When spin-lock sequences were applied to both  $J$  and NOE-transfers, the 2D TOCSY-ROESY and ROESY-TOCSY experiments [10, 16, 17] emerged.

A general problem associated with combined two-dimensional techniques is the increased number of correlations originating along different polarization transfer pathways. The probability of crosspeak overlap increases, and although the resulting spectra carry undoubtedly more information, this might be difficult to access. Moreover, since crosspeaks of different origin could differ in their signs, their mutual cancellation can occur. Some sort of spectral simplification is therefore highly desirable.

One way to achieve this is by applying selective pulses during the preparation period of combined 2D experiments [18–20]. Here, the number of coherences which evolve during the  $t_1$  period and are subjected to the first polarization transfer is considerably reduced. Correspondingly, there is a decreased probability of overlap, even after more signals have been generated by the second polarization transfer.

Another way of avoiding overlaps seen in two-dimensional spectra is to introduce the third dimension. This has been illustrated with the 3D NOESY-HOHAHA [21–25], 3D HOHAHA-NOESY [25–27], NOESY-COSY [28, 29], COSY-NOESY [28] and ROESY-TOCSY [23] experiments. A principal drawback, associated with homonuclear 3D techniques, is the low digital resolution achievable along the first and second spectral axes. This limitation can to certain extent be removed by implementing band selective pulses into the 3D homonuclear experiments [21, 26, 28–31].

In a move in the opposite direction, the overlaps resulting from concatenation of different polarization transfer mechanisms in combined 2D experiments can be eliminated by reducing the dimensionality of an experiment. Similarly to the successful transformation of basic 2D NMR techniques into their 1D counterparts [32–34], a conversion of combined 2D NMR techniques into their 1D analogs is feasible and has been explored by several groups [35–40]. From a different perspective this process can be seen as a twofold reduction of the dimensionality in a 3D experiment. Equally, concatenation of three polarization transfer steps in a single 1D experiment represents transformation of a possible 4D homonuclear experiment into its 1D analog.

One-dimensional spectra obtained in these experiments can be compared to 1D traces of  $n$ D NMR spectra but offering much better digital resolution and shorter acquisition times. On the negative side each “trace” needs to be acquired separately and thus, if several sites are to be inspected, a series of 1D experiments must be performed. In practice, this exercise is preceded by careful inspection of standard two-dimensional COSY, TOCSY, NOESY or ROESY spectra and only the ambiguous assignments are tackled by combined 1D techniques.

A more fundamental limitation lies in our ability to selectively excite individual multiplets – an essential part of a successful transformation of an  $n$ D experiment into its 1D analog. This requirement limits severely

application of 1D analogs of basic 2D techniques like 1D COSY, TOCSY or NOESY, which rely on a single selection step. However, for combined 1D experiments even if a complete overlap exists between resonances used for the first polarization transfer step, there is a possibility that the ambiguity will be removed during the second polarization transfer step. This puts less stringent requirements on signal separation in 1D spectra and broadens the application range for 1D NMR experiments which concatenate several polarization transfer steps.

So far, it has been argued that a combination of different polarization mechanisms in 1D experiments opens new possibilities for signal assignments. The realization that combined experiments can also be applied successfully to systems with a higher degree of overlap prompts us to explore concatenation of identical polarization transfer mechanisms as well. For example, when severe overlap prevents selective excitation of a single proton in a 1D TOCSY experiment, the desired signal selection might be achieved during the second TOCSY step in a 1D TOCSY-TOCSY experiment. Several experiments using exclusively a coherent polarization transfer mechanism are therefore included in this chapter, as well as the 1D NOESY-NOESY experiment – a concatenation of two incoherent polarization transfers steps.

Before presenting individual examples, let us focus briefly on general aspects of transformation of  $n$ D NMR techniques into their 1D analogs.

## 2. Transformation of $n$ D NMR techniques into their 1D analogs

### 2.1. Selective pulses and chemical-shift-selective filters

As pointed out in the Introduction, the essential part of a successful transformation of an  $n$ D experiment into its 1D analog is the selective excitation of spins. There are two distinct tools available for this purpose: selective pulses and chemical-shift-selective filters.

Many selective pulses have been designed during the last decade and the reader can find a special chapter devoted to this topic in this book. In short, the important criteria for choosing an appropriate selective pulse are their frequency characteristics, relaxation properties and the evolution of coupling constants during the long selective pulses. The following selective excitation pulses were used for most examples given in this chapter:  $90^\circ$  and  $270^\circ$  Gaussian [41, 42] and  $90^\circ$  half-Gaussian [43] pulse. The  $90^\circ$  Gaussian pulse was used when the evolution of  $J$ -couplings during the pulse was desired, while  $90^\circ$  half-Gaussian or a  $270^\circ$  Gaussian pulse were applied when  $J$ -coupling needed to be suppressed. For selective inversion of spins,  $180^\circ$  Gaussian or  $180^\circ$  rectangular DANTE-Z pulse [44] were employed. Although pulses with better excitation profiles are available at

present [45, 46] the above set was chosen mainly because of high tolerance of these pulses to fast spin–spin relaxation. This is especially true for the  $90^\circ$  half-Gaussian pulse. In order to remove the dispersive component of this pulse, it was usually followed by a  $90^\circ$  purging nonselective pulse [34]. When the  $270^\circ$  Gaussian pulse was used no purging of the dispersive component was used. In practice, there might be significant phase differences between different power levels of a transmitter used for the soft and hard pulses. These need to be calibrated and compensated for accurately in pulse sequences containing selective and nonselective pulses.

Selective pulses require individual multiplets to be well separated from one another, while chemical-shift-selective filters (CSSF) are able to resolve severely overlapping multiplets, with different chemical shifts [48–52]. Frequency selection is achieved during the CSSF by setting the transmitter frequency to the chemical shift of a selected proton and by acquiring a set of experiments by systematic incrementation of the chemical shift evolution period. The proton magnetization originating in the selected proton experiences no chemical shift evolution and is co-added constructively while the magnetization arising from other protons is co-added destructively and thus filtered out. The addition can be performed in the computer memory during acquisition, or by adding individual FIDs (or spectra) from the CSSF experiment originally stored separately, afterwards. Evolution of coupling constants during the entire filter must be constant. In homonuclear CSSFs this is achieved by gradual displacing of a  $180^\circ$  pulse from the centre of a constant time interval, e.g., the spin-echo interval of a multiple relay experiment. The whole process resembles the acquisition and processing of a constant time 2D experiment, the only difference is that instead of the second Fourier transformation individual CSSF spectra are added together. In addition to the analogy with 2D experiments, the CSSF can be compared to the rectangular DANTE pulse [53, 54]. The selectivity of both depends on their duration, while both produce side lobes and excitation sidebands. First zero in the absorption excitation profile of the CSSF occurs at  $1/2\tau_{\max}$ , where  $\tau_{\max} = n\Delta$  is the maximum duration of the filter;  $n$  is the number of increments and  $\Delta$  is the length of an increment of the CSSF. Excitation sidebands are found at  $\pm k/\Delta$  frequencies, where  $k$  is an integer. The larger the increment of the filter, the faster the desired selectivity is achieved and the number of necessary increments decreased. This brings the excitation sidebands closer to the carrier frequency. Nonetheless, as will be illustrated later, when the CSSF is applied for the second selection step, the magnetization has already been preselected by a selective pulse and excitation sidebands do not pose a problem. The need to acquire several FIDs in a CSSF experiment is perhaps a minor inconvenience in comparison with methods using selective pulses and may prolong the overall acquisition time. A more severe limitation for application of CSSFs stems from the

fact that they act only on the magnetization which is in the  $xy$  plane. CSSF based techniques are therefore not recommended for resolving close signals in molecules with fast spin–spin relaxation.

## 2.2. Concatenation of polarization transfer steps

There are different ways to achieve multiple concatenation of polarization transfer steps giving rise to selective 1D experiments which are likely to differ in the intermediate period connecting individual polarization transfer steps [35–40]. For experiments using only selective pulses for the signal selection, we have adopted a strategy whereby the magnetization of interest is stored along the  $z$  axis after the completion of each transfer. This approach has several advantages. First, it reduces the time the magnetization spends in the  $xy$  plane and makes the sequence more likely to succeed when applied to macromolecules with fast spin–spin relaxation. Second, the carrier frequency can be changed at this point of time without worrying how it will affect otherwise necessary phase coherence between individual steps, since the magnetization stored in the  $z$  axis has no phase memory. Third, it allows a choice from a wider range of selective pulses applicable to the  $z$  magnetization. In experiments when a selective pulse is applied to the  $xy$  magnetization only universal rotators [47] should be used.

A different situation is encountered when chemical-shift-selective filters are applied for the signal selection. Clearly, when used in simple 1D selective experiments [48–50] the power of CSSFs lies in their ability to separate severely overlapping multiplets. For application in 1D analogs of  $n$ D experiments [38], it is convenient to use CSSFs for the second selection step, when the magnetization was already preselected during the first step by a selective pulse and is in the  $xy$  plane. CSSF can then be incorporated into a sequence in a way such that no extra delays are introduced. It will be demonstrated later that when starting with only two overlapping signals it is not necessary to perform a complete CSSF experiment, instead, only two increments are sufficient to achieve the signal selection.

In general, 1D selective experiments with multiple polarization transfer steps can be performed by using the selective excitation exclusively at the beginning of the pulse sequence [55–57]. However, using this approach, the information obtained is ambiguous, e.g., the final nonselective NOESY transfer in a 1D TOCSY-NOESY experiment gives rise to many signals depending on the NOE contacts of all protons, magnetization of which had been created during the initial selective TOCSY transfer. These methods will not therefore be considered further. Truly selective experiments, which apply selection of the magnetization in both steps, retain all the advantages of one-dimensional experiments and the unambiguity of the 3D approach.

On the other hand when more than two polarization transfer steps are combined (1D analogs of 4D experiments) one can make a decision, without affecting the end result, as to whether the second, the third or both these steps should be selective. In order to avoid possible losses of magnetization during the selective pulses, due to either relaxation and/or nonperfect excitation profiles, it is usually possible to make one of these steps nonselective.

### 2.3. Pulsed field gradients

The recent introduction of pulsed field gradients (PFG) in high resolution NMR spectroscopy brought significant enhancement to the quality of NMR spectra [58, 59]. The main reason for this is that during the process of coherence selection by PFGs the unwanted coherences are dephased and the signal from them is not digitized. In principle, possible cancellation artifacts, present in traditional phase cycled experiments, are avoided. Elimination of extensive phase cycling means that many 2D experiments can be acquired with as little as one or two scans per  $t_1$  increment, providing the sensitivity is not a limiting step. This can speed up the acquisition of 2D experiments significantly. However, it is not that important for their 1D analogs where acquisition of multiple scans can be tolerated. The penalty which usually accompanies coherence pathway selection by PFGs is that one half of the signal is lost during the pulse sequence.

On the other hand, PFGs can be utilized in a different manner to achieve near complete suppression of unwanted coherences while still relying on some basic phase cycling for the final signal selection. This approach, sometimes referred to as coherence pathway rejection by pulsed field gradients [60], retains full sensitivity. It seems to be preferable for use in 1D NMR spectroscopy, where time saving due to elimination of phase cycling is not necessary. Cleaner spectra are expected from this method simply because cancellation artifacts from attenuated signals are scaled down accordingly. At the same time, no losses of magnetization due to molecular diffusion are encountered since the desired signal did not experience a cycle of de- and rephasing by PFGs.

There are several examples of 1D selective experiments [61–68], including combined 1D experiments [68, 69], in the literature which use pulsed field gradients. This subject has been reviewed thoroughly recently [69]. With one exception [67], all of them employ PFGs for coherence selection and are therefore liable to sensitivity losses as pointed out above. We have designed several selective 1D experiments which use pulsed field gradients for coherence pathway rejection [70]. They use the guidelines for concatenation of polarization transfer steps outlined in section 2.2 and are suitable for application to large molecules. Principal points of the transformation of phase-cycled selective experiments into their gradient-enhanced versions are outlined and illustrated on a 1D ge-NOESY-TOCSY experi-

ment in Section 3.6. Following this example, all phase-cycled experiments which combine TOCSY and NOESY polarization transfers steps can be easily transformed into their gradient-enhanced versions.

Since many spectrometers currently in use are not equipped with PFG modules, the examples given in this chapter focus on the phase-cycled experiments. Judging by comparison of noise levels in these spectra between regions which do and do not contain any signals, cancelation of unwanted signals is fairly good. Nevertheless, spikes from intense signals can be recognized and a considerable signal from water protons is almost always present in spectra acquired by purely phase cycled methods. On the other hand, gradient-enhanced methods described in Section 3.6 yielded artifact-free spectra.

### 3. 1D NMR experiments with multiple polarization transfer steps

Concatenation of polarization transfer steps in 1D NMR experiments is illustrated in the rest of this chapter using oligo- and polysaccharide samples. Carbohydrates give notoriously overlapped spectra in the region of 3–4 ppm. On the other hand, they feature reasonably resolved anomeric resonance between 4.5 and 5.5 ppm. These and other resolved signals are used as spectral windows in the analysis of carbohydrates and are very good candidates for the initial polarization transfer of selective 1D experiments. Bacterial polysaccharides are used to illustrate the usefulness of these techniques to molecules with short spin–spin relaxation times. They consist of relatively small repeating units but form large molecules. Their spectra resemble those of the corresponding oligosaccharides but with rather broad spectral lines.

Almost all spectra were acquired on a AMX-600 Bruker NMR spectrometer equipped with a 5 mm inverse broad-band probe. The only exception were the gradient-enhanced spectra acquired on an INOVA-600 Varian NMR spectrometer using a 5 mm triple-resonance probe with  $z$  gradients. The experimental details are given for each spectrum in the figure captions.

#### 3.1. 1D NOESY-TOCSY and 1D TOCSY-NOESY

The 1D NOESY-TOCSY experiment [39] shown in fig. 1(c) is a straightforward concatenation of 1D NOESY and TOCSY experiments [34] (figs 1(a), (b)). Since the NOE transfer takes place along the  $z$  axis, and thus has no phase memory, no phase correction for the second selective pulse is needed to compensate for the change of the r.f. frequency during the  $\tau_{\text{NOE}}$  interval. Nevertheless, any possible phase differences between the selective and consecutive nonselective pulses must be taken into account in both steps, by adjusting the phase of soft pulses.

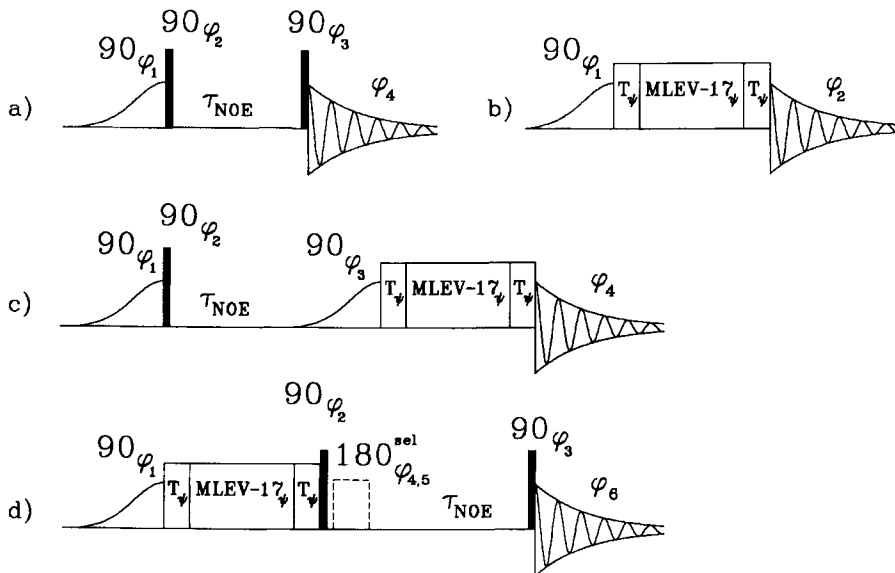


Fig. 1. Pulse sequences of 1D selective experiments. The shaped  $90^\circ$  pulses were half-Gaussian. The  $180^\circ$  selective pulses were produced by a DANTE-Z pulse train [44].  $T_\psi$  denotes the trim pulse of phase  $\psi$ .  $T_{\text{NOE}}$  stands for the NOE-mixing time.

(a) 1D NOESY and (b) 1D TOCSY experiments [34]. The following phase cycling was applied in (a):  $\phi_1 = x, -x$ ;  $\phi_2 = 8x, 8(-x)$ ;  $\phi_3 = 2x, 2(-x), 2(y), 2(-y)$ ;  $\phi_4 = x, 2(-x), x, y, 2(-y), y, -x, 2x, -x, -y, 2y, -y$ ; and (b):  $\phi_1 = y, -y$ ;  $\psi = x, 2(-x), x$ ;  $\phi_2 = y, -y$ .

(c) 1D NOESY-TOCSY experiment with both polarization transfer steps selective. The following phase cycling was applied:  $\phi_1 = x, -x$ ;  $\phi_2 = 8x, 8(-x)$ ;  $\phi_3 = 2x, 2(-x)$ ;  $\psi = 4y, 4(-y)$ ;  $\phi_4 = 2(-x, x, x, -x), 2(x, -x, -x, x)$ .

(d) 1D TOCSY-NOESY experiments. The  $180^\circ$  selective pulse consists of a DANTE-Z pulse train  $(\Theta^\circ(\phi_4) - \Delta - \Theta^\circ(\phi_5) - \Delta)_n$  where  $2n\Theta = 180^\circ$ . The following phase cycling was applied:  $\phi_1 = y, -y$ ;  $\phi_2 = 16y, 16(-y)$ ;  $\phi_3 = 4x, 4(-x), 4y, 4(-y)$ ;  $\phi_4 = 32x, 32(-x)$ ;  $\phi_5 = 8(x, x, -x, -x), 8(-x, -x, x, x)$ ;  $\psi = 2x, 4(-x), 2x$ ; the basic receiver phase cycle,  $\phi_6 = -x, 2x, -x, x, 2(-x), x$ , was incremented by  $90^\circ$  each eight scans. When the  $180^\circ$  selective pulse is omitted and a nonselective NOESY transfer is applied, all phases are the same as given above except for the basic receiver cycle,  $\phi_6$ , which is:  $2(x, -x), 2(-x, x)$ . The  $180^\circ$  DANTE-Z pulse can be replaced by a  $180^\circ(\phi_4)$  Gaussian pulse applied on- and off-resonance in blocks of two scans.

The sensitivity of this experiment depends to a large extent on the efficiency of the NOESY transfer. This is naturally high in macromolecules, therefore the 1D NOESY-TOCSY experiment is particularly suited for large molecules. The use of half-Gaussian pulses which are highly resistant to fast spin-spin relaxation together with the net transfer of magnetization in both steps, yielding inphase multiplets, is also in line with the intended application area.

By applying the NOESY step first, this experiment allows us to jump from one spin system to another or to overcome a bottleneck in TOCSY transfer caused by an occurrence of a small coupling constant in the chain of  $J$ -connectivities. Both these features are illustrated in 1D NOESY-TOCSY spectra of the type VI group B *Streptococcus* capsular polysaccharide (1).

The spin systems of individual carbohydrate residues are considered to be isolated, since the four-bond coupling constant across the glycosidic linkage is very small [71] and difficult to detect. Interglycosidic NOEs are therefore essential for establishing the sequence of monosaccharide units in oligo- and polysaccharides. However, because of spectral overlap between 3 and 4 ppm, it is often impossible to assign NOE crosspeaks between the anomeric and aglyconic protons unambiguously. Three signals were observed in the 1D NOESY spectrum of 1 (fig. 2(b)) after selective excitation of the H-1b proton. This is typical for NOESY spectra of  $\beta$ -D-hexopyranose residues, where two intraring protons, H-3 and H-5, are observed while the third belongs to the aglyconic proton of a neighbouring residue. In this particular molecule, the H-3b proton was identified on the basis of a TOCSY transfer from H-1b, however, assignment of the two other signals needed further attention. In a 1D NOESY-TOCSY experiment, the initial NOESY step from proton H-1b followed by a short TOCSY transfer from a proton at 3.8 ppm yielded resonances of H-1a, H-2a, H-4a and H-5a (fig. 2(c)) confirming that the signal at 3.8 belongs to proton H-3a.

The other signal seen in the 1D NOESY spectrum at 3.7 ppm must therefore belong to the H-5b. Indeed, when a selective TOCSY transfer in another 1D NOESY-TOCSY experiment was started from this proton only overlapping signals of H-6b and H-6b' near to that of H-5b were observed (fig. 2(d)). No transfer to H-4 occurred, because of the very small coupling constant  $J_{4,5}$  (<1 Hz) of this galactopyranose residue. The spectrum in fig. 2(d) illustrates the other possible application for the 1D NOESY-TOCSY technique – overcoming the bottleneck of the TOCSY transfer by a NOESY step. Because of very small  $J_{4,5}$  (<1 Hz) the transfer of magnetization from H-1b in a TOCSY experiment stopped at H-4b. The H-5b could, however, be reached by using its NOE contact with the anomeric proton of the same residue as seen in the 1D NOESY spectrum in fig. 1(b). A short TOCSY transfer ( $\approx$  20 ms) then directed the magnetization from H-5b to H-6b and H-6b'. It would have been otherwise difficult to obtain all these assignments, but using a simple 1D technique the task was completed quickly and unambiguously.

By reversing the order of polarization transfer steps, NOE contacts of signals hidden under the bulk of other resonances can be established in a 1D TOCSY-NOESY [39] experiment (fig. 1(d)). The necessary requirement is that an efficient TOCSY transfer can be made to a particular proton from

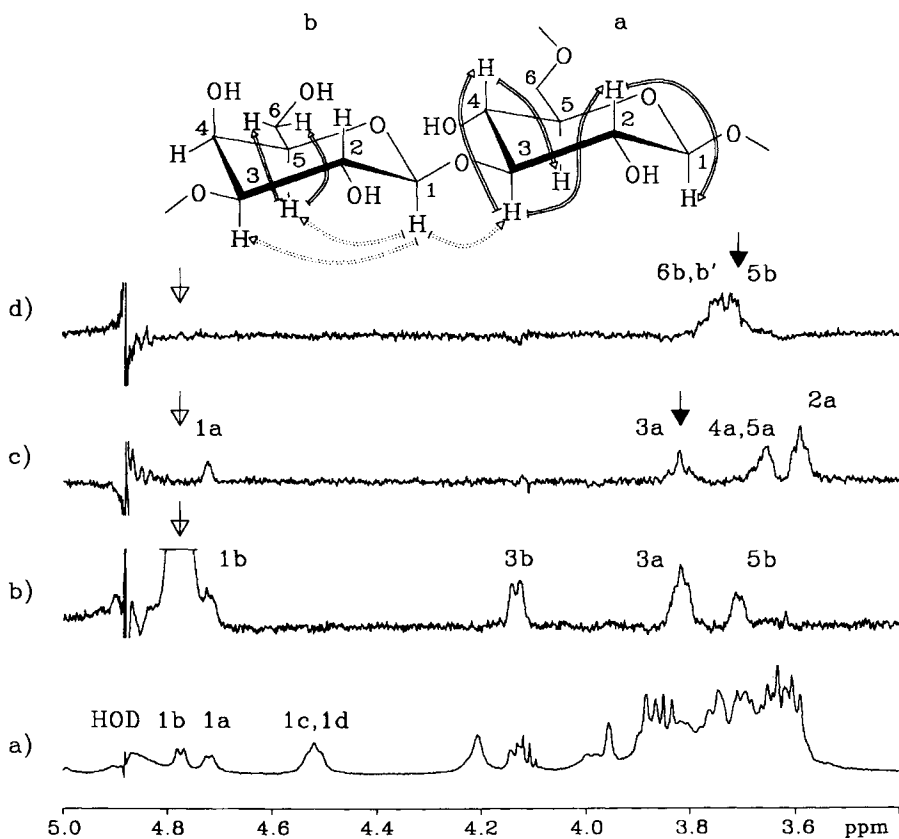


Fig. 2. (a) Partial  $^1\text{H}$  600 MHz spectrum (8 scans) of the type VI group B *Streptococcus* capsular polysaccharide (**1**) acquired on 5 mg of the sample at  $15^\circ\text{C}$  using water presaturation.

(b) 1D NOESY spectrum with selective excitation of H-1b. The duration of the half-Gaussian pulse was 50 ms,  $\tau_{\text{NOE}} = 50$  ms, 256 scans were acquired using the pulse sequence of fig. 1(a).

(c) 1D-NOESY-TOCSY with a selective NOESY transfer from H-1b and a selective TOCSY transfer from H-3a. Both half-Gaussian pulses were of 50 ms,  $\tau_{\text{NOE}} = 50$  ms, TOCSY mixing time was 26 ms including two trim pulses of 2.5 ms each. 4096 scans were acquired using the pulse sequence of fig. 1(c).

(d) The same as (c) except that the second selective pulse was applied at the frequency of H-5b.

Polarization transfer pathways for spectra (c) and (d) are depicted on a partial structure of **1** shown in the inset. Solid and dotted lines represent TOCSY and NOESY transfers, respectively. (Reprinted with adaptation with permission from ref. [39]. Copyright 1994 Academic Press, Inc.)

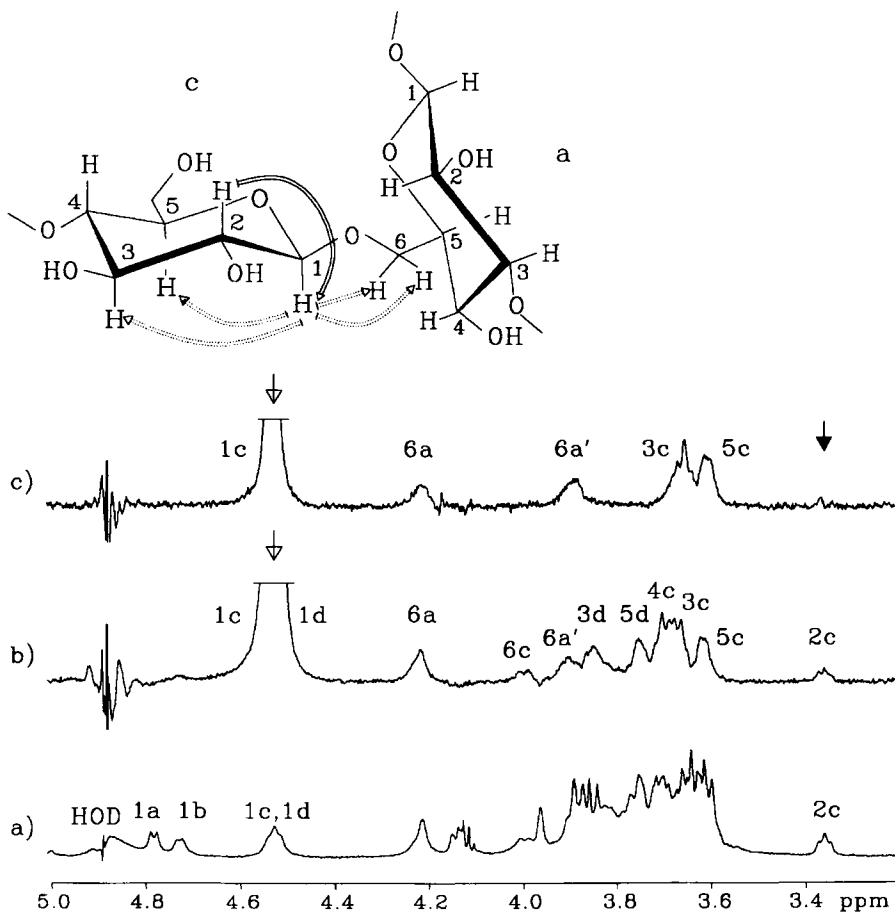


Fig. 3. (a) See the legend to fig. 2(a).

(b) 1D NOESY spectrum (pulse sequence of fig. 1(a)) with selective excitation of 1c and 1d protons. Parameters were the same as given in the legend to fig. 2(b), except that the number of scans was 1024.

(c) 1D TOCSY-NOESY spectrum with a selective TOCSY transfer from H-2c and a selective NOESY transfer from H-1c acquired using the pulse sequence of fig. 1(d). Parameters were the same as given in the legend to fig. 2(c), except the number of scans was 8192. The DANTE-Z pulse of 16 ms was used. Polarization transfer pathways for the spectrum (c) are depicted on a partial structure of **1** shown in the inset. Solid and dotted lines represent TOCSY and NOESY transfers, respectively. (Reprinted with adaptation with permission from ref. [39]. Copyright 1994 Academic Press, Inc.)

a proton of the same spin system whose resonance is resolved sufficiently to allow for a selective excitation.

In a 1D TOCSY-NOESY experiment [39], the proton magnetization is aligned along the spin-lock axis after the initial selective TOCSY step. The

subsequent nonselective pulse applied perpendicularly to the spin-lock axis brings the magnetization back to the  $z$  axis. Now the frequency of the carrier is changed and a selective  $180^\circ$  pulse applied on alternate scans. Once again there is no need to compensate for the change in the carrier frequency, since this occurred when the magnetization was aligned along the  $z$  axis. A simple rectangular selective inversion pulse produced in a DANTE-Z [44] manner was used. The components of this pulse were phased so that the overall effect was a  $180^\circ$ ,  $180^\circ$ ,  $0^\circ$ ,  $0^\circ$  selective pulse during the block of four scans. Alternatively, a selective  $180^\circ$  Gaussian pulse was applied on- and off-resonance on alternate pairs of scans to achieve the same effect. Both these methods yielded similar results.

The proposed 1D TOCSY-NOESY experiment is illustrated by the assignment of NOEs from anomeric protons H-1c and H-1d of the polysaccharide **1**. Because the resonances of H-1c and H-1d overlapped, this assignment was not possible from a 1D NOESY spectrum as shown in fig. 3(b). Although these protons differed in their chemical shifts, it was not possible to separate them by chemical-shift-selective filtration because of the very fast spin-spin relaxation of backbone protons (20–50 ms) in this polysaccharide. Instead, a 1D TOCSY-NOESY experiment was performed in which the initial TOCSY transfer from an isolated resonance of H-2c was followed by a selective NOESY transfer from H-1c. The 1D TOCSY-NOESY spectrum (fig. 3(c)) clearly separated NOE signals of the H-1c proton from those originating from the H-1d proton and established the linkage 1c  $\rightarrow$  6a.

This particular application was possible because of an isolated resonance of the H-2 proton. In a more typical situation, the TOCSY transfer would start on an anomeric resonance. After being directed to a proton thought to be involved in a glycosidic linkage the magnetization would then be subjected to the NOESY transfer. The presence or absence of transfer of magnetization to a different anomeric resonance would confirm or exclude the existence of a glycosidic linkage at this site.

### 3.2. 1D TOCSY-NOESY-TOCSY and 1D NOESY-TOCSY-NOESY

A more complicated situation occurs when it is not possible to excite selectively a proton which would be a good starting point for a 1D NOESY-TOCSY experiment. It might be possible, however, to build the magnetization of this proton via an initial TOCSY transfer. This leads to a 1D analog of 4D TOCSY-NOESY-TOCSY [39] (fig. 4(a)), which is formally obtained by replacing the final read pulse in the 1D TOCSY-NOESY experiment (fig. 1(d)) by an additional selective TOCSY step. Since all three building blocks of this sequence are linked together at a point when the magnetization is aligned along the  $z$  axis, no phase compensations for the frequency changes of the carrier are necessary. With this experimental scheme it is optional as to whether the NOESY step is performed in a selective or a

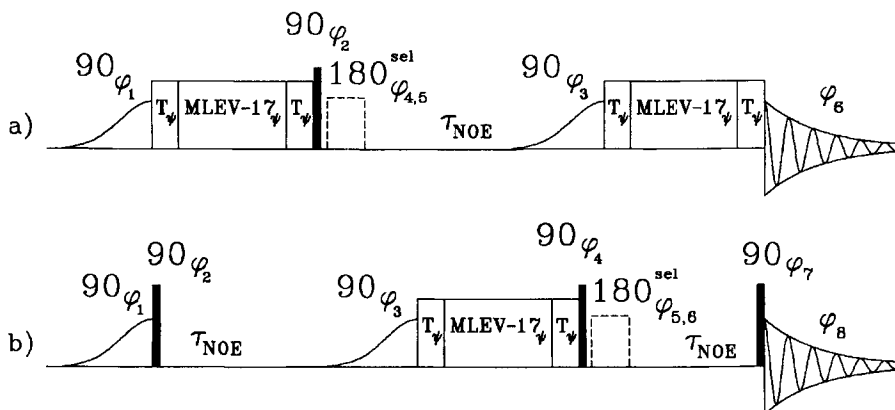


Fig. 4. Pulse sequences of 1D analogs of 4D experiments. The shaped  $90^\circ$  pulses were half-Gaussian. The  $180^\circ$  selective pulses were produced by a DANTE-Z pulse train.  $T_\psi$  denotes the trim pulse of phase  $\psi$ .  $\tau_{\text{NOE}}$  stands for a NOE-mixing time.

(a) 1D TOCSY-NOESY-TOCSY experiment. Phases were cycled as follows:  $\phi_1 = y, -y$ ;  $\phi_2 = 8y, 8(-y)$ ;  $\phi_3 = 2y, 2(-y)$ ;  $\phi_4 = 16y, 16(-y)$ ;  $\phi_5 = 2(4y, 4(-y)), 2(4(-y), 4y)$ ;  $\psi = 2(x, -x), 2(-x, x)$ . The receiver phase cycle,  $\phi_6$ , was:  $(-x, x, x, -x), 2(x, -x, -x, x), (-x, x, x, -x)$ . The DANTE-Z pulse can be replaced by a  $180^\circ(\phi_4)$  selective Gaussian pulse applied on- and off-resonance in blocks of four scans. When a nonselective NOESY transfer is used, the  $180^\circ$  selective pulse is omitted. All the phases are the same as given above except for the receiver cycle,  $\phi_6$ , which becomes:  $2(-x, x, x, -x), 2(x, -x, -x, x)$ .

(b) 1D NOESY-TOCSY-NOESY experiment. The following phase cycling was applied:  $\phi_1 = x, -x$ ;  $\phi_2 = 8x, 8(-x)$ ;  $\phi_3 = 2x, 2(-x)$ ;  $\phi_4 = x$ ;  $\phi_5 = x$ ;  $\phi_6 = 4x, 4(-x)$ ;  $\phi_7 = x$ ;  $\psi = 4y, 4(-y)$ ;  $\phi_8 = -x, 2x, -x, 2(x, -x, -x, x), (-x, 2x, -x)$ . On top of that, CYCLOPS was superimposed on the phase of the final read pulse ( $\phi_7$ ) and the receiver phase ( $\phi_8$ ) by applying  $90^\circ$  incrementation every 16 scans. The DANTE-Z pulse can be replaced by a  $180^\circ(\phi_5)$  selective Gaussian pulse applied on- and off-resonance on consecutive blocks of four scans. When the second NOE step is applied in a nonselective manner, the  $180^\circ$  selective pulse is omitted and the receiver is cycled according to  $\phi_8 = 2(-x, x, x, -x), 2(x, -x, -x, x)$ .

nonselective manner. If the  $180^\circ$  selective pulse is omitted, all the magnetization created during the first selective TOCSY step is transferred further in a subsequent nonselective NOESY step. The proton magnetization of one of the protons, which was created during the NOE mixing period, is then further subjected to the final selective TOCSY transfer. This introduces a certain ambiguity into the polarization transfer pathway of observed signals. However, in most circumstances it does not represent a problem, since the last TOCSY step is selective. To its advantage, such a sequence which contains one less selective pulse is simpler and shorter than a fully selective experiment.

The 1D TOCSY-NOESY-TOCSY experiment is illustrated on the assignment of proton resonances of the terminal sialic acid residue in the side chain of the capsular polysaccharide **1**. Because the coupling constant  $J_{6e,7e}$  is very small, the transfer of magnetization in a 1D TOCSY experiment stops at H-6e and a NOESY step is needed for magnetization to be transferred to H-7e. This is possible because of a gauche orientation between H-6e and H-7e. Resonances of H-8e and H-9e,9e' could then be reached via a consecutive TOCSY transfer. The experiment starts with a TOCSY transfer from the H-3e<sub>ax</sub> (fig. 5(b)). In the 1D TOCSY-NOESY spectrum, obtained using the pulse sequence depicted in fig. 1(d) without the selective 180° pulse, two NOE signals were located (fig. 5(c)). The signal of H-3b, which belongs to the adjacent galactopyranosyl residue, appeared due to the NOE contact between the H-3<sub>ax</sub>e and H-3b and is indicative of the 2e → 3b linkage. The other, more important signal of H-7e, stems from the intraresidue NOE contact between H-6e and H-7e. Signals of these two protons overlap partially. In the final 1D TOCSY-NOESY-TOCSY experiment, performed using the pulse sequence of fig. 4(a) without the selective 180° pulse, the second 90° half-Gaussian pulse was applied at the H-7e frequency. The magnetization was transferred from H-7e to H-8e, H-9e,9e'. Because of overlap between H-6e and H-7e resonances, a partial TOCSY transfer from H-6e caused signals of H-3<sub>ax</sub>e, 3<sub>eq</sub>e, 4e, 5e, and 6e also to appear in the spectrum.

The NOESY and TOCSY polarization transfers can also be arranged so that two NOESY steps are interrupted by one TOCSY transfer. This is useful for situations when a proton which is intended as a starting point for a 1D TOCSY-NOESY experiment cannot be selectively excited, nevertheless it has a NOE contact to an isolated proton. The 1D NOESY-TOCSY-NOESY sequence [72] (fig. 4(b)) is obtained by appending another NOESY step to the 1D NOESY-TOCSY pulse sequence of fig. 1(c). The last NOESY step can be either selective or nonselective depending whether a selective 180° pulse is applied after the nonselective 90° pulse at the end of the TOCSY transfer.

The 1D NOESY-TOCSY-NOESY experiment has been applied to locate a particular phosphorylation site in a complex oligosaccharide **2** [73]. The oligosaccharide, which was phosphorylated on several sites, consisted of 9 glycosyl residues and two amide-linked 3-hydroxytetradecanoic acids. It has been presumed that one of the phosphorylation sites is located on the side chain of the central  $\alpha$ -LD-heptose (residue a). Although the anomeric proton resonance of this heptose (H-1a) was isolated sufficiently for a selective excitation, it did not make a good starting point for a TOCSY transfer which stopped at H-2a. This was because of small coupling constant,  $J_{1,2}$ , and fast spin-spin relaxation caused by the presence of fatty acid chains in the molecule. Advantage was therefore taken from the presence of a

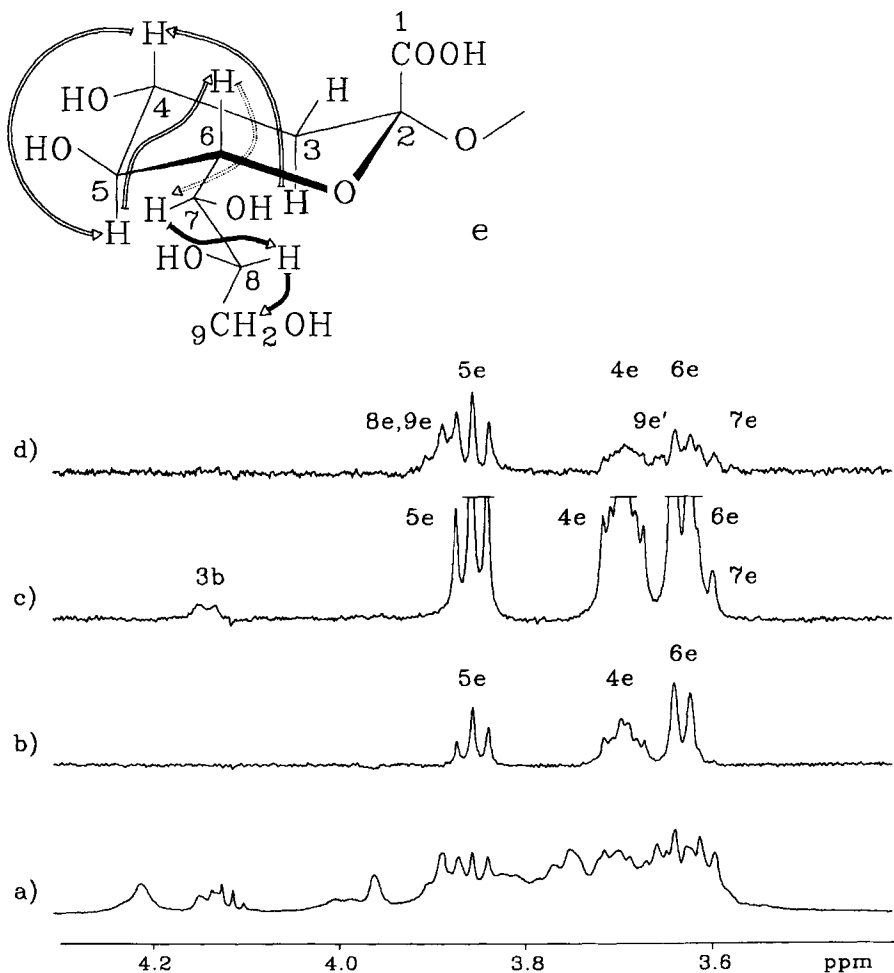


Fig. 5. (a) See the legend to the fig. 2(a).

(b)  $z$ -filtered 1D TOCSY (80) spectrum using selective excitation of  $H-3_{axa}$  by a 50 ms half-Gaussian pulse. A 82 ms spin-lock time, including two trim pulses each of 2.5 ms, was applied. In each of the 26 increments of the  $z$ -filter 80 scans were accumulated. Duration of one increment was 0.5 ms.

(c) 1D TOCSY-NOESY spectrum with selective TOCSY transfer from  $H-3_{axe}$  and a non-selective NOESY step (pulse sequence of fig. 1(d) without the selective  $180^\circ$  pulse). Duration of the TOCSY and NOESY mixing times were 82 and 200 ms, respectively. Number of scans was 16384.

(d) 1D TOCSY-NOESY-TOCSY spectrum with selective TOCSY transfer from  $H-3_{axe}$ , non-selective NOESY step and a final selective TOCSY transfer from  $H-7e$  acquired using the pulse sequence of fig. 5(a). Duration of the first TOCSY, NOESY and the second TOCSY step was 82, 200 and 48 ms, respectively. 50 ms half-Gaussian pulses were used and 24576 scans were acquired. Polarization transfer pathways for the spectrum (d) are depicted on a partial structure of **1** shown in the inset. Solid, dotted and filled lines represent the first TOCSY, the NOESY and the second TOCSY transfers, respectively. (Reprinted with adaptation with permission from ref. [39]. Copyright 1994 Academic Press, Inc.)

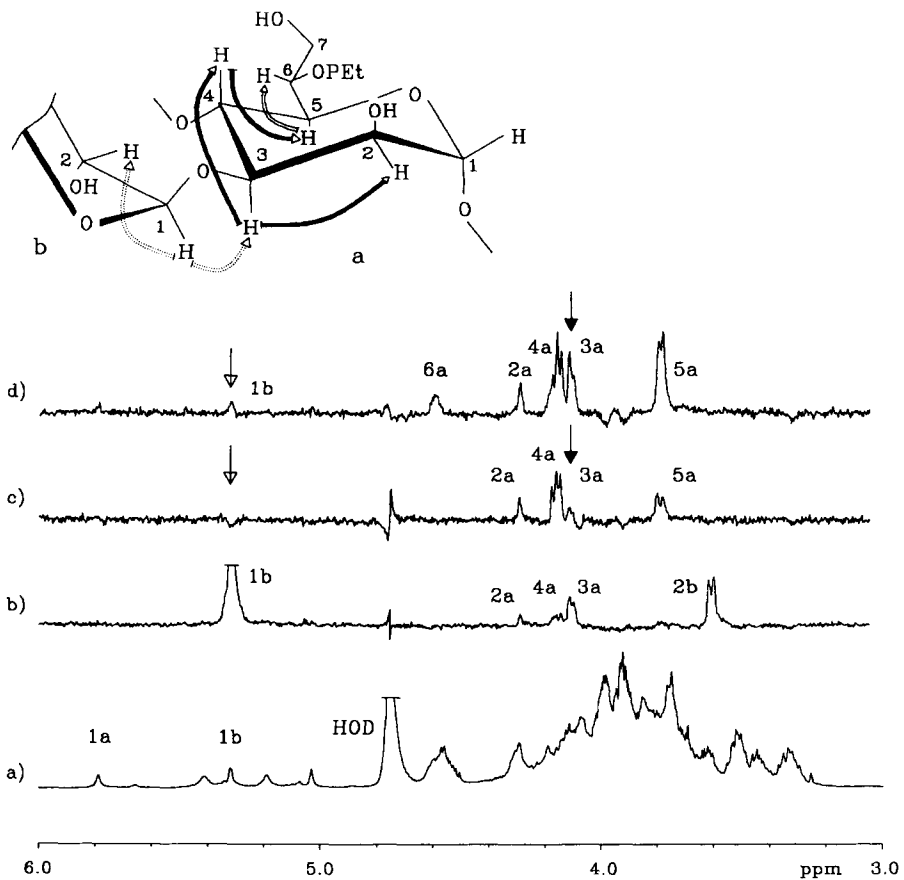


Fig. 6. (a) Partial 600 MHz  $^1\text{H}$  spectrum of an oligosaccharide **2**.

(b) A 32 scans 1D NOESY spectrum (pulse sequence of fig. 1(a)) with selective excitation of H-1b via 47 ms half-Gaussian pulse. The NOE mixing time was 250 ms.

(c) 1D NOESY-TOCSY spectrum (pulse sequence of fig. 1(c)) with an initial NOESY step as in (b) and a 95 ms TOCSY transfer preceded by a 47 ms half-Gaussian pulse applied at H-3. 5000 scans were accumulated.

(d) 1D NOESY-TOCSY spectrum (pulse sequence of fig. 4(b)). Nonselective transfer was applied for the second NOESY step (200 ms mixing time). The TOCSY mixing time was reduced to 48 ms in order to enhance the transfer to the H-5b proton compared to the (b) spectrum. Water presaturation was applied during the relaxation delay and the second NOE mixing time. The polarization transfer pathways are depicted on the partial structure of **2** given in the inset. Dotted, filled and solid lines are used for the first NOESY, TOCSY and the second NOESY transfer steps, respectively.

neighbouring  $\alpha$ -D-glucopyranose (residue b) known to be attached at C-3a. A selective NOE transfer from H-1b (pulse sequence of fig. 1(a)) yielded, besides H-2b, signals of H-2a,3a, and 4a of the heptose (fig. 6(b)). Higher order effects between the H-3a and H-4a caused build up of the magnetization of proton H-4a. Although the glycosidic linkage is located at C-3a, the NOE was observed also on H-2a which is due to its equatorial position. In a subsequent 1D NOESY-TOCSY experiment (pulse sequence of fig. 1(c)) a selective NOESY transfer from H-1b followed by a selective TOCSY from H-3a disclosed a new signal at 3.80 ppm assigned to H-5a (fig. 6(c)). The transfer of magnetization did not propagate to H-6a because of a small coupling constant  $J_{5a,6a}$ . In the final 1D NOESY-TOCSY-NOESY experiment, the TOCSY step was optimized for the H-3–H-5 transfer. The second NOESY transfer yielded a new signal at 4.6 ppm which appeared mainly due to the dipole–dipole interaction with H-5a. The signal at 4.6 ppm, which is according to a  $^{31}\text{P}$ – $^1\text{H}$  correlation spectrum coupled to phosphorus, was assigned to proton H-6. The last NOESY step of this 1D NOESY-TOCSY-NOESY experiment was nonselective because it was felt that the amount of sample (ca 2 mg) has reached the lower limit and the addition of another selective pulse might be critical. In general, this practice is not recommended and the last step of a multiple polarization transfer 1D experiment should be selective. The results provided by this series of selective experiments were crucial for locating the phosphorylation site in this residue.

### 3.3. 1D ROESY-TOCSY and 1D TOCSY-ROESY

For situations where the product of the resonance frequency and the overall correlation time of a molecule approaches unity NOE effects are close to zero. Under these circumstances the proximity of spins in space can still be inspected in the rotating frame by the ROESY experiment. This is usually the case for small oligosaccharides and oligopeptides at higher magnetic fields.

In a similar manner to the concatenation of NOESY and TOCSY transfers, it is possible to combine ROESY and TOCSY elements yielding 1D ROESY-TOCSY and 1D TOCSY-ROESY experiments [68] (fig. 7). Since the ROESY transfer is likely to be applied to smaller molecules with longer relaxation times,  $270^\circ$  Gaussian pulses were used in combined experiments containing the ROESY transfer. The  $270^\circ$  Gaussian pulse has much better phase profile than the  $90^\circ$  half-Gaussian pulse. Consequently, purging of the dispersive component was not applied in these sequences. Nevertheless, if required, these pulses can be replaced by  $90^\circ$  half-Gaussian pulses in the TOCSY step and a  $90^\circ$  half-Gaussian followed by a purging pulse in the ROESY step [34].

In both 1D ROESY-TOCSY and 1D TOCSY-ROESY experiments [72] (figs 7(c), (d)) magnetization was stored along the  $z$  axis at the joining point

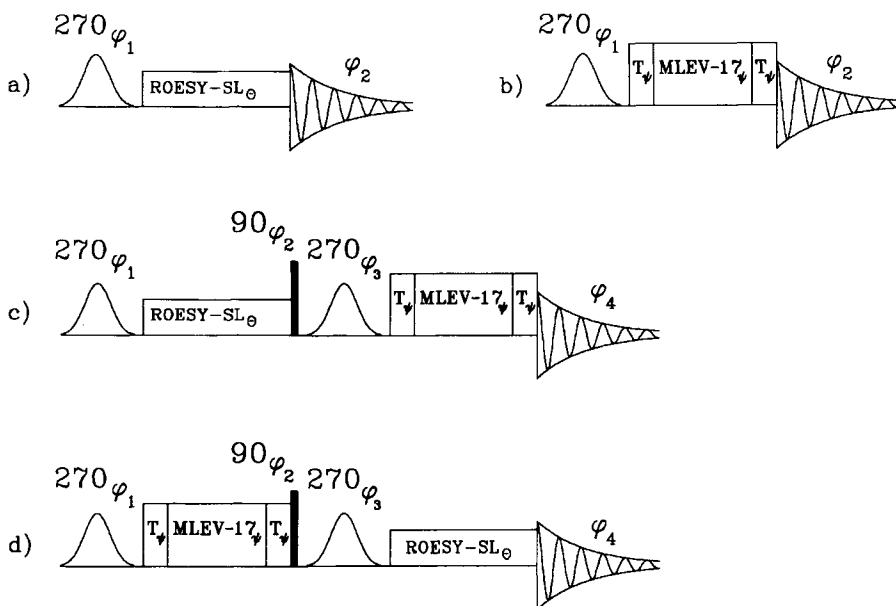


Fig. 7. Concatenation of ROESY and TOCSY polarization transfer steps.  $270^\circ$  Gaussian pulses were used in all sequences. Weak r.f. pulse ( $\gamma B_2/2\pi = 2.8$  kHz) applied off-resonance was used to generate a spin-lock field for the ROESY transfer. (a) 1D ROESY;  $\phi_1 = 2(y, -y)$ ;  $\theta = 2x, 2(-x)$ ;  $\phi_2 = 2(y, -y)$ . In addition all phases are shifted by  $90^\circ$  every 4 scans. (b) 1D TOCSY  $\phi_1 = y, -y$ ;  $\psi = 2x, 2(-x)$ ;  $\phi_2 = y, -y$ . (c) 1D ROESY-TOCSY and (d) 1D TOCSY-ROESY experiments. The following phase cycling was applied:  $\phi_1 = y, -y$ ;  $\phi_2 = 8y, 8(-y)$ ;  $\phi_3 = 2y, 2(-y)$ ;  $\theta = 16x, 16(-x)$ ;  $\psi = 2(x, -x), 2(-x, x)$ ;  $\phi_4 = 2(y, 2(-y), y), 2(-y, 2y, -y)$ .

of the two polarization transfer steps. This was achieved by a hard pulse applied perpendicular to the spin-lock axis. At this point the transmitter frequency was changed and the second selective pulse applied to a selected proton. A simple off-resonance low power pulse was used for the ROESY spin lock.

Both methods are illustrated on a model trisaccharide **3**, the partial structure of which is given in the inset of fig. 8. The intensity of ROEs of H-1b, as measured from the spectrum (fig. 8(b)) obtained by using the pulse sequence of fig. 7(a), was between 5–10%, which is considerably more than the intensity of NOEs in corresponding 1D NOESY spectra at 600 MHz. In-traring ROEs were observed to protons H-3b and H-5b<sub>ax</sub> including a three spin effect to H-5b<sub>eq</sub>. Small but noticeable TOCSY transfer occurred to protons H-2b and H-4b. ROE transfers across the glycosidic linkage were registered at H-4c and H-5c<sub>eq</sub>.

In the subsequent 1D ROESY-TOCSY experiment (pulse sequence of fig. 7(c)), a selective TOCSY transfer was applied from H-4c. During the

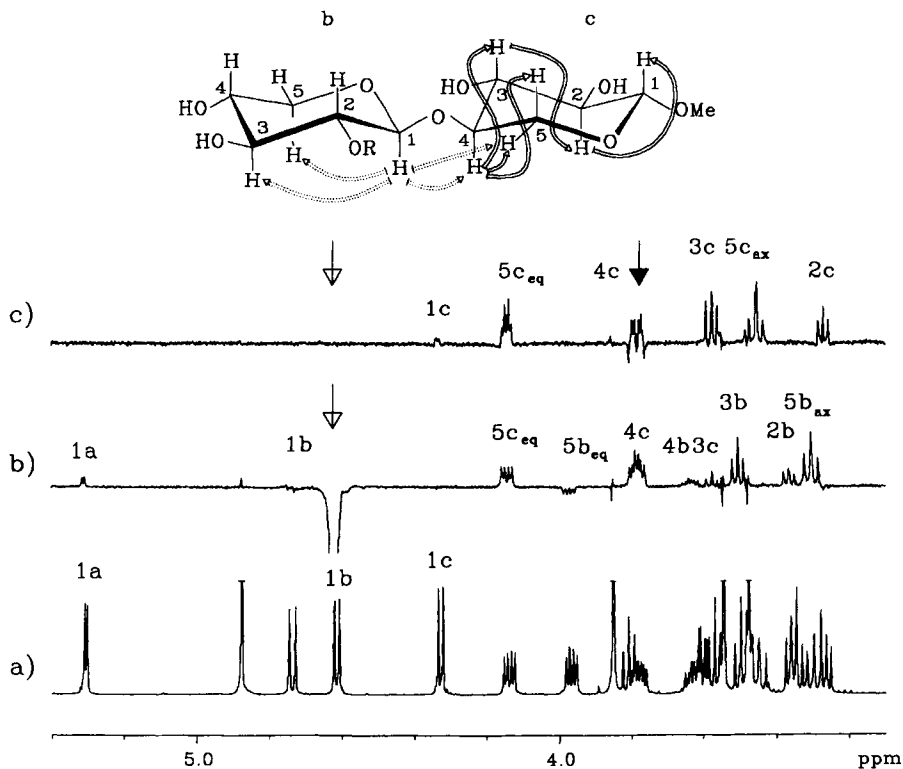


Fig. 8. 1D ROESY-TOCSY. (a)  $^1\text{H}$  spectrum of the oligosaccharide **3** (5 mg/0.5 ml  $\text{D}_2\text{O}$ ). (b) 1D ROESY spectrum of **3** acquired using the pulse sequence of fig. 7(a) with selective excitation of the H-1b proton. Duration of the  $270^\circ$  Gaussian pulse and the spin-lock pulse ( $\gamma B_2/\pi = 2.8$  kHz) was 49.2 ms and 0.5 s, respectively. The spin-lock pulse was applied 333.3 Hz downfield from the H-1b resonance. The time used for the frequency change was 3 ms. (c) 1D ROESY-TOCSY spectrum acquired using the pulse sequence of fig. 7(c) and the selective ROESY transfer from H-1b followed by a selective TOCSY transfer from H-4c. Parameters for the ROESY part were the same as in (b). A 49.2 ms Gaussian pulse was used at the beginning of the 29.07 ms TOCSY spin lock. 256 scans were accumulated. A partial structure of **3** is given in the inset. Solid and dotted lines represent TOCSY and ROESY transfers, respectively.

29 ms long spin-lock, the magnetization of H-4c which has been built up due to the ROE with H-1b, spread along the entire spin system of the ring c (fig. 8(c)).

The 1D TOCSY-ROESY experiment is illustrated on the same molecule using the pulse sequence of fig. 7(d). This time the magnetization of H-4c was generated during the initial selective TOCSY transfer from H-1c (fig. 9(b), pulse sequence of fig. 7(b)). In the subsequent 1D TOCSY-ROESY experiment, the ROE transfer from H-4c confirmed the expected

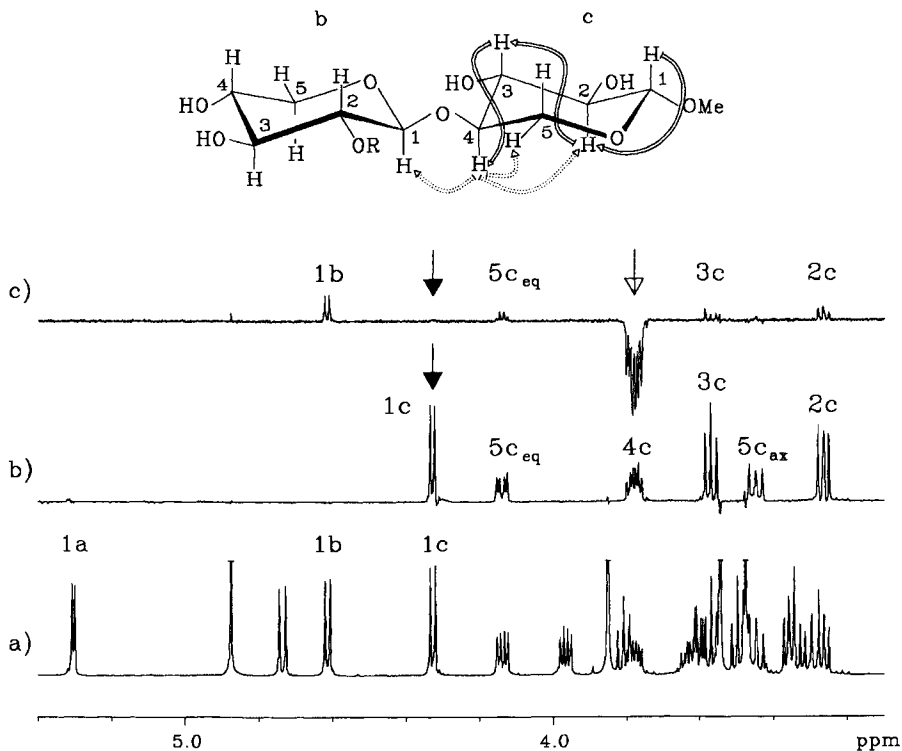


Fig. 9. 1D TOCSY-ROESY. (a)  $^1\text{H}$  spectrum of oligosaccharide **3** (5 mg/0.5 ml  $\text{D}_2\text{O}$ ). (b) 1D TOCSY spectrum acquired using the pulse sequence of fig. 7(b) and a selective excitation of H-1c by a 49.2 ms  $270^\circ$  Gaussian pulse. Duration of the spin lock was 132.7 ms including two 2.5 ms trim pulses. 32 scans were accumulated. (c) 1D TOCSY-ROESY spectrum acquired using the pulse sequence of fig. 7(d) with initial selective TOCSY transfer from H-1c and selective ROESY transfer from H-4c. Parameters for the TOCSY part were the same as in (b). A 49.2 ms  $270^\circ$  Gaussian pulse was used at the beginning of the ROESY transfer. A 500 ms ROESY spin-lock pulse ( $\gamma B_2/2\pi = 2.8$  kHz) was applied 1000 Hz downfield from the H-4c resonance. The time used for the frequency change was 3 ms. 128 scans were accumulated. A partial structure of **3** is given in the inset. Solid and dotted lines represent TOCSY and ROESY transfers, respectively.

spatial proximity of this proton to H-2c and H-5c<sub>eq</sub> within the same residue as well as that to the H-1b of the neighbouring ring (fig. 9(c)). A small amount of magnetization was transferred to the H-3c proton due to the TOCSY transfer.

#### 3.4. 1D TOCSY-TOCSY and 1D NOESY-NOESY

These two experiments are different from previously discussed techniques, since they are concatenations of two identical polarization transfer steps. There are various reasons why these experiments are beneficial to spec-

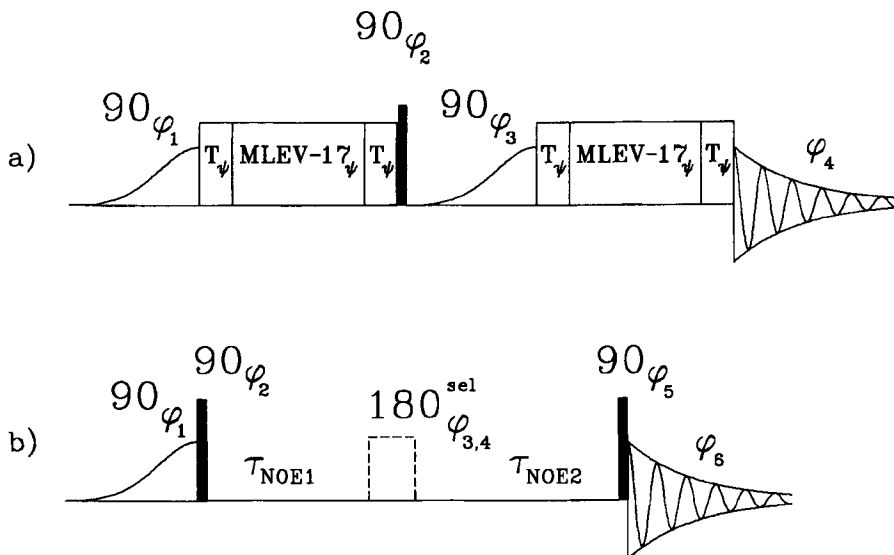


Fig. 10. Concatenation of two identical polarization steps.

(a) 1D TOCSY-TOCSY experiments with half-Gaussian pulses. The following phase cycling was applied:  $\phi_1 = y, -y$ ;  $\phi_2 = 8y, 8(-y)$ ;  $\phi_3 = 2y, 2(-y)$ ;  $\psi = 2(x, -x)$ ;  $\phi_4 = 2(y, 2(-y), y), 2(-y, 2y, -y)$ .

(b) 1D NOESY-NOESY experiments. The  $180^\circ$  selective pulse consists of a DANTE-Z pulse train  $(\Theta^\circ(\phi_3) - \Delta - \Theta^\circ(\phi_4) - \Delta)_n$  where  $2n\Theta = 180^\circ$ .  $\tau_{\text{NOE1}}$  and  $\tau_{\text{NOE2}}$  are the two NOE intervals. The following phase cycling was used:  $\phi_1 = x, -x$ ;  $\phi_2 = 16x, 16(-x)$ ;  $\phi_3 = x$ ;  $\phi_4 = 2x, 2(-x)$ ;  $\phi_5 = 4x, 4(-x), 4y, 4(-y)$ ; the receiver phase cycle  $\phi_6 = x, 2(-x), x, -x, 2x, -x, y, 2(-y), y, -y, 2y, -y$  was incremented by  $180^\circ$  every 16 scans. Alternatively, the DANTE-Z pulse can be replaced by a  $180^\circ \phi_3$  selective Gaussian pulse applied on- and off-resonance on consecutive blocks of two scans.

tral assignment and solving structural problems. The 1D TOCSY-TOCSY experiment is discussed first.

Let us consider a problem of selective excitation of two or three severely overlapping broad signals, a typical situation for large molecules, e.g., polysaccharides. Conventional means of selective excitations are bound to fail here. Both selective pulse and chemical-shift-selective filter, which would have a potential to resolve the degree of overlap, are too long compared to the life time of spins dictated by their short spin-spin relaxation times. On the other hand there is a possibility that some of the coupling partners of the overlapped protons will be reasonably separated and could be used as a convenient handle for disentangling the individual spin systems. It is therefore more appropriate to give up on attempts at selective excitation of one of the overlapping protons and to settle for a semiselective excitation of all of them for the first TOCSY step. When sufficiently isolated signals are discovered by varying the length of the mixing period,

the second TOCSY transfer is initiated from some of these protons during the second TOCSY step in a series of 1D TOCSY-TOCSY experiments.

Concatenation of two TOCSY steps in a 1D TOCSY-TOCSY experiment [72] is a straightforward matter (fig. 10(a)). After the initial TOCSY transfer, the magnetization is returned to the  $z$  axis by a nonselective  $90^\circ$  pulse applied perpendicularly to the spin-lock axis. The carrier frequency is changed and the second  $90^\circ$  selective pulse applied to a different proton followed by the second TOCSY spin-lock period.

The 1D TOCSY-TOCSY experiment is illustrated by the identification of two partial spin systems of a capsular polysaccharide **1**, starting with two overlapping protons H-1a and H-1b. A 20 ms half-Gaussian pulse was used in an exploratory 1D TOCSY experiment (pulse sequence of fig. 1(b)). It has been found (fig. 11(b)) that although the corresponding H-2 protons overlapped partially, H-3a and H-3b were separated completely. In the following 1D TOCSY-TOCSY experiments, using the pulse sequence of fig. 10(a), the second TOCSY transfer was initiated from protons H-3a and H-3b, respectively. The two spectra (fig. 11(c), (d)) clearly separate both partial spin system of **a** and **b** residues.

The 1D NOESY-NOESY experiment, which is an 1D analog of the 3D NOESY-NOESY technique [74], is able to differentiate between direct NOE signals and those which arise from spin diffusion. In fact, this technique can pin-point from which proton the spin diffusion arises. When spin-diffusion signals are identified and assigned, they are valuable supplement to regular NOESY peaks. Modification of the 1D NOESY experiment which leads to the 1D NOESY-NOESY technique [72] is shown in fig. 10(b). The mixing interval of a regular 1D NOESY experiment is divided into two parts separated by a  $180^\circ$  selective pulse applied on- and off-resonance on alternate two scans blocks. A proton which is suspected to be the source of spin diffusion is selectively inverted. The phase of receiver is modified accordingly and only NOEs from the selectively inverted proton, which have been built up during the second mixing period, are observed.

The use of 1D NOESY-NOESY experiment is illustrated with the O-chain polysaccharide (**4**) from *Proteus mirabilis* [75]. The 1D NOESY spectrum of **4**, acquired using selective excitation of H-1d and a mixing time of 200 ms (fig. 12(c)), showed more signals than expected for the anomeric proton of a  $\beta$ -D-hexopyranose. The 1D NOESY spectrum recorded using a very short mixing time of 25 ms (fig. 12(b)) suggested that significant spin diffusion took place during the 200 ms mixing time of the previous experiment. Three signals suspected to arise from spin diffusion are shaded in the 200 ms mixing time NOESY spectrum. Most likely, they originate from the intense NOE signals seen in the spectrum recorded with the short mixing time. These signals have been identified as belonging to protons H-3b, H-2d and H-3d. Two 1D NOESY-NOESY spectra with the selective inversion

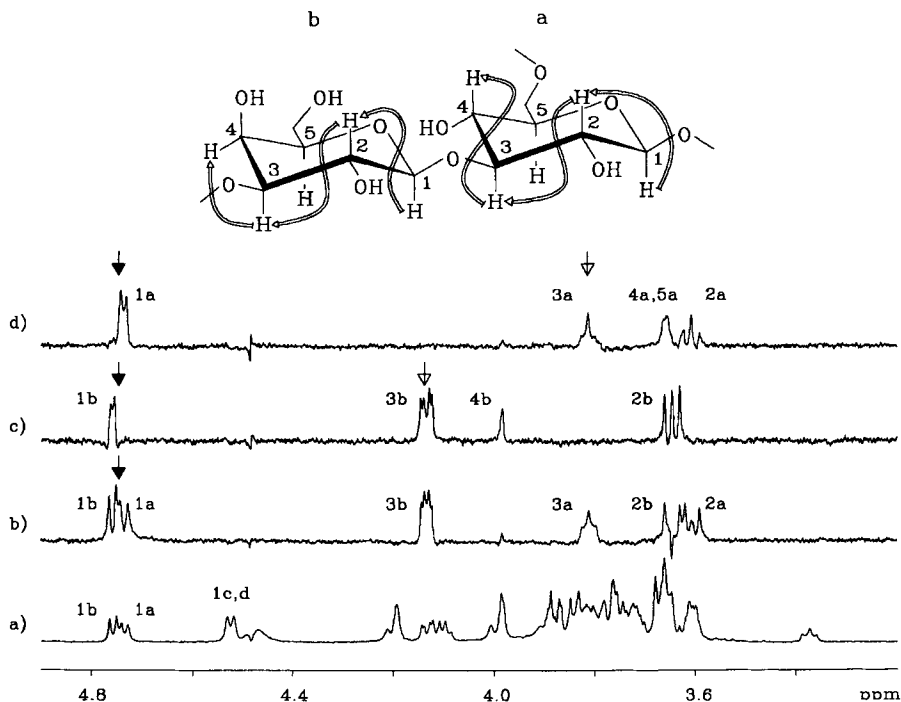


Fig. 11. 1D TOCSY-TOCSY experiment applied to polysaccharide **1**. A partial structure of **1** is given in the inset together with the polarization transfer pathways.

(a) Partial  $^1\text{H}$  600 MHz spectrum (8 scans) of **1** acquired on 5 mg of the sample at  $50^\circ\text{C}$  using water presaturation.

(b) 1D TOCSY spectrum acquired using the pulse sequence of fig. 1(b). A selective half-Gaussian pulse of 23.5 ms was applied midway between resonances 1a and 1b followed by a 54 ms spin-lock which includes two 2.5 ms trim pulses. 32 scans were collected.

(c), (d) 1D TOCSY-TOCSY spectra with the second polarization transfer from H-3b and H-3a, respectively, acquired using the pulse sequence of fig. 10(a). Duration of the second half-Gaussian pulse and the second spin-lock period were 23.5 and 45 ms, respectively. 256 and 1024 scans were accumulated in the (c) and the (d) spectrum, respectively. Faster relaxation in the **a** residues is the cause of the longer overall acquisition time in the (d) spectrum needed to achieve a comparable signal-to-noise ratio with the spectrum (c).

of H-2d/H-3d and H-3b protons, respectively, are shown in figs 12(d), (e). Indeed, all three signals suspected to originate from spin diffusion appeared in these spectra.

Overall, there is a wealth of spectral information in the spectra of fig. 12. Given the knowledge that the polysaccharide **4** is composed from  $\beta$ -D-galactopyranos residues only, several suggestions for its structure can be made by careful inspection of these spectra. Starting with a 25 ms 1D NOESY spectrum, because of their 1,3-diaxial arrangement with respect to the selectively excited proton H-1d, two of the signals belong to protons

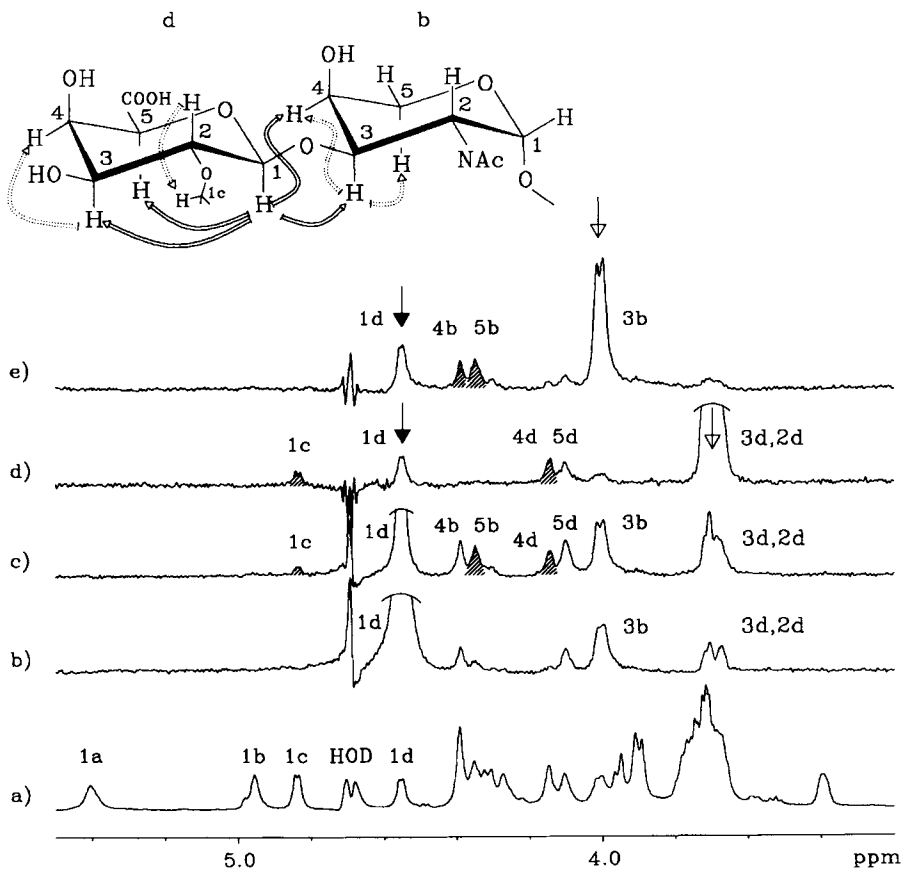


Fig. 12. Spin diffusion in 1D NOESY spectra of the polysaccharide **4**.

(a) Partial  $^1\text{H}$  spectrum of **4** (10 mg/0.5 ml  $\text{D}_2\text{O}$ ) acquired using 8 scans.

1D NOESY spectra (b) and (c) were acquired using the pulse sequence of fig. 1(a). A 59.2 ms half-Gaussian pulse was applied to proton H-1d. Mixing time was 25 ms in (b) and 200 ms in (c). Water presaturation was applied during the relaxation delay and the NOE mixing time.

1D NOESY-NOESY spectra (d) and (e) were acquired using the pulse sequence of fig. 10(b). A 59.2 ms half-Gaussian pulse was applied to H-1d in both experiments. H-2d/H-3d and H-3b were inverted by a 10 and 15 ms rectangular DANTE-Z pulse at the beginning of the second NOE period in (d) and (e), respectively. Duration of the first and second mixing period was 100 and 50 ms in both experiments. 512 scans were accumulated and the water saturation was applied during the relaxation delay and the second NOE mixing time. Signals which appeared due to the spin diffusion are shaded. A partial structure of **4** is given in the inset. Solid lines show the transfer of magnetization due to direct NOEs from H-1d. The dotted lines mark the origin of the spin diffusion signals.

of the **d** residue (H-3d, H-5d). The two other signals are most likely from the neighbouring residue. A signal at 3.70 ppm, was identified as that of the H-3d based on the 1D TOCSY transfer from proton H-1d. The same experiment revealed that H-2d and H-3d form a high order spin system and therefore the magnetization of the H-2d was also created in the previous NOESY experiment. The other intense signal at 4.00 ppm was assigned on the basis of a 1D TOCSY transfer from H-1b to proton H-3b. One of the less intense signals in the 25 ms NOESY spectrum is therefore most likely that of H-4b. It is well documented that the equatorial protons in the vicinity of the glycosidic linkage give NOE signals with the anomeric protons of the neighbouring unit. At this point it was, however, not clear which signal of the two low field resonances (4.4 and 4.07 ppm) in fig. 12(b) belongs to H-4b and which to H-5d. Neither was the origin and assignment of the spin diffusion signals in the 200 ms 1D NOESY spectrum apparent.

1D NOESY-NOESY spectrum acquired by selective inversion of the H-2d/H-3d protons (fig. 12(d)) showed expected 1,3-diaxial NOEs to H-1d and to the signal at 4.07 ppm seen also in the 25 ms NOE spectrum. This must therefore be the H-5d proton. The spin-diffusion signal at 4.14 ppm is that of the H-4d proton, since H-3d and H-4d are in the axial-equatorial relationship. The presence of a small spin-diffusion signal of H-1c in this spectrum suggested that the **c** and **d** rings are linked at 3d or 2d positions. The higher order effects are the source of this ambiguity. It has been established by other experiments, that the latter is the case. In the 1D NOESY-NOESY spectrum obtained by selective inversion of H-3b (fig. 12(e)) two more signals were observed besides that for the H-1d. The signal of H-4b appeared due to the axial-equatorial position with H-3b, and the signal of H-5b due to its 1,3-diaxial arrangement with H-3b. The assignment of these signals was based on appearance of H-4b in the 25 ms NOESY spectrum. The intensity of H-4b in the 200 ms 1D NOESY spectrum is a sum of the direct NOE transfer from H-1d and the spin diffusion from H-3b. Since the **b** residue is an  $\alpha$ -D-galactopyranose, there is no NOE to the H-1b proton in fig. 12(e).

As illustrated on this example, interpretation of NOESY spectra of polysaccharides might be complicated by the presence of spin-diffusion and higher order effects. 1D NOESY-NOESY experiment can provide some assistance in identification and assignment of spin-diffusion signals and thus prolong networks of spins experiencing NOE contacts beyond immediate neighbours normally detected in NOESY experiments.

### 3.5. Chemical-shift-selective filters in multiple polarization transfer experiments

As an alternative to selective pulses, chemical-shift-selective filters (CSSF) were successfully used in 1D COSY, 1D RELAY and 1D NOESY experiments when signals partially overlapping, but different in their chemical

shifts, were encountered [48–50]. Nevertheless, these techniques fail for completely degenerate signals. Under these circumstances, just as in the 1D TOCSY-TOCSY experiment, the signal selection can be achieved one or two steps further along the chain of  $J$ -coupled spins. In these experiments CSSFs can be used for the second selection step instead of a selective pulse. Since the CSSFs operate in the  $xy$  plane, and therefore are accompanied by evolution of  $J$ -couplings, it is advantageous to combine them with a polarization transfer mechanism operating via antiphase magnetization. Such experiments contain evolution intervals separated by polarization transfer pulses. Conveniently, CSSFs can be incorporated into one of these intervals.

The pulse sequences would typically start with a partially selective COSY transfer from all overlapping protons (e.g., anomeric, H-1) to the neighbouring (H-2) protons. If the chemical shift difference between H-2 protons is sufficient (approx.  $> 5$  Hz) the transverse magnetization is filtered through this spectral parameter prior to the next event in the sequence. The exact resonance frequencies of H-2 protons, which need to be known prior to the setting of the experiment are obtained in a preliminary 1D COSY experiment. In order to enable a CSSF, the nonselective COSY pulse must be applied at the frequency of one of the H-2 protons. The necessary phase relationship between the selective and nonselective COSY pulses is maintained by shifting the phase of a soft pulse by  $-2\pi(\nu_0 - \nu_2)\tau_0$ , where  $\nu_0$  and  $\nu_2$  are the frequencies of the soft and hard pulse, respectively, and  $\tau_0$  is the separation between these pulses in seconds. The filtration itself is achieved by a gradual displacement of a  $180^\circ$   $^1\text{H}$  pulse from the middle of a successive delay, which according to the need of a particular experiment, is optimized to yield maximum anti- or in-phase magnetization of the H-2 protons. After the filtration an appropriate polarization transfer mechanism is employed yielding experiments such as 1D COSY-RELAY, COSY-TOCSY or COSY-NOESY.

### 3.5.1. 1D COSY-RELAY and 1D COSY-TOCSY

In a 1D COSY-RELAY experiment [38] (fig. 13(a)) a multistep relay transfer is applied after the filtration. If the filtration is performed on the H-2 proton, the CSSF is incorporated into the first spin-echo. If there is not sufficient chemical shift separation between H-2 protons, the filter is shifted to the second spin-echo. The method is illustrated for the separation of the spin systems of two terminal  $\beta$ -glucopyranose residues of a modified LPS (5) containing a total of nine saccharide units [76]. The anomeric proton resonances of the two  $\beta$ -glycopyranoses overlapped almost completely, with a chemical shift difference of only 1.9 Hz, while the corresponding H-2 resonances were separated by 55.0 Hz. The length of the filtration interval,  $\tau_1$ , was adjusted to yield a maximum antiphase magnetization of H-2 pro-

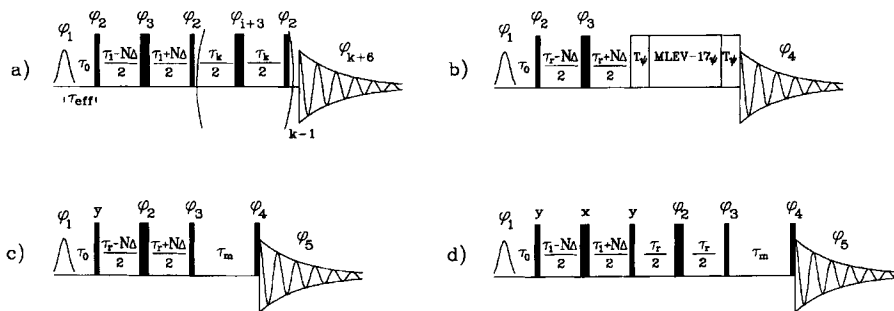


Fig. 13. Pulse sequences of combined NMR experiments which use chemical-shift-selective filtration for the second selective step. Thin bars represent  $90^\circ$  pulses, and thick bars  $180^\circ$  pulses. In all sequences a  $90^\circ$  Gaussian pulse of a duration  $\tau_{\text{sel}}$  was used for the initial selection of the magnetization.  $\tau_{\text{eff}} = \tau_{\text{sel}}/2 + \tau_0$ , for a doublet  $\tau_{\text{eff}} = 1/2J_{\text{HH}}$ ,  $k$  marks the number of relay steps,  $i = 1, \dots, k-1$ ,  $\tau_k$  intervals are optimized in order to yield a maximum antiphase magnetization for individual polarization transfer steps,  $\Delta$  is an increment of the CSSF and  $N$  goes from 0 to  $n$ ,  $n$  being the number of increments of the filter.  $\tau_r$  is optimized in order to refocus the magnetization prior to the TOCSY or NOESY steps,  $\tau_m$  is the NOE mixing interval. The  $\phi_1$  phase programmes given below must be corrected for the frequency change that might occur between the soft and the hard COSY pulses.

(a) 1D COSY-RELAY. The following phase programmes have been used:  $\phi_1 = 2(x, -x), 2(y, -y)$ ;  $\phi_2 = 4y, 4(-x)$ ;  $\phi_3 = 2x, 2(-x), 2y, 2(-y)$ ;  $\phi_4 = x$ ;  $\phi_5 = 8x, 8y$ ;  $\phi_6 = x$ ;  $\phi_7 = 2(y, -y), 2(-x, x)$ ;  $\phi_8 = 2(y, -y), 2(x, -x)$ ;  $\phi_9 = 2(y, -y), 2(-x, x), 2(-y, y), 2(x, -x)$ ;  $\phi_{10} = 2(y, -y), 2(x, -x), 2(-y, y), 2(-x, x)$ .

(b) 1D COSY-TOCSY;  $T_\psi$  denotes trim pulses of phase  $\psi$ . The following phases have been used:  $\phi_1 = 4(x, -x), 4(-x, x)$ ;  $\phi_2 = 16y$ ;  $\phi_3 = 8x, 8(-x)$ ;  $\psi = 2(y, -y), 2(-y, y), 2(y, -y), 2(-y, y)$ ;  $\phi_4 = 4(-x, x), 4(x, -x)$ . In addition, all the phases can be shifted by  $90^\circ$  making a 32 item phase cycling.

(c) 1D COSY-NOESY and (d) RELAY-NOESY with a CSSF on H-2s and back transfer to H-1 protons. The following phases have been used in (c) and (d) pulse sequences:  $\phi_1 = x, -x$ ;  $\phi_2 = 16x, 16(-x), 16y, 16(-y)$ ;  $\phi_3 = 8x, 8(-x)$ ;  $\phi_4 = 2x, 2(-x), 2y, 2(-y)$ ;  $\phi_5 = 2(x, -x, -x, x, y, -y, -y, y, -x, x, x, -x, -y, y, y, -y), 2(-x, x, x, -x, -y, y, -y, x, -x, -x, x, y, -y, -y, y)$ . (Reprinted with adaptation with permission from ref. [38].

Copyright 1993 ESCOM Science Publisher B.V.)

tons with respect to H-3 protons. Because the transverse magnetization of only two H-2 resonances was created by the initial selective COSY step, it was not necessary to run a complete CSSF for each spin system separately. Instead, more effectively, only two spectra were acquired which differed by  $180^\circ$  in the phase of one of the spin systems involved. In the first experiment a  $180^\circ$   $^1\text{H}$  pulse was applied in the middle of the  $\tau_1$  interval and in the second this pulse was displaced by  $0.25/(\nu_2 - \nu_2')$  from the centre of  $\tau_1$ , yielding a  $180^\circ$  chemical shift evolution for H-2' at  $\nu_2'$  which was off the carrier frequency  $\nu_2$ . The sum and the difference of these two spectra leaves the resonances of both glucose units separated.

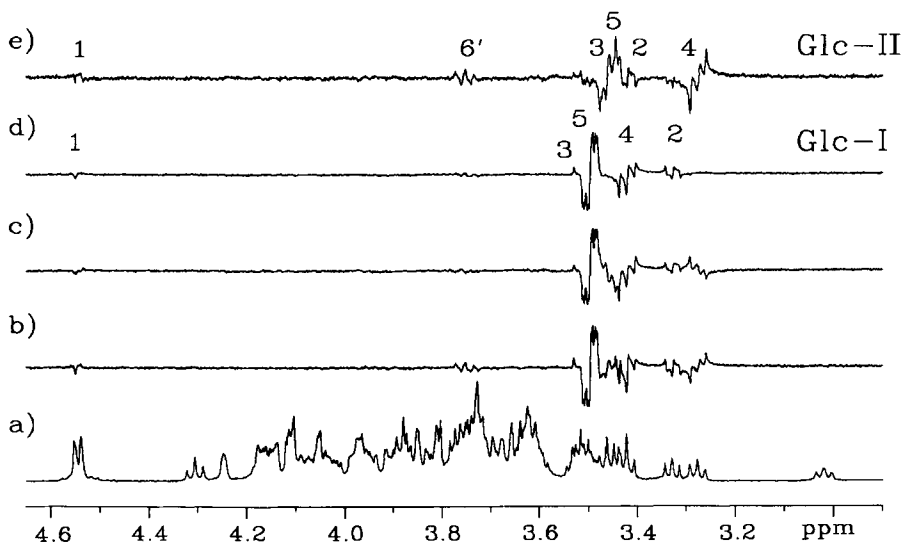


Fig. 14. 1D COSY-RELAY spectra of two terminal glucoses of oligosaccharide **5**. (a) Partial  $^1\text{H}$  spectrum of **5** at 600 MHz and 27°C. Spectra (b) and (c) were acquired using the pulse sequence in fig. 13(a) ( $k = 3$ ) with the initial polarization transfer from overlapping anomeric protons of terminal glucoses. Duration of the Gaussian pulse was 50 ms,  $\tau_0 = 39$  ms,  $\tau_1 = 50$  ms,  $\Delta = 9.09$  ms,  $\tau_2 = 50$  ms,  $\tau_3 = 40$  ms, number of scans was 64, relaxation delay and acquisition times were 2 and 1.4 s, respectively.  $N = 0$  for the first and  $N = 1$  for the second spectrum. (d) is the sum of (a) and (b), (e) is the difference between (a) and (b). (Reprinted with permission from ref. [38]. Copyright 1993 ESCOM Science Publisher B.V.)

One- to four-step 1D COSY-RELAY experiments were performed in order to obtain the assignment of resonances of both  $\beta$ -glucopyranose residues. The three-step RELAY spectra are shown before (figs 14(b), (c)) and after (figs 14(d), (e)) editing. Because of higher order effects associated with H-2 and H-3 resonances of Glc-II, the corresponding spectrum shows worse signal-to-noise ratio when compared to Glc-I subspectrum. A partial transfer of magnetization beyond H-5, to H-6', is observed in the Glc-II residue for the same reason.

Using the procedure described above, signals of two spin systems are accumulated during the entire experiment and the individual subspectra are obtained after editing of the original spectra. This provides a two-fold reduction in the total experimental time when compared to 1D experiments which employ two selective pulses for the selection of the magnetization transfer pathway.

Mixed phase lineshapes, typical for the multistep RELAY spectra, sometimes make the identification of individual signals difficult. At the same time, for extensive networks of coupled spins, the TOCSY transfer proved

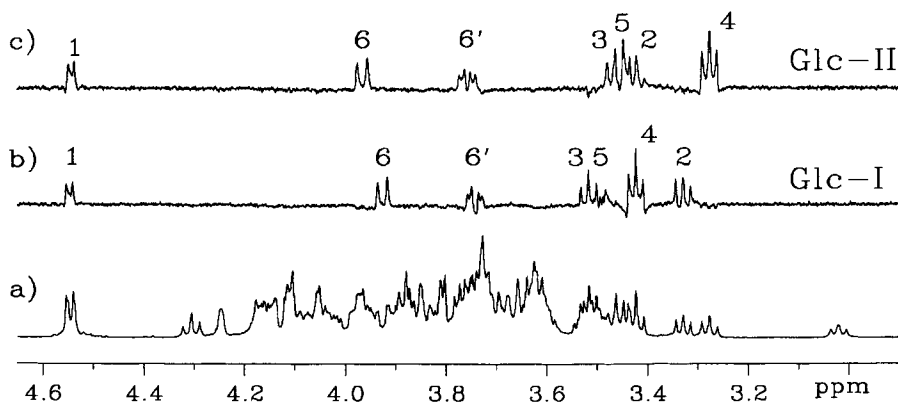


Fig. 15. 1D COSY-TOCSY spectra of the oligosaccharide **5** acquired using the pulse sequence of fig. 13(b) with the initial polarization transfer from overlapping anomeric protons of two terminal glucoses. (a) Partial  $^1\text{H}$  spectrum of **1** at 600 MHz after 8 scans. The summation (b) and subtraction (c) of two 1D COSY-TOCSY spectra acquired using the following parameters for the original spectra (not shown):  $\tau_{\text{scf}} = 50$  ms,  $\tau_0 = 39$  ms,  $\tau_r = 28$  ms,  $\Delta = 9.09$  ms, 2.5 ms trim pulse and the total mixing time of 87 ms. The relaxation delay was 2 s and the acquisition time was 1.4 s.  $N = 0$  in the first and  $N = 1$  in the second experiment. Number of scans was 128 in both spectra. (Reprinted with adaptation with permission from ref. [38]. Copyright 1993 ESCOM Science Publisher B.V.)

to be more effective. For these reasons it might be beneficial to apply a TOCSY transfer instead of a RELAY after the initial COSY and CSSF steps. This modification is described next.

In the 1D COSY-TOCSY experiment [38] (fig. 13(b)) the length of the filter, being the  $\tau_r$  interval, was adjusted to give maximum in-phase magnetization for the H-2 protons. The same procedure for separation of two subspectra was followed as in the previous 1D COSY-RELAY experiment. The results after the summation and subtraction of the original spectra are shown in figs 15(b), (c). Because of an absence of the chemical shift terms in the isotropic mixing Hamiltonian of the TOCSY transfer, the same signal-to-noise ratio was observed in 1D COSY-TOCSY spectra of both Glc-I and Glc-II despite the higher order effects seen in the Glc-II subspectrum. The TOCSY mixing time was optimized to yield maximum magnetization of H-6 protons. A shorter overall time was needed to build up the signals of all spins when compared to the 1D COSY-RELAY experiment.

### 3.5.2. 1D COSY-NOESY and RELAY-NOESY

Replacement of the TOCSY transfer in a 1D COSY-TOCSY experiment by the NOESY step yields a 1D COSY-NOESY sequence [38] (fig. 13(c)). The experiment is illustrated by the determination of NOEs from the H-7 proton of a terminal 3,6-dideoxy-4-C-(1-hydroxyethyl)-D-xylohexose (**6**)

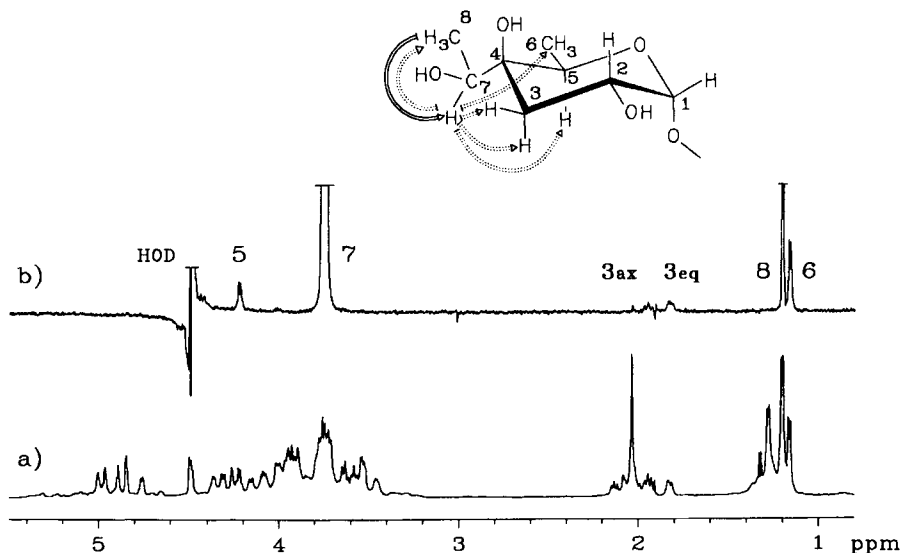


Fig. 16. 1D COSY-NOESY experiment on the polysaccharide **6** [77]. The structure of a terminal 3,6-dideoxy-4-C-(1-hydroxyethyl)-D-xylohexose is shown in the inset. The COSY transfer is depicted using the solid line, while a dotted line is used for the NOESY transfer. (a)  $^1\text{H}$  spectrum of **6** at 600 MHz and  $50^\circ\text{C}$ . (b) 1D COSY-NOESY spectrum acquired using the sequence of fig. 13(c) with the initial transfer of magnetization from H-8 and the following parameters:  $\tau_{\text{sel}} = 100$  ms,  $\tau_0 = 29$  ms,  $\tau_r = 32$  ms,  $\Delta = 0.5$  ms,  $N = 0, 1, \dots, 64$ ,  $\tau_m = 250$  ms. 32 scans were accumulated in each spectrum using an acquisition time of 1 s and a relaxation time of 4 s. Water suppression was applied in (a) but not in (b). (Reprinted with adaptation with permission from ref. [38]. Copyright 1993 ESCOM Science Publisher B.V.)

of a bacterial polysaccharide [77], which overlaps with other resonances in the  $^1\text{H}$  NMR spectrum. A 1D COSY-NOESY spectrum (fig. 16(b)) was therefore acquired with an initial COSY transfer from the  $\text{CH}_3$  (H-8) protons of the hydroxyethyl group. Since it overlapped with another  $\text{CH}_3$  resonances and was also close to additional  $\text{CH}_3$  signals, it was necessary to apply a complete CSSF at H-7, prior to the NOE mixing interval, by shifting the  $180^\circ$  pulse within a  $\tau_r$  interval in small steps instead of acquiring only two spectra as shown in previous examples. The length of the  $\tau_r$  interval was at the same time optimized to yield a maximum inphase magnetization of H-7. The resulting spectrum shows NOEs from H-7 to protons of two  $\text{CH}_3$  groups and several ring protons of the xylose.

An interesting possibility for assignment of NOEs from two or more overlapping anomeric protons is provided by a 1D RELAY-NOESY experiment [38] (fig. 13(d)). In this experiment the magnetization is transferred from H-1 protons to H-2 protons first and after a chemical-shift-selective

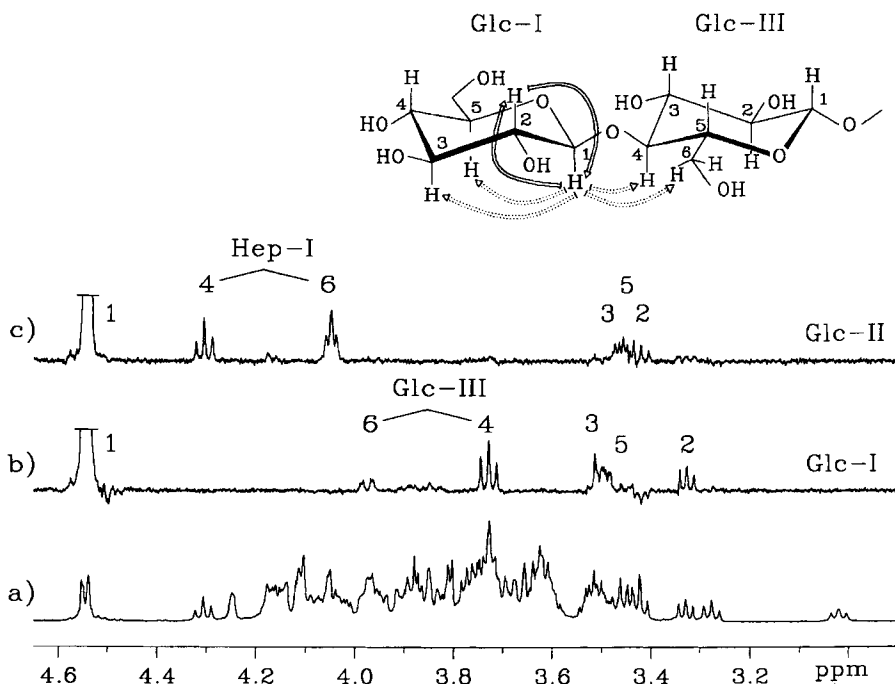


Fig. 17. 1D RELAY-NOESY spectra of the oligosaccharide **5** acquired using the pulse sequence of fig. 13(d) with the initial polarization transfer from overlapping anomeric protons of two terminal glucoses in **5**. (a) Partial  $^1\text{H}$  spectrum of **7** at 600 MHz after 8 scans. The following parameters were used to acquire the two original 1D RELAY-NOESY spectra (not shown):  $\tau_{\text{set}} = 50$  ms,  $\tau_0 = 39$  ms,  $\Delta = 9.09$  ms,  $\tau_1 = 120$  ms,  $\tau_r = 64$  ms,  $\tau_{\text{in}} = 400$  ms.  $N = 0$  in the first and  $N = 1$  in the second experiment, the relaxation delay was 2 s and the acquisition time was 1.4 s. Number of scans was 1024 in both spectra. The summation (b) and subtraction (c) of these spectra clearly separates NOEs from both overlapping anomeric protons. A partial structure of **5** is given in the inset. Polarization transfer pathways for the RELAY and NOESY transfers in Glc-I are shown using solid and dotted lines, respectively. (Reprinted with adaptation with permission from ref. [38]. Copyright 1993 ESCOM Science Publisher B.V.)

filtration at H-2 protons sent back to H-1 protons. A complete refocusing of H-1 protons, due to their doublet character, can be achieved during the refocusing interval prior to the NOE mixing. The method is illustrated using the oligosaccharide **5**. Two 1D RELAY-NOESY spectra were acquired using a different position of a  $180^\circ$   $^1\text{H}$  pulse during the filtration interval  $\tau_1$  similarly to the 1D COSY-RELAY and 1D COSY-TOCSY experiments on **5**. The sum and difference of the aforementioned experiments are shown in figs 17(b), (c). Based on this experiment, it was possible to establish the Glc-I  $\rightarrow$  Glc-III and Glc-II  $\rightarrow$  Hep-I sequence in the oligosaccharide **5**.

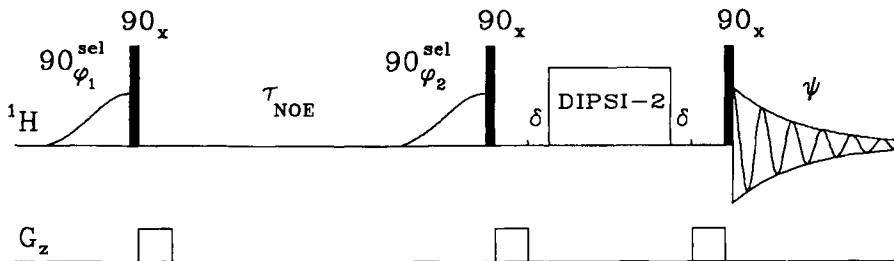


Fig. 18. The pulse sequence of a 1D ge-NOESY-TOCSY experiment.  $\tau_{\text{NOE}}$  is the NOE mixing time,  $\delta$  are optional delays which can be used for  $z$ -filtration [81] or for suppression of ROE effects in macromolecules ( $2 \times (\delta + \tau_{\text{grad}}) = 0.5 \times \text{mixing time}$ ). DIPSI-2 [78] sequence was used for isotropic mixing. Phases were cycled as follows:  $\phi_1 = 2x, 2(-x)$ ;  $\phi_2 = x, -x$ ;  $\psi = x, 2(-x), x$ . Rectangular PFGs,  $G_1 = 6$  Gauss/cm and  $G_1 = 7$  Gauss/cm, were applied along the  $z$  axis for  $\tau_{\text{grad}} = 1$  ms.

In all CSSF experiments filtration was performed immediately after the COSY step. Should there not be a sufficient chemical shift separation between H-2 protons, the magnetization could be further transferred along the spin system and filtered during one of the later spin-echoes. We note that such extensive transfer of magnetization can bring some signal attenuation due to the relaxation losses and a compromise setting of spin-echo intervals.

### 3.6. 1D ge-NOESY-TOCSY

The pulse sequence of a 1D ge-NOESY-TOCSY experiment [70] (fig. 18) follows the general principles outlined in section 2.3. After the two initial pulses the magnetization of the selectively excited proton is stored along the  $z$  axis. The magnetization of all other protons is, however, aligned along the  $y$  axis and dephased by the subsequent PFG. A significant part of this magnetization returns to the  $z$  axis during the long NOE interval due to spin-lattice relaxation. This is dephased again by another PFG applied after the next nonselective pulse, which has flipped this  $z$  magnetization back to the  $y$  axis. On the other hand, the magnetization of the proton which was selected for by the selective TOCSY transfer is kept along the  $z$  axis due to the preceding selective pulses. Isotropic mixing via DIPSI-2 sequence [78] takes place along the  $z$  axis and the created magnetization is flipped to the  $xy$  plane by the final nonselective  $90^\circ$  read pulse. The PFG applied immediately before the read pulse dephases all the  $xy$  magnetization which might have been created by the isotropic mixing sequence. A four scan phase cycling scheme is needed to remove the magnetization which has relaxed to the  $z$  axis mainly during the DIPSI sequence.

The 1D ge-NOESY-TOCSY experiment is illustrated using a LPS O-polysaccharide (7) isolated from *Proteus mirabilis* serotype O:57 [79]. The

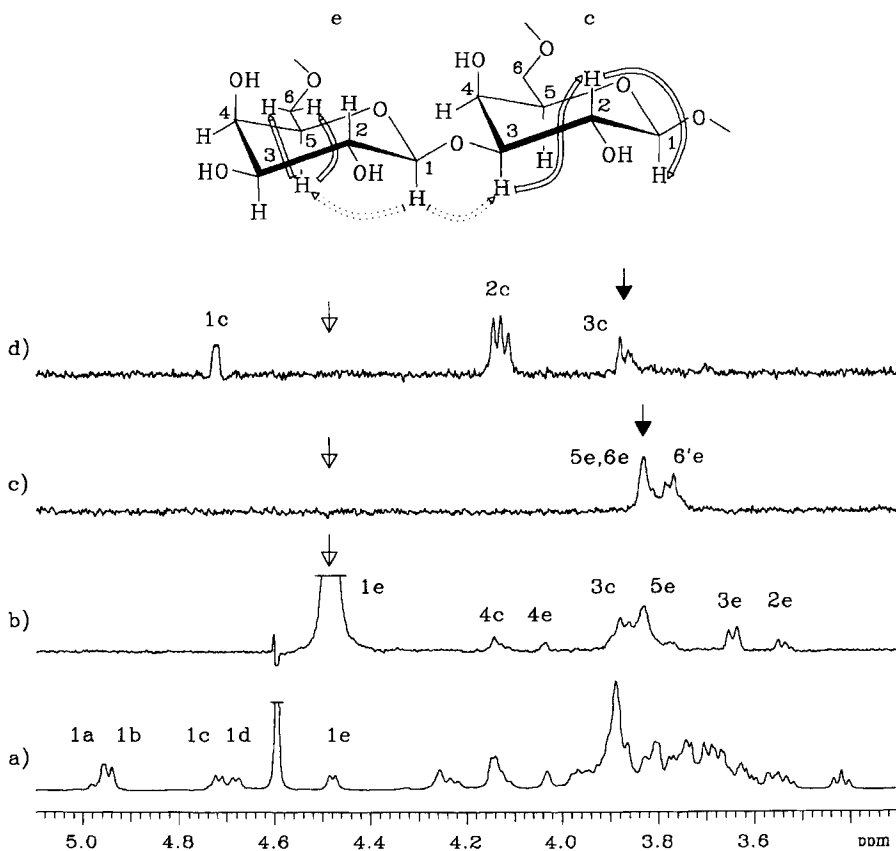


Fig. 19. (a) Partial 600 MHz  $^1\text{H}$  spectrum of **7** (8 scans).

(b) A 64 scan 1D ge-NOESY spectrum with selective excitation of H-1e via 45.5 ms half-Gaussian pulse. The NOE mixing time was 200 ms. A gradient-enhanced version of a 1D NOESY experiment, as described in the text, was used to acquire the spectrum.

(c) and (d) 1D ge-NOESY-TOCSY spectra of **7** (pulse sequence of fig. 18) with selective NOESY transfer from H-1e followed by a selective TOCSY transfer from H-5e in (c) and H-3c in (d). The first and the second selective pulses were half-Gaussian pulses of 45.5 and 72.1 ms, respectively. The NOE mixing time was 200 ms, while the TOCSY transfer was set to 25 ms in both spectra. The number of scans was 64 in (c) and 128 in (d). Polarization transfer pathways are depicted in the partial structure of **7** given in the inset. Dotted and solid lines were used to show the NOESY and TOCSY transfers, respectively.

1D NOESY spectrum (fig. 19(b)) of **7** after selective excitation of the H-1e proton showed several signals. Since this is an anomeric proton of a  $\beta$ -D-galactopyranose residue, the most intense signals seen in this spectrum should belong to protons H-3e, H-5e and to a proton from the neighbouring residue across the glycosidic linkage. The H-3e proton has been identified from a 1D TOCSY experiment starting at H-1e. Since the e residue is a

galactopyranose, the transfer stopped at H-4e and the assignment of the H-5e was not obtained. Two 1D ge-NOESY-TOCSY spectra, using the pulse sequence of fig. 18, were acquired with the TOCSY selective pulses applied at 3.84 and 3.88 ppm, respectively. Signals from higher order spin system of H-5e, H-6e,6e' were found in the first spectrum. Because of small coupling constant  $J(\text{H-4e}, \text{H-5e})$  no transfer to H-4e took place. The second spectrum showed, in addition to signal at 3.88 ppm, signals of H-1c, H-2c. No transfer was registered to proton H-4c because of the small coupling constant  $J(\text{H-3c}, \text{H-4c})$  of this galactopyranose residue. Based on these two experiments signals at 3.84 and 3.88 ppm were assigned to H-5e and H-3c protons respectively.

Other combinations of the ge-NOESY and ge-TOCSY sequences can be easily created following the above example of the 1D ge-NOESY-TOCSY. It should be noted that the amount of magnetization which returns to the  $z$  axis during mixing intervals is larger for the NOESY experiment, simply because this time interval is usually much longer than the one used for isotropic mixing. This makes the dephasing of the unwanted magnetization by a PFG applied after the first nonselective pulse of the NOESY sequence less effective than in the TOCSY experiment. As pointed out elsewhere [67], this can be reduced significantly by a  $180^\circ$  pulse applied in the middle of the NOE mixing interval. This procedure is recommended for experiments where the NOESY transfer constitutes the last step of a pulse sequence.

#### 4. Conclusions

It has been demonstrated that the concatenation of selective polarization transfer steps in 1D NMR experiments is yet another useful tool of NMR spectroscopy. Simple concatenation of several coherent and/or incoherent polarization transfer mechanisms results in a unique 1D experiment tailored for an individual spectral problem. Typical applications would include circumventing the bottleneck in polarization transfer of one mechanism by the other, and isolation of overlapping spin systems. The result is a one-dimensional spectrum acquired with high digital resolution and in a relatively short time. Selective pulses and chemical-shift-selective filters were used for the necessary signal selection. Since this process takes place in at least two stages, the signal separation required for concatenated experiments is less stringent compared to simple selective 1D experiments. Pulsed field gradients enhance the quality of the spectra, in particular the solvent peak suppression. Although especially useful for NMR spectroscopy of carbohydrates, the basic ideas behind these techniques are generally applicable across the whole field of high-resolution NMR spectroscopy.

## Acknowledgements

The author wishes to thank several people who were very helpful during various stages of the project. They are, in alphabetic order: E. Altman, P. Barlow, D.R. Bundle, V. Chandan, H.J. Jennings, G. Kogan, T. Liptaj, H. Masoud, L.L. MacLean, M.B. Perry and J.C. Richards. In particular he would like to acknowledge the contribution of Dr. J.-R. Brisson.

*Substantial parts of the text in sections 3.1. and 3.5 were reproduced with permission from D. Uhrín, J.-R. Brisson, G. Kogan and H.J. Jennings, J. Magn. Reson. Series B 104 (1994) 289, Copyright Academic Press, Inc., and from D. Uhrín, J.-R. Brisson and D.R. Bundle, J. Biomol. NMR 3 (1993) 367, Copyright ESCOM Science Publisher B.V., respectively.*

## References

- [1] J. Jeener, Ampere International Summer School, Basko Polje, Yugoslavia, 1971.
- [2] W.P. Aue, E. Bartholdi and R.R. Ernst, J. Chem. Phys. **64** (1976) 2229.
- [3] L. Braunschweiler and R.R. Ernst, J. Magn. Reson. **53** (1983) 529.
- [4] A. Bax and D.G. Davis, J. Am. Chem. Soc. **107** (1985) 2820.
- [5] J. Jeener, B.H. Meier, P. Bachmann and R.R. Ernst, J. Chem. Phys. **69** (1979) 4546.
- [6] A.A. Bothner-By, R.L. Stephens, J. Lee, C.D. Warren, R.W. Jeanloz, J. Am. Chem. Soc. **106** (1984) 811.
- [7] G. Wagner, J. Magn. Reson. **57** (1984) 497.
- [8] H. Kessler, S. Steuernagel, D. Gillissen and T. Kamiyama, Helv. Chim. Acta. **70** (1987) 726.
- [9] J. Cavanagh, J.J. Titman and J. Keeler, Magn. Reson. Chem. **26** (1988) 1093.
- [10] H. Kessler, G. Gemmecker and B. Haase, J. Magn. Reson. **77** (1988) 401.
- [11] H. Kessler, G. Gemmecker, B. Haase and S. Steuernagel, Magn. Reson. Chem. **26** (1988) 919.
- [12] H. Kessler, G. Gemmecker and S. Steuernagel, Angew. Chem. Int. Ed. Engl. **27** (1988) 564.
- [13] V. Basus and R.M. Scheek, Biochemistry **27** (1988) 2772.
- [14] B.R. Loefflant and J.F.G. Vliegthart, J. Magn. Reson. **89** (1990) 615.
- [15] J. Cavanagh and M. Rance, J. Magn. Reson. **87** (1990) 408.
- [16] M.P. Williamson, N.J. Murray and J.P. Waltho, J. Magn. Reson. **100** (1992) 593.
- [17] L. Poppe and J. Dabrowski, Biochem. Biophys. Res. Commun. **159** (1989) 618.
- [18] V. Sklenář and J. Fegion, J. Am. Chem. Soc. **112** (1990) 5644.
- [19] H. Schröder and E. Haslinger, Angew. Chem. Int. Ed. Engl. **32** (1993) 1349.
- [20] S.W. Homans, J. Magn. Reson. **90** (1990) 557.
- [21] H. Oschkinat, C. Griesinger, P.J. Kraulis, O.W. Sørensen, R.R. Ernst, A.M. Gronenborn and G.M. Clore, Nature **332** (1988) 374.
- [22] G.W. Vuister, R. Boelens and R. Kaptein, J. Magn. Reson. **80** (1988) 176.
- [23] G. Griesinger, O.W. Sørensen and R.R. Ernst, J. Magn. Reson. **84** (1989) 14.
- [24] G.W. Wuister, P. de Waard, R. Boelens, J.F.G. Vliegthart and R. Kaptein, J. Am. Chem. Soc. **111** (1989) 772.
- [25] J.-P. Simorre and D. Marion, J. Magn. Reson. **94** (1991) 426.

- [26] H. Oschkinat, C. Ciesler, A.M. Gronenborn and G.M. Clore, *J. Magn. Reson.* **81** (1989) 212.
- [27] H. Oschkinat, C. Ciesler, T.A. Holak, G.M. Clore and A.M. Gronenborn, *J. Magn. Reson.* **83** (1989) 450.
- [28] C. Griesinger, O.W. Sørensen and R.R. Ernst, *J. Am. Chem. Soc.* **109** (1987) 7227.
- [29] C. Griesinger, O.W. Sørensen and R.R. Ernst, *J. Magn. Reson.* **73** (1987) 574.
- [30] T.J. Rutherford and S.W. Homans, *Glycobiology* **2** (1992) 293.
- [31] T.J. Rutherford and S.W. Homans, *J. Magn. Reson. B* **106** (1995) 10.
- [32] D.G. Davis, A. Bax, *J. Am. Chem. Soc.* **107** (1985) 7197.
- [33] H. Kessler, H. Oschkinat, C. Griesinger and W. Bermel, *J. Magn. Reson.* **70** (1986) 106.
- [34] H. Kessler, U. Anders, G. Gemmecker and S. Steuernagel, *J. Magn. Reson.* **85** (1989) 1.
- [35] D. Boudot, C. Roumestand, F. Toma and D. Canet, *J. Magn. Reson.* **90** (1990) 221.
- [36] L. Poppe and H. van Halbeek, *J. Magn. Reson.* **96** (1992) 185.
- [37] S. Holmbeck, P. Hajduk and L. Lerner, *J. Magn. Reson. Series B* **102** (1993) 107.
- [38] D. Uhrín, J.-R. Brisson and D.R. Bundle, *J. Biomol. NMR* **3** (1993) 367.
- [39] D. Uhrín, J.-R. Brisson, G. Kogan and H.J. Jennings, *J. Magn. Reson. Series B* **104** (1994) 289.
- [40] K. Zangger and H. Sterk, *J. Magn. Reson. Series B.* **107** (1995) 186.
- [41] C. Bauer, R. Freeman, T. Frenkiel, J. Keeler and A.J. Shaka, *J. Magn. Reson.* **58** (1984) 442.
- [42] L. Emsley and G. Bodenhausen, *J. Magn. Reson.* **82** (1984) 211.
- [43] J. Friedrich, S. Davies and R. Freeman, *J. Magn. Reson.* **75** (1987) 390.
- [44] D. Boudot, D. Canet, J. Brondeau and J.-C. Boubel, *J. Magn. Reson.* **83** (1989) 428.
- [45] R. Freeman, *Chem. Rev.* **91** (1991) 1397.
- [46] L. Emsley, in: *Methods in Enzymology, Nuclear Magnetic Resonance, Part C, Vol. 239*, eds T.L. James and N.J. Oppenheimer (Academic Press, New York, 1994) p. 207.
- [47] P. Hajduk, D. Horita and L. Lerner, *J. Magn. Reson. A* **103** (1993) 40.
- [48] L.D. Hall and T.J. Norwood, *J. Magn. Reson.* **76** (1988) 548.
- [49] L.D. Hall and T.J. Norwood, *J. Magn. Reson.* **78** (1988) 582.
- [50] G. Batta and K.A. Kövér, *Tetrahedron* **47** (1991) 3535.
- [51] K.A. Kövér, D. Uhrín, G. Szalontai and G. Batta, *J. Magn. Reson. B* **101** (1993) 1.
- [52] D. Uhrín, A. Mele, K.A. Kövér, J. Boyd and R.A. Dwek, *J. Magn. Reson. A* **108** (1994) 160.
- [53] G. Bodenhausen, R. Freeman and G.A. Morris, *J. Magn. Reson.* **23** (1976) 171.
- [54] G.A. Morris and R. Freeman, *J. Magn. Reson.* **29** (1978) 433.
- [55] L. Poppe and J. Dabrowski, *Biochem. Biophys. Res. Commun.* **159** (1989) 618.
- [56] H. Schröder and E. Haslinger, *Liebigs Ann. Chem.* (1993) 751.
- [57] H. Schröder and E. Haslinger, *Liebigs Ann. Chem.* (1993) 959.
- [58] J. Keeler, R.T. Clowers, A.L. Davis and E. Laue, in: *Methods in Enzymology, Nuclear Magnetic Resonance, Part C, Vol. 239*, eds T.L. James and N.J. Oppenheimer (Academic Press, New York, 1994) p. 145.
- [59] L.E. Kay, *Curr. Opp. Struct. Biol.* **5** (1995) 681.
- [60] A. Bax and S. Pochapsky, *J. Magn. Reson.* **99** (1992) 638.
- [61] M.A. Bernstein and L.A. Trimble, *Magn. Reson. Chem.* **32** (1994) 107.
- [62] J. Stonehouse, P. Adell, J. Keeler and A.J. Shaka, *J. Am. Chem. Soc.* **116** (1994) 6037.
- [63] C. Dalvit and G. Bovermann, *Magn. Reson. Chem.* **33** (1995) 156.
- [64] P. Adell, T. Parella, F. Sanchez-Ferrando and A. Virgili, *J. Magn. Reson. Series B* **108** (1995) 77.

- [65] T. Facke and S. Berger, *J. Magn. Reson. Series A* **113** (1995) 257.
- [66] C. Dalvit, *J. Magn. Reson. Series A* **113** (1995) 120.
- [67] K. Stott, J. Stonehouse, J. Keeler, T.-L. Hwang and A.J. Shaka, *J. Am. Chem. Soc.* **117** (1995) 4199.
- [68] P. Adell, T. Parella, F. Sanchez-Ferrando and A. Virgili, *J. Magn. Reson. Series A* **113** (1995) 124.
- [69] T. Parella, *Magn. Reson. Chem.* **34** (1996) 329.
- [70] D. Uhrín and P.N. Barlow, *J. Magn. Reson.* **126** (1997) 248.
- [71] G. Batta, A. Liptak, *J. Am. Chem. Soc.* **106** (1984) 248.
- [72] D. Uhrín, unpublished results.
- [73] H. Masoud, D. Uhrín and J.C. Richards, unpublished results.
- [74] R. Boelens, G.W. Vuister, T.M.G. Koning and R. Kaptein, *J. Am. Chem. Soc.* **111** (1989) 8525.
- [75] D. Uhrín, V. Chandan and E. Altman, *Can. J. Chem.* **73** (1995) 1600.
- [76] H. Masoud and J.C. Richards, unpublished results.
- [77] V. Pavliak, D. Uhrín, J.-R. Brisson, A.O. Tzianabos, D.L. Kasper and H.J. Jennings, *Carb. Res.* **275** (1995) 333.
- [78] S.P. Rucker and A.J. Shaka, *Molecular Physics* **68** (1989) 509.
- [79] D. Uhrín, J.-R. Brisson, L.L. MacLean, J.C. Richards and M.B. Perry, *J. Biomol. NMR* **4** (1994) 615.
- [80] S. Subramanian and A. Bax, *J. Magn. Reson.* **71** (1987) 325.
- [81] M. Rance, *J. Magn. Reson.* **74** (1987) 557.

This Page Intentionally Left Blank

## chapter 4

---

# The Selective Reverse INEPT Experiment

---

Gareth A. Morris and Ian C. Clements

*Department of Chemistry  
University of Manchester  
Oxford Road, Manchester M13 9PL  
United Kingdom*

This Page Intentionally Left Blank

## 1. Introduction

There is a bewildering variety of multidimensional NMR techniques available to the modern NMR spectroscopist interested in structure elucidation, and used in a concerted fashion these provide efficient and economical tools for determining chemical structures. There is a trade-off implicit in the use of multidimensional experiments, between the volume of information that they provide and the minimum time taken to perform them; in most cases the extended experimental duration is more than compensated for by the wealth of structural information revealed. For a small proportion of structural problems, however, such experiments may provide far more information than is actually required, and where only a few critical parameters need to be measured they may represent a far from efficient use of spectrometer time.

Where multidimensional experiments provide an *embarras de richesse*, it may be preferable to exploit selective excitation methods [1] in order to focus on a few critical parameters or regions of a spectrum: the generality and broadband character of multidimensional spectroscopy are lost, but the ability to resolve individual signals may be improved and it may be possible to exploit the available nuclear signal in a significantly more effective way, improving sensitivity and reducing experiment time. Such experiments often have the added advantages of conceptual simplicity and ease of interpretation.

This chapter concerns a heteronuclear experiment, selective reverse INEPT, that provides a simple way to extract from a complex and overlapping proton spectrum the signals of those protons coupled to a particular heteronucleus. The heteronucleus will be assumed here to be carbon-13, although there are many other possibilities. There are at least three reasons for wanting to edit a proton spectrum in this way. One is to lift an unwanted degeneracy between two protons which have the same chemical shift but are bonded to different carbons, for example in order to measure a proton-proton coupling constant. Another is to allow a particular long-range proton-carbon-13 coupling constant to be measured, with good signal-to-noise ratio and without interference from overlapping signals. A third is to allow homonuclear proton-proton decoupling experiments to be carried out in a degenerate spin system, for example to determine the coupling se-

quence in a spin system containing a chain of coupled protons, two of which have the same shift. Two-dimensional experiments exist in all three cases that can provide the required information; for example, proton–proton multiplet structure in overcrowded spectra can be determined using an HMQC experiment [2] without heteronuclear decoupling in  $f_2$ , long-range proton–carbon-13 couplings can be extracted from HMBC spectra [3], and coupling sequences in degenerate systems can be traced using HMQC-TOCSY [4]. The advantages of using a selective experiment are that the minimum experiment duration is sharply reduced, coherence can be channeled where it will be most informative instead of being distributed across a range of signals, and the results of the 1D experiment can be significantly easier to analyze than the corresponding 2D spectrum.

There are of course many possible ways to achieve 1D spectral editing of carbon-13 satellites in proton NMR, particularly where an instrument is available that is equipped with actively shielded pulsed field gradients. For any given application there will often exist a more efficient experiment than selective reverse INEPT; on the other hand, selective reverse INEPT will give good results in a wide variety of applications, and is easy to set up and predictable in its results. Although advantage can be taken of pulsed field gradients where available, these are not essential to the success of the experiment, which can achieve clean editing without their assistance by the combined use of presaturation and phase cycling. Other polarization sequences can of course be substituted for INEPT, for example DEPT [5], but these generally require longer delays and hence give poorer signal-to-noise ratio where polarization is being transferred through long range couplings.

## 2. Experimental methods

The INEPT (Insensitive Nuclei Enhanced by Polarization Transfer) experiment [6, 7] was the first broadband pulsed experiment for polarization transfer between heteronuclei, and has been extensively used for sensitivity enhancement and for spectral editing. For spectral editing purposes in carbon-13 NMR, more recent experiments such as DEPT, SEMUT [8] and their various enhancements [9] are usually preferable, but because of its brevity and simplicity INEPT remains the method of choice for many applications in sensitivity enhancement, and as a building block in complex pulse sequences with multiple polarization transfer steps. The potential utility of INEPT in “inverse mode” experiments, in which polarization is transferred from a low magnetogyric ratio nucleus to protons, was recognized quite early [10]. The principal advantage of polarization transfer over methods such as heteronuclear spin echo difference spectroscopy is the scope it offers for presaturation of the unwanted proton signals, which allows clean spec-

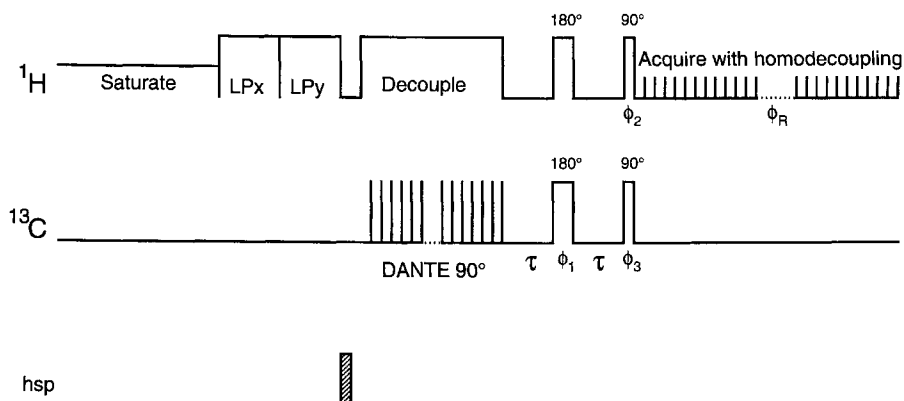


Fig. 1. Pulse sequence for selective reverse INEPT. The time-shared homonuclear decoupling during acquisition is optional, and a variety of simplifications may be made to the sequence depending on the instrument used and on the spin system under investigation, as discussed in the text. A DANTE sequence is shown as the selective  $90^\circ$  carbon-13 pulse, but this may be replaced by a soft pulse or some other form of selective excitation. Phase cycling for this sequence is summarized in table 1.

tra to be obtained without the need for pulsed field gradients and without placing excessive demands on instrument stability. Making the polarization transfer selective [11] allows the carbon-13 satellites for coupling to a given carbon to be extracted from a complex proton spectrum; by adjusting the delays involved in the pulse sequence, transfer can be achieved through one-bond couplings only, long range couplings only, or through both.

Figure 1 shows a general purpose selective reverse INEPT pulse sequence that is applicable to all three classes of problem mentioned above. The experiment starts with a period of modulated irradiation of the proton spins, with the proton transmitter approximately on resonance for the protons of interest, followed by pair of orthogonal proton spin lock pulses. The modulated irradiation gives a moderately efficient presaturation of all the proton magnetizations while allowing the nuclear Overhauser enhancement of the carbon magnetization to build up; coherent irradiation at exact proton resonance may be used if modulation is difficult to implement. The spin lock pulses purge the residual transverse magnetization left by the preirradiation, using the inhomogeneity of the proton radiofrequency field to disperse it as evenly as possible over the Bloch sphere. At this point a homospoil pulse may be applied, if available, to dephase further any remaining proton transverse magnetization. A short delay should be left for the main field  $B_0$  to settle if the  $Z_1$  shim coil, rather than a shielded gradient coil within the probe, is used to provide the homospoil pulse, as is generally the case on older spectrometers. Depending on the stability of the spectrometer used,

the natural abundance of the heteronucleus, and the dynamic range of the spectrum, it may be possible to dispense with one or more of the three sequence elements (the presaturation, the spin lock pulses and the homospoil pulse) used to attenuate the initial proton magnetization.

At this point the proton magnetization has been minimized, and the carbon-13 longitudinal magnetization is ready to be excited. A pulse or pulse sequence is applied to carbon-13 to generate carbon transverse magnetization, which is then allowed to evolve under the heteronuclear coupling until an antiphase state is obtained. For convenience, the carbon-13 transmitter is usually set to exact resonance where this is possible. For selective excitation a soft pulse, shaped or rectangular, or a DANTE sequence may be used; for semiselective excitation a band-selective pulse or a  $90^\circ$  pulse pair may suffice; for nonselective polarization transfer, a simple  $90^\circ$  pulse is used. The advantages of using DANTE rather than a soft pulse are that there is no need to change the carbon-13 transmitter power level, and that any problems with the carbon-13 radiofrequency phase varying with pulse amplitude are avoided. Proton irradiation is continued during the selective pulse or pulse sequence in order to decouple the carbon-13 from protons, and then the decoupling is gated off to allow the heteronuclear coupling to act during the  $2\tau$  delay.

The length of the delay  $2\tau$  depends on the nature of the spin system and on the coupling constant through which coherence is to be transferred. If protons are denoted  $I$  and carbon  $S$ , then for an  $I_nS$  spin system the polarization transferred varies as

$$S(2\tau) = \cos^{n-1}(2\pi J_{CH}\tau) \sin(2\pi J_{CH}\tau),$$

where  $J_{CH}$  is the carbon-13–proton coupling constant. For CH, CH<sub>2</sub> and CH<sub>3</sub> spin systems with a typical one-bond coupling  $^1J_{CH}$  of 135 Hz, the optimum values of  $2\tau$  are 3.70, 1.85 and 1.46 ms, respectively. The  $180^\circ$  carbon-13 and proton pulses may be omitted if  $2\tau$  is reasonably short (say  $<50$  ms) and the carbon transmitter is on exact resonance, since  $B_0$  field inhomogeneity and off-resonance effects should be of little importance in such circumstances. Where polarization transfer through the much smaller long range couplings is required, however, omitting the refocusing pulse is likely to lead to significant loss of signal (and, potentially, some interesting lineshapes, as the efficiency of polarization transfer will become spatially dependent). The coherence transfer is effected by the  $90^\circ$  proton and carbon-13 pulses, which generate transverse proton magnetization which is antiphase with respect to the carbon coupling; the order of the pulses is immaterial. At this point a further modulated spin echo could be used if proton magnetization in-phase with respect to carbon-13 were required, but this is rarely the case since a selective polarization transfer experiment

should not encounter any problems of overlap with extraneous signals in the proton spectrum.

Where the object of the experiment is to elucidate proton–proton connectivities in a spin system which is degenerate in the absence of carbon-13, during the delay  $2\tau$  the proton transmitter is moved to the frequency of the proton(s) to be irradiated, and immediately after the proton  $90^\circ$  pulse time-shared homonuclear decoupling is initiated. On most two-channel spectrometers this will require explicit programming of interleaved proton pulses and acquisition of data points, since the second channel will be set up to provide the carbon-13 pulses. Moving the proton transmitter frequency before the proton  $90^\circ$  pulse ensures phase coherence between the latter and the local oscillator (LO) reference frequency used in the spectrometer receiver, since the LO signal is often derived from the same source as the transmitter pulse. Spectrometers such as the Bruker AC series that derive the LO signal by changing the frequency of the transmitter synthesizer may require hardware modifications if pulses and data point acquisition are to be interleaved.

A typical time-sharing pattern at 500 MHz would be to give a  $1\ \mu\text{s}$  pulse, bracketed by  $10\ \mu\text{s}$  receiver gating delays, every  $200\ \mu\text{s}$  dwell time. The position of the pulse with respect to acquisition of a data point is not critical because of the smoothing effect of audio filtration. The amplitude of the pulse is adjusted to give the average irradiation strength  $\nu_2^{\text{eff}}$  required for homodecoupling, typically in the region of 10–50 Hz. If the amplitude of the proton pulses is  $\nu_0^{\text{eff}}$ , the pulse width  $\tau_p$  and the dwell time  $\tau_d$ , then

$$\nu_2^{\text{eff}} = \nu_0^{\text{eff}} \frac{\tau_p}{\tau_d}.$$

Since the duty cycle in the example given is about 0.5%, a proton pulse amplitude  $\nu_0^{\text{eff}}$  in the region of 2–10 kHz is required. If rapid level switching of the proton radiofrequency field strength is not available, then a constant amplitude may be used throughout the sequence, using adjustment of  $\tau_p$  to control  $\nu_2^{\text{eff}}$ , but care must be taken to avoid problems with the proton transmitter duty cycle or with power dissipation in the probe. In such circumstances it may be necessary to employ time-sharing in the preirradiation period as well as during data acquisition.

Table 1 summarizes a phase cycling scheme suitable for the sequence of fig. 1. Where possible the phase of the modulation scheme used for the preirradiation scheme should remain fixed from transient to transient, although this may be impractical in some spectrometers. The preirradiation and spin lock phases, and the phase of any homodecoupling irradiation during data acquisition, are all kept constant as the receiver phase is cycled. This suppresses any proton signals elicited by these fields, while phase alternation is used to cancel any remaining signals that do not originate with carbon-13

polarization. The phase cycling shown includes EXORCYCLE for the  $180^\circ$  carbon-13 refocusing pulse; this may improve the satellite signal strength obtained slightly, but also serves to improve the proton lineshape by favouring those regions of the sample which enjoy good carbon-13 radiofrequency field homogeneity. If necessary this effect could be amplified by using a  $540^\circ$  instead of a  $180^\circ$  refocusing pulse.

Where pulsed field gradient hardware is available, the sequence may be simplified significantly if a factor of two reduction in sensitivity can be

TABLE 1

Phase cycling scheme for the selective reverse INEPT pulse sequence of fig. 1. Phases are shown in multiples of  $90^\circ$ ; subscripts indicate that a given phase or bracketed block of phases should be repeated the stated number of times, e.g., the notation  $(01)_2 (13)_2$  indicates the sequence 0101 1313. Phases in the sequence of fig. 1 other than those listed above remain unchanged in successive transients.

$\phi_1$	$0_8 2_8 1_8 3_8$
$\phi_2$	$(0321 2103)_2 (2103 0321)_2$
$\phi_3$	1313 3131
$\phi_R$	0123

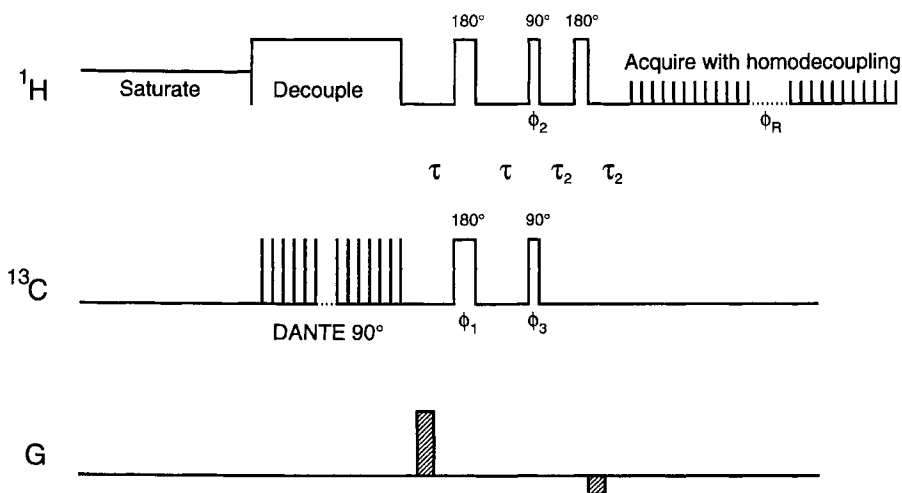


Fig. 2. Pulse sequence for selective reverse INEPT using pulsed field gradients to select the coherence transfer echo. The  $180^\circ$  pulse pair in the middle of the  $2\tau$  delay is not normally needed for  $\tau < 50$  ms, and the second proton  $180^\circ$  pulse and first  $\tau_2$  delay maybe omitted if a linear phase gradient in the resultant spectrum can be tolerated. The second field gradient pulse has an area  $(\gamma_C/\gamma_H)$  times that of the first.

tolerated. Using matched carbon-13 and proton gradient pulses to select the coherence transfer echo can give excellent suppression of unwanted proton signals even in the absence of preirradiation, spin lock pulses or phase cycling, although the preirradiation is still desirable in order to establish the nuclear Overhauser enhancement. The minimum sequence is shown in fig. 2; since the width of the spectrum of interest will normally be little more than a typical one-bond proton-carbon-13 coupling constant, the proton  $180^\circ$  pulse and first delay  $\tau_2$  may usually be dispensed with at the expense of a linear phase correction. There are, however, a number of more complex competing experiments to consider where pulsed field gradients are available, for example the SELINCOR experiment with pulsed field gradient coherence pathway selection [12]. A particularly versatile experiment would be to introduce selective or band-selective carbon inversion pulses into the excitation sculpting sequences of Shaka and coworkers [13].

### 3. Sample applications

The use of carbon-13 satellite spectra to gain access to proton-proton coupling constants in systems with degenerate chemical shifts has been common practice for many years [14]. The frequency displacement of  $(1/2)^1 J_{CH}$  introduced by the presence of a carbon-13 bonded to a given proton in an otherwise degenerate spin system is sufficient to render most couplings nearly first order. Figure 3 illustrates the use of a reverse INEPT experiment to reveal the long range and one-bond satellites in an aqueous solution

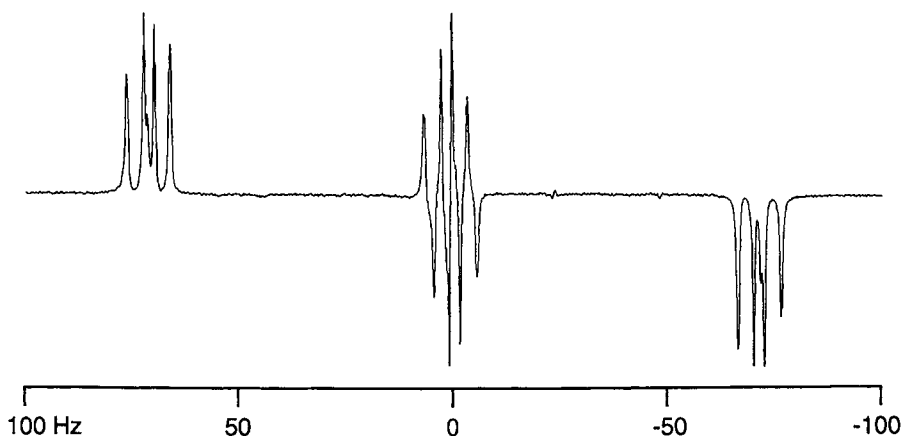


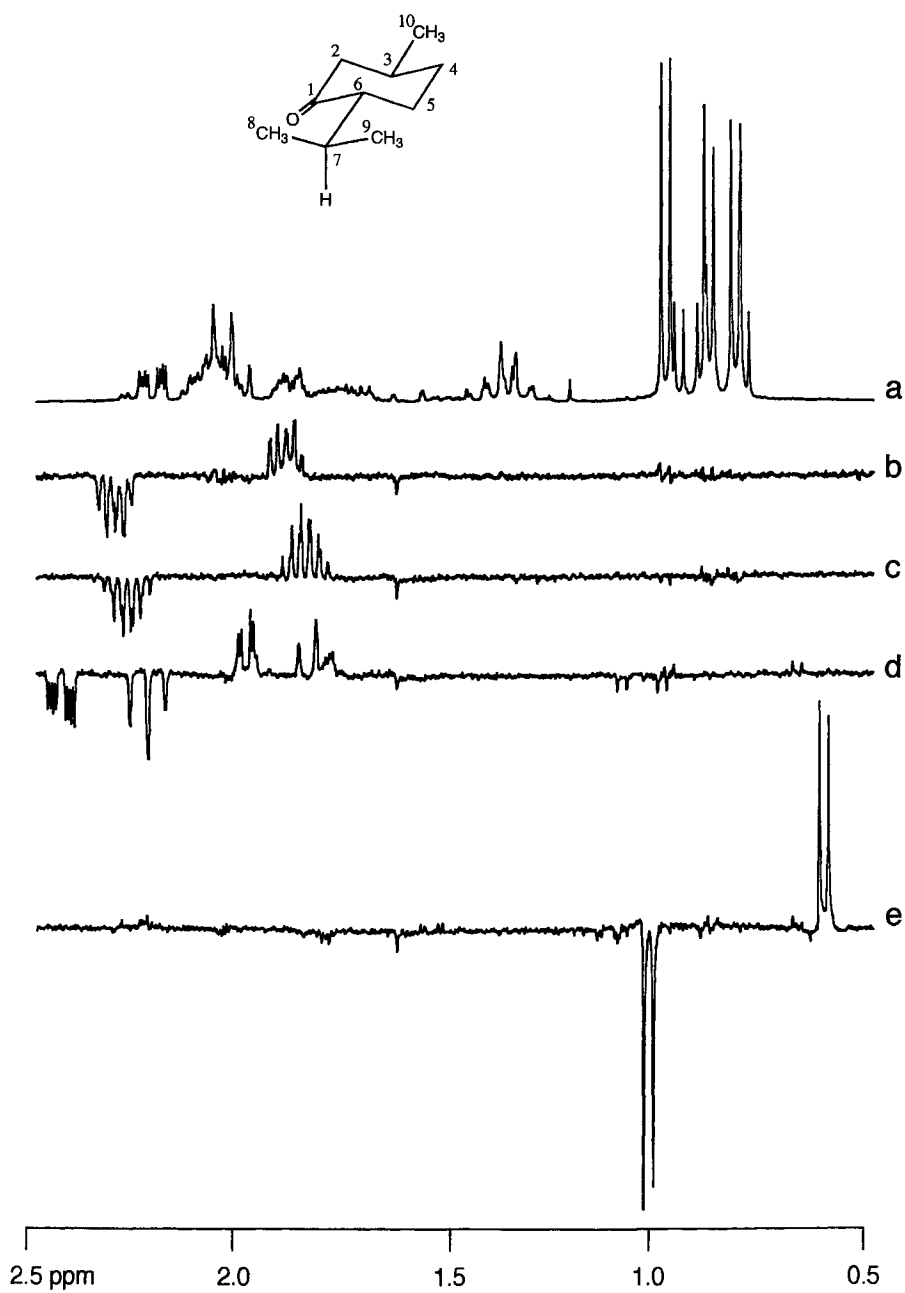
Fig. 3. Long range and one-bond carbon-13 satellite spectrum of a 5% w/w solution of ethanediol in  $D_2O$  at  $94^\circ C$ . 16 transients were measured on a Varian Associates Unity 500 spectrometer using the sequence of fig. 1, with 2.5 s presaturation, a  $\tau$  value of 100 ms, spin lock pulses of 450  $\mu s$ , no homospoil pulse, and no homodecoupling during acquisition.

of ethanediol at 500 MHz; proton multiplet structure appears in-phase, and carbon-13 in antiphase. The delay  $2\tau$  was set to 200 ms here in order to excite polarization transfer through both the one-bond and the two-bond couplings. The long range satellites in the centre of the spectrum arise from the isotopomer in which the methylene protons seen are bonded to  $^{12}\text{C}$  and the other methylene protons to  $^{13}\text{C}$ , and the one-bond satellites at the edges from the converse isotopomer in which  $^{13}\text{C}$  and  $^{12}\text{C}$  nuclei are exchanged.

This system is of interest because of the uncertainty of the position of the rotameric equilibrium [15]. The two vicinal coupling constants, 3.82 and 6.28 Hz, can be determined from this spectrum with good accuracy ( $\pm 0.02$  Hz). Unfortunately the interpretation of these values is far from straightforward. The Haasnoot equation [16] has an estimated accuracy of about  $\pm 0.5$  Hz; indeed model compound data for the  $-\text{OCH}_2\text{CH}_2\text{O}-$  fragment suggest that this may be an underestimate of the root mean square error. Using the recent reparametrization of the Haasnoot equation for aqueous solutions [17] to predict the coupling constants in rotamers with the oxygens gauche and trans, the only safe conclusion that can be drawn is that the contribution of trans rotamers in aqueous solution is less than 20%, corresponding to a minimum energy difference between gauche and trans rotamers of about  $2 \text{ kJ mol}^{-1}$ .

The combination of presaturation with phase cycling in the sequence of fig. 1 ensures that it remains suitable for use in older spectrometers with limited stability. Figure 4 shows illustrative spectra of a solution of menthone in acetone- $d_6$  obtained at 300 MHz. The normal proton spectrum of menthone is strongly coupled at 300 MHz, but the use of selective reverse INEPT to enforce selective filtering through individual carbon-13 sites ensures that at least one of the one-bond carbon-13 satellites is weakly coupled for each proton. Traces (b) and (c) illustrate the point; protons 6 and 7 are very strongly coupled in the normal proton spectrum, but all four multiplets in the two satellite spectra are approximately first order. The lifting of the degeneracy between H6 and H7 allows the vicinal coupling across the isopropyl-ring linkage, to be measured, and also reveals a long

→  
Fig. 4. (a) 300 MHz proton spectrum and (b)–(e) selective reverse INEPT spectra of 28% menthone (Aldrich) in acetone- $d_6$ , measured using a 5 mm sample in the 10 mm broadband probe of a Varian Associates XL300 spectrometer using the sequence of fig. 1. The sample contains substantial quantities of isomenthone, seen clearly in the methyl region of trace (a). Spectra (b) to (e) used selective excitation of carbon sites 6, 7, 2 and 8, respectively, with delays  $2\tau$  of 3.85, 3.85, 1.92 and 1.54 ms. 32 transients were used for each trace; no spin lock pulses or  $180^\circ$  pulses were used. Traces (b) to (e) have a vertical scale  $1000\times$  that of trace (a). No homodecoupling was used during acquisition.



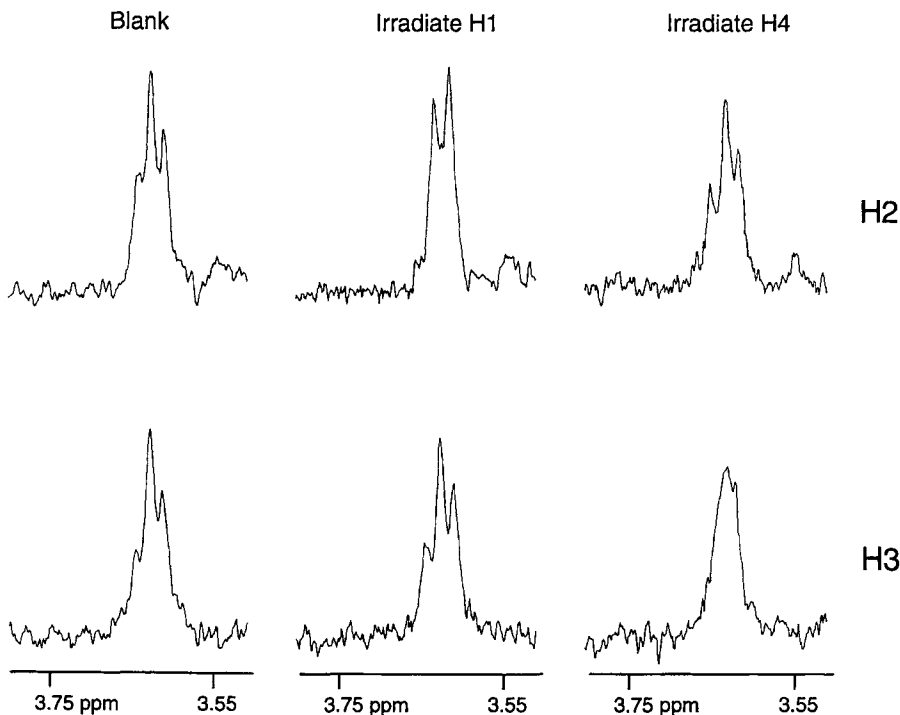


Fig. 5. Selective reverse INEPT spectra for the tigogenin glycoside **1**, using a 10% w/w solution in  $\text{dms}\text{-d}_6$ . A 5 mm inverse probe was used on a Varian Associates Unity 500 spectrometer. The sequence of fig. 1 was used to measure one-bond satellite spectra for the two carbon-13 sites known to be bonded to protons H2 and H3 of the branching glucose. Low field satellite multiplets are shown (left) without irradiation during data acquisition, and (centre and right) with time-shared homonuclear decoupling during acquisition of H1 and H4, respectively. 480 transients were recorded in 15 minutes for each of the 6 spectra. Quadrature spin lock pulses of 450  $\mu\text{s}$  were used following a preirradiation period of 1 s. A homospoil pulse of 8 ms duration was followed by a 12 ms recovery delay. Selective excitation used a DANTE train of 148 carbon pulses of 0.5  $\mu\text{s}$  width, with time-shared decoupling using 2.5  $\mu\text{s}$  pulses and a spectral width of 5 kHz.

range coupling of 1.2 Hz to H6. Frequently one satellite of a given proton is strongly coupled and one first order, as in trace 5(d) for methylene 2 of menthone: the high field satellites of both the protons are strongly coupled (as are the multiplets in the conventional proton spectrum), but the low field satellites are approximately first order.

The use of selective reverse INEPT with homonuclear decoupling is illustrated by fig. 5, which shows high field one-bond carbon-13 satellite spectra for protons H2 and H3 of the branching glucose of the pentasaccharide tigogenin glycoside **1** [18], 3-O-[[ $\beta$ -D-xylosyl(1  $\rightarrow$  3)] $\beta$ -D-xylosyl(1  $\rightarrow$  3)  $\beta$ -D-glucopyranosyl(1  $\rightarrow$  2)] $\beta$ -D-glucopyranosyl(1  $\rightarrow$

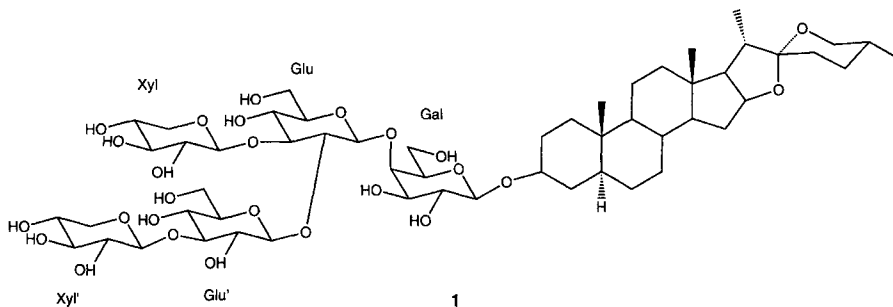


Fig. 6. Formula 1.

4)}}  $\beta$ -D-galactopyranosyl] (25R)-5 $\alpha$ -spirostan-3 $\beta$ -ol (see fig. 6). The usual 2D techniques of DQF COSY, TOCSY, HMQC and HMBC allow almost all of the proton and carbon resonances of **1** to be assigned. Unfortunately the relatively narrow range of proton chemical shifts in pyranose sugars, combined with the large trans diaxial coupling constants, makes strong coupling very common. The particular problem posed by the proton spectrum of **1** here is that the chemical shifts of protons H2 and H3 in the branching glucose are almost exactly degenerate. The chemical shifts of the carbons bound to protons H2 and H3 are known from the HMQC spectrum, and the sugars bound to these carbons can be identified from the long range couplings between the glucose ring carbons and the anomeric protons of the pendent sugars that are revealed by the HMBC spectrum. This leaves the problem of determining which of the two candidate carbons is bound to H2 and which to H3. The two protons are effectively indistinguishable in the normal spectrum, since the chemical shift difference is only about 0.002 ppm. In order to determine the sequence of coupled protons H1-H2-H3-H4 it is therefore necessary to lift the degeneracy by examining the proton spectra of isotopomers with carbon-13 in positions 2 and 3. Once H2 and H3 have been identified, the assignments of C2 and C3 follow from the HMQC data and hence the linkage pattern of the carbohydrate moiety of **1** can be established.

Selective excitation of the one-bond carbon-13 satellites corresponding to the two candidate carbon signals for C2 and C3 lifts the degeneracy, allowing a simple homonuclear decoupling experiment to be used to determine which of the protons is coupled to H1 and which to H4. Figure 3 shows for each of the two carbons the effect on the low field proton satellite of (left) no homonuclear decoupling; (centre) irradiating H1 during acquisition; and (right) irradiating H4. The collapse of the top centre and lower right multiplets shows clearly that the proton in the upper traces is H2 and that in the lower H3, establishing the assignments of the respective carbon-

13 signals and hence (through the long range couplings identified with the HMBC experiment) proving that C2 is linked to glucose and C3 to xylose.

#### 4. Discussion

The great majority of the structural questions that NMR is called upon to address can be tackled with a basic toolkit of perhaps a dozen one- and two-dimensional experiments. The challenge of making optimum use of scarce spectrometer time is to have the right experiments available for when the basic toolkit proves insufficient. The use of frequency selective experiments such as selective reverse INEPT allows simple questions about complex spin systems to be answered in a simple way, making good use of the available signal and hence minimizing demands on instrument time.

#### Acknowledgements

ICC thanks the EPSRC for a research studentship. The equipment used in this work was purchased with the aid of grants from the EPSRC and its predecessors, the University of Manchester, and the University of Manchester Institute of Science and Technology.

#### References

- [1] H. Kessler, S. Mronka and G. Gemmecker, *Magn. Reson. Chem.* **29** (1991) 527.
- [2] A. Bax, R.H. Griffey and B.L. Hawkins, *J. Magn. Reson.* **55** (1983) 301.
- [3] J. Stonehouse and J. Keeler, *J. Magn. Reson. Ser. A* **112** (1995) 43.
- [4] R.C. Crouch, R.B. McFadyen, S.M. Daluge and G.E. Martin, *Magn. Reson. Chem.* **28** (1990) 792.
- [5] D.M. Doddrell, D.T. Pegg and M.R. Bendall, *J. Magn. Reson.* **48** (1982) 323.
- [6] G.A. Morris and R. Freeman, *J. Am. Chem. Soc.* **10** (1979) 760.
- [7] G.A. Morris, *J. Am. Chem. Soc.* **102** (1980) 428.
- [8] O.W. Sørensen, S. Donstrup, H. Bildsøe and H.J. Jakobsen, *J. Magn. Reson.* **55** (1983) 347.
- [9] O.W. Sørensen, *Prog. NMR Spectrosc.* **21** (1989) 503.
- [10] R. Freeman, T.H. Mareci and G.A. Morris, *J. Magn. Reson.* **42** (1981) 341.
- [11] A.J. Shaka and R. Freeman, *J. Magn. Reson.* **50** (1982) 502.
- [12] T. Parella, F. Sanchez-Ferrando and A. Virgili, *J. Magn. Reson. Ser. A* **112** (1995) 106.
- [13] C. Emetarom, T.-L. Hwang, G. Mackin and A.J. Shaka, *J. Magn. Reson. Ser. A* **115** (1995) 137.
- [14] N.J. Sheppard and J.J. Turner, *Proc. R. Soc. London Ser. A* **252** (1959) 506.
- [15] S.R. Salman, R.D. Farrant, P.N. Sanderson and J.C. Lindon, *Magn. Reson. Chem.* **31** (1993) 585.
- [16] C.A.G. Haasnoot, F.A.M. De Leeuw and C. Altona, *Tetrahedron* **36** (1980) 2783.

- [17] C. Altona, R. Francke, R. De Haan, J.H. Ippel, G.J. Daalmans, A.J.A.W. Hoekzema and J. Van Wijk, *Magn. Reson. Chem.* **32** (1994) 670.
- [18] G. Pant, M.C. Purohit, G.A. Morris, A.G.W. Halstead and R.I.G. Thompson, *Magn. Reson. Chem.* **32** (1994) 213.

This Page Intentionally Left Blank

## chapter 5

---

# GROESY, Gradient-enhanced Selective 1D ROE Measurements

---

Pere Adell, Teodor Parella, Francisco Sánchez-Ferrando  
and Albert Virgili

*Departament de Química  
Universitat Autònoma de Barcelona  
08193 Bellaterra, Barcelona  
Catalonia, Spain*

This Page Intentionally Left Blank

## 1. Introduction

The quantitative measurement of homonuclear (interproton) Overhauser enhancements [1, 2] is usually a very important tool for the structure determination of organic molecules, in particular when dealing with stereochemical aspects such as configuration and conformation, due to the  $r^{-6}$  dependence of the enhancements.

$$\sigma_{ij}^{\text{NOE}} = \frac{\gamma^4 \hbar^2}{10r_{ij}^6} \left\{ \frac{6}{1 + 4w_0^2 \tau_c^2} - 1 \right\} \tau_c. \quad (1)$$

The simplest and most popular experimental method is the well known one-dimensional (1D) NOE difference procedure [3], which is very easily implemented in any spectrometer and which can be routinely set up even by novice spectrometer operators. However, this difference method is based on subtraction of the unperturbed spectrum from the NOE-containing one, both separately recorded, and therefore the required difference information contributes only a small part of the recorded signal. Furthermore, the difference spectrum is very sensitive to subtraction errors, as well as pulse imperfections or missettings, or other spectrometer instabilities, all of which often result in prominent phase distortions or other subtraction artifacts which prevent the accurate measurement of the desired NOE values. Therefore the reliable measurement (or even detection) of enhancements below 1% is not generally available using this difference method.

Two-dimensional methods, such as NOESY [4], can yield a wealth of NOE connectivities at once, by simple inspection of cross peaks and, in contrast with the 1D difference method, selective saturation of the target multiplet is not required. In addition, quantitative information can be obtained by integration of cross-peak volumes. Large, slow tumbling molecules such as proteins, with long correlation times  $\tau_c$ , give large, negative NOESY cross peaks, but small typical organic molecules, with much shorter correlation times  $\tau_c$ , usually give much smaller, positive NOESY peaks. In addition, the use of a single mixing time value (up to a few hundred milliseconds) in the NOESY sequence prevents the simultaneous achievement of the maximum NOE enhancements for all relaxation partners, in contrast

with the common situation in difference experiments, which are customarily obtained for organic compounds under saturation of the target multiplet for several seconds. As a result, 2D NOESY spectra of typical organic compounds show at most a few of the expected cross peaks, and quantitative measurements are not normally derived from such spectra.

Other 1D methods for measuring NOEs and relaxation rates use selective excitation [5]. For quantitative applications the transient NOE method [6] has been used for some time. In this method, the target multiplet is selectively inverted by means of a selective  $180^\circ$  pulse and, after a mixing time  $\tau_m$ , the analytical hard  $90^\circ$  pulse provides a measurement of the amount of NOE transferred during the mixing period from the inverted proton to each of its relaxation partners. The problem is that for highly selective, long  $180^\circ$  pulses, relaxation occurring during the pulse is no longer negligible. Therefore the results at short mixing times tend to be erratic, and relaxation rates (which are obtained from the initial slopes of the NOE vs.  $\tau_m$  plots) cannot be accurately measured in these cases.

Much better results are obtained using the 1D counterpart of NOESY [7]. In this method, after a first selective  $90^\circ$  pulse on the target multiplet, a fixed delay period is inserted in order to maximize in-phase transverse magnetization. A subsequent hard  $90^\circ$  pulse converts this maximized transverse magnetization into  $-z$  longitudinal magnetization, whose relaxation (now starting at the well defined time of the first hard pulse) is monitored after the mixing period  $\tau_m$  by the last hard  $90^\circ$  pulse, as before. Obviously, this 1D-NOESY method requires the same phase cycling procedures used for conventional 2D NOESY, and is therefore also based on difference spectroscopy, although in a more subtle way than the traditional 1D NOE difference method.

However, both NOE and NOESY experiments can fail for medium-sized molecules, in particular when using high field spectrometers, if their motional regime is close to the NOE null ( $\omega_0\tau_c \cong 1.12$ ; see eq. (1)).

The ROESY experiment [8] overcomes this problem by measuring cross-relaxation rates in the rotating frame. Their dependence on the correlation time,  $\tau_c$ , is now given by

$$\sigma_{ij}^{\text{ROE}} = \frac{\gamma^4 \hbar^2}{10r_{ij}^6} \left\{ \frac{3}{1 + \omega_0^2 \tau_c^2} + 2 \right\} \tau_c, \quad (2)$$

and therefore positive ROE enhancements are always observed for molecules of all sizes. In the conventional ROESY pulse sequence, after the initial  $90^\circ$  pulse which creates transverse magnetization, a spin-lock field is applied during the mixing time  $\tau_m$  in order to induce cross-relaxation in the rotating frame. However, if this spin-lock field is strong enough, it can also give rise to coherent magnetization transfer across  $J$ -coupled

spin networks, which would end up as TOCSY [9] peaks. Several types of spin-lock fields have been proposed to overcome these problems [10]. One of the most successful is T-ROESY [11], which effectively suppresses TOCSY contributions by using as the spin-locking field an on-resonance  $180^\circ(x)-180^\circ(-x)$  pulse train at moderately high power (i.e., bandwidth of a few kHz). Again, similarly to NOESY, there are 1D and 2D versions of the ROESY experiment using phase-cycling coherence selection.

## 2. Coherence selection using pulsed field gradients

The introduction of pulsed field gradients (PFGs) for coherence selection in high resolution NMR [12] as an alternative to conventional phase cycling [13] has suppressed many of the problems associated with difference spectroscopy in both 1D and 2D NMR, and has really opened up the way for 3D and 4D NMR measurements in reasonable spectrometer times. Gradients can conceivably be delivered from any direction in space, but most modern commercial spectrometers equipped for PFG work are usually limited to gradients in the  $z$ -axis direction. These can be delivered for rather short times (typically a few milliseconds), with a predefined shape (such as truncated Gaussian, for instance) and with peak amplitudes up to several Gauss per centimeter. The effect of a  $z$ -axis gradient of duration  $t_G$  and amplitude  $G_z$  (with its sign) on a coherence of order  $p$  (also with its sign) for a nucleus of gyromagnetic ratio  $\gamma$  would be to induce a dephasing,  $\Phi(z)$ , which would depend linearly on the  $z$  coordinate (i.e., position) of that particular nucleus according to

$$\Phi(z) = 2\pi p\gamma G_z t_G z. \quad (3)$$

Several such gradients  $G_i$ , all of equal duration, applied at different times in a particular pulse sequence would each contribute to the total dephasing of all coherence transfer pathways, except those for which  $\sum_i p_i \gamma_i G_i = 0$ , for which the cumulative dephasing would be null *at all positions*. These would be therefore selectively rephased at the end of the pulse sequence, while all others would remain permanently dephased and contribute nothing to the final detected signal. This is the basis of the use of pulsed field gradients for coherence selection. These gradient-selected spectra are usually artifact-free and can be obtained in dramatically short spectrometer times. For instance, since only the desired coherences reach the detector, 2D spectra can be obtained with a single scan per increment of  $t_1$ . In many cases solvent suppression is also very effectively achieved, thus improving the dynamic range. Virtually all known phase-cycled 1D, 2D and  $n$ D experiments, as well as their combinations, can be performed under gradient selection in much shorter total spectrometer time.

Combining selective excitation with PFG coherence selection yields gradient-enhanced 1D analogs of 2D experiments. Such a combination has been used for the accurate measurement of longitudinal NOEs by means of the GOESY experiment [14], a gradient-enhanced equivalent of the 1D-NOESY method referred to above. Ultra-high quality spectra are obtained with the GOESY method, because GOESY spectra show only the signals for the selectively perturbed proton (inverted) and that fraction of its relaxation partners which has indeed originated by cross relaxation. Therefore, without subtraction of any unperturbed spectrum, simple inspection of GOESY spectra shows directly the desired NOEs, which can thus be reliably observed even for values as small as 0.03% [14].

### 3. GROESY

We have developed GROESY [15], a gradient-selected version of the 1D-ROESY sequence, for the accurate measurement of cross-relaxation rates and Overhauser enhancements in the rotating frame. Gradient selection combined with T-ROESY spin lock ensure that only the target multiplet and the relevant Overhauser-enhanced signals will reach the detector, and therefore the receiver gain can be set to a high value, thus improving sensitivity. GROESY yields very clean, artifact-free one-dimensional spectra, very quickly obtained (typically less than five min. acquisition for a 50 mM

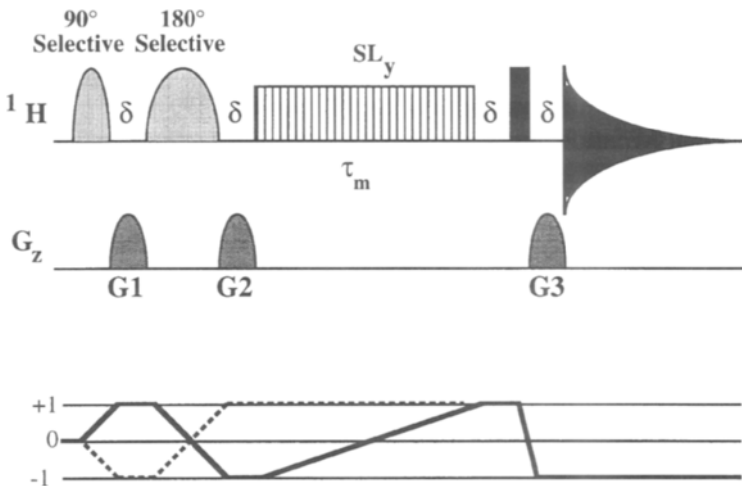


Fig. 1. Basic pulse sequence and CP diagram for gradient-based spin-locked 1D experiments. A  $1 : (-1) : 2$  gradient ratio selects N-type data (solid lines) while  $1 : (-1) : (-2)$  selects P-type data (dashed lines). When SL stands for a  $z$ -filtered DIPSI-2 pulse train, a ge-1D TOCSY is performed. On the other hand, when SL stands for a T-ROESY pulse train, a GROESY experiment is performed.  $\delta$  stands for the gradient length.

solution) without the need of a tedious and long phase-cycling procedure. GROESY spectra clearly display even very small Overhauser enhancements between protons separated up to 4 Å. Small indirect enhancements, which are normally not visible in conventional phase-cycled or transient NOE experiments, can be very clearly observed using moderately long mixing times.

The GROESY pulse sequence is shown in fig. 1. The 90° and 180° selective pulses are delivered on the target multiplet, which must be a well resolved one. The cluster  $G_1-180^\circ(\text{sel})-G_2$ , in which  $G_2 = -G_1$ , ensures dephasing of the magnetization of the selected spin, created by the first 90° selective pulse, and also avoids  $J$ -coupling evolution prior to the mixing period. Cross-relaxation occurs, under T-ROESY spin lock (SL), during the mixing period,  $\tau_m$ . The third gradient,  $G_3$ , rephases the effects of the first two gradients. Any chemical shift evolution during this third gradient is refocused by inserting a delay  $\delta$  (of duration equal to the gradient) and a 180° pulse prior to  $G_3$ . Such a chemical shift evolution, if present at the beginning of acquisition, would produce phase distortions in the resulting spectrum.  $N$ -type selection is achieved using a 1:(-1):2 gradient combination.

#### 4. Limitations

The advantages of GROESY have already been pointed out, and can be clearly appreciated in the quality of the spectra shown below. However, the method has also a certain number of limitations.

The hardware required for PFG work, although commercially available, is not usually included in the basic version of spectrometers. It consists of a gradient accessory, a gradient amplifier, a shielded probehead equipped with a  $z$ -gradient coil and a pulse shaper (which in itself is an integral part of the gradient accessory).

The target, i.e., the proton(s) selectively excited by the selective 90° and 180° pulses, must appear as a well resolved multiplet. From targets overlapping with other signals there is still a possibility to obtain clean GROESY spectra, using the so-called TORO (i.e., TOCSY-ROESY) method [16]. This requires a well resolved proton  $J$ -coupled to the overlapping target, and uses a selective optimized 1D-TOCSY transfer via  $J$ -coupling from the former to the target, followed by a selective 1D-ROESY from the latter, all under PFG coherence selection. Finally, if no coupling partner of the target appears as a well resolved multiplet, a gradient selected 2D-ROESY spectrum should still provide the desired Overhauser information.

In the presence of very strong coupling, i.e., protons displaying a large coupling constant with the target, TOCSY contributions might not be completely suppressed by a non optimized T-ROESY spin lock, and therefore

TOCSY peaks might appear in the GROESY spectrum as if truly due to cross-relaxation. This drawback can be corrected by means of a very careful calibration of the  $180^\circ$  pulses used for the T-ROESY spin-locking field.

Finally, due to the use of gradient coherence selection, approximately one half of the available signal is lost in GROESY spectra, in comparison with the conventional phase-cycled 1D-ROESY. However, the higher setting of the receiver gain and the far more tolerant stability requirements of GROESY result in final spectra of very high quality, which greatly compensates for this signal loss.

## 5. Experimental

As is the case in most gradient-enhanced pulse sequences, GROESY spectra should preferably be obtained with non-spinning samples. In our spectrometer, a Bruker ARX-400 equipped with an inverse broadband probehead incorporating a shielded Z-gradient coil, we have used the following experimental parameters:

- 1) The selective  $90^\circ$  and  $180^\circ$  pulses were of duration 20 and 40 ms, respectively, and shaped to a 5% truncated Gaussian.
- 2) The three gradients were all of 1 ms duration and shaped to a 5% truncated Gaussian. The peak amplitudes for  $G_1$ ,  $G_2$  and  $G_3$  were, respectively, 6,  $-6$  and 12 G/cm, approximately.
- 3) The T-ROESY SL field was achieved with an on-resonance  $180_x^\circ$ – $180_{-x}^\circ$  pulse train with an excitation bandwidth  $\gamma B_1/2\pi = 2.4$  kHz. We have used SL durations up to 600 ms.
- 4) A minimum two-step phase cycle was used by inverting the selective  $90^\circ$  pulse and the receiver phases on alternate scans. Exorcycle could also be applied on all  $180^\circ$  pulses.

Using these settings, we have been able to obtain very high quality GROESY spectra of reasonable amounts of substances (about 5–10 mg in 0.4–0.5 ml deuterated solvent) in less than ten minutes of spectrometer time. As shown below in several examples, these spectra allow the reliable measurement of very small Overhauser enhancements, both direct for two spins (i.e., positive) and indirect for three spins (i.e., negative). At least in one case, namely brucine [15], using a moderately long mixing time of 500 ms, we found a small but very clear positive four-spin indirect Overhauser enhancement, transmitted across two intermediate spins, which failed to appear when using other methods for the measurement of NOEs. This shows the usefulness of the GROESY method.

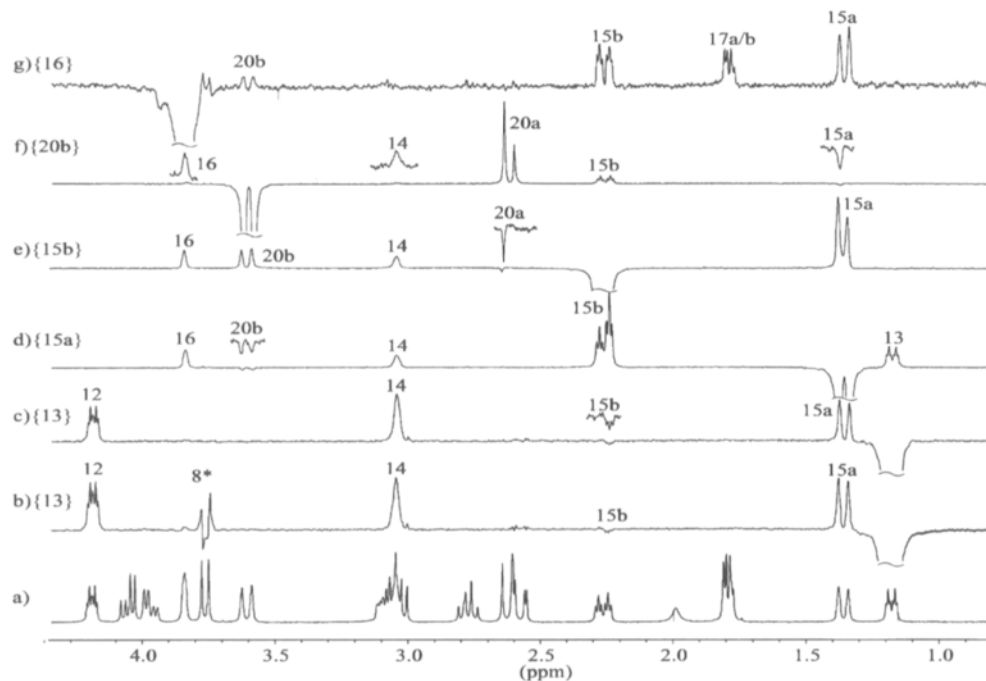


Fig. 2. GROESY spectra (aliphatic region) of strychnine, **1**, 50 mM in  $\text{CDCl}_3$ . (a) Normal spectrum; (b)–(g) GROESY spectra obtained by pulsing selectively the protons shown as {proton number} at the left part of each plot. Assignments shown on top of relevant peaks. Trace (b) was obtained using a non optimized setting for the  $180^\circ$  pulses of the T-ROESY spin-locking field, and displays a residual TOCSY signal for H-8 (starred), due to its high coupling constant with the target H-13 proton. Trace (c) was obtained after careful calibration of these  $180^\circ$  pulses, and shows perfect suppression of the residual H-8 TOCSY signal. All spectra were acquired in less than 5 min., using 128 scans, with the settings described in the Experimental section (see text).

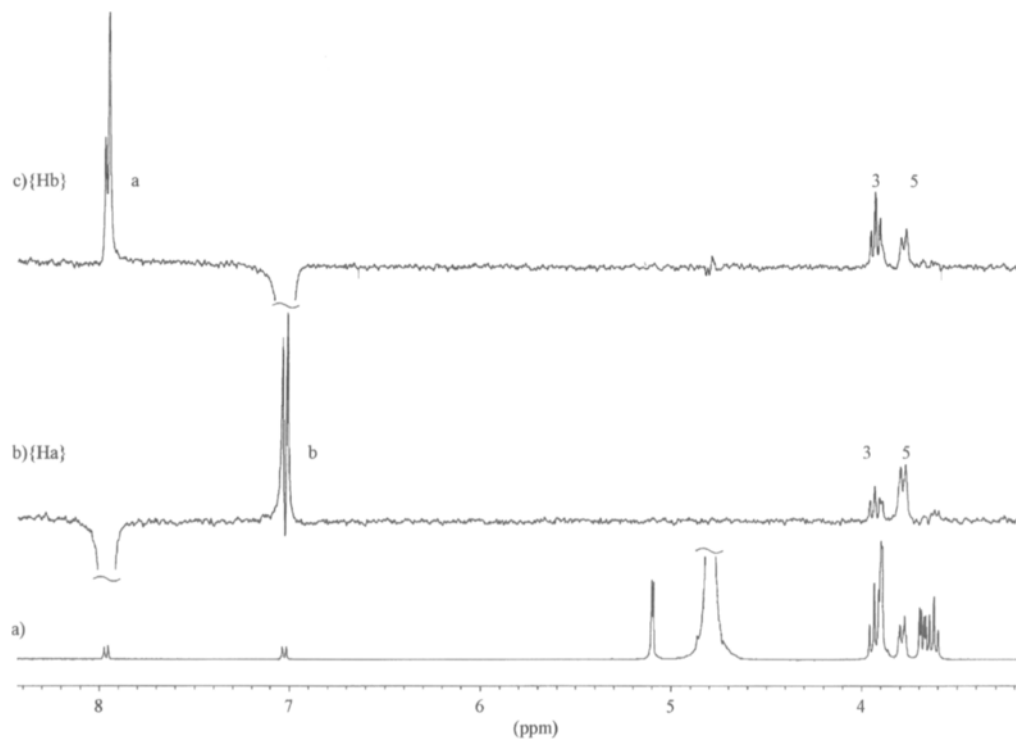


Fig. 3. GROESY spectra of the 1:1 inclusion complex of 4-hydroxybenzoic acid and  $\beta$ -cyclodextrin ( $\beta$ -CD), saturated solution in  $D_2O$ . (a): Normal spectrum; (b) and (c): GROESY spectra obtained after pulsing selectively the guest aromatic protons H-2 {Ha} and H-3 {Hb}, respectively. The inner H-3 and H-5 protons of  $\beta$ -CD are assigned on the traces. All spectra were acquired in about 40 min., using 1024 scans, with the settings described in the Experimental section (see text).

## 6. Examples

Figure 2 shows the aliphatic region of several GROESY spectra of a 50 mM sample of strychnine **1** in  $\text{CDCl}_3$ . All spectra were obtained with 128 scans, equivalent to less than 5 min. acquisition, using a SL mixing time of 600 ms. Both strong and weak Overhauser enhancements can be very easily observed, due to the high quality of the spectra. Thus trace (b), obtained by pulsing the H-13 proton, shows large positive enhancements for H-15a, H-14 and H-12, as well as a small indirect negative enhancement for H-15b (transferred via  $\text{H-13} \rightarrow \text{H-15a} \rightarrow \text{H-15b}$ ). The indirect nature of this enhancement is immediately evidenced by trace (d), in which perturbation of the H-15a proton results in a very large positive enhancement of the vicinal H-15b proton, as well as H-13, H-14 and H-16, and a sizeable indirect negative enhancement of H-20b (transferred via  $\text{H-15a} \rightarrow \text{H-15b} \rightarrow \text{H-20b}$ ). The trace with a smaller signal to noise ratio is trace (g), in which the relatively isolated H-16 proton was selected. However, clear positive enhancements can still be seen in trace (g) for protons H-15a, H-15b and H-17, as well as a smaller one on H-20b.

Trace (b) (fig. 2) also shows a prominent TOCSY peak for H-8, because of its very strong coupling with the antiperiplanar perturbed H-13 proton. This TOCSY peak could be filtered out by means of a very careful calibration of the  $180^\circ$  pulses used for the T-ROESY spin-locking field, as shown in trace (c).

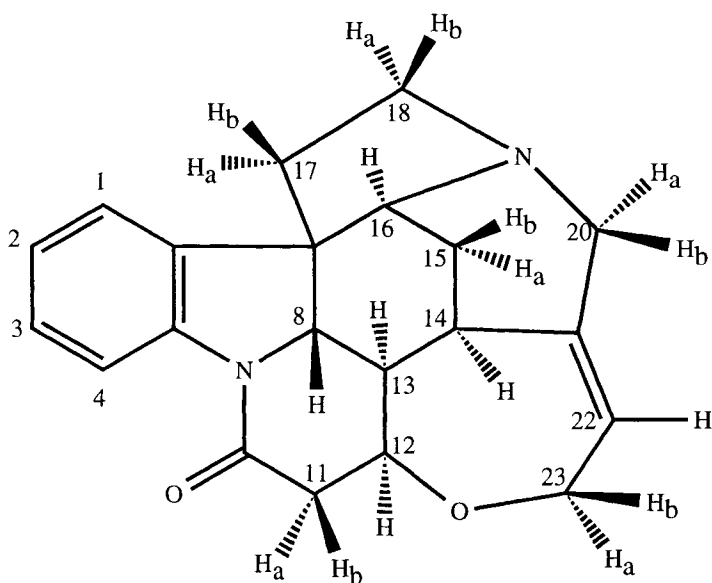


Fig. 4. Strychnine structure and numbering.

Figure 3 shows GROESY spectra of a D<sub>2</sub>O solution of the 1 : 1 inclusion complex of 4-hydroxybenzoic acid in  $\beta$ -cyclodextrin ( $\beta$ -CD). It must be recalled that cyclodextrins, owing to their high molecular weight, often lie close to the NOE-null motional regime, particularly in the less mobile solvents such as water. Thus, NOE determinations could easily fail in these cases, while ROESY enhancements, being always positive, should be easily measured. Therefore, GROESY is the method of choice for these medium-sized molecules.

The GROESY spectra shown in fig. 3 confirm fully the inner nature of the host-guest complex, because pulsing at any of the aromatic protons of the guest results in clear enhancements of the inner H-3 and H-5 protons of the host, but not at the remaining outer protons of  $\beta$ -CD. The perfect suppression of any residual HDO signal is also noteworthy.

## 7. Conclusion

The combination of selective excitation with pulsed field gradients for coherence selection has greatly simplified the design, testing and implementation of new pulse sequences producing cleaner and faster spectroscopic measurements. GROESY is one of the archetypal members of this new generation of NMR experiments which can produce in just a few minutes the results that a few years ago used to take painful hours to obtain. Undoubtedly, using these and other experimental breakthroughs, the NMR community will still produce many additional methodologies to improve the quality and information contents of their spectra.

## Acknowledgements

Financial support for this research was provided by DGICYT (Projects PB92-0630 and PB95-0636) and CIRIT-CICYT (Project QFN93-4427), and is gratefully acknowledged. P.A. thanks the Generalitat de Catalunya for a grant. We also thank the Servei de Ressonància Magnètica Nuclear, Universitat Autònoma de Barcelona, for allocating instrument time to this project.

## References

- [1] J.H. Noggle and R.E. Schirmer, *The Nuclear Overhauser Effect* (Academic Press, New York, 1971).
- [2] D. Neuhaus and M.P. Williamson, *The Nuclear Overhauser Effect in Structural and Conformational Analysis* (VCH, Weinheim, 1989).
- [3] J.K.M. Sanders and J.D. Mersh, *Prog. Nucl. Magn. Reson. Spectrosc.* **15** (1982) 353.
- [4] G. Wider, S. Macura, A. Kumar, R.R. Ernst and K. Wüthrich, *J. Magn. Re-*

- son. **56** (1984) 207.
- [5] R. Freeman, *Chem. Rev.* **91** (1991) 1397;  
J. Keeler, in: *Multinuclear Magnetic Resonance in Liquids and Solids – Chemical Applications*, NATO ASI Series C, Vol. 322, eds P. Granger and R.K. Harris (Kluwer, Dordrecht, 1990), p. 201.
- [6] M.P. Williamson and D. Neuhaus, *J. Magn. Reson.* **72** (1987) 369.
- [7] H. Kessler, H. Oschkinat, C. Griesinger and W. Bermel, *J. Magn. Reson.* **70** (1986) 106.
- [8] A. Bax and D.G. Davis, *J. Magn. Reson.* **63** (1985) 207.
- [9] L. Braunschweiler and R.R. Ernst, *J. Magn. Reson.* **53** (1983) 521;  
D.G. Davis and A. Bax, *J. Am. Chem. Soc.* **107** (1985) 2821.
- [10] C. Griesinger and R.R. Ernst, *J. Magn. Reson.* **75** (1987) 261;  
J. Cavanagh and J. Keeler, *J. Magn. Reson.* **80** (1988) 186;  
A. Bax, *J. Magn. Reson.* **78** (1988) 134;  
M. Rance and J. Cavanagh, *J. Magn. Reson.* **87** (1990) 363;  
H. Desveux, P. Berthault, N. Birli-  
rakis and M. Goldman, *J. Magn. Reson. A* **108** (1994) 219.
- [11] T.L. Hwang and A.J. Shaka, *J. Am. Chem. Soc.* **114** (1992) 3157;  
T.L. Hwang, M. Kadkhodaei, A. Mohebbi and A.J. Shaka, *Magn. Reson. Chem.* **30** (1992) S24;  
T.L. Hwang and A.J. Shaka, *J. Magn. Reson. B* **102** (1993) 155.
- [12] J. Keeler, R.T. Cloves, A.L. Davies and E.D. Laue, in: *Methods in Enzymology*, Vol. 239, eds T.L. James and N. Oppenheimer (Academic Press, San Diego, 1994), p. 145.
- [13] J. Keeler, in: *Multinuclear Magnetic Resonance in Liquids and Solids – Chemical Applications*, NATO ASI Series C, Vol. 322, eds P. Granger and R.K. Harris, (Kluwer, Dordrecht, 1990), p. 103.
- [14] J. Stonehouse, P. Adell, J. Keeler and A.J. Shaka, *J. Am. Chem. Soc.* **116** (1994) 6037.
- [15] P. Adell, T. Parella, F. Sánchez-Ferrando and A. Virgili, *J. Magn. Reson. B* **108** (1995) 77.
- [16] P. Adell, T. Parella, F. Sánchez-Ferrando and A. Virgili, *J. Magn. Reson. A* **113** (1995) 124.

This Page Intentionally Left Blank

## chapter 6

---

# The DANTE-Z Experiment

---

D. Canet

*Laboratoire de Méthodologie RMN  
(URA CNRS 406 – LESOC; FU CNRS E008 – INCM)  
Université Henri Poincaré, Nancy 1, B.P. 239  
54506 Vandoeuvre les Nancy Cedex  
France*

C. Roumestand

*Centre de Biochimie Structurale  
(UMR CNRS 9955 – U 414 INSERM/Université de Montpellier I)  
15 Avenue Charles Flahault  
34060 Montpellier Cedex  
France*

This Page Intentionally Left Blank

Selectivity has become one of the experimental procedures routinely used by the NMR spectroscopist [1, 2]. Its objective is to reduce the measuring time with 1D counterparts of 2D (or  $n$ D) experiments or to improve the spectral resolution in these latter experiments. Selectivity is usually achieved by a soft pulse or alternatively by a train of hard pulses of small flip angle (the DANTE experiment [3]). Both approaches are equivalent provided that the amplitude modulation of the soft pulse is implemented in the DANTE train through a modulation of pulse durations [4]. However, the simplest soft pulse, i.e., rectangularly shaped (or the equivalent DANTE train with pulses of identical durations) exhibits unwanted sinc oscillations on each side of the selected region with in addition a strong dispersive component. Both these drawbacks can be circumvented by the DANTE-Z variant [5], this experiment relying on the selective profile of the  $z$  magnetization component. As compared with the profiles of the transverse components, the one of longitudinal magnetization possesses the unique feature of much reduced sidelobes and, obviously, does not involve any disturbance from the other components of magnetization (fig. 1). In order to take full advantage of the  $z$  component profile (shown at the bottom of fig. 1), one must subtract it from a profile corresponding to the equilibrium magnetization and perfectly flat over the frequency zone of interest. This is achieved by the following basic phase cycle

$$[(\theta)_{x-\tau}-(\theta)_{\pm x-\tau}]_n(\pi/2)(Acq)_{\pm}, \quad (1)$$

where  $\theta$  stands for a pulse of small flip angle with  $2n\theta = \pi$ ,  $\tau$  being the classical precession interval of the DANTE sequence, and where the  $(\pi/2)$  pulse converts the longitudinal magnetization into transverse magnetization. The first step is just a standard DANTE inverting train whereas the second step leaves essentially the longitudinal magnetization at its equilibrium value over the frequency range of interest. Subtraction of these two results yields consequently a transverse magnetization whose profile reflects the one shown in the bottom of fig. 1. However, the DANTE trains generate unwanted dispersive components which can be eliminated by two further phase steps. The complete phase cycling is given in table 1, in accordance with the notations of the general DANTE-Z sequence given below

$$[(\theta)_{\varphi_1-\tau}-(\theta)_{\varphi_2-\tau}]_n(\pi/2)_{\varphi_3}(Acq)_{\varphi_4}. \quad (2)$$

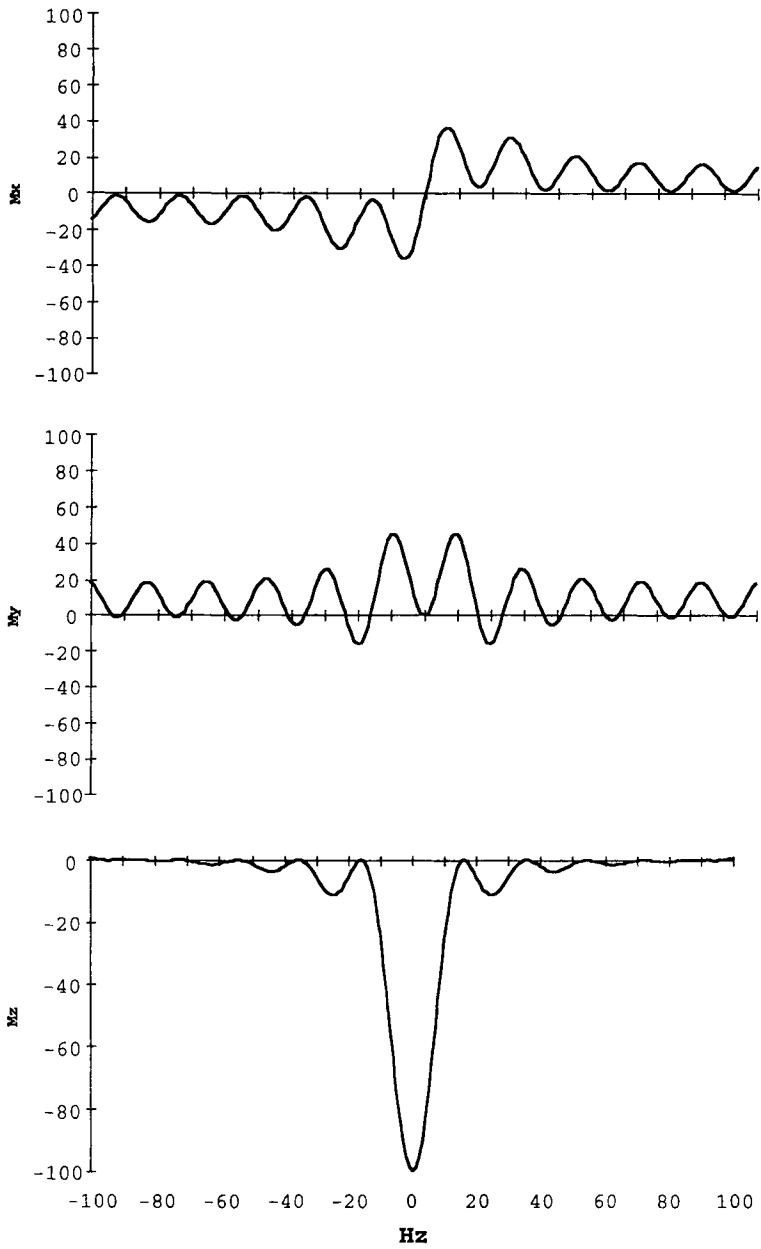


Fig. 1. A comparison of the profiles relative to the three components of magnetization after application of an inverting DANTE pulse train.

TABLE 1  
The four-step phase cycle  
of the DANTE-Z sequence.

$\varphi_1$	$\varphi_2$	$\varphi_3$	$\varphi_4$
$x$	$x$	$x$	$+$
$x$	$-x$	$x$	$-$
$x$	$x$	$-x$	$-$
$x$	$-x$	$-x$	$+$

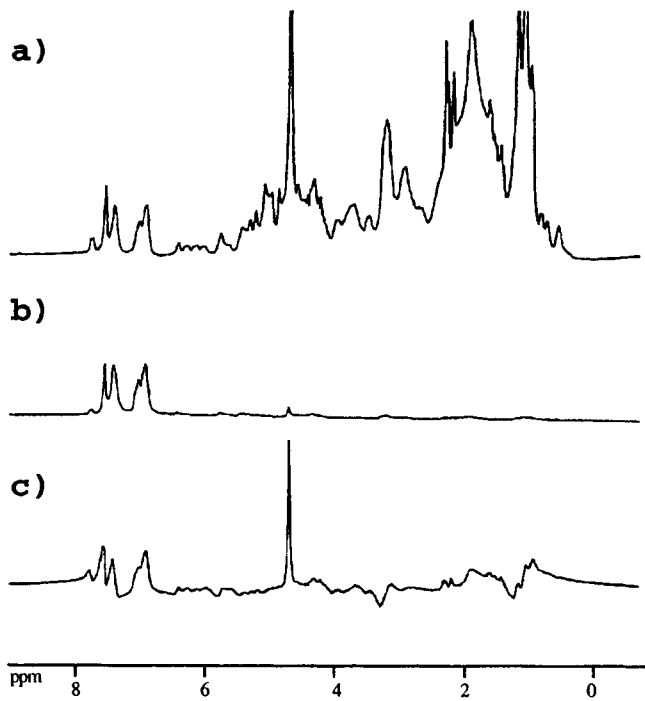
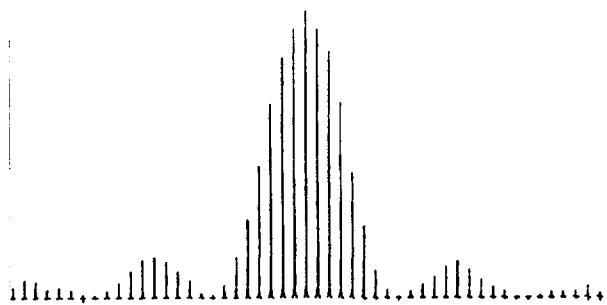
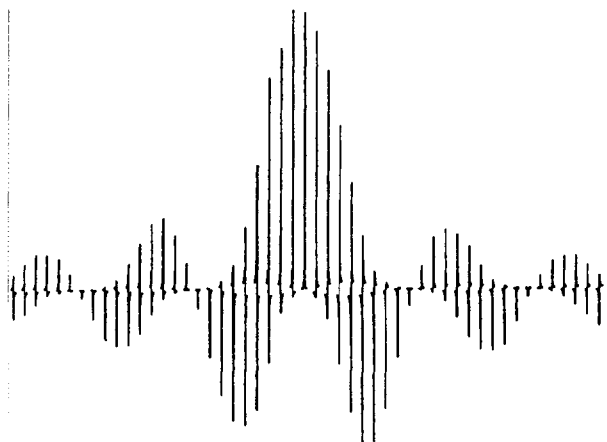
First of all, a four-step phase cycle may appear excessive. Fortunately, the two additional steps can be omitted by means of the application of a  $B_0$  gradient pulse prior to the  $\pi/2$  pulse [6], which has the virtue of defocusing unwanted dispersive components. Secondly, it remains the problem of unwanted (negative) excitations at frequencies equal to  $(2k + 1)/2\tau$  ( $k$  being an integer); those are specific of the DANTE-Z pulse train, since the classical DANTE train involves only positive sidebands at frequencies equal to  $k/\tau$ . Again, these negative sidebands can be canceled by a simple modification of the DANTE-Z sequence [6] which becomes

$$[(\theta)_x(\theta)_{\pm x-\tau}]_n(g_0)(\pi/2)_x(Acq)_{\pm}, \quad (3)$$

where  $(g_0)$  stands for a  $B_0$  gradient pulse, according to the above proposed procedure for limiting the number of phase cycling steps. As a consequence, eq. (3) represents the most efficient and simple version of the DANTE-Z sequence. However, because selectivity is ultimately governed by the total duration of the pulse train, and because the  $\tau$  value is dictated by the frequency of the first positive side-band (inherent to the classical DANTE pulse train),  $n$  must be multiplied by two and concomitantly each pulse length must be divided by two. This has to be done in order to obtain a selectivity identical to that of the original sequence.

The DANTE-Z sequence has been employed successfully as a 1D substitute in pseudo 3D experiments [7] and also as a “band-selective” technique in multidimensional experiments [8] in order to improve the spectral resolution. The efficiency of the DANTE-Z procedure over the simple DANTE sequence is illustrated by the spectra shown in fig. 2.

The quality of the profile pertaining to the selected region can be improved by a modulation of the pulse lengths within the pulse train, which mimics the amplitude modulation of a simple soft pulse [8]. Simple modulation schemes can be devised for attenuating or even suppressing the side-lobes in the vicinity of the selected region (as shown in fig. 3). Alternatively, more elaborated modulation schemes as those of the BURP family [9] can be run in the DANTE-Z mode [10]. This mode actually offers a



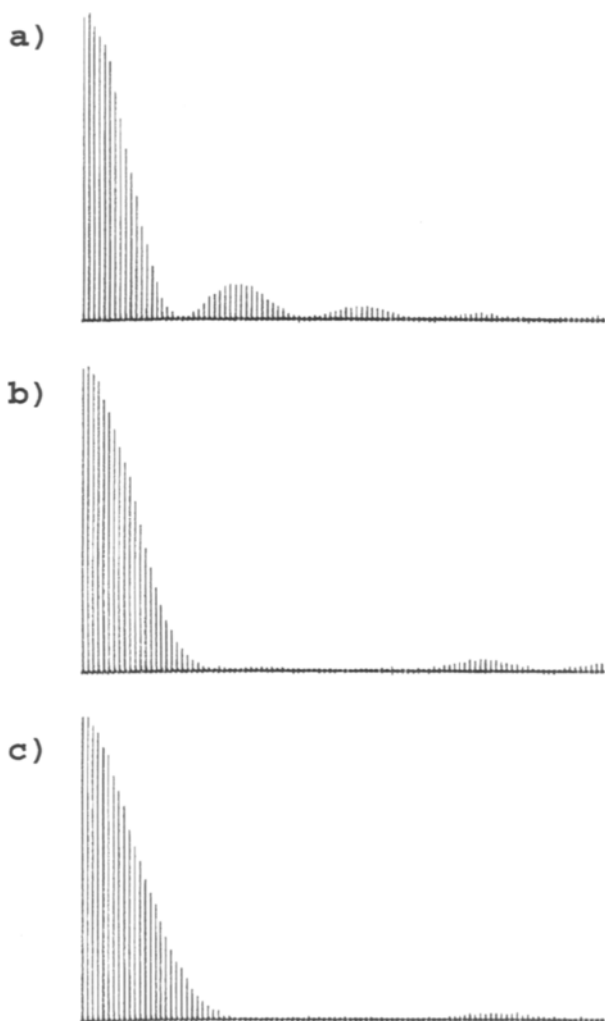


Fig. 3. Experimental profiles (same experimental setting as in fig. 2) (a) of the basic DANTE-Z sequence, (b) of DAZ 363, (c) of DAZ 22622 (the actual modulation schemes of DAZ 363 and DAZ 22622 can be found in ref. [7]).

←

Fig. 2. Left: Experimental profiles of the conventional DANTE sequence (top) and of the DANTE-Z sequence (bottom). The sample used was 5% H<sub>2</sub>O in D<sub>2</sub>O with a tiny amount of copper sulfate added (leading to a  $T_1$  of approximately 3 s). The different traces were obtained by shifting the carrier frequency in 50 Hz steps without readjustment of the spectrometer phase. For each experiment, four scans were acquired in order to perform the complete phase cycling of DANTE-Z. Right: (a) The conventional <sup>1</sup>H spectrum of a small protein (toxin  $\gamma$ :60 residues) in D<sub>2</sub>O at 318 K; (b) selection of the aromatic region by the conventional DANTE sequence; (c) same as (b) using the DANTE-Z procedure. Experiments were performed at 200 MHz using a “routine” AC200 Bruker spectrometer.

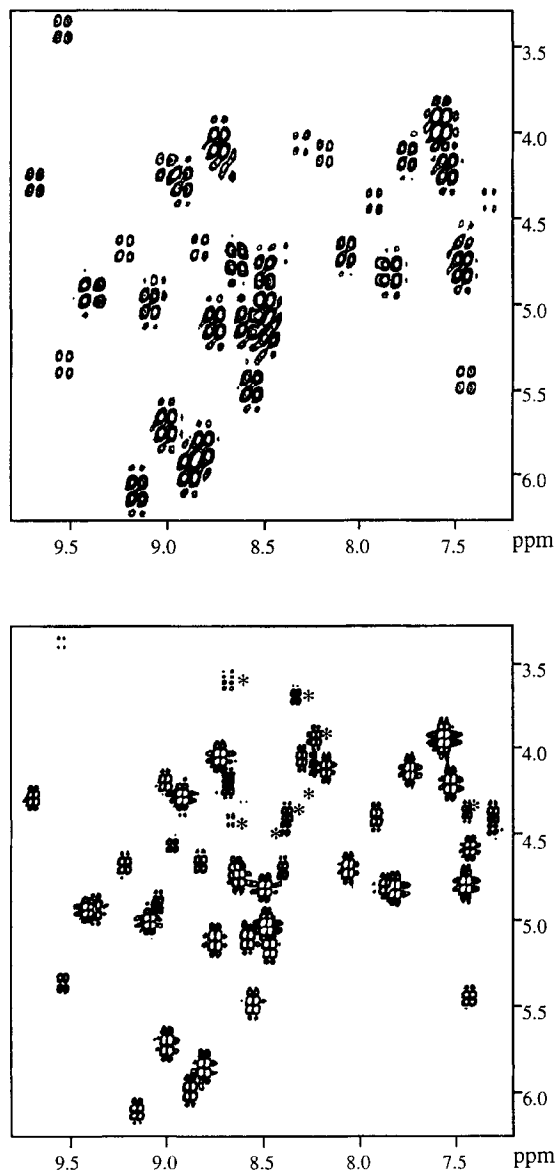


Fig. 4. Bottom: the Double-Band-Filtered COSY spectrum obtained by selection through DANTE-Z of the  $H_{\alpha}$  region (prior to the evolution interval) and by the selection through SPIN-PINGING [11] of the amide region (before the acquisition interval) of toxin  $\gamma$ . Top: the corresponding region of a standard COSY spectrum. Note, in the bottom diagram, the considerable increase in spectral resolution as well as the occurrence of additional cross-peaks (indicated with asterisks). Experiments were performed at 360 MHz (Bruker AMX360) in  $H_2O$  at 318 K. The 50 W "class C" amplifier of the proton channel was used as transmitter.

much more convenient way of setting the instrumental parameters of the sequence; the tedious calibration of BURP soft pulses reduces to the calibration of a  $90^\circ$  hard pulse [10]. The benefit of DANTE-Z is exemplified by the two-dimensional diagrams of fig. 4.

Finally, it can be mentioned that the ideas underlying the DANTE-Z methodology are closely related to the SPIN-PINGING sequence [11], in which the starting configuration is transverse magnetization. Both methods yield roughly the same results and present the same advantages. However, as far as the effects of relaxation phenomena are concerned, the DANTE-Z sequence appears to be slightly in favor [10].

## References

- [1] R. Freeman, *Chem. Rev.* **91** (1991) 1397.
- [2] H. Kessler, S. Mronka and G. Gemmecker, *Magn. Reson. Chem.* **29** (1991) 527.
- [3] G.A. Morris and R. Freeman, *J. Magn. Reson.* **29** (1978) 433.
- [4] J. Friedrich, S. Davies and R. Freeman, *J. Magn. Reson.* **75** (1987) 390.
- [5] D. Boudot, D. Canet, J. Brondeau and J.-C. Boubel, *J. Magn. Reson.* **83** (1989) 428.
- [6] C. Roumestand and D. Canet, *J. Magn. Reson. B* **106** (1995) 68.
- [7] D. Boudot, C. Roumestand, F. Toma and D. Canet, *J. Magn. Reson.* **90** (1990) 221.
- [8] C. Roumestand, D. Canet, N. Mahieu and F. Toma, *J. Magn. Reson. A* **106** (1994) 168.
- [9] H. Geen and R. Freeman, *J. Magn. Reson.* **93** (1991) 93.
- [10] C. Roumestand, J. Mispelter, C. Austruy and D. Canet, *J. Magn. Reson. B* **109** (1995) 153.
- [11] P. Xu, X.-L. Wu and R. Freeman, *J. Magn. Reson.* **83** (1989) 404.

This Page Intentionally Left Blank

## chapter 7

---

# One-Dimensional TOCSY and Related 1D Techniques

---

Tuck C. Wong

*Department of Chemistry*  
*University of Missouri*  
*Columbia, MO 65211*  
*USA*

This Page Intentionally Left Blank

## 1. Introduction

In the past two decades, numerous two-dimensional (2D) and multi-dimensional NMR techniques have been developed for the determination of homonuclear and heteronuclear spin correlations and the measurement of spin–spin coupling constants [1]. In many cases, especially for medium size molecules, many selective one-dimensional (1D) experiments enjoy distinct advantages over their 2D counterparts, when only a limited amount of correlation information is needed. The advantages include the much reduced experimental and data processing time, and reduced data storage requirements. One can also use substantially increased digital resolution over the corresponding 2D experiments. This is particularly important for samples where there are severely crowded spectral regions, and for the precise measurement of coupling constants.

In this chapter, the discussion will be focused on the 1D TOCSY (Total Correlation Spectroscopy) [2] experiment, which, together with 1D NOESY, is probably the most frequently and routinely used selective 1D experiment for elucidating the spin–spin coupling network, and obtaining homonuclear coupling constants. We will first review the development of this technique and the essential features of the pulse sequence. In the second section, we will discuss the practical aspects of this experiment, including the choice of the selective<sup>1</sup> (shaped) pulse, the phase difference of the hard and soft pulses, and the use of the *z*-filter. The application of the 1D TOCSY pulse sequence will be illustrated by examples in oligosaccharides, peptides and mixtures in Section 3. Finally, modifications and extensions of the basic 1D TOCSY experiment and their applications will be reviewed briefly in Section 4.

---

<sup>1</sup> The selective excitation is referred to alternatively as “semi-selective excitation”, e.g., in refs [5, 6]. It is semi-selective in the sense that for the 1D TOCSY experiment, the whole multiplet corresponding to a spin, rather than a component of the multiplet, is selectively excited. In this chapter, we will not make this distinction, and the term “selective” is used instead in this context.

## 2. Experimental/methodology

### 2.1. The pulse sequence

The pulse sequence for 1D TOCSY is a 1D modification of the original TOCSY experiment [2] introduced by Braunschweiler and Ernst. The TOCSY experiment was also referred to as HOHAHA (which stands for HOMonuclear HArtman-HAHn) by Bax and Davis [3]. The 1D TOCSY experiment was proposed by Bax and co-workers [4, 5], and by Kessler et al. [6]. The essential features of the pulse sequence involve the use of selective excitation of a desired resonance, followed by a homonuclear Hartman–Hahn (or isotropic) mixing period [2, 7]. That is, the unit  $P_{\text{nonselect}} - t_1$  in the 2D TOCSY pulse sequence is replaced by  $P_{\text{select}} - \tau$ , where  $P$  stands for a pulse (or pulses),  $t_1$  is the evolution period in the 2D experiment and  $\tau$  is a fixed delay.

Since most of the applications of the 1D TOCSY technique to date did not utilize pulsed field gradients (PFG) in the pulse sequence, we will discuss the non-gradient versions of the 1D TOCSY pulse sequence in more detail. The PFG versions will be briefly discussed in Section 4. In the Bax version of the pulse sequence [4, 5], the selective excitation is achieved by a selective  $180^\circ$  pulse followed immediately by a nonselective  $90^\circ$  pulse to create the transverse magnetization. The difference free induction decay (FID) is then obtained from the FID with the selective  $180^\circ$  pulse on-resonance minus the FID obtained with the selective excitation off-resonance (or with the selective  $180^\circ$  pulse turned off). In the Kessler version of the pulse sequence [6], a selective  $90^\circ$  or  $270^\circ$  pulse is used instead to create the transverse magnetization for the desired spin. Thus, there is no need to acquire a difference FID. Both versions of the pulse sequence are shown in fig. 1. For the isotropic (or Hartman–Hahn) mixing, the MLEV17 sequence [7, 8] is the most frequent choice [4, 5]. Other composite decoupling pulses (CPD), such as WALTZ17 [9] and DIPSI [10], have also been used. The MLEV17 mixing period is sandwiched between two trim pulses,  $T$ , typically of about 2–3 ms in duration. The trim pulses are used to capture the in-phase magnetization and to dephase the dispersive components.

The magnetization transfer in the TOCSY experiment involves the in-phase magnetization (as opposed to anti-phase magnetization such as in COSY). When a  $90^\circ$  Gaussian pulse is used for selective excitation, a delay period  $\tau$ , such that  $\tau + P/2 = 1/J$  (where  $P$  is the length of the Gaussian pulse), is sometimes added between the selective pulse and the isotropic mixing period to refocus the in-phase magnetization (for doublets) which has been converted to anti-phase magnetization at the end of the relatively long selective pulse. However, losses due to spin–spin relaxation during this delay and the difficulty in refocusing due to many other small couplings may make it undesirable to use such a delay. In practice, the duration of

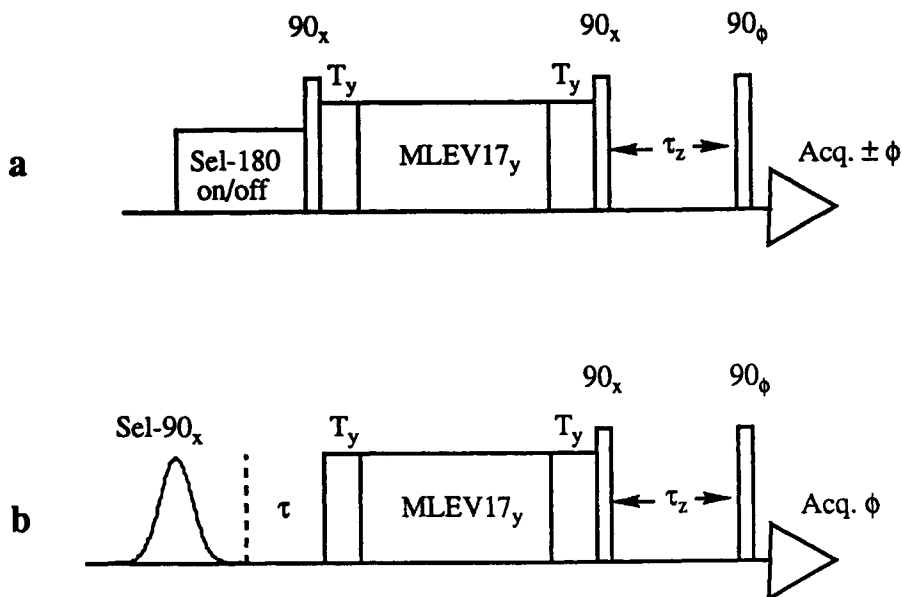


Fig. 1. The 1D TOCSY pulse sequence. (a) The Bax version; and (b) The Kessler version. The phase  $\phi$  for the last  $90^\circ$  pulse and the receiver is rotated synchronously along the four axes.

this delay should be optimized to give the best signals in each experiment. It is our experience that a short delay (in  $\mu\text{s}$ ) or no delay gives optimal signals in most cases.

In the 1D TOCSY experiment, usually a well-resolved signal is excited by the selective pulse, and then the magnetization will propagate during the isotropic mixing period through the spin coupling network, by direct coupling and by multiple step relays. By selectively exciting appropriately chosen signals, subspectra of the original complex spectrum corresponding to isolated spin subsystems in the molecule can be obtained. The subspectrum resembles a cross section through the corresponding 2D TOCSY spectrum, but usually with much improved digital resolution. The concept of subspectrum is most convenient for molecules such as peptides and oligosaccharides where spins (protons) from each amino acid or sugar residue form such an isolated spin system and are thus represented by such a subspectrum.

Homonuclear coupling constants can also be determined from these subspectra with good digital resolution and relative free of overlap of signals.

## 2.2. The choice of selective pulses

The soft (selective) pulse used for the selective excitation is usually either a Gaussian pulse [11], a purged half-Gaussian pulse (a half Gaussian pulse

followed by a hard  $90^\circ$  pulse which is  $90^\circ$  phase-shifted) [12], or a DANTE pulse train [13]. These shaped pulses or the DANTE pulse train can nowadays be easily generated in most of the modern spectrometers. The DANTE pulses do not require pulse shaping capabilities, and can thus be generated even in older spectrometers. The shaped pulses can be generated through a pulse shaping unit, generally referred to as the waveform generation unit or the waveform memory unit. Alternatively, these shaped pulses can also be generated by using a fast-switching linear attenuator to modulate the rf amplitude. When Gaussian shaped pulses are used for this purpose, the  $90^\circ$  pulse length is typically about 50–100 ms, depending on the selectivity desired. If the power level of the transmitter cannot be attenuated sufficiently to provide a  $90^\circ$  pulse long enough to fall in the 50–100 ms range, a  $270^\circ$  Gaussian pulse can be used instead to improve the selectivity. In addition, it has been shown that the self-refocusing (of the evolutions due to chemical shifts and  $J$  couplings) effects of the  $270^\circ$  Gaussian pulse improve the phasing properties of the multiplets and consequently it is easier to phase the resultant spectrum [14]. Thus, it was suggested that a  $270^\circ$  Gaussian pulse is preferred over a  $90^\circ$  Gaussian pulse of the same pulse length in 1D TOCSY and in other 1D selective techniques [14]. In our laboratory, a  $270^\circ$  Gaussian pulse of about 100 ms instead of a  $90^\circ$  Gaussian pulse is routinely used for this experiment. Extensive reviews of the various selective pulses for this and other selective techniques are available elsewhere [15].

When using the waveform generator to create the shaped pulses, the truncation level should be kept low to reduce the spurious excitation due to the discontinuity. Usually, a 1% truncation level (compared to the maximum amplitude of the shaped pulse) is recommended and is generally used.

The phase difference between the soft (selective) pulse and the hard (non-selective) pulse should also be determined and explicitly incorporated into the phases of the hard pulses in the pulse program. The phase difference can be determined by taking regular spectra of the actual sample using the hard pulse and the soft pulse, respectively. The on-resonance signal is phased to absorption mode by using the zero order phase correction only. The difference in the zero order phase corrections between these two spectra is the phase difference between the selective and the non-selective pulses. It should be noted that this phase difference changes with the change of sample or the pulse shape, and needs to be determined in each case.

The length of the MLEV17 mixing period usually ranges from 20 ms to as long as ca. 300 ms. The required length of the mixing period obviously depends on the magnitude of the  $J$  coupling and on the number of steps for the propagation of spin–spin coupling correlations through the coupling network. At short mixing times ( $\leq$  ca. 30 ms), only correlations due to a single step of propagation and relatively large spin–spin coupling are revealed. At longer mixing times, correlations due to small couplings and those due to

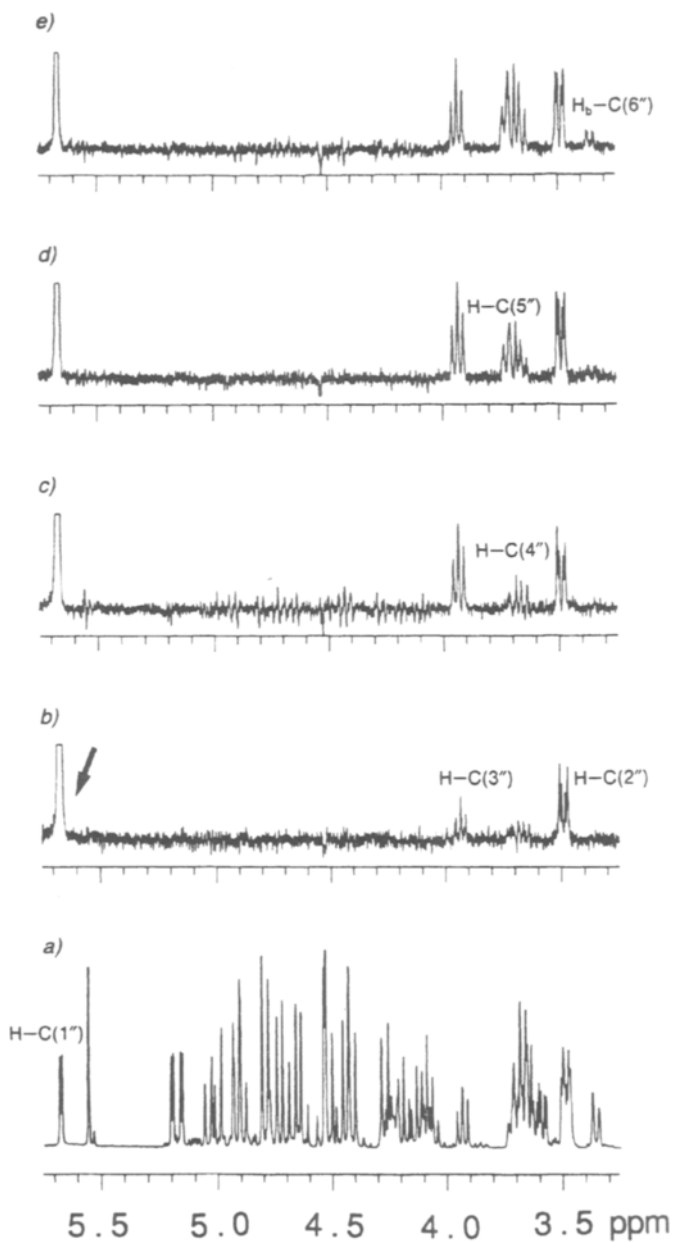


Fig. 2. (a) 400 MHz partial  $^1\text{H}$  spectrum of a trisaccharide in  $\text{CDCl}_3$ . (b)–(e) 1D TOCSY difference spectra with selective inversion of  $\text{H}_{1''}$  by a DANTE pulse train, and mixing times of 30, 60, 120 and 180 ms, respectively.  $10\tau_z$  values (of 16 scans each) were used for the  $z$ -filter. (Reproduced with permission from Wessel et al. [26a]. Copyright 1991 Verlag Helvetica Chimica Acta AG)

multi-step propagation will appear. Thus, by systematically increasing the mixing time in a series of 1D TOCSY experiments, the propagation of the correlations and thus the sequential connectivities in a coupling network can be completely deciphered. While it is also conceivable to perform 2D TOCSY at a number of mixing times, the reduced experimental time in the 1D version makes this procedure much more viable. This procedure is frequently not needed in, e.g., peptides where the distinction between  $\alpha$ ,  $\beta$  and  $\gamma$  spin etc. is usually relatively clear. Thus a single 1D TOCSY subspectrum obtained at a long mixing time ( $> 100$  ms) can usually reveal all the spins and their assignments in the coupling network (an amino-acid residue). It is, however, quite indispensable for assignments in carbohydrates and steroids, where the spins cannot be readily identified based on chemical shift considerations alone, and the sequential connectivity information is highly valuable in supplementing the “total correlation” spectra for unambiguous assignment. In fig. 2 such an application of the sequential connectivities to an oligosaccharide is demonstrated [26a].

### 2.3. *The use of the z-filter*

A  $z$ -filter [16, 17], which consists of two  $90^\circ$  pulses separated by a randomly varied delay  $\tau_z$  (fig. 1), is usually used between the isotropic mixing period and data acquisition to remove the dispersive contributions to the lineshape. As shown by Sorensen et al. [16], co-addition of the TOCSY FIDs from a number of varying  $\tau_z$  values removes the zero-quantum coherence (ZQC) contributions which are dispersive. This then leaves a pure absorption-mode spectrum. The removal of the dispersive contribution to the spectrum is particularly important if one wants to make accurate determinations of spin–spin coupling constants from the spectrum. Typically, up to about  $10\tau_z$  values, ranging from  $\mu\text{s}$  to about 20 ms, are used. The  $\tau_z$  values should cover the range of  $0-1/\delta_{\text{min}}$ , where  $\delta_{\text{min}}$  is the smallest frequency difference between the two coupled spins of interest [5]. Even with the use of the  $z$ -filter, the dispersive components may persist in short mixing times, but tend to disappear at longer mixing times, and the lineshape of the spectrum approaches perfect absorption mode [4].

One obvious disadvantage of using the  $z$ -filter is the additional experimental time required. Since a required number of scans for a complete phase cycle (usually 8 or 16 scans, depending on the phase cycling scheme) has to be made for each  $\tau_z$  value, a significant increase in the experimental time is needed. For practical purposes, if only spin correlations and assignment, rather than the accurate measurement of spin–spin coupling constants, are desired, one may consider using a limited number of  $\tau_z$  or to skip the  $z$ -filter altogether, especially if only long mixing time is used. The incorporation of pulsed field gradients (PFG) into this experiment [18, 19] (to be discussed

later in Section 4) can remove the need for phase cycling and the  $z$ -filter, and will substantially reduce the experimental time.

### 3. Applications

Since first proposed by Bax et al. [4, 5] and Kessler et al. [6], the 1D TOCSY technique has been gaining popularity among NMR spectroscopists as well as practicing chemists. The 1D TOCSY technique has been applied to the assignment of peptides [6, 12, 19–21], carbohydrates [22–34], steroids and alkaloids [35–43], carotenoids [44] and mixtures (of reaction products, isomers and diastereomers) [22b, 45–49]. The references cited here may represent only a small fraction of the work in the literature reporting the use of the 1D TOCSY technique.

By far the most frequent application of the 1D TOCSY technique has been found in the study of carbohydrates. There are several reasons for its popularity in carbohydrates. First, the signals of most of the protons on the sugar rings are usually crowded into the 3–4 ppm region. Thus for carbohydrates with several sugar rings, the overlap of signals in this region of primary interest is severe. High digital resolution offered in the 1D technique is essential for resolving these signals. Second, the chemical shifts of many of the ring protons are quite similar. The sequential connectivity information provided by 1D TOCSY performed at incremental mixing times is particularly useful for unambiguous assignment. There is one convenient spectroscopic feature for carbohydrates for selective 1D techniques in that the chemical shifts for the anomeric protons are usually well separated from those of the other protons, providing a suitable starting point for selective excitation and propagation through the spin coupling network.

An impressive example can be found in the study of the octasaccharide repeating unit of an O-specific polysaccharide isolated from *Hafnia alvei* strain 2 bacteria [25]. The corresponding signals from the three  $\alpha$ -glucose residues are only a few Hz apart, so are those from the two  $\beta$ -galactose residues. However, the 1D TOCSY shows remarkable selectivity, and the subspectra of all the residues were generated with little cross-talk between them (figs 3(a)–(h)). In contrast, the 3.4–3.9 ppm region of the corresponding 2D spectrum could not be analyzed due to severe overlap of the signals because of the much reduced digital resolution.

For most of the sugars, the propagation of the spin correlation is through a linear-spin system. A small coupling in the linear “chain” may cause a severe “bottleneck” in the propagation of the magnetization transfer. While magnetization transfer is very efficient in, e.g., glucose, where all the  $^3J$  are relatively large ( $\sim 7$  Hz), galactose, in which  $J_{45}$  is 1 Hz, is a common example of this “bottleneck” problem. An extremely long mixing time is usually needed to establish the correlations to protons  $H_5$  and  $H_6$  (starting



from the anomeric proton,  $H_1$ ) in galactose. Sometimes, even long mixing times fail to establish these correlations, causing difficulties in assignment. A special 1D TOCSY experiment, with two of the protons in the spin system simultaneously excited (by using the DANTE pulses), has been used to provide solutions to this problem [22a].

1D TOCSY was used extensively in the proton assignment and structural characterization of glycoalkaloids, such as saponins [29, 35, 37, 38], where the assignment of both the steroidal and the carbohydrate parts of the molecules can benefit from the sequential connectivity information provided by this technique.

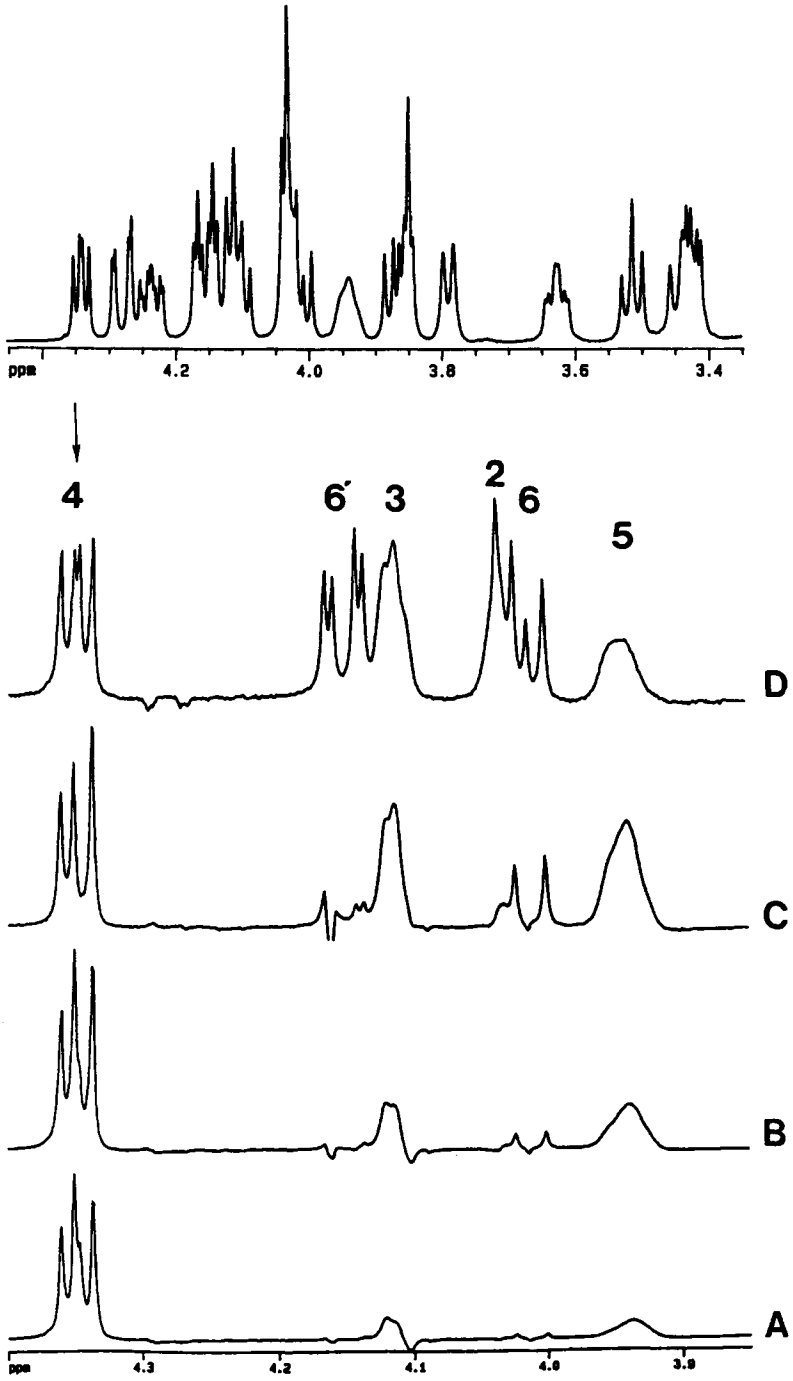
1D TOCSY is also ideal for the study of mixtures. In favorable situations, a subspectrum can be generated for each species, without interference signals from other components in the mixture, reducing much of the ambiguities. 1D TOCSY was applied in a study of three hydrolyzation products of carbohydrate-based surfactants, alkanoylgluconolactones [48]. The three products, the alkanoylglucono- $\gamma$ -lactone, the alkanoylglucono- $\delta$ -lactone, and the open-chain alkanoylgluconic acid, are structurally quite similar, with all the proton signals of interest in the narrow range of 3.4–4.3 ppm. In the 1D TOCSY experiment, by selectively exciting three separate signals, one in each of the three components, and by using incremental mixing times (fig. 4), the signals from these three compounds in the mixture were separately assigned and identified. Again, the results from 2D TOCSY and COSY were much more ambiguous due to overlapping of signals and the lower digital resolution.

Although in the above discussions, proton TOCSY was assumed, the 1D TOCSY is not limited to protons. In principle, this technique can be applied to any abundant spins. We are not aware, however, of any 1D TOCSY work on, e.g.,  $^{19}\text{F}$  or  $^{31}\text{P}$ .<sup>2</sup> Mons et al. have applied the  $^2\text{H}$ - $^2\text{H}$  1D TOCSY technique to assignment in perdeuterated compounds [50].

---

<sup>2</sup> 2D TOCSY experiments for  $^{19}\text{F}$  [W.I. Bailey, A.I. Kotz, P.L. McDaniel, D.M. Parees, F.K. Schweighardt, H.J. Yue and C. Anklin, *Anal. Chem.* **65** (1993) 752] and for  $^{11}\text{B}$  [D.J. Donohoe, D. Reed and A.J. Welch, *Polyhedron* **14** (1995) 961] have been reported. The corresponding 1D experiments should be equally feasible.

←  
Fig. 3. Top: Resolution-enhanced 600 MHz  $^1\text{H}$  NMR spectrum of the octasaccharide repeating unit from *Hafnia alvei* strain 2 O-specific polysaccharide. (a)–(g) 500 MHz 1D TOCSY subspectra with selective excitation of the respective anomeric proton resonances. (h) 1D TOCSY subspectrum with the H3eq resonance of the neuraminic acid residue selectively excited. (Reproduced (adapted) with permission from Gamian et al. [25]. Copyright 1991 American Chemical Society)



## 4. Extensions of the basic 1D TOCSY experiment

In the previous sections, only the basic, non-gradient 1D TOCSY pulse sequence, its experimental aspects and applications were described. In the following, the more recent modifications and extensions of the basic pulse sequence and their applicability to spectral assignments and structural elucidation will be briefly reviewed. Some of these more sophisticated techniques may not be as readily implementable as the basic 1D TOCSY experiments, and thus have not yet found wide applications in routine practice.

### 4.1. Gradient-enhanced 1D TOCSY

As of the writing of this manuscript, practically none of the published work utilizing the 1D TOCSY technique included the use of pulsed field gradients. However, several versions of the gradient-enhanced 1D-TOCSY pulse sequence have been published recently [18, 19]. The main advantage of the inclusion of the gradients is the elimination of the need for phase cycling. In addition, a spin-lock pulse and a pulse field gradient can be added at the end of the isotropic mixing period to dephase the ZQC [51] and thus removing the dispersive contributions to the lineshape. This obviates the need to use the time-consuming  $z$ -filter to obtain absorption line shape as discussed in the non-gradient versions of the experiment in Section 2. It was demonstrated that one-scan gradient-enhanced 1D TOCSY gives good suppression of undesired signals and good absorption lineshape [18].

### 4.2. $^1\text{H}$ chemical shift selective 1D TOCSY

An alternative to using selective pulses in selective 1D TOCSY has been proposed [52]. The frequency selection is instead accomplished by using a homonuclear ( $^1\text{H}$ ) chemical shift selective filter (CSSF) [53, 54]. The chemical shift filter for frequency selection consists of a non-selective  $90^\circ$  pulse which is set at the frequency of the selected signal, and a systematic increment of the chemical shift evolution between this pulse and the

←  
Fig. 4. Top: The regular 1D  $^1\text{H}$  spectrum of a mixture of alkanoylglucono- $\delta$ -lactone, alkanoylglucono- $\delta$ -lactone and alkanoylgluconic acid, resulting from the hydrolysis of the alkylglucono- $\delta$ -lactone. (A)–(D) 1D TOCSY subspectra of one of the components, alkanoylglucono- $\gamma$ -lactone, generated by selectively exciting the  $\text{H}_4$  signal (indicated by an arrow) at 4.336 ppm by a  $270^\circ$  Gaussian pulse of 105 ms. The truncation level was 1%. The subspectra for the other two components were similarly generated. The mixing time used was 20, 40, 80 and 120 ms, respectively. Note that at short mixing times, dispersive components persisted despite the use of the  $z$ -filter. However, at a long mixing time, an absorption lineshape was obtained. (Reproduced (adapted) with permission from Kwoh et al. [48]. Copyright 1995 Elsevier Science Publishing)

isotropic mixing period. The magnetization from this selected spin that is on-resonance is co-added coherently regardless of the chemical shift evolution, while magnetization from other spins is filtered out due to the chemical shift modulation of the off-resonance signals during the increment of the evolution in the experiment. The advantage of this method is that it does not require any additional hardware (for generating shaped pulses, for example). An application to the measurement of homonuclear coupling constants has been demonstrated [52].

#### 4.3. $^{13}\text{C}$ -filtered 1D TOCSY and 1D HMQC- and HSQC-TOCSY

The selective excitation of the proton signal can be achieved through a heteronuclear spin, to which the proton is bonded, by the HMQC or HSQC type of heteronuclear polarization transfer. Many versions of the 1D HMQC-TOCSY or HSQC-TOCSY have been proposed. The selective excitation of the desired heteronucleus can be accomplished by using a selective pulse on the heteronuclear signal [28, 42, 55], or by using either a proton or a  $^{13}\text{C}$  CSSF [52–54].

The  $^{13}\text{C}$ -filtered TOCSY (or heteronuclear-filtered TOCSY in general) or 1D HMQC-TOCSY and HSQC-TOCSY experiments are particularly useful for the determination of long-range heteronuclear coupling constants, which is vital to many aspects of conformational analysis of oligosaccharides [56]. Poppe et al. demonstrated the use of  $^{13}\text{C}$ -filtered 1D TOCSY to determine the stereospecific assignment of the C-6-methylene protons in the glycosidic linkage of oligosaccharides by making accurate measurements of several long range carbon–proton coupling constants, such as  $^3J(\text{C-4}, \text{H-6R})$  and  $^3J(\text{C-4}, \text{H-6S})$  [31], and Kövér et al. [52] used both the 1D  $^1\text{H}$ -CSSF TOCSY and the  $^{13}\text{C}$ -filtered TOCSY to determine the homo- and hetero-nuclear coupling constants in an enantiomeric mixture of amino-acids. These heteronuclear-filtered techniques are also beneficial when severe overlap of proton signals prevents the application of conventional 1D-TOCSY experimental based on direct selective excitation of proton signals.

Gradient enhanced versions of the 1D HMQC-TOCSY and 1D HSQC-TOCSY have also been published recently [31, 55].

#### 4.4. Double selective 1D TOCSY

“Doubly” selective 1D-TOCSY experiments have been proposed to specifically transfer in-phase magnetization from two designated spins [57, 58]. This transfer will only take place if the two spins are connected by a scalar coupling. This method is achieved by using a double-selective spin-lock after the selective excitation of transverse magnetization of a desired spin. The doubly selective spin-lock can be obtained by using cosine-modulated

selective pulses [57] or by using two interleaved DANTE sequences [58], one with pulses of constant phase, and the other with the phase incremented in small and equal steps to give the effects of an offset in frequency. This doubly selective 1D TOCSY technique has been applied to determine the coupling constants in peptides containing many identical amino-acid residues and are thus hampered by strongly overlapping signals [20, 57].

#### 4.5. 1D TOCSY-ROESY and 1D TOCSY-NOESY

The 1D TOCSY module has been used in many pseudo-3D experiments (or alternatively referred to as 1D analogues of 3D experiments in the literature) such as 1D TOCSY-NOESY or 1D TOCSY-ROESY experiments. The TOCSY part of these experiments are similar to that of a regular 1D TOCSY where a selective excitation of a desired signal is followed by a MLEV17-type isotropic mixing. The second polarization transfer (NOESY or ROESY) step can either be non-selective [29, 59–61] or selective [62–65].

These experiments provide identification of the through-bond spin coupling network as well as through-space proximity between spins. Examples of the application of these techniques have demonstrated the efficiency of these techniques in establishing the assignment, sequence and linkage site information for oligo- and poly-saccharides [59–60, 62–65], and for saponins [29].

The double-selective TOCSY-ROESY and TOCSY-NOESY techniques are particularly useful. They allow one to measure NOE and ROE correlations in spectra with high degree of overlap as often found in carbohydrates. In addition to the DANTE, DANTE-Z [66], and Gaussian pulses as described earlier for selective excitation, self-refocusing shaped pulses such as BURP (EBURP and UBURP) [67] have also been used for this purpose [64].

## References

- [1] R.R. Ernst, G. Bodenhausen and A. Wokaun, *Principles of Magnetic Resonance in One and Two Dimensions* (Clarendon Press, Oxford, 1987).
- [2] L. Baunschweiler and R.R. Ernst, *J. Magn. Reson.* **53** (1983) 521.
- [3] A. Bax and D.G. Davis, *J. Magn. Reson.* **65** (1985) 355.
- [4] D.G. Davis and A. Bax, *J. Am. Chem. Soc.* **107** (1985) 7197.
- [5] S. Subramanian and A. Bax, *J. Magn. Reson.* **71** (1987) 325.
- [6] H. Kessler, H. Oschkinat, C. Griesinger and W. Bermel, *J. Magn. Reson.* **70** (1986) 106.
- [7] A. Bax and D.G. Davis, *J. Magn. Reson.* **63** (1985) 207.
- [8] M.H. Levitt and R. Freeman, *J. Magn. Reson.* **43** (1981) 502; M.H. Levitt, R. Freeman and T.A. Frenkiel, *J. Magn. Reson.* **47** (1982) 328.
- [9] A.J. Shaka, J. Keeler, T. Frenkiel and R. Freeman, *J. Magn. Reson.* **52**

- (1983) 335.
- [10] J. Cavanaugh and M. Rance, *J. Magn. Reson.* **88** (1990) 72.
- [11] C.J. Bauer, R. Freeman, T. Frenkiel, J. Keeler and A.J. Shaka, *J. Magn. Reson.* **58** (1984) 442.
- [12] H. Kessler, U. Anders, G. Gemmecker and S. Steuernagel, *J. Magn. Reson.* **85** (1989) 1.
- [13] G.A. Morris and R. Freeman, *J. Magn. Reson.* **29** (1978) 433.
- [14] L. Emsley and G. Bodenhausen, *J. Magn. Reson.* **82** (1989) 211.
- [15] H. Kessler, S. Mronga and G. Gemmecker, *Magn. Reson. Chem.* **29** (1991) 527;  
R. Freeman, *Chem. Rev.* **91** (1991) 1397;  
W. Hull, in: *Two-Dimensional NMR Spectroscopy*, 2nd edition, eds W.R. Croasmun and R.M.K. Carlson (VCH Publishers, New York, 1994) Ch. 2.
- [16] O.W. Sorensen, M. Rance and R.R. Ernst, *J. Magn. Reson.* **56** (1984) 527.
- [17] M. Rance, *J. Magn. Reson.* **74** (1987) 557.
- [18] T. Facke and S. Berger, *J. Magn. Reson. Ser. A* **114** (1995) 32.
- [19] C. Dalvit and G. Bovermann, *Magn. Reson. Chem.* **33** (1995) 156.
- [20] K. Zangger and H. Sterk, *Magn. Reson. Chem.* **33** (1995) 421.
- [21] K. Zangger and H. Sterk, *J. Magn. Reson. Ser. B* **107** (1995) 186.
- [22] a) L. Poppe, J. Dabrowski, C.W. van der Lieth, M. Numata and T. Ogawa, *Eur. J. Biochem.* **180** (1989) 337;  
b) A. Ejchart, J. Dabrowski and C.W. van der Lieth, *Magn. Reson. Chem.* **30** (1992) S105.
- [23] F. Inagaki, I. Shimada, D. Kohda, A. Suzuki and A. Bax, *J. Magn. Reson.* **81** (1989) 186.
- [24] L. Poppe, J. Dabrowski, C.W. van der Lieth, K. Koike and T. Ogawa, *Eur. J. Biochem.* **189** (1990) 313;  
D. Acquotti, L. Poppe, J. Dabrowski, C.W. van der Lieth, S. Sonnino and G. Tettamanti, *J. Am. Chem. Soc.* **112** (1990) 7772;  
L. Poppe, J. Dabrowski and C. W. van der Lieth, *Biochem. Biophys. Res. Commun.* **174** (1991) 1169.
- [25] A. Gamian, E. Romanowska, U. Dabowski and J. Dabrowski, *Biochemistry* **30** (1991) 5032.
- [26] a) H.P. Wessel, G. Englert and P. Stangier, *Helv. Chim. Acta* **74** (1991) 682;  
b) H.P. Wessel, B. Meyer and G. Englert, *Carbohydr. Res.* **242** (1993) 141;  
c) H.P. Wessel and G. Englert, *J. Carbohydr. Chem.* **13** (1994) 1145.
- [27] S. Sabesan, J.O. Duus, S. Neira, P. Domaille, S. Kelm, J. C. Paulson and K. Bock, *J. Am. Chem. Soc.* **114** (1992) 8363.
- [28] R.A. Hoffman, J. Vanwijk, B.R. Leeftang, J.P. Kamerling, C. Altona and J.F.G. Vliegthart, *J. Am. Chem. Soc.* **114** (1992) 3710.
- [29] H. Schroder and E. Haslinger, *Liebigs Ann. Chem.* (1993) 959.
- [30] S. Saito, Y. Sasaki, T. Furumoto, S. Sumita and T. Hinomoto, *Carbohydr. Res.* **258** (1994) 59.
- [31] L. Poppe, S. Sheng and H. van Halbeek, *J. Magn. Reson.* **32** (1994) 97.
- [32] D.S. Himmelback, R.D. Hartley, W.S. Borneman, L. Poppe and H. van Halbeek, *Magn. Reson. Chem.* **32** (1994) 158.
- [33] A.J. Benesi, C.J. Falzone, S. Benerjee and G.K. Farber, *Carbohydr. Res.* **258** (1994) 27.
- [34] D. Uhrin, J.R. Brisson, L.L. MacLean, J.C. Richards and M.B. Perry, *J. Biomol. NMR* **4** (1994) 615.
- [35] W. Wilker and D. Leibfritz, *Magn. Reson. Chem.* **30** (1992) 645.
- [36] D.G. Davis and M.B. Thompson, *J. Lipid Res.* **34** (1993) 651.
- [37] R. Puri, T.C. Wong and R. Puri, *J. Nat. Prod.* **57** (1994) 587.
- [38] G. Bader, T. Danzandarjaa, K. Hiller, G. Reznicek, J. Jurenitsch, M. Golly, H. Schoder, M. Schubertsilavec and E. Haslinger, *Helv. Chim. Acta* **77** (1994) 1861.

- [39] R. Sawa, Y. Takahashi, T. Sawa, H. Naganawa and T. Takeuchi, *J. Antibiotics* **47** (1994) 1273.
- [40] N. Tabata, H. Tomada, R. Masuma, Y. Iwai and S. Omura, *J. Antibiotics* **48** (1995) 53.
- [41] D.E. Over, M. Bardet, J.C. Marchon and R. Ramasseul, *Magn. Reson. Chem.* **33** (1995) 224.
- [42] T. Facke and S. Berger, *Tetrahedron* **51** (1995) 3521.
- [43] K. Marat, J.F. Templeton, Y.Z. Ling, W.Y. Lin and R.K. Gupta, *Magn. Reson. Chem.* **33** (1995) 529.
- [44] J. Krane, T. Aakermann and S. Liaaen-Jensen, *Magn. Reson. Chem.* **30** (1992) 1169; G. Englert, T. Aakermann and S. Liaaen-Jensen, *Magn. Reson. Chem.* **31** (1993) 910.
- [45] J. Barluenga, R.P. Carlon, E. Pelaez, J. Joglar, F.L. Ortiz and S. Faustero, *Tetrahedron* **48** (1992) 9745.
- [46] T. Kanthimathi, Y. Moothy, C.N. Pillai and S. Subramanian, *Magn. Reson. Chem.* **32** (1994) 452.
- [47] B.T. Doan, B. Gillet, B. Blondel and J.C. Beloeil, *J. Magn. Reson. Ser. A* **114** (1995) 244.
- [48] D. Kwoh, D.J. Pocalyko, A.J. Carchi, B. Harirchian, L.O. Hargiss and T.C. Wong, *Carbohydr. Res.* **274** (1995) 111.
- [49] B.T. Doan, B. Gillet, B. Blondel and J.C. Beloeil, *J. Magn. Reson. Ser. A* **114** (1995) 244.
- [50] H.-E. Mons, K. Bergander and H. Gunther, *Magn. Reson. Chem.* **31** (1993) 509.
- [51] A.L. Davis, G. Estcourt, J. Keeler, E.D. Laue and J.J. Titman, *J. Magn. Reson. Ser. A* **105** (1993) 167.
- [52] K. Kövér, D. Jiao, D. Uhrin, P. Forgö and V.J. Hruby, *J. Magn. Reson. Ser. A* **106** (1994) 119.
- [53] G. Otting, *J. Magn. Reson.* **86** (1990) 496.
- [54] L.D. Hall and T.J. Norwood, *J. Magn. Reson.* **76** (1988) 548; **78** (1988) 582.
- [55] T. Parella, F. Sanchez-Ferrando and A. Virgili, *J. Magn. Reson. Ser. A* **114** (1995) 32.
- [56] C. Morat, F.R. Tavel and M.R. Vignon, *Magn. Reson. Chem.* **26** (1988) 264.
- [57] R. Konrat, I. Burghardt and G. Bodenhausen, *J. Am. Chem. Soc.* **113** (1991) 9135.
- [58] E. Kupce and R. Freeman, *J. Am. Chem. Soc.* **114** (1992) 10671.
- [59] L. Poppe and J. Dabrowski, *Biochem. Biophys. Res. Commun.* **59** (1989) 618.
- [60] E. Katzenellenbogen, E. Romanowska, U. Dabrowski and J. Dabrowski, *Eur. J. Biochem.* **200** (1991) 401.
- [61] P. Adell, T. Parella, F. Sanchez-Ferrando and A. Virgili, *J. Magn. Reson. Ser. A* **113** (1995) 124.
- [62] D. Boudot, C. Roumestand, F. Toma and D. Canet, *J. Magn. Reson.* **90** (1990) 221.
- [63] L. Poppe and H. van Halbeek, *J. Magn. Reson.* **96** (1992) 185.
- [64] S. Holmbeck, P. Hajduk and L. Lerner, *J. Magn. Reson. Ser. B* **102** (1993) 107.
- [65] D. Uhrin, J.-R. Brisson, G. Kogan and H.J. Jennings, *J. Magn. Reson. Ser. B* **104** (1994) 289.
- [66] D. Boudot, D. Canet, J. Brondeau and J.-C. Boubel, *J. Magn. Reson.* **83** (1989) 428.
- [67] H. Geen and R. Freeman, *J. Magn. Reson.* **93** (1991) 93.

This Page Intentionally Left Blank

## chapter 8

---

# Use of High Power Spin-Lock Purge Pulses in High Resolution NMR Spectroscopy

---

Gottfried Otting

*Department of Medical Biochemistry and Biophysics  
Karolinska Institute  
S-171 77 Stockholm  
Sweden*

This Page Intentionally Left Blank

## 1. Introduction

Spin-lock pulses are radiofrequency pulses with nominal flip-angles much larger than  $360^\circ$ . Because of the spatial inhomogeneity of the radiofrequency field  $B_1$ , a spin-lock pulse produces a continuous distribution of effective flip-angles across the sample. Consequently, in-phase magnetization with a phase different from the spin-lock axis is defocused while the magnetization aligned with the spin-lock axis passes the spin-lock pulse unaffected. There is a close analogy between spin-lock pulses and pulsed magnetic field gradients (PFG) which is perhaps most strikingly manifested by the fact that short spin-lock pulses can be used for coherence order selection in 2D spectra recorded with a single scan per FID [1]. There are, however, also important differences. For example, spin-lock pulses effect a transfer of magnetization via scalar couplings in TOCSY experiments [2] and magnetization transfer by NOE in ROESY experiments [3]. These side-effects are minimized, if the spin-lock pulses are short. To achieve coherence order selection by a short spin-lock pulse, the pulse must therefore be of high power to obtain good averaging of the magnetization by the radiofrequency field inhomogeneity. Alternatively, the probehead can be equipped with a second radiofrequency coil which is designed to produce an inhomogeneous  $B_1$  field [4].

On conventional probeheads, the  $B_1$  field of the  $^1\text{H}$  radiofrequency coil is sufficiently inhomogeneous that high-power spin-lock pulses of about 0.5 to 3 ms duration largely defocus the magnetization which is not aligned along the spin-lock axis. During these short time periods, TOCSY and ROE effects are weak and can be neglected. The spin-lock pulses are most readily applied, if their power is the same as for hard  $90^\circ$  proton pulses, since this ensures the phase coherence of the spin-lock pulse with the other pulses in the pulse sequence without any phase adjustments.

In the following, three different experiments are discussed, where short, high-power spin-lock pulses are used to purge the spectrum from undesired resonances. The experiments are (i) the  $^{13}\text{C}$  HSQC experiment [5], (ii) experiments with  $^{13}\text{C}$  half-filter elements [6], and (iii) NOESY and ROESY experiments for the observation of water–protein NOEs [7]. In the first two experiments, spin-lock purge pulses are used to suppress the signals from

protons not directly bound to  $^{13}\text{C}$ . In the last experiment, spin-lock pulses are used to suppress the solvent signal immediately before the detection period.

## 2. $^{13}\text{C}$ HSQC with spin-lock purge pulses

The HSQC (heteronuclear single quantum coherence) pulse sequence originally proposed by Bodenhausen and Ruben in 1980 [5] correlates the chemical shifts of heteronuclei like  $^{13}\text{C}$  and  $^{15}\text{N}$  with their directly bonded protons. The experiment combines excellent sensitivity with high spectral resolution, since it uses proton magnetization both as starting magnetization and for detection, and heteronuclear couplings are decoupled in both frequency dimensions. Furthermore, the evolution of  $^1\text{H}$ - $^1\text{H}$  couplings is suppressed during the evolution period  $t_1$  leading to singlets in the  $F_1$  frequency dimension. These characteristics make the HSQC experiment most useful for the detection of  $^{13}\text{C}$ - $^1\text{H}$  and  $^{15}\text{N}$ - $^1\text{H}$  correlations at natural isotopic abundance. Because of the low natural abundance of  $^{13}\text{C}$  and  $^{15}\text{N}$ , however, most of the  $^1\text{H}$  magnetization comes from protons which are bound to  $^{12}\text{C}$  and  $^{14}\text{N}$ . Imperfect suppression of this magnetization results in strong bands of  $t_1$  noise which can totally obscure the weak  $^{13}\text{C}$ - $^1\text{H}$  and  $^{15}\text{N}$ - $^1\text{H}$  correlation peaks. A single spin-lock purge pulse inserted into the HSQC pulse sequence defocuses most of the undesired proton magnetization while maintaining the proton magnetization of the protons bound to  $^{13}\text{C}$  or  $^{15}\text{N}$  [8].

## 3. Pulse sequence and product operator description

Figure 1 shows the pulse sequence of the  $^{13}\text{C}$  HSQC experiment supplemented by a spin-lock pulse to suppress the signals from  $^{12}\text{C}$ -bound protons. The experiment is readily described in terms of Cartesian product operators [9]. For a two spin system consisting of a proton spin  $H$  coupled to a  $^{13}\text{C}$  spin  $C$ , the relevant coherence transfer pathway is

$$\begin{aligned}
 H_z &\xrightarrow{90_y^\circ(H)} H_x \xrightarrow{\tau/2-180_x^\circ(H,C)-\tau/2} 2H_y C_z \xrightarrow{\text{SL}_y(H)} 2H_y C_z \\
 &\xrightarrow{90_x^\circ(H), 90_x^\circ(C)} -2H_z C_y \xrightarrow{t_1/2-180_x^\circ(H)-t_1/2} 2H_z C_y \cos(\Omega_C t_1) \\
 &\xrightarrow{90_x^\circ(H,C)} -2H_y C_z \cos(\Omega_C t_1) \xrightarrow{\tau/2-180_x^\circ(H,C)-\tau/2} H_x \cos(\Omega_C t_1). \quad (1)
 \end{aligned}$$

In writing eq. (1), relaxation was neglected and the delay  $\tau$  was assumed to match  $1/[2J(^1\text{H}, ^{13}\text{C})]$ . Equation (1) shows that the signal is modulated

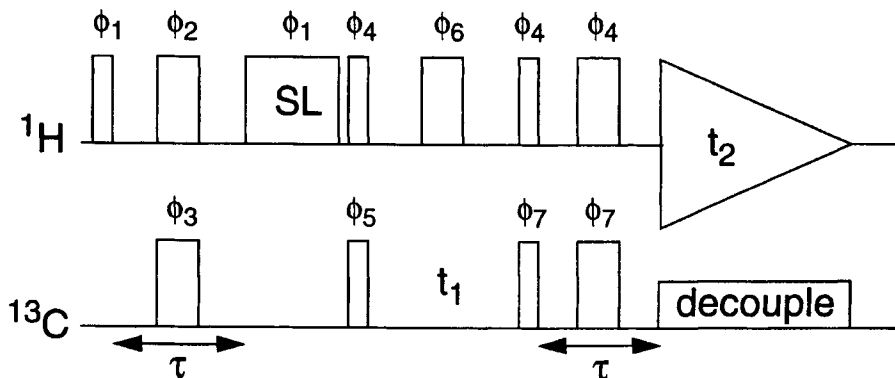


Fig. 1. Pulse sequence of the  $^{13}\text{C}$  HSQC experiment with a spin-lock pulse for the suppression of signals from protons not bound to  $^{13}\text{C}$ . Narrow and wide bars denote  $90^\circ$  and  $180^\circ$  pulses, respectively. The spin-lock pulse is labeled SL.  $\tau$  is set to  $1/[2J(^{13}\text{C}, ^1\text{H})]$ . The detection period is symbolized by a triangle. Phase cycle:  $\phi_1 = 8(y)$ ;  $\phi_2 = 2(x, x, y, y)$ ;  $\phi_3 = \phi_4 = \phi_7 = 8(x)$ ;  $\phi_5 = 4(x, -x)$ ;  $\phi_6 = 4(x), 4(-x)$ ; acquisition =  $2(x, -x, -x, x)$ . The phases of the  $^{13}\text{C}$  pulses before  $t_1$  ( $\phi_3$  and  $\phi_5$ ) are subjected to the States-TPPI scheme [38].

with the  $^{13}\text{C}$  frequency  $\Omega_C$  in  $F_1$  and with the  $^1\text{H}$  frequency in the  $F_2$  dimension. It also demonstrates that in the absence of  $^{13}\text{C}$ - $^{13}\text{C}$  couplings, all scalar couplings are decoupled during  $t_1$ , since the  $180^\circ(H)$  pulse refocuses the  $^1\text{H}$ - $^{13}\text{C}$  couplings, and the  $H_z$  operator contained in the term  $2H_zC_y$  is inert with respect to  $^1\text{H}$ - $^1\text{H}$  couplings. During signal detection,  $^{13}\text{C}$  broadband decoupling can be applied to prevent the evolution of the term  $H_x$  with respect to the heteronuclear couplings. Note that the spin-lock pulse (denoted SL) does not change the coherence and therefore does not spoil the sensitivity of the experiment.

The magnetization from  $^{12}\text{C}$ -bound protons is suppressed by the spin-lock purge pulse. Denoting the operators of a proton 2-spin system as  $H_A$  and  $H_B$ , the product operator calculation yields

$$\begin{aligned}
 H_{Az} &\xrightarrow{90_y(H)} H_{Ax} \\
 &\xrightarrow{\tau/2-180_x(H,C)-\tau/2} H_{Ax} \cos(\pi J\tau) + 2H_{Ay}H_{Bz} \sin(\pi J\tau) \\
 &\xrightarrow{SL_y(H)} (H_{Ax} \cos \beta - H_{Az} \sin \beta) \cos(\pi J\tau) \\
 &\quad + (2H_{Ay}H_{Bz} \cos \beta + 2H_{Ay}H_{Bx} \sin \beta) \sin(\pi J\tau). \quad (2)
 \end{aligned}$$

Averaging over all possible flip angles  $\beta$  which result from the spin-lock pulse, all signals from eq. (2) cancel. It can be shown that this holds for

proton spin systems of any size in the absence of scalar coupling to a  $^{13}\text{C}$  spin [10].

In practice, the suppression of the signals from  $^{12}\text{C}$ -bound protons is not complete. In part, this arises from imperfections of the  $180^\circ(H)$  pulse in the delay  $\tau$ . If the chemical shift evolution is not refocused, pure proton terms are generated which pass the spin-lock purge pulse. Therefore, the suppression of the signals from  $^{12}\text{C}$ -bound protons is improved by applying the Excorcycle [11] phase cycle to this  $180^\circ(H)$  pulse [10]. To keep the phase cycle short, only the first two steps of Excorcycle can be used. The selection of the  $^{13}\text{C}$ - $^1\text{H}$  correlations is further improved by phase cycling at least one of the  $90^\circ(C)$  pulses (fig. 1).

Since water protons are not bound to  $^{13}\text{C}$  or  $^{15}\text{N}$  nuclei, the water signal is also suppressed by the spin-lock purge pulse. In practice, the suppression of the water signal is sufficient to record HSQC spectra of protein samples dissolved in mixtures of 95%  $\text{H}_2\text{O}/5\%$   $\text{D}_2\text{O}$  without any further water suppression scheme [12]. For optimum water suppression the carrier frequency must be at the frequency of the water resonance. On resonance, the phase of the water magnetization is not affected by imperfections of the first  $180^\circ(H)$  pulse, so that no solvent magnetization ends up along the axis of the spin-lock purge pulse.

#### 4. Experimental example

Figure 2 shows the  $^{15}\text{N}$  HSQC experiment recorded with a cyclosporin mutant at natural isotopic abundance without  $^{15}\text{N}$  decoupling during acquisition. The spin-lock purging yields a spectrum virtually free of  $t_1$ -noise, where besides the cross peaks of the four amide protons even small signals from a minor conformational species are visible. The cross peaks are singlets in the indirectly detected dimension and doublets of doublets in the acquisition dimension due to the  $\alpha$  proton–amide proton coupling constant and the one-bond  $J(^1\text{H}, ^{15}\text{N})$  coupling constant.

#### 5. Comparison with the HMQC experiment

Because of the favorable cross-peak multiplet fine-structure, the HSQC experiment offers superior spectral resolution over the HMQC (heteronuclear multiple quantum coherence) experiment [13, 14]. On the other hand, the HMQC experiment works with fewer pulses and is thus less prone to pulse imperfections. The real advantage of the HSQC experiment is for measurements of samples at natural isotopic abundance and without the use of pulsed field gradients, since the HSQC experiment lends itself to purging with a spin-lock pulse. Spin-lock purging in the HMQC experiment

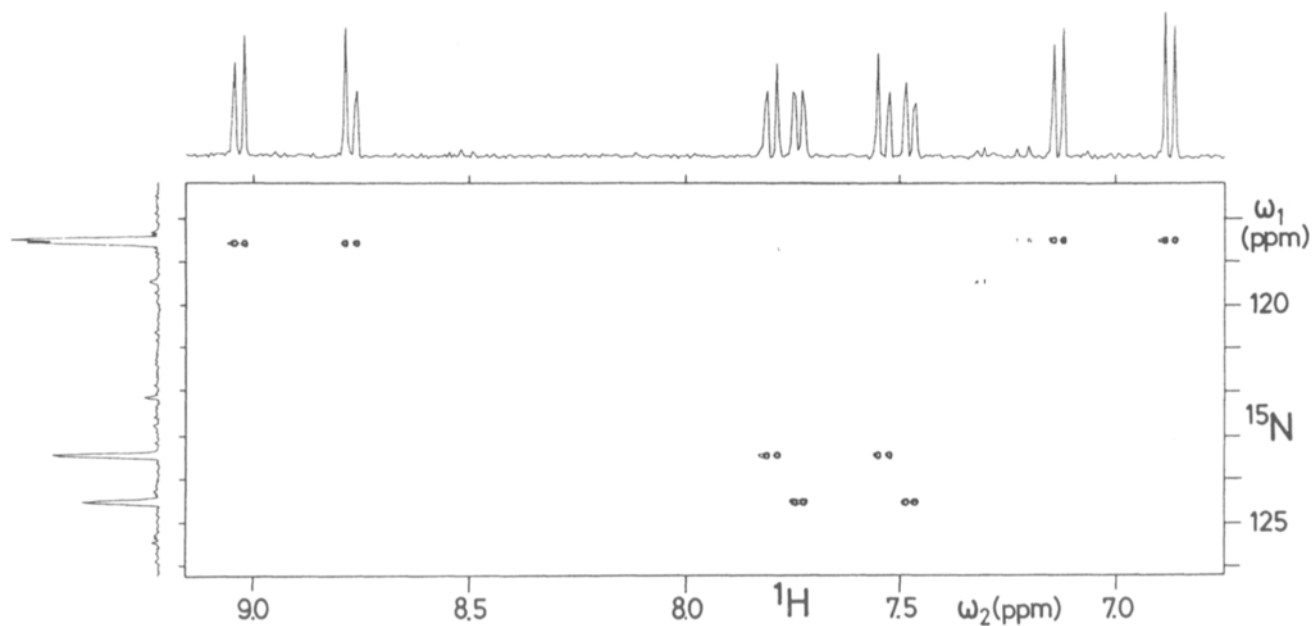


Fig. 2.  $^{15}\text{N}$  HSQC spectrum of a 75 mM solution of Pro<sup>3</sup>-cyclosporin in  $\text{CDCl}_3$  at natural isotope abundance using the pulse sequence of fig. 1 without  $^{15}\text{N}$  decoupling during acquisition.  $\tau = 5.7$  ms, SL = 2.5 ms. An additional, short spin-lock pulse was used right before signal detection [8]. The projections are shown at the top and on the left. (Reproduced by permission of Academic Press from Otting and Wüthrich [8])

is possible only at the expense of additional pulses, e.g., by replacing the excitation pulse by a TANGO sequence [15]. The situation looks different, when heteronuclear long-range correlations are to be measured. The HMQC pulse sequence is based on a simple spin-echo sequence, where the proton magnetization reaches the receiver independent of the presence of  $^1\text{H}$ - $^1\text{H}$  couplings. When choosing a longer defocusing delay  $\tau$  in the HSQC experiment to achieve correlations via small multiple bond heteronuclear couplings, the  $^1\text{H}$ - $^1\text{H}$  couplings will evolve significantly during the time period  $\tau$ . It can be shown that all  $^{13}\text{C}$ - $^1\text{H}$  long-range correlations are still present in the "long-range HSQC" experiment even in the presence of the spin-lock purge pulse, albeit mostly at decreased intensity [10]. Yet, the purging effect achieved by the spin-lock pulse may be essential to overcome the otherwise limiting  $t_1$ -noise on unstable spectrometers [10].

## 6. Pulse programme for a Bruker DMX NMR spectrometer

```

30m ze
1 60m do:f2           ;f1 is the proton channel,
                    ;f2 is the carbon channel
2 3m
3 10u
d1 p11:f1 p12:f2    ;d1=relaxation delay, p11=power level  $^1\text{H}$ ,
                    ;p12=power level  $^{13}\text{C}$ 
(p1 ph1):f1         ;p1=90 degree  $^1\text{H}$  pulse
d2                  ;d2=1/(4J( $^1\text{H}$ ,  $^{13}\text{C}$ ))
(d12 p1*2 ph2):f1 (p2*2 ph3):f2 ;p2=90 degree  $^{13}\text{C}$  pulse,
                    ;d12=p2-p1
d2
(p20 ph1):f1        ;spin-lock pulse, p20=0.5-3 ms
4u                  ;phase setting delay
(p1 ph4):f1 (p2 ph5):f2
d0                  ;d0=incremented  $t_1$  delay
(p1*2 ph6):f1
d0
(p1 ph4):f1 (p2 ph7):f2
d2
(d12 p1*2 ph4):f1 (p2*2 ph7):f2
d2 p112:f2          ;power for  $^{13}\text{C}$  decoupling during acquisition
go=1 ph0 cpds2:f2   ;acquisition with broadband decoupling
30m do:f2 wr #0 if #0 ip3 zd ;write FID, increment phase 3
                    ;for States-TPPI

```

```

30m ip5                ;increment phase 5 for States-TPPI
lo to 2 times 2
3m id0                 ;increment  $t_1$ 
lo to 3 times 10
exit
ph1 = 1
ph2 = 0 0 1 1
ph3 = 0
ph4 = 0
ph5 = 0 2
ph6 = 0 0 0 0 2 2 2 2
ph7 = 0
ph0 = 0 2 2 0

```

## 7. $^{13}\text{C}$ half-filter with spin-lock purge pulse

$^{13}\text{C}$  half-filter elements are designed to separate the signals of  $^{13}\text{C}$ -bound protons from the signals of  $^{12}\text{C}$ -bound protons [6]. The name indicates that the selection acts only on one of the two frequency axes in a two-dimensional experiment. Experiments with  $^{13}\text{C}$  half-filters are mostly used with  $^{13}\text{C}$  enriched samples. At natural isotopic abundance, the subspectrum with the  $^{13}\text{C}$ -bound protons would usually be obscured by the  $t_1$  noise from the predominating signals of the  $^{12}\text{C}$ -bound protons. In this situation, a spin-lock purge pulse significantly improves the selection of the resonances of the  $^{13}\text{C}$ -bound protons, because it greatly helps to suppress the signals of the  $^{12}\text{C}$ -bound protons. As a drawback, the subspectrum with the  $^{12}\text{C}$ -bound protons is lost. At natural isotopic abundance, however, this subspectrum would be virtually identical to the unedited spectrum.

Selecting the  $^{13}\text{C}$ -bound protons before performing a homonuclear two-dimensional experiment enables to measure small heteronuclear coupling constants [16]. Such an experiment with a sample of natural isotopic abundance was first published by Otting and Wüthrich in 1990, where the  $^{13}\text{C}$  half-filter element with spin-lock purge pulse was used to select the  $^{13}\text{C}$ -bound protons in a small protein in aqueous solution [6]. Later applications illustrated the usefulness of the same  $^{13}\text{C}$  half-filter element with smaller molecules [17, 18].

## 8. Pulse sequence and product operator description

As an illustration of the use of the  $^{13}\text{C}$  half-filter element for the measurement of small  $^1\text{H}$ - $^{13}\text{C}$  coupling constants, consider the TOCSY experiment

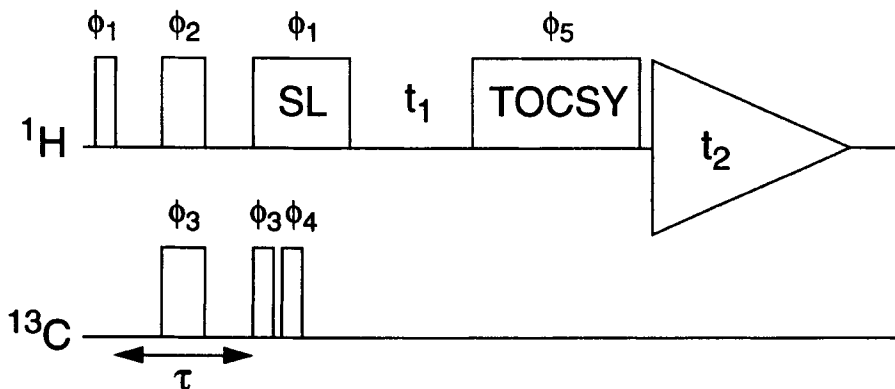


Fig. 3. Pulse sequence of a TOCSY experiment with  $^{13}\text{C}(\omega_1)$  half-filter. The spin-lock pulse and the TOCSY mixing sequence are identified by SL and TOCSY, respectively.  $\tau$  is set to  $1/[2J(^{13}\text{C}, ^1\text{H})]$ . Phase cycle:  $\phi_1 = \phi_3 = 8(x)$ ;  $\phi_2 = 2(x, x, y, y)$ ;  $\phi_4 = 4(x, -x)$ ;  $\phi_5 = 4(x), 4(-x)$ ; acquisition =  $2(x, -x, -x, x)$ . The phases of the  $^1\text{H}$  pulses before  $t_1$  ( $\phi_1$  and  $\phi_2$ ) are subjected to States-TPPI [38].

with  $^{13}\text{C}(\omega_1)$ -half-filter. The name indicates that the half-filter element is applied before the evolution time  $t_1$ , which limits the editing effect to the  $F_1$  frequency axis. The pulse sequence is shown in fig. 3. The half-filter element corresponds to the sequence  $\tau/2-180^\circ(H, C)-\tau/2-\text{SL}(H), 90^\circ(C)-90^\circ(C)$  which is inserted between the  $90^\circ$  excitation pulse and the evolution time  $t_1$  of the pulse sequence of the conventional two-dimensional TOCSY experiment. The delay  $\tau$  is  $1/[2(J(^1\text{H}, ^{13}\text{C})]$ , where  $J(^1\text{H}, ^{13}\text{C})$  denotes the one-bond  $^1\text{H}-^{13}\text{C}$  coupling constant. Note the similarity of the half-filter element with the first part of the  $^{13}\text{C}$  HSQC pulse sequence. Like in the HSQC experiment, the spin-lock pulse purges the signals from protons not bound to  $^{13}\text{C}$ . The selected proton magnetization is antiphase with respect to the directly bonded proton after the delay  $\tau$ , and the same product operator description applies up to this point as for the HSQC experiment (eqs (1) and (2)). The  $90^\circ(C)$  pulses are applied either with the same or with opposite phase, resulting, respectively, in an effective  $180^\circ$  or  $0^\circ$  pulse. Since a  $180^\circ(C)$  pulse inverts the sign of the antiphase proton magnetization, the cycling of the receiver phase together with the phase of one of the  $90^\circ(C)$  pulses supports the selection of the antiphase magnetization.

The purpose of the  $^{13}\text{C}(\omega_1)$ -half-filter is to start the TOCSY experiment only with the magnetization of protons bound to  $^{13}\text{C}$ . No further  $^{13}\text{C}$  pulses are applied after the start of the evolution time  $t_1$ . For the description of the multiplet fine-structure of the resulting cross-peaks, it is instructive to consider a 3-spin system with the operators  $H_A$ ,  $H_B$  and  $C$  denoting the spins of two protons and one carbon. Starting from antiphase magnetiza-

tion  $2H_{Ax}C_z$  the following relevant terms are obtained by the end of the evolution time:

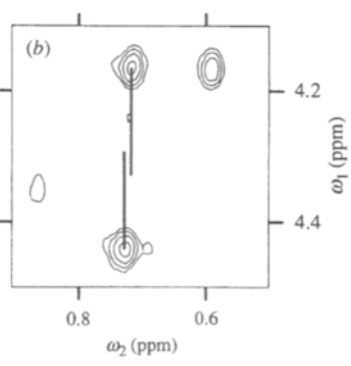
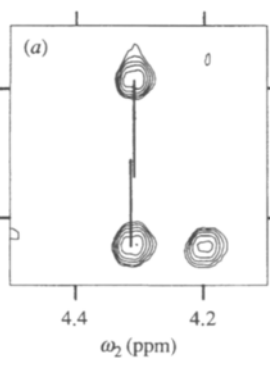
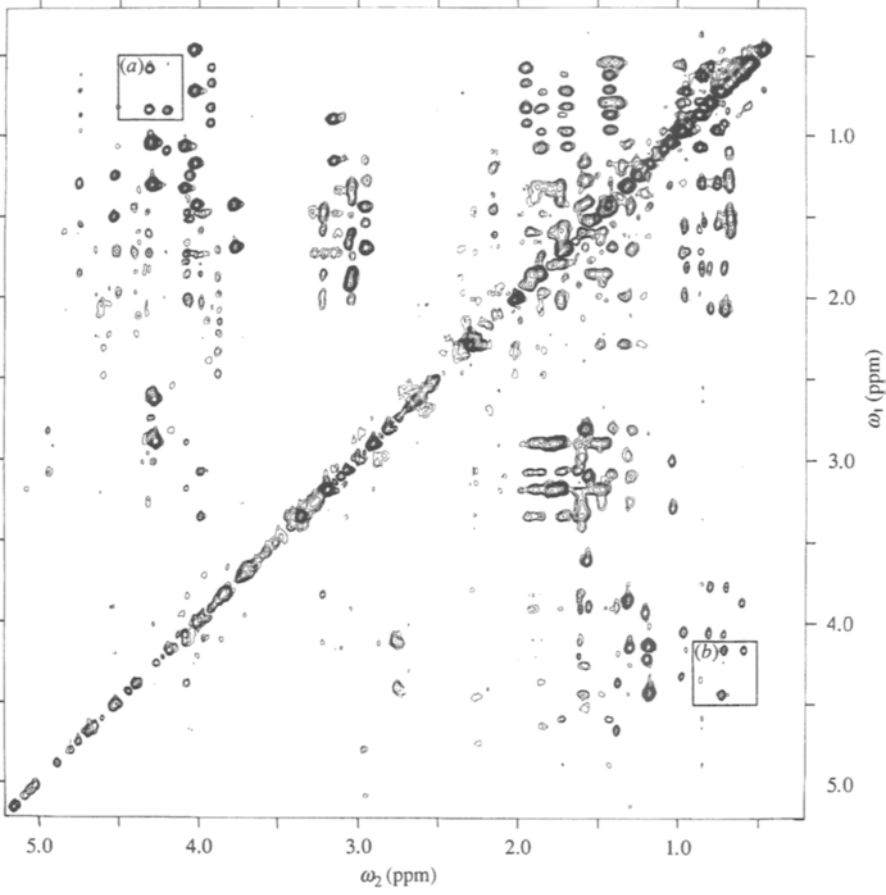
$$2H_{Ax}C_z \xrightarrow{t_1} 2H_{Ax}C_z \cos(\Omega_A t_1) \cos(\pi J_{HC} t_1) - H_{Ax} \sin(\Omega_A t_1) \sin(\pi J_{HC} t_1), \quad (3)$$

where  $J_{HC}$  denotes the one-bond  $^1\text{H}$ - $^{13}\text{C}$  coupling constant and  $^1\text{H}$ - $^1\text{H}$  couplings are disregarded. A TOCSY mixing sequence selecting proton magnetization along the  $x$ -axis for coherence transfer carries the magnetization from proton A to proton B without affecting the spin state of the  $^{13}\text{C}$  nucleus, which simply corresponds to exchanging the operator  $H_A$  for the operator  $H_B$  on the right hand side of eq. (3). The resulting cross peak multiplet fine-structure with respect to the  $^{13}\text{C}$  spin is a 1:1 superposition of an absorptive in-phase and an absorptive antiphase doublet in both frequency dimensions. Thus, while each term on the right hand side of eq. (3) represents a cross peak with four multiplet components each, two of the four multiplet components cancel in the superposition. The remaining two multiplet components are shifted in the  $F_1$  frequency dimension by the one-bond  $^1\text{H}$ - $^{13}\text{C}$  coupling constant between spin  $H_A$  and  $C$  and in  $F_2$  by the  $^1\text{H}$ - $^{13}\text{C}$  coupling constant between spin  $H_B$  and  $C$  in the characteristic way of an E.COSY type multiplet fine-structure [19]. Additional homonuclear  $^1\text{H}$ - $^1\text{H}$  couplings do not alter the basic E.COSY type pattern. The displacement of the multiplet components along the  $F_2$  frequency axis makes it easy to measure small heteronuclear multiple bond coupling constants with high digital resolution. Since one-bond  $^1\text{H}$ - $^{13}\text{C}$  coupling constants are large and well resolved, the digital resolution in the  $F_1$  frequency dimension is not critical.

In writing eq. (3), relaxation was neglected. Since antiphase magnetization relaxes more rapidly than in-phase magnetization, relaxation during  $t_1$ , the mixing time, and during  $t_2$  can produce an inequilibrium between the two terms. However, the relaxation effect becomes troublesome only for larger molecules with fast relaxation rates, when the linewidth of the proton signal is larger than the heteronuclear coupling constant. In this situation, it may be difficult to assess whether the in-phase multiplet component dominates the cross peak which would bias the measurement of the multiple bond  $^1\text{H}$ - $^{13}\text{C}$  coupling constant towards too small values.

## 9. Experimental example

Figure 4 shows a TOCSY spectrum with  $^{13}\text{C}(\omega_1)$ -half-filter recorded with the small globular protein bovine pancreatic trypsin inhibitor (BPTI) using the pulse sequence of fig. 3. Although proton multiplets are usually difficult



to resolve in protein spectra, the E.COSY type displacements of the multiplet components are readily observed in the spectrum. The inserts a and b show expansions of the  $^1\text{H}$ - $^1\text{H}$  cross peak between the  $\gamma$ -methyl group and the  $\alpha$ -proton of Ile19. The cross peaks are split in the  $F_1$  frequency dimension by the one-bond  $^1\text{H}$ - $^{13}\text{C}$  coupling constant of the  $\gamma\text{CH}_3$  group and the  $\alpha\text{CH}$  group, respectively. The relative displacements of the two multiplet components in the  $F_2$  frequency dimension reflect the three-bond  $^1\text{H}$ - $^{13}\text{C}$  couplings between the  $\gamma$ -carbon and the  $\alpha$ -proton (insert (a)), and the  $\alpha$ -carbon and the  $\gamma$ -protons (insert (b)).

### 10. Pulse programme for a Bruker DMX NMR spectrometer

```

30m ze
1 60m do:f2          ;f1 is the proton channel,
                    ;f2 is the carbon channel
2 3m
3 10u
  d1 p11:f1 p12:f2  ;d1=relaxation delay, p11=power level  $^1\text{H}$ ,
                    ;p12=power level  $^{13}\text{C}$ 
  (p1 ph1):f1      ;p1=90 degree  $^1\text{H}$  pulse
  d2                ;d2=1/(4J( $^1\text{H}$ ,  $^{13}\text{C}$ ))
  (d12 p1*2 ph2):f1 (p2*2 ph3):f2 ;p2=90 degree  $^{13}\text{C}$  pulse,
                    ;d12=p2-p1
  d2
  (p20 ph1):f1 (p2 ph3 2u p2 ph4):f2 ;p20=spin-lock pulse
                    ;(0.5-3 ms)
  d0                ;d0=incremented  $t_1$  delay
  (p7 ph5):f1      ;500 us trim pulse
4 (2u p1 ph6 d3 p1*2 ph7 d3 p1 ph6):f1 ;MLEV-17 TOCSY
                    ;mixing sequence
  (2u p1 ph8 d3 p1*2 ph9 d3 p1 ph8):f1 ;d3=2.6*p1

```

←

Fig. 4. TOCSY spectrum with  $^{13}\text{C}(\omega_1)$  half-filter recorded with bovine pancreatic trypsin inhibitor (BPTI) at natural isotope abundance using the pulse sequence of fig. 3. Protein concentration 20 mM in  $\text{D}_2\text{O}$ , pD 4.6,  $36^\circ\text{C}$ .  $\tau = 3.4$  ms, spin-lock pulse = 2 ms, TOCSY mixing time = 60 ms. The mixing sequence of the clean-TOCSY experiment was used [39]. Positive and negative levels are plotted without distinction. Two spectral regions containing the  $\gamma\text{CH}_3$ - $\alpha\text{CH}$  and  $\alpha\text{CH}$ - $\gamma\text{CH}_3$  cross-peaks of Ile19 are plotted on an enlarged scale in inserts (a) and (b). The separation of the two vertical lines drawn in inserts (a) and (b) indicate the heteronuclear coupling constants  $^3J(\alpha\text{H}, \gamma\text{C})$  and  $^3J(\gamma\text{H}, \alpha\text{C})$ , respectively. (Reproduced by permission of Cambridge University Press from Otting and Wüthrich [6])

```

(2u p1 ph8 d3 p1*2 ph9 d3 p1 ph8):f1
(2u p1 ph6 d3 p1*2 ph7 d3 p1 ph6):f1
(2u p1 ph8 d3 p1*2 ph9 d3 p1 ph8):f1
(2u p1 ph8 d3 p1*2 ph9 d3 p1 ph8):f1
(2u p1 ph6 d3 p1*2 ph7 d3 p1 ph6):f1
(2u p1 ph6 d3 p1*2 ph7 d3 p1 ph6):f1
(2u p1 ph8 d3 p1*2 ph9 d3 p1 ph8):f1
(2u p1 ph6 d3 p1*2 ph7 d3 p1 ph6):f1
(2u p1 ph6 d3 p1*2 ph7 d3 p1 ph6):f1
(2u p1 ph8 d3 p1*2 ph9 d3 p1 ph8):f1
(2u p1 ph6 d3 p1*2 ph7 d3 p1 ph6):f1
(2u p1 ph6 d3 p1*2 ph7 d3 p1 ph6):f1
(2u p1 ph8 d3 p1*2 ph9 d3 p1 ph8):f1
(2u p1 ph8 d3 p1*2 ph9 d3 p1 ph8):f1
(2u p1*0.66 ph5):f1
lo to 4 times lo ;l0=(mixing time)/(p8*147.86+34us)
go=1 ph0 ;acquisition
30m wr #0 if #0 ip1 zd ;write FID,
;increment phase 1 for States-TPPI
30m ip2 ;increment also phase 2 for
;States-TPPI

lo to 2 times 2
3m id0 ;increment t1
lo to 3 times 11
exit
ph1=0
ph2=0 0 1 1
ph3=0
ph4=0 2
ph5=0 0 0 0 2 2 2 2
ph6=0 0 0 0 2 2 2 2
ph7=1 1 1 1 3 3 3 3
ph8=2 2 2 2 0 0 0 0
ph9=3 3 3 3 1 1 1 1
ph0=0 2 2 0

```

Quadrature images in the  $F_2$  dimension can be suppressed by expanding the 8-step phase cycle to 32 steps or 16 steps, respectively, using CYCLOPS [20] or 2-step CYCLOPS [21]. In the CYCLOPS scheme, the phases of all  $^1\text{H}$  pulses are simultaneously incremented by  $90^\circ$ ,  $180^\circ$  and  $270^\circ$ . In the 2-step CYCLOPS scheme, the incrementation of the pulse phases is limited to the  $90^\circ$  step.

## 11. Solvent signal suppression by spin-lock pulses

Spin-lock pulses can be used to suppress an intense solvent signal within a few milliseconds. As a general strategy a pair of spin-lock pulses can be used which are separated by a short free precession delay and phase shifted by  $90^\circ$  relative to each other. The carrier frequency is set to the frequency of the solvent signal. The first spin-lock pulse serves to select the in-phase magnetization aligned along the phase of the spin-lock pulse. During the following delay, the magnetization of the solute protons precess with respect to the solvent magnetization. The following spin-lock pulse selects the magnetization along the axis orthogonal to the phase of the first spin-lock. With the carrier on the solvent resonance, the solvent magnetization does not precess between the two spin-lock pulses and is therefore eliminated by the second, phase-shifted spin-lock pulse.

Solvent suppression by the use of spin-lock pulses has originally been developed for the observation of water–protein NOEs in NOESY and ROESY experiments [7]. These experiments are performed with protein solutions in  $H_2O$  with 5–10%  $D_2O$  added for the field-frequency lock. Without water suppression, the water resonance would be by far the biggest signal requiring low receiver gain settings for which the signal-to-noise ratio is poor. Since the water signal gives rise to a strong band of  $t_1$  noise, water–protein NOEs can be observed only in the cross-section taken along the  $F_2$  frequency axis at the  $F_1$  chemical shift of the water signal. This means that the water signal must be suppressed only after the magnetization has been transferred from the water to the protein protons during the NOE mixing period. In this application, spin-lock pulses represent one of the fastest techniques to suppress the water signal before acquisition.

## 12. Pulse sequence and product operator description

The use of spin-lock pulses for water suppression is illustrated with the NOESY and ROESY pulse sequences (fig. 5). Using the Cartesian product operator description [9], the effect of the NOESY pulse sequence of fig. 5(A) is readily illustrated:

$$\begin{aligned}
 I_z &\xrightarrow{90_x^\circ} -I_y \xrightarrow{t_1} -I_y \cos(\Omega t_1) \xrightarrow{90_x^\circ} -I_z \cos(\Omega t_1) \\
 &\xrightarrow{\tau_m - 90_x^\circ} I_y \cos(\Omega t_1) \xrightarrow{SL_y} I_y \cos(\Omega t_1) \\
 &\xrightarrow{\tau} [I_y \cos(\Omega \tau) - I_x \sin(\Omega \tau)] \cos(\Omega t_1)
 \end{aligned}$$

$$\xrightarrow{\text{SL}_x} -I_x \sin(\Omega\tau) \cos(\Omega t_1), \quad (4)$$

where SL denotes the spin-lock pulses and unobservable terms have been dropped. Equation (4) shows that the use of the spin-lock pulses results in a non-uniform excitation profile in the  $F_2$  dimension which is zero at the carrier frequency ( $\Omega = 0$ ) and at multiples of  $\Omega/(2\pi) = \pm 1/(2\tau)$ . The water signal is suppressed by setting the carrier frequency at the water resonance. If  $\tau$  is set to the inverse of the sweep width in Hz, the first minima of the excitation function are at the ends of the spectrum. Because of the sine shape of the excitation function, the signals on either side of the suppressed water resonance appear with opposite sign. For improved spectral representation, the sign of the signals in one half of the spectrum can be reversed before plotting.

The first spin-lock pulse in equation 4 apparently does not alter the magnetization. Its function is to ensure the desired coherence transfer pathway by defocusing any magnetization which is not aligned along the  $y$  axis.

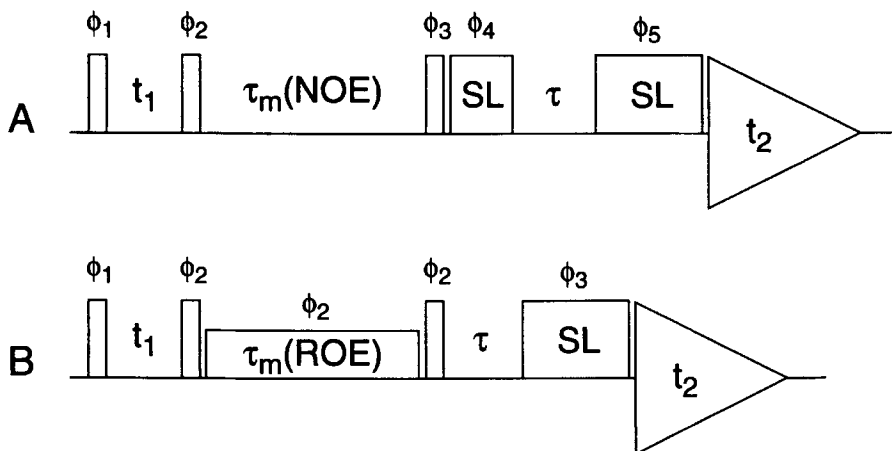


Fig. 5. Pulse sequences of NOESY and ROESY with spin-lock purge pulses for water suppression. (A) NOESY pulse sequence. The spin-lock pulses are typically of length 0.5 ms and 2 ms, and  $\tau = 1/\text{SW}$ , where SW is the spectral width in the acquisition dimension. Phase cycle:  $\phi_1 = 8(x, -x)$ ;  $\phi_2 = 4(x, x, -x, -x)$ ;  $\phi_3 = \phi_5 = 4(x), 4(y), 4(-x), 4(-y)$ ;  $\phi_4 = 4(y), 4(-x), 4(-y), 4(x)$ ; acquisition =  $x, -x, -x, x, y, -y, -y, y, -x, x, x, -x, -y, y, y, -y$ . (B) ROESY pulse sequence. The spin-lock pulse SL is typically 2 ms long, and  $\tau = 1/\text{SW}$ . The mixing time consists either of a low-power spin-lock or of a series of small flip-angle pulses separated by delays [40]. Phase cycle:  $\phi_1 = 4(x, -x)$ ;  $\phi_2 = 2(y, y, -y, -y)$ ;  $\phi_3 = 4(x), 4(-x)$ ; acquisition =  $4(x, -x)$ . The phase of the  $^1\text{H}$  pulse before  $t_1$  ( $\phi_1$ ) is subjected to States-TPPI [38] in both the NOESY and the ROESY pulse sequence.

This is of particular importance for the water magnetization in the NOESY experiment, since radiation damping during the mixing time usually turns the water magnetization into a position which is difficult to predict [22]. The complications caused by radiation damping are avoided, if the transverse components of the water magnetization during the mixing time are defocused by a  $B_0$ -field gradient [23]. This enables to run the NOESY experiment without the first spin-lock pulse [24]. Self-shielded gradients are not required in this experiment, since a 2 ms  $z$ -gradient every 30 ms during the mixing time is sufficient to suppress radiation damping and eddy currents have largely decayed after 30 ms even if the gradients are applied via the room temperature shim system. In the ROESY pulse sequence (fig. 5(B)) the mixing period replaces the first spin-lock pulse of the NOESY pulse sequence (fig. 5(A)) and the water signal is suppressed with only a single spin-lock purge pulse.

### 13. Experimental example

Figure 6 shows the spectral region from a NOESY spectrum of BPTI which contains the NOEs between the water signal in  $F_1$  and the protein resonances in  $F_2$ . The spectral region around the  $F_2$  frequency of the water resonance is not plotted, because this region is obscured by  $t_1$  noise from the water signal. The assignment of the water-protein cross-peaks is hampered by spectral overlap in the one-dimensional protein spectrum. The assignment problem can be solved by three-dimensional experiments, where intra-protein correlations with the water-protein cross-peaks are observed in the third dimension [7].

### 14. Pulse programmes for a Bruker DMX NMR spectrometer

```

;noesy
  30m ze
1 30m
2 3m
3 10u
  d1 p11 : f1      ;d1=relaxation delay, p11=power level 1H
  (p1 ph1) : f1   ;p1=90 degree 1H pulse
  d0              ;d0=incremented  $t_1$  delay
  (p1 ph2) : f1
  d8              ;d8=mixing time
  (p1 ph3) : f1
  4u              ;phase switching delay
  (p5 ph4) : f1   ;spin-lock pulse, p5=500us-1ms

```

```

d2                ;free precession delay, e.g., d2=1/(sweep width)
(p6 ph5):f1       ;spin-lock pulse, p6=2ms-3ms
go=1 ph0          ;acquisition
30m wr #0 if #0 ip1 zd ;write FID,
                  ;increment phase 1 for States-TPPI

lo to 2 times 2
3m id0           ;increment t1
lo to 3 times 11
exit
ph1=0 2
ph2=0 0 2 2
ph3=0 0 0 0 1 1 1 1 2 2 2 2 3 3 3 3
ph4=1 1 1 1 2 2 2 2 3 3 3 3 0 0 0 0
ph5=0 0 0 0 1 1 1 1 2 2 2 2 3 3 3 3
ph0=0 2 2 0 1 3 3 1 2 0 0 2 3 1 1 3

;roesy
30m ze
1 30m
2 3m
3 10u
d1 p11:f1         ;d1=relaxation delay, p11=power level 1H
(p1 ph1):f1       ;p1=90 degree 1H pulse
d0                ;d0=incremented t1 delay
(p1 ph2):f1
4 (8u 4up ph2 8u):f1 ;spin-lock pulse by a DANTE pulse train
lo to 4 times 10 ;mixing time=10*20us
(p1 ph2):f1
d2                ;free precession delay, e.g., d2=1/(sweep width)
(p6 ph3):f1       ;spin-lock pulse, p6=2ms-3ms
go=1 ph0          ;acquisition
30m wr #0 if #0 ip1 zd ;write FID,
                  ;increment phase 1 for States-TPPI

lo to 2 times 2
3m id0           ;increment t1
lo to 3 times 11
exit
ph1=0 2
ph2=1 1 3 3
ph3=0 0 0 0 2 2 2 2
ph0=0 2

```

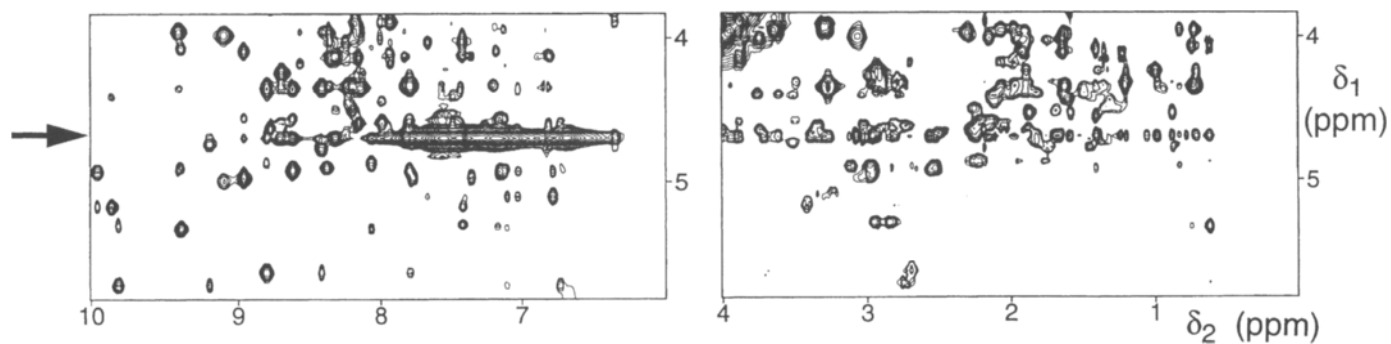


Fig. 6. Selected spectral regions of a NOESY spectrum of BPTI recorded with the pulse sequence of fig. 5(A), except that the first spin-lock pulse was omitted and a  $B_0$  gradient was applied during the NOESY mixing time. Protein concentration 20 mM in 90%  $H_2O$  / 10%  $D_2O$ , pH 6.9, 36°C. The relaxation reagent GdDTPA-BMA was added at a concentration of 750  $\mu M$  to enhance the relaxation of the water protons. Spin-lock pulse 2 ms,  $\tau_m(\text{NOE}) = 50$  ms,  $\tau = 190$   $\mu s$ . Positive and negative levels were plotted without distinction. The arrow identifies the cross section containing the intermolecular water–protein cross peaks. (Reproduced by permission of the American Chemical Society from Otting and Liepinsh [41].)

The phase cycle of both pulse programmes may be expanded four-fold or two-fold by the use of CYCLOPS [20] or 2-step CYCLOPS [21], respectively, to suppress quadrature images in the  $F_2$  dimension.

## 15. Alternatives to spin-lock purge pulses

### 15.1. Pulsed field gradients

In almost all cases, the purging function of spin-lock purge pulses can be achieved equally well or better by the use of pulsed field gradients along the axis of the main magnetic field (PFG). However, PFGs require that the probehead is equipped with self-shielded gradient coils which, as a rule, somewhat decreases the sensitivity of the probehead. Typical PFGs are 0.5 to 2 ms long, i.e., not significantly shorter than spin-lock purge pulses. PFGs suppress undesired coherences best, if they are applied to transverse coherence and used for coherence order selection [25, 26].

Excellent results are routinely obtained when applying PFGs to the transverse  $^{13}\text{C}$  coherence in a  $^{13}\text{C}$  HMQC experiment which is conducted at natural isotopic abundance [27]. Under those circumstances, however, half of the coherence transfer pathways are rejected by the PFGs. More complicated acquisition schemes and additional pulses in the sequence are required to restore the full sensitivity [26, 28, 29]. Spin-lock purge pulses may not purge as well as PFGs, but they are easier to use and don't interfere with a phase-sensitive recording.

PFGs are also the basis for the elegant water suppression scheme called WATERGATE [30] or the excitation sculpting scheme proposed by Hwang and Shaka [31]. These sequences give excellent results, if the selective  $180^\circ$  pulse applied to the water resonance is relatively short. Their main drawback seems to be associated with the fact, that a selective pulse of a few milliseconds duration disturbs a rather wide spectral region around the water resonance. Using longer, more selective pulses leads to increased relaxation and worse quality of water suppression with the WATERGATE sequence. Although the water suppression scheme using spin-lock purge pulses results in a non-ideal excitation profile, it seems to be superior for the observation of rapidly relaxing signals close to the water signal.

The defocusing of the water magnetization by spin-lock purge pulses results in incomplete recovery of the water magnetization between subsequent scans, if the repetition rate is much shorter than the relaxation rate of the water signal. Since the attenuation of the water signal is transferred to any proton of the solute which exchanges rapidly with the water, these proton signals are attenuated as well. To recover the full magnetization between the scans, a paramagnetic relaxation reagent may be used. For example, Gd-diethylenetriamine pentaacetic acid-bismethylamide [Gd(DTPA-BMA)]

at a concentration of 0.75 mM reduces the  $T_1$  relaxation time of the water protons to about 430 ms without much influence on the ease of water suppression [32]. GdDTPA-BMA is a standard contrast reagent used in clinical MR imaging. The compound is uncharged and does not interact significantly with plasma proteins.

### 15.2. BIRD pulse

A BIRD pulse sandwich [33] followed by a delay can be used to suppress the magnetization from  $^{12}\text{C}$ -bound protons [34]. The BIRD pulse sequence is  $90_x^\circ(H) - \tau - 180_y^\circ(H, C) - \tau - 90_x^\circ(H)$ . With the delay  $\tau$  set to  $1/(2J)$ , where  $J$  is the one-bond  $^1\text{H}$ - $^{13}\text{C}$  coupling constant, the effect of the sequence is to invert the magnetization of the  $^{12}\text{C}$ -bound protons but not that of the  $^{13}\text{C}$ -bound protons. During the following delay, the inverted magnetization relaxes back towards the positive  $z$ -axis. The 2D pulse sequence is started at the time point where the magnetization of the  $^{12}\text{C}$ -bound protons is zero.

This suppression scheme has been shown to work well together with  $^{13}\text{C}$  HMQC experiments of small molecules at natural  $^{13}\text{C}$  abundance. Even cleaner spectra are obtained, if the BIRD sequence is combined with  $^{13}\text{C}$  HSQC experiments already containing a spin-lock purge pulse. Drawbacks of the BIRD pulse scheme are the fact that the relaxation delay between scans cannot be chosen freely anymore and that complete suppression of all  $^{12}\text{C}$ -bound proton signals is impossible, if they have different relaxation times. Furthermore, the BIRD pulse scheme is not applicable to molecules in the slow motional regime, since negative NOEs between the inverted proton spins and the non-inverted  $^{13}\text{C}$ -bound proton spins would reduce the magnetization of the latter.

## 16. Conclusion

Although radiofrequency coils are designed for optimum radiofrequency field homogeneity, the spatial distribution of the radio frequency field over the sample is still sufficiently inhomogeneous that their defocusing effect is virtually complete after only 0.5 to 3 ms. Spin-lock purge pulses are thus versatile tools for the suppression of undesired magnetization. They are often used with the experiments discussed above, but also in many other applications, e.g., as trim pulses preceding and following TOCSY mixing sequences [35], for water suppression in 3D NOESY-HSQC experiments [12], for water suppression by total scrambling of magnetization (e.g., [36]), and for the suppression of radiation damping [37].

## References

- [1] C.J.R. Counsell, M.H. Levitt and R.R. Ernst, *J. Magn. Reson.* **64** (1985) 470.
- [2] D.G. Davis and A. Bax, *J. Am. Chem. Soc.* **107** (1985) 2820.
- [3] A.A. Bothner-By, R.L. Stephens, J. Lee, C.D. Warren and R.W. Jeanloz, *J. Am. Chem. Soc.* **106** (1984) 811.
- [4] W.E. Maas, F.H. Laukien and D.G. Cory, *J. Magn. Reson. A* **103** (1993) 115.
- [5] G. Bodenhausen and D. Ruben, *Chem. Phys. Lett.* **69** (1980) 185.
- [6] G. Otting and K. Wüthrich, *Quart. Rev. Biophys.* **23** (1990) 39.
- [7] G. Otting, E. Liepinsh, B.T. Farmer II and K. Wüthrich, *J. Biomol. NMR* **1** (1991) 209.
- [8] G. Otting and K. Wüthrich, *J. Magn. Reson.* **76** (1988) 7870.
- [9] O.W. Sørensen, G.W. Eich, M.H. Levitt, G. Bodenhausen and R.R. Ernst, *Prog. NMR Spectrosc.* **16** (1983) 163.
- [10] S. Mattila, A.M.P. Koskinen and G. Otting, *J. Magn. Reson. B*, in press.
- [11] G. Bodenhausen, R. Freeman and D.L. Turner, *J. Magn. Reson.* **27** (1977) 511.
- [12] B.A. Messerle, G. Wider, G. Otting, C. Weber and K. Wüthrich, *J. Magn. Reson.* **85** (1989) 608.
- [13] A. Bax, R.H. Griffey and B.L. Hawkins, *J. Magn. Reson.* **55** (1983) 301.
- [14] A. Bax, M. Ikura, L.E. Kay, D.A. Torchia and R. Tschudin, *J. Magn. Reson.* **86** (1990) 304.
- [15] K. E. Kövér, O. Prakash and V. Hruby, *J. Magn. Reson.* **99** (1992) 426.
- [16] G. T. Montelione, M. E. Winkler, P. Rauenbuehler and G. Wagner, *J. Magn. Reson.* **82** (1989) 198.
- [17] W. Willker, U. Wollborn and D. Leibfritz, *J. Magn. Reson. B* **101** (1993) 83.
- [18] U. Wollborn, W. Willker and D. Leibfritz, *J. Magn. Reson. A* **103** (1993) 86.
- [19] C. Griesinger, O.W. Sørensen and R.R. Ernst, *J. Chem. Phys.* **85** (1986) 6837.
- [20] D.I. Hoult and R.E. Richards, *Proc. R. Soc. Lond. A* **344** (1975) 311.
- [21] G. Otting, *J. Magn. Reson.* **86** (1990) 496.
- [22] G. Otting and E. Liepinsh, *J. Biomol. NMR* **5** (1995) 420.
- [23] J.L. Leroy, D. Broseta and M. Guéron, *J. Mol. Biol.* **184** (1985) 165.
- [24] G. Otting, E. Liepinsh and K. Wüthrich, *J. Am. Chem. Soc.* **114** (1992) 7093.
- [25] R.E. Hurd, *J. Magn. Reson.* **87** (1990) 422.
- [26] J. Keeler, R.T. Clowes, A.L. Davis and E.D. Laue, *Meth. Enzymol.* **239** (1994) 145.
- [27] R.E. Hurd and B.K. John, *J. Magn. Reson.* **91** (1991) 648.
- [28] L.E. Kay, P. Kcifer and T. Saarinen, *J. Am. Chem. Soc.* **114** (1992) 10663.
- [29] J. Schleucher, M. Schwendinger, M. Sattler, P. Schmidt, S.J. Glaser, O.W. Sørensen and C. Griesinger, *Angew. Chem. Int. Ed. Engl.* **32** (1993) 1489.
- [30] M. Piotto, V. Saudek and V. Sklenář, *J. Biomol. NMR* **2** (1992) 661.
- [31] T. Hwang and A.J. Shaka, *J. Magn. Reson. A* **112** (1995) 275.
- [32] G. Otting and E. Liepinsh, *J. Magn. Reson. B* **107** (1995) 192.
- [33] J.R. Garbow, D.P. Weitekamp and A. Pines, *Chem. Phys. Lett.* **93** (1982) 504.
- [34] A. Bax and S. Subramanian, *J. Magn. Reson.* **67** (1986) 565.
- [35] A. Bax and D.G. Davis, *J. Magn. Reson.* **65** (1985) 355.
- [36] H. Molinari and S. Mammi, *J. Magn. Reson.* **90** (1990) 355.
- [37] G. Otting, *J. Magn. Reson. B* **103** (1994) 288.
- [38] D. Marion, M. Ikura, R. Tschudin and A. Bax, *J. Magn. Reson.* **85** (1989) 393.

- [39] C. Griesinger, G. Otting, K. Wüthrich and R.R. Ernst, *J. Am. Chem. Soc.* **110** (1988) 7870.
- [40] H. Kessler, C. Griesinger, R. Kerssebaum, K. Wagner and R.R. Ernst, *J. Am. Chem. Soc.* **109** (1987) 607.
- [41] G. Otting and E. Liepinsh, *Acc. Chem. Res.* **28** (1995) 171.

This Page Intentionally Left Blank

## chapter 9

---

# Decoupled HMBC (D-HMBC), an Improved Version of HMBC

---

Haruo Seto

*Institute of Molecular and Cellular Biosciences  
University of Tokyo  
Yayoi, Bunkyo-ku, Tokyo 113  
Japan*

Kazuo Furihata

*Division of Agriculture and Agricultural Life Sciences  
University of Tokyo  
Yayoi, Bunkyo-ku, Tokyo 113  
Japan*

This Page Intentionally Left Blank

Heteronuclear multiple bond correlation (HMBC) [1, 2] is one of the most powerful NMR techniques and is now being widely used for structural analysis of complicated molecules. Since it detects  $^{13}\text{C}$ - $^1\text{H}$  long range couplings by the most sensitive NMR nucleus ( $^1\text{H}$ ) by using an inverse detection, its sensitivity is particularly high when the  $^1\text{H}$  signals to be observed appear as sharp lines such as methyl groups. Good examples are seen in the structure determination of microbial polyketide metabolites with many methyl groups such as desertomycin [2] and erythromycin [3].

On the other hand, when  $^1\text{H}$ -signals appear as broad lines due to complicated splitting such as consecutive methylene groups, HMBC suffers from a considerable loss of sensitivity. As a consequence, detection of the cross peaks becomes difficult with, for example, complicatedly split methylene proton signals. This problem arises when the power mode data processing causes cancellation between inphase and antiphase signal components and when the separation of these components with broad signal shapes is small. This situation, which will become more serious for the structural studies of natural products available only in tiny quantity, can be overcome by a new technique, decoupled HMBC (D-HMBC) [4], which gives spectra with improved signal to noise ratio by implementation of  $^{13}\text{C}$ -decoupling during signal acquisition. This article will give detailed explanation of this technique.

The pulse sequences of D-HMBC and HMBC are compared in fig. 1. Relative to HMBC, an additional delay time ( $\Delta$ ) is introduced after the  $^{13}\text{C}$   $90_x^\circ$  pulse to refocus the  $^1\text{H}$  magnetization, and wide band decoupling (MPF) [5] for the  $^{13}\text{C}$  nucleus is employed in D-HMBC. As a result of this modification, a fan out of the  $^1\text{H}$  magnetization is prevented during  $\Delta_2$  in the HMBC pulse sequence. Thus, the spectra can be acquired in the phase sensitive mode by suppressing the decrease of signal to noise ratio due to poor digital resolution (for data processing, see later).

This pulse sequence is essentially the same as that used for HMQC [6]. It should be noted, however, that since the quaternary carbonyl signals appearing at the lowest field (as low as 230 ppm for the ketone carbonyl function) must also be decoupled in this experiment, the decoupling band width required is wider than that used for HMQC which requires the decoupling of only protonated carbons resonating in the range of 0 ~ 140 ppm. To achieve this wide range decoupling, we usually employ MPF decoupling [5] with

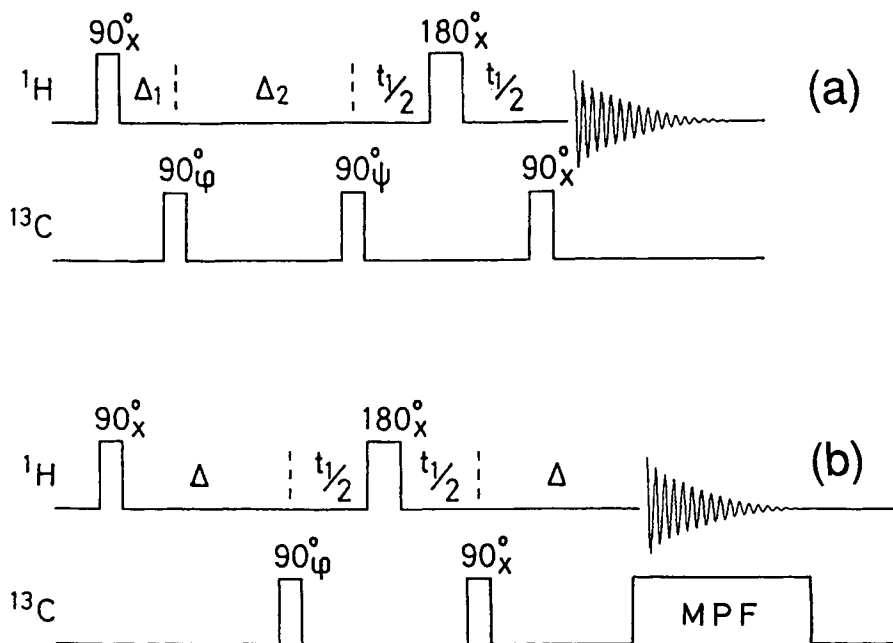


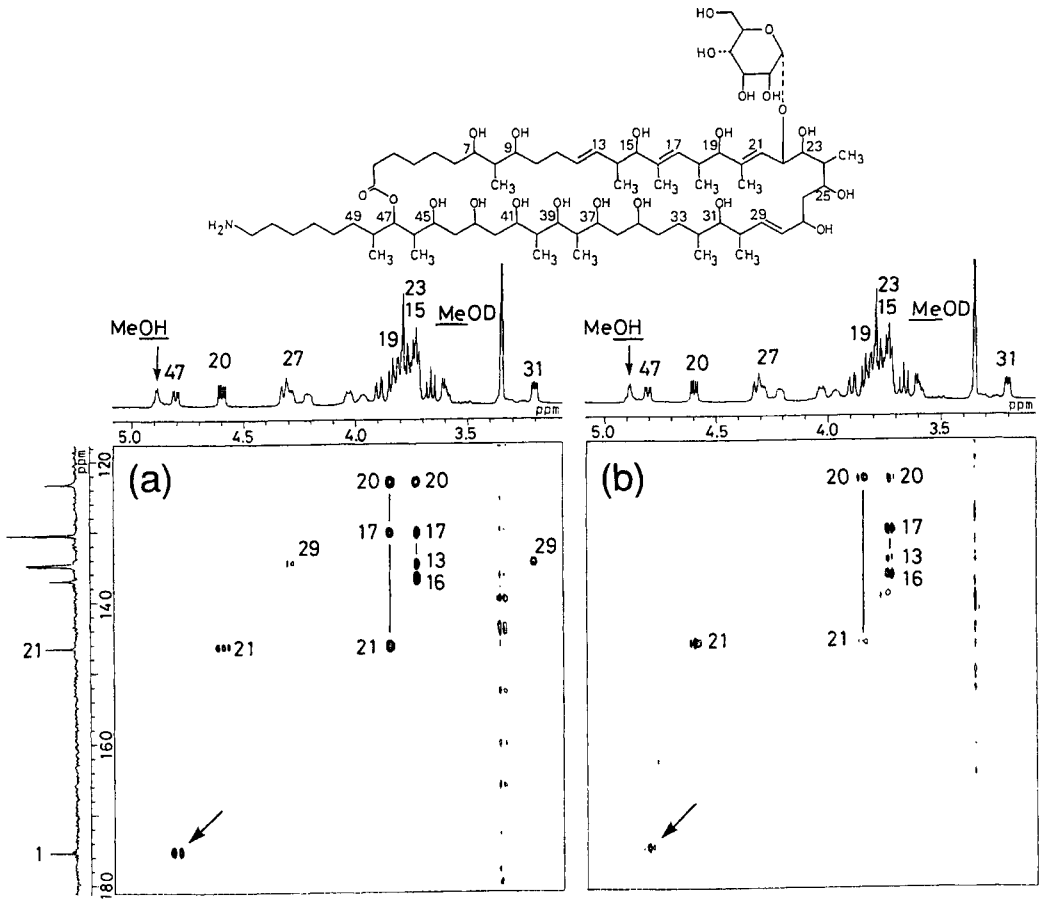
Fig. 1. Pulse sequences of HMBC (a) and D-HMBC (b). Delay times,  $\Delta_1$ ,  $\Delta_2$  and  $\Delta$  were set to 3.5, 50 ~ 60 and 50 ~ 60 ms, respectively.

the decoupler power being set to 2 W resulting in complete decoupling of the direct  $^{13}\text{C}$ - $^1\text{H}$  splittings. This decoupling mode can be replaced by new decoupling techniques [7-9] reported recently.

For D-HMBC experiments, we usually omit the low pass  $J$ -filter (the first  $90^\circ$  pulse for  $^{13}\text{C}$  nucleus in the HMBC pulse sequence) aiming to suppress the cross peaks due to the direct  $J_{\text{C-H}}$  correlation, but it can be implemented if desirable. In the D-HMBC spectra, the cross peaks between directly bonded  $^{13}\text{C}$  and  $^1\text{H}$  do not, in most cases, hinder the easy analysis of the spectra, because these cross peaks appear as singlets. On the contrary, these peaks even contribute to easy NMR spectral analysis when HMQC spectral data are not in hand.

Figure 2 compares the HMBC and D-HMBC spectra of an antibiotic monazomycin [10]. It is seen that several cross peaks, which cannot be ob-

Fig. 2. D-HMBC (a) and HMBC (b) spectra of monazomycin. The experimental conditions were as follows;  $t_1 \times t_2 = 256 \times 512$  points,  $t_1 \times t_2 = 23000 \times 4500$  Hz, times =  $96 \times 2$ , pulse delay = 1.2 s,  $\Delta = 120$  ms. The sample (30 mg) was dissolved in 0.4 ml of  $d_6$ -DMSO.



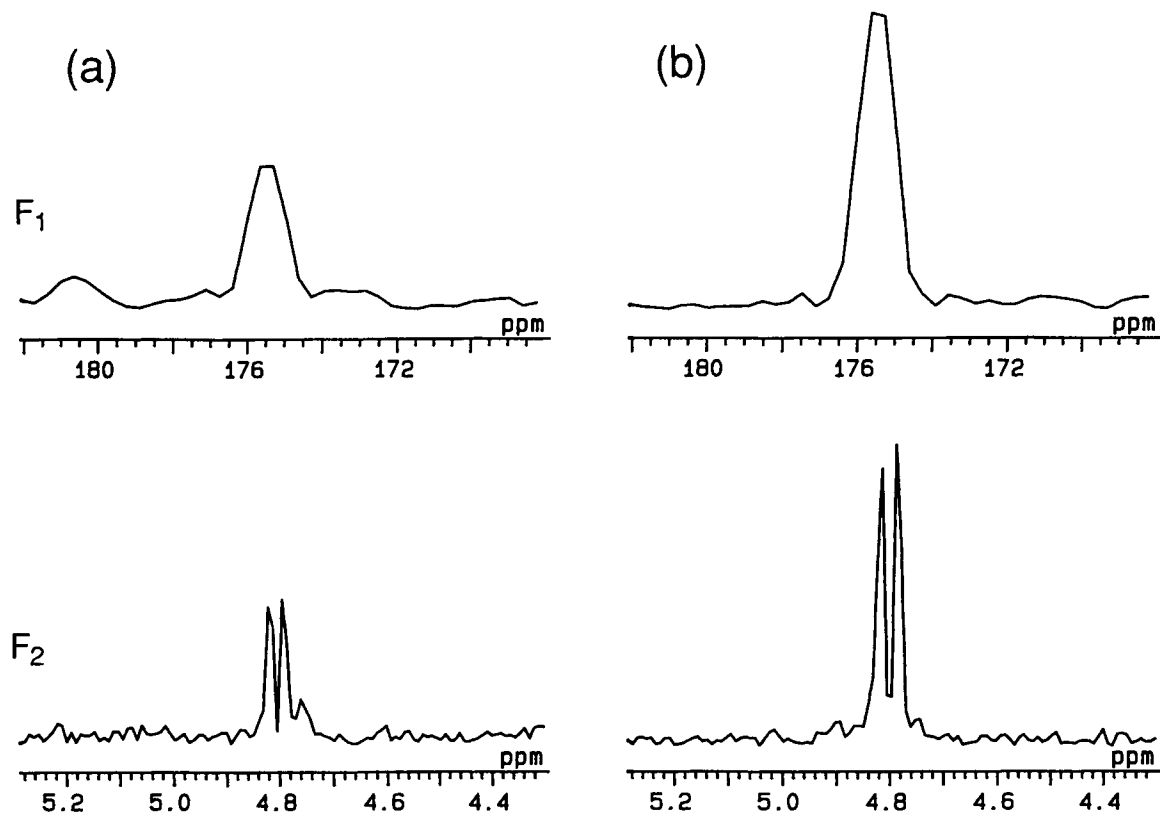


Fig. 3. Comparison of  $F_1$  and  $F_2$  slices between HMBC (a) and D-HMBC (b) spectra of monazomycin. These spectra were prepared at the same recorder gain.

served in the HMBC spectrum (fig. 2(b)), appear between H-19 and C-17, H-27 and H-31 and C-29 in the D-HMBC spectrum (fig. 2(a)). In addition, it should be noted that although the cross peak between the carbonyl carbon (C-1) and oxymethine proton (H-47) is considerably weak in fig. 2(b), its intensity is increased by approximately two folds in fig. 2(a) (shown by arrows). According to our experiences, observation of the cross peak between the ester carbonyl carbon and its appended oxymethine ( ${}^3J_{\text{C-O-C-H}}$ ) in the macrolide system by HMBC is very often hampered due to the small coupling constant between them. Consequently the appearance of this cross peak with the ester carbonyl carbon is an important outcome of the D-HMBC technique.

This improvement is clearly seen in the  $F_1$  and  $F_2$  slices of the same D-HMBC spectrum shown in fig. 3. The intensities of both the  ${}^1\text{H}$ - and  ${}^{13}\text{C}$ -signals in the D-HMBC spectrum are approximately twice as strong as those in the conventional HMBC spectrum. In addition, the resolution is improved in the D-HMBC spectrum. Note that the splitting of the proton signals in the  $F_2$  axis is caused by  ${}^1\text{H}$ - ${}^1\text{H}$  spin coupling and not by  ${}^1\text{H}$ - ${}^{13}\text{C}$  coupling.

Another advantage of D-HMBC is that it facilitates the observation of  ${}^{13}\text{C}$ - ${}^1\text{H}$  long range couplings with small coupling constants. For example, when applied to structural analysis of a thiopeptide compound, promothiocin B produced by *Streptomyces* sp. [11], long range couplings between  ${}^{13}\text{C}$  and  ${}^1\text{H}$  separated by four or five bonds were observed when the delay time was set to 120 ms or 500 ms as shown in figs 4 and 5(b). In addition, very small long range couplings through three bonds (smaller than 2 Hz) which could not be observed by HMBC were detected by D-HMBC. The cross peaks observed in the D-HMBC spectrum with shorter delay time ( $\Delta = 120$  ms) also appeared when longer delay time ( $\Delta = 500$  ms) was employed. However, it should be emphasized that since the long delay time causes considerable decrease of signal to noise ratio, shorter delay time ( $\Delta = 60$  ms) is generally recommended for most experiments.

The successful observation of such long range couplings in the D-HMBC spectra of promothiocin B is obviously ascribed to the sharp shapes of the relevant signals (aromatic and methyl protons) and good planarity of the involved spin systems resulting in relatively large long range couplings through four or five bonds.

Another important fact to be pointed out is that the sample was dissolved in DMSO, which is one of the most unfavorable solvents for observing small long range couplings. The high viscosity of this solvent causes rapid signal decay due to short transverse relaxation time ( $T_2$ ) during long delay time, and makes it difficult to observe small long range couplings. Therefore, long range couplings through four or five bonds in saturated

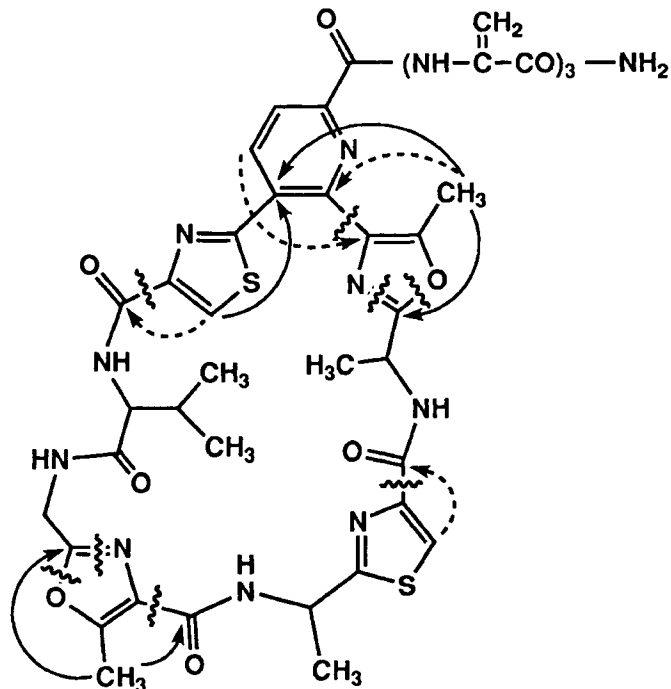


Fig. 4. Long range couplings observed in the D-HMBC spectra of promothiocin B.  $\Delta = 120$  ms for dotted arrows and  $\Delta = 500$  ms for arrows.

systems is generally difficult, if not possible, due to very small coupling constants.

The successful observation of such small long range coupling correlations enabled to connect partial structures of promothiocin established by conventional NMR techniques (fig. 4). It is important to note that these correlations could not be observed in the HMBC spectra even when the same delay time was employed due to poor signal to noise ratio (data not shown). It should also be emphasized that considerably good signal to noise ratio was obtained notwithstanding such long delay time. Thus the undesirable effect of transverse relaxation on signal to noise ratio may be alleviated in the case of D-HMBC.

The D-HMBC pulse sequence can also be used in combination with the pulse field gradient (PFG) technique [12]. Figure 5(c) shows the successful observation of cross peaks between the methyl group at C-5 of an oxazole unit and adjacent carbons in promothiocin. These cross peaks are hidden by the strong  $t_1$  noise of the solvent peak in the HMBC and D-HMBC spectra. The above results clearly indicate that D-HMBC is a quite useful technique for structural studies of complicated natural products.

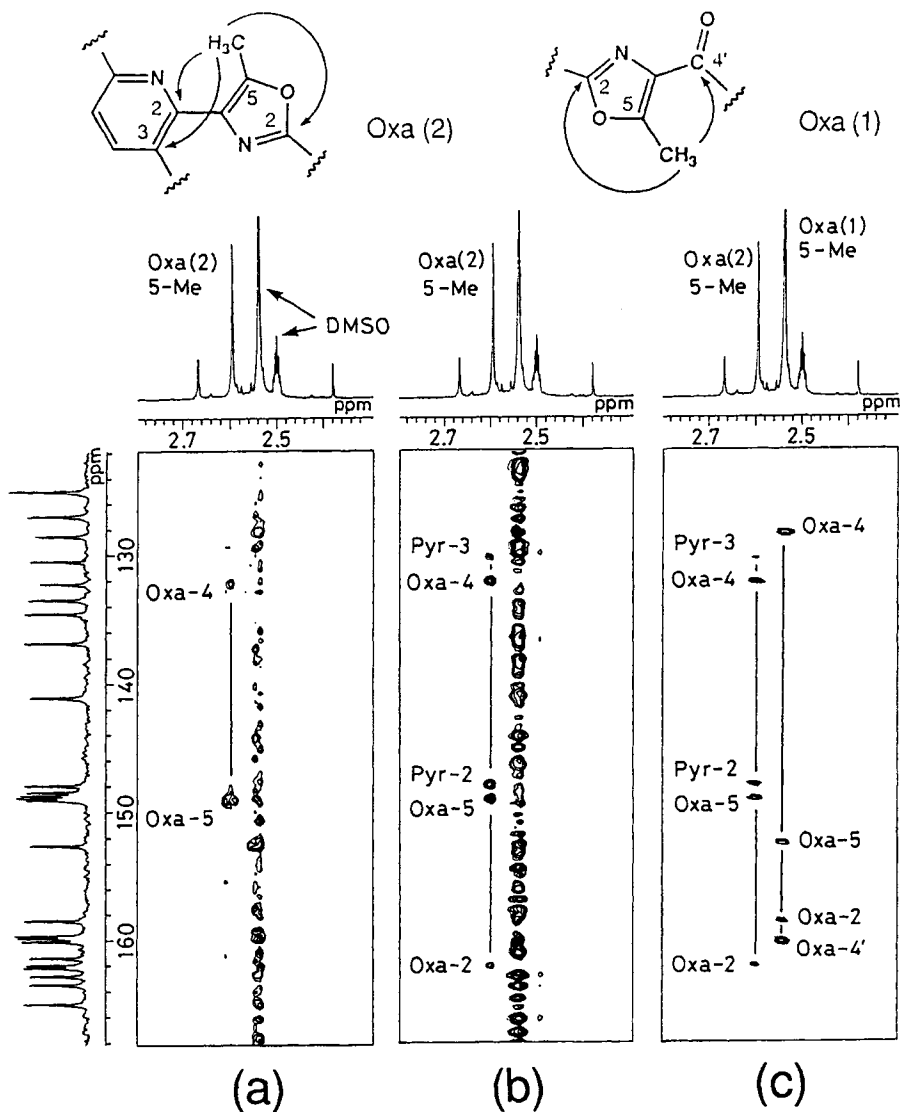


Fig. 5. Comparison of HMBC, D-HMBC and Field Gradient D-HMBC spectra of promethocin B showing long range  $^{13}\text{C}$ - $^1\text{H}$  couplings between methyl protons and relevant carbons of two oxazole units. Delay time was set to 500 ms. The sample (20 mg) was dissolved in 0.4 ml of  $\text{d}_6$ -DMSO.

## 1. Comparison of PFG and D-HMBC

It may be necessary to mention the relationship between PFG and D-HMBC. PFG is an especially suitable method to observe HMBC spectra with suppressed  $t_1$  noise, and enables to detect very weak cross peaks which could

not be detected by HMBC. Therefore, the results obtained by employing the D-HMBC technique can be more easily acquired by the use of the PFG technique. However, since considerable loss of the signal to noise ratio due to the fan out of the  $^1\text{H}$  magnetization (see above) cannot be avoided, it is worthy to try to take D-HMBC spectra when the expected signals cannot be detected by the PFG method. When the signals disappear due to cancellation between inphase and antiphase signals and not due to short  $T_2$ , D-HMBC may give better results. These two situations can be discriminated by taking 1D spin echo spectra. For NMR instruments not equipped with PFG, D-HMBC will always give better results than conventional HMBC.

## 2. Data processing of HMBC spectra

It may be useful to make some explanations on data processing to prepare good D-HMBC spectral data. Sine-bell window is usually employed for processing of HMBC data to give power-mode spectra as shown in fig. 6(a), because they consist of absorption-mode (*cosine*) and dispersion mode (*sine*) signals for both the  $t_1$  and  $t_2$  axes. This procedure causes a considerable loss of signal to noise ratio when cross peaks appear as broad ones and when digital resolution is poor as used for ordinary HMBC measurement.

In contrast, NMR data collected by the States method [13] consist of real ( $S_x$ ) and imaginary ( $S_y$ ) components (fig. 6(b)) which are independently obtained during signal acquisition. The data are Fourier transformed along  $t_2$  axis ( $t_2 \rightarrow F_2$ ). Then the imaginary data ( $I_{r,s}$ ) of  $S_x(t_1, F_2)$  and real data ( $R_{i,c}$ ) of  $S_y(t_1, F_2)$  are exchanged to give  $R_{r,c}$  and  $R_{i,c}$  of  $S_x(t_1, F_2)$  and  $I_{r,s}$  and  $I_{i,s}$  of  $S_y(t_1, F_2)$ . Here r, i, c and s represent real, imaginary, *sine* and *cosine*, respectively. Fourier transformation of  $S_x(t_1, F_2)$  along the  $t_1$  axis gives a pure-absorption mode spectrum as shown in fig. 7(a), where most signals in the  $^1\text{H}$ -spectrum ( $F_2$  axis) are out of phase due to  $J$ -modulation by  $^1\text{H}$ - $^1\text{H}$  couplings. Thus, these data must be recorded in power-mode at the sacrifice of signal to noise ratio and signal resolution.

In order to overcome this problem, the half-absorption mode has been proposed by Bax [14] to take advantage of the phase-mode data processing. In this method,  $R_{s,c}$  of  $S_x(F_1, F_2)$  and  $I_{c,s}$  of  $S_y(F_1, F_2)$  prepared from the data acquired by the States method are exchanged, and the final  $t_2$  axis data containing dispersion component (*sine*) are presented in the power-mode, and the  $t_1$  axis data in the pure absorption-mode as follows;

$$S_{R,I} = \sqrt{R_{c,c}^2 + I_{c,s}^2}$$

This half-absorption mode is also employed for data processing of the D-HMBC spectra with a modification that  $t_2$  and  $t_1$  axes data are treated in

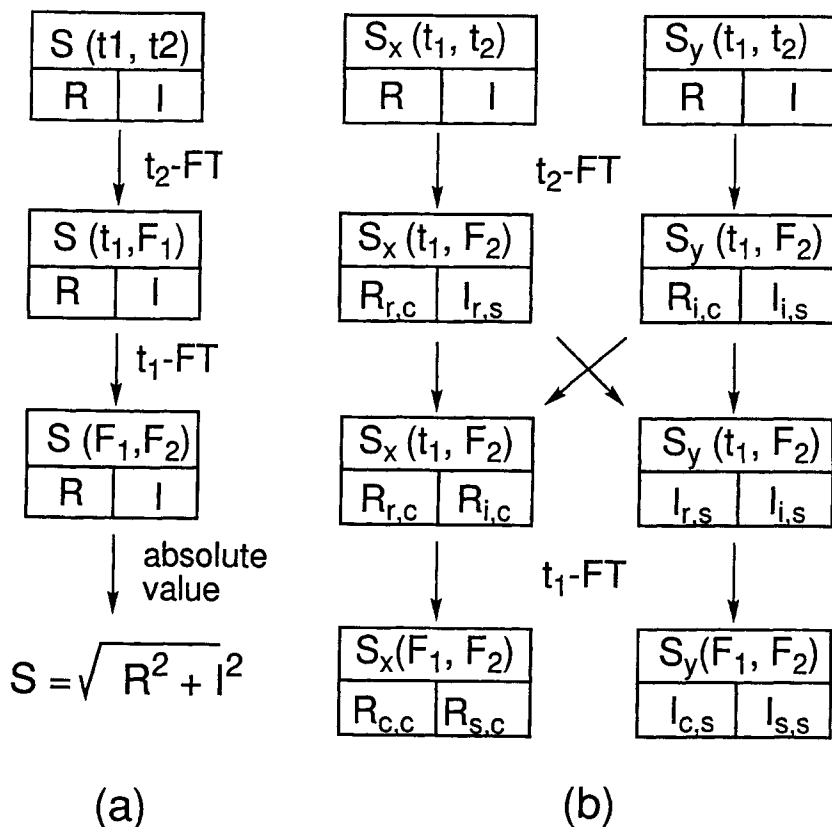


Fig. 6. Data processing procedures used for preparation of absolute or phase-sensitive mode spectra.

the opposite manner, namely  $t_2$  data in the pure absorption-mode and  $t_1$  data containing dispersion component in the power-mode [13]. This procedure requires the phase adjustment of the  $t_2$  axis data to be made before Fourier transformation. The  $t_1$  data containing dispersion component are processed using sine-bell window and presented in the power-mode as follows;

$$S_{R,R} = \sqrt{R_{c,c}^2 + I_{s,c}^2}$$

Figure 7 demonstrates the effects of window functions on the signal to noise ratio of the  $S_{R,R}$  spectrum (for D-HMBC) and  $S_{R,I}$  spectrum.  $S_{R,R}$  spectra shown in fig. 7(c) revealed marked decrease of  $t_1$ -noise in the range between 0.8 to 1.1 ppm. Processing of  $S_{R,R}$  spectral data, however, requires somewhat tedious phase adjustment of the  $F_2$  spectrum. In order to achieve this easily, it is recommended to take a 1D-NMR spectrum at first under

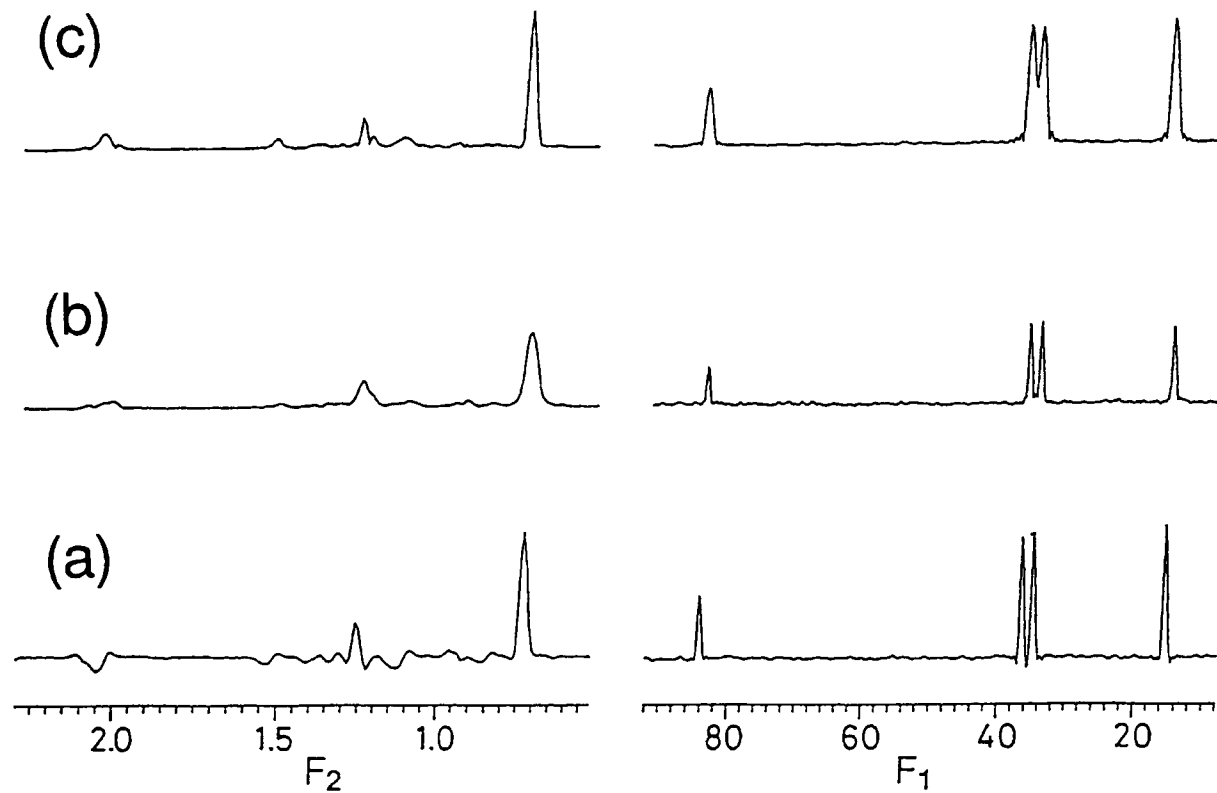


Fig. 7. Comparison of the effects of sinebell and exponential windows used for preparation of power-mode and half absorption-mode spectra. The sample utilized was a polyether antibiotic portmicin [15] (20 mg), which was dissolved in 0.4 ml of  $C_6D_6$ .

the same condition as for the D-HMBC experiment and to determine the parameters for phase correction of the D-HMBC spectrum.

Figure 7(b) shows  $S_{R,R}$  spectral data with improved resolution with regard to the  $F_1$  spectrum. It is seen that better signal to noise ratio can be obtained by  $S_{R,R}$  treatment at a slight sacrifice of signal resolution of  $F_1$  axis as compared with  $S_{R,I}$  mode. However, since improved signal to noise ratio is generally more important than signal resolution,  $S_{R,R}$  processing is preferable from practical view point.

### 3. Important point to get good D-HMBC spectra

One of the most important experimental parameters for taking good D-HMBC spectra is the setting of delay time. To observe cross peaks with  $^1\text{H}$ -signals of concern, it is highly recommended to check the effects of  $T_2$  on the signal decay by taking 1D-spin echo spectra of the target compound. Failure to observe spin echo signals under a given experimental condition means that the employed delay time was not appropriate, and thus shorter delay time must be set for the 2D experiment.

### References

- [1] M.F. Summers, L.G. Marzilli and A. Bax, *J. Am. Chem. Soc.* **108** (1986) 4285.
- [2] A. Bax, A. Aszalos, Z. Dinya and K. Sudo, *J. Am. Chem. Soc.* **108** (1986) 8056.
- [3] H. Seto, K. Furihata and M. Ohuchi, *J. Antibiot.* **41** (1988) 1158.
- [4] K. Furihata and H. Seto, *Tetrahedron Lett.* **36** (1995) 2817.
- [5] T. Fujiwara, T. Anai, N. Kurihara and K. Nagayama, *J. Magn. Reson. A* **104** (1993) 103.
- [6] A. Bax and S. Sabramanian, *J. Magn. Reson.* **67** (1986) 565.
- [7] R. Fu and G. Bodenhausen, *J. Magn. Reson.* **117** (1995) 324.
- [8] M. R. Bendall, *J. Magn. Reson.* **112** (1995) 126.
- [9] E. Kupce and R. Freeman, *J. Magn. Reson.* **117** (1995) 246.
- [10] H. Nakayama, K. Furihata, H. Seto and N. Otake, *Tetrahedron Lett.* **22** (1981) 5217.
- [11] B.-S. Yun, T. Hidaka, K. Furihata and H. Seto, *J. Antibiot.* **47** (1994) 510.
- [12] R.E. Hurd and B.K. John, *J. Magn. Reson.* **91** (1991) 648.
- [13] D.J. States, R.A. Haberkorn and D.J. Ruben, *J. Magn. Reson.* **48** (1982) 286.
- [14] A. Bax and D. Marion, *J. Magn. Reson.* **78** (1988) 186.
- [15] H. Seto, K. Furihata, K. Saeki, N. Otake, Y. Kusakabe, C. Xu and J. Clardy, *Tetrahedron Lett.* **28** (1987) 3357.

This Page Intentionally Left Blank

# chapter 10

---

## Optimal Acquisition and Presentation of HoMQC Spectra

---

István Pelczer

*Department of Chemistry  
Frick Laboratory  
Princeton University  
Princeton, NJ 08544  
USA*

Karl D. Bishop

*Department of Chemistry  
Michigan State University  
East Lansing, MI 48824  
USA*

Methods for Structure Elucidation by High-Resolution NMR  
Edited by Gy. Batta, K.E. Kövér and Cs. Szántay, Jr.  
© 1997 Elsevier Science B.V. All rights reserved

This Page Intentionally Left Blank

## 1. Introduction

Multidimensional NMR spectroscopy includes three major families of correlation techniques: through-bond, through space and exchange correlations [1]. A very interesting and information rich version of through bond correlations is HOmonuclear Multiple-Quantum Correlation spectroscopy (HoMQC). It could also be termed as MQ-COSY, but in order to clearly distinguish MQ correlations from multiple-quantum filtered-, or MQF-COSY we prefer to use the term HoMQC. This method establishes connectivities between spins which have resolved coupling [2–6]. Technical implementation of the HoMQC experiment is relatively simple and is well known [2, 5, 6]. The basic pulse sequence consists of three pulses separated by the MQ excitation delay and the evolution time  $t_1$ , respectively. A refocusing inversion pulse is commonly applied in the middle of the MQ excitation delay in order to remove chemical shift modulation of MQ coherences. Various alterations of this basic composition are possible, but the structure of the final correlation map usually does not change, therefore we are not going to discuss it in here any further.

It is somewhat puzzling that the HoMQC techniques are not more widely used in NMR spectroscopy. The utility of these experiments, including three-dimensional variants [7, 8] has been well demonstrated on several different molecular systems. The power of such applications can be illustrated briefly by the following recent examples. It was shown that two 2D experiments, NOE and 2Q-HoMQC, were sufficient to allow the assignment of 139 of the 143 non-exchangeable protons of a DNA hexadecamer duplex [9]. In order to obtain this information with the conventional methods, several COSY and RELAY-COSY or TOCSY spectra with varying spin-lock times would have been necessary. Also, a novel all-homonuclear 3D-NOE/2QC spectrum led to full assignment of non-exchangeable protons in a 24-mer RNA hairpin with no isotope labeling required [7].

Multiple-quantum correlation spectra provide information about through-bond connectivities as all COSY type experiments do. In addition, direct topology information is also available from the same spectrum through *remote* and *combination* peaks [5]. Correlation peaks between spins with small chemical shift difference can be examined, too, since there are no diagonal peaks. In this sense, a correlation of MQ coherences with those

of single-quantum (SQ) coherences is closely analogous to heteronuclear correlations. (Correlation of MQ/MQ frequencies would only be possible in a three dimensional MQ/MQ/SQ experiment.) In spite of their rich information content HoMQC spectra are significantly underutilized. One reason for the reluctance in its use may be that HoMQC spectra seem to require a disproportional investment in terms of acquisition time and data size in comparison with conventional COSY experiments.

There is a common understanding that HoMQC spectra need a large frequency window in the remote dimension due to the sum frequencies of individual contributions to the multiple-quantum coherence order (with the exception of that for zero-quantum, or 0Q-HoMQC spectra, where difference frequencies count). Of course, this would make such correlations disadvantageous for practical reasons, since sufficient digitization in the remote dimension is always costly in time [10]. In this work we show that in most cases, especially in those of important biomolecules such as proteins and nucleic acids, optimal acquisition conditions can be achieved by taking advantage of appropriate aliasing without producing severe overlap of important correlation peaks. As a result, HoMQC spectra often require the same (or less) overall acquisition time than that for common COSY spectra. Similarly, data size is not a significant problem either. Should the comparison be normalized to the information content, HoMQC spectra are definitely superior, especially if various coherences were selected through data processing instead of using hard-wired phase cycling procedures. An alternative will also be mentioned where no "selection" is necessary, by placing the carrier off resonance.

Spectral rearrangement of double-quantum correlations in combination with dispersive phasing along the direct acquisition dimension (DA phasing [11]) will also be discussed briefly. Such rearrangements lead to 2Q-HoMQC frequency domain spectra which can be symmetrized with conventional software tools in order to highlight direct correlation peaks against others, improve signal-to-noise and resolution. COSY type (diagonally symmetric) presentation of pure phase 2Q-HoMQC spectra through data processing also becomes available.

## 2. Discussion

### 2.1. Aliasing in the remote dimension

Aliasing is a term for choosing slower digitization than required by the Nyquist-theorem to cover the full spectral window, while sign discrimination is accomplished by simultaneous acquisition of real and imaginary phase components (called also "complex" acquisition) [10, 12]. Sequential acquisition for sign discrimination (either TPPI, or the Redfield–Kunz

approach) leads to a different way of “folding” [10, 12] which offers advantageous behavior only in carefully adjusted special circumstances [13]. In the following, simultaneous acquisition will be assumed except when noted otherwise.

We should keep in mind that when the acquisition is S/N limited only data size can be reduced by aliasing. Spectral resolution and signal-to-noise will remain the same whether full size or reduced spectral window was chosen for the remote dimension if sensitivity, which is determined by the overall number of scans, has to be kept constant. For correct comparison  $t_1^{\max}$  should be the same, of course. For example, it is equivalent to acquire  $2K^*$  points and 32 scans averaged for every  $t_1$  increment with 200  $\mu\text{s}$  dwell time (corresponds to 5000 Hz spectral window,  $t_1^{\max} = 409.6$  ms), or  $1K^*$  points and 64 scans per increment with 400  $\mu\text{s}$  dwell time. The double dwell time (in other words half digitization speed) corresponds to 2500 Hz window, i.e., single aliasing, but  $t_1^{\max} = 409.6$  ms; therefore spectral resolution remains the same. Time domain data size was cut by half. However, in order to retain the same sensitivity, twice as many scans should be acquired for each  $t_1$  increment. Please note, that relaxation conditions in  $t_1$  will be the same in both cases; only digitization speed was altered. In such a S/N limited case opening up the spectral window in the remote dimension with proportionally less number of acquisitions per increment may still offer some advantage due to better noise reduction by the “oversampling” effect [14–16].

Aliasing in the remote dimension is truly worthwhile only if the sample concentration is high enough to collect only the minimum number of scans per increment required for proper coherence selection; in other words, the acquisition is not S/N limited. If so, aliasing offers a proportional saving in acquisition time and data size for a given spectral resolution.

It has been shown that 2D-INADEQUATE spectra (in fact,  $^{13}\text{C}$ ,  $^{13}\text{C}$ -2Q-HoMQC at natural  $^{13}\text{C}$  abundance) [17] can be acquired most economically with equal spectral windows for both the direct and remote dimensions [18]. This is based on the fact that aliasing in the remote dimension (provided that simultaneous acquisition was used for quadrature sign discrimination [10]) will transfer cross peaks from outside of the selected frequency range into areas which would otherwise be empty. An alternative approach, which is related to the historically well known SECSY method [19] reduces the resonance frequencies in the remote dimension by delayed acquisition [20]. It leads to diagonally symmetrical frequency domain spectra which can be symmetrized using most conventional software tools [21]. However, this experimental approach has been shown to be less sensitive than that of the original version [18]. Alternatively, there are possible methods of data processing which may allow symmetrization using conventional software tools (see later).

The 2D-INADEQUATE spectra are very simple in characteristics; only AB type correlations will show up [17]. However, in a more general case, when more than two spins can interact, the connectivity pattern becomes more complex, including remote and combination peaks [5]. Such peaks can be largely suppressed using a read pulse other than ninety-degrees (60 or 120 degree pulses are most efficient) in order to simplify the HoMQC spectrum similar to that in 2D-INADEQUATE [4, 6]. Remote and combination peaks carry, however, important additional connectivity and topological information [5] and are very much worthwhile to retain. Combination peaks may show up in two-quantum spectra first as derivatives of four-quantum transitions. They are barely seen in most HoMQC spectra of biomolecules due to the usually insufficient number of mutually coupled spins and fast relaxation of higher number of quanta. Therefore we shall focus on direct and remote peaks in the following discussion. On fig. 1 theoretical 2Q and 3Q correlation patterns (direct and remote peaks) of an ambient AMPX spin system are shown. It is quite obvious that significant segments of these cor-

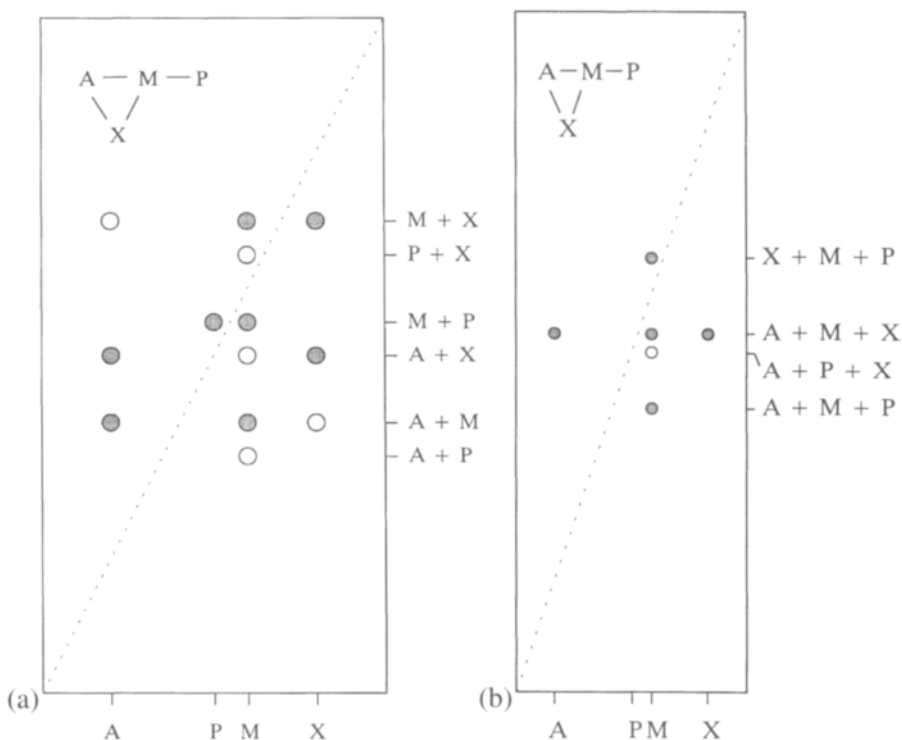


Fig. 1. Schematic 2Q (a) and 3Q (b) correlation maps for an ambient AMPX spin system. Direct correlation peaks are denoted with filled circles, while remote peaks are shown with open circles. Full remote dimensions are presented with no aliasing or folding.

relation maps remain blank; therefore single aliasing would not jeopardize any important information.

### 2.2. *Position of the carrier in the direct acquisition dimension*

The carrier position in the directly detected dimension may seem to be important; however, in most cases it is not critical whatsoever. The one exception is when no quadrature detection in the remote dimension is desired (see below). In a general scenario the carrier can be placed anywhere in the spectral region of interest with no significant penalty on overall acquisition time. The only important requirement to be fulfilled is that the pulse(s) should cover the desired frequency range with sufficient uniformity (see also below).

In the directly acquired dimension the spectral window can be opened up to cover all frequencies of interest on both sides of the carrier with a proportional increase in the overall data size. As an alternative, it may be sufficient to open the (audio)filters to allow signals to alias to empty regions (if any) with no intensity loss. Carrier shift using time domain tools in data processing can be applied to restore a more convenient arrangement of the spectrum [10].

In the remote (or indirectly acquired) dimension(s) there are no actual filters, so aliasing can be used at will.

### 2.3. *No quadrature detection in the remote dimension*

One may use no quadrature detection in the remote dimension at all, thereby accepting some degree of overlap of correlation regions [22]. By judicious placing of the carrier within the spectral region of interest, one can solve many correlation patterns. This approach is, however, limited to relatively sparse spectra and needs careful planning ahead.

One can avoid overlap in the remote dimension if the carrier was moved away sufficiently from the spectral region of interest. In this case there will be no need for explicit quadrature detection neither in the direct, nor in the remote dimension, while pure phase character is still retained. Two-channel (e.g., quadrature) detection in the direct acquisition dimension offers, however, a sensitivity advantage of factor of  $\sqrt{2}$  [23] with no extra cost in acquisition time, so it is worthwhile to retain.

With the carrier off-resonance coherence selection may be completely omitted, too, because most SQ and various MQ cross peaks will appear shifted from each other in the remote dimension. The separation is a function of the distance between the individual (SQ) resonances and the carrier. All number of quanta, including 0Q correlations, can be covered by removing the refocusing  $180^\circ$  pulse in the middle of the MQ excitation delay. This introduces modulation of cross peak intensities by the chemical shift, too, however [6].

There are two limitations for using the off-resonance approach. RF pulse strength is one of these, as it defines the frequency range which can be covered with reasonable uniformity. This becomes a more difficult issue when other than  $^1\text{H}$  spectra are concerned, such as the case of  $^{13}\text{C}$ ,  $^{13}\text{C}$ -HoMQC [16, 24, 25]. The applicable pulse power is limited by the hardware, especially by the probe. In such cases application of adiabatic pulses may provide a promising alternative to cover large frequency windows.

The other, not nearly as significant disadvantage is that of increasing data size in the time domain. When the carrier is moved outside of the spectral window of interest the spectral window to be covered is increased by a factor of two (or more). Consequently, twice as many data points should be acquired for the same resolution. Nevertheless it means no increase in the acquisition time ( $t_n^{\text{max}}$ ) if no quadrature detection in the remote dimension will be required [10]. Acquisition of real and imaginary components of the time domain signal for actual quadrature detection in the remote detection is entirely equivalent to acquiring singlature data with double digitization speed in order to cover twice as much of the spectral window in the frequency space. In summary, overall size of time domain data will be increased by a factor of two at least. However, final size of the frequency domain spectrum remains the same because half of the processed spectrum is mirror image of the other half and can be thrown away during processing.

#### *2.4. Various numbers of quanta by data processing*

It is possible to perform coherence selection during data processing rather than using phase cycling or gradient selection procedures in data acquisition. It will increase the size of the time domain data and increase the complexity of the data processing procedure [10, 16, 26]. Acquisition time will not have to be compromised in a common case; one just replaces addition-subtraction steps in the phase cycling procedure with the same in data processing afterwards. In the following we do not address this in detail, but want to underline that various HoMQC spectra discussed separately may be derived from a single acquisition through linear combination of subsets of the time domain data.

#### *2.5. 2Q- and 3Q-HoMQC in combination*

The most practical and useful HoMQC methods are the 2Q- and 3Q-HoMQC techniques. In combination they offer extensive information about connectivity and topology through chemical bonds for most biomolecules. 2Q-HoMQC spectra are perhaps most important because they reveal the smallest coupled clusters in spin systems where at least two spins are connected with reasonable coupling constants. In addition a great variety of other connectivities will usually show up. Sensitivity of 2Q spectra is also

greater than that of higher quanta. 3Q spectra are less crowded than that of 2Q and can reveal connectivity for quite complex spin-systems [27]. Total number of spins connected in a single cross peak pattern can be significantly higher than the basic number of quanta in the experiment through remote (and combination) peaks, provided that resolved couplings of sufficient size exist between them [5, 6].

2Q and 3Q correlations can be utilized in combination with highest efficiency. In some cases more than one spectrum of each is worthwhile to acquire because cross peak intensity is an explicit function of all coupling constants involved [6, 27, 28]. Coherences of higher order than 3Q exhibit significantly reduced sensitivity. Also, few spin systems in biologically relevant molecules allow sufficient communication between multiple spins to allow observation of higher order spin systems.

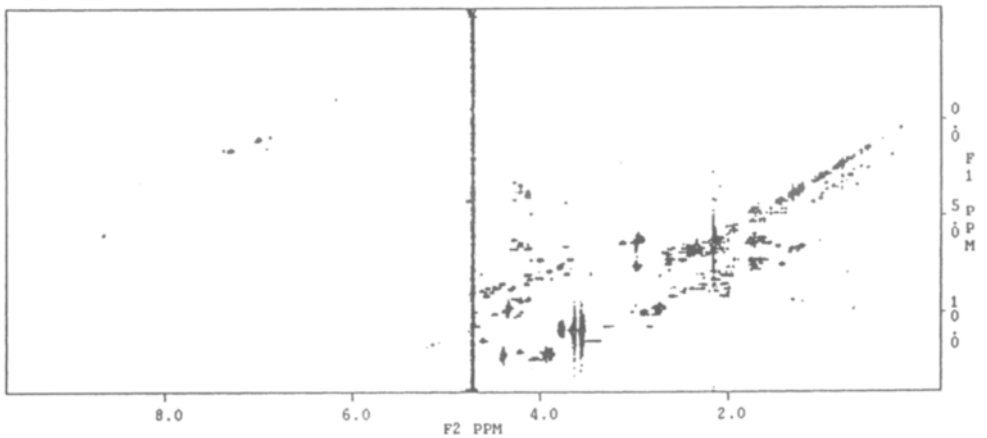
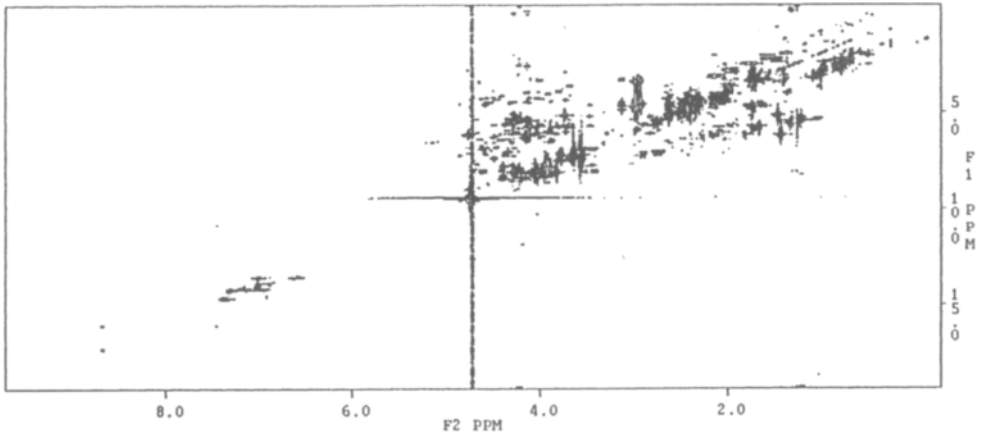
### 3. Practical examples

#### 3.1. Proteins

$^1\text{H}$  NMR protein spectra in  $\text{D}_2\text{O}$  offer an obvious example where the remote dimension in a HoMQC experiment can be chosen equal to (or even less than) that for the direct acquisition dimension, which covers all resonances. In such samples there is practically no through bond communication between the low field section (aromatic resonances) and that of the rest of the spectrum. Therefore, there is no risk of overlapping important correlation regions of the spectrum if single (or sometimes as much as double) aliasing is applied to 2Q and 3Q spectra, respectively. As the carrier is placed on the residual water signal usually, some of the correlation peaks will be aliased. In order to achieve a visually more appealing and easier to analyze spectrum the spectral window can be shifted using simple time domain tools [10]. An example is shown in fig. 2, which presents both  $^1\text{H}$  2Q- and 3Q-HoMQC spectra of rabbit uteroglobin in  $\text{D}_2\text{O}$ .

Very much the same applies to  $^{13}\text{C},^{13}\text{C}$ -HoMQC spectra of  $^{13}\text{C}$ -labeled proteins. When fractional labeling is used [24, 25] there is no difference from regular 2D-INADEQUATE spectra; only AB coupling systems will be seen. Full labeling, commonly available these days for biomolecules, has its advantages due to more extended spin systems and additional topological information available [28] as mentioned above. The structure of these spectra is quite similar to that of proton HoMQC of proteins with the same options for aliasing. 2Q- and 3Q-HoMQC spectra complement each other very well in such systems both for proton and carbon.

COSY type  $^1\text{H}$  NMR experiments for  $\text{H}_2\text{O}$  samples are established primarily to reveal coupling connectivities between exchangeable *NH* protons and those in the alpha position. The chemical shift difference of these pro-



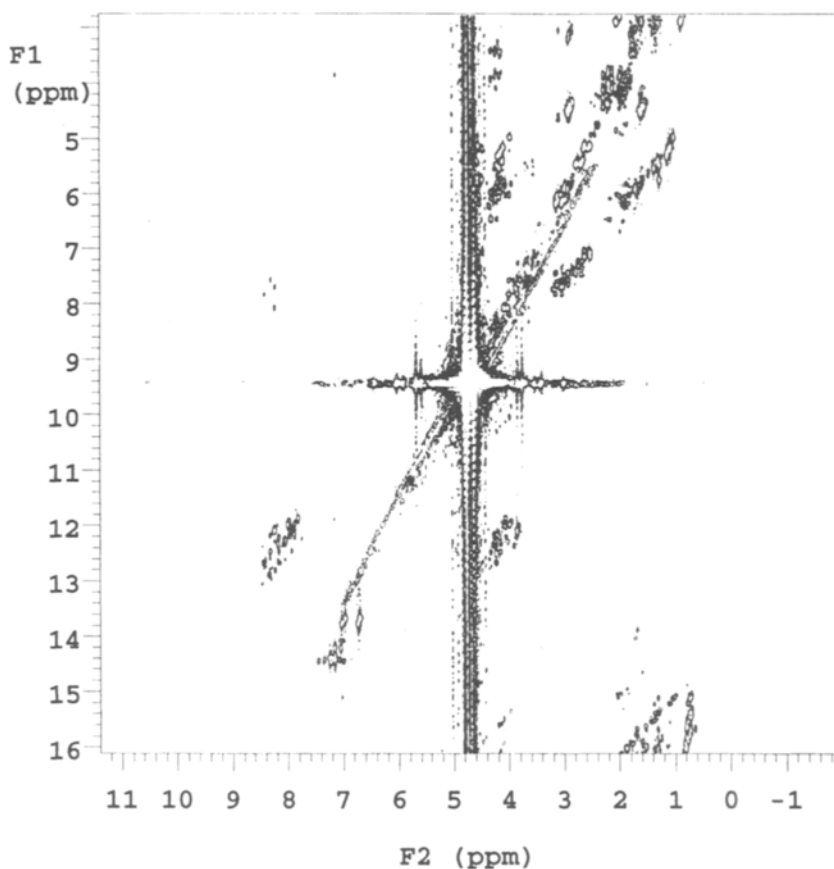


Fig. 3. 2Q-HoMQC spectrum of *apo*-cytochrome *c* in 93% H<sub>2</sub>O at pH = 6 and 0.48 mM concentration. The spectrum was acquired with 30 ms 2Q excitation delay overnight on a Varian Unity/INOVA 600 MHz instrument using gradient MQ selection and no additional water suppression (I.P., unpublished). Equal spectral windows were set for both dimensions.

tons is in the range of ca. 3.5–5 ppm, and their double-quantum frequency falls between those of aromatic protons and the carrier position (center) in the remote dimension. Therefore equal spectral windows will always be adequate for mapping the  $NH\text{-}\alpha CH$  direct connectivities. Unique  $NH\{\alpha\text{-}$

Fig. 2. <sup>1</sup>H, <sup>1</sup>H-2Q-HoMQC (top) and 3Q-HoMQC (bottom) spectra of rabbit uteroglobin in D<sub>2</sub>O [16]. Spectral windows for the direct and remote dimensions are the same in each case. For the 3Q spectrum the frequency window in the remote dimension was shifted by half inverting every other complex points in time domain [10] in order to bring all high-field correlations together for easier analysis.

$CH'$ ,  $CH''$ } remote correlations for Gly residues will show up in a position approximately mirror image to  $F_1 = 0$ .

Figure 3 presents an example of such a situation. The 2Q-HoMQC spectrum of apo-cytochrome *c* was acquired in 93%  $H_2O$  at 480  $\mu M$  concentration on a Varian Unity/INOVA 600 MHz NMR instrument overnight, using a pulse sequence with gradient coherence selection and weak gradient spin-echo during excitation delays and the evolution period [29], respectively (I.P., not published). The spectral windows were 8 kHz both in  $F_2$  and  $F_1$ .

3Q-HoMQC spectra will not provide information about direct correlation of the exchangeable  $NH$  protons other than those of Gly  $\{NH, \alpha-CH', CH''\}$  peaks which are easy to recognize in the 2Q spectra. Remote  $\alpha CH\{NH, \beta CH\}$  correlations represent valuable connectivity and topology information and opportunity for assignment of the corresponding  $\beta CH$  [27]. Such peaks will be relatively close to the  $F_1 = 0$  location and require no wide frequency window in this dimension at all.

### 3.2. DNA

One of the most attractive examples of using aliasing for HoMQC spectra is provided by the carrier of genetic information, DNA. In nucleic acids exchangeable protons have no resolved coupling contacts to other protons, therefore only  $D_2O$  samples will be considered in the following. The resonances in the  $^1H$  spectrum of such molecules commonly are at chemical shifts which make it very feasible to use efficient aliasing, in turn reducing the overall size and/or acquisition time. We have recently demonstrated that aliasing by a factor of two is straightforward and leads to no loss of information with the direct, or the very informative remote peaks [9]. Figure 4 presents a practical example of a DNA hexadecamer duplex without and with aliasing applied. It is quite apparent that almost no overlap of important resonances on the 2D spectrum should be expected.

### 3.3. RNA

RNA, which is rapidly becoming the target of many current NMR structural studies, has unique spectral features. Almost all the protons are crowded together within a ca. 1.5 ppm range. The only exceptions are  $H1'$  and base protons, and those of resonances exchangeable with water. This dramatically reduces the spectral window to be covered when HoMQC spectra are concerned. At the same time, correlations are arranged in a way which again allows extensive aliasing with no loss of information. Due to the largely linear topology of coupled protons in the sugar ring the only remote correlations which point out of the narrow region of 1.5 ppm mentioned above are those direct connectivities between  $H1'$  and  $H2'$ , as well as remote  $H2'\{H1', H3'\}$  correlations. As soon as the chemical shift difference

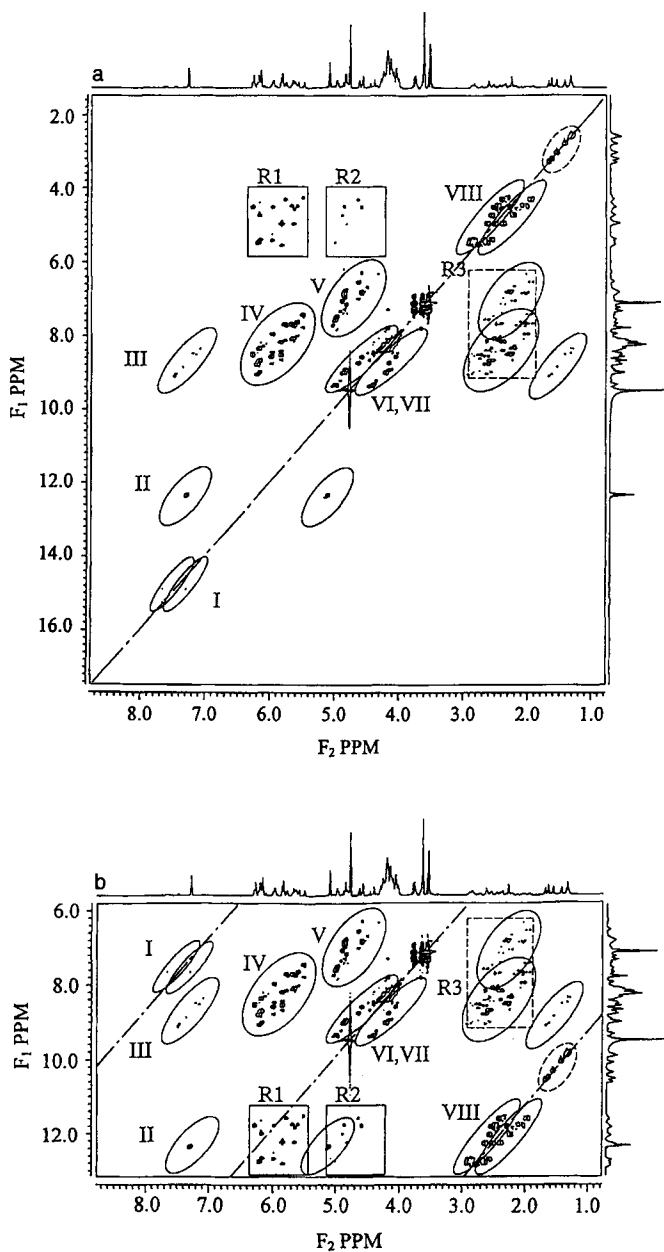


Fig. 4. 2Q-HoMQC of the DNA  $[d(AAATATAGCTATATTT)]_2$  at 500 MHz and 25°C without (top) and with (bottom) aliasing. The 2Q pseudo-diagonal is denoted by dot-dashed lines. Regions for direct correlations and remote correlations are highlighted by ellipsoids and rectangles, respectively. For more details see ref. [9]. (Copyright Academic Press, with permission)

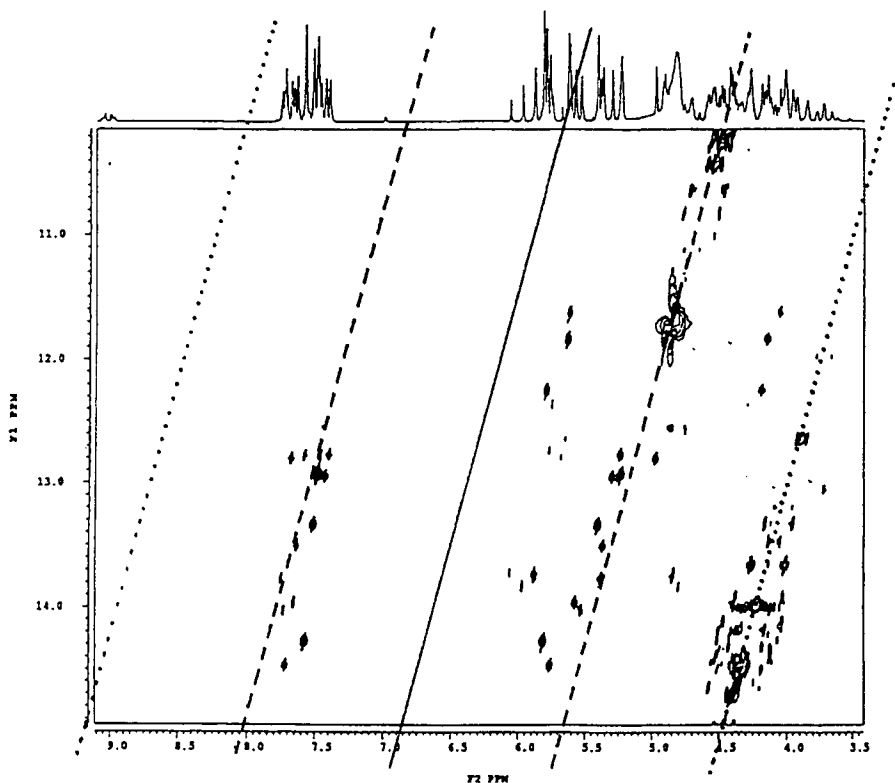


Fig. 5. Multiple aliasing for 2Q-HoMQC of a 24-mer RNA hairpin [7]. The spectrum was acquired in  $D_2O$  with presaturation of the residual water signal. Relevant sections of the 2Q pseudo-diagonal are denoted with solid line (no aliasing), dashed line (single aliasing), dotted line (double aliasing).

of  $H2'$  and  $H3'$  is relatively small, these remote peaks show up in the same area where direct  $\{H1', H2'\}$  peaks can be found. All other  $^1H$  resonances occupy such fortunate locations for RNA that multiple aliasing can easily be used, as it is illustrated in fig. 5 for a 24-mer RNA hairpin structure in  $D_2O$ . Multiple aliasing is especially helpful when three-dimensional extensions of HoMQC techniques are concerned, as was shown for the same sample recently [7].

### 3.4. Other structures

There are other structures which have well dispersed resonances and extensive set of resolved couplings. In some cases it may be unreasonable to use aliasing, because it might move important correlation regions on top of each other, introducing serious overlap. However, such systems are quite rare (are sought to be subjects of illustrations in textbooks); the strategy

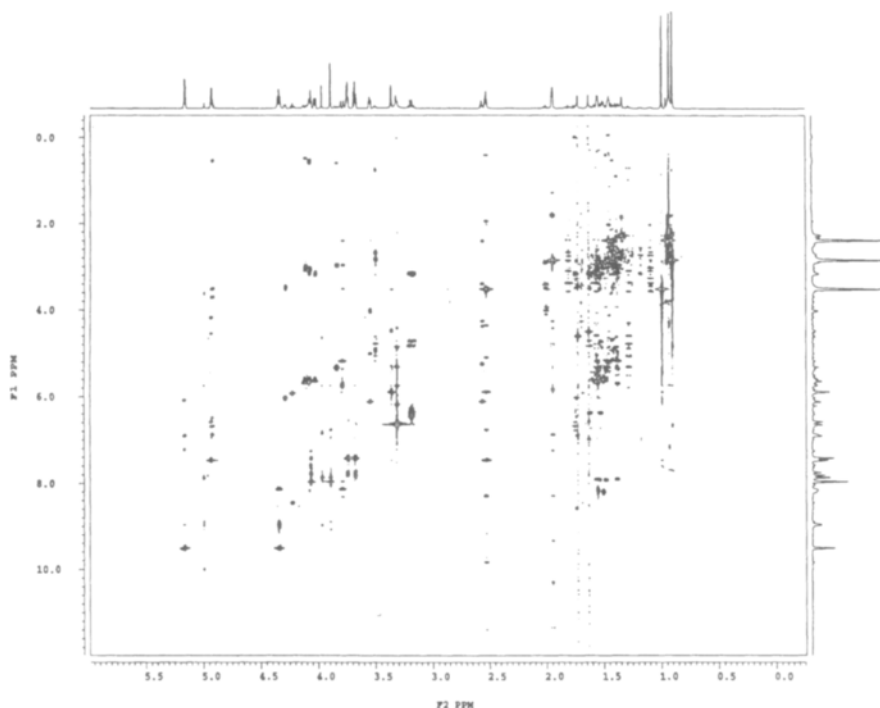


Fig. 6. 2Q- (this page) and 3Q- (next page) HoMQC spectra of the major component of primycin [30] acquired in methanol- $d_4$  on a Bruker DRX-800 (800 MHz) instrument (Biozentrum, J.W. Goethe-Universität, Frankfurt, Germany). For each spectrum equal spectral windows were chosen for the direct and remote dimensions.

presented in this work can therefore be applied with no significant risk most of the time.

As an example of a more dispersed system,  $^1\text{H}$  2Q- and 3Q-HoMQC spectra of the cyclic antibiotic primycin [30] recorded at 800 MHz [31] are shown in fig. 6. This molecule has a sequence of alternating  $\text{CH}(\text{OH})$  and  $\text{CH}_2$  groups, establishing correlations both within, and between the two extreme regions of the spectrum. The spectral windows could be still chosen to be equal with no serious overlap introduced on the final spectrum.

#### 4. Symmetric 2Q-HoMQC spectra through data processing

Aliasing in the remote dimension is most beneficial when the number of acquisitions for each increment can be kept to a minimum. Should the number of scans be increased beyond the minimum, opening up the spectral window in the remote dimension may be a better choice than increasing the number of scans per increment. However, this will result in a larger data size.

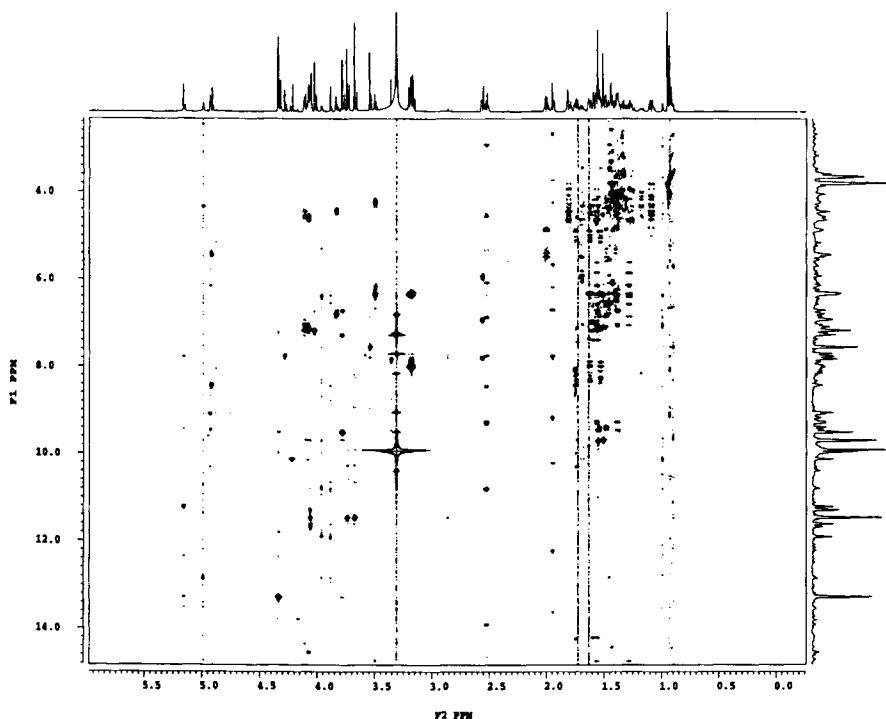


Fig. 6. (Continued)

Should at least a full spectral window be acquired for a 2Q-HoMQC spectrum, there are interesting possibilities for data manipulation through processing.

Pairwise symmetry of cross peaks to a single pseudo-diagonal applies only to the direct correlation peaks in 0Q- and 2Q-HoMQC spectra. All other peaks, and those in correlations of higher number of quanta, occupy systematic and predictable positions, of course, but their relative location can not be expressed in terms of mirror image symmetry of some kind.

Symmetry relationship of cross peak locations has been used for improving the quality of correlation spectra for quite a long time in NMR spectroscopy both for diagonally [21] and laterally symmetric spectra [22]. Such data processing procedures have their advantage but may introduce artifacts and remove real information and therefore should be used with caution [10]. 2Q-HoMQC spectra can be symmetrized directly using the appropriate symmetry function [33], but most commercial software do not provide such option. Also, fine structure of the direct correlation peaks in 2Q-HoMQC spectra is antisymmetric in the SQ dimension which requires extra attention.

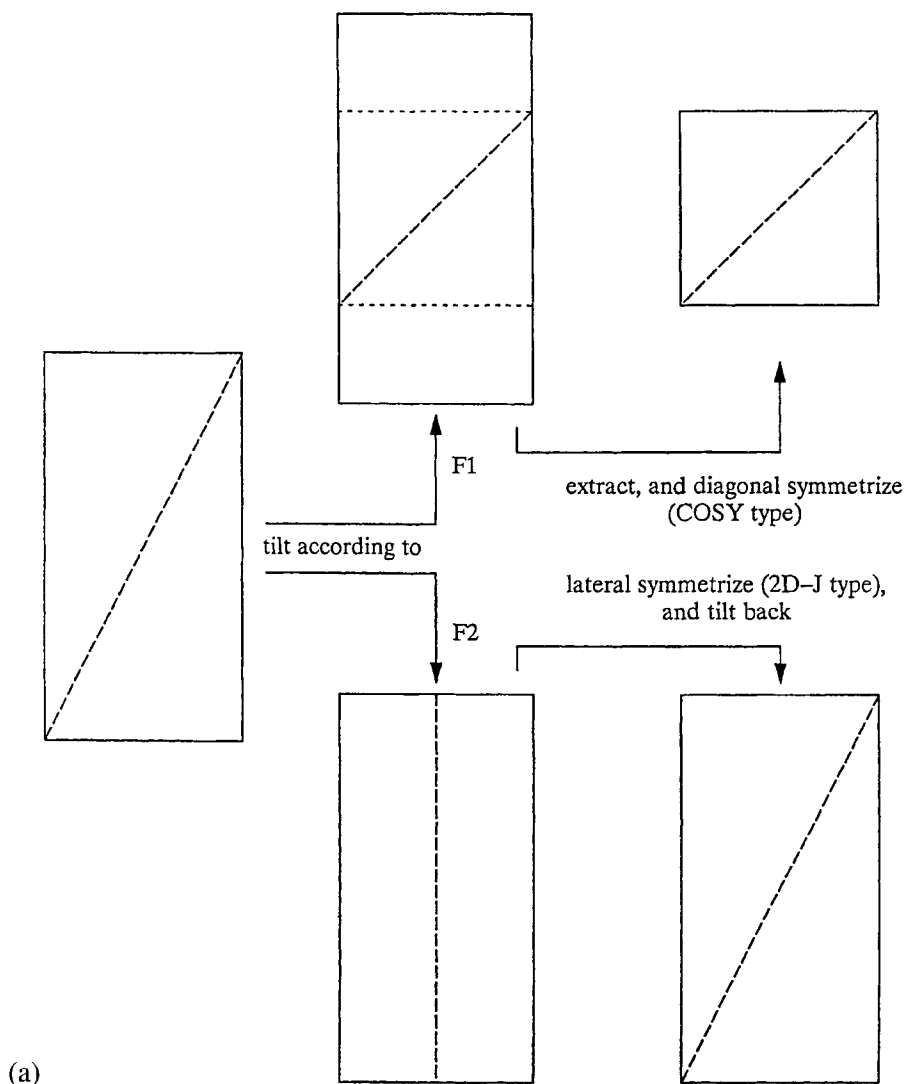
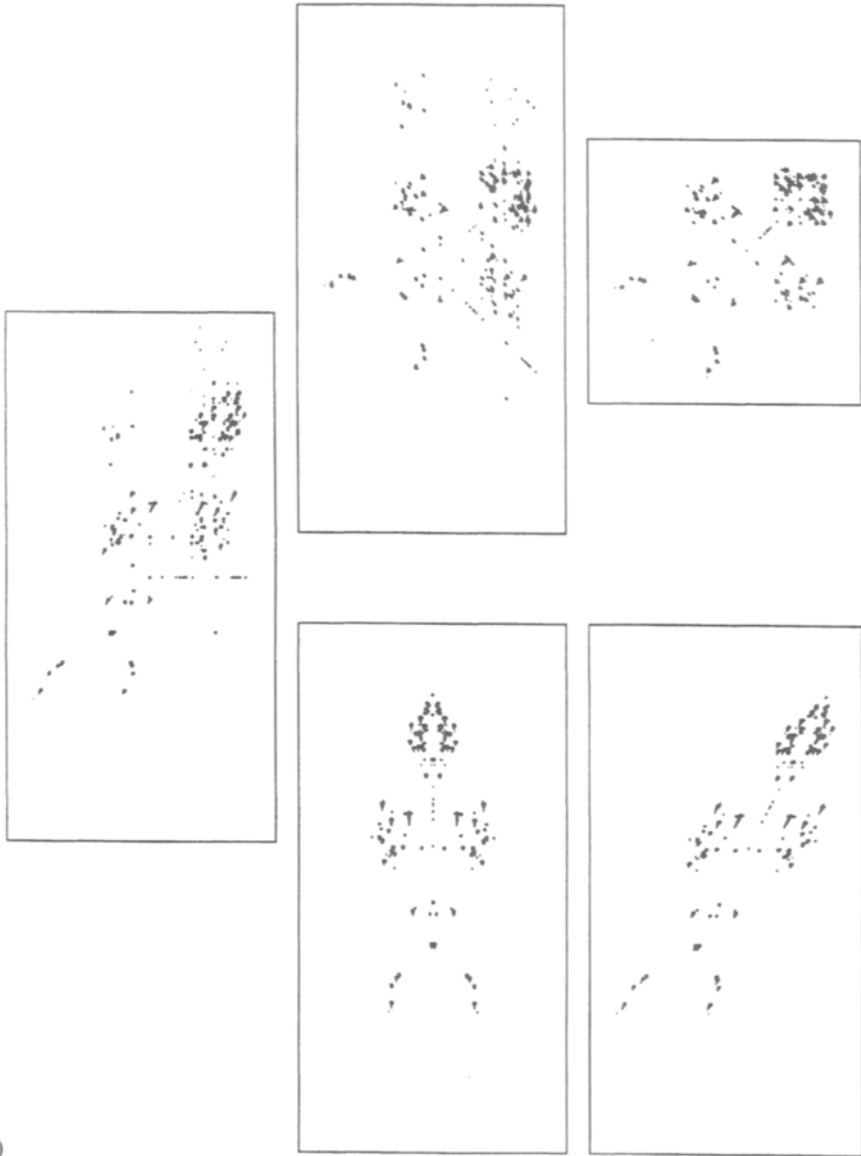


Fig. 7. Diagonal or lateral rearrangement followed by symmetrization of the 2Q-HoMQC of cyclosporin A, acquired at 500 MHz in benzene- $d_6$  at room temperature. (a) Scheme for rearrangement and symmetrization of the full 2Q-HoMQC spectrum. Additional processing may include extraction of a diagonally symmetric correlation map (as shown here) or reverse tilting in order to restore the original arrangement. (b) The same procedure was applied on the real spectrum after DA phasing [11]. Remote peaks and artifacts are both removed from the final output.



(b)

Fig. 7. (Continued)

Frequency domain rearrangement of 2Q-HoMQC spectra leading to a diagonally symmetric correlation map was proposed earlier [34] which relies on uniform excitation of MQ coherence [35]. We have introduced an enhanced alternative approach which removes the antisymmetric character of low resolution cross peaks by simple dispersive phasing [11]. Then the spectra can be rearranged easily either in the frequency domain or the time domain and can be symmetrized by conventional software tools. Rearrangement is possible either in  $F_2$  or  $F_1$ . The output spectrum can undergo lateral [32] or diagonal [21] symmetrization, respectively. An inverse rearrangement may follow in order to reconstruct the original spectrum, which will have enhanced signal-to-noise and yet has the resolution of the pure phase spectrum. In the same time it is clean of most artifacts and all but the direct correlation peaks. Alternatively, the spectrum with diagonal symmetry can be compared directly to other conventional homonuclear correlation spectra, such as COSY, NOESY, etc.

The two alternative strategies are both illustrated on fig. 7 using a 2Q-HoMQC spectrum of cyclosporin A in benzene- $d_6$ .

## 5. Summary

Aliasing of HoMQC spectra is possible and is advantageous for most samples of biomolecules, especially if the data acquisition is not S/N limited. Optimal acquisition should take into account positioning the carrier, quadrature detection in the remote dimension, and arrangement of correlation regions if (multiple) aliasing was used. In this paper it is shown that most important biomolecules have correlation patterns suitable for at least single aliasing in  $^1\text{H}$ ,  $^1\text{H}$ -HoMQC experiments. Similar behavior of  $^{13}\text{C}$ ,  $^{13}\text{C}$ -HoMQC spectra is also discussed. Other structures may allow use of similar aliasing with no significant risk of confusing overlap on the final HoMQC spectrum. Data processing techniques are presented which lead to more convenient arrangement of the frequency domain data for visualization and analysis, including application of common symmetrization tools.

The utility of HoMQC spectra is enhanced by the application of the acquisition, processing and presentation techniques discussed in this review. By demonstrating the application and utility of the optimized HoMQC to proteins, DNA and RNA in multidimensional experiments, it is the hope of the authors that a more uniform acceptance of the methods described here will commence.

## Acknowledgments

Contribution to many related work and partial financial support is greatly appreciated to Prof. P.N. Borer (Syracuse University, NY). This presentation

has relevance to several projects conducted at Syracuse University, NY, with assistance from former students Ke Yu Wang, M. Szafranski, and several others.

Prof. H. Rüterjans (J.W. Goethe-Universität, Frankfurt, Germany) provided essential research opportunities in his laboratory (I.P., visiting), which is greatly appreciated. Thanks are due to R. Winkelmann and S. Geschwindner for their assistance in preparation of the uteroglobin sample and in data acquisition.

Kind permission for using the 2Q-HoMQC spectrum of apo-cytochrome c was received from Prof. Jannette Carey (Princeton University, NJ), while Xinshan Kang (Princeton University) contributed with preparation of the sample. This work was supported, in part, by the Exxon Education Foundation (I.P.). Special thanks are due to Lee Bickerstaff for critical reading of the manuscript.

## References

- [1] C. Griesinger, O.W. Sørensen and R.R. Ernst, *J. Magn. Reson.* **84** (1989) 14–63.
- [2] G. Bodenhausen, *Prog. NMR Spectrosc.* **14** (1981) 137–173.
- [3] M. Munowitz and A. Pines, *Science* **233** (1986) 525–531.
- [4] T.H. Mareci and R. Freeman, *J. Magn. Reson.* **51** (1983) 531–535.
- [5] L. Braunschweiler, G. Bodenhausen and R.R. Ernst, *Mol. Phys.* **48** (1983) 535–560.
- [6] T.H. Mareci, *Principles of Multiple-Quantum Spectroscopy*, in: *Pulse Methods in 1D and 2D Liquid-Phase NMR*, ed. W.S. Brey (Academic Press, New York, 1988) Ch. 4.
- [7] P.N. Borer, Y. Lin, S. Wang, M.W. Roggenbuck, J. Gott, O.C. Uhlenbeck and I. Pelczer, *Biochemistry* **34** (1995) 6488–6503; I.M.A. Nooren, K.Y. Wang, P.N. Borer and I. Pelczer, *J. Biomol. NMR* (in press); P.N. Borer, L. Pappalardo, D.J. Kerwood and I. Pelczer, *NMR-based Structure Determination for Unlabeled RNA and DNA*, in: *Advances in Biophysical Chemistry*, ed. C.A. Bush, **6** (1997) 173–216.
- [8] Y.Q. Gossler, K.P. Howard and J.H. Prestegard, *J. Magn. Reson., Ser. B* **101** (1993) 126–133; J. Chung, J.R. Tolman, K.P. Howard and J.H. Prestegard, *J. Magn. Reson., Ser. B* **102** (1993) 137–147.
- [9] K.D. Bishop, P.N. Borer and I. Pelczer, *J. Magn. Reson., Ser. B* **110** (1996) 9–15.
- [10] I. Pelczer and S. Szalma, *Chem. Rev.* **91** (1991) 1507–1524; I. Pelczer and B.G. Carter, *Data processing in Multidimensional NMR*, in: *Protein NMR Protocols* (series: *Methods in Molecular Biology*, Vol. 60), ed. D.G. Reid (Humana Press, NJ, 1997) Ch. 4.
- [11] I. Pelczer, K.D. Bishop, G.C. Levy and P.N. Borer, *J. Magn. Reson.* **91** (1991) 604–606.
- [12] R. Freeman, *A Handbook of Nuclear Magnetic Resonance* (Longman/Wiley, New York, 1987).
- [13] S.J. Archer, D.M. Baldisseri and D.A. Torchia, *J. Magn. Reson.* **97** (1992) 602–606.
- [14] J.-M. Nuzillard and R. Freeman, *J. Magn. Reson., Ser. A* **110** (1994) 252–256.

- [15] R.A. Beckman and E.R.P. Zuiderweg, *J. Magn. Reson., Ser. A* **113** (1995) 223–231.
- [16] I. Pelczer, R. Winkelmann, S. Geschwindner and H. Rüterjans, Poster #MP98 (Abstr. p. 115), 37th ENC, Pacific Grove, CA, USA, March 17–22, 1996.
- [17] A. Bax, R. Freeman and S.P. Kempell, *J. Amer. Chem. Soc.* **102** (1980) 4849–4851.
- [18] A. Bax and T.H. Mareci, *J. Magn. Reson.* **53** (1983) 360–363.
- [19] K. Nagayama, K. Wüthrich and R.R. Ernst, *Biochem. Biophys. Res. Commun.* **90** (1979) 305–311.
- [20] D.L. Turner, *J. Magn. Reson.* **49** (1982) 175–178.
- [21] R. Baumann, A. Kumar, R.R. Ernst and K. Wüthrich, *J. Magn. Reson.* **44** (1981) 76–83;  
R. Baumann, G. Wider, R.R. Ernst and K. Wüthrich, *J. Magn. Reson.* **44** (1981) 402–406.
- [22] M. Rance, W.J. Chazin, C. Dalvit and P.E. Wright, *Methods in Enzymology* **176** (1989) 114–134.
- [23] E.O. Stejskal and J. Schaefer, *J. Magn. Reson.* **14** (1974) 160–169.
- [24] B.H. Oh, W. Westler, P. Darba and J.L. Markley, *Science* **240** (1988) 908–911.
- [25] J.L. Markley, *Methods in Enzymology* **176** (1989) 12–64.
- [26] R. Ramachandran, P. Darba and L.R. Brown, *J. Magn. Reson.* **78** (1988) 56–68.
- [27] W.J. Chazin, *J. Magn. Reson.* **91** (1991) 517–526.
- [28] I. Pelczer, R. Winkelmann, S. Geschwindner and H. Rüterjans, Poster #MoP 152 (Abstr. p.123), XVIIth International Conference on Magnetic Resonance in Biological Systems (ICMRBS), Keystone, CO, August 18–23, 1996.
- [29] V. Sklenár, *J. Magn. Reson., Ser. A* **114** (1995) 132–135.
- [30] J. Frank, Gy. Dékány and I. Pelczer, *Tetrahedron Lett.* **33** (1992) 7393–7396.
- [31] I. Pelczer and J. Frank, in preparation.
- [32] J.D. Mersh and J.K.M. Sanders, *J. Magn. Reson.* **50** (1982) 171–174.
- [33] P.H. Bolton, *J. Magn. Reson.* **68** (1986) 180–184.
- [34] E.R.P. Zuiderweg, *J. Magn. Reson.* **66** (1986) 153–156.
- [35] M. Rance, O.W. Sørensen, W. Lupin, H. Kogler, K. Wüthrich and R.R. Ernst, *J. Magn. Reson.* **61** (1985) 67–80.

This Page Intentionally Left Blank

# chapter 11

---

## High Resolution Diffusion Ordered Spectroscopy

---

Gareth A. Morris and Hervé Barjat

*Department of Chemistry  
University of Manchester  
Oxford Road, Manchester M13 9PL  
United Kingdom*

Methods for Structure Elucidation by High-Resolution NMR  
Edited by Gy. Batta, K.E. Kövér and Cs. Szántay, Jr.  
© 1997 Elsevier Science B.V. All rights reserved

This Page Intentionally Left Blank

## 1. Introduction

NMR is generally the method of choice for the structure elucidation of total unknowns, provided that relatively pure samples are available. It is a great deal less effective at tackling mixtures of unknowns: coupled spin systems can readily be picked out using 2D methods such as COSY and TOCSY, but there is no general way of deciding which isolated spin systems belong to which species. A typical example of a mixture analysis problem that currently consumes a great amount of NMR time is that presented by body fluids [1] (e.g., urine, cerebrospinal fluid, plasma). Other examples of mixtures that present pressing problems include biological tissue extracts (e.g., perchloric acid extracts), natural product extracts, cell culture extracts and cell-free suspensions. The usual approach at present for tackling such mixtures involves laborious separation followed by NMR spectroscopy of individual fractions. Newer techniques such as LC-NMR show promise but make heavy demands on instrument time and require considerable extra hardware and chromatographic expertise.

One very promising, and so far relatively neglected, potential solution to the problem of unknown mixtures is the use of pulsed field gradient NMR to identify signals with a common diffusion coefficient. This was demonstrated for carbon-13 NMR as long ago as 1981 by Stilbs [2], but has only been applied to practical problems more recently. By accurate fitting of the signal decay in pulsed field gradient spin echo spectra as a function of gradient strength, in order to determine diffusion coefficients, it is possible to construct a 2D spectrum in which one domain is the normal spectrum, and the other disperses signals according to diffusion coefficient. All signals from a given molecule should appear at the same diffusion coefficient, allowing the resolution of the spectra of complex mixtures into subspectra from individual components, which could then be identified using the now classical apparatus of multiple pulse NMR. Quite small variations in molecular size can be sufficient to allow the resolution of resonances from different species; differences in diffusion coefficient as small as 1% can readily be detected. The technical challenge is to optimize the separation of the signals in the diffusion domain while retaining good spectral resolution in the NMR domain. In the past such Diffusion-Ordered Spectroscopy (DOSY) spectra [3–8] have been mostly restricted to low resolution in both diffusion and

spectral domains: the methods described here might by analogy be termed high resolution or HR-DOSY. The sensitivity of the technique is very good; instrumental time demands are comparable to those for  $T_1$  measurement or for the more sensitive 2D NMR methods (e.g., TOCSY).

## 2. Experimental methods

To date most attempts to exploit differential diffusion rates have concentrated on systems with very wide ranges of diffusion coefficient, because of the difficulty of extracting multiple Gaussian decay constants from the decays of overlapping signals, and have used specialist hardware producing relatively large field gradients (see for example refs. [3] to [8]). Such spectrometer systems are best suited to mixtures involving materials of high molecular weight, which have relatively broad lines; this means that the disturbance of static field homogeneity by gradient coils etc. is of little importance. For high resolution NMR of small molecules, in contrast, it is essential to maintain excellent static field homogeneity in order to be able to resolve closely-spaced signals, but the demands on field gradient strength are much more moderate because all the components of a mixture have relatively fast diffusion.

Recent developments in adding pulsed field gradient capabilities to commercial high resolution spectrometers offer sufficient gradient strength to perform satisfactory diffusion measurements on small molecules (<1 kDa) without compromising NMR lineshape or sensitivity. Provided that the NMR performance of the pulsed field gradient system is sufficiently good that individual signals are still well-resolved, the problem of deconvoluting overlapping Gaussian decays with different decay constants does not arise, and a simple two or three parameter fit can suffice. This opens up the possibility of achieving high resolution in both the spectral and the diffusion domains of a DOSY 2D spectrum. The potential significance of such experiments for the analysis of mixtures of small molecules is only just beginning to be appreciated [5, 9].

Suitable instrumentation for high resolution DOSY experiments might consist of a high field, high resolution spectrometer, and a probe with actively shielded pulsed field gradients of at least  $10 \text{ G cm}^{-1}$  ( $0.1 \text{ T m}^{-1}$ ). High field strength is important if proton spectra are to be sufficiently well-resolved for signals to be accurately quantifiable without interference from overlap, while active shielding of the pulsed field gradient is necessary if lineshape distortions due to slow field recovery are to be avoided. Since proton NMR is the most obvious area in which to use HR-DOSY (although there are other interesting possibilities), the presence of scalar coupling needs to be taken into account when selecting a pulse sequence for measuring echo attenuation by pulsed field gradients. If echo modulation by

coupling is to be avoided, the periods for which the magnetization is transverse must be kept to a minimum. One possibility would simply be to use a short  $90^\circ-\tau-180^\circ-\tau$  echo sequence, keeping  $\tau$  to a few milliseconds, but this would require very powerful field gradient pulses indeed. A simpler solution is to exploit the freedom given by the relatively long spin-lattice relaxation times of small molecules and use a stimulated echo sequence. This extends the timescale of diffusion during the pulse sequence while allowing the periods during which the magnetization evolves under the scalar coupling to be kept to a minimum. Extending the diffusion time from milliseconds to tenths of a second greatly reduces the demands on field gradient strength.

The conventional stimulated echo pulse sequence [10] may be extended without significant loss of sensitivity (beyond the factor of two inherent in the use of a stimulated echo) by the addition of a pair of  $90^\circ$  pulses bracketing a short delay; this gives the LED sequence [11] of Gibbs and Johnson, which increases the time available for recovery from the second field gradient pulse. A final addition to give the practical sequence of fig. 1 is to add a few dummy gradient pulses at the start of the sequence for “gradient presaturation”; this may improve the reproducibility of the gradient pulses with some systems. The short phase cycle of table 1 suffers from unwanted coherence transfer pathways, but is generally adequate if the gradient pulses are not too weak; the minimum recommended cycle for practical purposes is the full 16 steps. The full phase cycle of table 2 enforces the desired coherence pathway throughout the sequence, and hence should be usable with any gradient pulse strength. The minimum recommended cycle is 16 steps, with further improvements being obtained up to the full cycle of 256 steps. Although field gradient pulses may be used in the delays  $\tau_D$  and  $\tau_S$  to select zero order coherence during these delays, this is a risky proceeding and it is preferable to rely on phase cycling, since unwanted coherence pathways may generate spurious echoes for particular values of diffusion encoding gradients.

A further enhancement of the LED sequence which reduces very significantly the perturbation of the field-frequency lock, and hence improves the lineshape and the reproducibility of signals, is to use bipolar gradient pulses during the delays  $\tau$  of the sequence of fig. 1, with two equal and opposite gradient pulses bracketing a  $180^\circ$  pulse [12]. This BPLED sequence has two advantages: the disturbance of the main field is reduced, since the slow components of the perturbations caused by the two pulses cancel approximately; and the deuterium transverse magnetization responsible for the lock signal does not experience a  $180^\circ$  pulse, and hence refocuses as a gradient echo, rather than being spoiled as in the basic LED sequence. The bipolar LED sequence may, however, run the risk of causing systematic errors, underestimating diffusion because those regions of the sample which do not

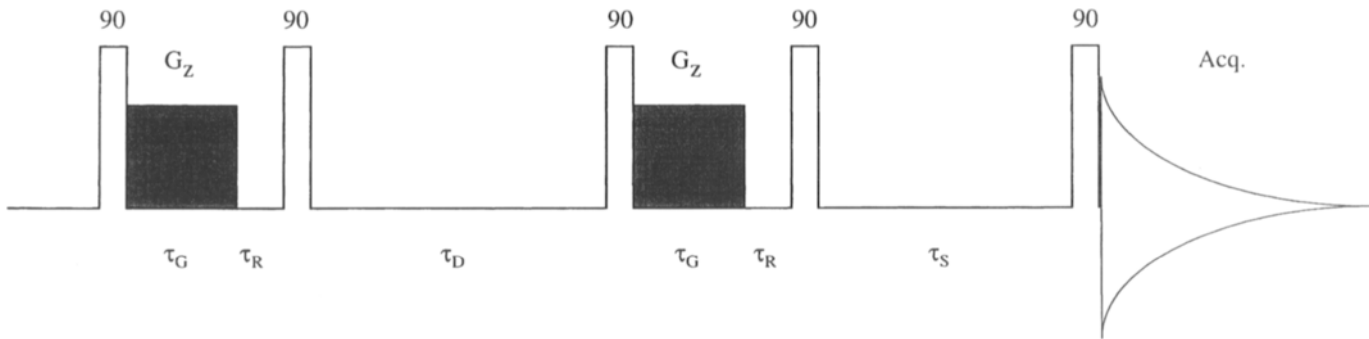


Fig. 1. LED pulse sequence for the measurement of stimulated echoes attenuated by diffusion. Typical values for delays and pulse widths are 5 ms for the gradient pulse widths  $\tau_G$ , 2–3 ms for the recovery time  $\tau_R$ , 0.1 s for the diffusion time  $\tau_D$ , and 5 ms for the storage time  $\tau_S$ . Phase cycling for this sequence is given in table 1 and table 2.

TABLE 1  
Simple phase cycling for the LED  
sequence of fig. 1. Phases are  
shown in multiples of  $90^\circ$ .

$\phi_1$	0
$\phi_2$	02
$\phi_3$	0
$\phi_4$	0022
$\phi_5$	0000 1111 2222 3333
$\phi_R$	0220 1331 2002 3113

TABLE 2  
Full phase cycling for the LED se-  
quence of fig. 1. Phases are shown in  
multiples of  $90^\circ$ ; subscripts indicate  
that a given phase should be repeated  
the stated number of times, e.g., the  
notation  $0_4 1_4 2_4 3_4$  indicates the se-  
quence 0000 1111 2222 3333.

$\phi_1$	0123
$\phi_2$	0
$\phi_3$	$0_{64} 1_{64} 2_{64} 3_{64}$
$\phi_4$	$0_{16} 1_{16} 2_{16} 3_{16}$
$\phi_5$	$0_4 1_4 2_4 3_4$
$\phi_R$	$\phi_1 - \phi_2 - \phi_3 + \phi_4 + \phi_5$

experience a full  $180^\circ$  pulse between the two antiphase gradient pulses will not be spatially labeled. It is therefore important to apply EXORCYCLE phase cycling to at least one of the  $180^\circ$  pulses.

Having set up spectrometer and pulse sequence, spectra are then acquired with a range of field gradient pulse areas. Since it is important to keep systematic errors to an absolute minimum, it is best to use interleaved acquisition, cycling through the different gradient pulse areas during time averaging, reducing the effects of any field or temperature drifts over the course of the experiment. The number of different pulse areas to use depends on the range of diffusion coefficients to be covered and on the balance between systematic and random errors, but will typically be in the range of 10 to 30. As in any quantitative experiment, there is a balance to be struck when choosing a repetition rate between signal-to-noise ratio and accuracy, but in DOSY experiments a delay of  $1-2 T_1$  suffices provided that care is taken to establish a steady state before acquiring data. In contrast to experiments such as inversion recovery, DOSY only requires that each pulse sequence start with the same longitudinal magnetization, and not that the spin system be fully relaxed. Depending on the concentration of the

sample, the nucleus being observed, and the accuracy sought in the diffusion domain, DOSY experiments may require anything from a minute or two to overnight.

### 3. Data analysis

Once the spin echo spectra as a function of gradient pulse area have been acquired, the problem is to extract the information on relative diffusion coefficients as efficiently as possible. The simplest situation, and the one to which DOSY is best suited, is where the signals of different species in the sample under study give rise to distinct, well-resolved signals. Here the intensities of the different signals can be determined rapidly and unambiguously either by peak height measurement or by integration. Diffusion coefficients can then be extracted by fitting a Gaussian to the observed decay, using two parameters (amplitude and diffusion coefficient); a third parameter (DC offset) may be added if the spectra have a constant baseline error.

However, before going on to consider in detail how best to analyze well-resolved spectra it is useful to look at the difficulties posed by less tractable systems. The problem of overlapping signals may appear in weak, medium or strong forms. The weak form is where signals with significantly different bandshapes or centre frequencies are partially overlapping. Here it should be possible to use iterative fitting methods to extract from the experimental data values for the relative contributions of the two different components to the overlapping signals in different spectra. The labour involved, both for the experimenter in formulating the fitting problem and for the computer system in carrying out the fit, is considerably greater than that involved in peak picking, but the data obtained should be reasonably accurate.

The problem in its medium strength form occurs where there is overlap between signals with similar bandshapes and centre frequencies but different NMR properties such as relaxation rates. Here it may be possible to combine relaxation and diffusion measurements into an experiment which is three-dimensional in the time domain (diffusion time, relaxation delay and acquisition time) but two-dimensional in the frequency domain. The relative contributions of the different signals to the bandshape can be separated by fitting the time-domain data to a suitable function of the relaxation rate and diffusion coefficient, an approach which has proved feasible for water in heterogeneous systems [13]. Here the accuracy of the diffusion coefficients obtained is likely to suffer by comparison with those for well-resolved signals, but 10% or so should be a reasonable target to aim for where the overlapping signals have significantly different relaxation properties.

The strong form of the problem, where signals overlap which are effectively indistinguishable by NMR, is much less amenable. Here the only

recourse is to try to decompose the measured signal as a function of gradient into a superimposed set of two or more Gaussians. Although very sophisticated computer methods for such a decomposition are available [4], this is a notoriously difficult problem and the fitting process is only reliable for the separation of signals with very different diffusion coefficients.

Having extracted, by fair means or foul, a diffusion coefficient for each significant component of the spectrum, a two-dimensional DOSY spectrum may be constructed by taking the bandshape of a given signal from the first (lowest gradient area) spectrum, and convoluting it in a second dimension with a Gaussian line centred at the calculated diffusion coefficient and with a width determined by the estimated error in diffusion coefficient obtained from the fitting process. A reasonable compromise here is to use a Gaussian constant in the diffusion domain equal to twice the estimated standard error; a purist might argue for half this value, but a pragmatist would wish signals with equal true diffusion coefficients to overlap strongly in the diffusion domain. The choice of bandshape from the 1D spectrum inevitably is somewhat arbitrary; a simple algorithm is to ascribe to a given peak all the intensity in the 1D spectrum either side of the peak, until either the signal falls to 1% of its maximum value, or a point midway between two peaks is reached. Where the spectrum is not sufficiently well-resolved for individual peak heights to be used as the basis for extracting diffusion coefficients and some sort of decomposition using iterative fitting is used, the bandshapes to use as the basis of the DOSY spectrum may be obtained directly from the fitting process.

The success or otherwise of the construction of a DOSY spectrum hinges on the relative accuracy of the diffusion coefficients obtained, so it is vital to minimize the contributions made by systematic errors; in a well-conducted proton experiment with good signal-to-noise ratio these will generally predominate over the very small random errors. Two important sources of distortion of the Gaussian dependence of echo signal peak height on field gradient pulse area are changes in the spectrometer lineshape as a function of gradient strength, and errors in the effective gradient amplitude. Fortunately each leaves internal evidence in the experimental spectrum that may be used to deduce a suitable correction for these systematic errors.

Some change in the signal lineshape as the applied field gradients increase is inevitable even with the best apparatus, whether arising from the direct perturbation of the main field caused by the eddy currents left by the gradient pulse, or from the disturbance of the field-frequency lock caused by the momentary loss of the deuterium signal. The effects of such perturbations will be felt equally by all signals in a spectrum, so by comparing the lineshapes of a given signal in successive spectra it should be possible to deduce the changes taking place. The simplest way to translate this information into a corrected dataset is to use the reference deconvolution

or FIDDLE algorithm [14]. Here a reference signal is chosen for which a theoretical lineshape is known, for example a chemical shift reference such as TMS; the experimental spectrum is deconvoluted by the lineshape of the reference signal, and then reconvoluted by the ideal lineshape. In practice the manipulations take place largely in the time domain for computational convenience, and considerable care must be taken to avoid errors caused by truncation of the reference signal, but these methods are now comparatively well-established (see Chapter 14). The result is a corrected spectrum in which the instrumental contribution to the lineshapes of the signals has been removed. This process is applied to all the spin echo spectra, taking care to ensure that the integrals of the signals remain unaffected, yielding a set of spectra in which the constancy of the lineshape from spectrum to spectrum ensures that the measured peak heights accurately reflect the signal intensities.

Deviations in the effective experimental field gradient pulse areas from the values specified may be corrected by an analogous process, this time in the second domain of the experiment. Since the decay of a single signal as a function of field gradient pulse area is known to be pure Gaussian for unbounded diffusion, any deviation from a Gaussian must be attributable to errors either in the signal amplitude or in the gradient. If random errors in the amplitudes are small, as they should be in a spectrum with good signal-to-noise ratio, and systematic errors have been corrected with FIDDLE, then the remaining deviations can be attributed to errors in the field gradient. A well-resolved signal with relatively slow diffusion and good signal-to-noise ratio is therefore selected as a reference. If the assumption is made that this signal does in fact have a strict Gaussian dependence on gradient strength, then the actual field gradient pulse areas experienced by the spins can be deduced from the signal amplitudes, provided that there is sufficient signal in each spectrum. The gradient strengths determined by this process can then be used to replace the nominal values in fitting the remaining signals. This procedure sacrifices some absolute accuracy in the determination of diffusion coefficient for what can be a significant improvement in the relative accuracy, which is the more important parameter for HR-DOSY since it is this which determines the ability to resolve signals in the diffusion domain. A useful extension to this process is to pool information from the decays of a number of signals, or even all the signals, in order to extract a more accurate set of corrections to the nominal gradient strengths. Although they are typically only a fraction of a percent, the corrections are quite significant in high field proton DOSY because of the good signal-to-noise ratio typically enjoyed by spectra. Once the contributions made by lineshape distortions and gradient errors have been corrected, it is possible to achieve standard errors on diffusion coefficient fits of well below 1%.

#### 4. Examples

Figure 2 shows a stacked plot of a series of 30 500 MHz proton spectra of a mixture of choline chloride, acetone and TSP (sodium 3-trimethylsilylpropionate) in  $D_2O$ , chosen to give a well-resolved proton spectrum. The spectra were measured using the LED sequence of fig. 1 for a range of values of pulsed field gradient varying linearly up to  $0.15 \text{ mT m}^{-1}$ . 16 transients were measured for each value of gradient, using delays  $\tau_G = 5 \text{ ms}$ ,  $\tau_R = 5 \text{ ms}$ ,  $\tau_D = 200 \text{ ms}$  and  $\tau_S = 50 \text{ ms}$ , with a delay of 15 s between transients. The upper limit of field gradient pulse area used was chosen to be rather higher than would be usual for DOSY, in order to make the different Gaussian decay rates of the different signals more obvious.

To construct the DOSY spectrum, the first twenty raw free induction decays were Fourier transformed and then deconvoluted with the FIDDLE algorithm using the TMS signal as reference, with a target lineshape of a Lorentzian 1.5 Hz wide at half height; the remainder of the data were discarded. Each spectrum was baseline corrected, and the peak heights of all the signals in the corrected spectra were then collated, and the decay of each signal fitted using two parameters to an exponential function of the square of field gradient pulse area. The decays of the three strongest signals were then used to compute the average deviation from the Gaussian curves of each of the nominal pulsed field gradient areas, and the calculation was repeated for all the signals using the recalibrated gradient areas. The diffusion coefficients thus obtained were then used to construct the 2D DOSY spectrum of fig. 3, as described earlier. The average standard error in diffusion coefficient obtained from the Gaussian fitting after the gradient calibration was approximately 0.2%.

Figure 4 shows a 500 MHz high resolution DOSY spectrum of a perchloric acid extract of gerbil brain, and illustrates the potential utility of DOSY in analyzing mixtures such as tissue extracts. Fifteen spectra were measured with the LED sequence using 512 transients per spectrum, in a total time of 10 hours. FIDDLE reference deconvolution using the DSS (sodium 3-trimethylsilylpropanesulfonate) line as reference and internal gradient calibration were used in the construction of the DOSY spectrum from measurements on 116 peaks. The assignments of a number of common metabolites are marked on the spectrum; as expected, the observed diffusion coefficients reflect the different sizes of the various species. The increased widths in the diffusion domain compared to those seen in fig. 3 reflect the poorer signal-to-noise ratio of the 1D spectra obtained

Figure 5 shows a 500 MHz DOSY spectrum of a sample of spearmint oil in deuteriochloroform, with TMS as reference. Essential oils such as spearmint represent a particular challenge for DOSY, since so many of the

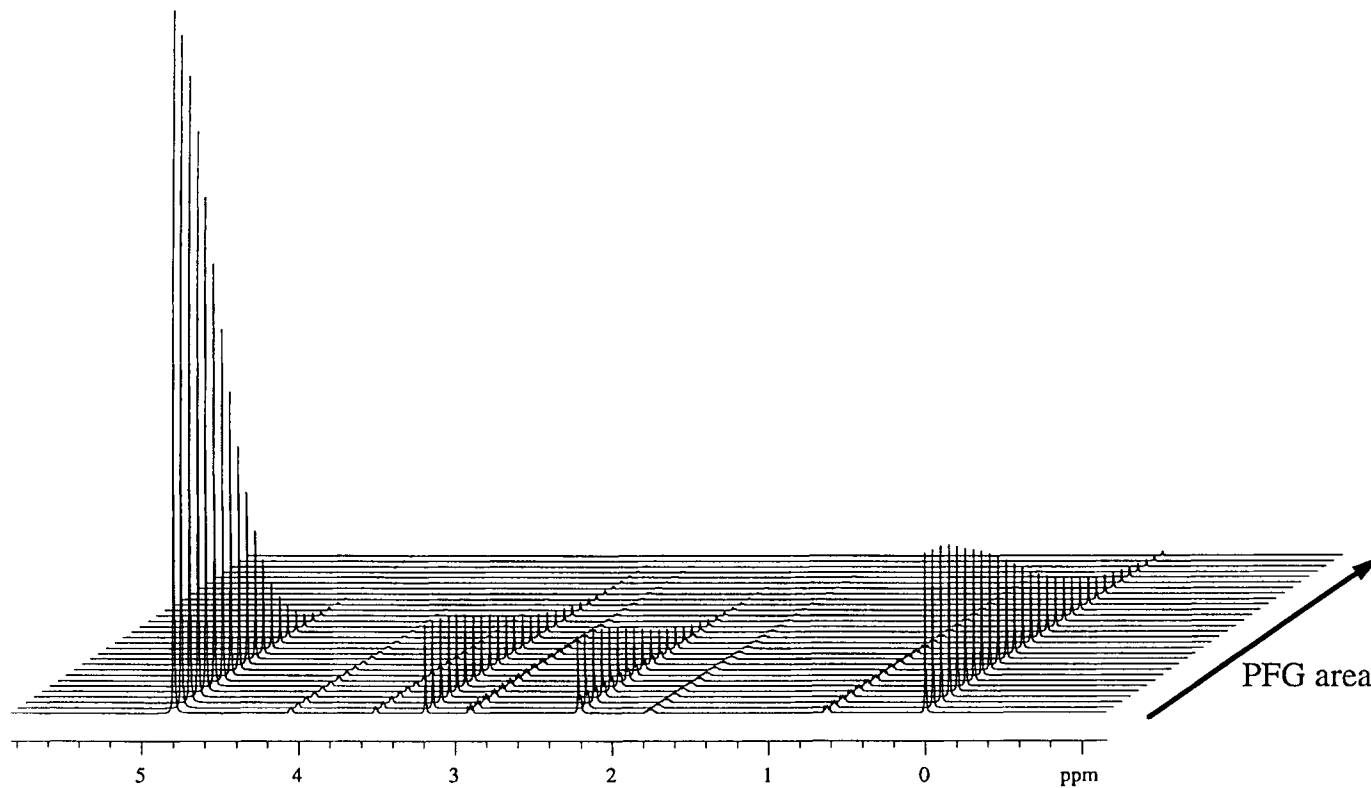


Fig. 2. 500 MHz pulsed field gradient stimulated echo spectra of a mixture of choline chloride, acetone and TSP in  $D_2O$ , obtained using the LED sequence as described in the text. A signal from an unidentified impurity is visible just to high field of the acetone resonance.

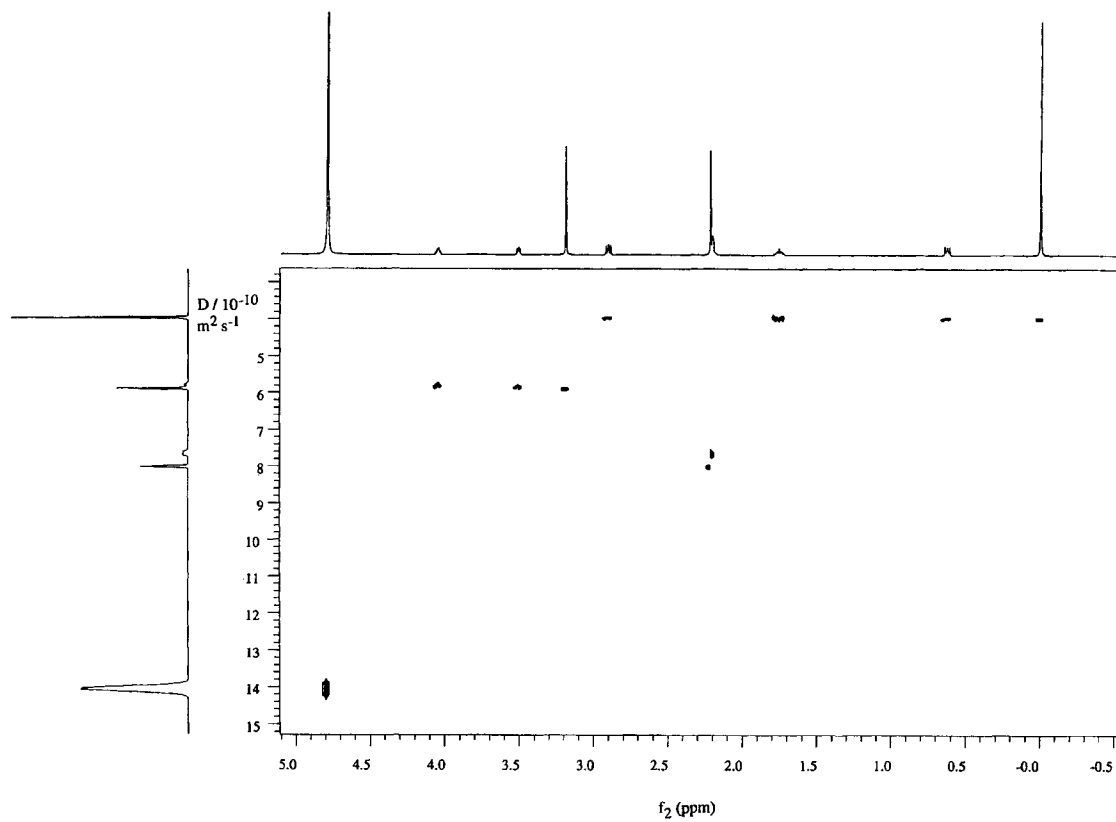


Fig. 3. DOSY spectrum constructed from the data of fig. 2. The first spectrum of the set of 30 is shown at the top, and a projection of the DOSY spectrum onto the diffusion axis at the left.

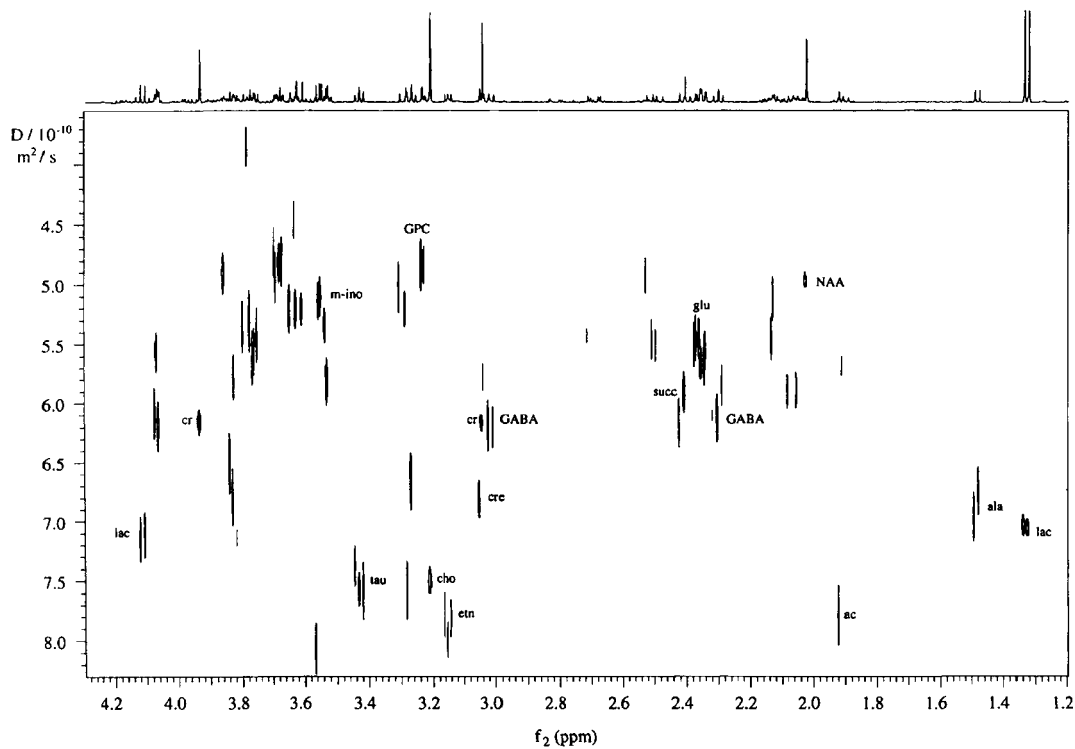


Fig. 4. 500 MHz DOSY spectrum of a  $D_2O$  solution of a perchloric acid extract of gerbil brain. Assignments of selected signals are indicated as follows: ac = acetate; ala = alanine; cho = choline; cr = creatine; cre = creatinine; etn = ethanolamine; GABA =  $\gamma$ -aminobutyric acid; glu = glutamate; GPC = glycerophosphocholine; lac = lactate; m-ino = *myo*-inositol; NAA = N-acetylaspartate; succ = succinate; and tau = taurine. (Raw data kindly provided by Drs. S.C. Smart, A.G. Swanson and S.C.R. Williams)

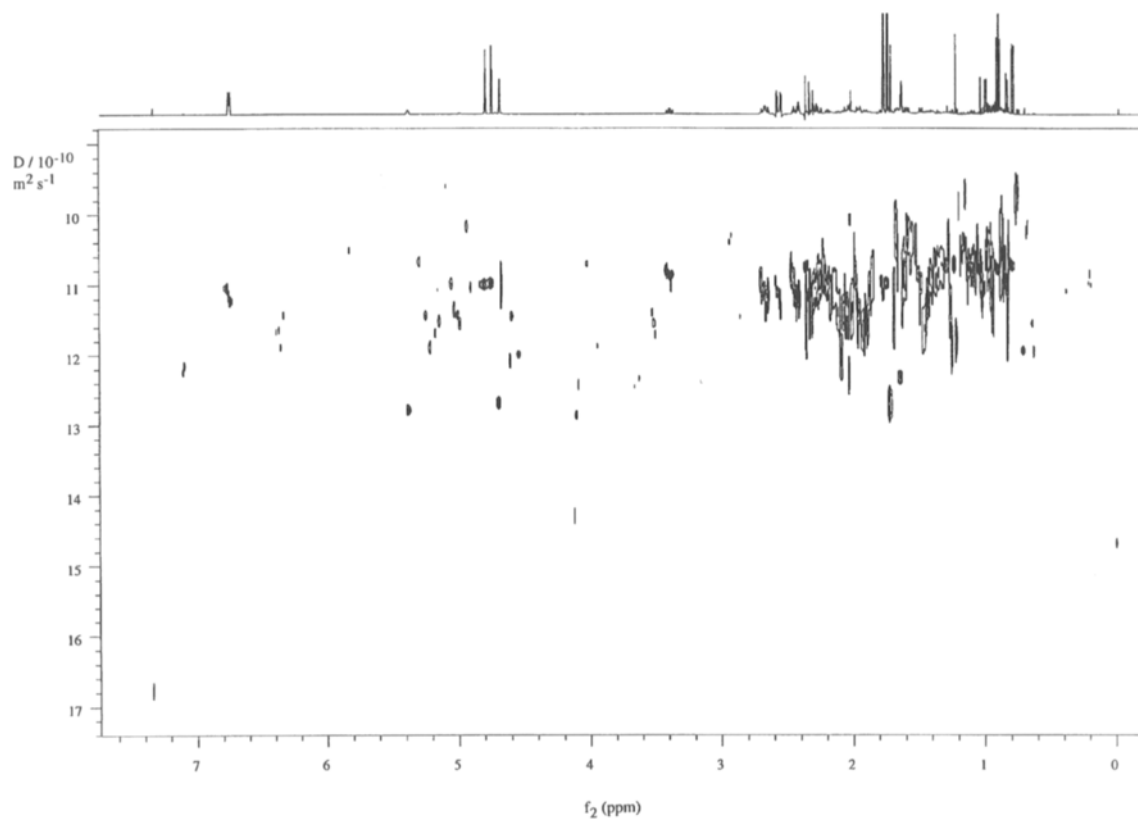


Fig. 5. 500 MHz DOSY spectrum of a solution of spearmint oil in deuteriochloroform, obtained overnight using the BPPLD sequence. (Sample kindly provided by Dr. A.S.F. Boyd)

constituents are monoterpenes with similar or identical molecular masses. 20 spectra of 384 transients were measured overnight with the BPPLIED sequence [12], using delays  $\tau_G = 5$  ms,  $\tau_R = 0.1$  ms,  $\tau_D = 250$  ms and  $\tau_S = 50$  ms, with a delay of 7 s between transients. The experimental data were processed using FIDDLE with a target lineshape of a 1.35 Hz wide Lorentzian, and field gradient calibration was carried out using pooled data from 8 peaks. Standard errors for some diffusion coefficients estimated from the fitting process were as low as 0.3%, giving very good apparent resolution in the diffusion domain. One of the principal limitations of this type of spectrum, in which the signals are relatively poorly resolved in the spectral domain, is, however, the systematic perturbation of the apparent diffusion coefficients because of crosstalk between signals. The standard errors obtained from the fitting algorithm assume a single diffusion coefficient; the standard error on the apparent diffusion coefficient obtained by fitting a composite signal formed from two resonances with similar diffusion coefficients will be significantly less than the difference in diffusion coefficient. Thus care must be taken in interpreting high resolution DOSY spectra where signals overlap.

## 5. Discussion

Three obvious areas in which progress is to be looked for are the use of more complex pulse sequences and further dimensionality in order to improve resolution, the development of better numerical methods for extracting accurate diffusion parameters from overlapping signals, and the systematic manipulation of sample composition to increase the amount of information obtained. The principal limitation of HR-DOSY as it stands is the need to resolve individual signals in the spectral domain. Although very good results are achievable using conventional proton NMR, the small chemical shift range sets clear limits on the complexity of mixtures susceptible to HR-DOSY analysis. It should be possible to extend the basic experiment to edited spectra, to other nuclei, and to higher dimensions; these approaches should improve usable resolution by at least an order of magnitude. Editing of proton stimulated echo spectra by multiple quantum or spin topology filtration should improve proton resolution very considerably while retaining excellent sensitivity. Combining stimulated echo and INEPT pulse sequences allows HR-DOSY carbon-13 spectra to be constructed without the need for a fourfold increase in gradient strength; this carries a sensitivity penalty, but gives a very big increase in NMR resolution. One of the most exciting possibilities is to add a PFG stimulated echo to 2D sequences such as DQFCOSY or HMQC, giving a 3D DOSY-COSY or DOSY-HMQC spectrum. The time demands are considerably less than those of most 3D experiments, since only 10–20 increments suffice for the

diffusion dimension. The gain in spectral resolution is accompanied by a big increase in the structural information obtained from the spectrum, allowing multiple structure determinations to be carried out on a single sample of a complex mixture.

The problem of improving the treatment of overlapping spectra has already been discussed briefly above. It seems unlikely that any spectacular progress will be made with the strong form of the overlap problem: the decomposition of overlapping exponential or Gaussian decays is a classic crux, and despite great efforts the results presently obtainable have standard errors far too big to be of use in high resolution DOSY. Prospects look much better, however, for the weak and medium forms of the problem; by paying a price either in analysis time or experimental time it should be possible to obtain usable results in these two cases. In systems which do not offer scope for three-dimensional experiments, whether for lack of sample or lack of exploitable correlations between spins, direct analysis of overlapping spin echo spectra remains the most hopeful avenue to pursue.

The third area in which significant advances should be possible is in the manipulation of sample properties to increase the interpretable information offered by HR-DOSY. The principal methods that compete with DOSY are the classical approach of bulk separation followed by spectroscopy on the fractions produced, which is both time-consuming and labour-intensive, and LC-NMR, which demands special hardware. One of the strengths of HPLC is the scope for manipulating retention time by changing the composition of the static and mobile phases. This suggests the possibility of manipulating diffusion coefficients by changing the solvent (by analogy with the chromatographic mobile phase) or by adding cosolvents to associate with solutes and hence slow their diffusion selectively (by analogy with the stationary phase). A very simple experiment that should be revealing with ionic species would be to change the pH or ionic strength and monitor the diffusion changes produced. It should also prove much simpler to interpret the absolute diffusion coefficients obtained with DOSY in such experiments than it is to interpret retention times.

The HR-DOSY method outlined here is potentially a very powerful tool for the NMR analysis of complex mixtures. There are significant technical challenges in its successful implementation, but early results suggest that the method could greatly reduce the labour involved in analyzing complex mixtures such as biofluids and tissue extracts.

### **Acknowledgements**

HB thanks the EPSRC and Pfizer Central Research for a research studentship and research associateship (GR /K16296). Equipment used in this work was purchased with the aid of grants from the EPSRC and its pre-

decessors and the University of Manchester. Helpful discussions with Drs. A.G. Swanson and S.C.R. Williams are gratefully acknowledged. The sample for fig. 5 was kindly provided by Dr. A.S.F. Boyd.

## References

- [1] J.K. Nicholson and I.D. Wilson, *Prog. NMR Spectrosc.* **21** (1989) 449.
- [2] P. Stilbs, *Anal. Chem.* **53** (1981) 2135.
- [3] K.F. Morris and C.S. Johnson, Jr., *J. Am. Chem. Soc.* **114** (1992) 3139.
- [4] K.F. Morris and C.S. Johnson, Jr., *J. Am. Chem. Soc.* **115** (1993) 4291.
- [5] D. Wu, W.S. Woodward and C.S. Johnson, Jr., *J. Magn. Reson. Ser. A* **104** (1993) 231.
- [6] D. Schulze and P. Stilbs, *J. Magn. Reson. Ser. A* **105** (1993) 54.
- [7] G.R. Newkome, J.K. Young, G.R. Baker, R.L. Potter, L. Audoy, D. Cooper, C.D. Weis, K. Morris and C.S. Johnson, Jr., *Macromolecules* **26** (1993) 2394.
- [8] A. Chen, D.H. Wu and C.S. Johnson, *J. Am. Chem. Soc.* **117** (1995) 7965.
- [9] H. Barjat, G.A. Morris, S.C. Smart, A.G. Swanson and S.C.R. Williams, *J. Magn. Reson., Ser. B* **108** (1995) 170.
- [10] E.L. Hahn, *Phys. Rev.* **80** (1950) 580.
- [11] S.J. Gibbs and C.S. Johnson, Jr., *J. Magn. Reson.* **93** (1991) 395.
- [12] D.H. Wu, A.D. Chen and C.S. Johnson, *J. Magn. Reson., Ser. A* **115** (1995) 260.
- [13] D. van Dusschoten, P.A. de Jager and H. Van As, *J. Magn. Reson., Ser. A* **116** (1995) 22.
- [14] G.A. Morris, *J. Magn. Reson.* **80** (1988) 547.

## chapter 12

---

# Chemical Exchange Measurements in NMR

---

Alex D. Bain and G.J. Duns

*Department of Chemistry  
McMaster University  
Hamilton, ON  
Canada L8S 4M1*

Methods for Structure Elucidation by High-Resolution NMR  
Edited by Gy. Batta, K.E. Kövér and Cs. Szántay, Jr.  
© 1997 Elsevier Science B.V. All rights reserved

This Page Intentionally Left Blank

## 1. Introduction

Most molecules are not fixed, rigid structures in solution. Chemical bonds may bend and rotate, so the atomic geometry will change. Even at room temperature, weak bonds may break and re-form, so that atoms exchange positions. The average structure of the molecule remains the same, but the detailed structure can be quite dynamic. Because Nuclear Magnetic Resonance (NMR) is so sensitive to chemical bonding, the dynamics can have dramatic effects on the NMR spectrum. There is a timescale associated with an NMR spectrum, so a range of rates (typically  $1-10^5 \text{ s}^{-1}$ ) can be studied relatively easily. Many of the interesting dynamic processes in molecules fit nicely into this rate window. NMR therefore offers one of the best ways of studying chemical exchange.

This chapter is aimed at giving an overview of the principles of chemical exchange and a review of the methods for measuring it by NMR. For each method we give the principles of the method, some indication of the theory behind it, a description of how data are analyzed, and finally some experimental results, details and opinions. This covers the familiar coalescence methods, as well as several other ways for extracting rates which are readily implemented on FT NMR spectrometers. Each has its applicable range of rates and its strengths and weaknesses. It is clear that the appropriate technique should be used and that a combination of several methods will give better results. The aim here is to describe the various techniques available, and to offer some of our opinions on which ones should be used.

The measurement of exchange rates is important, since it gives us vital information on the transition state between reagents and products. Absolute rate theory states that the rate is given by eq. (1), in which  $k$ ,  $h$  and  $R$  are Boltzmann's, Planck's and the gas constants, and  $T$  is the absolute temperature. The transmission coefficient,  $\kappa$ , is usually taken as 1. The thermodynamic functions  $\Delta G$ ,  $\Delta H$  and  $\Delta S$  represent the change between the initial and transition states.

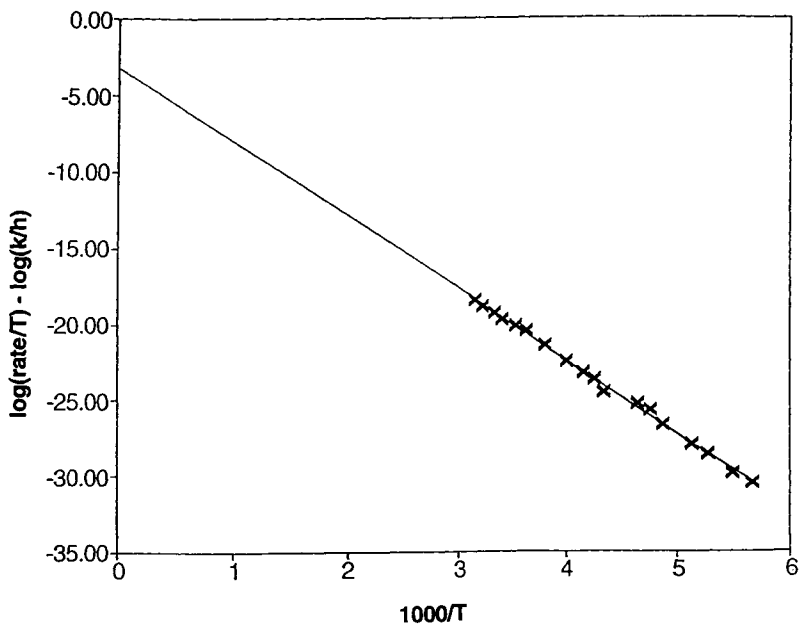


Fig. 1. Eyring plot of  $\log(\text{rate}/T) - \log(k/h)$  vs.  $(1/\text{temperature})$  for the chemical exchange of the aldehyde proton in furfural. Crosses represent measured rates and the straight line is the best fit to eq. (1) in the text.

$$\begin{aligned} \text{rate} &= \kappa \frac{kT}{h} e^{-\Delta G/RT} \\ &= \kappa \frac{kT}{h} e^{\Delta S/R} e^{-\Delta H/RT}. \end{aligned} \quad (1)$$

An Eyring plot of  $\log(\text{rate}/T)$  vs.  $1/T$  (fig. 1) should give a straight line with a slope equal to  $-\Delta H/R$  and an intercept related to  $\Delta S$ . Many good measurements of  $\Delta H$  are available in the literature, but values of  $\Delta S$  are less reliable, since an extrapolation back to  $1/T = 0$  in the Eyring plot is involved. Figure 1 shows rate measurements over a temperature range of 140 K, yet still there is a considerable extrapolation. However, measurements of reactions rates still provide the best way of studying the all-important transition state in a reaction.

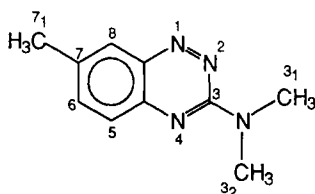
The determination of the thermodynamic activation parameters for dynamic processes contributes to an overall understanding of the bonding and conformational details of exchanging molecules. NMR has extensively been used, and a variety of methods have been developed for this purpose [1–5]. In order to obtain reliable data, it is essential to measure rates of exchange over as wide a range of temperatures (and thus rates or time scales) as possible [3–6]. The NMR chemical exchange time scale may be considered to consist of three distinct regimes: the slow, intermediate, and fast exchange. These time scales may be defined, for the simplest case of two exchanging sites 1 and 2 with equal populations, i.e.,



in terms of the ratio of the rate constant  $k$  to the chemical shift separation (in frequency, not ppm) between the sites,  $\Delta\nu_{1,2}$ . In slow exchange, the rate is much less than the separation, so the normal spectrum is observed with a slight broadening of the lines due to the dynamics. As the rate goes up, the lines broaden more and eventually coalesce, as is characteristic of intermediate exchange (fig. 2). Finally, fast exchange is the regime when the rate is much greater than the separation. In this case there is a single line at the average chemical shift, but it still has some residual width due to exchange. In general, any particular method of rate measurement will be useful only over a restricted range of temperatures. A combination of techniques is essential in order to accomplish a complete and thorough dynamic NMR study [7–11].

The effects of intermediate exchange on the appearance of the lineshapes are already familiar [1–12]. From the observation of exchange-broadened lineshapes, measurements of rates at the coalescence temperature have been widely used to estimate energy barriers for intramolecular exchange processes [1, 3, 4, 6]. Complete lineshape analysis methods, in which calculated lineshapes are compared to the corresponding experimental spectra to determine exchange rates, have been used for studies of exchanging systems of varying complexity [3–5, 13–16]. With the inclusion of any relevant scalar couplings, and allowances for any temperature dependence of the chemical shifts in the corresponding formulation, lineshape methods are best suited to the intermediate exchange regime [3–5]. Indeed, complete lineshape analysis methods can sample an exchange process over all three regimes of the NMR exchange time scale, and are in theory applicable over a range of rates encompassing approximately  $10\text{--}10^3 \text{ s}^{-1}$ .

The intermediate exchange regime may, however, represent only a narrow region of an accessible exchange process. At the extremes, neglect of long-range couplings and other effects can introduce pernicious biases into the measurements [17]. Also, in unequally populated cases, the mi-



3-Dimethylamino-7-methyl-1,2,4-benzotriazine

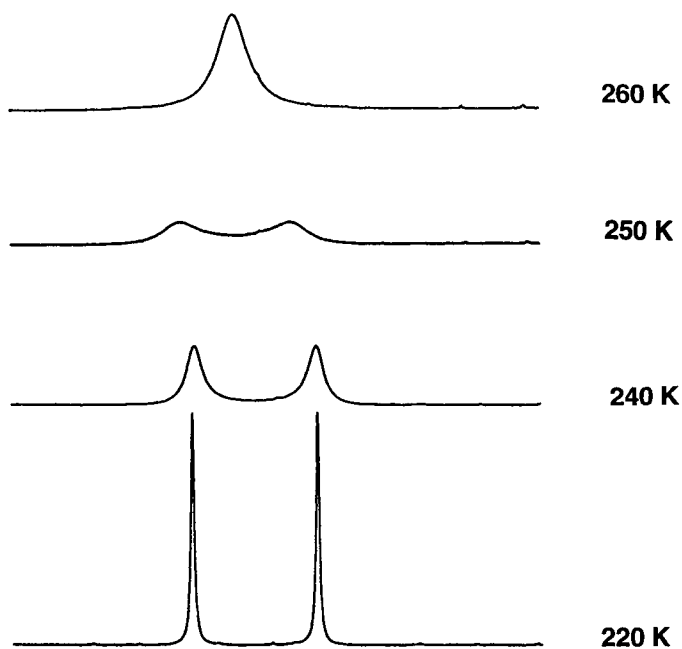


Fig. 2. Experimental NMR lineshapes for the two N-methyl signals in 3-Dimethylamino-7-methyl-1,2,4-benzotriazine. We are grateful to C.J.L. Lock and T. Fauconnier for a gift of the sample.

nor component broadens proportionately faster (fig. 3), so that it becomes unobservable quite quickly. Thus, in order to expand the lower and upper limits of accessible rate measurement, it is necessary to employ methods other than lineshape analysis. For systems possessing either relatively high or low barriers, or those compounds characterized by thermal instability, the slow or fast exchange regimes may be the only ones which can be studied. It has recently been shown that a complete study of chemical exchange in relatively straightforward exchanging systems is best accomplished using a combination of NMR methods, each best suited to a particular regime of

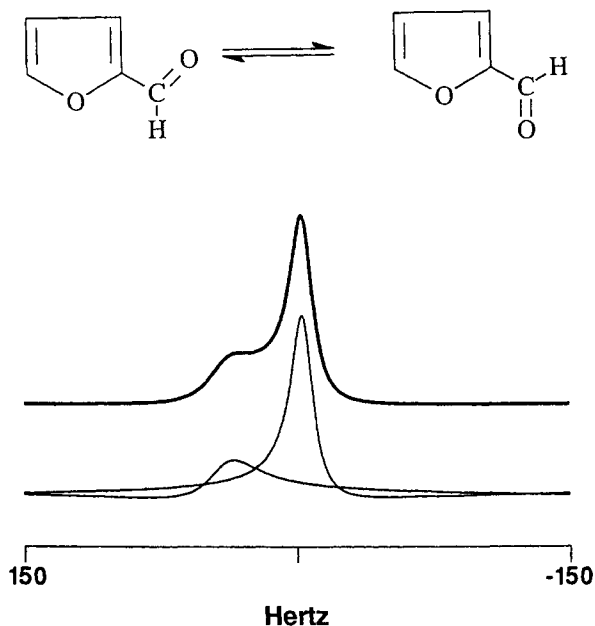


Fig. 3. Simulation of the lineshape of the aldehyde proton in furfural in the intermediate exchange region, and its constituents (lower lines). The lineshape consists of two components, each normal NMR lineshapes but distorted in position, phase, intensity by the dynamics.

the exchange time scale [10, 11]. Such a combination of methods provides the widest possible range of temperatures over which reliable rate data can be obtained.

One simple example of chemical exchange is furfural (fig. 3). This is a classic case of chemical exchange between unequally populated sites [18–20]. We have chosen an unequally-populated two-site case because it shows almost all of the important phenomena, but is easy to understand and repeat. The fact that the equilibrium constant is not equal to 1 in this exchange means that both the exchange rate and the populations of the two sites are temperature dependent. Furthermore, since the minor site broadens relatively quickly, this means that the range of rates over which lineshape methods are useful is quite small. Finally, the barrier in furfural ( $\Delta H^* = 40 \pm 1 \text{ kJ mol}^{-1}$ ,  $\Delta S^* = 27 \pm 5 \text{ J K}^{-1} \text{ mol}^{-1}$  in acetone) is such that the three regimes of chemical exchange are accessible in the  $-100^\circ\text{C}$  to  $+100^\circ\text{C}$  range that is convenient for typical solvents and spectrometers.

In this chapter, we discuss NMR methods for rate measurements in all three regimes. First we discuss a new way of looking at the coalescing lineshapes in intermediate exchange. Then we cover standard and alternative NMR methods for studies of slow and fast chemical exchange. For many

systems undergoing slow chemical exchange, the exchange may be too slow to result in apparent broadening of the resonances of the exchanging sites, but may be comparable in magnitude to the spin-lattice relaxation rates. The selective inversion technique exploits the effects of exchange rates which are comparable to spin-lattice relaxation times for application to studies of slow exchange, and provides the optimal means for probing slow exchange systems of varying complexity. For systems undergoing fast chemical exchange, the upper limit of accessible rate measurement is largely determined by the ability to measure the spin-spin relaxation time  $T_2$ , or the intrinsic linewidth, of narrow lines. The offset-saturation method provides a convenient and facile way of measuring  $T_2$ , and has proven to be a useful technique for obtaining rates of exchange which are beyond the upper limit of lineshape analysis. This combination of techniques can yield excellent data over a wide range of rates.

## 2. Lineshapes in the intermediate exchange regime

### 2.1. Principles

In the intermediate exchange regime, the rate constant is comparable to the difference in Larmor frequency between the two sites ( $\omega_A - \omega_B$ ). In this region, the spectra may be observed as broad overlapping peaks which coalesce to a broad singlet at higher temperatures or faster exchange rates. Indeed, the observation of lineshapes bearing characteristics of intermediate exchange is the classical indicator of an exchange process occurring [3]. It is difficult to make approximations to the lineshape equations to obtain a simple closed form of the exchange equations for evaluating the lifetimes  $\tau_A$  and  $\tau_B$  in the intermediate exchange region. Early procedures attempted for determining intermediate exchange rates using closed form solutions of the lineshape equation proved very susceptible to systematic errors and thus no longer find use [3, 6].

One important relationship which has survived from the earliest days of DNMR [1] and which is still used to estimate exchange rates is the relationship between the exchange rate  $k_c$  which is the rate that just results in coalescence of the A and B signals into a broad, single, flat-topped absorption. From differentiation of the lineshape equation, it is possible to obtain the simple expression [1]

$$k_c = \pi(\nu_A - \nu_B)/\sqrt{2}, \quad (3)$$

which is applicable only for equally-populated ( $p_A = p_B = 0.5$ ) systems, and when the signal separation ( $\nu_A - \nu_B$ ) is large compared with the linewidths at half-height for A and B. The use of eq. (3) to obtain the

exchange rate and corresponding thermodynamic data at the coalescence temperature depends on the ability to adequately control the temperature and obtain the coalescence point accurately. The exclusive use of rate data based on coalescence measurements is often used to obtain thermodynamic parameters for rate processes. The parameter  $\Delta G$  in eq. (1) is often quoted, which is tantamount to quoting the exchange rate itself. To be consistent,  $\Delta G$  values are often reported at a standard temperature such as 273 K. With associated errors and the fact that it represents only a single rate and corresponding temperature, the use of the rate at coalescence should not stand by itself to represent accurate data for an exchanging system. A more complete kinetic study should be carried out when possible [3, 6].

The most accurate method for obtaining rates in the intermediate region and which is applicable over the largest range of rates is the generation of the lineshape and direct comparison with the corresponding experimental spectrum, either visually or ideally by an iterative procedure [3–5, 21]. Such comparisons of observed and calculated spectra are accomplished most preferably by a computerized complete lineshape fitting method using a least-squares comparison of the observed and computed normalized absorption intensities over an appropriate frequency range at suitable frequency intervals, with the exchange rate as the important variable [3, 6, 13, 22].

In many of these descriptions of lineshapes, chemical exchange lineshapes are treated as a unique phenomenon, rather than simply another example of relaxation effects on lineshapes. This is especially true for lineshapes in the intermediate time scale, where severe broadening or overlapping of lines may occur. The complete picture of exchange lineshapes can be somewhat simplified, following Reeves and Shaw [13], who showed that for two sites, the lineshape at coalescence can always be described by two NMR lines. This fact can be exploited to produce a clarified picture of exchange effects on lineshapes and to formulate a new method for the calculation of exchange lineshapes [16, 23]. This method makes use of the fact that lineshapes, even near coalescence, retain Lorentzian characteristics [13] (fig. 3). These lines, or coherences, are each defined by an intensity, phase, position, and linewidth, and for each line in the spectrum, the contribution of that particular line to the overall free induction decay (FID) or spectrum can be calculated.

## 2.2. Theory

Various theoretical formalisms have been used to describe chemical exchange lineshapes. The earliest descriptions involved an extension of the Bloch equations to include the effects of exchange [1, 2, 12]. The Bloch equations formalism can be modified to include multi-site cases, and the effects of first-order scalar coupling [3, 13, 24]. As chemical exchange is merely a special case of general relaxation theories, it may be compre-

hensively treated by quantum mechanical or density matrix formulations. The exchange theory of nuclear spins in magnetic resonance in quantum mechanical terms has been developed, based largely on the early work of Kaplan [25] and Alexander [26, 27], who derived a complete solution for the lineshape of the steady state spectrum using density matrix techniques. Further extensions of the quantum mechanical formulation of exchange using Liouville-space superoperator techniques have been made [4, 15, 28]. Sophisticated quantum mechanical formalisms of exchange have since been refined and form the basis for computer programs for which generate lineshapes to fit NMR spectra with chemical exchange [3, 4, 15, 22, 29, 30]. These theories will not be discussed here in detail, but are significant for their accurate description of exchanging lineshapes. The density matrix formalism provides the most complete description of exchange effects, with the ability to accommodate perturbations such as second-order coupling effects [2–5, 22, 25, 31], although the accompanying algorithms may be computationally intensive, limiting the applicability in cases such as systems having multiple sites.

The basis of the approach presented here is a re-examination of the transition probability [23]. A familiar example is shown in fig. 4, which shows the simulated lineshape due to mutual exchange in an AB system [32]. It is clear that the static spectrum of an AB spin system at equilibrium is made up of four transitions whose intensities are proportional to the transition probabilities. All the other spectra in fig. 4 are of the same spin system, with different rates of mutual exchange. The traditional approach to exchange has been to treat these as single lineshapes – to calculate the total signal at any given frequency. The dynamic spectra are then traced as a function of frequency [1, 2, 22, 28, 30, 33–35]. In contrast, we prefer [16, 23] to regard all these spectra as the sum of four transitions [13]. The signal at any given frequency is the sum of the contributions of the four lines. Furthermore, we can deal with the four transitions in the time domain, as we would do with a pulse Fourier transform spectrum. The results are the same, of course, but the re-formulation clarifies the concepts and simplifies the solution.

In order to define the transitions in fig. 4, we need to go back and examine the transition probability, which is usually given by time-dependent perturbation theory [36]. If  $\phi_i$  is the initial state,  $\phi_f$  the final state and  $I_x$  the perturbation, then the transition probability is given in eq. (4). Two factors make up the transition probability, and they are complex conjugates, so the intensity is real. In the generalization presented here, these two factors have a physical interpretation: they are the projections of the individual transitions along the total magnetization. In a dynamic system, the two factors are not complex conjugates, so the lineshapes in fig. 4 are more complicated. In spite of this, we may still treat them as transitions, as in the static case.

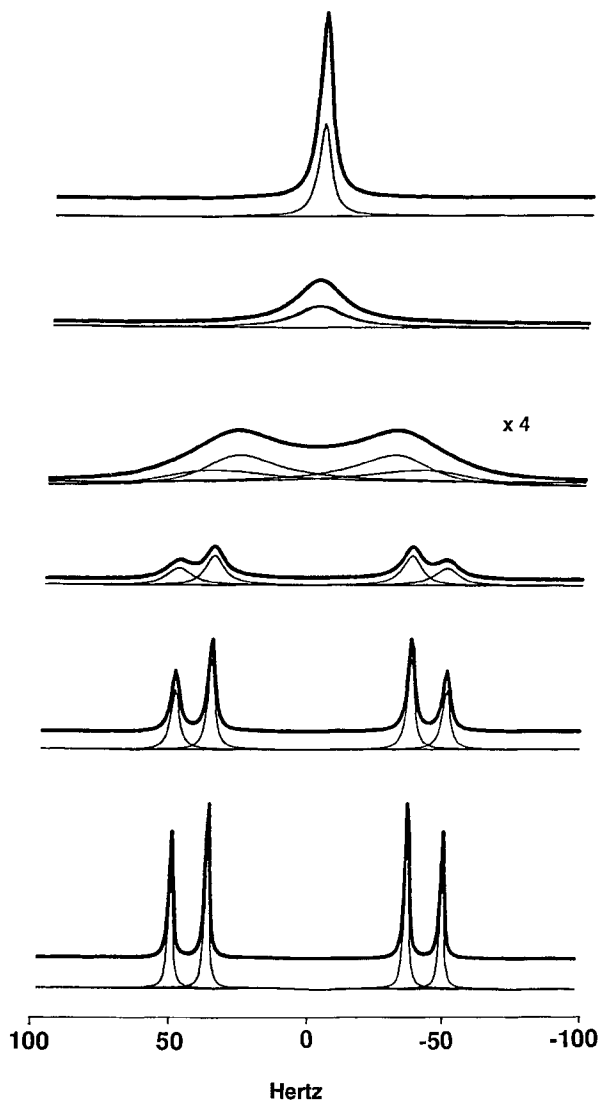


Fig. 4. Simulations of the mutual exchange in an AB spin system, along with the components of each lineshape. All the spectra in this figure are the sum of four lines.

$$\begin{aligned}
 \text{Transition Probability} &\propto |\langle \phi_f | I_x | \phi_i \rangle|^2 \\
 &= \langle \phi_f | I_x | \phi_i \rangle^* \langle \phi_f | I_x | \phi_i \rangle.
 \end{aligned}
 \tag{4}$$

In a pulse NMR experiment, the  $z$  magnetization is flipped into the  $xy$  plane, and the individual transitions start to precess. During the detection,

the total  $xy$  magnetization of the spin system is measured as a function of time. In physical terms, one of the factors in eq. (4) comes from the fact that the total  $z$  magnetization (converted to  $xy$  magnetization by the first pulse) must be divided amongst the individual NMR coherences. Each line in the spectrum gets its share of coherence before it starts precessing. The other factor comes from how visible each transition is to the detector. If we have a pulse experiment, the spin manipulations fit “between” the two factors in eq. (4). The initial magnetization is divided into the individual coherences, these are manipulated by the pulse sequence, and then the signal is detected. The two factors are complex conjugates, so the line intensities are real. In a dynamic system the two factors are no longer equal, and the transition probability has both real and imaginary parts. The real and imaginary terms give the intensity and phase distortions that are common in pulse experiments. All the spectra in fig. 4 are made up of four transitions; the only difference is the character of the transition probability.

The fundamental equation is the equation of motion for the density matrix,  $\rho$ , [37] as in eq. (5).

$$i \frac{\hbar}{2\pi} \frac{\partial}{\partial t} \rho = [H, \rho]. \quad (5)$$

It is more convenient to re-express this equation in Liouville space [37–39], in which the density matrix becomes a vector, and the commutator with the Hamiltonian becomes the Liouville superoperator. We will use bold-face upper-case italic letters to denote superoperators. Equation (5) becomes:

$$i \frac{\hbar}{2\pi} \frac{\partial}{\partial t} \rho = \mathbf{L}\rho. \quad (6)$$

If we use frequency units ( $\hbar/2\pi = 1$ ), then the formal solution to (6) is given in (7), in which  $\exp()$  denotes the exponential of a matrix:

$$\rho(t) = \exp(-i\mathbf{L}t)\rho(0). \quad (7)$$

Relaxation or chemical exchange can be easily added in Liouville space, by including a Redfield matrix,  $\mathbf{R}$ , for relaxation, or a kinetic matrix,  $\mathbf{K}$ , to describe exchange. The equation of motion becomes:

$$\rho(t) = \exp\{(-i\mathbf{L} - \mathbf{R} - \mathbf{K})t\}\rho(0). \quad (8)$$

In NMR, we detect the magnetization in the  $xy$  plane, so we may say that we always measure the expectation value of the  $I_x$  operator. It may be a

function of several time variables, including the time during the acquisition, but it is always given by (9):

$$\langle I_x(t) \rangle = \text{trace}(I_x \rho(t)). \quad (9)$$

In Liouville space, both the density matrix and the  $I_x$  operator become vectors. The scalar product of these Liouville space vectors is the trace of their product as operators. Therefore, the NMR signal, as a function of a single time variable,  $t$ , is given by (10), in which the parentheses denote a Liouville space scalar product:

$$\text{NMR Signal} = (I_x | \rho(t)). \quad (10)$$

We start at equilibrium. In the high-temperature approximation, the equilibrium density operator is proportional to the weighted sum of the  $I_z$  operators, which we will call  $F_z$ . We assume that a simple, non-selective pulse has been used at the start of the experiment. This rotates the equilibrium  $z$  magnetization onto the  $x$  axis. After the pulse the density matrix is therefore given by  $F_x$ , and it will evolve as in equation (7) or (8). If we substitute (8) into (10), we get the NMR signal as a function of time  $t$ , as given by (11). The detector sees each spin (but not each coherence!) equally well.

$$\begin{aligned} \text{NMR Signal} &= (I_x | \exp\{(-i\mathbf{L} - \mathbf{R} - \mathbf{K})t\} F_x) \\ &= (I_x | \exp\{(-i\mathbf{L} - \mathbf{R} - \mathbf{K})t\} | F_x). \end{aligned} \quad (11)$$

This equation can be solved several ways [40]. One method involves diagonalizing the Liouville matrix,  $i\mathbf{L} + \mathbf{R} + \mathbf{K}$ . The matrix,  $i\mathbf{L} + \mathbf{R} + \mathbf{K}$ , is precisely the matrix that Binsch deals with [22, 35]. If  $\mathbf{U}$  is the matrix with the eigenvectors as columns, and  $\mathbf{\Lambda}$  is the diagonal matrix with the eigenvalues down the diagonal, then we can write (11) as (12). This is similar to other eigenvalue problems in quantum mechanics, such as the transformation to normal co-ordinates in vibrational spectroscopy.

$$\text{NMR Signal} = (I_x | \mathbf{U}^{-1} \exp(-i\mathbf{\Lambda}t)\mathbf{U} | F_x). \quad (12)$$

Note that the Liouville matrix,  $i\mathbf{L} + \mathbf{R} + \mathbf{K}$  may not be Hermitian, but it can still be diagonalized. Its eigenvalues and eigenvectors are not necessarily real, however, and the inverse of  $\mathbf{U}$  may not be its complex-conjugate transpose. If we allow complex numbers in the equation, (12) is a general result. Since  $\mathbf{\Lambda}$  is a diagonal matrix we can expand in terms of the individual eigenvalues,  $\lambda_j$ . We can also apply  $\mathbf{U}^{-1}$  (“backwards”)

to  $I_x$ , and obtain equation (13). This is the basis of defining the transition probability in a dynamic system.

$$\text{NMR Signal} = \sum_j (\mathbf{U}^{-1}I_x)_j^* (\mathbf{U}F_x)_j e^{i\lambda_j t}. \quad (13)$$

The quantities  $(\mathbf{U}^{-1}I_x)_j$  and  $(\mathbf{U}F_x)_j$  in (13) are projections of the eigenvector  $j$  along  $I_x$ . From the above equations, we can interpret these as follows. The term  $(\mathbf{U}F_x)_j$  is the amount that the transition  $j$  received from the total  $x$  magnetization, created from the equilibrium state, and  $(\mathbf{U}^{-1}I_x)_j$  is how much that transition contributes to the observed signal. These two terms may not be equal, as we see in exchanging systems. This general approach forms the basis of the description of dynamic NMR lineshapes.

### 2.3. Data analysis

Equation (13) gives us a complete way of calculating the lineshape of any exchanging system, coupled or uncoupled. Using this method, or any of the standard programs, such as DNMR3, a lineshape can be calculated for a given set of kinetic and spin parameters. On most modern spectrometers, the data structure for the spectrum is well-documented, so comparisons between calculated and experimental spectra is relatively easy. The parameters can then be changed so that a best fit is obtained.

### 2.4. Experimental

The principles of getting good spectra in the intermediate exchange region are well-known and essentially the same as those for obtaining any one-dimensional spectra. The temperature must be stable, and accurately known. Modern spectrometers are able to maintain temperatures within ranges of about  $\pm 0.2$  K, which is normally sufficient but not ideal. The magnet must be shimmed well, so that the lineshape can be ascribed to chemical exchange effects and not shimming, which will affect even the broad lines. To this end, a compound such as TMS is often added to the sample to provide a lineshape reference [41]. Waiting at least  $5T_1$  between scans is often not needed, except to maximize the signal, since the  $T_1$ 's of the two sites are averaged by the exchange. Saturation will affect the whole lineshape uniformly. Finally, near coalescence the spectrum will be very broad, and the associated FID will decay very quickly. In this case, it is useful to broaden the sweep width, which is equivalent to increasing the digitization rate. In the time domain, this means more data points are collected during the fast-decaying FID, and so it is better defined. In the frequency domain, there is much more baseline in the spectrum, so that recognizing a broad line against the baseline, and phasing it, become easier. With these precautions, good lineshapes should be obtained.

### 3. The selective inversion experiment for slow chemical exchange

In the slow exchange regime, well below the coalescence temperature, the exchange rate  $k$  is less than the chemical shift difference the sites  $\Delta\nu_{1,2}$ , and the characteristic resonances for each site are separately resolved. Below a certain temperature, the exchange rates may be too slow to result in apparent exchange broadening of the resonances. In such cases, lineshape analysis methods are of limited usefulness, and other methods are required for accurate measurements of the exchange rates. One of the early methods, due to Hoffman and Forsén [32, 42–44] used the competition between spin relaxation and chemical exchange. Over the past decade or so, there has been widespread use of two-dimensional techniques, such as application of the NOESY-type pulse sequence, to study slow exchange processes. When chemical exchange is the mode of magnetization transfer, these 2D experiments are known as EXSY, or 2D exchange spectroscopy [37, 45]. These EXSY experiments produce a map in which cross peaks indicate which sites are exchanging with each other, giving a clear and unambiguous picture of the overall exchange pathways or processes. These pictorial depictions of chemical exchange are a definite advantage when elucidating the exchange processes in complicated multi-site exchange systems [46–54]. For qualitative mapping of exchange networks, EXSY is clearly the method of choice.

We feel that two-dimensional exchange spectroscopy, however, may not be the optimal methodology for the extraction of quantitative information or exchange rates. In order to obtain values of the exchange rates using EXSY, it is necessary to measure cross peak volumes, generally as a function of mixing time. In general, volumes are more difficult to measure than areas [55–62], with errors arising from factors such as spectrometer noise, digitization, and truncation [56, 63, 64]. In addition, the important parameter in 2D EXSY experiments, the mixing time, is dependent on the rate of exchange and on the spin-lattice relaxation time  $T_1$ . Several studies have shown that the ability to obtain useful information from EXSY-type experiments is dependent on optimal setting of the mixing time [50, 54, 65–68]. Too short a mixing time results in small or negligible cross peaks, while a mixing time that is too long may result in a loss of signal intensity due to  $T_1$  relaxation, and provides the potential for higher order peaks to appear. In addition, multiple two-dimensional experiments are time-consuming, and require large amounts of spectrometer disk space. With these limitations in mind, alternatives to two-dimensional exchange spectroscopy for measuring reliable rate data in the slow exchange regime must be considered, and can be found in applications of relaxation spectroscopy techniques.

If exchange rates are of the same order as the spin-lattice relaxation times, we can measure one relative to the other. This fact can be exploited, using

double-resonance techniques or generalizations of the inversion-recovery experiment to separate the competing effects of spin-lattice relaxation and chemical exchange, and ultimately determine the exchange rate. The pioneering experiments in this area were undertaken by Hoffman and Forsén [32, 42–44], who introduced a transient or time-dependent double-resonance saturation-transfer method which could be implemented on continuous-wave NMR spectrometers. They demonstrated that, for the simplest case of two exchanging sites, saturation of the resonance of site 1 with a second rf field resulted in the fluctuation in intensity of the second unsaturated resonance (site 2) as a function of time. The corresponding rate of exchange could be determined from an analysis of the time dependence of the magnetizations, using the Bloch equations incorporating chemical exchange. Hoffman and Forsén demonstrated that their method was capable of extending the lower limit of rate measurement to below the limit accessible by conventional single resonance techniques, particularly for exchange lifetimes in the range 1–10 s.

The advent of pulse FT NMR spectroscopy and the relative ease with which spin-lattice relaxation time measurements can be performed on modern spectrometers has seen an increased use of pulse FT techniques analogous to the saturation transfer method for the study of slow chemical exchange. Many related techniques have been developed, as modern pulse methods permit facile and versatile manipulation of a spin system in concert with direct observation of the exchange process. Generalizations of the inversion-recovery experiment for  $T_1$  measurement have proven to be amenable to the study of slow exchange processes [48, 69–74]. Selective inversion experiments in particular exploit the advantages of pulse FT NMR and have proven to be of extreme utility in the determination of rates in systems undergoing slow exchange, largely supplanting the classic saturation-transfer method.

Selective inversion experiments for the determination of slow exchange rates are analogous to the saturation-transfer method in that they involve selective manipulation of one of the exchanging sites, while observing the subsequent effect on the second site as a function of time [48, 69, 70]. Chemical exchange, if present, will provide an alternative route to normal spin relaxation processes which a spin system undergoes, if perturbed at the start of an experiment. The rate of relaxation will depend on both the exchange rate  $k$  and the spin-lattice relaxation rate  $(T_1)^{-1}$  (fig. 5).

An important point is that the initial non-equilibrium state largely determines the relative contributions of exchange and normal spin-lattice relaxation to the re-establishment of equilibrium. We have a good deal of control over the initial state, so we can enhance or suppress particular processes. For example, if the magnetizations in both sites are inverted, the return to equilibrium will be dominated by spin relaxation providing the

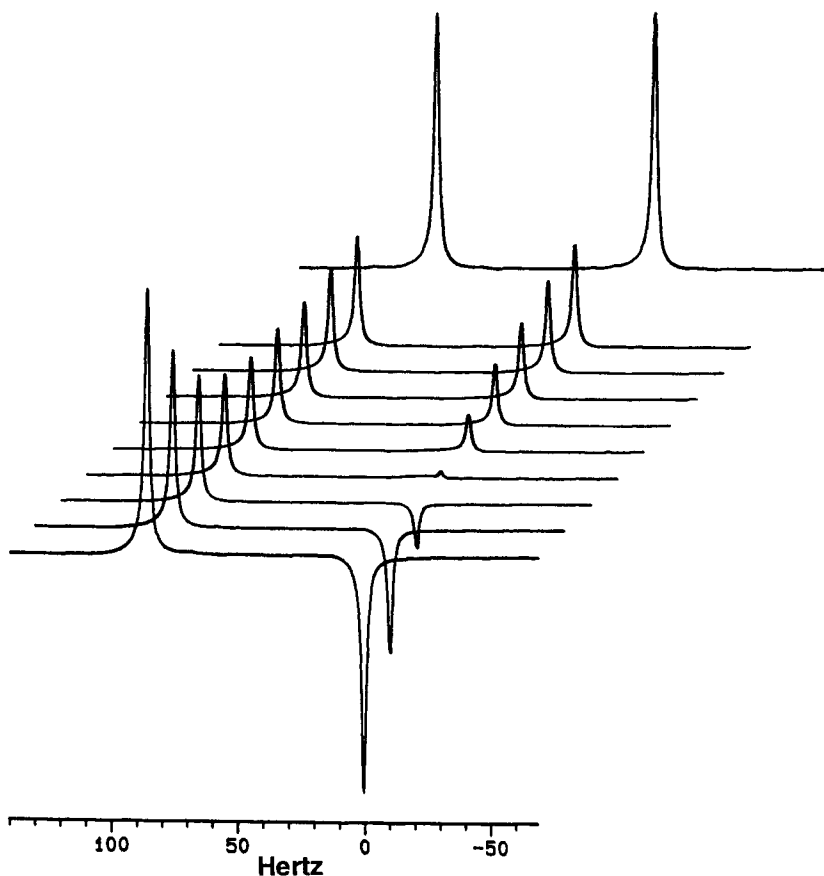


Fig. 5. Relaxation of the N-methyl signals in 3-Dimethylamino-7-methyl-1,2,4-benzotriazine (fig. 2), following a selective inversion of the low-frequency line. The spectra were taken at 220 K on a Bruker AC300 spectrometer.

relaxation rates for both sites are similar. For a simple two-site system undergoing slow exchange, the application of a non-selective inversion pulse sequence such as the common  $180^\circ$ - $\tau$ - $90^\circ$  experiment results in the inversion of the initial  $z$  magnetization after the  $180^\circ$  pulse, which will then return to equilibrium along the  $z$  axis at a rate determined mainly by the relaxation rate  $(T_1)^{-1}$ . Thus, the initial magnetization of sites 1 and 2 will be  $M_{z1}(0)$  and  $M_{z2}(0)$  respectively, with the equilibrium magnetizations being  $M_{z1}(\infty)$  and  $M_{z2}(\infty)$  for site 1 and site 2 respectively. Immediately following the  $180^\circ$  pulse, the initial conditions will be  $M_{z1}(0) = -M_{z1}(\infty)$  and  $M_{z2}(0) = -M_{z2}(\infty)$ . The non-selective experiment is relatively insensitive to the exchange rate,  $k$ . Exchange tends to equalize the two lines, and they start out equal and are equal at infinity in this experiment. However,

if site 1 is selectively inverted (fig. 5), so that  $M_{z1}(0) = -M_{z1}(\infty)$  but  $M_{z2}(0) = M_{z2}(\infty)$ , exchange strongly effects the relaxation. Site 1 relaxes more quickly than in the non-selective experiment under both spin-lattice relaxation and exchange, and site 2 shows a transient behavior, as in figs 5 and 8.

The quantitative analysis of selective inversion experiments can be accomplished by considering the formal equations for coupled relaxation and exchange. This formalism permits the construction of a parameterized model in matrix formulation containing the relaxation and exchange rates [70]. For an exchanging system with  $n$  sites, the general process of spin relaxation coupled with chemical exchange can be described in terms of the time dependence of the magnetizations as in equation (14).

$$\frac{\partial}{\partial t} \begin{bmatrix} M_1(\infty) & - & M_1(t) \\ \vdots & - & \vdots \\ M_n(\infty) & - & M_n(t) \end{bmatrix} = -\mathbf{A} \begin{bmatrix} M_1(\infty) & - & M_1(t) \\ \vdots & - & \vdots \\ M_n(\infty) & - & M_n(t) \end{bmatrix}. \quad (14)$$

In this equation the matrix  $\mathbf{A}$  is defined by equations (15):

$$\mathbf{A} = \begin{bmatrix} R_1 & -k_{21} & -k_{31} & \cdots & -k_{n1} \\ -k_{12} & R_2 & -k_{32} & \cdots & -k_{n2} \\ \vdots & \vdots & \vdots & \cdots & \vdots \\ -k_{1n} & -k_{2n} & -k_{3n} & \cdots & R_n \end{bmatrix}. \quad (15)$$

The diagonal elements of  $\mathbf{A}$  are given in equation (16),

$$R_i = \frac{1}{T_{1i}} + \sum_{l \neq i} k_{il}, \quad (16)$$

where  $R_i$  is the relaxation rate of site  $i$ ,  $T_{1i}$  is the spin-lattice relaxation time of site  $i$ , and  $k_{ij}$  is the rate of exchange from site  $i$  to site  $j$ . This formulation effectively ignores off-diagonal relaxation terms, which give rise to nuclear Overhauser effects. Note that since the principle of detailed balance applies, this kinetic scheme will determine the relative values of the equilibrium magnetizations [74].

The formal solution to the coupled set of differential equations presented in equation (14) is given by equation (17) [75].

$$\begin{bmatrix} M_1(\infty) & - & M_1(t) \\ \vdots & - & \vdots \\ M_n(\infty) & - & M_n(t) \end{bmatrix} = \exp(-\mathbf{A} \cdot t) \begin{bmatrix} M_1(\infty) & - & M_1(0) \\ \vdots & - & \vdots \\ M_n(\infty) & - & M_n(0) \end{bmatrix}$$

$$= \mathbf{U} \exp(-\mathbf{A} \cdot t) \mathbf{U}^{-1} \begin{bmatrix} M_1(\infty) & - & M_1(0) \\ \vdots & - & \vdots \\ M_n(\infty) & - & M_n(0) \end{bmatrix}. \quad (17)$$

In this equation,  $\mathbf{A}$  is the relaxation matrix in eq. (14),  $\Lambda$  is the diagonal matrix of the eigenvalues, and  $\mathbf{U}$  is the matrix with the eigenvectors of  $\mathbf{A}$  as its columns. Note that this is identical to eq. (8), except that now all the frequencies are zero.

For a two-site equally populated system, the solution to eq. (17) is relatively straightforward. In this case, the return to equilibrium for the magnetization in site A can be solved analytically [75] as given by

$$M(\infty) - M_1(t) = \frac{1}{2} [e^{-(R+2k)t} + e^{-Rt}] [M(\infty) - M_1(0)] \\ + \frac{1}{2} [e^{-(R+2k)t} + e^{-Rt}] [M(\infty) - M_2(0)]. \quad (18)$$

In eq. (18),  $M_1(t)$  and  $M_2(t)$  are the magnetizations at time  $t$  for sites 1 and 2 respectively,  $M(\infty)$  is the equilibrium value of the magnetization in either site,  $R$  is the spin-lattice relaxation rate ( $= 1/T_1$ ) for the two sites, which are assumed to be equal, and  $k$  is the exchange rate. For a larger system, numerical solutions are readily available with standard eigenvalue methods [42–44].

#### 4. Data analysis

The exchange rates  $k_i$  can be obtained from selective inversion experiments and the use of eqs (17) or (18) by two different methods. The first method is a non-linear least-squares iterative procedure, in which initial guessed values of the exchange rates and other parameters are put into a model. The resulting calculated set of data is then compared to that of the observed data set. A new set of parameters is then calculated, with the parameters varied until the sums of squares of the differences between the observed and calculated data, as defined by the appropriate  $\chi^2$  function, is minimized, or a convergence criteria is met [76–78]. This minimization procedure can be accomplished using linearization, Marquardt, or steepest-descent methods [77, 78]. The second method of data analysis is to invert the equation and attempt to solve for the matrix elements directly, which can prove to be a somewhat complicated and potentially unstable procedure [46, 47, 79–81]. We prefer to analyze the selective inversion experiments using the first method, which is robust and provides a convenient way of estimating the parameters and their associated error. For the simplest two-site equally-

populated case, incorporating the five parameters  $M(\infty)$ ,  $M_1(0)$ ,  $M_2(0)$ ,  $R$  and  $k$  into a parameterized model allows facile determination of the rate constant by non-linear methods [70, 75]. The relaxation rate  $R$  is best determined directly from a separate inversion-recovery experiment in order to obtain the input value for that particular parameter.

As mentioned above, the non-linear least-squares fitting procedure allows an estimate of the errors in the parameters for a fit to a particular set of data. In non-linear problems, it is impossible to define an exact definition of the error associated with any particular parameter, since the parameters are not statistically independent [76–78, 82]. In many instances, for example, for the comparison of rates in multi-site processes, the errors may be important as the data themselves, so that accurate determination of the errors as well as the rates may be critical [74]. The non-linear least-squares method essentially provides a built-in determination of errors from the iterative procedure, in the form of the variance-covariance matrix of the data [76, 78]. Ignoring the off-diagonal elements (covariances) and taking the diagonal elements to be the variances of the parameters gives a simple but inaccurate way of determining parameter error. A more accurate way of calculating parameter error is to define, in parameter space, an ellipsoidal ( $\chi^2$ ) surface determined by the required confidence level. A confidence region for a single parameter can be determined by projecting the entire surface onto the appropriate parameter axis, to give an estimate of the error of a particular parameter without influence from other values [76, 78, 83, 84].

#### 4.1. *Experimental methods*

The initial states of the spin system in a selective-inversion experiment can be created using various selective excitation pulse sequences such as the DANTE experiment [85, 86], or more sophisticated types of shaped pulses. A form of the  $90^\circ - \tau - 90^\circ$  sequence [48, 87], (compare the 1–1 sequence for solvent elimination, or the NOESY experiment) offers the advantage of offering two variable parameters, namely the rf transmitter offset and the delay time  $\tau$ . Both parameters can be varied independently to create a variety of initial selective excitation conditions. This is particularly advantageous in the study of exchanging systems having multiple sites or multiple pathways for the overall exchange process [48]. For more complicated exchanging systems, such as those with multiple sites or pathways, the ability to choose the initial perturbation(s) from the variety of available initial conditions is a definite advantage. The sites in a multiple exchange process pathway can be observed individually, by choosing the appropriate initial perturbation, and the times at which the relaxing magnetizations are sampled. These factors allow for considerable control over the experiment [75].

In principle there are “best” sets of initial conditions for sampling for a given process, and these can be found by inspecting the matrix of partial

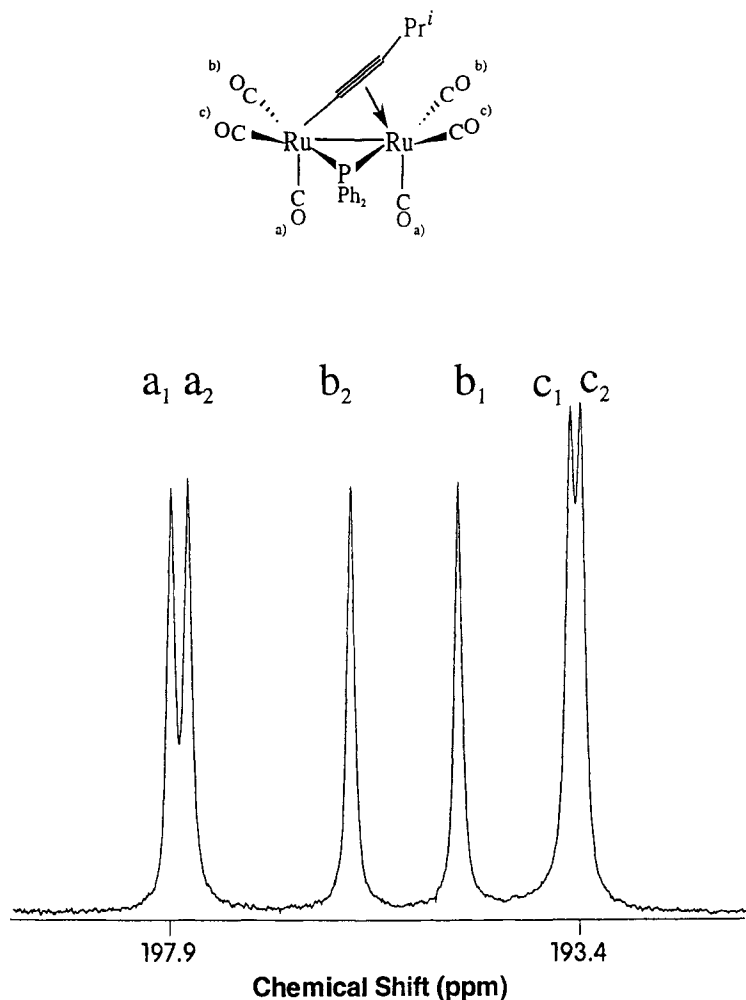


Fig. 6. Structure and  $^{13}\text{C}$  NMR spectrum in the carbonyl region of the molecule  $\text{Ru}_2(\text{CO})_6(\mu_2\text{-PPh}_2)(\mu_2\text{-}\eta^1:\eta^2\text{-C}\equiv\text{C-}i\text{-Pr})$  at 300 K. There are three distinguishable carbonyl species at this temperature, and each signal is split by coupling to  $^{31}\text{P}$ .

derivatives with respect to the parameters [48, 75, 88]. In practice, we find the experiment very robust, and that a wide variety of experimental conditions all give good data.

One example is the set of dynamic processes going on in  $\text{Ru}_2(\text{CO})_6(\mu_2\text{-PPh}_2)(\mu_2\text{-}\eta^1:\eta^2\text{-C}\equiv\text{C-}i\text{-Pr})$ . The molecule (fig. 6) is asymmetric in the absence of any dynamics, but near 300 K the alkyne flips back and forth (“windshield wiper motion”) quickly, so that the carbonyls on either side are equivalent. Each carbonyl is coupled to phosphorus, so if the carbonyls do not scramble amongst themselves, there are six lines in the carbonyl

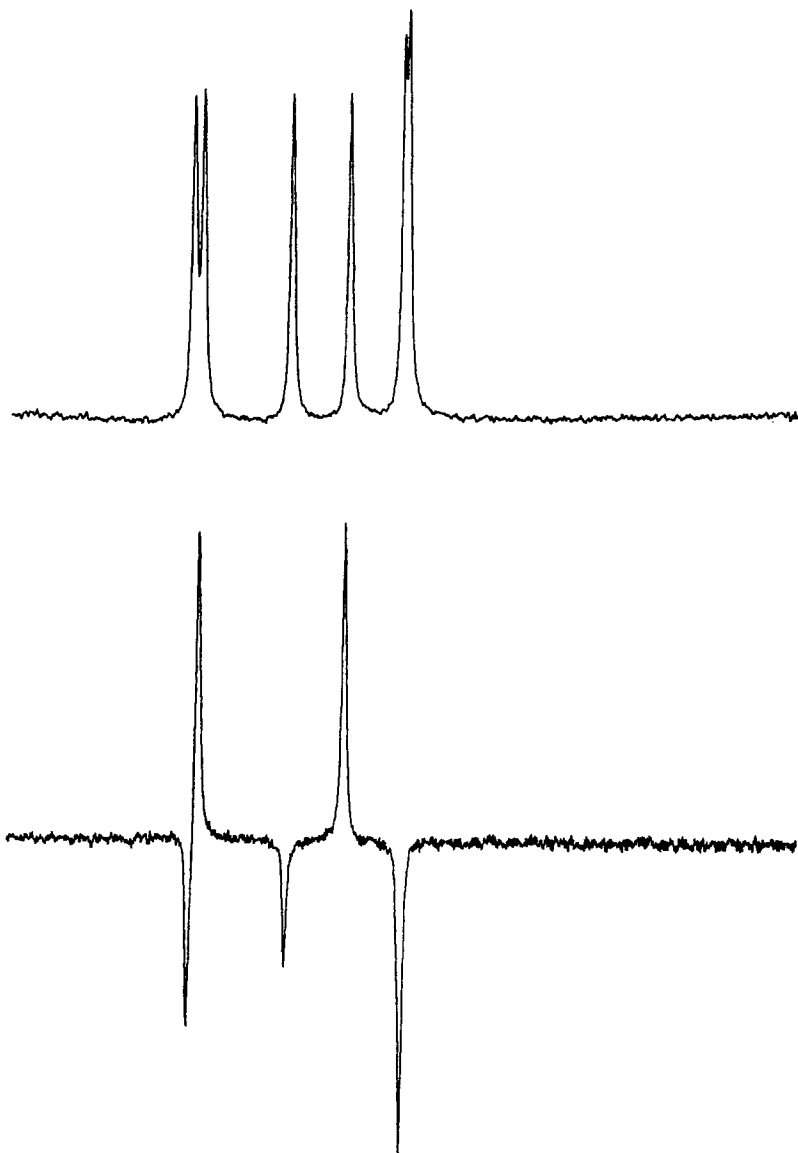


Fig. 7. The equilibrium spectrum (top) and the spectrum immediately after a selective inversion (bottom) of the molecule in fig. 6.

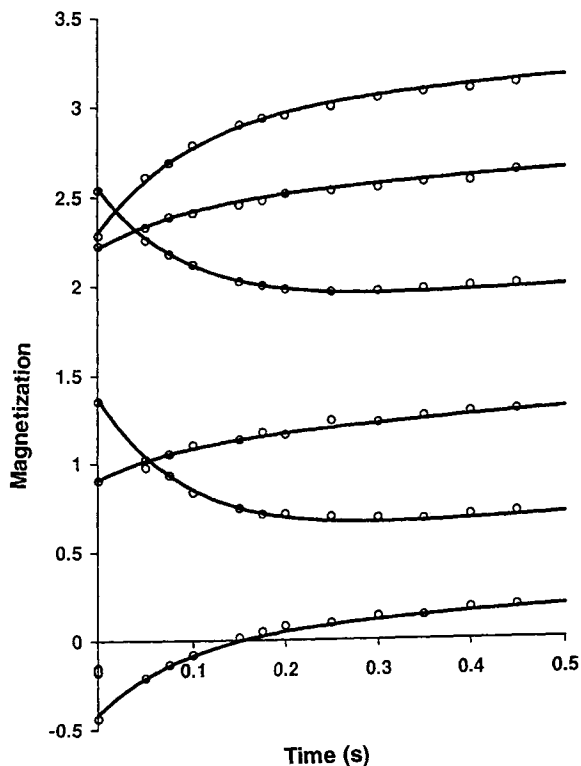


Fig. 8. Intensities as a function of time (circles) and best fit values (solid lines) of the six lines in the carbonyl spectrum of  $\text{Ru}_2(\text{CO})_6(\mu_2\text{-PPh}_2)(\mu_2\text{-}\eta^1\text{:}\eta^2\text{-C}\equiv\text{C-}i\text{-Pr})$ , following a selective inversion. The lines have been offset along the  $y$  axis for the sake of clarity.

region. The issue is whether the carbonyls scramble in a concerted rotation, or whether there are three independent pair-wise exchanges [48, 74].

There are 22 parameters in the model for this system. Each of the six lines in the spectrum has a relaxation rate,  $1/T_1$ , and values for the magnetization at equilibrium and at the start of the experiment,  $M(\infty)$  and  $M(0)$ . The data used were peak heights rather than integrals. Even though the  $M(\infty)$  should all be the same, they are slightly different because of differences in width. The carbonyl scrambling is defined by three pairwise rates of exchange, plus the  $^{31}\text{P}$  relaxation rate. The relaxation rates of the carbonyls and the phosphorus can be determined separately, so they were not allowed to vary, but the  $M(0)$ ,  $M(\infty)$  and the three rates (15 parameters) were all varied. This involves many parameters, but  $M(0)$  and  $M(\infty)$  seem to be sufficiently well determined, so they do not affect the fitting very much. Figure 6 shows the agreement between the observed data and the best-fit calculation.

The pairwise rates are presumed to be the same in both the forward and backward directions. The fact that the lines in the spectrum are all equally intense places little restriction on the three pairwise rates. The principle of detailed balance shows that the symmetry of the individual processes (i.e., equal forward and reverse rates) is sufficient to ensure that all the lines have equal intensity at equilibrium.

A series of selective inversions was performed on the compound, using the simple  $\pi/2-\tau-\pi/2$  excitation sequence, in which the two pulses are hard. Our experience is that the quality of the data does not seem to depend as critically as we thought [48] on the choice of initial conditions. Most reasonable perturbations, so long as they are not completely non-selective (fig. 7), seem to give similar data. Figure 8 shows the reassuring quality of the fit between the observations and the model, which is available from only 13 one-dimensional spectra. The data were then analyzed to see if the concerted mechanism was appropriate, as indeed it was.

## 5. Measurements of fast exchange rates by the offset-saturation experiment

In the fast exchange regime, the exchange rates are large such that  $k > \Delta\nu_{1,2}$ . The resulting spectrum for a two-site exchanging system is single averaged line, with chemical exchange being the dominant line broadening mechanism in the immediate post-coalescence region. As the exchange rate increases, the line will decrease in width until it is dominated by other spin-spin relaxation mechanisms. The lineshape may contain a significant contribution from magnetic field inhomogeneities [89], and in cases where fast exchange is present, the problems inherent in the measurement of accurate  $T_2$  values limit the accuracy of exchange rates measured from linewidth measurements or lineshape fits. The measurement of accurate exchange rates in the fast exchange regime is thus primarily dependent on the ability to measure linewidths, or the spin-spin relaxation time  $T_2$ , with minimal error.

The spin echo method of Hahn [90], a product of his pioneering work on pulsed NMR, provides a viable alternative to the direct measurement of linewidths for obtaining  $T_2$  by eliminating the effects of magnetic field inhomogeneity. The more sophisticated CPMG spin echo experiment combines the modifications of Carr and Purcell [91] for minimizing the effects of molecular diffusion in spin echo experiments by the application of a combination of  $90^\circ$  and  $180^\circ$  pulses, and of Meiboom and Gill [92], who solved the problem of cumulative  $\pi$  pulse imperfections by introducing a  $90^\circ$  phase shift between the  $\pi/2$  and  $\pi$  pulses. The CPMG experiment has become the standard experiment for measuring accurate values of the spin-spin transverse relaxation time  $T_2$  [93, 94].

As chemical exchange results in a modulation of the Larmor frequency of the exchanging nuclei and an attenuation of the echo amplitudes, the exchange process can be affected by changing the pulse repetition rate in a spin-echo experiment. Spin-echo techniques were accordingly shown to be suitable for studies of fast chemical exchange, having the potential for extending the upper limit of accessible rate measurement above that of lineshape analysis, to rates on the order of  $10^4 \text{ s}^{-1}$  [95–98]. The CPMG or spin-echo sequences are, however, susceptible to several sources of error, including rf phase, baseline fluctuations and off-resonance effects [94, 99–101], so that the use of these methods for obtaining reliable measurements of fast chemical exchange rates is possible, but requires very careful control over many experimental parameters. Furthermore, many spectrometers will not tolerate pulse repetition times of less than a millisecond. As a result, these methods may be intimidating to the non-specialist who wishes to acquire fast rate data for a particular fluxional system of interest.

Measurements of the spin-lattice relaxation time in the rotating frame,  $T_{1\rho}$ , can also give exchange rates up to two orders of magnitude greater than the upper limit of the lineshape method, providing that the spectrometer is capable of producing rf of the sufficient required strength [102]. Both the spin-echo and  $T_{1\rho}$  methods can provide absolute rate measurements, rather than the rate relative to the frequency difference between sites. By observing the  $T_2$  as a function of pulse repetition rate in a CPMG experiment, or the dependence of  $T_{1\rho}$  on the size of the spin-locking rf field, an absolute value for the exchange rate can be obtained. Despite the claims of considerably extending the upper range of accessible rate constants, the  $T_{1\rho}$  method appears to have undergone very limited application [98, 103, 104], probably due to the somewhat specialized nature of the technique. A simple yet reliable method for measurement of fast chemical exchange rates beyond the upper limit of lineshape analysis is accordingly desired.

An alternative method for measuring  $T_2$  was originally proposed by Bain, Martin and Ho [105]. This method is based on the formation of a steady state in the spin system by irradiation with an rf field, with interpretation of the data obtained from the Bloch equations in the presence of saturation. The method has been called the offset-saturation experiment [83]. The original form of the experiment [105] involves saturation of the resonance of a single spin system without coupling, at some offset from resonance ( $\omega_0 - \omega$ ) with an rf field, for a time period on the order of  $5T_1$  to allow the formation of a steady state. The irradiation is then gated off and a  $90^\circ$  observation pulse applied (fig. 9). The FID is acquired and Fourier transformed to give a spectrum which provides a measure of the partially saturated  $z$  magnetization. This procedure is repeated for several different values of the irradiation resonance offset, and the value of  $T_2$  can be obtained by analysis of the curve of  $M_z$  as a function of irradiation offset (fig. 10) by consid-

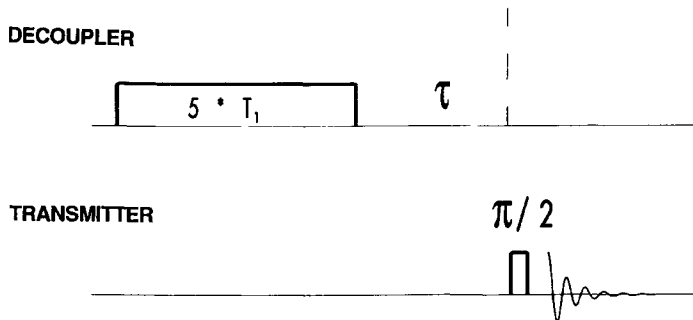


Fig. 9. Pulse sequence for the offset-saturation experiment for measuring  $T_1$  and  $T_2$  simultaneously.

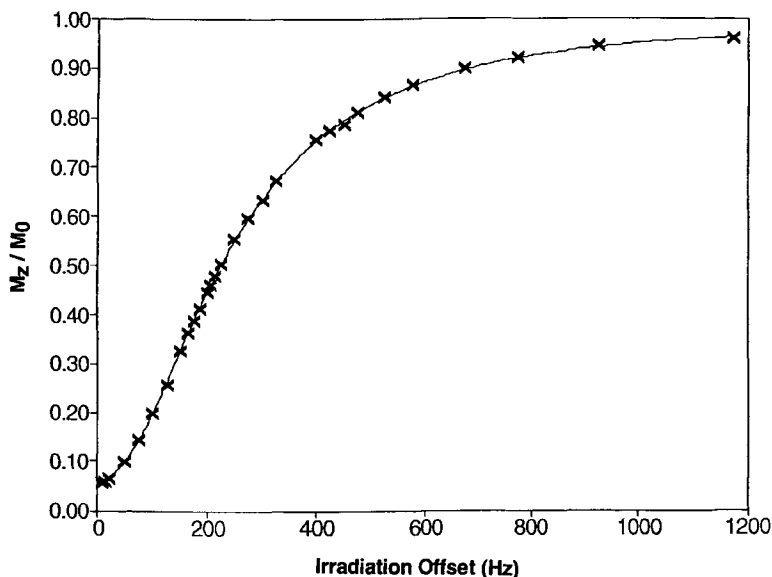


Fig. 10. Plot of partially saturated  $z$  magnetization as a function of irradiation offset in the offset-saturation experiment. The crosses represent experimental values and the line is the best fit to eq. (20).

ering the Bloch equations in the presence of saturation [106]. Significantly, provided that the value of  $B_2$  is sufficiently large, the  $T_2$  obtained will be the true or natural spin-spin relaxation time  $T_2$ , independent of magnetic field inhomogeneities [89, 105].

Pulse schemes similar to that of the offset-saturation method, often with a homospoil gradient pulse to destroy any  $x$ - $y$  magnetization, have been utilized in off-resonance  $T_{1\rho}$  experiments to study intermediate molecular motions in biological systems [107-111] and inorganic compounds [112] from

low-frequency relaxation time measurements, and to study cross-relaxation or magnetization transfer contrast effects in heterogeneous systems [106, 113–118]. The term “Z spectroscopy” has been given to such experiments which are concerned with measuring the  $z$  component of the magnetization [114]. Using a modification of the basic offset-saturation experimental procedure [83, 105], the technique can also be used to measure both  $T_1$  and  $T_2$  simultaneously. The insertion of a delay time  $\tau$ , which is some fraction of the spin-lattice relaxation time  $T_1$  after the irradiation is gated off and prior to the  $90^\circ$  observation pulse will allow the  $z$  magnetization to partially relax. This pulse scheme is illustrated in fig. 9. The minimum intensity in the plot of  $M_z$  as a function of irradiation offset will be at some non-zero minimum value, as in fig. 10. The fact that the  $z$  magnetization is partially relaxed can be used to determine the  $T_1$  by a slight modification to the steady-state solution to the Bloch equations for  $M_z$ . This simple experiment provides a way of measuring both  $T_1$  and  $T_2$  simultaneously.

### 5.1. Theory

The experiment is simply based on the Bloch equations [105]. The expression for  $M_z$  in the usual form is given in eq. (19):

$$M_z = M(\infty) \frac{1 + T_2^2(\omega - \omega_0)^2}{1 + T_2^2(\omega - \omega_0)^2 + (\gamma B_2)^2 T_1 T_2}. \quad (19)$$

The experiment assumes the rf magnetic field is saturating

$$\gamma B_2^2 \frac{T_1}{T_2} \gg 1,$$

and the system is allowed to relax for some time,  $\tau$ , before the  $z$  magnetization is measured. The equation for the curve of  $z$  magnetization plotted as a function of decoupler irradiation offset, as derived from the Bloch equations for  $M_z$  in the presence of saturation, is given by eq. (20):

$$M_z = M(\infty) \left( 1 - \frac{(\gamma B_2)^2 T_1 / T_2}{(\omega - \omega_0)^2 + (\gamma B_2)^2 T_1 / T_2} e^{-\tau/T_1} \right). \quad (20)$$

In this equation,  $M(\infty)$  is the equilibrium magnetization, and  $B_2$  is the strength of the irradiating or decoupling rf field.

### 5.2. Data analysis

The resulting values of  $T_1$  and  $T_2$  are determined by means of a non-linear least squares fit, using a parameterized model based on eq. (20). For a given

set of irradiation resonance offset values and corresponding intensities, pre-acquisition delay  $\tau$ , peak resonance position and calibrated value of the irradiating rf field  $B_2$  are used as input parameters [83]. As for the case of the selective-inversion experiments, the use of a non-linear fitting procedure to determine the relaxation times allows for reasonable estimation of the errors in the fitted parameters [83]. In this procedure, three parameters in eq. (19) are varied, namely,  $M(\infty)$ ,  $(\gamma B_2)^2 T_1 / T_2$ , and  $e^{-1/T_1}$ . Using the best-fit values of  $(\gamma B_2)^2 T_1 / T_2$  and  $e^{-1/T_1}$  and the calibrated value of  $B_2$ , both  $T_1$  and  $T_2$  are obtained from the nonlinear least-squares procedure, together with a determination of the errors as the 95% confidence limits, for the fitted parameters. Figure 10 shows the results of such a fitting.

### 5.3. Experimental

It is essential for the determination of accurate  $T_2$  values using the offset-saturation method that the irradiating field  $B_2$  be calibrated as accurately and precisely as possible without spending a disproportionate amount of experimental time calibrating the decoupler. The single-spin double resonance experiment [119–122] best fulfills these criteria. This experiment requires no special hardware or software considerations and is accordingly relatively simple to implement, with rapid interpretation of the data. The single-spin double-resonance method involves the irradiation of a single spin with a second rf field, as provided by a homodecoupler, while acquiring the signal. The irradiation process results in the creation of an effective magnetic field,  $B_{\text{eff}}$ . The magnetization  $\mathbf{M}$  is aligned along the effective field  $B_{\text{eff}}$ , which is oriented in the  $x$ - $z$  plane at some angle with respect to the  $z$  axis. When the total magnetization  $\mathbf{M}$  is perturbed from its steady-state orientation along the effective field, it will precess about the effective field as it relaxes back to its equilibrium position. The signal detected in the  $x$ - $y$  plane as a result of the projection of  $\mathbf{M}$  onto the  $x$ - $y$  plane results in the observation of two resonances or satellite peaks (fig. 11), as a result of precession about the effective magnetic field  $B_{\text{eff}}$  [32, 119, 123]. These satellite peaks will be symmetrically displaced about the irradiation frequency, and are inverted in phase with respect to each other when the irradiation is not far removed from resonance. The precession in one case will be of the same phase as the Larmor precession around the effective field, while the other spin transition of opposite phase results from precession in the opposite sense around the effective field [32, 119, 123]. The relative intensities of the two satellites vary with irradiation resonance offset. The magnitude of the irradiating field manifests itself in a rather straightforward manner in single-spin double-resonance spectra, which provides a convenient and facile method for the determination of  $B_2$ . The magnitude of the irradiating field  $\gamma B_2 / 2\pi$  (in Hz) can be determined from the distance between the satellites  $\omega_A$  and  $\omega_B$  as [83, 119, 120].

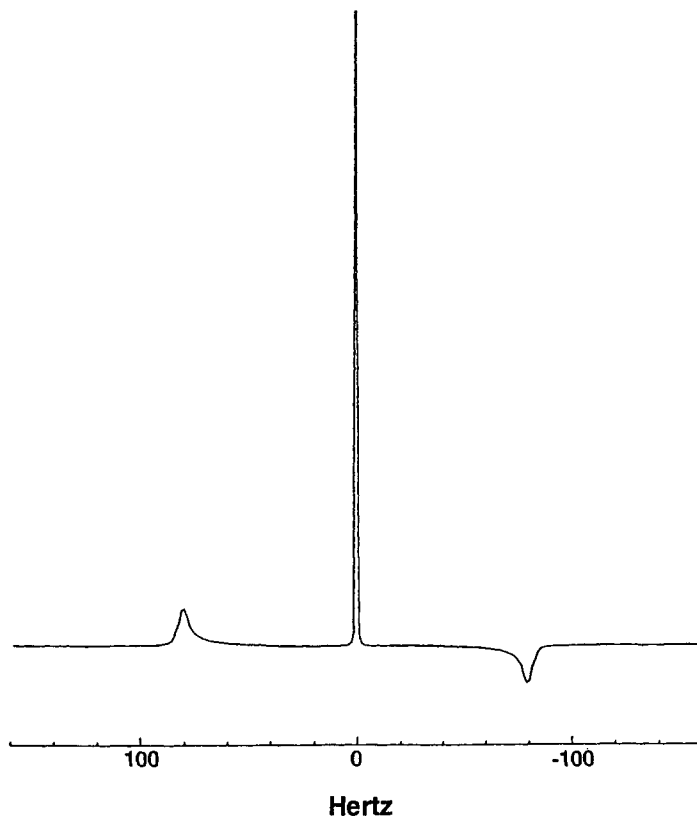


Fig. 11. Single-spin double-resonance experiment for the calibration of irradiation power. The proton line in chloroform is irradiated with the homonuclear decoupler. The strong central feature is at the irradiation frequency, and the separation of the two satellites is given by eq. (21).

$$\frac{\gamma B_2}{2\pi} = \left( \frac{(\omega_A - \omega_B)^2}{4} - (\omega_0 - \omega_2)^2 \right)^{1/2}. \quad (21)$$

Pulsed homodecoupling, which is employed on the majority of modern high resolution FT NMR spectrometers, involves a time sharing of the irradiation and acquisition so that the irradiation is actually on for a short period of time, appearing as a series of regularly repeated identical pulses, interrupted by signal acquisition. The equivalence of continuous wave radiation to a series of soft rf pulses [124] is important to establish in order that the pulsed single-spin double resonance experiment can be used to calibrate the homodecoupler field  $B_2$  which is used as the irradiating field in offset-saturation experiments. It has been shown analytically that the observed or calibrated value of  $B_2$  determined by the single-spin double-resonance ex-

periment is equal to the product of the instantaneous value of  $B_2$  (the value per individual pulse) and the spectrometer duty cycle in the limit of small duty cycles, (on the order of 20% or less) which are normal for most high-resolution NMR spectrometers. It is possible to calibrate  $B_2$  quickly and with good accuracy and precision using the single-spin double-resonance experiment, using several different values for the irradiation resonance offset ( $\omega_0 - \omega_2$ ), which permits the determination of an average value for  $B_2$ , together with a standard deviation. An example of a single-spin double resonance experiment is shown in fig. 11, for the irradiation of the proton in a sample of chloroform in  $\text{CDCl}_3$ . In this instance, the value of  $B_2$  (as  $\gamma B_2/2\pi$  in units of Hz) is 79.4 Hz.

An example of the offset-saturation method applied to an exchanging system is given in fig. 9, for the *chair-chair* inversion of cyclohexane. In the neglect of any scalar couplings between protons, cyclohexane represents a two-site equally populated exchanging system, for which many dynamic NMR studies have been presented using a variety of methods [3, 5], including lineshape analysis [10, 14, 125], spin echo [96],  $T_{1\rho}$  [102], and saturation transfer [10] techniques. These studies have resulted in a range of values for the activation energy of the ring-inversion process, with values of the activation energy in the range of 40–50 kJ/mol. The aforementioned study of Anet and Bourne [10] using a combination of lineshape analysis and saturation transfer methods on a sample of  $\text{C}_6\text{D}_{11}\text{H}$ , is considered to be the most comprehensive analysis. In spite of the numerous studies of cyclohexane, relatively few have provided rate information for temperatures above approximately 260 K; the  $T_{1\rho}$  study of cyclohexane by Deverell and co-workers gave rates on the order of  $10^3 \text{ s}^{-1}$  at a maximum temperature of 243.5 K.

With the offset-saturation method, the magnetic field inhomogeneity contribution is excluded from  $T_2^*$ . Thus, in the fast exchange regime, the rate constant  $k$  for an equally populated system can be determined from the relaxation times measured for the exchange-averaged resonance using the offset-saturation technique can be calculated using eq. (22).

$$\begin{aligned}
 k &= \frac{(\pi\Delta\omega_{1,2})^2}{2} T_2^{\text{exch}} \\
 &= \frac{(\pi\Delta\omega_{1,2})^2}{2} \left[ \frac{1}{T_2^{\text{obs}}} - \frac{1}{T_1} \right]^{-1}.
 \end{aligned}
 \tag{22}$$

In this equation,  $\Delta\omega_{1,2}$  is the chemical shift separation between the exchanging sites, such as the protons in axial and equatorial sites in cyclohexane, and  $T_2^{\text{exch}}$  is the exchange contribution to the observed  $T_2$ ,  $T_2^{\text{obs}}$  in eq. (22), which is the  $T_2$  determined from the offset-saturation experiment. The ex-

change contribution to the observed  $T_2$  is obtained simply by subtracting all other contributions from other  $T_2$  relaxation mechanisms to the observed  $T_2$  in the form of  $T_1$ , assuming that relaxation occurs by a dipole–dipole mechanism for protons in the molecules studied in the examples present herein. The advantage of using the offset-saturation method for applications to exchanging systems, with the ability to simultaneously measure both  $T_1$  and  $T_2$ , is thus apparent.

A plot of the  $z$  magnetization ( $M_z/M_\infty$ ) as a function of the irradiation resonance offset is given for an offset saturation experiment on a sample of degassed cyclohexane ( $C_6H_{12}$ ) in  $CDCl_3$  at a temperature of 303 K. At this temperature, the cyclohexane resonance was noticeably narrow; at 280 K, the linewidth of the cyclohexane  $^1H$  resonance was approximately 1.2 Hz, compared to a width of 0.5 Hz for the internal TMS standard. From the resulting values of  $T_1$  and  $T_2$ , and the measured low-temperature axial-equatorial chemical shift difference of 45.4 Hz at 100 MHz used in eq. (22), the rate at 293 K was determined to be  $1.94 \times 10^5 \text{ s}^{-1}$ . Thus, rates on the order of  $10^5$  or  $10^6 \text{ s}^{-1}$  are accessible in relatively simple systems using the offset-saturation method.

A further illustrative example of the offset-saturation method applied to a more complicated system undergoing fast exchange is presented for the case of 2-furaldehyde (furfural) in acetone- $d_6$ , which exchanges between (OO)-*cis* and (OO)-*trans* sites. In this particular system, the two sites are unequally populated, and the region of intermediate exchange is quite narrow. The fast exchange regime is entered at relatively low temperatures (approximately 220 K), rendering lineshape methods of limited application for this system, highlighting the applicability of the offset-saturation technique in this particular system. As this system possesses unequal populations of the exchanging sites, a knowledge of the equilibrium constant is necessary in order to determine the rate constants for the exchange process. The equilibrium constant can be readily obtained from the exchange-averaged chemical shift at the appropriate temperature in the fast exchange regime. For a two-site system in the fast exchange limit, the single exchange-averaged line will occur at the population-weighted mean resonance frequency, which may be given in terms of the chemical shifts and populations for each of the individual sites [3, 6, 126] as

$$\omega_{\text{obs}} = p_1\omega_1 + p_2\omega_2, \quad (23)$$

where  $\omega_{\text{obs}}$  is the experimentally observed or exchange-averaged resonance,  $p_1$  and  $p_2$  are the temperature-dependent fractional populations of sites 1 and 2 respectively, such that  $p_1 + p_2 = 1$ , and  $\omega_1$  and  $\omega_2$  are respectively the chemical shifts for the individual sites 1 and 2.

Expressions for determining rate constants from exchange contributions to observed linewidth for unequally populated systems in the fast exchange limit have been derived from the formal solutions to the Bloch equations modified for chemical exchange [3, 127–129]. These equations relate each rate constant to the site populations, chemical shift difference between sites, and spin relaxation times  $T_1$  and  $T_2$ . For example, the forward rate  $k_{1,2}$  is given by [3, 127]:

$$k_{1,2} = p_1 p_2^2 (\Delta\omega_{1,2})^2 \left( \frac{1}{T_2^*} - \frac{1}{T_1} \right)^{-1}, \quad (24)$$

where  $\Delta\omega_{1,2}$  is the chemical shift difference between sites 1 and 2 in units of radians per second. In eq. (24), it is assumed that  $T_1 = T_2$  in the absence of exchange, and that the fast exchange values of  $T_1$  for each site are equal, i.e.,  $T_1 = T_{2A} = T_{2B}$ . These approximate expressions were scrutinized by numerical calculations by Gutowsky and co-workers [130] and shown to be accurate for the determination of fast exchange rates, but are subject to serious systematic errors if used to obtain rates in the region near coalescence. Accordingly, the offset-saturation technique should be employed only in the fast exchange region well above the point of coalescence, at temperatures above the point of maximum exchange broadening.

A plot of the  $z$  magnetization ( $M_z/M_\infty$ ) as a function of the irradiation resonance offset is given in fig. 10 for an offset saturation experiment performed on the aldehydic proton of furfural for a degassed sample of furfural in acetone- $d_6$  at a temperature of  $262.5 \pm 0.5$  K.

The preceding examples illustrate that the offset-saturation method can successfully be used with some degree of facility, to measure exchange rates in systems undergoing fast chemical exchange. Rates on the order of  $10^5 \text{ s}^{-1}$ , which are beyond the upper bounds of lineshape analysis, have been determined using the relaxation times measured using the offset-saturation technique. Applications to date have been restricted to 2-site exchanging systems, although the potential exists to extend both theory and methodology to multi-site processes. In addition, successful application of the offset-saturation method to obtain rate data for systems undergoing fast exchange requires prior knowledge of the chemical shift separation.

## 6. Conclusions

In order to use chemical exchange measurements to study transition states, we need accurate rates over a wide range of temperatures. In NMR terms, this means covering the three regimes: slow exchange, intermediate exchange and fast exchange. In favourable cases, this means that ranges of

reliable reaction rates run over five orders of magnitude. This sort of data gives excellent values of the thermodynamic functions of the activated complex – errors in  $\Delta H$  of less than 1 kJ mol<sup>-1</sup> and errors in  $\Delta S$  of a few J/K.

In the slow exchange region, where the spectra are well-resolved and the rates are comparable to relaxation times, two-dimensional methods such as EXSY give excellent information on the exchange mechanism. However, for quantitative measurement of the exchange rate, we feel one-dimensional selective-inversion relaxation experiments are the best way to get good data. If a spin is selectively perturbed, it can return to equilibrium by a combination of chemical exchange and spin-lattice relaxation. We feel that this experiment gives the best data since the exchange is observed directly, and there is a good model of the process. Rates can be measured with an accuracy of a few percent.

When the lines in the spectrum are broad and starting to coalesce, we are in the intermediate exchange region. The best way to measure rates here is to simulate the lineshape and compare it, visually or numerically, with the observed spectrum. Several ways of calculating the lineshape are available, but we like the formulation that treats the spectrum always as a sum of transitions, rather than as a single lineshape.

In fast exchange, we must measure  $T_2$  for the coalesced line, and then calculate the exchange rates from that. Standard CPMG and  $T_{1\rho}$  methods may be difficult to implement, but the offset-saturation experiment can be done on essentially any spectrometer. These  $T_2$  measurements can often extend the high-temperature side of the Eyring plot by substantial amounts, particularly in the case of unequally populated systems. Taken together with the other methods, they provide excellent data.

Chemical exchange studies by NMR offer all sorts of exciting possibilities for examining the fluxionality of molecules. We can determine the mechanism of the reaction by seeing which sites are exchanging with which other sites. Various NMR experiments allow us to measure the rates, provided they are in the wide range of about 1–10<sup>5</sup> s<sup>-1</sup>. With these rate measurements over a wide temperature range, we can get excellent values of the activation parameters. All of this gives insight into what holds molecules together.

## References

- [1] H.S. Gutowsky and C.H. Holm, J. Chem. Phys. **25** (1956) 1228.
- [2] H.M. McConnell, J. Chem. Phys. **28** (1958) 430.
- [3] J. Sandstrom, Dynamic NMR Spectroscopy (Academic Press, London, 1982).
- [4] J.I. Kaplan and G. Fraenkel, NMR of Chemically Exchanging Systems (Academic Press, New York, 1980).
- [5] L.M. Jackman and F.A. Cotton, Dynamic Nuclear Magnetic Resonance Spectroscopy (Academic Press, New York, 1975).

- [6] I.O. Sutherland, *Ann. Rep. NMR Spectrosc.* **4** (1971) 71.
- [7] M. Schlabach, H.H. Limbach, E. Bunnenberg, A.Y.L. Shu, B.R. Tolf and C. Djerassi, *J. Am. Chem. Soc.* **115** (1993) 4554.
- [8] J. Braun, M. Schlabach, B. Werhle, M. Kocher, E. Vogel and H.H. Limbach, *J. Am. Chem. Soc.* **116** (1994) 6593.
- [9] M. Schlabach, H.H. Limbach, E. Bunnenberg, A.Y.L. Shu, B.-R. Tolf and C. Djerassi, *J. Am. Chem. Soc.* **115** (1993) 4554.
- [10] F.A.L. Anet and A.J.R. Bourn, *J. Am. Chem. Soc.* **89** (1967) 760.
- [11] A.D. Bain, G.J. Duns, S. Ternieden, J. Ma and N.H. Werstiuk, *J. Phys. Chem.* **98** (1994) 7458.
- [12] H.S. Gutowsky, D.W. McCall and C.P. Slichter, *J. Chem. Phys.* **21** (1953) 279.
- [13] L.W. Reeves and K.N. Shaw, *Can. J. Chem.* **48** (1970) 3641.
- [14] P.T. Inglefield, E. Krakower, L.W. Reeves and R. Stewart, *Mol. Phys.* **15** (1968) 65.
- [15] S. Szymanski, M. Witanowski and A.M. Gryff-Keller, in: *Annual Reports on NMR Spectroscopy*, ed. G.A. Webb (Academic Press, London, 1978) p. 227.
- [16] A.D. Bain and G.J. Duns, *J. Magn. Reson. A* **112** (1995) 258.
- [17] T. Drakenberg and R.E. Carter, *Org. Magn. Reson.* **7** (1975) 307.
- [18] K.-I. Dahlqvist and S. Forsén, *J. Phys. Chem.* **69** (1965) 4062.
- [19] R.J. Abraham and T.M. Siverns, *Tetrahedron* **28** (1972) 3015.
- [20] A.D. Bain, G.J. Duns, F. Rathgeb and J. Vanderkloet, *J. Phys. Chem.* **99** (1995) 17338.
- [21] F. Bloch and A. Siegert, *Phys. Rev.* **57** (1940) 522.
- [22] D.A. Kleier and G. Binsch, *J. Magn. Reson.* **3** (1970) 146.
- [23] A.D. Bain and G.J. Duns, *Can. J. Chem.* **74** (1996) 819.
- [24] L.W. Reeves and K.N. Shaw, *Can. J. Chem.* **49** (1971) 3671.
- [25] J.I. Kaplan, *J. Chem. Phys.* **28** (1958) 278.
- [26] S. Alexander, *J. Chem. Phys.* **37** (1962) 967.
- [27] S. Alexander, *J. Chem. Phys.* **37** (1962) 974.
- [28] R.M. Lynden-Bell, *Prog. Nucl. Magn. Reson. Spectrosc.* **2** (1967) 163.
- [29] K.-I. Dahlqvist and S. Forsén, *J. Phys. Chem.* **73** (1969) 4124.
- [30] D.S. Stephenson and G. Binsch, *J. Magn. Reson.* **32** (1978) 145.
- [31] H.S. Gutowsky, R.L. Vold and E.J. Wells, *J. Chem. Phys.* **43** (1965) 4107.
- [32] R.E. Hoffman and S. Forsén, *Prog. Nucl. Magn. Reson. Spectrosc.* **1** (1966) 15.
- [33] R.G. Gordon and R.P. McGinnis, *J. Chem. Phys.* **49** (1968) 2455.
- [34] C.S. Johnson, *Adv. Magn. Reson.* **1** (1965) 33.
- [35] D.S. Stephenson and G. Binsch, *J. Magn. Reson.* **30** (1978) 625.
- [36] R.K. Harris, *Nuclear Magnetic Resonance Spectroscopy* (Pitman Books, London, 1983).
- [37] R.R. Ernst, G. Bodenhausen and A. Wokaun, *Principles of Nuclear Magnetic Resonance in One and Two Dimensions* (Clarendon Press, Oxford, 1987).
- [38] U. Fano, in: *Lectures on the Many Body Problem*, Vol. 2, ed. E.R. Caianiello (Academic Press, New York, 1964) p. 217.
- [39] A.D. Bain, *Prog. Nucl. Magn. Reson. Spectrosc.* **20** (1988) 295.
- [40] I. Najfeld and T.F. Havel, *Adv. Appl. Math.* **16** (1995) 321.
- [41] A. Gibbs and G.A. Morris, *J. Magn. Reson.* **91** (1991) 77.
- [42] S. Forsén and R.A. Hoffman, *J. Chem. Phys.* **39** (1963) 2892.
- [43] S. Forsén and R.A. Hoffman, *J. Chem. Phys.* **40** (1964) 1189.
- [44] R.A. Hoffman and S. Forsén, *J. Chem. Phys.* **45** (1966) 2049.

- [45] J. Jeener, B.H. Meier, P. Bachmann and R.R. Ernst, *J. Chem. Phys.* **71** (1979) 4546.
- [46] G.E. Hawkes, L.Y. Lian, E.W. Randall, K.D. Sales and S. Aime, *J. Chem. Soc. Dalton Trans.* (1985) 225.
- [47] G.E. Hawkes, L.Y. Lian, E.W. Randall, K.D. Sales and S. Aime, *J. Magn. Reson.* **65** (1985) 173.
- [48] A.D. Bain and J.A. Cramer, *J. Magn. Reson. A* **103** (1993) 217.
- [49] D.L. Turner, *J. Magn. Reson.* **61** (1985) 28.
- [50] E.W. Abel, T.P.J. Coston, K.G. Orrell, V. Sik and D. Stephenson, *J. Magn. Reson.* **70** (1986) 34.
- [51] C.L. Perrin and R.K. Gipe, *J. Am. Chem. Soc.* **106** (1984) 4036.
- [52] R. Willem, *Prog. Nucl. Magn. Reson. Spectrosc.* **20** (1987) 1.
- [53] K.G. Orrell, V. Sik and D. Stephenson, *Prog. Nucl. Magn. Reson. Spectrosc.* **22** (1990) 141.
- [54] C.L. Perrin and T. Dwyer, *Chem. Rev.* **90** (1990) 935.
- [55] G.H. Weiss and J.A. Ferretti, *J. Magn. Reson.* **55** (1983) 397.
- [56] R. Nadjari and J.-Ph. Grivet, *J. Magn. Reson.* **98** (1992) 259.
- [57] G. Wider, R.R. Ernst, A. Kumar, S. Macura and K. Wüthrich, *J. Magn. Reson.* **56** (1984) 207.
- [58] R.G.S. Spencer, A. Horska, J.A. Ferretti and G.H. Weiss, *J. Magn. Reson. B* **101** (1993) 294.
- [59] S. Macura, *J. Magn. Reson. A* **112** (1995) 152.
- [60] T.A. Holak, J.N. Scarsdale and J.H. Prestegard, *J. Magn. Reson.* **74** (1987) 546.
- [61] M.S. Broido, T.L. James, G. Zon and J.W. Keepers, *Eur. J. Biochem.* **150** (1985) 117.
- [62] W. Denk, R. Baumann and G. Wagner, *J. Magn. Reson.* **67** (1986) 386.
- [63] G.H. Weiss, R.A. Byrd and J.A. Ferretti, *J. Magn. Reson.* **71** (1987) 97.
- [64] G.H. Weiss, J.E. Kiefer and J.A. Ferretti, *J. Magn. Reson.* **97** (1992) 227.
- [65] K.G. Orrell and V. Sik, *Ann. Rep. NMR Spectrosc.* **19** (1987) 79.
- [66] H.L. Pardue, *Anal. Chimica Acta* **216** (1989) 69.
- [67] L.J. Farrugia and S.E. Rae, *Organometallics* **11** (1992) 196.
- [68] C.L. Perrin, *J. Magn. Reson.* **82** (1989) 619.
- [69] H. Gesmar and J.J. Led, *J. Magn. Reson.* **68** (1986) 95.
- [70] D.R. Muhandiram and R.E.D. McClung, *J. Magn. Reson.* **71** (1987) 187.
- [71] M. Grassi, B.E. Mann, B.T. Pickup and C.M. Spencer, *J. Magn. Reson.* **69** (1986) 92.
- [72] B.E. Mann, *Organometallics* **11** (1992) 481.
- [73] B.E. Mann, B.T. Pickup and A.K. Smith, *J. Chem. Soc. Dalton Trans.* (1989) 889.
- [74] A.D. Bain and J.A. Cramer, *J. Magn. Reson. A* **118** (1996) 21.
- [75] A.D. Bain and J.A. Cramer, *J. Phys. Chem.* **97** (1993) 2884.
- [76] W.H. Press, B.P. Flannery, S.A. Teukolsky and W.T. Vetterling, *Numerical Recipes in C. The Art of Scientific Computing* (Cambridge University Press, Cambridge, 1988).
- [77] N.R. Draper and H. Smith, *Applied Regression Analysis* (Wiley, Toronto, 1981).
- [78] G.A.F. Seber and C.J. Wild, *Non-linear Regression* (Wiley, New York, 1989).
- [79] B.T. Bulliman, P.W. Kuchel and B.E. Chapman, *J. Magn. Reson.* **82** (1989) 131.
- [80] R.E. Engler, E.R. Johnston and C.G. Wade, *J. Magn. Reson.* **77** (1988) 377.
- [81] X.A. Mao, *Chem. Phys.* **175** (1993) 237.
- [82] G.E.P. Box, W.G. Hunter and J.S. Hunter, *Statistics for Experimenters* (Wiley, New York, 1978).
- [83] A.D. Bain and G.J. Duns, *J. Magn. Reson. A* **109** (1994) 56.
- [84] A. Celmins, *J. Magn. Reson.* **50** (1982) 373.

- [85] G. Bodenhausen, R. Freeman and G.A. Morris, *J. Magn. Reson.* **23** (1976) 171.
- [86] G.A. Morris and R. Freeman, *J. Magn. Reson.* **29** (1978) 433.
- [87] F.D. Riddell, S. Arumugam and B.G. Cox, *J. Chem. Soc. Chem. Commun.* (1987) 1890.
- [88] A.D. Bain, *J. Magn. Reson.* **89** (1990) 153.
- [89] A. Abragam, *The Principles of Nuclear Magnetism* (Clarendon Press, Oxford, 1961).
- [90] E.L. Hahn, *Phys. Rev.* **80** (1950) 580.
- [91] H.Y. Carr and E.M. Purcell, *Phys. Rev.* **94** (1954) 630.
- [92] S. Meiboom and D. Gill, *Review of Scientific Instruments* **29** (1958) 688.
- [93] E. Fukushima and S.B.W. Roeder, *Experimental Pulse NMR* (Addison-Wesley, Don Mills, Ontario, 1981).
- [94] R. Freeman and H.D.W. Hill, in: *Dynamic Nuclear Magnetic Resonance Spectroscopy*, eds L.M. Jackman and F.A. Cotton (Academic Press, New York, 1975) p. 131.
- [95] Z. Luz and S. Meiboom, *J. Chem. Phys.* **39** (1963) 366.
- [96] A. Allerhand and H.S. Gutowsky, *J. Chem. Phys.* **42** (1965) 1587.
- [97] M. Bloom, L.W. Reeves and E.J. Wells, *J. Chem. Phys.* **42** (1965) 1615.
- [98] L.W. Reeves, in: *Dynamic Nuclear Magnetic Resonance Spectroscopy*, eds L.M. Jackman and F.A. Cotton (Academic Press, 1975) p. 83.
- [99] R.L. Vold, R.R. Vold and H.E. Simon, *J. Magn. Reson.* **11** (1973) 283.
- [100] D.G. Hughes and G. Lindblom, *J. Magn. Reson.* **26** (1977) 469.
- [101] D.G. Hughes, *J. Magn. Reson.* **26** (1977) 481.
- [102] C. Deverell, R.E. Morgan and J.H. Strange, *Mol. Phys.* **18** (1970) 553.
- [103] P. Stilbs and M. Moseley, *J. Magn. Reson.* **31** (1978) 55.
- [104] S. Chopra, R.E.D. McClung and R.B. Jordan, *J. Magn. Reson.* **59** (1984) 361.
- [105] A.D. Bain, W.P.Y. Ho and J.S. Martin, *J. Magn. Reson.* **43** (1981) 328.
- [106] S.D. Wolff and R.S. Balaban, *Magn. Reson. Med.* **10** (1989) 135.
- [107] T.L. James, G.B. Matson and I.D. Kuntz, *J. Am. Chem. Soc.* **100** (1978) 3590.
- [108] T.L. James and S.P. Sawan, *J. Am. Chem. Soc.* **101** (1979) 7050.
- [109] T.L. James, *J. Magn. Reson.* **39** (1980) 141.
- [110] G.H. Caines, T. Schleich and J.M. Ryzewski, *J. Magn. Reson.* **95** (1991) 558.
- [111] G.H. Caines and T. Schleich, *J. Magn. Reson.* **95** (1991) 457.
- [112] T.L. James and G.B. Matson, *J. Magn. Reson.* **33** (1979) 345.
- [113] J. Grad, D. Mendelson, F. Hyder and R.G. Bryant, *J. Magn. Reson.* **86** (1990) 416.
- [114] J. Grad and R.G. Bryant, *J. Magn. Reson.* **90** (1990) 1.
- [115] R.G. Bryant and L.C. Coolbaugh, *J. Magn. Reson. B* **101** (1993) 121.
- [116] T.L. Ceckler and R.S. Balaban, *J. Magn. Reson.* **93** (1991) 572.
- [117] A. Knuttel and R.S. Balaban, *J. Magn. Reson.* **95** (1991) 309.
- [118] G.A. Morris and G.A. Freemont, *Magn. Reson. Med.* **28** (1992) 97.
- [119] W.A. Anderson, *Phys. Rev.* **102** (1956) 151.
- [120] J.D. Baldeschweiler, *J. Chem. Phys.* **40** (1964) 459.
- [121] N.R. Krishna, *J. Chem. Phys.* **63** (1975) 4329.
- [122] G. Tomlinson, *J. Magn. Reson.* **52** (1983) 374.
- [123] N.R. Krishna and S.L. Gordon, *Phys. Rev. A* **6** (1972) 2059.
- [124] A.D. Bain and G.J. Duns, *Bull. Magn. Reson.* **15** (1993) 64.
- [125] D. Hofner, S.A. Lesko and G. Binsch, *Org. Magn. Reson.* **11** (1978) 179.
- [126] E.L. Eliel, *Chem. Ind.* (1959) 568.
- [127] L.H. Piette and W.A. Anderson, *J. Chem. Phys.* **30** (1959) 899.

- [128] S. Meiboom, Z. Luz and D. Gill,  
J. Chem. Phys. **27** (1957) 1411.
- [129] T.J. Swift and R.E. Connick, J.  
Chem. Phys. **37** (1962) 307.
- [130] A. Allerhand, H.S. Gutowsky, J.  
Jonas and R. Meinzer, J. Am. Chem.  
Soc. **88** (1966) 3185.

This Page Intentionally Left Blank

# chapter 13

---

## Homonuclear Two-Dimensional Cross-Relaxation Spectroscopy

---

Nenad Juranić, Zsolt Zolnai and Slobodan Macura

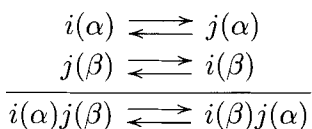
*Department of Biochemistry and Molecular Biology  
Mayo Graduate School  
Mayo Clinic and Foundation, Rochester, MN 55905  
USA*

This Page Intentionally Left Blank

## 1. Introduction

Dynamic processes generally are examined in terms of migration of suitable labels from an initial to a final state. A choice of labels that do not interfere with the basic exchange processes allows process dynamics to be observed during equilibrium conditions. Nuclear magnetization is a convenient label for the study of exchange processes because it does not perturb observed processes and one can label a large number of fragments by their respective resonance frequencies. Pulsed Fourier nuclear magnetic resonance (NMR) spectroscopy allows all resonance frequencies to be recorded simultaneously. Two-dimensional (2D) Fourier NMR spectroscopy traces resonance frequencies in two domains and is an excellent method for studying exchange processes; one domain can be attributed to the initial state and the other to the final state. A cross talk between different frequencies in the time domain indicates that exchange has taken place between the spin sites with the respective frequencies. 2D exchange spectroscopy [1–3] is a convenient tool for studying dynamic processes in liquids. It is best suited for elucidation of the slow incoherent magnetization transfer processes such as chemical exchange and cross-relaxation.

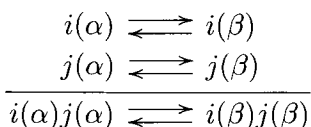
In the chemical exchange mechanism, the nuclear spin magnetization migrates together with the spin, which changes the site ( $i \rightleftharpoons j$ ) but not polarization ( $\alpha, \beta$ ):



In the cross-relaxation mechanism, the spin changes polarization ( $\alpha \rightleftharpoons \beta$ ) but not the site ( $i, j$ ):

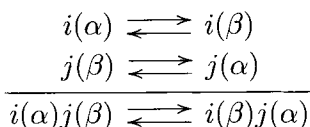
extreme-narrowing regime

(small molecules)



spin-diffusion regime

(macromolecules or low temperatures)



In the laboratory frame of reference, the net effects of the chemical exchange and the cross-relaxation are indistinguishable in the spin-diffusion regime. The individual contributions of each cannot be determined from a single exchange experiment.

### 1.1. Cross-relaxation

Cross-relaxation originates from dipole–dipole interactions between pairs of nuclear spins. Random molecular motion of the spin magnetic moments at one site (resonance frequency) induces magnetic transitions in the spins at another site. The net effect is a migration of the magnetization between the sites. Magnitude of the effect depends on the proximity of the interacting spins and the type and frequency of the motion that modulates their interaction. It also depends on whether the magnetization is longitudinal or transverse, i.e., whether magnetization exchange takes place in the laboratory or in the rotating frame [4]. The nuclear Overhauser effect (NOE) [5, 6] is an experimental manifestation of the cross-relaxation. It represents change in the intensity of one resonance line while the other line is saturated. The effect described originally by Overhauser [7] arose from electron–nuclear cross-relaxation. The NOE was described first by Solomon [4, 8].

The cross-relaxation rates between two spins can be experimentally measured in the laboratory ( $\sigma^n$ ) and in the rotating frame ( $\sigma^r$ ). They depend on interspin distance  $r$  and correlation time  $\tau_c$  that modulates the dipole–dipole interaction [4]:

$$\sigma^n = f^n(\tau_c)r^{-6}, \quad (1a)$$

$$\sigma^r = f^r(\tau_c)r^{-6}. \quad (1b)$$

The functions  $f^n(\tau_c)$  and  $f^r(\tau_c)$  depend on the type of molecular motion, and for a rigid body with isotropic motion, they become [9, 10]:

$$f^n(\tau_c) = q \left[ \frac{6}{1 + 4\omega_0^2\tau_c^2} - 1 \right] \tau_c, \quad (2a)$$

$$f^r(\tau_c) = q \left[ \frac{3}{1 + \omega_0^2\tau_c^2} + 2 \right] \tau_c, \quad (2b)$$

where  $q = 0.1(\mu_0/4\pi)^2\hbar^2\gamma^4$  (for protons  $q = 5.688 \times 10^{10} \text{ \AA}^6 \text{ s}^{-2}$ ) and  $\omega_0$  is the resonance frequency in rad/s. Figure 1 shows a contour plot of the cross-relaxation rates versus correlation time and interproton distance, according to eqs. (1) and (2). For  $\omega_0\tau_c > \sqrt{5}/2$ ,  $\sigma^n$  is negative, directly

proportional to the correlation time and inversely proportional to the sixth power of interspin distance  $r$  (solid lines in fig. 1). At  $\omega_0\tau_c = \sqrt{5}/2 \approx 1.14$ , the cross-relaxation disappears, i.e.,  $\sigma^n$  is zero. For  $\omega_0\tau_c < 1.14$ ,  $\sigma^n$  is positive and shows a distinct maximum at

$$\omega_0\tau_c = \sqrt{\frac{\sqrt{21}}{4} - 1} \approx 0.382.$$

One can notice a mirror symmetry at contour lines in the vicinity of zero cross-relaxation rate. Near zero, the laboratory-frame cross-relaxation rate can be enhanced either by an increase or by a decrease of temperature.

The cross-relaxation in the rotating frame (dashed lines in fig. 1) monotonically increases with correlation time. For  $\omega_0\tau_c < 0.382$  two cross-relaxation rates,  $\sigma^n$  and  $\sigma^r$ , have similar dependence on correlation time, and at the limit when  $\omega_0\tau_c \rightarrow 0$ , "the extreme narrowing limit," their ratio

$$S = \sigma_{ij}^n / \sigma_{ij}^r \quad (3)$$

tends toward unity (fig. 1, top).

For macromolecules (or small molecules in viscous solvents at a low temperature) in a high magnetic field,  $\omega_0\tau_c \gg 1$ . At this "spin-diffusion limit" the rotating-frame cross-relaxation rate is twice as fast as in the laboratory frame, and the rates are of the opposite sign,  $S = -1/2$  (fig. 1, top).

Also note that for  $\omega_0\tau_c \gg 1$ , the laboratory-frame cross-relaxation is independent from the overall relaxation. In the rotating frame, however, the cross-relaxation is an integral part of the overall relaxation process. In addition, the rotating-frame intragroup relaxation may become a dominant relaxation mechanism, and in larger molecules (or at lower temperatures) it may quench the rotating-frame cross-relaxation.

A distinctly different behavior of the two cross-relaxation rates at  $\omega_0\tau_c > 0.382$  in the two frames is crucial for determination of the correlation time [9, 11].

## 1.2. Chemical exchange

The chemical exchange, in NMR sense, reflects all processes of intermolecular and intramolecular rearrangements that occur while the observed spins change their magnetic environments [12, 13]. However, for 2D exchange spectroscopy, only the slow processes in which the observed spins change their resonance frequencies are observable. Here, slow refers to an exchange rate  $k_{ij}$  between sites  $i$  and  $j$  that is smaller than the difference between

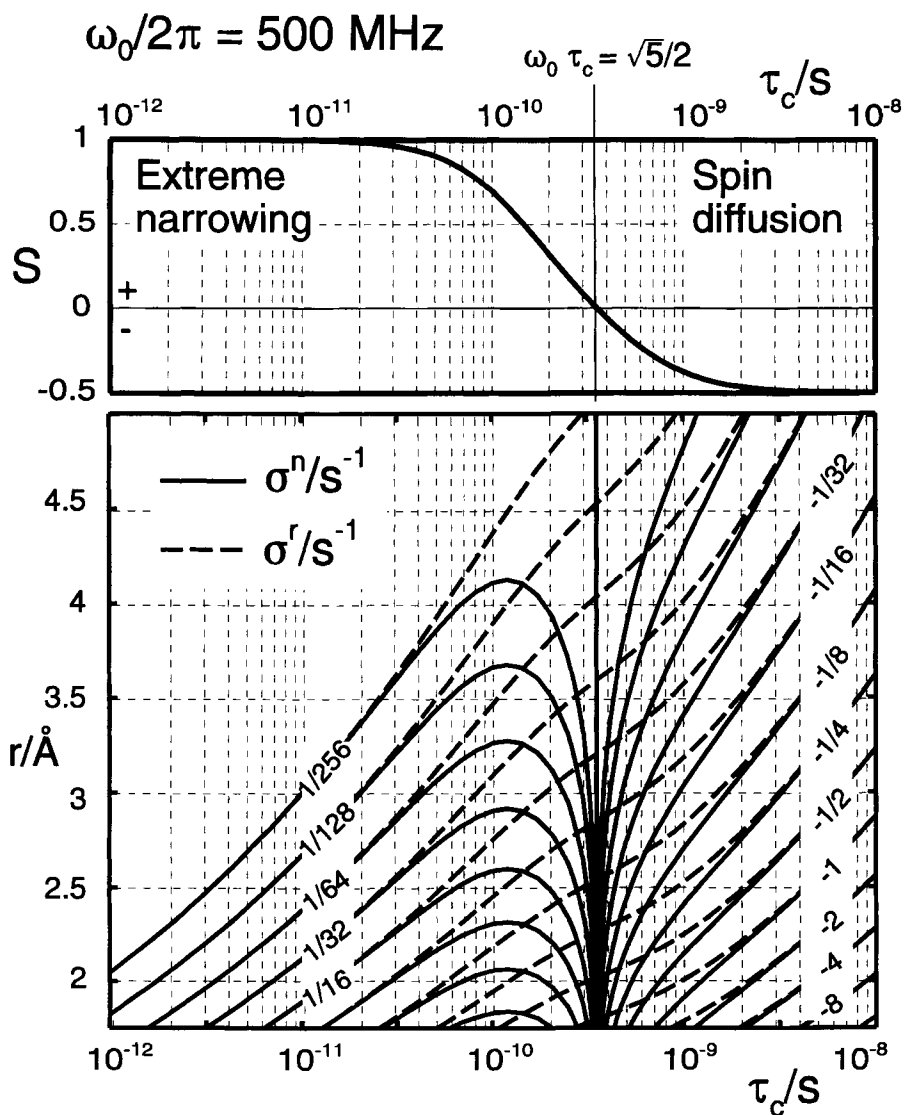


Fig. 1. Contour plot of the dependence of the cross-relaxation rate in the laboratory frame,  $\sigma^n$  (solid line), and rotating frame,  $\sigma^r$  (dashed line), on the interproton distance,  $r$ , and correlation time,  $\tau_c$ . Rigid body isotropic motion is assumed (eqs. (1) and (2)). Top panel shows the dependence of the ratio of the two cross-relaxation rates on correlation time.  $\sigma^r$  is always positive, whereas  $\sigma^n$  is positive for  $\omega_0\tau_c < \sqrt{5}/2$  and negative for  $\omega_0\tau_c > \sqrt{5}/2$ .  $\omega_0$  is resonance frequency.

the resonance frequencies at the two exchange sites; i.e., the exchange does not influence the shapes and positions of the individual resonance lines,  $k_{ij} \ll |\omega_i - \omega_j|/2\pi$ . The lower limit for the exchange processes is imposed by the  $T_1$  spin relaxation. To be observable at all, the rate of an exchange process must be larger than or comparable to the  $T_1$  relaxation rate,  $k_{ij} \geq R_i, R_j$ . Unlike the cross-relaxation, the chemical exchange does not depend on the frame of reference in which it occurs. Some processes with rates high enough to make them not amenable for study by the exchange spectroscopy ( $k_{ij} \geq |\omega_i - \omega_j|/2\pi$ ) can be studied by the NMR relaxation time measurements [14, 15] or by the line-shape analysis [16, 17].

### 1.3. Coherent magnetization transfer

Coherent magnetization transfer takes place through the network of scalar coupling. It is a prerequisite for most modern NMR experiments [3]. The coherence transfer can be observed both in laboratory and rotating frame, and it can contribute to magnetization transfer in 2D exchange experiments done in either frame. In 2D exchange experiments it is an undesirable artifact. Several methods have been proposed for elimination of the coherent magnetization transfer from exchange experiments [18–21]. These methods distinguish between the coherent and the incoherent transfer on the basis of differences in their time evolution. The coherent magnetization transfer takes place only at well-defined frequencies, e.g.,  $\sin(\omega_i\tau_m)$ , whereas the incoherent transfer continues steadily according to eq. (8) (see below).

In the laboratory-frame NOE experiments the coherent transfer can be eliminated by a random variation of mixing time within a range that represents a small fraction of the total mixing time. In these conditions, the  $\sin(\omega_i\tau_m)$  terms average to zero, and the incoherent exchange averages to a nonzero value.

Elimination of the coherence transfer from the rotating-frame experiments is more difficult, because transferred magnetization evolves as  $\sin^2(\omega_i\tau_m)$ . The modulation of mixing time is ineffective, because it does not average the coherent signal to zero. However, some other dissimilarities between the two transfer mechanisms can be used to separate these two effects in the rotating-frame experiments. Most notable is a dependence of the coherent transfer on the  $B_1$  radiofrequency (RF) field resonance offset and strength. The coherent transfer is highly sensitive to the effective field strength, and if the field strength is small compared to the frequency difference between the coupled spins, the coherent transfer is virtually absent [22–24]. If the RF field strength at the frequencies of the coupled nuclei is different because of the resonance offset effects, the coherence transfer will be strongly suppressed. This sensitivity to the resonance offset from the  $B_1$  field has been used for suppression of the coherence transfer artifacts in magnetiza-

tion exchange experiments [25]. The same artifacts can be eliminated by a multipulse sequence [26, 27].

#### 1.4. Influence of temperature

The dependence of chemical exchange rate constant  $k$  on temperature  $T$  can be expressed by the Arrhenius equation:

$$k = A \exp\left(-\frac{\Delta E_k^a}{RT}\right), \quad (4)$$

where  $A$  is the frequency factor,  $\Delta E_k^a$  is the activation energy, and  $R$  is the gas constant. A dependence of the cross-relaxation rate constant on temperature can be obtained by exploiting its dependence on the correlation time. If one neglects the anomalous behavior of  $\sigma^n$  at  $\omega_0\tau_c \sim 1$ , the cross-relaxation rate constants are proportional to correlation time,  $\tau_c$ . A good approximation for correlation time dependence on temperature is

$$\tau_c = \tau_c^0 \exp\left(+\frac{\Delta E_\tau^a}{RT}\right), \quad (5)$$

where  $\Delta E_\tau^a$  is the activation energy for a process that leads to the spin reorientation in an external magnetic field. Thus, for  $\omega_0\tau_c \ll 1$  and  $\omega_0\tau_c \gg 1$ ,

$$\frac{k}{\sigma} \sim \exp\left(-\frac{\Delta E_k^a + \Delta E_\tau^a}{RT}\right), \quad (6)$$

Even a small temperature change may have a profound effect on the relative contributions of the chemical exchange and cross-relaxation mechanisms in the exchange spectra [28]. Because the two processes, chemical exchange and cross-relaxation, are unrelated, the total sensitivity of the  $k/\sigma$  ratio is hard to predict. The temperature dependence of correlation time enables scanning of the whole range of mobility, from the extreme-narrowing limit at high temperatures to the spin-diffusion limit at low temperatures, using the same sample [29–31].

## 2. Basic experiments

The incoherent magnetization exchange can be measured if the relative orientation of magnetization vectors is constant during exchange, irrespective of their absolute orientation with regard to the external magnetic field. Traditionally, the magnetization exchange has been observed in the laboratory frame, i.e., during the exchange period (mixing time) with the magnetization vectors aligned along an external magnetic field. Such a 2D experiment

is known as NOESY (nuclear Overhauser effect spectroscopy), if applied to observe the cross-relaxation, or EXSY (chemical exchange spectroscopy) if applied to monitor the chemical exchange.

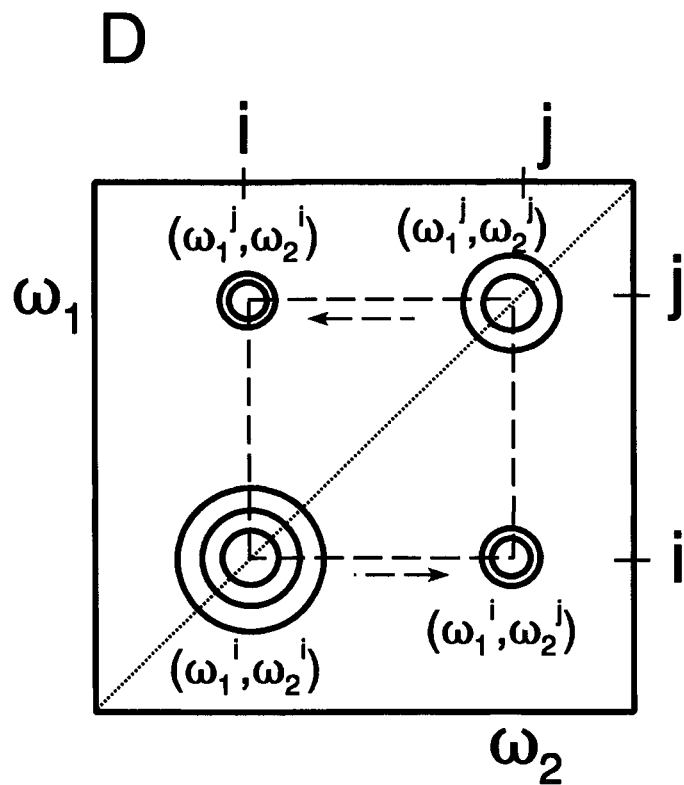
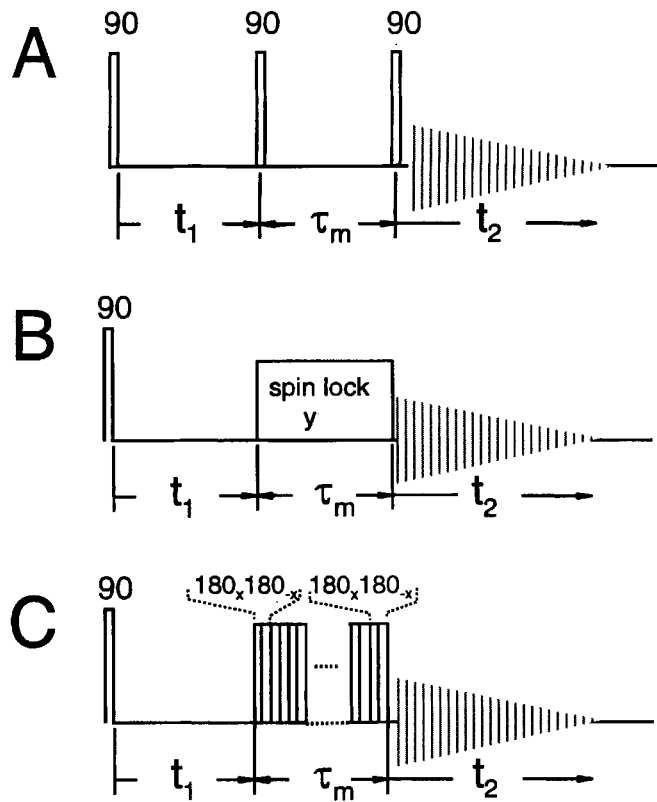
Another possibility for monitoring the cross-relaxation (and chemical exchange) is to keep the magnetization components during exchange in a transverse plane aligned by a constant “spin lock” RF pulse. The 2D cross-relaxation experiment is then called ROESY (rotating frame Overhauser effect spectroscopy). If instead of a constant RF pulse a sequence of pulses is used to “spin lock” the magnetization components during the exchange, the actual path of magnetization vectors may be complex and exchange can be considered to take place in the laboratory and in the rotating frame. Depending on the “spin-locking” pulse sequence design, the pulse sequences have different names [32]. Below, we will describe the T-ROESY (transverse ROESY) sequence in which the magnetization is constantly flipped between the two frames of reference, with a major goal of the coherent magnetization transfer elimination from a 2D exchange spectrum [27].

### 2.1. NOESY (EXSY)

The basic experiment of 2D exchange spectroscopy [2, 33–35] is shown in fig. 2(A). The first pair of  $90^\circ$  pulses, separated by the time interval  $t_1$ , creates a frequency-labeled longitudinal magnetization. After the second  $90^\circ$  pulse, the longitudinal magnetization migrates among various sites during the mixing time  $\tau_m$ . A result of this migration is recorded during the detection time  $t_2$  that begins after a third  $90^\circ$  pulse. By repeating the experiment with systematic incrementation of the evolution period  $t_1$ , a series of frequency-modulated, nonequilibrium states is created. After magnetization exchange during the mixing time  $\tau_m$ , one detects the signal  $s(t_1, t_2)$  that on 2D Fourier transformation yields the 2D exchange spectrum  $S(\omega_1, \omega_2)$ , as shown in fig. 2(D). The diagonal peaks at positions  $\omega_1 = \omega_2 = \omega^i$  and  $\omega_1 = \omega_2 = \omega^j$  indicate a fraction of magnetization that did not migrate during the mixing time. The cross peaks at symmetrical positions around the diagonal,  $(\omega_1 = \omega^i, \omega_2 = \omega^j)$  and  $(\omega_1 = \omega^j, \omega_2 = \omega^i)$ , originate from the fraction of magnetization that migrated between sites  $i$  and  $j$  during the mixing time.

### 2.2. ROESY

Figure 2(B) shows an equivalent pulse scheme used for studying exchange processes in the rotating frame [22, 36–38]. As in the above experiment, the first  $90^\circ$  pulse, followed by the incremental delay  $t_1$ , creates a frequency-labeled transverse magnetization that is projected onto the rotating-frame axis ( $x$  or  $y$ ) by a spin-locking pulse of duration  $\tau_m$ . While the magnetization is spin locked, exchange will occur. As in the previous case, the data



acquisition within time domain  $t_2$  is repeated with systematic incrementation of the evolution period  $t_1$ , generating a time domain signal  $s(t_1, t_2)$  that on 2D Fourier transformation yields the exchange spectrum  $S(\omega_1, \omega_2)$ .

### 2.3. T-ROESY

This experiment monitors the magnetization exchange in both frames simultaneously [26, 27]. A series of  $180^\circ(x)$   $180^\circ(-x)$  pulses during the mixing time causes the magnetization to oscillate between the two frames. The resulting magnetization exchange rate constant  $L$  is the average of exchange rates in two frames [26, 27, 32],

$$L_{ij}^{\text{rf}} = -\frac{1}{2}(\sigma_{ij}^{\text{n}} + \sigma_{ij}^{\text{r}}) + k_{ij}. \quad (7)$$

The main purpose of the T-ROESY experiment is suppression of the coherence magnetization transfer [27]. The experiment is close to one designed for elimination of the cross-relaxation from the chemical exchange [26, 39]. There, in a spin-diffusion regime, the weights of laboratory- and rotating-frame cross-relaxations are optimized in such a way that the terms inside the parentheses in eq. (7) cancel each other, and the chemical exchange becomes the only process to give rise to cross peaks in a 2D spectrum.

## 3. Quantitative relationships

For the analysis of a cross-peak evolution during mixing time, it is convenient to represent the 2D exchange spectrum as a matrix of peak volumes  $\mathbf{A}(\tau_m)$  that depends on the mixing time  $\tau_m$ . For  $\tau_m = 0$ , no magnetization exchange takes place, and, consequently,  $\mathbf{A}(0)$  represents a diagonal matrix with elements proportional to the equilibrium populations of the individual spin sites. The volume matrix of the exchange spectrum recorded with an

←

Fig. 2. Basic sequence of two-dimensional exchange spectroscopy. (A) NOESY: monitors cross-relaxation in the laboratory frame,  $\sigma^{\text{n}}$ . (B) ROESY: monitors cross-relaxation in the rotating frame,  $\sigma^{\text{r}}$ . (C) T-ROESY: monitors cross-relaxation under the influence of RF field. Because on average, magnetization is half of the time in the laboratory frame and half in the rotating frame,  $\sigma^{\text{rf}} = (\sigma^{\text{n}} + \sigma^{\text{r}})/2$ . Magnetization transfer due to chemical exchange is invariant to the frame of reference and thus can be observed in either experiment. (D) Geometry of 2D exchange spectrum. Spectrum is symmetric along the main diagonal which contain lines of nonexchanged magnetization components. Volumes of symmetrically positioned peaks are proportional to the amount of transferred magnetization. Magnetization exchange takes place horizontally; parent diagonal and descendant cross peak have the same  $\omega_1$  frequency.

arbitrary (fixed) mixing time  $\mathbf{A}(\tau_m)$  depends on the equilibrium populations  $\mathbf{A}(0)$ , on the mixing time  $\tau_m$ , and on the dynamic matrix  $\mathbf{L}$  [2, 3, 33]

$$\mathbf{A}(\tau_m) = \mathbf{e}^{\mathbf{L}\tau_m} \cdot \mathbf{A}(0). \quad (8)$$

Each element  $L_{ij}$  of the dynamic matrix  $\mathbf{L}$  expresses the rate of magnetization exchange between the sites  $i$  and  $j$ . The exchange spectra in the rotating and the laboratory frame have the same general appearance, but their detailed characteristics depend on the nature of  $\mathbf{L}$ , i.e., on the mechanism of magnetization transfer. The elements  $L_{ij}$  of the dynamic matrix contain terms corresponding to two possible mechanisms: (i)  $k_{ij}$ , the chemical exchange rate and (ii)  $R_{ij}$ , the cross-relaxation rate,

$$L_{ij} = k_{ij} - \sigma_{ij}. \quad (9)$$

In a matrix form,

$$\mathbf{L} = \mathbf{K} - \mathbf{R}, \quad (10)$$

where  $\mathbf{K}$  is the kinetic matrix and  $\mathbf{R}$  is the relaxation matrix.

Traditionally, the analysis of  $\mathbf{L}$  in terms of cross-relaxation spectroscopy (as  $\mathbf{R}$ ) or chemical exchange spectroscopy (as  $\mathbf{K}$ ) has been treated separately, both by full matrix analysis and by initial buildup rate analysis. The interference between two processes of the magnetization transfer has been avoided, either by careful selection of the system under study or by varying the exchange and cross-relaxation rates in an adjustment of the sample conditions. For rigid molecules  $\sigma_{ij} \gg k_{ij}$ , and for extreme narrowing or fast exchange (or both)  $k_{ij} \gg \sigma_{ij}$ . In these conditions  $\mathbf{L}$  can be separated easily into  $\mathbf{R}$  and  $\mathbf{K}$  according to eqs (9) and (10). More recently, the separation of the two processes by spectroscopic means has been facilitated by the development of 2D and ND techniques [26, 39–41].

### 3.1. Full matrix analysis

The dynamic matrix  $\mathbf{L}$  can be obtained by the full matrix analysis, solving eq. (8) [42–47]:

$$\mathbf{L} = \frac{1}{\tau_m} \ln [\mathbf{A}(\tau_m)\mathbf{A}(0)^{-1}]. \quad (11)$$

The principle of detailed balance (and the micro reversibility) [48] requires that 2D exchange spectrum  $\mathbf{A}(\tau_m)$  is always symmetric. The matrix  $\mathbf{A}(0)$  represents a 2D exchange spectrum recorded at  $\tau_m = 0$ . It is a diagonal

matrix with elements proportional to the equilibrium populations of the respective spin sites,

$$\mathbf{A}(0) = A_0 \cdot \text{diag}\{n_1, \dots, n_N\}. \quad (12)$$

$A_0$  is the spectral peak volume of a single proton and  $n_i$  is the number of protons at the spin site  $i$ . Obviously, when different spin sites have different populations, i.e.,  $n_i \neq n_j$ , neither the product matrix  $\mathbf{A}(\tau_m) \mathbf{A}(0)^{-1}$  nor the exchange matrix  $\mathbf{L}$  is symmetric, eq. (11). This also follows from the principle of detailed balance [28, 48],

$$\begin{aligned} \mathbf{L} \cdot \text{diag}\{n_1, \dots, n_N\} &= (\mathbf{L} \cdot \text{diag}\{n_1, \dots, n_N\})^T \\ &= \text{diag}\{n_1, \dots, n_N\} \cdot \mathbf{L}^T, \end{aligned} \quad (13)$$

or in a scalar form,

$$n_j L_{ij} = n_i L_{ji}. \quad (14)$$

Note that

$$\frac{L_{ij}}{n_i} = \frac{L_{ji}}{n_j} = L_{ij}^0 \quad (15)$$

and

$$L_{ij}^0 = L_{ji}^0. \quad (16)$$

In the case of cross-relaxation

$$\sigma_{ij} = -L_{ij}^0. \quad (17)$$

Because  $\text{diag}\{n_1, \dots, n_N\}$  is positive definite, the quasi-symmetric matrix  $\mathbf{L}$  has  $N$  real eigenvalues, whereas the eigenvectors corresponding to two different eigenvalues are  $\text{diag}\{n_1, \dots, n_N\}$ -orthogonal:

$$\langle u_i, \text{diag}\{n_1, \dots, n_N\} \cdot u_j \rangle = 0, \quad i \neq j, \quad (18)$$

where  $\langle \cdot, \cdot \rangle$  denotes the scalar product of two (column) vectors. From eq. (11) it follows that the dynamic matrix  $\mathbf{L}$  is a function of two matrices that correspond to two exchange spectra obtained from the experiments recorded at mixing times  $\tau_m$  and 0. The most convenient way for calculating the elements of the dynamic matrix uses the eigensystem of  $\mathbf{A}(\tau_m) \mathbf{A}(0)^{-1}$ . The

matrix  $\mathbf{A}(\tau_m)\mathbf{A}(0)^{-1}$  that corresponds to a normalized exchange spectrum can be written as

$$\mathbf{A}(\tau_m)\mathbf{A}(0)^{-1} = \mathbf{U}\Gamma(\tau_m)\mathbf{V}^T, \quad (19)$$

where  $\Gamma(\tau_m)$  is a diagonal matrix whose elements  $\gamma_i(\tau_m)$  are the eigenvalues of the normalized spectral matrix  $\mathbf{A}(\tau_m)\mathbf{A}(0)^{-1}$ ,

$$\Gamma(\tau_m) = \text{diag}\{\gamma_1(\tau_m), \dots, \gamma_N(\tau_m)\}, \quad (20)$$

and the matrices  $\mathbf{U}$  and  $\mathbf{V}$  are its left and right modal matrix. Because  $\mathbf{A}(\tau_m)\mathbf{A}(0)^{-1}$  is quasi-symmetric,

$$\mathbf{U} = \text{diag}\{n_1, \dots, n_N\} \cdot \mathbf{V}. \quad (21)$$

The left and right eigenvectors are biorthogonal

$$\langle \mathbf{u}_i, \mathbf{v}_j^T \rangle = \sum_{\ell} u_{i\ell} v_{\ell j}^T = \delta_{ij} \quad (22)$$

( $\delta_{ij}$  denotes the Kronecker delta:  $\delta_{ij} = 1$  for  $i = j$  and  $\delta_{ij} = 0$  for  $i \neq j$ ).

The left and right eigenvectors are equal only when the populations at all spin sites are the same. As a result of the invariance of modal matrices to matrix functions, the dynamic matrix  $\mathbf{L}$  can be written as

$$\mathbf{L} = \mathbf{U}\mathbf{A}\mathbf{V}^T = \text{diag}\{n_1, \dots, n_N\}\mathbf{V}\mathbf{A}\mathbf{V}^T, \quad (23)$$

where

$$\mathbf{A} = \text{diag}\{\lambda_1, \dots, \lambda_N\}. \quad (24)$$

The eigenvalues of  $\mathbf{L}$  and  $\mathbf{A}(\tau_m)\mathbf{A}(0)^{-1}$  are related by [49, 50]:

$$\lambda_i = \frac{1}{\tau_m} \ln \gamma_i(\tau_m). \quad (25)$$

Thus, full matrix analysis comprises calculation of eigenvectors and eigenvalues of the dynamic matrix over the eigenvectors and eigenvalues of the normalized spectral matrix  $\mathbf{A}(\tau_m)\mathbf{A}(0)^{-1}$ . Then,

$$L_{ij} = \sum_{\ell} u_{i\ell} v_{\ell j}^T \lambda_{\ell} = \sum_{\ell} n_i v_{i\ell} v_{\ell j}^T \lambda_{\ell} \quad (26)$$

and

$$|\Delta L_{ij}| \approx \Delta a \left\{ \sum_{r,s} (n_i v_{ir} v_{sj}^T)^2 \left[ \left( \frac{(1 - \delta_{\lambda_r \lambda_s})(\lambda_r - \lambda_s)}{e^{\lambda_r \tau_m} - e^{\lambda_s \tau_m}} \right)^2 + \left( \frac{\delta_{\lambda_r \lambda_s}}{\tau_m e^{\lambda_r \tau_m}} \right)^2 \right] \right\}^{1/2}. \quad (27)$$

Equation (27) expresses an error in the dynamic matrix element  $L_{ij}$  obtained from full matrix analysis if the error in peak volumes is  $\Delta a$  [50]. It also assumes that volume errors are equal for all peaks and are uncorrelated:  $\Delta a$  is volume error normalized to the volume of a single spin at  $\tau_m = 0$ . Modern computer programs (Matlab, Mathematica, Mapple) can calculate the dynamic matrix from eq. (11) directly.

The main disadvantage of the full matrix analysis is that it requires volume integrals of *all* spectral peaks, including the diagonal.

### 3.2. Initial buildup rate analysis

For sufficiently short mixing times, the expansion of eq. (8) into a Taylor series [33, 51–55]

$$\begin{aligned} \mathbf{A}(\tau_m) \mathbf{A}(0)^{-1} &= e^{\mathbf{L}\tau_m} \\ &= \mathbf{1} + \mathbf{L}\tau_m + \frac{1}{2}(\mathbf{L}\tau_m)^2 + \frac{1}{6}(\mathbf{L}\tau_m)^3 + \dots \end{aligned} \quad (28)$$

can be truncated after the linear term. Then, the experimentally obtained spectrum,  $\mathbf{A}(\tau_m)$  directly maps the elements of the dynamic matrix, and

$$\frac{a_{ij}(\tau_m)}{n_i a_{jj}(0)} = \frac{a_{ij}(\tau_m)}{n_j a_{ii}(0)} \approx \delta_{ij} + L_{ij}^0 \tau_m. \quad (29a)$$

In practice, owing to the low sensitivity, longer mixing times are used. Then the higher-order terms of Taylor expansion must be taken into account and eq. (29a) becomes

$$\begin{aligned} \frac{a_{ij}(\tau_m)}{n_i a_{jj}(0)} &= \delta_{ij} + L_{ij}^0 \tau_m + \frac{1}{2} \sum_k n_k L_{ik}^0 L_{kj}^0 \tau_m^2 + \dots \\ &= \frac{a_{ij}(\tau_m)}{n_j a_{ii}(0)}. \end{aligned} \quad (29b)$$

The quadratic and higher-order terms in eq. (29b),  $L_{ik}L_{kj}$ ,  $L_{ik}L_{k\ell}L_{\ell j} \dots$  which represent two-, three-, ... step transfer, respectively, are a source of

error in the analysis of the linear term. The nonlinear terms can overwhelm the desired linear term by the magnitude of individual  $L_{k\ell}$  terms, by the large number of exchange pathways  $k, \ell$ , or by the long mixing times (large  $\tau_m$ ). A significant practical improvement in the buildup analysis can be achieved if cross peaks are normalized with their respective diagonals at the same mixing time (instead at zero mixing time) [56]. Then the experiment at  $\tau_m = 0$  is not necessary and, more importantly, the buildup curves are not sensitive to external relaxation up to the second order in  $\tau_m$  [54, 55]

$$\begin{aligned} \frac{a_{ij}(\tau_m)}{n_i a_{jj}(\tau_m)} &= \delta_{ij} + L_{ij}^0 \tau_m + \left( \frac{1}{2} \sum_k n_k L_{ik}^0 L_{kj}^0 - n_j L_{ij}^0 L_{jj}^0 \right) \tau_m^2 + \dots \\ &= \frac{a_{ij}(\tau_m)}{n_j a_{ii}(\tau_m)}. \end{aligned} \quad (30)$$

When diagonal elements have distinctly different relaxation rates, i.e.,

$$n_j a_{ii}(\tau_m) \neq n_i a_{jj}(\tau_m), \quad (31)$$

then the results depend on a diagonal peak selection. In that case it is best to use the geometric mean of the diagonal peak volumes:

$$\frac{a_{ij}(\tau_m)}{\sqrt{n_i n_j a_{ii}(\tau_m) a_{jj}(\tau_m)}} \approx \delta_{ij} + L_{ij}^0 \tau_m + \frac{1}{2} \sum_{k \neq i, j} n_k L_{ik}^0 L_{kj}^0 \tau_m^2. \quad (32)$$

If cross peaks are of unequal volumes,  $a_{ij}(\tau_m) \neq a_{ji}(\tau_m)$ , owing to short repetition time or spectral distortions, it is best to normalize the geometric mean of the cross peaks by the geometric mean of their respective diagonals. Although approximate, eq. (30) is useful because errors of peak volumes often exceed errors introduced by the truncated Taylor expansion. The limitations and criteria for the validity of Taylor expansion are described elsewhere [55].

#### 4. Practical aspects of 2D exchange spectroscopy

Compared to other multidimensional experiments the exchange experiments are fairly simple and, thus, easy to optimize. Experiments are robust with regard to the pulse imperfections and miscalibration. All artifacts except coherence transfer can be removed with standard phase cycling of RF pulses and receiver. The coherence transfer can be removed by appropriate pulse sequences, preferably with T-ROESY.

The mixing time,  $\tau_m$ , is the only parameter that needs to be optimized. It ranges from a few milliseconds (in paramagnetic systems) to a few seconds

(in small molecules). As a rule of thumb, the mixing time should be of the order of the relaxation time  $T_1$ . Practically, it can be determined from the first increment in the 2D experiment ( $t_1 = 0$ ). The longest meaningful mixing time is the one in which the first increment gives observable peaks at resonances of interest. This signal is equivalent to the sum of cross and diagonal peaks along the selected frequency. If it is negligibly small, either both diagonal and cross peaks are equal to zero or cross peaks are equal to the diagonal (but with the opposite sign). Neither of these is favorable; thus, a shorter mixing time should be selected. Once the range of  $\tau_m$  is found, selection of the mixing time depends on the type of analysis of the exchange spectra. The initial buildup rate analysis requires short mixing times such that  $L_{ij}\tau_m \ll 1$  for all spin pairs. The full matrix analysis allows longer mixing times but such that  $a_{ij}(\tau_m) < a_{ii}(\tau_m), a_{jj}(\tau_m)$ . When any cross peak becomes commensurate to its diagonal within the noise level, the full matrix analysis fails [28, 50].

## 5. Quantitative interpretation of exchange spectra

Quantitative analysis of exchange spectra directly provides data about the chemical exchange and the cross-relaxation rates. Whereas the chemical exchange rate constants are used directly, the cross-relaxation rates are usually processed further for determination of interproton distances and correlation times.

### 5.1. Determination of interproton distances

Interproton distances can be calculated directly from eq. (1):

$$r = \left( \frac{f^n(\tau_c)}{\sigma^n} \right)^{1/6} \quad (33a)$$

or

$$r = \left( \frac{f^r(\tau_c)}{\sigma^r} \right)^{1/6} . \quad (33b)$$

Equations (33a) and (33b) are of limited value because, most often,  $f(\tau_c)$  is not known. Therefore, to determine interproton distance one has to eliminate the correlation time dependence. One possibility is to calibrate cross-relaxation rate by comparing the cross-relaxation rate of a spin pair with known distance  $\sigma_{\text{std}}, r_{\text{std}}$ :

$$r = r_{\text{std}} \left( \frac{\sigma_{\text{std}}}{\sigma} \right)^{1/6} . \quad (34)$$

Measurement of the cross-relaxation rate in either the laboratory or the rotating frame suffices. This assumes that the respective correlation time function,  $f(\tau_c)$ , is the same for all spin pairs. If the calibration of the cross-relaxation rate is not feasible (e.g., no suitable spin pair, spectral overlap, motion not isotropic, molecule has internal mobility), the value of  $f(\tau_c)$  for each spin pair (or for a group of selected pairs), i.e., the correlation time, must be explicitly determined.

### 5.2. Determination of correlation time

Cross-relaxation rates in the two frames,  $\sigma^n$  and  $\sigma^r$ , can provide estimates of  $r$  and  $f(\tau_c)$  for the observed spin pair [9–11]. Because the ratio of cross-relaxation rates from the two frames,  $S(\tau_c)$  (eq. (3)), does not depend on the distance, it can be used for determination of the correlation time. For the rigid body isotropic motion, the ratio is:

$$S(\tau_c) = \frac{(5 - 4\omega_0^2\tau_c^2)(1 + \omega_0^2\tau_c^2)}{(1 + 4\omega_0^2\tau_c^2)(5 + 2\omega_0^2\tau_c^2)} \quad (35)$$

and is depicted in the top panel of fig. 1. In two limiting cases, i.e., spin diffusion  $\omega_0\tau_c \gg 1$  and extreme narrowing  $\omega_0\tau_c \ll 1$ , the ratio takes the values  $-1/2$  and  $+1$ , respectively. As the ratio is a continuous, monotonically decreasing function of the correlation time, it has a unique inverse.

Thus, from the measured cross-relaxation rates,  $\sigma^n$  and  $\sigma^r$ , the ratio  $S(\tau_c)$  is calculated and from it (eq. (35)) the corresponding correlation time,  $\tau_c$  [9, 10]. However, reliable values of correlation times can be obtained only within the limited range of  $\omega_0\tau_c$  [11].

## 6. Two-dimensional cross-relaxation spectroscopy of small rigid molecule: Cyclo(Pro-Gly)

Cyclo(Pro-Gly) (fig. 3) is a convenient model for demonstration of various aspects of 2D exchange spectroscopy. It is small rigid molecule with 10 protons, of which 8 are spectroscopically well resolved. It is well dissolved in dimethyl sulfoxide (DMSO)/water mixtures and stable at a broad range of temperatures. We used a 10 mM solution of cyclo(Pro-Gly) in 70/30 volume/volume mixture of DMSO/water. This solvent mixture is suitable for the cross-relaxation studies because it is rather viscous even at room temperature and does not freeze down to 223 K [29, 30]. Thus, molecules dissolved in this mixture can be studied at a broad range of temperatures (correlation times).

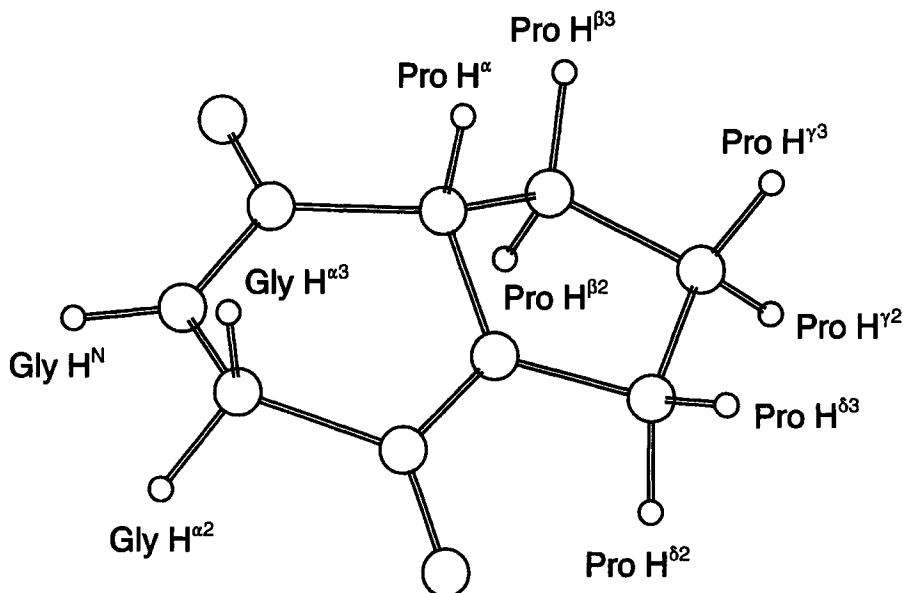


Fig. 3. Energy-minimized molecular structure (CHARMm ver. 23) of cyclo(prolyl-glycine), cyclo(Pro-Gly).

### 6.1. Spectroscopic artifacts and their elimination

Figure 4 shows four 2D spectra of cyclo(Pro-Gly) in which cross-relaxation plays an important role. Spectra were recorded at  $T = 263$  K, the temperature at which laboratory frame NOE is vanishingly small. In TOCSY (HO-HAHA) spectrum (fig. 4(A)), cross peaks appear among the spin groups that are directly coupled, and at longer mixing times, also among the spin groups that have at least one common coupling partner. For example, Gly  $H^N$  (8.2 ppm) is directly coupled with Gly  $H^{\alpha 2}$  (3.6 ppm) and Gly  $H^{\alpha 3}$  (4.0 ppm) and TOCSY cross peaks appear at the crossings of these frequencies. On the other hand, Pro  $H^{\alpha}$  (4.1 ppm) is not coupled with Pro  $H^{\delta 2, \delta 3}$  (3.3 ppm), but at 55-ms mixing time cross peaks appear between them due to the couplings in the proline side chain  $H^{\alpha}-H^{\beta}-H^{\gamma}-H^{\delta}$ . Cross peaks also can appear among unsuspected coupling partners. For example, cross peaks between Pro  $H^{\alpha}$  and Gly  $H^{\alpha 3}$  are genuine peaks resulting from the five-bond coupling across the peptide bond  ${}^5J_{\alpha\alpha'} = 3.0$  Hz [57]. Because the coupling partners usually are close in space, the cross-relaxation cross peaks appear at the same positions as the TOCSY peaks, interfering with each other in the exchange spectra. The simplest way to observe such interference in NOESY spectra is to record a spectrum with zero mixing time or, as shown in fig. 4(B), to record a spectrum at temperature at which the laboratory cross-relaxation rate is vanishingly small. Then, all the cross peaks stem

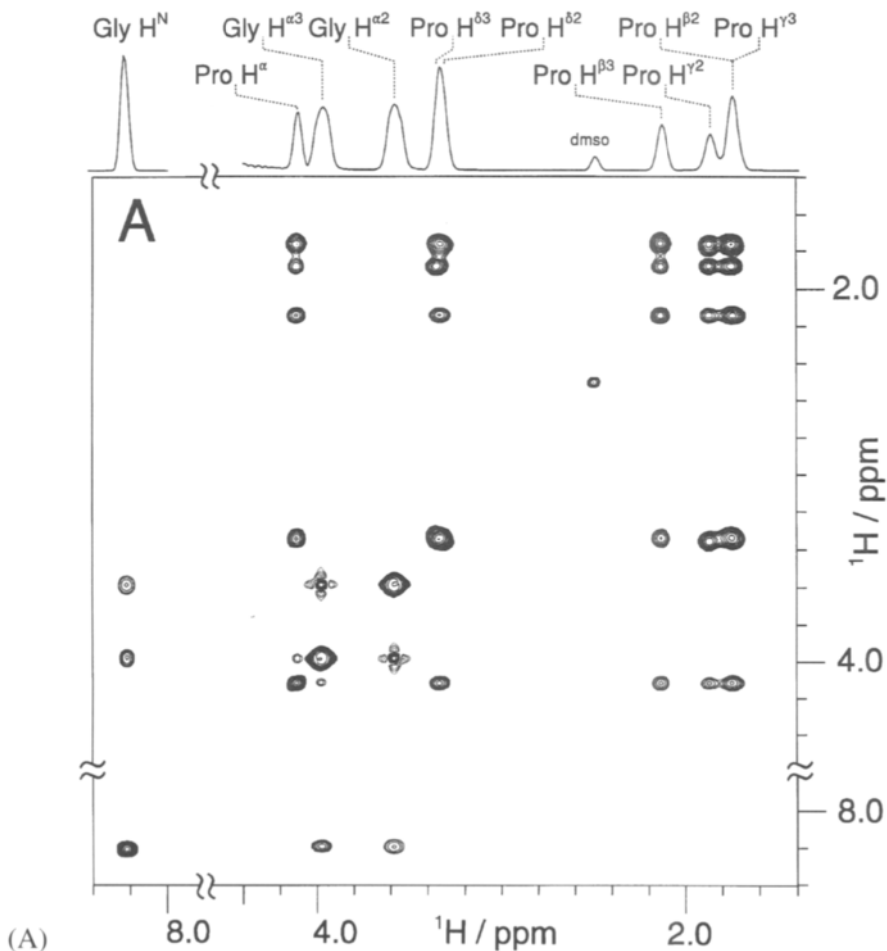


Fig. 4. Two-dimensional (2D) spectra of cyclo(Pro-Gly), 10 mM in 70/30 volume/volume DMSO/H<sub>2</sub>O mixture at  $\omega_0/2\pi = 500$  MHz and  $T = 263$  K. (A) TOCSY,  $\tau_m = 55$  ms. (B) NOESY,  $\tau_m = 300$  ms. (C) ROESY,  $\tau_m = 300$  ms,  $B_1 = 5$  kHz. (D) T-ROESY,  $\tau_m = 300$  ms,  $B_1 = 10$  kHz. Contours are plotted in the exponential mode with the increment of 1.41. Thus, a peak doubles its intensity every two contours. All spectra are recorded with 1024 data points, 8 scans per  $t_1$  increment, 512  $t_1$  increments; repetition time was 1.3 s and  $t_{90} = 8$   $\mu$ s;  $512 \times 512$  time domain data set was zero filled up to  $1024 \times 1024$  data points, filtered by Lorentz to Gauss transformation in  $\omega_2$  domain ( $GB = 0.03$   $LB = -3$ ) and  $80^\circ$  skewed  $\sin^2$  in  $\omega_1$ , yielding a 2D Fourier transformation  $1024 \times 1024$  data points real spectrum. (Continued on subsequent pages)

from the scalar coupling. With standard phase rotation schemes [18, 58] zero-quantum coherence is the only source of the magnetization transfer. In the NOESY spectrum recorded with  $\tau_m = 300$  ms in fig. 4(B), cross peaks appear only between the geminal pairs Gly H $^{\alpha 2}$ /Gly H $^{\alpha 3}$ , Pro H $^{\beta 2}$

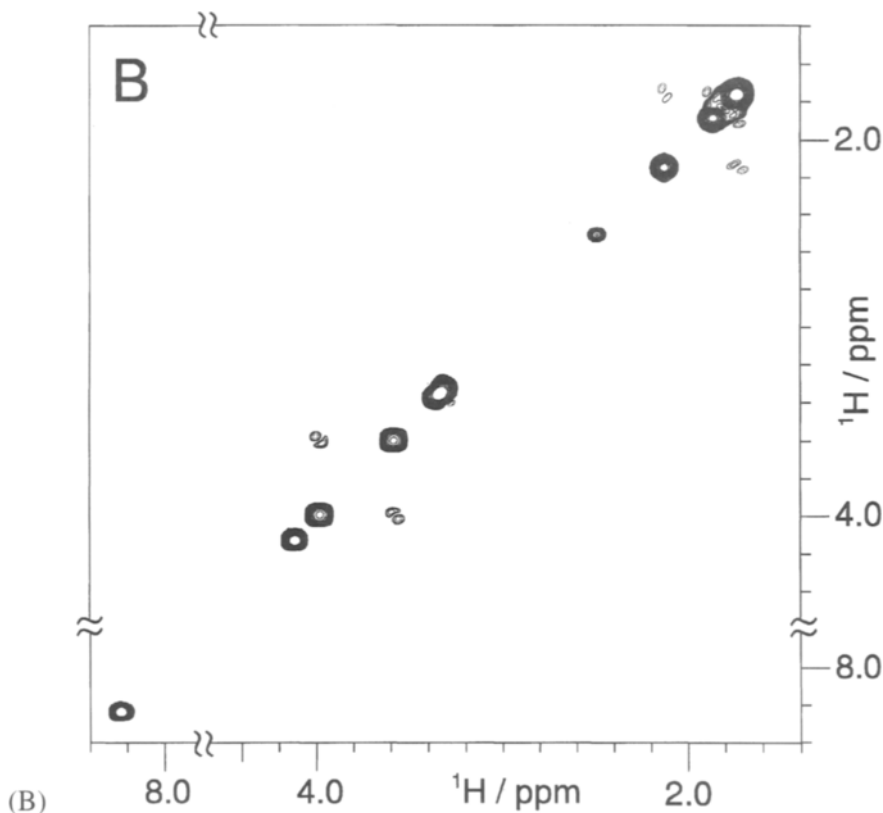


Fig. 4. (Continued)

(1.7 ppm)/Pro H $^{\beta 3}$  (2.2 ppm), and Pro H $^{\gamma 2}$  (2.9 ppm)/Pro H $^{\gamma 3}$  (1.7 ppm) because they have the largest coupling constants. The zero quantum coherence transfer function may be complex and it is hard to predict when and which cross peak will occur. These so called “*J* peaks” are easy to identify in the phase-sensitive spectra because of their differential character. *J* cross peaks are out of phase with regard to genuine cross-relaxation peaks and have zero integral intensity. Thus, even if not removed from the exchange spectrum they do not distort integral intensity of genuine exchange peaks. They can be removed easily by modulation of the mixing time [18, 20] or by insertion of a randomly positioned 180° pulse in the mixing period [19].

More serious are the coherence transfer cross peaks in ROESY spectra because the coherence peaks are in phase with the genuine cross-relaxation peaks and thus may modulate intensity of the genuine peaks. To emphasize the effect of coherence transfer peaks (now TOCSY peaks) we do the ROESY experiment with  $\tau_m = 300$  ms and with a spin-lock field of 5 kHz (fig. 4(C)). Besides positive diagonal peaks (thick contours), several pairs

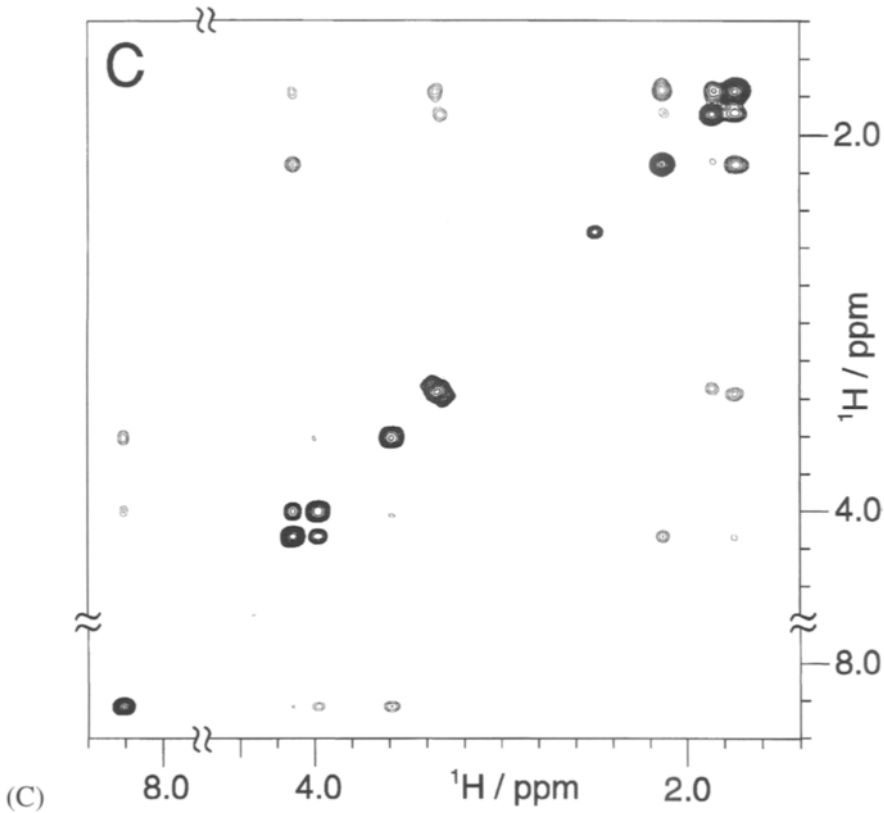


Fig. 4. (Continued)

of negative (thin contours) ROESY peaks appear. The basic problem for interpretation of such a spectrum is that relative cross-peak intensities do not reflect spin proximity. Besides, some genuine cross-relaxation peaks can be exactly compensated with the TOCSY cross peaks. For example, cross peaks between the geminal pair Gly H<sup>α2</sup>/Gly H<sup>α3</sup> are barely visible although the two protons are at the shortest possible distance, 1.77 Å. Thus, for a quantitative interpretation of the ROESY spectra it is necessary to eliminate TOCSY peaks completely or to reduce analysis to the noncoupled spin pairs.

The easiest way to reduce the amplitude of TOCSY cross peaks in the ROESY spectra is to record a spectrum with minimal spin-lock power [23]. The other possibility is to modulate the frequency of the spin-lock field [25]. However, the most convenient way is to apply a series of 180° pulses instead of a single continuous-wave pulse during the mixing time, as is done in the T-ROESY experiment. Figure 4(D) shows the T-ROESY spectrum of cyclo(Pro-Gly) recorded with  $\tau_m = 300$  ms. Although the

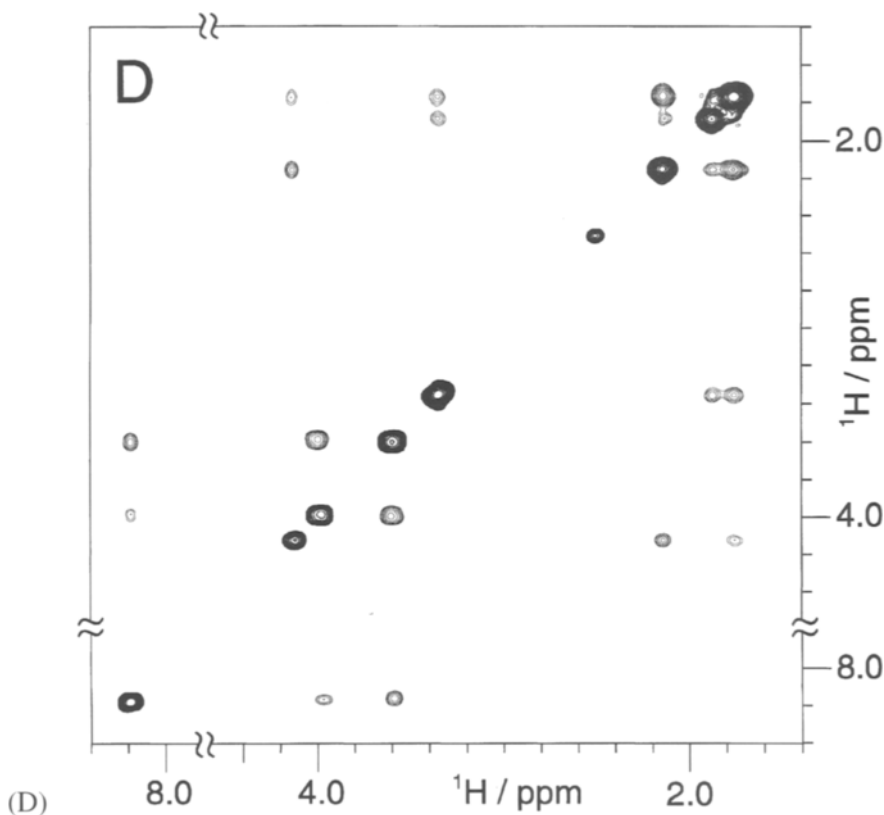


Fig. 4. (Continued)

efficacy of the effective magnetization transfer is one half of the efficacy of the ROESY experiment, eq. (7), the T-ROESY spectrum exhibits more of the ROESY-type cross peaks. As expected, the strongest cross peaks are between geminal pairs Gly  $H^{\alpha 2}$ /Gly  $H^{\alpha 3}$  and Pro  $H^{\beta 2}$ /Pro  $H^{\beta 3}$ .

The efficacy of T-ROESY in eliminating the TOCSY cross peaks can be judged best from comparison of the cross peaks between Pro  $H^{\alpha}$  and Gly  $H^{\alpha 3}$  in the ROESY and T-ROESY spectra. These two spins are more than 3 Å apart (table 1) and cross-relaxation cross peaks can hardly be observed at the mixing times used. However, because they are coupled they can produce TOCSY cross peaks (fig. 4(A)). These, coherence transfer cross peaks are even more pronounced in the ROESY spectrum (fig. 4(C)), most notably as a result of the excessively long mixing time,  $\tau_m = 300$  ms. In the T-ROESY experiment, with the same mixing time, these coherence transfer peaks are virtually absent. However, some coherence transfer peaks may survive even in T-ROESY, notably among these the spins with a small chemical shift difference. For example, the positive (thick contours) cross

TABLE 1  
Interproton distances and cross-relaxation rates from the energy minimized molecular model of cyclo(Pro-Gly).

	Pro H <sup>β3</sup>	Pro H <sup>β2</sup>	Pro H <sup>γ3</sup>	Pro H <sup>γ2</sup>	Pro H <sup>δ2</sup>	Pro H <sup>δ3</sup>	Gly H <sup>N</sup>	Gly H <sup>α3</sup>	Gly H <sup>α2</sup>	
Pro H <sup>α</sup>	3.993 <sup>a</sup>	2.410 <sup>b</sup>	3.036	2.872	3.884	3.395	3.883	3.871	3.118	4.258
Pro H <sup>β3</sup>	-1.152	12.377	1.761	2.411	2.733	4.126	4.046	4.997	5.263	5.937
Pro H <sup>β2</sup>	-0.288	-7.579	11.498	3.028	2.405	3.919	3.101	4.310	5.045	5.175
Pro H <sup>γ3</sup>	-0.403	-1.149	-0.293	12.951	1.760	2.347	3.006	6.168	5.470	6.203
Pro H <sup>γ2</sup>	-0.066	-0.541	-1.165	-7.584	12.885	2.817	2.388	6.254	6.125	6.386
Pro H <sup>δ2</sup>	-0.147	-0.046	-0.062	-1.350	-0.451	11.220	1.770	5.826	4.571	4.999
Pro H <sup>δ3</sup>	-0.066	-0.051	-0.254	-0.306	-1.219	-7.331	11.057	5.289	4.818	4.675
Gly H <sup>N</sup>	-0.067	-0.014	-0.035	-0.004	-0.004	-0.006	-0.010	3.585	2.708	2.342
Gly H <sup>α3</sup>	-0.246	-0.011	-0.014	-0.008	-0.004	-0.025	-0.018	-0.573	9.853	1.775
Gly H <sup>α2</sup>	-0.038	-0.005	-0.012	-0.004	-0.003	-0.014	-0.022	-1.366	-7.219	10.441
Pro H <sup>α</sup>	Pro H <sup>β3</sup>	Pro H <sup>β2</sup>	Pro H <sup>γ3</sup>	Pro H <sup>γ2</sup>	Pro H <sup>δ2</sup>	Pro H <sup>δ3</sup>	Gly H <sup>N</sup>	Gly H <sup>α3</sup>	Gly H <sup>α2</sup>	

<sup>a</sup> Cross-relaxation rates, in s<sup>-1</sup>, are calculated from interproton distances with  $\omega_0/2\pi = 500$  MHz,  $\tau_c = 4$  ns,  $R_{ex} = 1.426$  s<sup>-1</sup> (external relaxation rate) by use of eq. (1a).

<sup>b</sup> Interproton distances in Å.

peaks between Pro H<sup>2</sup> and Pro H<sup>3</sup> are TOCSY peaks that are not removed owing to their small chemical shift difference and the large coupling constants.

The general conclusion (from the presented examples) is that all three cross-relaxation experiments, NOESY, ROESY, and T-ROESY, have advantages and limitations. NOESY is the simplest and less prone to coherence transfer interference than ROESY. Its main disadvantage is that there is an intermediate motional regime in which laboratory-frame cross-relaxation is vanishingly small. The ROESY experiment is efficient in every motional regime but is sensitive to the coherent magnetization transfer. The T-ROESY experiment as a combination of NOESY and ROESY is mainly free from the coherence transfer artefacts but is less efficient than either of them. Its main limitation, however, is of a technical nature. Namely, to invert efficiently all magnetization vectors in a given chemical shift range one needs to apply strong 180° pulses during the whole mixing period. This requirement may be harmful to the NMR probe or the sample.

Therefore, for a complete characterization of the cross-relaxation network, it is best to do all three experiments and to extract from each of them information that can be interpreted unambiguously. If the number of possible experiments is limited, then in the extreme-narrowing and the spin-diffusion regime it is best to record NOESY and in the intermediate motional regime ROESY or T-ROESY spectra.

### 6.2. High temperature versus low temperature cross-relaxation spectroscopy

When sample stability permits free choice of temperature, an appropriate question is what working temperature to choose. At high temperatures (extreme-narrowing limit), the cross-relaxation is much slower and thus much longer mixing times are necessary to obtain cross-relaxation spectra with decent cross peaks. At low temperatures (in the spin-diffusion limit), cross-relaxation is much faster and high-quality cross-relaxation spectra can be obtained with much shorter mixing times. The basic disadvantage of this low temperature limit is that, because of the spin diffusion, some indirect “false” cross peak can appear as well. Figure 5 shows NOESY spectra of cyclo(Pro-Gly) at two different temperatures, recorded with the optimal mixing times. At high temperature,  $T = 298$  K, mixing time on the order of seconds is necessary to get a sizeable cross peak. At low temperatures,  $T = 233$  K, mixing times on the order of a few hundred milliseconds are sufficient. In addition, at low temperature much higher repetition rates can be used (1 s at 233 K vs. 3 s at 298 K, fig. 5), which leads toward a significant increase in data collection efficacy. Although much richer in the number of cross peaks and their size, the low-temperature NOESY spectra are more difficult to interpret. For example, the cross peaks between H<sup>β3</sup>

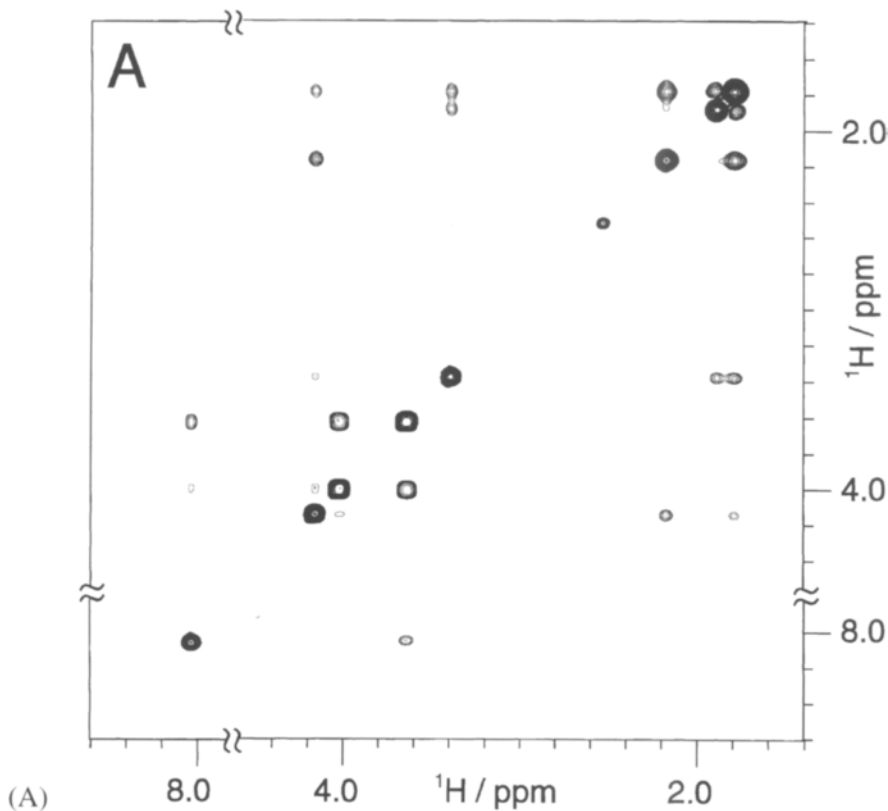


Fig. 5. NOESY spectrum of cyclo(Pro-Gly) at  $\omega_0/2\pi = 500$  MHz in the two motional regimes. (A) Extreme narrowing,  $T = 298$  K,  $\tau_m = 1.0$  s, repetition delay 3 s. (B) Spin diffusion,  $T = 233$  K,  $\tau_m = 300$  ms, repetition delay 1 s. Data sizes and processing are the same as in fig. 4. (Continued on the next page)

(2.2 ppm) and Pro  $H^{\gamma 2}$  (1.9 ppm) are small at  $T = 298$  K and of moderate size at  $T = 233$  K. From the known interproton distance,  $r_{\beta 3, \gamma 2} = 2.73$  Å (table 1), these peaks should be an order of magnitude smaller than the peaks between the geminal protons ( $r = 1.77$  Å);  $(1.77/2.73)^6 \approx 0.1$ . Comparing  $H^{\beta 3}/H^{\gamma 2}$  cross peaks with geminal Gly  $H^{\alpha 2}/H^{\alpha 3}$  peaks at two temperatures, one can see that the high-temperature spectrum is closer to the expectation than the low-temperature one. Apparently, at the low temperature and the long mixing time used, the contribution of spin diffusion becomes significant (see below).

To get better insight into the importance of temperature selection, we have recorded a series of NOESY spectra of cyclo(Pro-Gly) at different temperatures. The dashed lines in fig. 6 show theoretical dependence of the laboratory frame cross-relaxation rate on the correlation time (according to

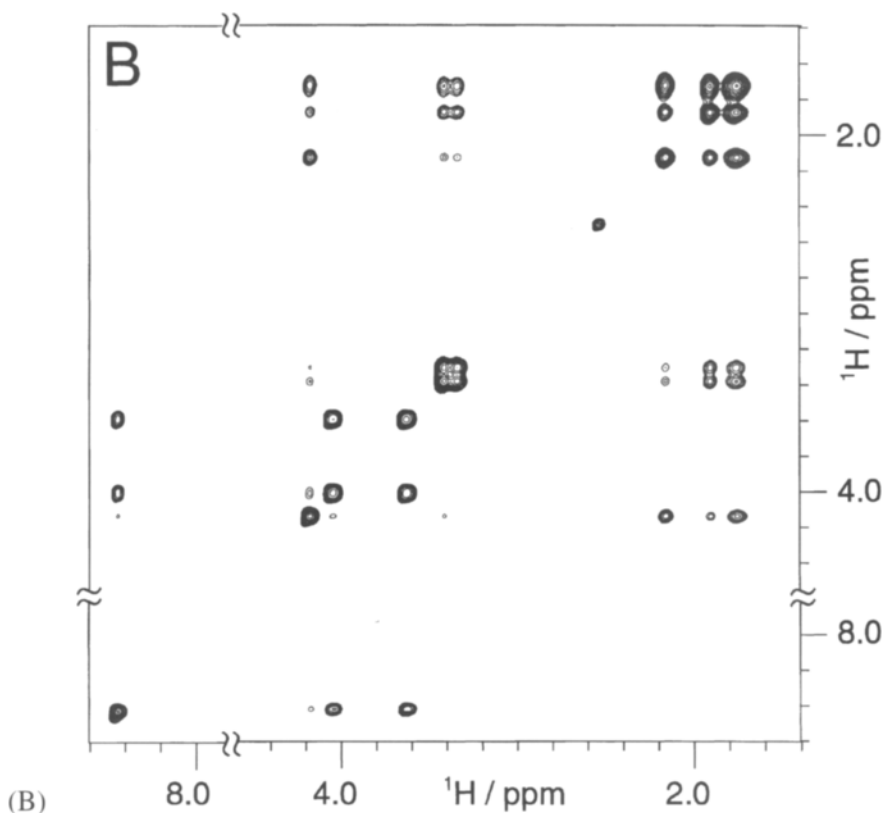
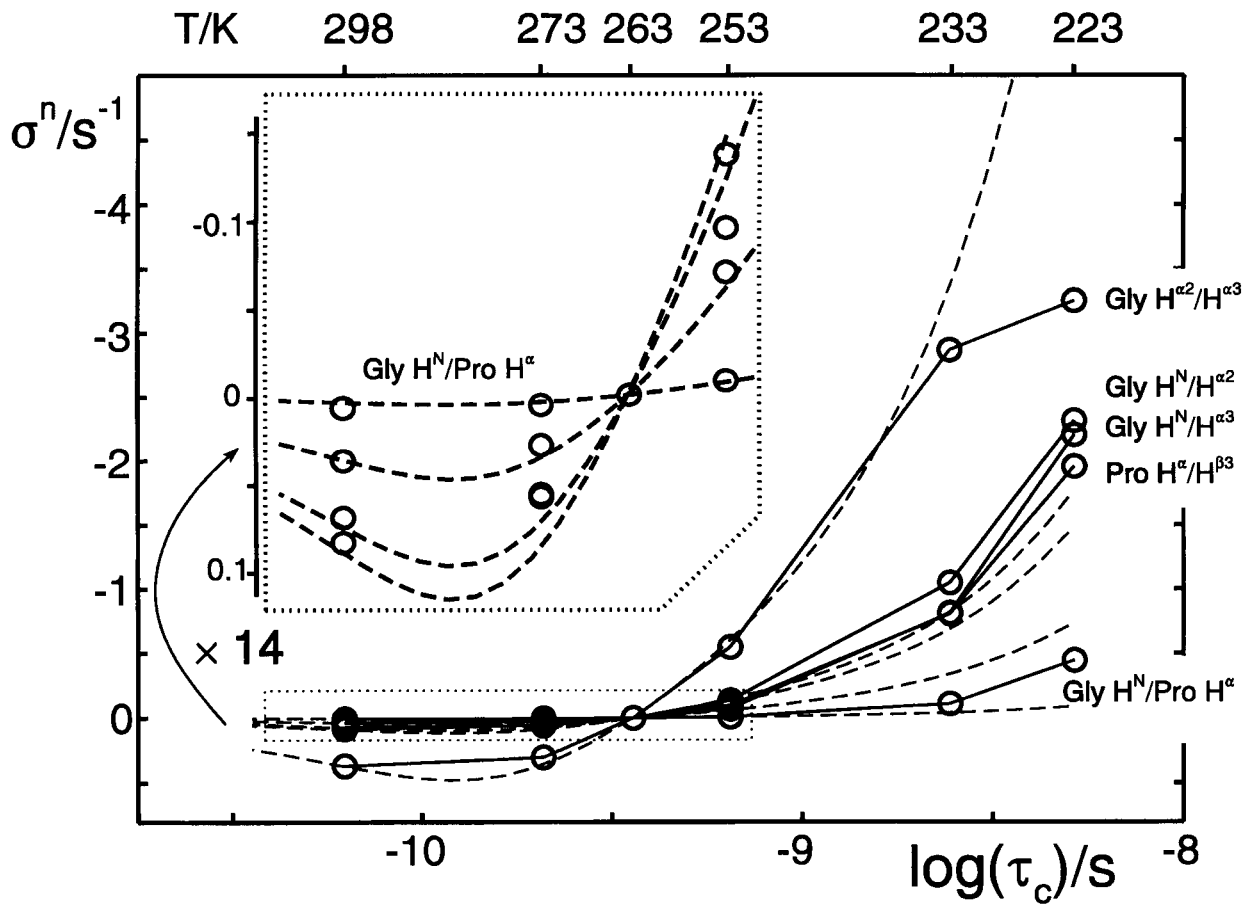


Fig. 5. (Continued)

eqs (1a) and (2a) for five representative spin pairs in cyclo(Pro-Gly). The circles represent  $\sigma^n$  cross-relaxation rates calculated from the NOESY spectra recorded at indicated temperatures with  $\tau_m = 300$  ms. Equation (32), with the linear term only, is used to calculate  $\sigma^n$  from the peak volumes. Experimental points are plotted as a function of  $1/T$ , according to eq. (5). The agreement between the experimental and theoretical  $\sigma^n$  values is remarkable at high temperatures, as the insert in fig. 6 shows. This indicates that in the extreme narrowing motional regime where all the complications of spin-diffusion are absent, a reliable estimate of the cross-relaxation rates can be obtained even from a linear approximation of buildup curve (eqs (30) and (32)). As the temperature decreases, agreement between the theoretical curves and  $\sigma^n$  from the linear buildup approximation using only one point at  $\tau_m = 300$  ms becomes less favorable, and at  $T = 223$  K none of the calculated  $\sigma^n$  values agrees with the theoretical prediction. This essentially results from the increased contribution of the spin diffusion at low temperature that makes linear approximation of buildup curves unsatisfactory.



Besides the advantage of the high-temperature measurements for quantitative interpretation of NOESY spectra, fig. 6 also indicates a special role of the high temperature maximum (note that positive cross-relaxation rates increase downward) of  $\sigma^n$ . If the NOESY spectrum can be recorded at several temperatures around the  $\sigma^n$  maximum, than calculated cross-relaxation rates can be used to obtain simultaneously the correlation time and the interproton distances without the necessity of any other knowledge. A typical problem in the cross-relaxation experiments is that cross-relaxation rate depends on two parameters,  $\tau_c$  and  $r$  (eq. (1a)), and to calculate one of them the other must be independently known. However, the position of the maximum uniquely determines correlation time, and its height uniquely determines interproton distances.

In conclusion, if temperature can be chosen freely, the best one is around the high-temperature maximum of  $\sigma^n$ . Then, the NOESY spectrum has the highest possible sensitivity but is still free of spin diffusion. Low-temperature spectroscopy can increase sensitivity immensely, but quantitative data analysis requires either the full matrix or the buildup curve analysis.

### 6.3. Coping with spin diffusion

In the spin diffusion motional regime (small molecules at low temperatures or macromolecules at all temperatures) the cross-relaxation is so efficient that it can hardly be limited to a single-step magnetization transfer. The multistep magnetization transfer is known as spin diffusion. It manifests differently in NOESY and ROESY spectra, as can be illustrated by writing eq. (29b) explicitly for the process of cross relaxation:

$$\frac{a_{ij}(\tau_m)}{n_j a_{ii}(0)} = -\sigma_{ij}^{n,r} \tau_m = \frac{1}{2} \sum_k n_k \sigma_{ik}^{n,r} \sigma_{kj}^{n,r} \tau_m^2 + \dots \quad (36)$$

←

Fig. 6. Normalized cross-peak volumes of five representative spin pairs from NOESY spectra of cyclo(Pro-Gly) at different temperatures, recorded with  $\tau_m = 300$  ms. Circles, cross-relaxation rates calculated from eq. (27a) using only the linear term. Dashed lines were drawn according to eqs (1a) and (2a) using  $\omega_0/2\pi = 500$  MHz (actual resonance frequency) and interproton distances,  $r$ , from the model (table 1). Solid lines connect the points of one spin pair at different temperatures. Experimental temperatures indicated at the top are superimposed on the correlation time axis according to eq. (5):  $\log \tau_c \sim 1/T$ . Reciprocal temperature axis is scaled and shifted to produce the best visual overlap of the theoretical curves and experimental data points. Inset represents the indicated region around the cross-relaxation rate maximum in the extreme-narrowing regime, magnified 14 times.

The linear term represents a direct magnetization transfer. The higher-order terms represent multistep magnetization transfer. Terms of even order are negative and terms of odd order are positive; in the spin-diffusion regime,  $\sigma^n$  is negative and  $\sigma^r$  is positive. Thus, in NOESY experiments superposition of different terms is additive and in ROESY experiments, subtractive. In NOESY the spin diffusion enhances existing peaks and creates a new cross peaks even between the distant peaks, whereas in ROESY experiment the spin diffusion diminishes the direct (negative) cross-peaks and gives rise to the “false”-positive cross peaks among distant spins.

For quantitative interpretation of cross-relaxation spectra in the spin-diffusion regimes it is necessary to take spin diffusion into account. From the mathematical point of view, this means that the Taylor series in eq. (36) must be used without truncation. In other words, the basic formula, eq. (8), must be used and the full spectral matrix must be analyzed.

Table 2 shows the full NOESY spectral matrix of cyclo(Pro-Gly),  $A(\tau_m = 80 \text{ ms}) A(0)^{-1}$ , recorded at  $T = 233 \text{ K}$ . All cross peaks are integrated from the 2D experiment using Felix (Biosym), and overlapping peaks of Pro  $H^{\beta 2}$  and Pro  $H^{\gamma 3}$  were separated after integration into two components in the proportion obtained from the 3D [ $^1\text{H}$ - $^{13}\text{C}$ ] HMQC-NOESY experiment recorded in similar conditions. Cross peaks between Pro  $H^{\beta 2}$  and Pro  $H^{\gamma 3}$  that also overlap in the 3D experiment were reconstructed from the known distance (table 1). Volume integration error,  $\Delta a = 0.015$  (eq. (27)), is estimated from deviation from zero of the cross-peak integrals at  $\tau_m = 0$ .

Even a superficial analysis of the data in table 2 points out some interesting problems of the full matrix analysis. First, there is a question whether 80 ms is the optimal mixing time. Many cross-peak volumes are vanishingly small or are of the size comparable to the integration error. This suggests that longer mixing time might be better. However, relative intensities between cross and diagonal peaks from geminal protons are already close to one half. This suggests that mixing time should not be prolonged because cross peaks become commensurate with the respective diagonal for any pair in the multispin system, errors in all calculated cross-relaxation rates become immense, and the whole procedure fails [28, 50]. Thus, even with mixing time not far from optimum (strictly speaking, there is no single optimal mixing time [50]), the full matrix analysis may be successful only if the integration error is small enough so that volumes of small cross-peaks can be measured. A large integration error is, perhaps, the principal reason for the volume matrix asymmetry. The matrix must be symmetric to get real valued eigenvalues and cross-relaxation rates. Cross-relaxation rates and their error limits (table 3), are obtained directly from eqs (11) and (27) using Matlab (Mathworks Inc.). Interproton distances, also shown in table 3, are calculated from eq. (32) by using Gly  $H^{\alpha 2}/H^{\alpha 3}$  distance as a standard.

TABLE 2  
Normalized peak volumes,  $a_{ij}(\tau_m)/a_{jj}(0)$  from NOESY spectrum of cyclo(Pro-Gly) at  $\tau_m = 80$  ms and  $T = 233$  K.

	Pro H $^\alpha$	Pro H $^{\beta 3}$ (a)	Pro H $^{\beta 2}$	Pro H $^{\gamma 3}$ (a)	Pro H $^{\gamma 2}$	Pro H $^{\delta 2}$	Pro H $^{\delta 3}$	Gly H $^N$	Gly H $^{\alpha 3}$	Gly H $^{\alpha 2}$
Pro H $^\alpha$	0.814 <sup>b</sup>	0.065	0.035	0.027	0.009	0.000	0.009	0.003	0.002	-0.005
Pro H $^{\beta 3}$	0.050	0.410	0.186	0.036	0.045	0.005	0.007	-0.003	-0.001	-0.001
Pro H $^{\beta 2}$	0.027	0.200	0.462	0.034	0.048	0.007	0.013	-0.002	-0.001	-0.001
Pro H $^{\gamma 3}$	0.021	0.039	0.034	0.418	0.222	0.048	0.036	0.000	0.000	0.000
Pro H $^{\gamma 2}$	0.005	0.029	0.038	0.177	0.576	0.033	0.049	0.002	0.000	-0.001
Pro H $^{\delta 2}$	0.016	0.010	0.008	0.052	0.038	0.469	0.263	0.001	0.000	-0.003
Pro H $^{\delta 3}$	0.012	0.008	0.013	0.036	0.050	0.244	0.538	0.000	0.000	0.000
Gly H $^N$	0.006	0.001	0.003	0.001	0.002	0.001	0.002	0.752	0.053	0.080
Gly H $^{\alpha 3}$	0.020	0.001	0.001	0.001	-0.002	0.000	0.000	0.049	0.524	0.255
Gly H $^{\alpha 2}$	0.010	0.001	-0.001	0.000	-0.001	0.000	0.000	0.079	0.257	0.483

(a) Integrated volumes of overlapping resonances Pro H $^{\beta 3}$ /Pro H $^{\gamma 2}$  are separated in the proportion obtained from three dimensional HMQC-NOESY spectrum (not shown) recorded in the same conditions.

(b) Volume integration error,  $\Delta a = \sqrt{\langle \Delta V_{ij}^2(0) \rangle / \langle V_{jj}(0) \rangle}$ , is determined from the integrals at the position of cross peaks of the spectrum recorded at  $\tau_m = 0$ . The same position and size of the integration window are used as for  $\tau_m = 80$  ms;  $\Delta a$  is estimated from the statistical distribution around zero of cross-peak integrals obtained at  $\tau_m = 0$ ;  $\Delta a = 0.015$ .

TABLE 3

Cross-relaxation rates and interproton distances in cyclo(Pro-Gly) from the full matrix analysis of NOESY spectrum recorded at  $\tau_m = 80$  ms and  $T = 233$  K. Cross-relaxation rates are obtained from the volumes shown in table 2 according to eq. (11) by Matlab (Mathworks Inc). Error limits were obtained from eq. (27) with  $\Delta a = 0.015$  (table 2).

	Pro H $^\alpha$	Pro H $^{\beta 3}$	Pro H $^{\beta 2}$	Pro H $^{\gamma 3}$	Pro H $^{\gamma 2}$
Pro H $^\alpha$	2.64 <sup>a</sup> $\pm$ 0.26 <sup>b</sup>	2.42 <sup>c</sup> $\pm$ 0.13 <sup>d</sup>	2.90 $\pm$ 0.64	2.83 $\pm$ 0.46	6.70 $\pm$ 3.77
Pro H $^{\beta 3}$	-1.15 $\pm$ 0.38	12.67 $\pm$ 0.59	1.85 $\pm$ 0.02	2.55 $\pm$ 0.21	2.70 $\pm$ 0.51
Pro H $^{\beta 2}$	-0.39 $\pm$ 0.36	-5.89 $\pm$ 0.57	11.00 $\pm$ 0.55	2.72 $\pm$ 1.01	2.58 $\pm$ 0.20
Pro H $^{\gamma 3}$	-0.46 $\pm$ 0.38	-0.84 $\pm$ 0.60	-0.58 $\pm$ 0.58	12.28 $\pm$ 0.62	1.88 $\pm$ 0.02
Pro H $^{\gamma 2}$	0.00 $\pm$ 0.38	-0.60 $\pm$ 0.60	-0.80 $\pm$ 0.58	-5.30 $\pm$ 0.62	7.98 $\pm$ 0.62
Pro H $^{\delta 2}$	-0.10 $\pm$ 0.36	-0.11 $\pm$ 0.56	-0.04 $\pm$ 0.54	-1.20 $\pm$ 0.57	-0.39 $\pm$ 0.57
Pro H $^{\delta 3}$	-0.15 $\pm$ 0.36	-0.05 $\pm$ 0.56	-0.25 $\pm$ 0.54	-0.44 $\pm$ 0.57	-0.93 $\pm$ 0.57
Gly H $^N$	-0.07 $\pm$ 0.26	-0.01 $\pm$ 0.37	-0.01 $\pm$ 0.36	-0.01 $\pm$ 0.38	-0.04 $\pm$ 0.38
Gly H $^{\alpha 3}$	-0.22 $\pm$ 0.34	-0.01 $\pm$ 0.53	-0.01 $\pm$ 0.51	0.00 $\pm$ 0.54	0.00 $\pm$ 0.54
Gly H $^{\alpha 2}$	-0.01 $\pm$ 0.35	-0.01 $\pm$ 0.54	-0.01 $\pm$ 0.52	0.00 $\pm$ 0.55	0.00 $\pm$ 0.55
	Pro H $^\alpha$	Pro H $^{\beta 3}$	Pro H $^{\beta 2}$	Pro H $^{\gamma 3}$	Pro H $^{\gamma 2}$

<sup>a</sup> Cross-relaxation rates,  $\sigma^n$ , from the volume matrix, table 2, by eq. (11).

<sup>b</sup> Absolute errors,  $\Delta\sigma^n$ , from eq. (23).

<sup>c</sup> Distances,  $r$ , from cross-relaxation rates by eq. (33a), assuming  $\tau_c = 4.0 \times 10^{-9}$  s, and  $\omega_0/2\pi = 500$  MHz.

<sup>d</sup> Absolute errors,  $\Delta r$ , from  $|\Delta\sigma^n/\sigma^n| = |\Delta r/r|/6$ .

Comparing experimental cross-relaxation rates from table 3 with cross-relaxation rates from the model (table 1), one can see that discrepancy beyond the estimated error limits exists only for proton  $\gamma$  and  $\delta$  geminal pairs. Because the differences are not far from  $3\Delta\sigma^n$ , it is hard to interpret them in more detail. A relatively large discrepancy between the diagonal elements can be explained by the fact that in the model calculations uniform external relaxation rate was assumed for all spins ( $R_{ex} = 1.426$  s $^{-1}$ ).

Observed agreement between the experimental and model cross-relaxation rates within the estimated error limits confirms validity of the full matrix analysis procedure but not necessarily its usefulness. Namely, the agreement is achieved mainly within the broad limits of cross-relaxation rate errors. Errors span the range 0.25 to 0.62 s $^{-1}$  but are clustered around the values 0.35 s $^{-1}$  and 0.55 s $^{-1}$ . All the errors involving cross-relaxation rates of Pro H $^\alpha$  and Gly H $^N$  are clustered around 0.35 s $^{-1}$ . This is mainly because

TABLE 3

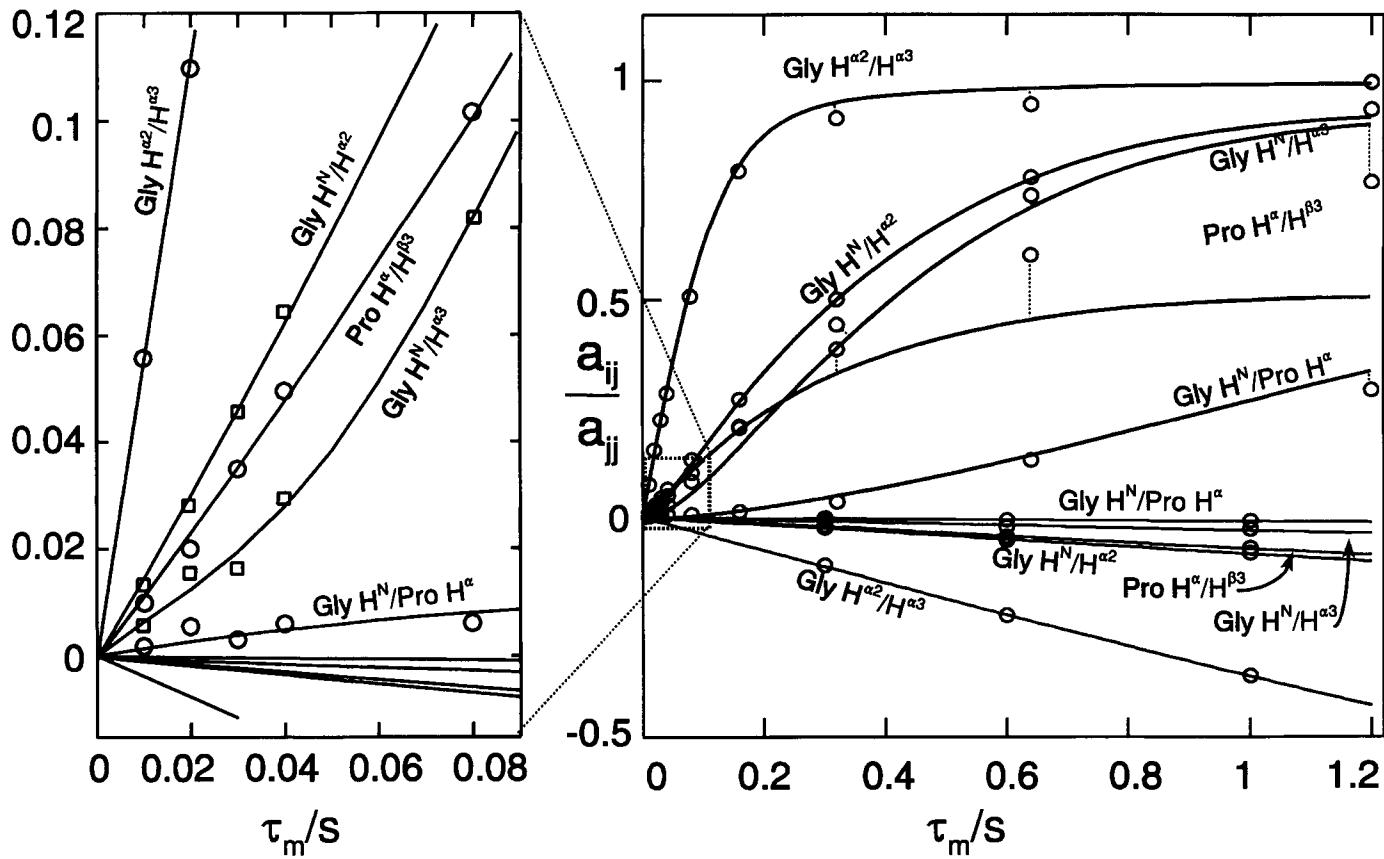
(Continued) Distances were obtained from cross-relaxation rates from eq. (33a) with  $\tau_c = 4.0$  ns and  $\omega_0/2\pi = 500$  MHz; correlation time was determined from eq. (1a) using Gly H $^{\alpha 2}$ /H $^{\alpha 3}$  spin pair:  $\sigma = -7.22$  s $^{-1}$  (from build up rate analysis of a series of spectra, table 4);  $r = 1.77$  Å (from model, table 1). Interproton error limits were obtained from the errors of respective cross-relaxation rates:  $|\Delta r/r| = |\Delta\sigma/\sigma|/6$ .

Pro H $^{\delta 2}$	Pro H $^{\delta 3}$	Gly H $^N$	Gly H $^{\alpha 3}$	Gly H $^{\alpha 2}$
3.66 ± 1.38	3.40 ± 3.52	3.86 ± 2.46	3.20 ± 0.72	5.06 ± 7
3.59 ± 8	4.09 ± 7	5.56 ± 21	5.32 ± 44	5.01 ± 104
4.23 ± 6	3.12 ± 1.10	5.32 ± 7	5.51 ± 32	5.76 ± 39
2.41 ± 0.17	2.85 ± 0.93	5.57 ± 94	6.21 ± 58	7.48 ± 145
2.90 ± 0.60	2.52 ± 0.19	4.33 ± 104	6.75 ± 129	6.98 ± 177
11.46 ± 0.53	1.80 ± 0.02	4.70 ± 60	7.16 ± 15	7.52 ± 30
-6.91 ± 0.53	9.55 ± 0.53	5.38 ± 30	7.08 ± 22	10 ± 18
-0.02 ± 0.35	-0.01 ± 0.35	3.67 ± 0.25	2.65 ± 0.27	2.32 ± 0.10
0.00 ± 0.50	0.00 ± 0.50	-0.68 ± 0.34	9.91 ± 0.47	1.80 ± 0.02
0.00 ± 0.52	0.00 ± 0.51	-1.51 ± 0.34	-6.98 ± 0.49	11.13 ± 0.50
Pro H $^{\delta 2}$	Pro H $^{\delta 3}$	Gly H $^N$	Gly H $^{\alpha 3}$	Gly H $^{\alpha 2}$

these two protons are relatively isolated and their cross-relaxation with one partner is not much perturbed by the interaction with the other. On the other hand, all cross-relaxation rates involving two geminal protons have the errors around 0.55 s $^{-1}$ . This is understandable because all these protons are involved in the fast magnetization exchange with the nearby partners. Even a small error in one peak volume propagates to the cross-relaxation rate of all members of the cross-relaxation network [50].

In going from the cross-relaxation rates to the interproton distances the relative error reduces and is six times smaller because of the sixth-power dependence. Error limits for the distances shorter than 3 Å are meaningful but for the larger distances are unacceptably high. The large error limits indicate the obvious fact that distances cannot be measured for those spin pairs for which cross-peaks of appreciable volume are not detected.

The present analysis clearly indicates that besides a complete peak volume matrix the full matrix analysis requires high accuracy of integrated peak volumes. Therefore, a good signal-to-noise ratio and good methods for peak volume integration are the main prerequisites for a successful full matrix analysis.



In practice, the full matrix analysis is rarely applicable because of spectral overlap and because of the global error propagation. In full matrix analysis all the elements are interconnected and the error in one volume element propagates into all cross-relaxation rates. This property is not favorable in practical situations in which a part of the spectrum may be ill-defined although a good portion of the spectrum is of a satisfactory quality. Then, the more favorable analysis is localized, i.e., errors are confined within respective cross-relaxation rates. However, such analysis is possible only on data in which spin diffusion is not dominant.

The relevance of the spin diffusion can be judged by comparison of the linear and quadratic terms in eq. (36). The linear term dominates when  $|\sigma_{ij}|\tau_m \ll 1$  or, more precisely, when

$$\sum_k n_k \sigma_{ik} \sigma_{kj} \tau_m^2 < 1. \quad (37)$$

Then, eq. (29a) that contains only a linear term can be used. The condition from eq. (37) can be met by reducing either  $\tau_m$  or  $\sigma_{ik}$ . An experimental example is presented in fig. 7, which contains buildup rates of five selected spin pairs of cyclo(Pro-Gly). At room temperature, molecular motion is in the extreme narrowing limit and cross-relaxation rates are rather small. Then, at mixing times as long as 1 s the cross-peak buildup is still linear in time. The cross-relaxation rates calculated according to eq. (32), with the linear term only, are shown in table 4,  $\sigma_{298}^{\text{bu}}$ . Even for the largest cross-relaxation rate, the product  $|\sigma|\tau_m$  is less than one in the mixing time range used. For comparison, table 4 shows the cross-relaxation rates calculated from the model,  $\sigma_{298}^{\text{geo}}$ . Correlation time was varied until the best agreement with a single correlation time ( $\tau_c = 4.65 \times 10^{-11}$  s) was found for all cross-relaxation rates. Experimental cross-relaxation rates yield the interproton distances  $r_{298}^{\text{bu}}$ , which are in perfect agreement with the distances from the model.

When the cross-relaxation rates are inherently large (low-temperature or macromolecular), then a series of experiments with short mixing times must be performed. Buildup of cross-peak intensities of selected spin pairs in cyclo(Pro-Gly) at low temperature,  $T = 233$  K, is shown also in fig. 7.

←

Fig. 7. Buildup rate analysis of NOESY spectra at  $T = 298$  K ( $\tau_m = 0.3$  s, 0.6 s, 1 s) and  $T = 233$  K ( $\tau_m = 10$  ms, 20 ms, 30 ms, 40 ms, 80 ms, 160 ms, 320 ms, 640 ms, 1.2 s). Lines are drawn according to eq. (8) with a dynamic matrix from the energy minimized model (table 1). High-temperature data (negative slopes) are linearly fitted according to eq. (30). Low-temperature data (positive slopes) are fitted by eq. (30); only points with  $a_{ij}/a_{jj} < 0.2$  were used (inset).

TABLE 4  
Buildup analysis of selected spin pairs in cyclo(Pro-Gly) from the data shown in fig. 7.

	$\sigma_{298}^{\text{bu}}$	$\sigma_{298}^{\text{geo}}$	$\sigma_{233}^{\text{bu}}$	$\sigma_{233}^{\text{FMA}}$	$\sigma_{233}^{\text{geo}}$	$r_{298}^{\text{bu}}$	$r_{233}^{\text{bu}}$	$r_{233}^{\text{FMA}}$	$r^{\text{geo}}$
Gly H $^{\alpha 2}$ -Gly H $^{\alpha 3}$	0.38	0.38	-7.67	-6.98	-7.22	1.77	1.77	1.80	1.77
Gly H $^{\text{N}}$ -Gly H $^{\alpha 3}$	0.03	0.03	-0.68	-0.68	-0.57	2.71	2.65	2.65	2.71
Gly H $^{\text{N}}$ -Gly H $^{\alpha 2}$	0.08	0.07	-1.45	-1.51	-1.37	2.29	2.33	2.32	2.34
Pro H $^{\alpha}$ -Pro H $^{\beta 3}$	0.07	0.06	-1.27	-1.15	-1.15	2.35	2.39	2.42	2.41
Gly H $^{\text{N}}$ -Pro H $^{\alpha}$	0.01	0.004	-0.15	-0.07	-0.07	3.32	3.41	3.86	3.87

$\sigma_{298}^{\text{bu}}$  Cross-relaxation rate from buildup, fig. 7;  $T = 298$  K.

$\sigma_{298}^{\text{geo}}$  Cross-relaxation rate from geometry;  $\tau_c = 4.65 \times 10^{-11}$  s,  $\omega_0/2\pi = 500$  MHz,  $T = 298$  K.

$\sigma_{233}^{\text{bu}}$  Cross-relaxation rate from buildup, fig. 7;  $T = 233$  K.

$\sigma_{233}^{\text{FMA}}$  Cross-relaxation rate from full matrix analysis, table 3.

$\sigma_{233}^{\text{geo}}$  Cross-relaxation rate from geometry;  $\tau_c = 4.0 \times 10^{-9}$  s,  $\omega_0/2\pi = 500$  MHz,  $T = 233$  K.

$r_{298}^{\text{bu}}$  Interproton distance from  $\sigma_{298}^{\text{bu}}$ ;  $r_{\alpha 2/\alpha 3} = 1.77$  Å.

$r_{233}^{\text{bu}}$  Interproton distance from  $\sigma_{233}^{\text{bu}}$ ;  $r_{\alpha 2/\alpha 3} = 1.77$  Å.

$r_{233}^{\text{FMA}}$  Interproton distance from  $\sigma_{233}^{\text{FMA}}$ .

$r^{\text{geo}}$  Interproton distance from energy minimized-molecular model.

At low temperature, mixing times of about 1 s are excessively long. This can be seen from the buildup curve for geminal pair Gly H $^{\alpha 2}$ /H $^{\alpha 3}$ , which reached saturation around 300 ms.

At mixing times longer than 300 ms, the cross-peak volume and diagonal peak volume are almost the same and only a lower limit of the cross-relaxation rate can be estimated. Because the transfer process has taken place to the completion, data at  $\tau_m > 300$  ms do not contain information on the rate by which the cross and diagonal peak volumes were equilibrated. Thus, valuable information can be obtained only at shorter mixing times. The inset in fig. 7 shows expansion of the normalized cross-peak intensities for the first 80 ms of mixing time. There, only the fastest cross-relaxation rate between geminal protons has fulfilled the condition from eq. (37) and thus can be calculated by the linear approximation of eqs (30) and (32). All other spin pairs are influenced by spin diffusion and the second order approximation must be used, eqs (30) and (32). Results of such analysis are presented in table 4,  $\sigma_{233}^{\text{bu}}$ , in comparison with the cross-relaxation rates obtained from the full matrix analysis,  $\sigma_{233}^{\text{FMA}}$ , and from the molecular model,  $\sigma_{233}^{\text{geo}}$ . Converted into interproton distances, all cross-relaxation rates agree.

## References

- [1] B.H. Meier and R.R. Ernst, *J. Am. Chem. Soc.* **101** (1979) 6441.
- [2] J. Jeener, B.H. Meier, P. Bachmann and R.R. Ernst, *J. Chem. Phys.* **71** (1979) 4546.
- [3] R.R. Ernst, G. Bodenhausen and A. Wokaun, *Principles of Nuclear Magnetic Resonance in One and Two Dimensions* (Oxford University Press, New York, 1987).
- [4] I. Solomon, *Phys. Rev.* **99** (1955) 559.
- [5] J.H. Noggle and R.E. Schirmer, *The nuclear overhauser effect Chemical applications* (Academic Press, New York, 1971).
- [6] D. Neuhaus and M. Williamson, *The Nuclear Overhauser Effect in Structural and Conformational Analysis* (VCH Publishers, New York, 1989).
- [7] A.W. Overhauser, *Phys. Rev.* **91** (1953) 476.
- [8] I. Solomon and N. Bloembergen, *J. Chem. Phys.* **25** (1956) 261.
- [9] D.G. Davis, *J. Am. Chem. Soc.* **109** (1987) 3471.
- [10] B.T. Farmer II, S. Macura and L.R. Brown, *J. Magn. Reson.* **80** (1988) 1.
- [11] C. Isernia, L. Paolillo, E. Russo, A. Pastore, G. Zanotti and S. Macura, *J. Biomolecular NMR* **2** (1992) 573.
- [12] H.S. Gutowsky and C.H. Holm, *J. Chem. Phys.* **25** (1956) 1228.
- [13] H.M. McConnell, *J. Chem. Phys.* **28** (1958) 430.
- [14] L.W. Reeves, in: *Advances in Physical Organic Chemistry*, ed. V. Gold (Academic Press, London, 1965) p. 187.
- [15] J. Jen, *Adv. Mol. Relaxation Processes* **6** (1974) 171.
- [16] K.V. Vasavada, J.I. Kaplan and B.D.N. Rao, *J. Magn. Reson.* **41** (1980) 467.
- [17] B.D.N. Rao, in: *Methods in Enzymology*, Vol. 176, eds N.J. Oppenheimer and T.L. James (Academic Press, San Diego, 1989).
- [18] S. Macura, Y. Huang, D. Suter and R.R. Ernst, *J. Magn. Reson.* **43** (1981) 259.
- [19] S. Macura, K. Wüthrich and R.R. Ernst, *J. Magn. Reson.* **47** (1982) 351.
- [20] S. Macura, K. Wüthrich and R.R. Ernst, *J. Magn. Reson.* **46** (1982) 269.
- [21] M. Rance, G. Bodenhausen, G. Wagner, K. Wüthrich and R.R. Ernst, *J. Magn. Reson.* **62** (1985) 497.
- [22] A. Bax and D.G. Davis, *J. Magn. Reson.* **63** (1985) 207.
- [23] H. Kessler, C. Griesinger, R. Kerssebaum, K. Wagner and R.R. Ernst, *J. Am. Chem. Soc.* **109** (1987) 607.
- [24] A. Bax, *J. Magn. Reson.* **77** (1988) 134.
- [25] J. Cavanagh and J. Keeler, *J. Magn. Reson.* **80** (1988) 186.
- [26] J. Fejzo, W.M. Westler, S. Macura and J.L. Markley, *J. Magn. Reson.* **92** (1991) 20.
- [27] T.-L. Hwang and A.J. Shaka, *J. Am. Chem. Soc.* **114** (1992) 3157.
- [28] S. Macura, J. Fejzo, W.M. Westler and J.L. Markley, *Bull. Magn. Reson.* **16** (1994) 73.
- [29] A. Motta, D. Picone, T. Tancredi and P.A. Temussi, *J. Magn. Reson.* **75** (1987) 364.
- [30] S.W. Fesik and E.T. Olejniczak, *Magn. Reson. Chem.* **25** (1987) 1046.
- [31] N. Juranic, S. Macura, V. Likic and N. Kostic, *Inorg. Chem.* **34** (1995) 938.
- [32] S. Macura, J. Fejzo, C.G. Hoogstraten, W.M. Westler and J.L. Markley, *Isr. J. Chem.* **32** (1992) 245.
- [33] S. Macura and R.R. Ernst, *Mol. Phys.* **41** (1980) 95.
- [34] A. Kumar, R.R. Ernst and K. Wüthrich, *Biochem. Biophys. Res. Commun.* **95** (1980) 1.
- [35] Y. Huang, S. Macura and R.R. Ernst, *J. Am. Chem. Soc.* **103** (1981) 5327.
- [36] J. Hennig and H.H. Limbach, *J. Magn. Reson.* **49** (1982) 322.
- [37] A.A. Bothner-By, R.L. Stephens, J. Lee, C.D. Warren and R.W. Jeanloz, *J. Am. Chem. Soc.* **106** (1984) 811.

- [38] L.R. Brown and B.T. Farmer II, in: *Methods in Enzymology, Nuclear Magnetic Resonance, Part A: Spectral Technique and Dynamics*, Vol. 176, eds N.J. Oppenheimer and T.L. James (Academic Press, San Diego, 1989) p. 199.
- [39] J. Fejzo, W.M. Westler, S. Macura and J.L. Markley, *J. Am. Chem. Soc.* **112** (1990) 2574.
- [40] D.G. Davis and A. Bax, *J. Magn. Reson.* **64** (1985) 533.
- [41] J. Fejzo, W.M. Westler, S. Macura and J.L. Markley, *J. Magn. Reson.* **92** (1991) 195.
- [42] J. Bremer, G.L. Mendz and W.J. Moore, *J. Am. Chem. Soc.* **106** (1984) 4691.
- [43] R. Boelens, T.M.G. Koning and R. Kaptein, *J. Mol. Struct.* **173** (1988) 299.
- [44] B.A. Borgias and T.L. James, in: *Methods in Enzymology, Nuclear Magnetic Resonance, Part A: Spectral Techniques and Dynamics*, Vol. 176, eds N.J. Oppenheimer and T.L. James (Academic Press, San Diego, 1989) p. 169.
- [45] R. Boelens, T.M.G. Koning, G.A. Van der Marel, J.H. Van Boom and R. Kaptein, *J. Magn. Reson.* **82** (1989) 290.
- [46] B.A. Borgias and T.L. James, *J. Magn. Reson.* **87** (1990) 475.
- [47] B.R. Leeftang and M.J. Kroon-Batenburg, *J. Biomol. Nmr.* **2** (1992) 495.
- [48] M. Starzak, *Mathematical Methods in Chemistry and Physics* (Plenum Press, New York and London, 1989).
- [49] X.A. Mao, *Chem. Phys.* **175** (1993) 237.
- [50] S. Macura, *J. Magn. Reson.* **112** (1995) 152.
- [51] A. Kumar, G. Wagner, R.R. Ernst and K. Wüthrich, *J. Am. Chem. Soc.* **103** (1981) 3654.
- [52] S.G. Hyberts and G. Wagner, *J. Magn. Reson.* **81** (1989) 418.
- [53] A. Majumdar and R.V. Hosur, *Biochem. Biophys. Res. Commun.* **159** (1989) 886.
- [54] J. Fejzo, Zs. Zolnai, S. Macura and J.L. Markley, *J. Magn. Reson.* **82** (1989) 518.
- [55] J. Fejzo, Zs. Zolnai, S. Macura and J.L. Markley, *J. Magn. Reson.* **88** (1990) 93.
- [56] S. Macura, B.T.I. Farmer and L.R. Brown, *J. Magn. Reson.* **70** (1986) 493.
- [57] N. Juranic, V. Likic, T. Parac and S. Macura, *J. Chem. Soc. Perkin Trans.* **2** (1993) 1805.
- [58] G. Wider, S. Macura, A. Kumar, R.R. Ernst and K. Wüthrich, *J. Magn. Reson.* **56** (1984) 207.

# chapter 14

---

## Reference Deconvolution

---

Gareth A. Morris and Hervé Barjat

*Department of Chemistry  
University of Manchester  
Oxford Road, Manchester M13 9PL  
United Kingdom*

Methods for Structure Elucidation by High-Resolution NMR  
Edited by Gy. Batta, K.E. Kövér and Cs. Szántay, Jr.  
© 1997 Elsevier Science B.V. All rights reserved

This Page Intentionally Left Blank

## 1. Introduction

Suppose that a pulse Fourier transform proton NMR experiment is carried out on a sample containing acetone and ethanol. If the instrument is correctly operated and the  $B_0$  field perfectly uniform, then the result will be a spectrum in which each of the lines has a Lorentzian shape, with a width given by the natural limit  $1/(\pi T_2)$ . Unfortunately such a result is an unattainable ideal: the most that any experimenter can hope for is to shim the field sufficiently well that the sample experiences only a narrow distribution of  $B_0$  fields. The effect of the  $B_0$  inhomogeneity is to superimpose an instrumental lineshape on the natural lineshapes of the different resonances; the true spectrum is convoluted by the instrumental lineshape.

In principle we could deconvolute the experimental spectrum with the instrumental lineshape, if that were known, to recover the true spectrum. In our example we have some good experimental evidence as to the form of the instrumental lineshape: since the acetone signal is (apart from small carbon-13 satellites) a singlet, its experimental shape is just the instrumental lineshape convoluted by a Lorentzian of width  $1/(\pi T_2^{\text{ac}})$ , where  $T_2^{\text{ac}}$  is the spin-spin relaxation time of the acetone protons. How can we use this experimental evidence to correct the imperfect experimental spectrum? The simplest way to deconvolute one function  $f_1(\omega)$  by another  $f_2(\omega)$  is to Fourier transform the ratio of their inverse Fourier transforms:

$$f(\omega) = \text{FT}^- \left[ \frac{\text{FT}^+ \{f_1(\omega)\}}{\text{FT}^+ \{f_2(\omega)\}} \right], \quad (1)$$

where  $\text{FT}^-$  indicates (discrete) Fourier transformation and  $\text{FT}^+$  the corresponding inverse transformation. In our case, since the experimental lineshape of the acetone signal is the convolution of the instrumental lineshape and the natural shape, to recover the true spectrum we actually need to deconvolute the experimental spectrum with the experimental acetone lineshape and then reconvolute it with the natural lineshape. This process may be termed reference deconvolution; here the acetone serves to provide a reference signal for which the ideal form is easily calculated.

We can find the experimental lineshape by taking the raw experimental spectrum and zeroing all but the acetone signal, taking care to ensure that what remains includes all the acetone signal but no other signals. To find the natural acetone lineshape we need to estimate the spin–spin relaxation time  $T_2^{\text{ac}}$ ; this estimate is not critical, since any discrepancy will simply lead to a slight increase or decrease in the widths of the Lorentzian lines in our corrected spectrum. If the raw experimental free induction decay is  $s_e(t)$  and the corresponding spectrum  $S_e(\omega)$ , then the time-domain form of the reference signal is

$$s_r(t) = \text{FT}^+ \{II(\omega_L, \omega_R)S_e(\omega)\}, \quad (2)$$

where  $II(\omega_L, \omega_R)$  is the Dirichlet function, unity between  $\omega_L$  and  $\omega_R$  and zero elsewhere. The ideal reference signal  $s_i(t)$  is the inverse Fourier transform of the ideal acetone lineshape  $S_i(\omega)$

$$s_i(t) = \text{FT}^+ \{S_i(\omega)\}, \quad (3)$$

so a corrected free induction decay  $s_c(t)$  can be calculated using the complex ratio  $R(t)$  of  $s_i(t)$  and  $s_r(t)$ :

$$s_c(t) = s_e(t) \times R(t) = s_e(t) \times \frac{s_i(t)}{s_r(t)}. \quad (4)$$

In practice  $S_i(\omega)$  must include small contributions from long range carbon-13 satellites as well as the main central singlet if the deconvolution is to be accurate; the time-domain ideal reference signal  $s_i(t)$  may be found either by explicit inverse Fourier transformation or by direct calculation in the time domain. The choice of the reference region  $\omega_L$  to  $\omega_R$  is critical; too narrow a region will exclude part of the experimental acetone lineshape, too wide a region runs the risk of incorporating other signals and increases the amount of unwanted noise included.

The corrected free induction decay  $s_c(t)$  will transform to a spectrum  $S_c(\omega)$  in which not only the acetone signal but also all the ethanol signals have had the instrumental contributions to their lineshapes removed. Provided that the reference region  $\omega_L$  to  $\omega_R$  gives a complete and accurate representation of the experimental acetone lineshape, our deconvolution process should allow us to obtain a clean corrected spectrum even when the shimming is far from ideal. There are of course limitations on this process. If the experimental lineshape is very broad, it will clearly not be possible to obtain a corrected spectrum in which the lines are very narrow without some sort of penalty. Here the limiting factor is signal-to-noise ratio: since  $S_i(\omega)$  is much sharper than  $S_e(\omega)$ , the ratio of their inverse Fourier

transforms will become very large as  $t$  increases, amplifying the noise in the later part of  $s_e(t)$ . It is sometimes helpful to think of the process of reference deconvolution as a slightly more sophisticated version of the familiar process of resolution enhancement, tailored to the exact form of the experimental lineshape.

A less obvious limitation stems from the form of eq. (1). If the inverse Fourier transform of the experimental acetone lineshape drops to zero, (1) will become indeterminate. This places an upper limit on the degree of improvement in resolution obtainable with reference deconvolution which depends on the exact form of the instrumental lineshape. An obvious case which causes problems is a split lineshape which consists of two identical components  $\Delta\omega$  apart; the inverse Fourier transform of this lineshape will fall to zero at times  $(2n+1)\pi/(2\Delta\omega)$ . Fortunately neither of these two limitations is too restrictive in practice. Reference deconvolution in the form described has a wide range of uses, from correcting severe lineshape distortions in *in vivo* spectra, where shimming is very difficult and local variations in magnetic susceptibilities of tissues further distort  $B_0$ , to correcting the much smaller distortions in lineshape found in a well-shimmed high resolution spectrometer, that nevertheless can prevent the reliable detection and quantitation of small signals in the presence of larger ones.

There are, however, many other ways in which reference deconvolution can be used to enhance the results of NMR experiments. The effect of poor shimming is to convolute the true spectrum with an instrumental lineshape; this corresponds in the time domain to multiplying the free induction decay by a (complex) error function  $E(t)$ . Many of the other things that can – and do – go wrong in NMR experiments also correspond to multiplying the free induction decay, for example the generation of spinning or mains frequency modulation sidebands, phase errors caused by pulse phase irreproducibility, amplitude errors caused by variation in probe tuning or receiver gain, etc. In each case all the signals in an experimental spectrum suffer in exactly the same manner, and hence in each case it is possible to correct the error by reference deconvolution. Reference deconvolution can thus also be used to ensure exact comparability between experimental spectra where this is important, for example in difference spectroscopy or between the successive increments of a two-dimensional experiment. The earliest published uses of reference deconvolution were for lineshape correction [1, 2] in high resolution NMR, but subsequent workers have independently developed the technique for difference rapid scan cross-correlation NMR [3, 4] and *in vivo* NMR [5]. Several improvements on the crude algorithm for pulse FT NMR outlined above have been developed [6, 7], and applied to difference spectroscopy [8] and to 2D NMR [9]; the technique has also been applied in IR spectroscopy [10]. Reference deconvolution algorithms have been given a variety of names, including RLSA (Reference LineShape

Adjustment) [3], FIDDLE (Free Induction Decay Deconvolution for Lineshape Enhancement) [6] and QUALITY (QUAntification improvement by converting Lineshapes to the Lorentzian TYpe) [5].

## 2. Practical implementation

The main problem in constructing a viable algorithm for reference deconvolution is to extract the complete reference signal from the experimental spectrum, without contamination from other signals. The difficulty is that both the real and imaginary parts of the reference signal are required; while the absorption mode signal has a relatively narrow base and is usually unencumbered by overlap, the dispersion mode signal is far wider, falling off only hyperbolically with frequency, making overlap far more likely. The need to make the reference region of the spectrum extracted very wide also means that relatively large amounts of noise are included in the experimental reference signal, degrading the accuracy of the eventual deconvolution. One compromise is to set a narrow reference region, truncating the dispersion mode part of the reference signal, but then attempt to supply the missing signal by extrapolation [6]. This can be surprisingly effective, but compromises both the accuracy and the basic linearity of reference deconvolution, and has now been supplanted by a method which avoids the need to extract the dispersion mode signal from the experimental spectrum by exploiting the Hilbert transform relation between the absorption mode and dispersion mode parts of a causal signal [11].

If an experimental signal  $s_e(t)$  of  $N$  complex points ( $N$  real and  $N$  imaginary measurements) is Fourier transformed, it will yield a discrete spectrum in which there are  $N$  real (e.g., absorption mode) and  $N$  imaginary (dispersion mode) points. As expected there is no change in the overall amount of information: half of the information in the  $2N$  measurements that make up the experimental time-domain signal ends up in the real part of the spectrum and half in the imaginary. Suppose now that a further  $N$  complex zeroes are appended to  $s_e(t)$  before Fourier transformation. Now there will be  $2N$  real data points in the spectrum and  $2N$  imaginary. There has been no increase in the total information content of the spectrum, but now the real and imaginary parts of the spectrum are correlated: all  $N$  complex points in the time domain contribute to the real part of the spectrum, and all  $N$  points contribute to the imaginary part. The imaginary part is therefore redundant, the real spectrum containing all the original information in  $s_e(t)$ . If the real part of the spectrum alone were to be subjected to inverse Fourier transformation, the imaginary part being set to zero, the result would be a time-domain function consisting of  $s_e(t)$  followed by a reflected replica, since the transform of a pure real function must be symmetric in the time

domain. Zeroing the second half of the inverse Fourier transform would then leave just the original time-domain signal  $s_e(t)$ .

The way to ensure a clean extraction of an experimental reference signal is thus to zero-fill the experimental free induction decay  $s_e(t)$  once before Fourier transformation, zero completely the imaginary part of the resultant spectrum, and zero all but the reference region  $\omega_L$  to  $\omega_R$  of the real part [7]. Inverse Fourier transformation then gives a symmetric time-domain signal, the first half of which is the required experimental reference signal  $s_r(t)$ :

$$s_r(t) = \text{FT}^+ [H(\omega_L, \omega_R) \times \text{FT}^- \{s_e(t) + Z(t, 2t)\}] \times H(0, t), \quad (5)$$

where  $s_e(t)$  extends from time 0 to  $t$ , and the function  $Z$  appends zeroes from time  $t$  to  $2t$ . The corrected free induction decay is then once again

$$s_c(t) = s_e(t) \times \frac{s_i(t)}{s_r(t)}, \quad (6)$$

but now the reference region  $\omega_L$  to  $\omega_R$  only needs to encompass the absorption mode reference signal and not the dispersion mode. The complete algorithm is summarized in fig. 1.

The Hilbert transform reference deconvolution algorithm just described is simple to implement and robust in use, and makes only modest demands on data processing capacity; a typical deconvolution takes only three to four times as long as a normal Fourier transformation. There are, however, a number of useful extensions to the basic method, for use with distorted experimental data or for specific experiments. The simplest extension is to add a dc correction to the reference region before inverse Fourier transformation; this reduces any errors caused by baseline distortion in the experimental spectrum. Spectra with severe rolling baselines can be dealt with by applying a suitable spline or polynomial correction to a zero-filled raw experimental spectrum, and then inverse Fourier transforming this spectrum to give a baseline corrected experimental free induction decay  $s_e^b(t)$  which can be subjected to reference deconvolution as normal. Reference deconvolution can be used to ensure exact comparability between spectra in difference experiments: in nuclear Overhauser effect difference spectroscopy, for example, if the control and irradiated spectra are both deconvoluted using the same ideal lineshape, artefacts in the difference spectrum due to instrumental instability can be eliminated [8].

The same logic can be applied in multidimensional spectroscopy, to decrease  $t_1$ -noise; in favourable cases  $t_1$ -noise can be reduced by an order of magnitude, allowing weak cross-peaks to be detected [9]. The 2D experiments for which  $t_1$ -noise poses the greatest problem are those which require strong signals to be nulled, either by phase cycling or by the use

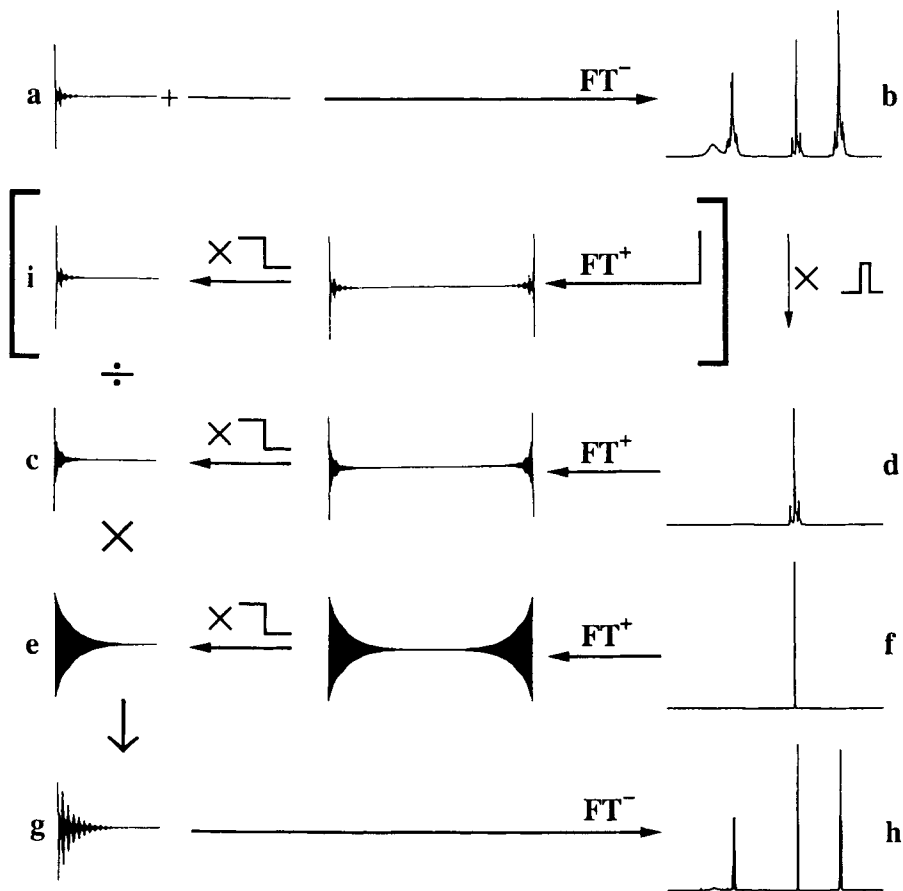


Fig. 1. Schematic illustration of the Hilbert transform algorithm for reference deconvolution. The raw experimental spectrum  $S_c(\omega)$  (b) is produced by Fourier transforming the zero-filled experimental free induction decay, its imaginary part is zeroed and the real part of the reference signal (d) is extracted. Inverse Fourier transformation and truncation yields the time-domain reference signal (c)  $s_r(t)$ ; the corresponding ideal signal (e)  $s_i(t)$  is produced either by direct calculation or by inverse Fourier transformation of the ideal reference lineshape  $S_i(\omega)$ . Multiplying the experimental free induction decay (a) (or if necessary the truncated inverse transform (i) of a baseline-corrected version of  $S_c(\omega)$ ) by the complex ratio of (e) and (c) gives a corrected free induction decay (g) which Fourier transforms to the corrected spectrum (h)  $S_c(\omega)$ . (Reproduced, with permission, from *Signal Treatment and Signal Analysis in NMR*, ed. D.N. Rutledge, Elsevier, Amsterdam, 1996)

of pulsed field gradients. A typical example is the HMBC experiment [12], in which long-range couplings between protons and carbon-13 give rise to cross peaks, but the intense signals from protons not enjoying long range couplings to carbon-13 have to be suppressed. In this experiment the  $t_1$ -noise is dominated by the imperfect suppression of the unwanted signals,

caused by instrumental irreproducibility [13, 14], so the principal problem is signal irreproducibility within the phase cycle for a particular  $t_1$  increment rather than signal variation from increment to increment. Both types of variation can be cured by splitting the phase cycling for the HMBC experiment into two halves, giving signals with the same phase for protons with couplings to carbon-13 but opposite phases for uncoupled protons. Reference deconvolution (with a reference signal which has no long range couplings) is used [9] to ensure that any variation in signal amplitude, phase or lineshape between the two halves of the signal for a given  $t_1$  increment is corrected, so that when the signals from the two halves of the phase cycling are combined the unwanted signals are rigorously suppressed, and the desired signals show no spurious variation as a function of  $t_1$ .

The requirement that the reference signal be a singlet can be an inconvenient one, for example where a precious sample must not be contaminated with a reference material, or *in vivo* where it is not possible to add a reference. The problem with using more than one signal as a composite reference is that interference between the components of the reference can lead to the reference signal falling to zero at certain times. This is a particular problem for common multiplets, since all first order multiplet patterns other than the singlet lead to zeroes in the time domain. It is however still possible to make use of multiplet signals as references if interpolation is used to deduce the value of the correction function  $R(t)$  for those regions of time where the reference signal falls close to zero. This process demands careful attention to detail, as close to the zeroes in the time domain small discrepancies between the ideal bandshape and the true bandshape of the reference signal can lead to big errors in  $R(t)$ . However, in spectra with good signal-to-noise ratio, the quality of deconvolution obtainable with a doublet reference signal is very nearly as good as that with a singlet [15].

### 3. Applications

Figure 2 illustrates the use of the FIDDLE algorithm of fig. 1 for the correction of gross field homogeneity errors in a 300 MHz proton spectrum; the example chosen is that used in the Introduction and in fig. 1, a sample containing acetone and ethanol. Severe field inhomogeneity was produced by missetting the shim currents, resulting in a dissymmetric lineshape with strong spinning sidebands. A reference region 300 Hz wide around the acetone signal in the raw experimental spectrum of fig. 2(a) was excised using the Hilbert transform method described earlier, and the ideal lineshape  $S_1(\omega)$  was chosen to be a Lorentzian of full width 1 Hz at half height. Figure 2(b) shows the result of deconvolution; the spinning sidebands are suppressed and all the signals have a clean Lorentzian lineshape. A Gaussian instrumental lineshape can be achieved by substituting a Gaussian ideal reference

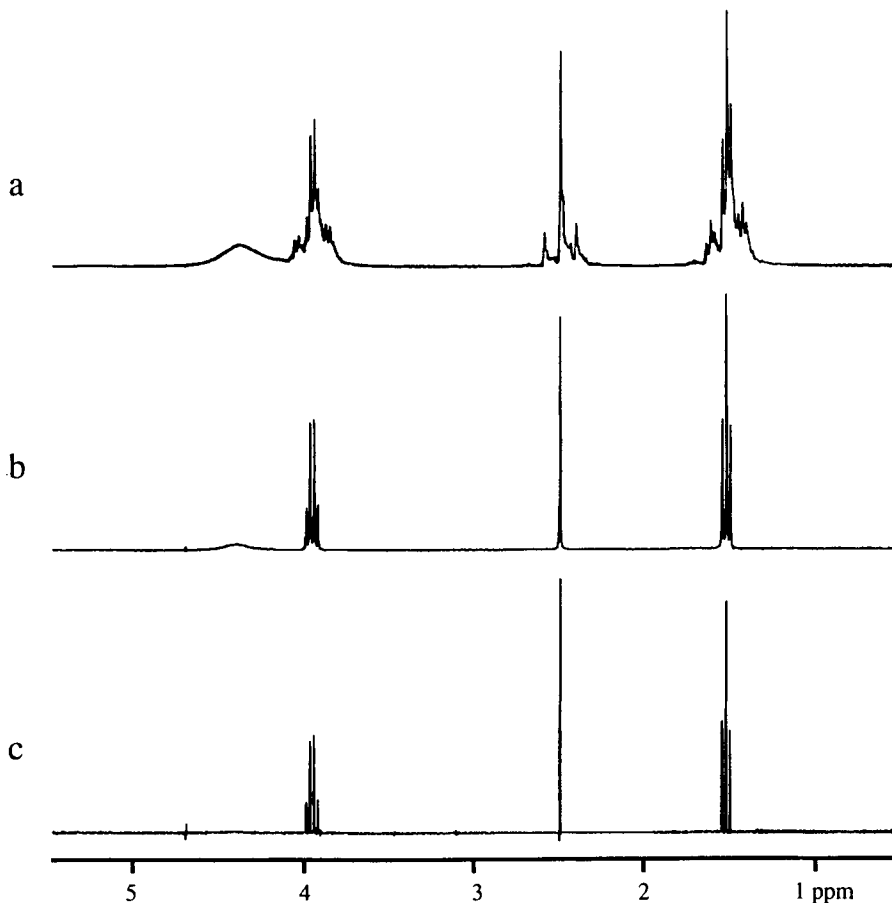


Fig. 2. (a) Raw 300 MHz proton spectrum of a mixture of acetone and ethanol in deuteriochloroform; (b) after reference deconvolution using the acetone signal as reference and an ideal lineshape of a 1 Hz wide Lorentzian; and (c) after reference deconvolution with an ideal lineshape characterized by a negative Lorentzian width of 0.1 Hz and a Gaussian width of 0.4 Hz. The 0.1 Hz Lorentzian term represents the approximate difference in natural linewidth between the ethanol and acetone signals, and is responsible for the “wings” on the acetone signal.

lineshape for a Lorentzian, corresponding to a Gaussian envelope for  $s_i(t)$ . The best compromise between resolution and signal-to-noise ratio is achievable by combining reference deconvolution with resolution enhancement by choosing an envelope for  $s_i(t)$  which is an exponential rising with a time constant equal to the  $T_2$  of the signals of interest, multiplied by a Gaussian decay. Figure 2(c) shows such a spectrum, in which the ethanol lines are now Gaussians with a full width at half height of 0.4 Hz. Note that the relative integrals of the signals remain constant during the deconvolution

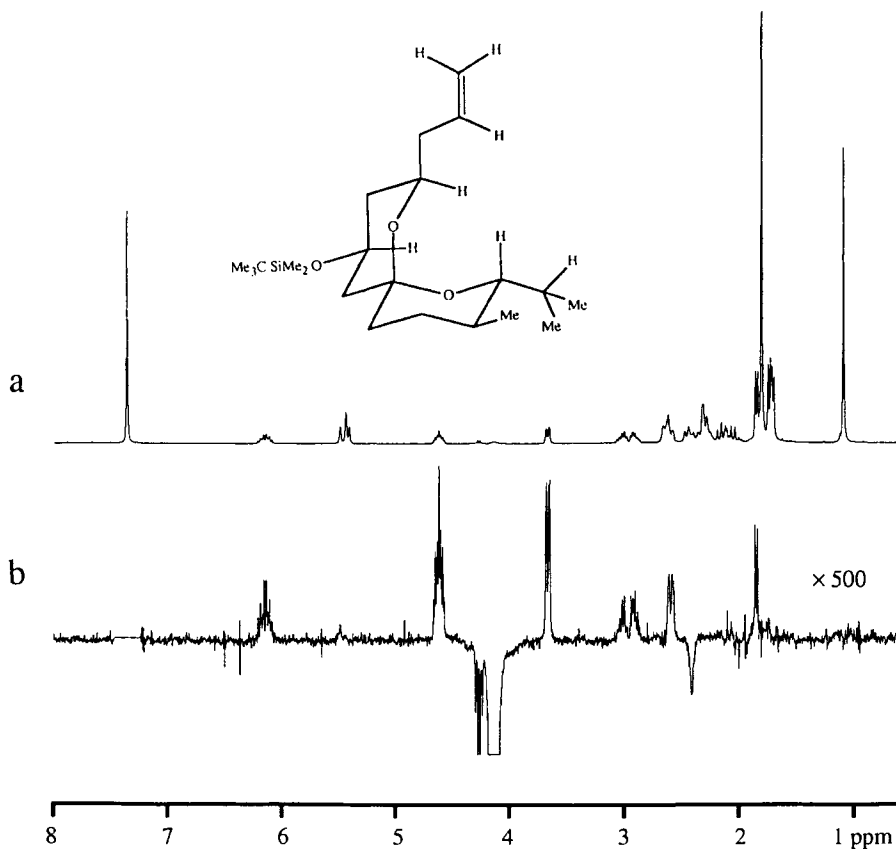


Fig. 3. (a) 300 MHz proton spectrum of the molecule shown, and (b) 500-fold expanded NOE difference spectrum obtained using reference deconvolution to enforce identical reference lineshapes (2 Hz Lorentzian) for the chloroform signals in the irradiated and unirradiated spectra. Note the complete absence of the usual “up-down” difference artefacts in trace (b), even for the sharp singlet methyl signals; the remaining artefacts are largely homodecoupler spikes.

process; the apparent reduction in the relative intensity of the broad OH singlet at 4.4 ppm arises from the peak heights of the remaining signals increasing as their widths decrease. As expected, the price paid for the increase in resolution is a corresponding reduction in signal-to-noise ratio.

The use of reference deconvolution for the correction of artefacts in nuclear Overhauser effect difference spectroscopy [9] is illustrated by the spectra of fig. 3. The experimental technique used here differs slightly from that normally encountered in using a control spectrum in which the preirradiation is gated off rather than shifted in frequency, and in keeping the decoupler and transmitter at the same frequency. These modifications were

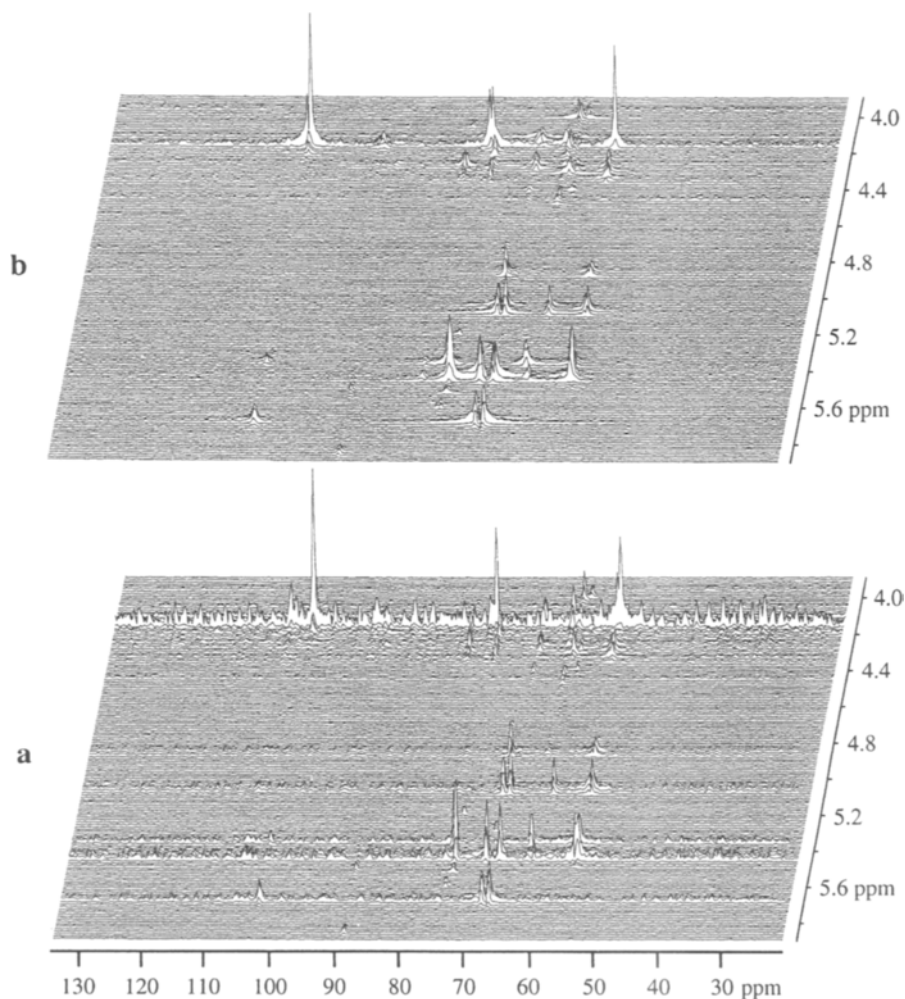


Fig. 4. (a) Conventional 500 MHz HMBC spectrum of sucrose octaacetate in deuteriochloroform, and (b) HMBC spectrum with  $t_1$ -noise corrected by reference deconvolution. (Reproduced, with permission, from *Signal Treatment and Signal Analysis in NMR*, ed. D.N. Rutledge, Elsevier, Amsterdam, 1996)

made in order to remove the effects of off-resonance steady-state transverse magnetization generated by the preirradiation. In normal NOE difference spectra the spurious difference signals caused by instrumental drifts and instabilities are sufficient to swamp such effects, but once reference deconvolution is used to compensate for such irreproducibility the steady-state effects become clearly visible if shifted rather than gated preirradiation is used. The normal spectrum of the target molecule is shown in fig. 3(a), and the corrected NOE difference spectrum with a 500-fold vertical expan-

sion in fig. 3(b). The chloroform signal appears in the difference spectrum as a completely blank section of baseline, since the deconvolution process is specifically designed to ensure that the chloroform signals in the two spectra cancel exactly. Difference artefacts in the rest of the spectrum are reduced from typical levels of around 0.5% for sharp signals to less than 0.02%, significantly increasing the effective internuclear distance range of the experiment.

Figure 4 shows an example of the reduction in  $t_1$ -noise in the HMBC experiment that can be achieved with reference deconvolution. Protiochloroform was used to provide a reference in a solution of sucrose octaacetate in deuteriochloroform. Figure 4(a) shows part of a stacked plot of a conventional HMBC spectrum measured on a 500 MHz spectrometer, and fig. 4(b) the same data corrected by reference deconvolution. The level of  $t_1$ -noise seen in fig. 4(a) is typical of a good quality phase cycled HMBC spectrum. Both spectra were obtained from the same dataset, acquired with the split phase cycling discussed in the preceding section. For fig. 4(a) the two halves of the dataset were simply added; for the spectrum of fig. 4(b), for each  $t_1$  increment the data for each half of the phase cycling were deconvoluted separately using the same ideal lineshape (a Gaussian of width 5 Hz) and amplitude and then combined, suppressing the unwanted signals. The corrected data were doubly Fourier transformed to give the spectrum shown, with the  $t_1$ -noise greatly reduced.

#### 4. Discussion

Data processing methods for enhancing the results of NMR experiments can be roughly divided into those that are mathematically linear, such as conventional sensitivity or resolution enhancement using appropriate time-domain weighting functions, and those that are nonlinear, such as maximum entropy or (despite its name) linear prediction. Nonlinear methods suffer from the disadvantage that there is no simple relationship between the data going in and the results coming out, with the consequence that it is all too easy to obtain misleading results. Considerable care is needed if reliable results are to be obtained from such methods. Reference deconvolution is, to a very good approximation, linear, involving little if any falsification of the incoming data; rather, prior knowledge about the spectrum (the form of the ideal reference signal) is used to factorize the spectrum into a corrected spectrum and an instrumental lineshape.

Reference deconvolution is unusual among data processing methods in using internal evidence to repair the damage done to the spectral data by instrumental imperfections; parenthetically, it may be noted that the form of the correction function  $R(t)$  itself can be a useful guide to instrumental fault-finding. The principal uses of reference deconvolution are in the pro-

duction of very high quality spectra, whether for the reliable detection of minor components of mixtures, for the accurate measurement of very small nuclear Overhauser effects, or for the detection of weak HMBC cross-peaks. There is also a good case for using reference deconvolution as a routine tool whenever resolution enhancement is to be applied to a high resolution spectrum, since all too often enhancing the resolution of an apparently well-shimmed spectrum leads to the appearance of spurious splittings.

### Acknowledgments

This work has been generously supported by Glaxo Group Research, Pfizer Central Research and by the EPSRC and its predecessors. The contributions of Dr. A. Gibbs and Mr. C. England to the development of the FIDDLE software used are gratefully acknowledged. H.B. thanks the EPSRC for a research studentship and a research associateship (GR /K16296).

### References

- [1] R.R. Ernst, R. Freeman, B. Gestblom and T.R. Lusebrink, *Mol. Phys.* **13** (1967) 283.
- [2] J. Taquin, *Rev. Phys. Appl.* **14** (1979) 669.
- [3] J.M. Wouters and G.A. Petersson, *J. Magn. Reson.* **28** (1977) 81.
- [4] J.M. Wouters, G.A. Petersson, W.C. Agosta, F.H. Field, W.A. Gibbons, H. Wyssbrod and D. Cowburn, *J. Magn. Reson.* **28** (1977) 93.
- [5] A.A. de Graaf, J.E. van Dijk and W.M.M.J. Bovée, *Magn. Reson. Med.* **13** (1990) 343.
- [6] G.A. Morris, *J. Magn. Reson.* **80** (1988) 547.
- [7] A. Gibbs and G.A. Morris, *J. Magn. Reson.* **91** (1991) 77.
- [8] G.A. Morris and D. Cowburn, *Magn. Reson. Chem.* **27** (1989) 1085.
- [9] A. Gibbs, G.A. Morris, A.G. Swanson and D. Cowburn, *J. Magn. Reson. Ser. A* **101** (1993) 351.
- [10] M.I. Rogojerov and M.G. Arnaudov, *Vibr. Spectrosc.* **3** (1992) 239.
- [11] E. Bartholdi and R.R. Ernst, *J. Magn. Reson.* **11** (1973) 9.
- [12] A. Bax and M.F. Summers, *J. Am. Chem. Soc.* **108** (1986) 2093.
- [13] G.A. Morris, *J. Magn. Reson.* **78** (1988) 281.
- [14] G.A. Morris, *J. Magn. Reson.* **100** (1992) 316.
- [15] H. Barjat, G.A. Morris, A.G. Swanson, S. Smart, and S.C.R. Williams, *J. Magn. Reson. Ser. A* **116** (1995) 206.

## chapter 15

---

# The Super Fast Inversion Recovery (SUFIR) Experiment

---

D. Canet, P. Mutzenhardt

*Laboratoire de Méthodologie RMN  
(URA CNRS 406 - LESOC; FU CNRS E008 - INCM) Université Henri Poincaré  
Nancy 1, B.P. 239  
54506 Vandoeuvre les Nancy Cedex  
France*

J.-B. Robert

*Centre de Recherches sur les Très Basses Températures  
Laboratoire associé à l'Université J. Fourier-Grenoble I/CNRS  
B.P. 166  
38042 Grenoble Cedex  
France*

Methods for Structure Elucidation by High-Resolution NMR  
Edited by Gy. Batta, K.E. Kövér and Cs. Szántay, Jr.  
© 1997 Elsevier Science B.V. All rights reserved

This Page Intentionally Left Blank

A commonly used method of measuring longitudinal relaxation times in multiline spectra, almost as old as Fourier transform NMR, is the inversion recovery experiment [1] which can be schematized by the pulse sequence

$$[(\pi)-\tau-(\pi/2)-\text{Acq}-T_w]_n. \quad (1)$$

By means of the  $\pi$  pulse, the experiment starts with the complete inversion of nuclear magnetization which remains longitudinal. This is followed by an interval  $\tau$  during which magnetization tends to recover toward its equilibrium value. The  $(\pi/2)$  pulse allows for reading the state of longitudinal magnetization by transforming it into detectable transverse magnetization whose Fourier transform yields peak amplitudes as a function of  $\tau$ . Under ideal conditions, these amplitudes obey the relationship

$$S(\tau) = M_0[1 - 2 \exp(-\tau/T_1)], \quad (2)$$

where  $M_0$  represents the equilibrium magnetization.

The signal is measured for an appropriate set of  $\tau$  values (generally in the range  $0-2T_1$ ), leading to the  $T_1$  value associated with each line in the spectrum, provided that the other unknown in (2),  $M_0$ , has been determined independently or is deduced from the actual experimental data. The drawback of the method lies in a waiting time  $T_w$  of the order of  $5T_1$  which must be inserted before starting again a new sequence so that longitudinal magnetization is allowed to recover to its full equilibrium value. At first sight, this appears mandatory whenever accumulations have to be performed for improving the signal-to-noise ratio. Of course, this can lead to prohibitive overall measuring times.

A first improvement, aiming at reasonable measuring times [2], consists of choosing an arbitrary waiting time  $T_w$  (though of the order of  $T_1$ ). This is the Fast Inversion Recovery method whose results must be analyzed according to

$$S(\tau) = M_0[1 - K \exp(-\tau/T_1)], \quad (3)$$

where  $K \leq 2$  is a parameter to be determined from experimental data.

The method is reliable provided that, during  $T_w$ , any transverse magnetization is irreversibly destroyed by transverse relaxation. It is highly efficient

when one is dealing with long relaxation times in systems which require a somewhat large number of accumulations. Optimal conditions of operation have been discussed in several papers [3–6].

However, the above method may still be too lengthy in cases of very diluted species or whenever a large number of measurements have to be performed (for instance, as will be mentioned below, if  $T_1$  has to be monitored over a large temperature range with small step variations). The proposed method, SUFIR [7] (for SUper Fast Inversion Recovery), rests on the comparison of *one* reference spectrum with *one* partially relaxed spectrum, both spectra (or their associated fids) being obtained in identical instrumental conditions. This constraint amounts to obtaining the partially relaxed spectrum immediately after the reference spectrum. Moreover, since one point of the recovery curve is acquired, the longitudinal magnetization evolution is assumed to be purely monoexponential. The basic SUFIR sequence corresponds to a one-shot experiment and can be schematized as follows

$$\left[ \begin{array}{cc} (\pi/2)-\tau-(\pi)-\tau-(\pi/2)-\tau- & \\ \vdots & \vdots \\ S_1 & S_2 \end{array} \right]_n \quad (4)$$

The sequence is repeated  $n$  times in order to improve the signal-to-noise ratio. Each elementary step involves three intervals of strictly identical duration  $\tau$ . During the first and the last of these intervals the receiver is open and the corresponding fids ( $S_1$  and  $S_2$ , respectively, which denote the amplitude of the signal under study) are stored and accumulated in separate memory blocks. Since  $S_1$  and  $S_2$  are alternatively acquired, this insures that they will be affected in the same way by any instrumental drift. Unwanted transverse magnetization which could possibly contribute to the signal is eliminated by a proper phase cycling. Details can be found in the original publication [7]. Because the three evolution intervals have equal duration, the longitudinal relaxation time associated with each line is easily derived by examining the magnetization value  $M_z$  as a function of time. Denoting by  $M(0)$  the magnetization at time  $t = 0$ , one has  $M_z(t) = M_0 - [M_0 - M(0)] \exp(-t/T_1)$ . Thus with  $E_1 = \exp(-\tau/T_1)$ , we obtain  $S_1 = M_0(1 - E_1)$  and  $S_2 = M_0(1 - E_1)^2$ , which finally lead to  $T_1$ :

$$T_1 = -\tau / \ln(1 - S_2/S_1). \quad (5)$$

We now consider the uncertainty in  $T_1$  determined by this procedure. The first cause of inaccuracy may be an inappropriate choice of  $\tau$ , with respect to the expected  $T_1$  values. It can be shown that the optimal choice of  $\tau$  is  $1.3 T_1$ , whereas the relative uncertainty  $\Delta T_1/T_1$  does not exceed twice the

optimal relative uncertainty provided that  $\tau$  lies in the range  $0.5T_1-3T_1$ ; this corresponds indeed to a reasonable " $T_1$  dynamic range". The second cause of inaccuracy may be a low signal-to-noise ratio. Assuming that the optimal  $\tau$  value has been selected (i.e.,  $\tau = 1.3 T_1$ ), we obtain for the relative  $T_1$  uncertainty

$$\frac{\Delta T_1}{T_1} \approx \frac{12}{\{S/N\}_1}, \quad (6)$$

where  $\{S/N\}_1$  stands for the signal-to-noise ratio relative of the reference spectrum (stored in block 1). Thus a reasonable accuracy requires a  $S/N$  ratio of ca. 200.

Data analysis can be fully automated. This proves valuable as long as one is dealing with a large series of measurements. In order to get rid of the tedious task of phasing spectra, either the magnitude or the power spectra are calculated. In the former case, formula (5) is directly applied while in the latter case, where genuine linewidth is preserved, the square root of the signal heights must be used. The output of the corresponding algorithm provides directly the  $T_1$  values.

Regarding the efficiency of the method, it was shown [7] that for a typical carbon-13  $T_1$  determination in a surfactant, the measuring time was shortened by a factor as large as 40 with respect to the Fast Inversion Recovery experiment. In some circumstances, it turns out that SUFIR is the only tractable method. As a first example, fig. 1 shows the two SUFIR spectra obtained for the  $C_{60}$  fullerene dissolved in  $CS_2$  to the extent of ca. 1 mg in 1 ml (10 mm o.d. sample tube) [8]. The experiment was run at 50 MHz ( $^{13}C$  resonance frequency) leading to a  $T_1$  value of 153 s. Obviously such a long relaxation time, together with a weak sensitivity, rules out the use of any other method. A second example is provided by the study of carbon-13 longitudinal relaxation times in derivatives of quinoline [9]. Probing these relaxation times as a function of temperature  $T$  may reveal changes in the liquid structure and (or) motion through a plot of  $\ln(T_1)$  as a function of  $1/T$ . This is a somewhat tiny effect which manifests itself by a break in the considered plot, requiring accurate  $T_1$  determinations and an extensive series of measurements as a function of  $T$ . This is exemplified in fig. 2. Measuring times as short as possible are recommended, especially with regard to possible drifts of the temperature regulation system. Again, the SUFIR method proved to possess this unique feature of celerity.

The SUFIR method has been successfully used in this laboratory for about ten years, implying that its reliability has been frequently checked. The only precaution concerns the timing which must be perfectly stable without disturbance caused by the data storage in alternate memory blocks. Finally,

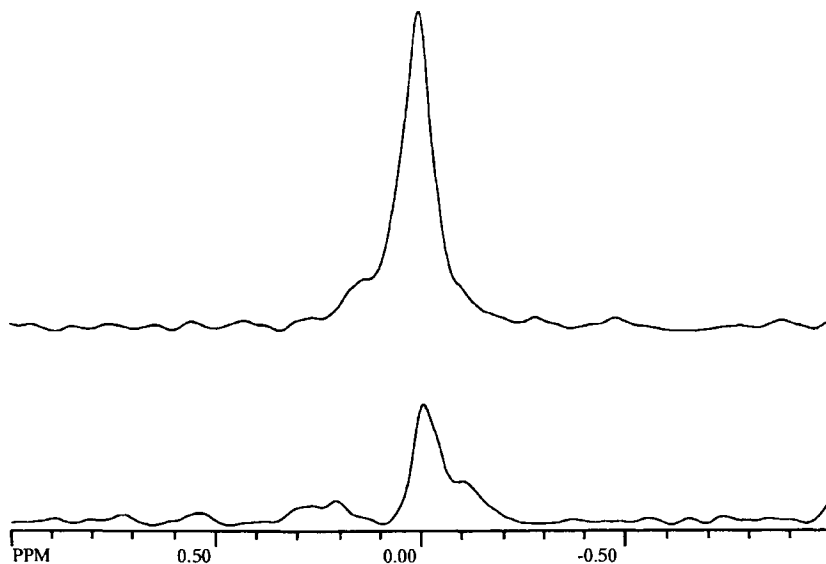


Fig. 1. Use of the SUFIR method in extreme conditions: the two spectra correspond to  $S_1$  and  $S_2$  (see text) of a dilute species (1 mg of the  $C_{60}$  fullerene dissolved in 1 ml of carbon disulfide) possessing an unusually long relaxation time. The SUFIR sequence was repeated for 232 scans with  $\tau = 150$  s.

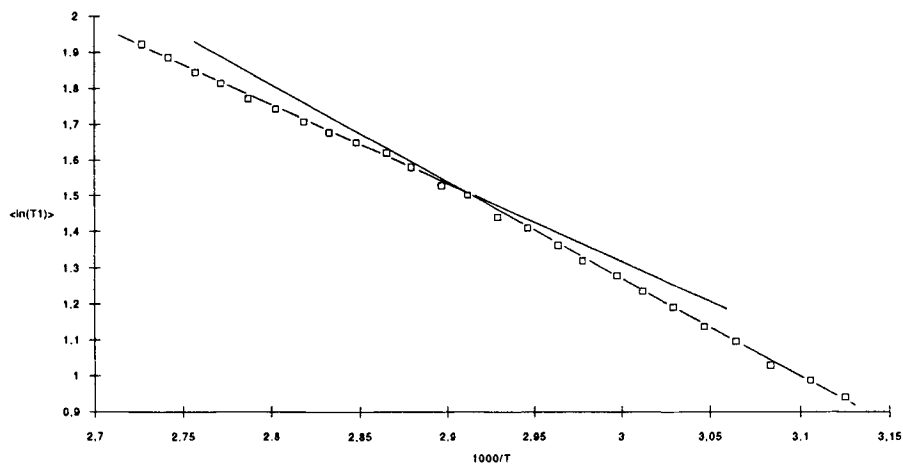


Fig. 2. Plot, as a function of the inverse of temperature, of the average of  $\ln(T_1)$  for all protonated carbons in quinazoline. The break indicates a change in the liquid structure and (or) motion.

it can be mentioned that a related approach has been recently published [10], indicating the real need of a fast and accurate procedure for measuring longitudinal relaxation times.

*Details about SUFIR programs running on Bruker spectrometers can be obtained from Pierre.Mutzenhardt@meth-rmn.u-nancy.fr*

## References

- [1] R.L. Vold, J.S. Waugh, M.P. Klein and D.E. Phelps, *J. Chem. Phys.* **48** (1968) 3831.
- [2] D. Canet, G.C. Levy and I.R. Peat, *J. Magn. Reson.* **18** (1975) 199.
- [3] G.H. Weiss, R.K. Gupta, J.A. Ferretti and E.D. Becker, *J. Magn. Reson.* **38** (1980) 369.
- [4] E.D. Becker, J.A. Ferretti, R.K. Gupta and G.H. Weiss, *J. Magn. Reson.* **37** (1980) 381.
- [5] G.H. Weiss and J.A. Ferretti, *J. Magn. Reson.* **61** (1985) 490.
- [6] G.H. Weiss and J.A. Ferretti, *J. Magn. Reson.* **61** (1985) 499.
- [7] D. Canet, J. Brondeau and K. El-bayed, *J. Magn. Reson.* **77** (1988) 483.
- [8] D. Canet, J.-B. Robert and P. Tekely, *Chem. Phys. Lett.* **212** (1993) 483.
- [9] D. Jalabert, J.-B. Robert, D. Canet and P. Tekely, *Mol. Phys.* **79** (1993) 673.
- [10] H. Zhao, W.M. Westler and J.L. Markley, *J. Magn. Reson. A* **112** (1995), 139.

This Page Intentionally Left Blank

# chapter 16

---

## Measurements of Relaxation Rates for Low Natural Abundance $I = 1/2$ Nuclei

---

Jozef Kowalewski and Lena Mäler

*Division of Physical Chemistry  
Arrhenius Laboratory  
Stockholm University  
S-106 91 Stockholm  
Sweden*

This Page Intentionally Left Blank

## 1. Introduction

The concept of “relaxation time” was introduced into the terminology of nuclear magnetic resonance in 1946 by Bloch in his famous equations of motion for nuclear magnetization [1]. The phenomenological Bloch equations assume the magnetization component along the external magnetic field (the longitudinal magnetization) to relax exponentially to its equilibrium value. The time constant for the process is called the spin-lattice or longitudinal relaxation time, and is denoted  $T_1$ . The magnetization components perpendicular to the magnetic field (the transverse magnetization) are also assumed to relax in an exponential manner to an equilibrium value of zero. The time constant for this process is called the spin-spin or transverse relaxation time and is denoted  $T_2$ . The inverse of a relaxation time is referred to as relaxation rate.

The discovery of Fourier Transform NMR spectroscopy opened up possibilities for NMR studies of low natural abundance, low magnetogyric ratio spin 1/2 nuclei, such as carbon-13 or nitrogen-15 (the spins of such nuclei will in the remainder of this paper be denoted I, while the proton spins will be called S. In fully fluorinated compounds the spins S might denote fluorines). Measurement of nuclear spin relaxation times, in particular  $T_1$  in multi-line  $^{13}\text{C}$  spectra, has been an important and active field of research from the early days of FT NMR [2, 3]. Similar measurements for other low-natural abundance, spin-1/2 nuclei gained impetus later, as the sensitivity of commercially available instrumentation kept improving [3]. There are several reasons for the interest in measurements of this type, apart from the simplicity and elegance of the experiment as such. First of all, at least approximate knowledge of the relaxation times is necessary for optimal design of even the simplest time-domain NMR experiments. Second, the relaxation measurements carry chemically interesting information on the dynamics of molecular motions in the liquid state. The specific issues within this field that can be studied by NMR relaxation measurements include the anisotropy of reorientational motions, the extent and dynamics of internal motions, the effects of intermolecular interactions etc. [3].

This chapter is not meant to provide a comprehensive literature review on the methodology of relaxation measurement. Thus, the list of references is by no means complete but rather reflects the personal taste of the authors.

The layout of this chapter is as follows. The aspects of relaxation theory of interest for this article are summarized very briefly in Section 2. Section 3 deals with general aspects of relaxation measurements, including polarization transfer techniques for improving the sensitivity. Sections 4, 5 and 6 cover measurements of  $T_1$ ,  $T_2$  and the nuclear Overhauser enhancement, respectively.

## 2. Relaxation theory

The theory of nuclear spin relaxation (see monographs by Slichter [4], Abragam [5] and McConnell [6] for comprehensive presentations) is usually formulated in terms of the evolution of the density operator,  $\sigma$ , for the spin system under consideration from some kind of a non-equilibrium state, created normally by one or more radio-frequency pulses, to thermal equilibrium, described by  $\sigma^T$ . Using the Bloch–Wangsness–Redfield (BWR) theory, usually appropriate for the liquid state, we can write [7, 8]:

$$\frac{d\sigma}{dt} = -R(\sigma - \sigma^T). \quad (2.1)$$

$R$  is called the relaxation superoperator. Expanding the density operator in a suitable basis (e.g., product operators [7]), the  $\sigma$  above acquires the meaning of a vector in a multidimensional space, and eq. (2.1) is thereby converted into a system of linear differential equations.  $R$  in this formulation is a matrix, sometimes called the relaxation supermatrix. The elements of  $R$  are given as linear combinations of the spectral density functions  $J_i^{\mu\mu'}(\omega)$ , taken at frequencies  $\omega_k$  corresponding to the energy level differences in the spin system.

$$R_{\kappa\lambda} = \sum_{\mu, \mu'} \sum_i J_i^{\mu\mu'}(\omega_k). \quad (2.2)$$

The indices  $\kappa\lambda$  in the lhs above denote a pair of basis operators, coupled by the element  $R_{\kappa\lambda}$ . The indices  $\mu$  and  $\mu'$  denote individual interactions (dipole–dipole, anisotropic shielding etc); the double sum over  $\mu$  and  $\mu'$  indicates the possible occurrence of interference terms between different interactions [9]. The spectral density functions are in turn related to the time-correlation functions (TCFs), the fundamental quantities in non-equilibrium statistical mechanics. The time-correlation functions depend on the strength of the interactions involved and on their modulation by stochastic processes. The TCFs provide the fundamental link between the spin relaxation and molecular dynamics in condensed matter. In many common cases, the TCFs and the spectral density functions can, to a good approximation, be

expressed as products of an interaction strength factor and a factor dependent on the modulation dynamics.

The elements of the relaxation matrix connecting the elements of  $\sigma$  corresponding to different coherence orders vanish [7]. Thus,  $R$  can in general be written in a block-diagonal form, with the populations separated from coherences. Using the product operator language, the basis vectors containing one or more  $I_z$  or  $S_z$  operators are not coupled to any basis vectors that do not contain such terms. The relaxation processes within the populations block, corresponding to the longitudinal relaxation, are described by a block which in a general case contains diagonal as well as off-diagonal elements. The diagonal elements can be called the auto-relaxation rates (or the leakage rates) and the off-diagonal elements are called cross-relaxation rates. The solutions of eq. (2.1), with  $R$  containing the diagonal and off-diagonal elements, can be written as linear combinations of exponentials. The longitudinal relaxation processes are therefore in general multi- rather than single-exponential. In other words, the concept of  $T_1$  – the time-constant for a simple exponential process – can only be used under certain conditions.

The relaxation processes within the coherences block (the generalized transverse relaxation) are in a way simpler, in particular if there are no degeneracies and if the lines in the spectrum do not overlap (the absence of degeneracy and overlap is a simple way of formulating the validity condition of the secular approximation in the BWR theory). In this case, and using the basis of single transition operators, the transverse  $R$  block is diagonal, i.e., each coherence relaxes as a single exponential (with its own time constant  $T_2$ ) and each line has a simple Lorentzian shape. In the language of the product operators, which is often more convenient, the off-diagonal elements of the relaxation supermatrix connecting the in-phase and anti-phase multiplet components (such as, for example,  $I_x$  and  $2I_xS_z$ ) can be different from zero. This corresponds, in experimental terms, to a different linewidth within a multiplet, a phenomenon called differential line broadening. This is a signature of interference or cross-correlation effects. The transverse relaxation measurements are in general more difficult to perform than longitudinal relaxation studies. We shall return to this point in Section 5 of this chapter.

In the case of low natural abundance spin  $1/2$  nuclei, certain simplifications are possible for the longitudinal relaxation. The low natural abundance means that we do not need to be bothered by the interaction between I nuclei, which only very rarely reside close to each other in the same molecule. The interaction with the S spins (protons) is obviously present, and is one of the main causes of the I-spin relaxation. However, if the protons are saturated by the double resonance irradiation, then the longitudinal relaxation for I-nuclei carrying not more than a single proton is predicted by

the theory to be single exponential. The  $T_1$  concept is therefore rigorously valid, and the corresponding relaxation rate is given by:

$$R_1 = T_1^{-1} = R_{1DD} + R_{1CSA} + R_{1SR} + R_{1SC} + R_{1P}, \quad (2.3)$$

where the additive terms on the right-hand-side of eq. (2.3) represent the dipole–dipole (DD), the chemical shift anisotropy (CSA), the spin-rotation (SR), the scalar (SC) and the paramagnetic (P) mechanisms of relaxation, respectively. In general, the different contributions to the relaxation rate are magnetic-field dependent, through the frequency dependence of the spectral densities in eq. (2.2). In most (but not all!) cases, it is possible to define a fast motion (or extreme narrowing) region in which all the relevant spectral densities are very close to the zero-frequency limit.

The dipolar interaction with the directly bonded proton is usually the dominant relaxation mechanism for proton-carrying carbon or nitrogen nuclei. The dipolar IS interaction, in combination with the saturation of the S-spins, gives rise to the nuclear Overhauser effect. The discussion of this effect is deferred to section 6 of this chapter. The role of the CSA terms differs very much from one system to another; in general,  $R_{1CSA}$  is proportional to the square of the magnetic field. The spin rotation and the scalar term are usually negligible for  $^{13}\text{C}$  and  $^{15}\text{N}$  (except for very small molecules, where the SR mechanism can be of a certain importance, or for carbons directly bonded to bromine, where the SC mechanism may be operative). The expressions for various rate terms can be found in textbooks [5, 6] and reviews [3, 8]. The  $R_{1P}$  term represents the interaction with paramagnetic materials, either added on purpose or in the form of impurities and dissolved oxygen. When undesired, the paramagnetic contribution to the relaxation rate can be suppressed by appropriate sample handling. It is important to note that the interference terms, corresponding to  $\mu \neq \mu'$  in eq. (2.2), do not appear in eq. (2.3).

For  $^{13}\text{C}$  nuclei in groups such as methylene or methyl (or for other  $\text{IS}_n$  ( $n > 1$ ) systems containing magnetically equivalent protons), complications can arise even under proton decoupling because of the interference effects between two dipolar IS interactions. A discussion of these problems is beyond the scope of this chapter. A comprehensive presentation has been given in a review by Werbelow and Grant [10].

### 3. Relaxation measurements – general considerations

An experiment intended to measure a relaxation rate consists in general of three elements: the preparation period, the relaxation period and the detection period. The scheme differs a little from the famous four-period division of two-dimensional experiments [7]. In the case of two-dimensional

relaxation experiments, the evolution and mixing periods of the 2D language can be, depending on the specific experiment design, parts of any of the three periods in the present terminology.

The preparation period consists of the creation of a non-equilibrium state and, possibly, of the frequency labeling in 2D experiments. Usually, the preparation period should be designed in such a way that in the created non-equilibrium state, the population differences or coherences under consideration deviate as much as possible from the equilibrium values. During the relaxation period, the coherences or populations evolve towards an equilibrium (or a steady-state) condition. The behavior of the spin system during this period can be manipulated in order to isolate one specific type of process. The detection period can contain also the mixing period of the 2D experiments. The purpose of the detection period is to create a signal which truthfully reflects the state of the spin system at the end of the relaxation period. As always in NMR, sensitivity is a matter of prime concern.

In the  $T_1$  relaxation experiment on a heteronucleus,  $I$ , such as carbon-13 or nitrogen-15, the measurement is usually performed under broadband decoupling of protons throughout the experiment. The continuous broadband proton decoupling has important advantages from the point of view of all the above-mentioned requirements. It enhances the steady-state  $I$ -spin signal by a factor of  $1 + \eta$ , the nuclear Overhauser enhancement (NOE) [11]. The details behind dipolar relaxation and measurement of heteronuclear NOE's will be presented in section 6. Here, we note that the NOE enhancement improves the performance of the preparation as well as the detection periods. Moreover, as mentioned in the theory section, broadband decoupling simplifies the behavior of the spin system during the relaxation period, as it isolates the relaxation of the  $I$ -spin Zeeman magnetization.

For small molecules, inside the extreme narrowing limit region, the relaxation of  $I = {}^{13}\text{C}$ ,  ${}^{15}\text{N}$  nuclei is usually dominated by dipole-dipole interaction with directly attached protons, and the heteronuclear NOE is substantial. There are, however, cases when other ways of improving the sensitivity are needed. For nuclei with negative magnetogyric ratio, such as  ${}^{29}\text{Si}$  or  ${}^{15}\text{N}$ , the conventional NOE-enhanced method may not be the best choice since  $\eta$  is always negative and a situation when  $|1 + \eta| < 1$  can occur for unfavorable combinations of relaxation mechanisms and/or dynamic conditions. For measurements on  ${}^{13}\text{C}$ , one may have problems with sensitivity when dealing with larger molecules, outside the extreme narrowing limit, where NOE's are very small.

There are several ways to address the problem of sensitivity enhancement, and numerous experiments to increase sensitivity have been invented. The most common approach has been to use a polarization transfer sequence to transfer magnetization from the protons directly bonded to a heteronucleus to that nucleus, in order to achieve a strongly polarized state at the be-

gining of the relaxation period. This has usually been done practically by including in the experiment an INEPT [12] (Insensitive Nuclei Enhanced by Polarization Transfer) or a DEPT [13] (Distortionless Enhancement by Polarization Transfer) sequence before the delay,  $\tau$ , during which relaxation is allowed to take place. With the use of a refocused INEPT experiment one can obtain a maximum increase in the heteronucleus signal by a factor of  $\gamma_{\text{H}}/\gamma_{\text{I}}$ . For carbon-13, this implies a signal increase by a factor of 4. If the NOE is small, it is evident that there is some signal to gain from doing this type of experiment. Kowalewski and Morris [14] used an INEPT-enhanced  $T_1$  relaxation experiment on  $\text{I} = {}^{13}\text{C}$ ,  ${}^{15}\text{N}$ ,  ${}^{29}\text{Si}$  nuclei and found a reduction in the experimental time needed when using the INEPT enhanced sequence as compared to using the NOE enhanced methods. Another reason for preferring a polarization transfer experiment is the fact that the waiting period needed between scans is dependent on the proton relaxation, and not the relaxation of the I nucleus. For  ${}^{29}\text{Si}$  or  ${}^{15}\text{N}$ , spin-lattice relaxation time measurements may not be possible to perform at all with the conventional methods due to very long  $T_1$  relaxation of the  ${}^{29}\text{Si}$  and  ${}^{15}\text{N}$ . With the INEPT enhanced method it was however shown to be possible to rather easily measure  $T_1$  for the insensitive nuclei.

To further increase the sensitivity of a relaxation experiment, one can choose to optimize the detection period performance by detecting the more sensitive nucleus, i.e., the proton. This is usually referred to as indirect, or inverse detection. Such spin-lattice relaxation experiments have been proposed by Kay et al. [15] and by Sklenar et al. [16]. Both groups examined the sequences involving the preparation using the NOE enhancement as well as the  ${}^1\text{H}$  to  ${}^{13}\text{C}$  polarization transfer step. After the relaxation period,  $\tau$ , the heteronuclear magnetization was transferred back to the protons for detection. There is, however, a drawback in doing this experiment as the proton spectra are often more crowded than the I spin spectra. This drawback is often less serious for smaller molecules, where the signals may be separated well enough in the proton spectrum to yield relaxation parameters corresponding to individual heteronuclei. In such case, it may be favorable to do the one-dimensional inverse-detection experiment.

For relaxation studies of biomolecules in solution (which is no specialty of the authors of this chapter), it is often essential to use inverse-detection schemes to obtain reasonable sensitivity. Furthermore, besides problems with poor sensitivity, the carbon-13 and nitrogen-15 spectra are often too crowded to allow measurement of individual relaxation rates for different I nuclei, either by direct detection or by indirectly detecting the protons. If this is the situation, one can spread out the I nuclei signals for better resolution of individual resonances by detecting a two-dimensional  ${}^1\text{H}$ -I correlation spectrum. Relaxation experiments of this type can be considered a modification of the double polarization-transfer IS correlation experiment [7, 17];

they were proposed in late eighties by Nirmala and Wagner [18, 19] and by Kay et al. [20]. After some modifications [21], they have become a standard tool for the determination of relaxation rates of larger biomolecules. The basic idea is to use the initial INEPT (or DEPT) polarization transfer from  $^1\text{H}$  to I, then label the coherences by their carbon or nitrogen frequencies, allow relaxation to take place during the  $\tau$  period, and then apply a reversed INEPT (or DEPT) sequence to bring back the magnetization to the protons. The idea of proton detection is again that one should observe the more sensitive nucleus to gain overall sensitivity. Thus, there are in fact several reasons for doing a two-dimensional relaxation experiment: to gain sensitivity with the polarization transfer and to increase the resolution in the carbon or nitrogen spectrum by spreading out the peaks in two dimensions. The recent advancement in the biomolecule-oriented methodology involves the use of pulsed-field gradient techniques [22, 23].

There are drawbacks in the use of a polarization enhancement experiment. First, it requires accurate determination of several parameters such as pulse lengths and delays depending on the  $J$ -coupling constant. Obviously, such an experiment can produce artifacts, and the gain in sensitivity may not be as high as the theoretical predictions. Kay et al. [15] and Sklenar et al. [16] suggested using the DEPT sequence for the polarization transfer instead of the INEPT, since DEPT contains fewer pulses and delays and consequently would produce fewer artifacts. The DEPT sequence has also been proposed in the original two-dimensional experiments of Nirmala and Wagner [18, 19]. Second, the problem with proton detection in a two-dimensional experiment is related to removing signals from the protons attached to a carbon-12, which requires long phase-cycling schemes.

In both the one-dimensional carbon- or proton-detected INEPT polarization transfer experiment and the two-dimensional proton-detected experiment, one needs to optimize the polarization transfer delay with an estimate of the coupling constant. In addition, the refocusing delay,  $\Delta'$ , must be set separately for an IS and IS<sub>2</sub> spin system. For an IS spin system, the optimum delay is  $\Delta' = (1/4)J_{\text{IS}}$ , whereas for an IS<sub>2</sub> system the delay should be set to  $\Delta' = (1/8)J_{\text{IS}}$  to get maximum polarization transfer. If one is interested in, for instance, the determination of relaxation parameters for carbons carrying two protons as well as for CH carbons, this requires separate experiments.

#### 4. Spin-lattice relaxation time measurements

A simple way to prepare a non-equilibrium state of the longitudinal magnetization is to invert the equilibrium magnetization (or its NOE-enhanced counterpart) by a  $\pi$  pulse. This preparation is used in the “classical” inversion-recovery (IR) method as described by Vold et al. [24] in the early

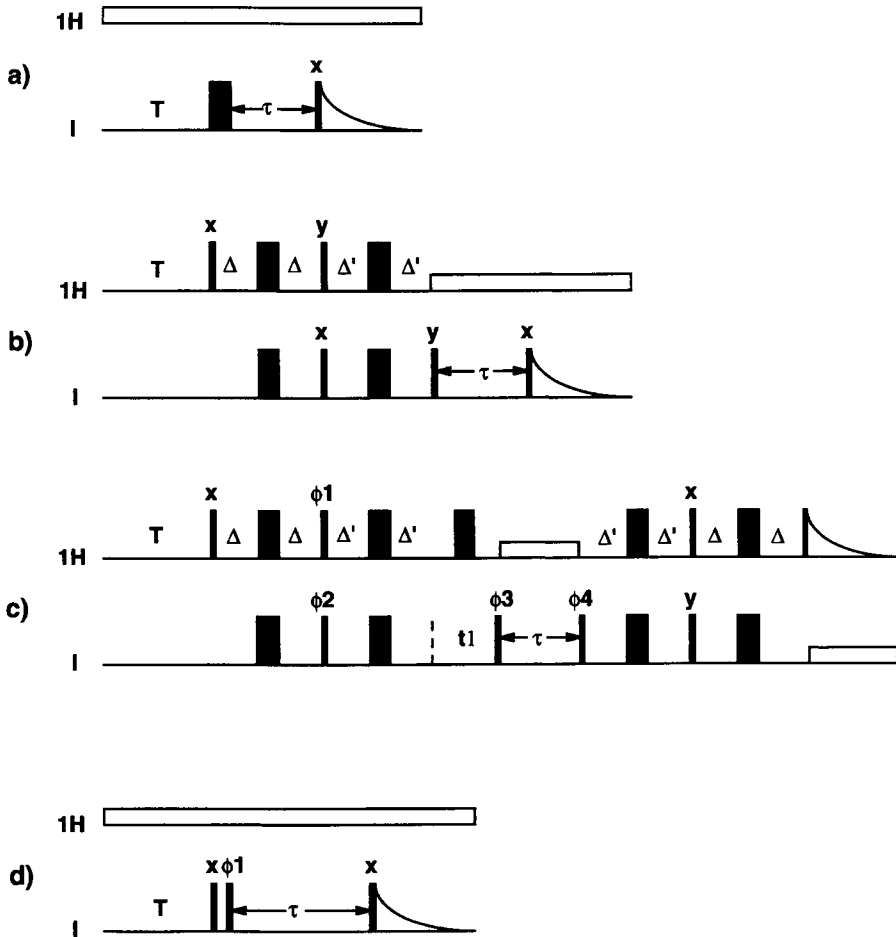


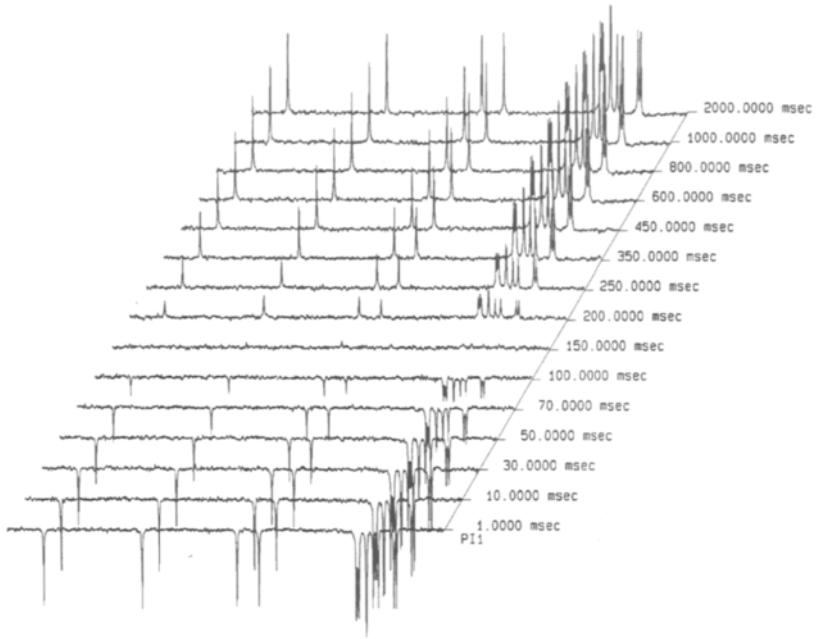
Fig. 1. Pulse sequences for determining spin-lattice relaxation time constants. Thin bars represent  $\pi/2$  pulses and thick bars represent  $\pi$  pulses. (a) The inversion-recovery sequence, (b) the INEPT-enhanced inversion recovery, (c) a two-dimensional proton-detected INEPT-enhanced sequence and (d) the CREPE sequence.  $T$  is the waiting period between individual scans. In (b) and (c),  $\Delta$  is set to  $(1/4)J_{\text{IH}}$  and  $\Delta'$  is set to  $(1/4)J_{\text{IH}}$  to maximize the intensity of IH heteronuclei and to  $(1/8)J_{\text{IH}}$  to maximize the intensity of  $\text{IH}_2$  spins. The phase cycling in (c) is as follows:  $\phi_1 = 8(y), 8(-y)$ ;  $\phi_2 = 4(x), 4(-x)$ ;  $\phi_3 = -y, y$ ;  $\phi_4 = 2(x), 2(-x)$ ; Acq =  $x, 2(-x), x, -x, 2(x), -x, -x, 2(x), -x, x, 2(-x), x$ . The one-dimensional version of the proton-detected experiment can be obtained by omitting the  $t_1$  delay. In sequence (d), the phase  $\phi_1$  is chosen as increments of  $2\pi/16$  in a series of 16 experiments.

days of carbon-13 NMR (cf. fig. 1(a)). In the terminology of the preceding section, the preparation period consists of the waiting period  $T$  and the  $\pi$ -pulse;  $\tau$  is the relaxation period, and the final pulse, together with the signal acquisition, constitutes the detection period. The whole sequence may

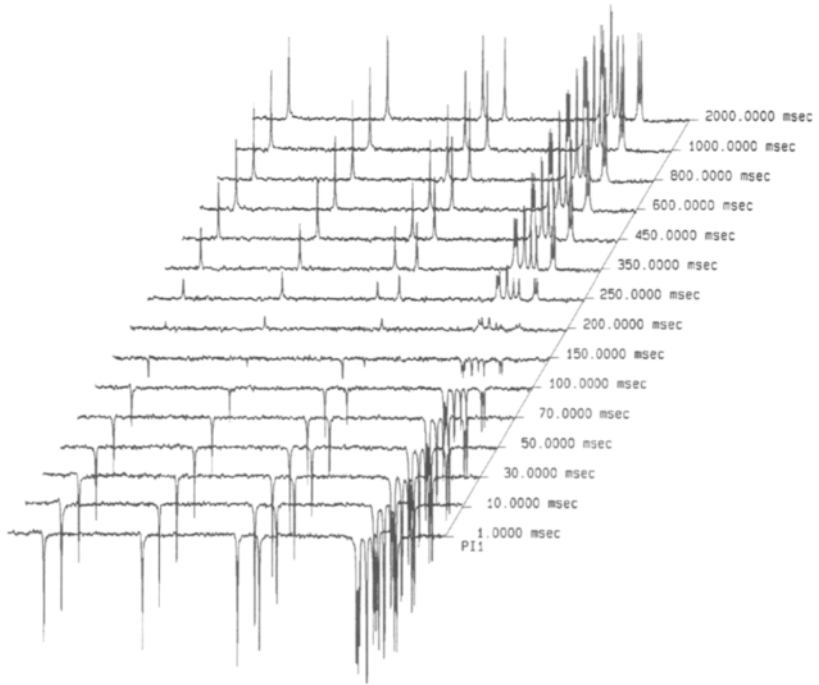
be repeated several times for a given relaxation period, in order to obtain an adequate signal/noise ratio. The  $T_1$  determination requires a repetition of the whole experiment for a series of different  $\tau$ -values. The waiting period at the beginning of the preparation period has to be larger than  $5T_1$ , which can be time-consuming if  $T_1$  of the I-spin is long. Canet and coworkers [25] have proposed a modification of the IR technique, called fast inversion-recovery, FIR, where the waiting period is shorter (of the order of  $1-2 T_1$ ) and the whole experiment is performed under steady-state conditions. Combination of the FIR technique with continuous broadband proton decoupling gives an efficient and robust experiment. Two simple and effective improvements of the basic scheme should be mentioned here: the use of a composite  $\pi$ -pulse to improve the inversion performance with the radiofrequency off-resonance [26], and phase-cycling to reduce artifacts [27].

In this section, a comparison between the various available methods will be presented from the viewpoint of optimizing the resulting precision and accuracy in the  $T_1$  values in the shortest length of experimental time. Clearly, preferences vary with the system under investigation. For small or medium-sized molecules, it is often sufficient to use the conventional IR or FIR methods to detect, for instance, carbon-13 relaxation. In a comparative study by Becker et al. [28] it was shown that the FIR technique is the most time-saving when comparing methods that use the NOE as signal enhancement. It may, however, be of interest to clarify whether there is any gain in sensitivity or in experimental time when performing polarization-enhanced experiments, as compared to the NOE-enhanced experiments. In a recent study from our laboratory, FIR and INEPT-enhanced carbon-13  $T_1$  relaxation experiment (the pulse sequence is shown in fig. 1(b)) were compared using the trisaccharide melezitose [29] and spectra obtained by the two methods are shown in fig. 2. As the NOE for the carbon was found to be in the range of 1.60–1.71 at the magnetic field-strength and temperature of the comparison, it is clear that, for this molecule, there should in principle be some signal intensity to be gained by using the INEPT-enhanced method. This was also found to be the case, which is evident from examining the spectra in fig. 2. The question still remains whether the quality of the relaxation data obtained differs between the two methods. In the above-mentioned study, it was found that the sets of relaxation times obtained with the two methods were nearly identical, within the error limits, and furthermore it was shown that the errors (standard deviations of the non-linear least-squares fit) of the  $T_1$  values were similar in magnitude for the two data sets. One may conclude that for molecules of this size there is no real reason for performing the polarization-transfer enhanced experiments.

As for inverse-detected one-dimensional relaxation measurements, there are problems related to the removal of proton signals originating from  $^1\text{H}$  not bound to  $^{13}\text{C}$  nuclei and to the fact that the  $^1\text{H}$  spectrum is in general



(a)



(b)

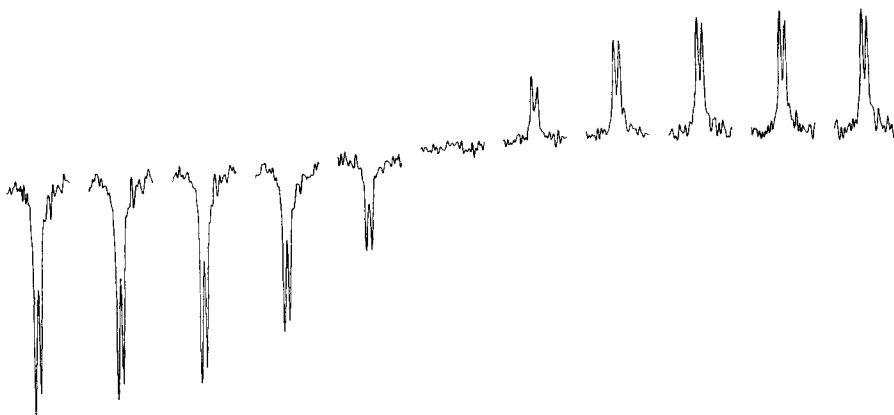


Fig. 3. Proton-detected carbon-13 spin-lattice relaxation for the pentasaccharide *p*-trifluoroacetamidophenyl-2,6-di-O- $[\beta$ -D-galactopyranosyl-(1  $\rightarrow$  4)-O-2-acetamido-2-deoxy- $\beta$ -D-glucopyranosyl] $\alpha$ -D-mannopyranoside. The measurements were performed with the two-dimensional method proposed by Skelton et al. [21], modified to obtain a one-dimensional pulse sequence. The figure shows the measurements for C1 in the 2-acetamido-2-deoxy-glucopyranose residue attached at position 2 on the mannopyranose residue.

more difficult to analyze in terms of well-separated signals. In consequence, the inverse detection schemes are usually not to be preferred for  $T_1$  relaxation measurements on small molecules. There are exceptions from this rule, though. In one of our studies, on a pentasaccharide [30], the carbon-13 spectra of two sugar units were completely overlapping, while the proton spectra could be resolved. The results of one-dimensional, proton-detected  $T_1$  measurement on this molecule are displayed in fig. 3. The pulse sequence employed is shown in fig. 1(c). Since the experiment was run in one dimension,  $t_1$  was not incremented.

For larger molecules the situation is different because of the more complicated spectra and because of the smaller NOE enhancements. Two-dimensional inverse-detection experiments are usually the only practical solution to performing relaxation measurements in larger systems, such as biomolecules. In principle, it should be possible to obtain the same signal-to-noise ratio by two-dimensional and one-dimensional methods in

←  
Fig. 2. Carbon-13 spin-lattice relaxation for melezitose, O- $\alpha$ -D-glucopyranosyl-(1  $\rightarrow$  3)- $\beta$ -D-fructofuranosyl-(2  $\rightarrow$  1)- $\alpha$ -D-glucopyranoside. Figure (a) shows spectra as a function of  $\tau$  obtained by the FIR method and (b) shows spectra obtained by the INEPT-enhanced experiment. Both series were acquired with 1024 transients, and in the same length of experimental time.

the same amount of time. In practice, however, the 2D methods are very time-consuming, because one two-dimensional data set has to be collected for every  $\tau$  value, which is equivalent in principle to performing a three-dimensional experiment, with the relaxation period being the third dimension.

Most relaxation measurements are conducted in such a way as to record the resulting magnetization after a variable delay,  $\tau$ , during which the initially created state is allowed to relax. In the spin-lattice relaxation experiment, the  $T_1$  relaxation time can be evaluated by non-linear three-parameter fitting of the following expression [31] to the intensities:

$$S_\tau = S_\infty \left[ 1 - A \exp\left(-\frac{\tau}{T_1}\right) \right], \quad (4.1)$$

where  $S_\tau$  is the measured signal intensity at the time  $\tau$ , and  $S_\infty$  is the equilibrium magnetization at very high  $\tau$ -values. The need for a three-parameter fitting procedure is evident if the FIR method is used, as the equilibrium magnetization will never be attained between individual scans, but rather a steady state. In the FIR experiment, the factor  $A = 2(1 - \exp(-T/T_1))$ , where  $T$  is the waiting period between transients. In some of the two-dimensional inverse-detection methods, the high- $\tau$  limit of the measured intensity is zero, and a two-parameter fit is adequate.

There are, however, other procedures one can think of for obtaining a relationship between the measured intensities and the  $T_1$  relaxation time constant. Recently, a novel procedure was proposed which involves the creation of different states of initial magnetization and the detection of the resulting magnetization after a constant relaxation period,  $\tau$  [32]. The experiment was named CREPE (Constant Relaxation Period). Different initial states are created by altering the phase of the second pulse,  $\phi_1$ , in the pulse sequence displayed in fig. 1(d). This enables the creation of a spread in the amount of created  $z$ -magnetization. The relationship between the amount of initial  $z$ -magnetization and the resulting longitudinal magnetization after a relaxation period is linear, with a slope depending on the longitudinal relaxation rate.  $T_1$  can thus be calculated from the slope of the straight line obtained by plotting pairs of initial and final magnetizations according to:

$$S_\tau = S_i \exp\left(-\frac{\tau}{T_1}\right) + S_\infty \left[ 1 - \left(-\frac{\tau}{T_1}\right) \right]. \quad (4.2)$$

It was argued that by the use of this method it is possible to increase the precision in the  $T_1$  value by a factor of two, as compared to what can be obtained by the FIR method with the same measurement time. With the constant-relaxation-period method, the number of systematic errors should decrease, since both the initial and final states are recorded for every phase,

TABLE I  
Results from  $T_1$  measurements with the CREPE method and the FIR method for selected carbons in melezitose at 7.05 T and 303 K.

Carbon	$T_1$ (ms)		
	CREPE <sup>a</sup>	CREPE <sup>b</sup>	FIR <sup>c</sup>
C-1g <sup>3</sup>	154 ± 14	168 ± 3	163 ± 2
C-1g <sup>2</sup>	164 ± 16	170 ± 5	152 ± 5
C-3f	150 ± 15	163 ± 3	157 ± 7
C-5f	170 ± 8	163 ± 4	153 ± 4

<sup>a</sup> CREPE experiment with  $\tau = 50$  ms and 10 pairs of initial and final magnetizations.

<sup>b</sup> CREPE experiment with  $\tau = 200$  ms and 16 pairs of initial and final magnetizations.

<sup>c</sup> FIR experiment with 16  $\tau$  increments.

$\phi_1$ , in the experiment. A comparison between  $T_1$  values obtained with the two methods for selected carbons in the carbohydrate melezitose, using a Varian Unity U300 spectrometer operating at 7.05 T, is presented in table 1. The CREPE experiment was performed with two different values of  $\tau$ , one shorter than  $T_1$  and one longer than  $T_1$ . Virtually no difference in  $T_1$  errors was found between the experiments performed with the two  $\tau$ -values. The CREPE experiment was also performed with different numbers of recorded magnetization pairs. Comparing the results, it was seen that the precision with which the  $T_1$  value could be measured, related to standard deviations of the fit to eq. (4.2), suffered dramatically when the number of magnetization pairs was decreased from 16 to 10. The CREPE experiment with 16 intensity pairs showed somewhat lower errors than the FIR sequence recorded with the same experimental time. It should also be noted that the relaxation times in table 1, obtained by the FIR and CREPE methods, in some cases differ from each other by more than the sum of the standard deviations of the two values.

Summing up, it may be concluded that for small molecules, with a relatively large heteronuclear NOE, the most efficient way of measuring  $T_1$  is by means of the Fast Inversion Recovery method. When the NOE is weak, signal gain may be achieved by performing polarization transfer experiments. For macromolecules, the use of proton-detected two-dimensional methods is necessary, both from the viewpoint of gaining signal-to-noise ratio, but also to increase the resolution by spreading out the signals in two dimensions. The novel experiment utilizing a constant relaxation period works well, and accurate  $T_1$  values can be obtained. It should, however, be pointed out that the method seems to be sensitive to the experimental setup, e.g., choosing the phases for the creation of the initial magnetization states.

## 5. Spin–spin relaxation rate measurements

The spin–spin relaxation rate,  $R_2 = T_2^{-1}$  with  $T_2$  defined by the Bloch equations [1], is simply related to the width  $\Delta\nu_{1/2}$  of the Lorentzian line at the half-height:  $\Delta\nu_{1/2} = 1/\pi T_2$ . Thus, it is in principle possible to determine  $T_2$  by measuring the linewidth. This approach has been demonstrated to work for carbon-13, provided the magnetic field homogeneity is very carefully shimmed [33]. The more usual practice, however, is to suppress the inhomogeneous broadening caused by the spread of the magnetic field values and thus resonance frequencies over the sample volume, by the spin-echo technique. Such experiments are in general more difficult to perform than the spin-lattice relaxation time measurements, as described in the previous section. The most common echo sequence, the  $(\pi/2)-\tau-(\pi)-\tau$ -echo, was originally proposed by Carr and Purcell [34] and modified (by introducing phase shifts) by Meiboom and Gill [35]. After the initials of the four authors, the modified sequence is widely known as the CPMG method. The details of the behavior of the spin isochromats under the spin-echo sequence can be found in modern NMR monographs [36] and will not be repeated here. We wish, on the other hand, to mention two interesting modifications of the basic sequence, the first one being the use of composite  $\pi$ -pulses, proposed by Levitt and Freeman [37]. Another modification is connected with the state of the spin system at the beginning of the echo-sequence, which is normally the equilibrium state. A modification replacing the equilibrium by a steady-state condition, similar to the fast inversion-recovery scheme [25], has been suggested by Forster [38] but does not seem to have gained any popularity.

The variation of the delay  $\tau$  in the spin-echo sequence results in a series of echo signals with amplitude decaying as  $\exp(-\tau/T_2)$ . The sequence in its simplest form is susceptible to artifacts, due to chemical exchange [39] and diffusion [39–41], and it is common practice to measure  $T_2$  by repeating the  $(\tau-(\pi)-\tau)$  part of the sequence a variable number of times while using a constant value of  $\tau$ . The relaxation rate is obtained by estimating the time constant of the exponential decay  $\exp(-t/T_2)$ , where  $t$  is the total time between the initial  $(\pi/2)$  pulse and the peak of the echo signal. This is in principle very simple, but one question arises immediately: should the duration of the repetitive  $\pi$ -pulses be included when calculating  $t$ ? Our way of answering this question is that it is essential, for performing a successful CPMG experiment, to have sufficient transmitter power to produce  $\pi$ -pulses of so short duration that it can safely be neglected in comparison with the delay  $\tau$ .

Performing the CPMG experiment on a spin system with homonuclear coupling introduces the complication of echo modulation by the scalar couplings [4, 5, 7, 36]. This makes transverse proton relaxation measurements

in most organic compounds rather impractical. We turn therefore to the case of a carbon-13, or another low natural abundance spin-1/2 nucleus, in a sample containing S-spins (normally protons) in high abundance. If only pulses at the resonance frequency of the I spins are used, the heteronuclear IS coupling behaves similarly to a chemical shift between the I spins carrying the  $\alpha$  and the  $\beta$  S-spins, and as such becomes refocused by the  $\pi$ -pulses [4, 5, 7, 36]. The heteronuclear couplings, however, cause other problems. First, we have the splitting of the I resonance into multiplets, which reduces the sensitivity and complicates the analysis. This problem is simple to solve: we only need to use the broadband S-spin decoupling during the acquisition of the I-spin echo signal. The second problem is more subtle and relates to the behavior of the coherences during the train of the  $\pi$ -pulses. As mentioned in the theory section, the relaxation of the in-phase I spin coherence,  $I_+$ , is coupled to the relaxation of the antiphase coherence,  $2I_x S_z$ . The transverse relaxation in such a two-spin system is thus characterized by two eigenvalues of the  $2 \times 2$  relaxation matrix. If the interference between the DD and the CSA interactions is not completely negligible (and in many cases of practical importance [42–44] it is not), then the two eigenvalues are different and the relaxation is biexponential. The trick used for suppressing the biexponentiality of the longitudinal relaxation – broadband S-spin decoupling during the whole relaxation period – is not practicable, because the broadband decoupling schemes destroy the transverse magnetization and prevent refocusing [45]. There are other means of suppressing the DD-CSA interference, but they put higher demands on the instrumentation.

One way to handle this problem, within the framework of the CPMG scheme, is to add proton pulses at judiciously chosen points in the train of the carbon  $\pi$ -pulses [42, 43]. An example of such a sequence is given in fig. 4(a). An important issue when setting up experiments of this type is the duration  $\delta$  between the pulses. On the one hand, it should be small compared to  $(1/2)J_{IS}$  [43]. On the other hand, it should be much longer than the relevant pulse widths. It is difficult to simultaneously fulfill both these requirements rigorously with typical high-resolution equipment, and some compromise has to be settled on.

An alternative method to get rid of the biexponentiality of the transverse I spin relaxation is to use the basic experimental scheme known as the measurement of “ $T_1$  in the rotating frame” or  $T_{1\rho}$ , instead of the CPMG approach. This was proposed, for the purpose of carbon-13 studies, by Ohuchi et al. [46] already in the late seventies. The general relation between  $T_2$ ,  $T_{1\rho}$  and other related quantities was discussed in that work and in the important paper by Vega [47]. The basic idea of the  $T_{1\rho}$  measurements is illustrated in fig. 4(b). After the initial ( $\pi/2$ ) I-spin pulse, the phase of the radiofrequency field is switched by  $90^\circ$ . The transverse mag-

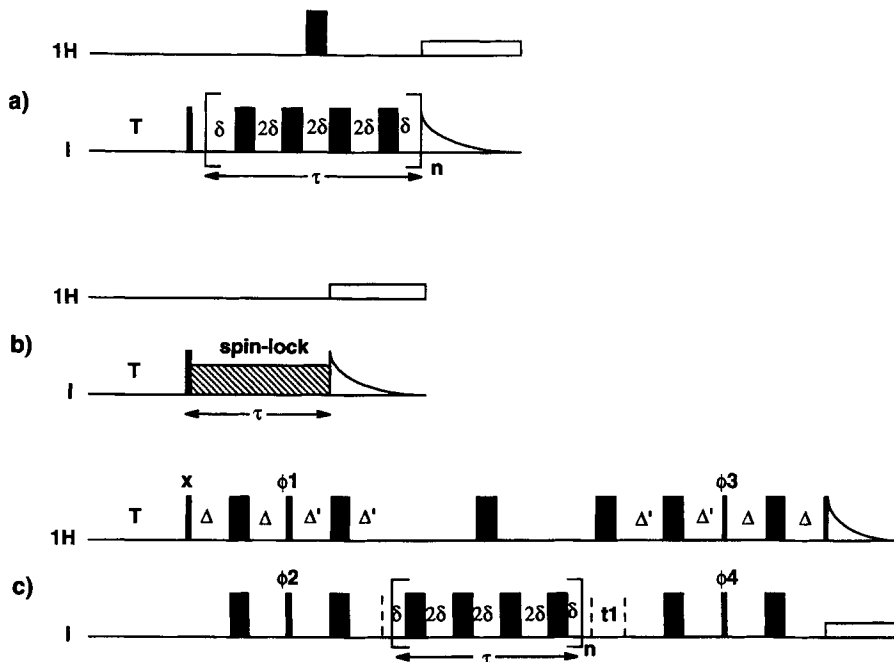


Fig. 4. Pulse sequences for determining spin-spin relaxation time constants. Thin bars represent  $\pi/2$  pulses and thick bars represent  $\pi$  pulses. (a) the CPMG sequence, (b) the spin-lock sequence used for determining  $T_{1\rho}$  and (c) a two-dimensional proton-detected INEPT-enhanced CPMG.  $T$  is the waiting period between individual scans. The pulse train during the  $\tau$  period is used for suppression of cross-correlation effects, and the delay  $\delta$  is set to  $< (1/2)J$ . The delay  $\Delta$  in (c) is set to  $(1/4)J_{IH}$  and  $\Delta'$  is set to  $(1/8)J_{IH}$  to maximize the intensity of IH heteronuclei and to  $(1/8)J_{IH}$  to maximize the intensity of IH<sub>2</sub> spins. The phase cycling in (c) is as follows:  $\phi_1 = y, -y$ ;  $\phi_2 = 2(x), 2(-x)$ ;  $\phi_3 = 4(x), 4(-x)$ ;  $\phi_4 = 8(x), 8(-x)$ ; Acq =  $x, 2(-x), x, -x, 2(x), -x, -x, 2(x), -x, x, 2(-x), x$ . The one-dimensional version the proton-detected experiment can be obtained by omitting the  $t_1$  delay.

netization created by the initial pulse is directed along the  $90^\circ$  phase-shifted radiofrequency field  $B_1$  and is “locked” along it. One can say (sacrificing some stringency) that the quantization axis of the I-spins is turned to be along the  $B_1$  field, and the relaxation can be pictured as being similar to the longitudinal relaxation along an axis defined in the rotating frame of reference; this explains the origin of the name. The application of the I-spin irradiation has the effect of decoupling the I and S spins. Thus, we only need to bother about the in-phase coherence  $I_+$ , and the problems of the biexponential relaxation are suppressed. In practice, the  $T_{1\rho}$  experiments are rather demanding. The  $B_1$  field is applied continuously over an extended period of time, which may be impossible to do with the full transmitter power. Thus, a capability of fast switching of the transmitter

power level (as well as the phase) should be available. In the case of a multi-line I spectrum, there is another complication. The amplitude of the  $B_1$  field should not be reduced too much during the spin-lock period, in order to maintain the spin lock condition for all the I nuclei characterized by different resonance frequencies. This requirement is formulated as  $\gamma B_1 \gg \delta\nu$ , where  $\delta\nu$  is the resonance offset in angular frequency units, and it is actually quite stringent. In practice, one finds it sometimes necessary to repeat the experiment with several different carrier frequencies in order to attain the proper spin-lock conditions for all the I-spin resonances [48]. In summary, our experience with the modified CPMG and  $T_{1\rho}$  experiments for carbon-13 is that their performances are rather comparable [48].

If the condition  $\gamma B_1 \gg \delta\nu$  is not fulfilled, then the experiment is called the “off-resonance spin-lock” or “ $T_{1\rho}$  experiment in a tilted rotating frame”. The experiments of this type, employing off-resonance conditions to a variable extent, have actually been proposed as a tool for varying the frequencies at which the spectral densities are being sampled [49]. The advantage of this approach is that it provides a means of estimating the rotational correlation time for macromolecules in solution.

The basic schemes for studying the transverse relaxation of carbon-13 or nitrogen-15, discussed above, can be combined with polarization transfer techniques in very much the same way as their longitudinal relaxation counterparts, discussed in the previous section. The advantages of the increased sensitivity and resolution, offset in a system-dependent way by the increased experimental complexity and the need for performing a full two-dimensional experiment, are fully analogous to the case of  $T_1$  measurements. An example of a 2D sequence of the CPMG-type, using the double INEPT-type transfer and inverse detection is shown in fig. 4(c) [42, 43]. Similar varieties based on the principles of the  $T_{1\rho}$  experiments have also been proposed [44, 50].

## 6. Cross-relaxation rates – heteronuclear NOE measurements

For a spin-1/2 nucleus, such as carbon-13, the relaxation is often dominated by the dipole–dipole interaction with directly bonded proton(s). As mentioned in the theory section, the longitudinal relaxation in such a system deviates in general from the simple description based on Bloch equations. The complication – the transfer of magnetization from one spin to another – is usually referred to as cross-relaxation. The cross-relaxation process is conveniently described within the framework of the extended Solomon equations. If cross-correlation effects can be neglected or suitably eliminated, the longitudinal dipole–dipole relaxation of two coupled spins, such

as a  $^{13}\text{C}$ - $^1\text{H}$  pair, can be described by a set of two coupled differential equations [51]:

$$\begin{aligned}\frac{d}{dt}\langle M_{\text{Cz}} \rangle &= -\rho_{\text{C}}\langle M_{\text{Cz}} - M_{\text{Cz}}^0 \rangle - \sigma_{\text{CH}}\langle M_{\text{Hz}} - M_{\text{Hz}}^0 \rangle, \\ \frac{d}{dt}\langle M_{\text{Hz}} \rangle &= -\sigma_{\text{CH}}\langle M_{\text{Cz}} - M_{\text{Cz}}^0 \rangle - \rho_{\text{H}}\langle M_{\text{Hz}} - M_{\text{Hz}}^0 \rangle.\end{aligned}\quad (6.1)$$

The terms  $\rho_{\text{C}}$  and  $\rho_{\text{H}}$  correspond to  $1/T_{1\text{C}}$  and  $1/T_{1\text{H}}$ , respectively, and  $\sigma_{\text{CH}}$  is the cross-relaxation rate. It should be stressed that the simplicity of the above equation is a consequence of the rareness of the I spins and of the dominant strength of the dipolar interaction between directly bonded nuclei. The situation for homonuclear proton spin systems is often more complicated, since the protons usually constitute a much larger spin system, and a separation into distinct two-spin systems may be not valid in this case. The broadband irradiation of the protons yields, in a steady state,  $M_{\text{Hz}} = 0$  and  $M_{\text{Iz}} = M_{\text{Iz}}^0(1 + \eta)$ . The factor  $1 + \eta$  is called, as introduced above, the nuclear Overhauser enhancement factor. The NOE factor is related in a simple way to the equilibrium magnetizations of the I- and S-spins (which are proportional to the magnetogyric ratios  $\gamma_{\text{I}}$  and  $\gamma_{\text{S}}$ ), the cross-relaxation rate and the relaxation rate of the I-spin:

$$\eta = \frac{\gamma_{\text{S}} \sigma_{\text{IS}}}{\gamma_{\text{I}} \rho_{\text{I}}}. \quad (6.2)$$

Thus, if  $\rho_{\text{I}}$  is known, then the measurement of  $\eta$  provides the  $\sigma_{\text{CH}}$  value. Under extreme narrowing conditions, the heteronuclear NOE reaches a maximum value (minimum for  $\gamma_{\text{I}} < 0$ ) and can be used to determine the dipole-dipole contribution to the total relaxation rate:

$$1 + \eta = 1 + \frac{\gamma_{\text{S}}}{2\gamma_{\text{I}}} \frac{R_{1\text{DD}}}{R_1}. \quad (6.3)$$

The ‘‘classical’’ method for determining the heteronuclear NOE factor for a I- $^1\text{H}$  spin system, the gated decoupling technique, was proposed by Freeman et al. [52]. The NOE factor is evaluated by taking the ratio of the signal intensity,  $S_{\infty}$ , of the heteronucleus after a long ( $>5T_1$ ) period of broadband decoupling of protons to the signal intensity,  $S_0$ , obtained with the decoupling switched on immediately prior to the observe pulse. Clearly, this can lead to systematic errors in the measurement of either the signal intensity obtained with a short irradiation delay or in the experiment with a long irradiation delay. Furthermore, in the measurement of heteronuclear NOE’s, it is important to choose the waiting period (which we in this context can call equilibration delay) in an appropriate way. The acquisition is

usually done with proton decoupling, and it is important to attain complete relaxation of the heteronuclear magnetization between individual scans. In order to improve the accuracy of the NOE factors, the dynamic NOE sequence [52, 53] can be used to obtain a series of NOE build-up spectra as a function of the time between switching on the decoupler and the observe pulse. A non-linear fit of peak intensities can thus provide the NOE factor [53]. This procedure should minimize systematic errors, and the fit provides an estimate of the relative error in the NOE parameters.

A few comments regarding NOE measurements for larger molecules or biomolecules in aqueous solution are appropriate. The methods of choice, for sensitivity and resolution reasons, for these systems in water solution are usually inverse-detected experiments. The experiments consist basically of an equilibration delay and a saturation on/off step, followed by the I spin  $90^\circ$  pulse, I spin frequency-labeling, polarization transfer to the protons and proton detection. In addition, some form of water signal suppression is usually applied. The goal is to obtain accurate estimates of the signal intensities with and without a proton saturation period at the beginning of the sequence, but obtaining a NOE-free intensity turns out to be rather complicated in  $^{15}\text{N}$  experiments on peptides and proteins. The main complication is due to chemical exchange between the amide protons, whose resonances report the behavior of the nitrogens, and the solvent water protons. This exchange process has several consequences. One issue that needs to be considered is the length of the equilibration delay: it should be rather long, to allow full relaxation of not only the amide protons, but also the water protons. Otherwise, the partial saturation of the water signal will reduce the intensity of the signal which is supposed to be free of the NOE and increase the estimated magnitude of the  $1 + \eta$  value [20]. As discussed by Skelton et al. [21], the NOE's can be corrected for this effect [54]. The second issue is the effect of the water suppression. The NOE-free signal should be obtained without any irradiation of the protons between the equilibration delay and the first I spin pulse. In the original work of Kay et al. [20], a short period of water presaturation through a selective pulse is inserted at this point of time. In spite of using selective saturation of the water signal, one may have problems with measuring NOEs due to exchange between water protons and the amide protons. An alternative way is therefore to apply a water suppression scheme just before the acquisition [55]. The use of pulsed field gradients to suppress the solvent saturation-transfer artifact in heteronuclear NOE measurements has also been suggested [22, 23, 56–58]. Another problem encountered in heteronuclear NOE measurements, discussed by Neuhaus and van Mierlo [55], is of a more trivial nature: the difference in the proton irradiation conditions between the spectra with and without the NOE creates a non-negligible temperature change in the salt-containing aqueous solutions.

## Acknowledgements

This work has been supported by the Swedish Natural Science Research Council. The grant of the U300 instrument time at the Swedish NMR Center is gratefully acknowledged.

## References

- [1] F. Bloch, *Phys. Rev.* **70** (1946) 460.
- [2] D.A. Wright, D.E. Axelson and G.C. Levy, in: *Topics in Carbon-13 NMR Spectroscopy*, Vol. 3, ed. G.C. Levy (Wiley, New York, 1979).
- [3] J. Kowalewski, *Ann. Rep. NMR Spectr.* **22** (1990) 307; **23** (1991) 289.
- [4] C.P. Slichter, *Principles of Magnetic Resonance* (Springer, Berlin, 1989).
- [5] A. Abragam, *The Principles of Nuclear Magnetism* (Oxford University Press, Oxford, 1961).
- [6] J. McConnell, *The Theory of Nuclear Magnetic Relaxation in Liquids* (Cambridge University Press, Cambridge, 1987).
- [7] R.R. Ernst, G. Bodenhausen and A. Wokaun, *Principles of Nuclear Magnetic Resonance in One and Two Dimensions* (Clarendon Press, Oxford, 1987).
- [8] R.L. Vold and R.R. Vold, *Progr. NMR Spectr.* **12** (1978) 79.
- [9] S. Szymanski, A.M. Gryff-Keller and G. Binsch, *J. Magn. Reson.* **68** (1986) 399.
- [10] L.G. Werbelow and D.M. Grant, *Adv. Magn. Reson.* **9** (1977) 189.
- [11] J.H. Noggle and R.E. Schirmer, *The Nuclear Overhauser Effect* (Academic Press, New York, 1971).
- [12] G.A. Morris and R. Freeman, *J. Am. Chem. Soc.* **101** (1979) 760.
- [13] D.M. Doddrell, D.T. Pegg and M.R. Bendall, *J. Magn. Reson.* **48** (1982) 323.
- [14] J. Kowalewski and G.A. Morris, *J. Magn. Reson.* **47** (1982) 331.
- [15] L.E. Kay, T.L. Jue, B. Bangerter and P.C. Demou, *J. Magn. Reson.* **73** (1987) 558.
- [16] V. Sklenar, D. Torchia and A. Bax, *J. Magn. Reson.* **73** (1987) 375.
- [17] G. Bodenhausen and D.J. Ruben, *Chem. Phys. Lett.* **69** (1980) 185.
- [18] N.R. Nirmala and G. Wagner, *J. Am. Chem. Soc.* **110** (1988) 7557.
- [19] N.R. Nirmala and G. Wagner, *J. Magn. Reson.* **82** (1989) 659.
- [20] L.E. Kay, D.A. Torchia and A. Bax, *Biochemistry* **28** (1989) 8972.
- [21] N.J. Skelton, A.G. Palmer, M. Akke, J. Kördel, M. Rance and W.J. Chazin, *J. Magn. Reson. B* **102** (1993) 253.
- [22] N.A. Farrow, R. Muhandiram, A.U. Singer, S.M. Pascal, C.M. Kay, G. Gish, S.E. Shoelson, T. Pawson, J.D. Forman-Kay and L.E. Kay, *Biochemistry* **33** (1994) 5984.
- [23] K.T. Dayie and G. Wagner, *J. Magn. Reson. A* **111** (1994) 121.
- [24] R.L. Vold, J.S. Waugh, M.P. Klein and D.E. Phelps, *J. Chem. Phys.* **48** (1968) 3831.
- [25] D. Canet, G.C. Levy and I.R. Peat, *J. Magn. Reson.* **18** (1975) 199.
- [26] M.H. Levitt and R. Freeman, *J. Magn. Reson.* **33** (1979) 473.
- [27] R.R. Vold and G. Bodenhausen, *J. Magn. Reson.* **39** (1980) 363.
- [28] E.D. Becker, J.A. Ferretti, R.K. Gupta and G.H. Weiss, *J. Magn. Reson.* **37** (1980) 381.
- [29] L. Mäler, J. Lang, G. Widmalm and J. Kowalewski, *Magn. Reson. Chem.* **33** (1995) 541.
- [30] L. Mäler, G. Widmalm and J. Kowalewski, *J. Biomol. NMR*, **7** (1996) 1.
- [31] J. Kowalewski, G.C. Levy, L.F. Johnson and L. Palmer, *J. Magn. Reson.* **26** (1977) 533.

- [32] H. Zhao, W.M. Westler and J.L. Markley, *J. Magn. Reson. A* **112** (1995) 139.
- [33] A. Allerhand and M. Dohrenwend, *J. Am. Chem. Soc.* **107** (1985) 6684.
- [34] H.Y. Carr and E.M. Purcell, *Phys. Rev.* **94** (1954) 630.
- [35] S. Meiboom and D. Gill, *Rev. Sci. Instrum.* **29** (1958) 688.
- [36] J.K.M. Sanders and B.K. Hunter, *Modern NMR Spectroscopy* (Oxford University Press, Oxford, 1993).
- [37] M.H. Levitt and R. Freeman, *J. Magn. Reson.* **43** (1981) 65.
- [38] M.J. Forster, *J. Magn. Reson.* **84** (1989) 580.
- [39] L.W. Reeves, in: *Dynamic Magnetic Resonance*, eds L.M. Jackman and F.A. Cotton (Academic Press, New York, 1975) p. 83.
- [40] P. Stilbs, *Progr. NMR Spectr.* **19** (1987) 1.
- [41] P.T. Callaghan, *Principles of Nuclear Magnetic Resonance Microscopy* (Clarendon Press, Oxford, 1991).
- [42] A.G. Palmer, N.J. Skelton, W.J. Chazin, P.E. Wright and M. Rance, *Mol. Phys.* **75** (1992) 699.
- [43] L.E. Kay, L.K. Nicholson, F. Delaglio, A. Bax and D.A. Torchia, *J. Magn. Reson.* **97** (1992) 359.
- [44] J.W. Peng, V. Thanabal and G. Wagner, *J. Magn. Reson.* **95** (1991) 421.
- [45] R. Freeman and H.D.W. Hill, *J. Chem. Phys.* **54** (1971) 3367.
- [46] M. Ohuchi, T. Fujito and M. Imanari, *J. Magn. Reson.* **35** (1979) 415.
- [47] A.J. Vega, *J. Magn. Reson.* **65** (1985) 252.
- [48] J. Kowalewski and G. Widmalm, *J. Phys. Chem.* **98** (1994) 28.
- [49] T. Schleich, C.F. Morgan and G.H. Caines, *Methods Enzymol.* **176** (1989) 386.
- [50] J.W. Peng, V. Thanabal and G. Wagner, *J. Magn. Reson.* **94** (1991) 82.
- [51] I. Solomon, *Phys. Rev.* **99** (1955) 559.
- [52] R. Freeman, H.D.W. Hill and R. Kaptein, *J. Magn. Reson.* **7** (1972) 327.
- [53] J. Kowalewski, A. Ericsson and R. Vestin, *J. Magn. Reson.* **31** (1978) 165.
- [54] G.M. Clore, P.C. Driscoll, P.T. Wingfield and A.M. Gronenborn, *Biochemistry* **29** (1990) 7387.
- [55] D. Neuhaus and C.P.M. Van Mierlo, *J. Magn. Reson.* **100** (1992) 221.
- [56] A. Ross, M. Czisch, T. Zink and T.A. Holak, *J. Magn. Reson. B* **102** (1993) 314.
- [57] S. Grzesiek and A. Bax, *J. Am. Chem. Soc.* **115** (1993) 12593.
- [58] Y.-C. Li and G.T. Montelione, *J. Magn. Reson. B* **105** (1994) 45.

This Page Intentionally Left Blank

---

# Subject Index

---

- acetone 311
- activation energy 272
- acquisition
  - delayed 191
  - sequential acquisition 190
  - – with TPPI, Redfield–Kunz approach 190
  - simultaneous acquisition 190, 191
  - S/N limited 191
- aliasing and folding
  - in remote dimension 191
  - multiple 200
  - of HoMQC spectra 190
  - single and double 191, 195
- alkanoylgluconolactones
  - 1D TOCSY of 141
- Arrhenius equation 272
  
- $B_0$  field
  - inhomogeneity 305, 311
- BIRD pulse 169
  - in HMQC experiments 169
- Bloch 242, 327
  - equations 253
- Bovine pancreatic trypsin inhibitor (BPTI)
  - TOCSY spectrum with  $^{13}\text{C}(\omega_1)$  half-filter 159
- BURP pulses
  - in DANTE-Z mode 125
- BWR theory 328
  
- carbon-13 327, 331, 332
  - satellite 94, 100
  - spin-lattice relaxation time 332
- carrier position (frequency) 57
  - in acquisition dimension 193
  - off-resonance 190, 194
- cembrene
  - selective INADEQUATE spectra of 37
  
- chemical shift selective filter (CSSF) 56, 57, 144
  - excitation profile of 56
  - frequency selection with 56
  - in multiple polarization transfer experiments 77
  - selectivity of 56
- cinnamic aldehyde
  - heteronuclear multiple selective COSY of 39
- coherence
  - order 111, 329
  - selection 190, 194
    - – during data processing 190, 194
    - – N-type selection 113
    - – using phase cycling 111, 190
    - – using pulsed field gradient (PFG) 58, 98, 143, 194, 198
  - single-quantum (SQ) 190
  - transfer 271
    - – artifacts suppression 271
    - transfer pathway 111
    - zero-quantum (0Q) (ZQC) 190, 138
- combined 1D experiments 55
  - transformation of  $n$ D NMR techniques into 55
  - with multiple polarization transfer steps 59
- correlation
  - AB type, in 2D-INADEQUATE 192
  - through-bond (spin–spin coupling) 53, 136, 145, 189
    - through space (NOE, ROE) 53, 145
- correlation time 69, 109, 268
  - determination of 282
    - – COSY-NOESY, 1D 81
    - – – of a bacterial polysaccharide 82
    - – COSY-RELAY, 1D 78
    - – – of a modified LPS 78
  - temperature dependence 272

- COSY
- MQ-COSY 189
  - MQF-COSY 189
  - RELAY-COSY 189
  - type presentation of pure phase 2Q-HoMQC spectra 190
- COSY-TOCSY, 1D 78
- coupling
- strong 100, 102
  - weak 100
- coupling constant
- carbon-carbon, one-bond, long-range 35, 36
  - proton-proton (homonuclear) 93, 99, 133, 135, 138
  - proton-carbon, long-range 44, 94, 144
- cross-relaxation 267
- heteronuclear
    - - NOE measurements 343
    - - - biomolecules 345
    - - - - chemical exchange 345
    - - - - - water solution 345
    - - - - - dynamic NOE sequence 345
    - - - - - systematic errors 345
    - - - - - extreme narrowing 344
    - - - - - gated decoupling 344
    - - - - - Solomon equations 343
    - - - - - steady state 344
  - homonuclear
    - - high temperature 289
    - - influence of temperature 272
    - - low temperature 289
    - - rigid molecule 282
    - - rotating frame 269
- cyclohexane 256
- *chair-chair* inversion 256
  - rate of inversion 257
- cyclo(Pro-Gly) 282
- cyclosporin 154
- 2Q-HoMQC spectrum of 205
- DANTE 246
- DANTE-Z 123
  - - band-selective technique 125
  - - dispersive component 123
  - - flip angle 123
  - - gradient pulse (PFG) 125
  - - in pseudo 3D 125
  - - relaxation 129
  - - sinc oscillations 123
  - - selective  $z$  profile 123
- data processing
- of HMBC spectra 182
  - reference deconvolution 305-316
  - States-method 182
  - symmetrization 191, 205
  - - lateral, diagonal 202, 205
  - to disentangle the superimposed responses (spectra) 21, 42
- data size
- reduced by aliasing 191
- decoupling
- time-shared homonuclear 97, 102
- degenerate
- chemical shift 99
  - spin system 93
- density operator 328
- desertomycin 175
- difference
- double 37, 41
  - NOE 109
  - spectroscopy 110, 111
  - spectrum 109
- diffusion ordered spectroscopy (DOSY) 211
- with high resolution (HR-DOSY) 211
  - - data analysis 216
  - - - decomposition 217
  - - - errors on diffusion coefficients 218
  - - - FIDDLE algorithm 218
  - - - Gaussian fit of decay 216
  - - - iterative fitting 217
  - - - systematic errors 217
  - -  $^{13}\text{C}$  NMR 224
  - -  $^1\text{H}$  NMR 212
  - - LED sequence 213
  - - - BPPLIED 213
  - - - interleaved acquisition 215
  - - - phase cycling 213
  - - - repetition rate 215
  - - on small molecules 212
  - - - examples 219
  - - - - extract of gerbil brain 219
  - - - - spearmint oil 219
  - - - - manipulation of sample 225
  - - spin echo 212, 213
  - - - stimulated 213
- dipole-dipole interaction 268
- Dirichlet function 306
- dispersive phasing (DA phasing) 190, 205
- DNA hexadecamer duplex 189
- HoMQC spectrum of, without and with aliasing 198
- DSS (sodium 3-trimethylsilylpropanesulfonate)
- in DOSY 219

- duty cycle 97
- dynamic processes 267
- dwelt time 97, 191
  
- equilibrium 267
  - constant 257
- erythromycin 175
- ethanediol 100
- ethanol 311
- evolution
  - of chemical shift 113, 144
  - – during CSSF 56, 79
  - of heteronuclear coupling 96
  - of homonuclear coupling during CSSF 78
- exchange
  - chemical 229, 267, 269
  - data analysis 240
  - experimental conditions 240
  - – baseline 240
  - – lineshape reference 240
  - – waiting time 240
  - incoherent magnetization 272
  - influence of temperature 240, 272
  - intermediate 234
  - – lineshape analysis 231
  - intermolecular 269
  - intramolecular 269
  - timescale 231
  - – fast 231
  - – slow 231, 269
  - EXSY (chemical exchange spectroscopy) 273
  - – mixing time 280
  - – practical aspects 280
  - – quantitative interpretation 281
- excorcycle
  - in HSQC with spin-lock 154
- eyring plot 230, 259
  
- fast-switching linear attenuator 136
- FIDDLE (reference deconvolution)
  - in DOSY 218
- Fourier 267
  - inverse Fourier transform 305
  - pulse FT methods for  $T_1$  242
- frame
  - rotating 268
  - – ROESY (rotating frame Overhauser effect spectroscopy) 273
  - – elimination of the coherence transfer from 271
- fullerene 321
  
- furfural (2-furaldehyde)
  - fast exchange in acetone- $d_6$  233
  
- Ge-NOESY-TOCSY, 1D 84
  - of LPS O-polysaccharide 84
- Gibbs free-energy 235
- GOESY 112
- gradient enhanced 58, 59, 112
- GROESY 109–118
  
- Haasnoot equation 100
- Hilbert transform 308, 309
- HoMQC (homonuclear multiple-quantum correlation spectroscopy) 189–206
  - $^{13}\text{C}$ ,  $^{13}\text{C}$ -HoMQC spectrum 191, 194, 195
  - $^1\text{H}$ ,  $^1\text{H}$ -HoMQC spectra 189–206
  - 2Q-HoMQC 189, 190, 194
  - 3Q-HoMQC 194
  - symmetric 2Q-HoMQC spectrum 201
- half-filter ( $^{13}\text{C}$ )
  - E-COSY pattern 159
  - $^1\text{H}$ - $^{13}\text{C}$  coupling constant 159
  - pulse sequence 158
  - TOCSY with 158
  - to measure small heteronuclear coupling constants 157
  - with spin-lock purge pulse 157
- heteronuclear
  - long-range couplings 175
  - multiple bond correlation (HMBC) 175
  - – decoupled version (D-HMBC) 175
  - – phase sensitive 175
  - – low-pass  $J$ -filter 176
  - –  $t_1$ -noise 180
  - multiple quantum correlation (HMQC) 175, 176
- HMQC 154
  - TANGO in 156
- HMQC-, HSQC-TOCSY 144
- HSQC 154
  - comparison with the HMQC experiment 154
  - for small multiple bond heteronuclear couplings 156
  - $^1\text{H}$ - $^{15}\text{N}$ , in cyclosporin 154
  - pulse programme 156
  - with spin-lock purge pulse 156
  
- INADEQUATE, 2D 191
- inclusion complex

- of 4-hydroxybenzoic acid in  $\beta$ -cyclodextrin ( $\beta$ -CD) 118
- GROESY spectra of 118
- INEPT, 1D, selective reverse 93–104
- initial slope 110
- initial buildup rate analysis 279
- cross peaks normalized with their respective diagonals 280
- Taylor series 279
- - higher-order terms 279
- interference 329
- inversion recovery (IR) 333
- fast IR (FIR) 319, 333, 335
- off-resonance effects 335
- - composite pulse 335
- - phase cycling 335
- SUFIR 319–323
- three-parameter fitting 338
  
- J*-coupled spin network 110, 111
  
- kinetic
- matrix **K** 238
  
- line broadening
- differential 329
- lineshape
- absorption 138
- correction in *in vivo* spectra 307
- correction in high resolution NMR, in difference spectroscopy, in 2D NMR 307
- dispersive contributions to 138, 143
- Gaussian 311, 312
- instrumental (experimental) 305, 306
- Lorentzian, natural 305, 312
- mixed phase 80
- Lineshape analysis 231
- coalescence point 235
- DNMR3 program 240
- intermediate exchange regime 234
- iterative 235
- Lorentzian 235
- theory 235
- - density matrix formalism 236
- - transition probability 236
- - - phase distortion 238
- - - perturbation theory 237
- - - real and imaginary 238
- - - time domain 236
- Liouville 238
- matrix  $i\mathbf{L} + \mathbf{R} + \mathbf{K}$  239
- - eigenvalues 239
- - eigenvectors 239
- - - projections of 240
- Hermitian 239
- space 238
- - scalar product in 239
- superoperator **L** 238
- local oscillator (LO) 97
- long-range couplings
- in D-HMBC experiment 175
- low-pass filter 45
  
- magnetization
- antiphase 78
- in-phase 78, 81
- longitudinal, transverse 268
- transfer
- - coherent 110, 271
- - - elimination 271
- - incoherent 267
- - propagation of 139
- magnetogyric ratio 332
- magnitude spectrum
- in SUFIR 321
- menthone 100
- migration 268
- mixing time 110
- isotropic 81, 134
- random variation 271
- with MLEV17, WALTZ17, DIPSI 84, 134, 136
- mixture analysis
- LC-NMR 211
- DOSY 211
- - HR-DOSY 212
- - instrumental time 212
- of body fluids 211
- molecular motion 268
- monazomycin 176
- motional regime 269
- extreme-narrowing 269
- spin-diffusion 269
- multidimensional NMR, *see also* specific NMR experiments
- 2D (two-dimensional) 189–206
- - HMBC 94, 103
- - HMQC 94, 103
- - HMQC-TOCSY 94
- - INADEQUATE 191
- - NOESY 109
- - NOESY-TOCSY 53

- ROESY 110
- ROESY-TOCSY 54
- TOCSY 103, 189
- TOCSY-NOESY/ROESY 53
- 3D (three-dimensional)
- 3D COSY-NOESY, ROESY-TOCSY 54
- 3D HOHAHA-COSY 42
- 2D analog of 42
- 3D-NOE/2QC 189
- 3D NOESY-HOHAHA, HOHAHA-NOESY, NOESY-COSY 54
- 4D (four-dimensional)
- 1D analog of 54, 57, 58, 64
- reference deconvolution in 309–311
- multiple-quantum (MQ)
- coherences 189
- correlation of 190
- excitation delay 189, 193
- multiple-quantum correlation spectra 189–206
- direct, remote and combination peaks, in 189, 192, 195, 198, 200
- multiplet
- antiphase 8, 39, 96
- in-phase 8, 39, 60, 96
  
- nitrogen-15 327, 331
- spin-lattice relaxation time 332
- NOESY (nuclear Overhauser effect spectroscopy) 273
- artifacts
- *J*-peaks 285
- zero mixing time 283
- cross-relaxation rate 276
- dynamic matrix 276
- error in 279
- exchange rate 276
- full matrix analysis 276
- interproton distances 281
- quantitative 275
- spin-diffusion 293
- NOESY, 1D 110
- NOESY-NOESY, 1D 72, 74
- NOESY-TOCSY, 1D 59
- NOESY-TOCSY-NOESY, 1D 64, 66
- to locate phosphorylation site in an oligosaccharide 66
- non selective inversion recovery 243
- nuclear Overhauser effect (NOE) 109–118, 268
- direct enhancement 114
- indirect enhancement 113, 114
- interglycosidic 61
- NOE null 110
- reference deconvolution in NOE difference spectroscopy 313–315
- steady-state NOE 27, 331
- transient NOE 110, 27
- nucleic acid 198
- Nyquist-theorem 190
  
- O-chain polysaccharide
- from *Proteus mirabilis* 74
- 1D NOESY-NOESY of 74
- O-specific polysaccharide
- octasaccharide repeating unit of 139
- 1D TOCSY subspectra of 139
- off-resonance effect 96
- offset-saturation experiment 250
- application for  $T_1$  and  $T_2$  measurement 251–253
- data analysis 253
- experimental 254
- calibration of  $B_2$  field 254–256
- fast exchange region 259
- magnetic field inhomogeneity 256
- theory 253
- oversampling 191
  
- peracetylated triglucose
- 1D TOCSY subspectra of 30
- phase
- correction 136
- difference between soft and hard pulses 56, 136
- phase cycling 110
- EXORCYCLE 98, 114
- split phase cycling 311, 315
- polarization 267
- transfer
- by DEPT, SEMUT, INEPT 3, 332
- coherent 53
- concatenation of 57
- double 332
- for  $I_nS$  spin system 96
- incoherent 53
- multiple 57, 59
- population 329
- portmicin 184
- power spectra
- in SUFIR 321
- presaturation
- of proton magnetization 95
- primycin
- 2Q- and 3Q-HoMQC spectra of 201

- product operator 328
  - for HSQC 152
  - for half filter 157–159
- promethiocin B 179
- protein
  - 2Q- and 3Q-HoMQC spectra of, rabbit uteroglobin 195
  - 2Q-HoMQC spectrum of, apo-cytochrome *c* 198
- purging
  - spin-lock 151
- pseudo-3D experiment 145
- pulse
  - adiabatic 194
  - homospoil 95
  - purge 39, 40
  - spin lock 95, 143
  - trim 134
- pulsed field gradient (PFG) 333
  - amplitude of 111
  - duration of 111
  - effect of 111
    - dephase, rephase 58, 84, 86, 111, 113
  - excitation sculpting 168
  - for coherence pathway rejection 58
  - for coherence selection 58, 99, 111, 198
    - *N*-type selection 113
  - for suppression of unwanted coherences 58
  - in DANTE-Z 123
  - in solvent suppression 168
    - paramagnetic relaxation reagent 168, 169
    - WATERGATE 168
- pulse sequence
  - for HSQC with spin-lock 153
  - with gradient coherence selection 99, 111, 198
  - with multiple selective excitation 21–49
    - principle of 23
    - selective 1D and 2D experiments 21–49
    - with selective excitation, *see also* specific 1D NMR experiments
      - 1D TOCSY 28, 134
      - GROESY 111
      - selective reverse INEPT 95
      - SELINCOR 41, 99
- quadrature detection
  - no quadrature, in remote dimension 193
  - quadrature sign discrimination 191
- quinoline 321
- Redfield 238
  - matrix *R* 238
  - elements 329
    - anti-phase 329
    - in-phase 329
- reference deconvolution 305–316
  - in difference spectroscopy, NOE 309, 313–315
  - in multidimensional spectroscopy 309–311
  - reference signal 305, 308
    - absorption mode of, dispersion mode of 308
- reference deconvolution algorithms 308
  - FIDDLE (Free Induction Decay Deconvolution for Lineshape Enhancement) 311
  - QUALITY (QUAntification improvement by converting Lineshapes to the Lorentzian Type) 308
  - RLSA (Reference LineShape Adjustment) 307, 308
- relaxation
  - auto 329
  - BWR theory 328
  - cross 329
  - cross-correlation 329
  - chemical shift anisotropy (CSA) 330
  - dipolar 330
  - during selective pulses 14, 15
  - *I* = 1/2 nuclei 327
    - low natural abundance 327
  - interference 329
  - inverse detection 332
    - biomolecules 332
  - longitudinal ( $T_1$ ) 14, 30
  - longitudinal, transverse 268, 327
  - measurements 330
  - multi-exponential 329
  - paramagnetic 330
  - rates 327
  - scalar (SC) 330
  - spin-lattice 327
  - spin rotation (SR) 330
  - spin-spin ( $T_2$ ) 305
- RELAY-NOESY, 1D 81
  - of oligosaccharide 83
- resolution
  - digital 22, 54, 135
  - enhancement 307, 312
  - spectral 191
- RNA
  - HoMQC spectrum of 24-mer RNA hairpin, multiple aliasing 198

- ROE, ID 109–118
- ROESY (Rotating frame Overhauser Effect Spectroscopy) 273
- T-ROESY (transverse ROESY) 275
  - suppression of the coherence magnetization transfer in T-ROESY 275
  - TOCSY peaks 285
  - spin-lock power 285, 286
- ROESY experiment 110
- ROESY-TOCSY, ID 69
- Rotameric equilibrium 100
- rotating frame 251
- cross-relaxation rate 110, 112
  - spin-lattice relaxation time  $T_{1\rho}$  251
  - off-resonance  $T_{1\rho}$  252
- $\text{Ru}_2(\text{CO})_6(\mu_2\text{-PPh}_2)(\mu_2\text{-}\eta^1\text{:}\eta^2\text{-C}\equiv\text{C-}i\text{-Pr})$
- alkyne flips 247
  - concerted mechanism 249
  - carbonyl scrambling 249
- saturation transfer method 242
- Bloch equations 242
- selective experiments
- heteronuclear
    - – 1D heteronuclear NOE 23, 31
    - – 1D heteronuclear one-bond, long-range COSY 23, 37
    - – 1D HMQC-, HSQC-TOCSY 144
    - – 1D INADEQUATE 23, 35
    - –  $^{13}\text{C}$ -filtered 1D TOCSY 144
    - – selective 2D HMBC 23, 44
    - – selective reverse INEPT 93–104
    - – SELINCOR 99
    - – SELINQUATE 36
  - homonuclear, *see also* specific 1D experiments
    - – 1D TOCSY 22, 23, 28, 133
    - – GROESY 109–118
    - – selective 2D TOCSY-COSY 23, 42
- selective inversion recovery method 241
- experimental methods 246
    - – DANTE 246
    - – initial conditions 246
  - Hoffman-Forsén method 241
  - mass balance 244
  - NOE 244
  - quantitative analysis 244
    - – matrix method 245
    - – non-linear least-squares 245
    - – – errors in parameters 246
    - – – – confidence region 246
  - slow exchange conditions 241
    - – comparison with EXSY 241
    - – initial state 242
    - two-site system 245
  - selective (soft) /semiselective (band-selective) pulses 3–17, 55, 56, 135, 136
    - calibration of 11
    - DANTE 22, 96, 136
    - DANTE-Z 55, 64, 145
    - dispersive component of 56, 69
    - evolution of coupling during 55
    - excitation profile of 6
    - frequency response of 5
    - on-resonance, off-resonance 24, 64, 74
    - phase distortions caused by 12
    - rectangular pulse 6, 10, 11
    - relaxation during 14, 15, 134
    - self-refocusing during 8, 136
    - shaped pulses
      - – E-BURP-1/2, I-BURP2 5, 10, 11, 145
      - – for excitation, for inversion, for refocusing 3–16
      - – Gaussian 4, 10, 11, 55, 56, 69, 114, 134
      - – Gaussian cascades ( $G^3$  and  $G^4$ ) 6
      - – half-Gaussian 55, 56, 60, 69
      - – purged half-Gaussian 135, 136
      - – Quaternions cascades ( $Q^3$  and  $Q^5$ ) 4–6, 12
    - transition region of 4–6, 11
    - universal/non-universal pulses 6, 10, 57
- sensitivity 191, 193
- enhancement by polarization transfer 94
  - of 2Q-HoMQC and 3Q-HoMQC spectra 194
- sequential connectivities 138, 139
- shielded probehead 114
- signal
- on-resonance, off-resonance 144
- signal-to-noise (S/N) ratio (*see also* sensitivity) 191, 306, 312, 313
- in inversion recovery experiment 319
- silicon-29 332
- spin-lattice relaxation time 332
- solvent signal suppression 86, 111
- by pulsed field gradients (PFG) 168
  - by spin-lock pulses 163
    - – product operator description 163–165
    - – pulse sequence 164
    - – water suppression 163
    - – in NOESY and ROESY 165
    - – radiation damping 165
- spectral density 328
- spectral editing 23, 80
- in proton spectrum 93

- spin coupling network 7, 29, 135
- spin diffusion 74
- spin echo
  - in DOSY 213
- spin-lock
  - field 110, 111
  - axis 64, 70
  - pulse 95
  - – double-selective 145
  - – by cosine-modulated selective pulse 144
  - – by interleaved DANTE 145
  - purge pulses 151
  - – in HMQC experiment 154
  - – for  $^{13}\text{C}$  HSQC experiment 151
  - –  $^{13}\text{C}$  half filter 151, 157
  - – side-effects 151
  - – water–protein NOEs 151
  - – – NOESY and ROESY 151
  - spatial inhomogeneity of  $B_1$  151
  - T-ROESY 114
- spin ping
  - related to DANTE-Z 129
- spinning sidebands
  - suppression of 311
- stochastic processes 328
- Streptococcus capsular polysaccharide 61
  - 1D NOESY-TOCSY spectra of 61
  - 1D TOCSY-NOESY spectra of 64
  - 1D TOCSY-NOESY-TOCSY of 66
  - 1D TOCSY-TOCSY of 74
- strychnine
  - GROESY spectra of 117
- subspectrum 24, 80, 135, 139
  - 2D COSY subspectra 43, 44
  - of peracetylated triglucose, 1D TOCSY 30
- subsystem
  - isolated spin 28, 29, 42, 135
- subtraction error 109
- sucrose octaacetate 315
- SUFIR 319–323
  - data analysis 321
  - elimination of transverse magnetization 320
  - optimal choice of tau 320
  - partially relaxed spectrum 320
- sugar 337
  - melezitose (trisaccharide) 335
- $T_1$  (spin-lattice relaxation time) 327
  - measurement
  - – constant relaxation time period method (CREPE) 338
  - – – comparison of methods 339
  - – fast inversion recovery (FIR) 335
  - – inversion recovery (IR) 333
  - – rotating frame ( $T_{1\rho}$ ) 341–343
  - – SUFIR (super fast inversion recovery) 319–323
  - – – uncertainty in  $T_1$  320
  - $T_{1\rho}$  341–343
    - spin-lock 342, 343
    - – off-resonance 343
  - $T_2$  (spin–spin relaxation time) 234, 250, 251, 340
    - Lorentzian line 340
    - spin echo 250, 251, 340
    - – artifacts due to 340
    - – – chemical exchange 340
    - – – spin diffusion 340
    - – inhomogeneous broadening 340
    - CPMG method 250, 251, 340
    - – DD/CSA interference 341
    - – duration of pi pulse 340
    - – heteronuclear couplings 341
    - – homonuclear couplings 340
    - – pulse repetition rate 251
    - – 2D sequence 343
    - $T_{1\rho}$  method 341–343
    - offset-saturation method 234, 250
- thermodynamic functions 229
  - activation parameters 231
  - theory 229
- tigogenin glycoside 102
  - selective reverse INEPT spectra of 102
- time correlation function (TCF) 328
  - stochastic processes 328
- $t_1$ -increment 111, 191
- $t_1$ -noise 309
  - reduction of, in HMQC experiment 309–311, 315
- TOCSY
  - with  $^{13}\text{C}$  ( $\omega_1$ ) half filter 157, 158
- TOCSY, 1D 133
  - applications of 138
  - $^{13}\text{C}$ -filtered 144
  - double selective 144
- TOCSY-NOESY, 1D 59, 145
  - double-selective 145
- TOCSY-NOESY-TOCSY, 1D 64
- TOCSY-TOCSY, 1D 72
- TORO (TOCSY-ROESY), 1D 69, 113, 145,
  - double-selective 145
- trajectories 6, 15
- T-ROESY 111–113

- truncation level 136
- two-dimensional, 2D 267, 330, 331
  - detection 330, 331
  - evolution 330, 331
  - preparation 330, 331
- water–protein NOEs 151
- waveform generation unit 136
- zero-fill 309
- z-filter 138
- z-gradient coil 114

This Page Intentionally Left Blank